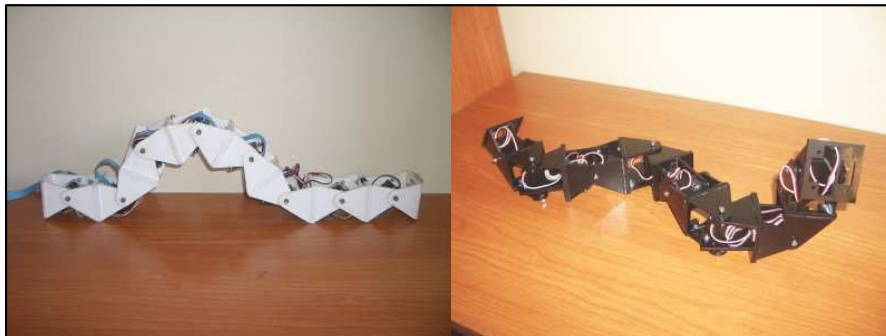


UNIVERSIDAD AUTÓNOMA DE MADRID
ESCUELA POLITÉCNICA SUPERIOR



Ph.D. Thesis

MODULAR ROBOTICS AND LOCOMOTION: APPLICATION TO LIMBLESS ROBOTS



Author:
JUAN GONZÁLEZ GÓMEZ
Telecommunication Engineer

Supervisor:
Dr. EDUARDO BOEMO SCALVINONI

Translator:
TREVOR WALTER ROUTLEY

Madrid, 2008

Acknowledgements

So many people have helped me, guided me and motivated me during these years of doctoral study that there is no room to express my thanks to all of them.

Firstly I would like to thank my supervisor, Eduardo Boemo who had confidence in me and permitted me to pioneer the investigation in Spain of Modular Robotics. Many thanks as well to Francisco Gómez (Paco) for his recommendations, his constant interest and his corrections. For me he has been like a second director of studies. Also thanks are due to professor Andrés Perez-Urbe of the Haute Ecole d'Ingénierie et de Gestion du Canton de Vaud (HEIG-VD), Switzerland and professor Jianwei Zhang of Hamburg University for his favourable comments. Many thanks also to Dave Calkins of San Francisco State University for writing the fantastic prologue to the thesis.

Many thanks to all my colleagues in the laboratory: Sergio López-Buedo, the great living encyclopaedia who was always willing to share freely of his knowledge and help. Gustavo Sutter and Elías Todorovich for all the good advice and suggestions that they have given me. Estanislao Aguayo and Jose Alberto Hernández for their help with Octave/Matlab and why not, for Iván González, with whom I have shared conversations, congresses, summer courses, times of relaxation, and why not admit it, the occasional party.

I want to also thank Miguel Ángel García for all his help and support, Susana Holgado, Javier Garrido and Guillermo González de Rivera for including me in the robotics workshops and other robotics information events at EPS, Pablo Varona, Francisco de Borja and Fernando Herrero for their interest in my investigations and for opening the doors to computational neuroscience and Profesor Miguel López of the Biology Faculty for given his valuable time to advise me. Also many thanks to Juana Calle for her help in fighting 'red tape'.

Many thanks to all my colleagues of the TAMS group of the University of Hamburg, for the way in which they received me and the good times we had together: Tim Baier, Sascha Jockel, Andreas Mäder, Manfred Grove and Daniel Westhoff. Special thanks to Tatjana Tetsis (Lu) for her logistic help and to Professor Jianwei Zhang for allowing me to be part of his group for three months. I am specially indebted to Houxiang Zhang who adopted me as his disciple and shared with me his wisdom. Since then we have continued to work together.

I must thank all those who have invited me to demonstrate my robots in different events, congresses and seminars, as well as all those who have freely given of their time to show me around their laboratories, share with me their investigations and advise me. Arturo Morgado of the UCA (Cádiz), Julio Pastor of the UAH (Alcalá de Henares), Javier de Lope of the UPM, Fernando Remiro of the IES Juan de la Cierva, Cristina Urdiales of the UMA (Málaga), Juan Pablo Rozas of the UCLM (Ciudad Real), Vicente Matellán of the Universidad de León, Jose María Cañas of the URJC, Juan Carlos Pérez of the ITI (Valencia), Gloria Martínez of the UJI (Castellón), Javier Asensi of Eventronic (Alicante), Frank Kirchner, Dirk Spenneberg and Jose de Gea of the University of Bremen and Erik Maehle and Adam El Sayed of the University of Lübeck.

This thesis would not have been possible without the input of those robotics fanatics who share my passion and those of whom I have learnt so much in informal occasions. Jose Pichardo, Ricardo Gómez, Jose Jaime Ariza, Ángel Hernández (Mif), Javier Herrero, David Yáñez, Iñaki Navarro, Isaac Barona and in general all the companions of ARDE. Many thanks also to Chris for all his comments. Rafael Treviño merits a special mention for the MRSuite tool design, not only has he been inspirational, but also of enormous help in the thesis. Many thanks.

I would like to give special thanks to two people for their help during these years and for all that I have learnt from them. One is Alejandro Alonso with whom I have shared conferences and congresses, very interesting conversations and visits to research centres. The other is Andrés Prieto-Moreno with whom I have been collaborating for more than 14 years. He is a never failing fount of information and inspiration and knows how to give to his designs that grace that makes them seem so simple. Many thanks.

Finally I must give thanks to my parents, Juan and Virginia and my sister Virginia, for all their unconditional help and the effort they have made so that I can sit here writing these lines. Most of all my fulsome gratitude to Mercedes, my wife, for the sacrifice she has made so that I could work on the thesis. Thank you for being there in the most difficult moments ;-)

Juan,
Madrid, September 2008

Preface

Snakes aren't the kind of cuisine most people look for when ordering, but the speciality of the house was Juan González-Gómez's amazing servo-driven snakebot. All snake robots I've ever seen –even Gavin Miller's amazing bots- cheat. They replicate a snake's motion, be it sinusoidal, caterpillar, or side-winding, but always with wheels on the bottom to eliminate friction and help the bot along. Gonzalez, however, perfected a system that most closely replicates how snakes really move. There are no wheels on his robots. Just his own servo housings. Watching a snake robot skitter across the floor is always cool. But when you pick up Juan's bot and realize that it's got no wheels and can still move the same way any snake can, you're truly awed. Even more inspiring is the fact that his bots are totally modular. You can have as few as two modules or as many as 256 – good for both garter snakes and anacondas.

Dave Calkins,

President of the Robotics Society of America,

Lecturer of the Computer Engineering Program at San Francisco State University

Founder of ROBOLympics/RoboGames - the International all-events robot competition

Abstract

This thesis deals with the locomotion of modular robots concentrating specifically on the study of configurations with one dimensional topology, that we call apodal robots. The problem we face is how to co-ordinate the movement of the articulations of these robots so that they can move as easily in one as in two dimensions.

One of the biggest challenges is to develop a robot that is as versatile as possible and is able to move from one place to another over various types of terrain, even the roughest and most broken. This is of special importance where the environment is unknown, such as the exploration of the surface of other planets, navigation in hostile environments or in search and rescue operations.

To increase versatility of movement, modular robotics proposes the creation of robots based on basic modules. Each configuration would have different locomotive characteristics that must be studied. If also the modules were self configuring, the robots could constantly be selecting the optimum configuration for each environment.

One type of controller used is bio-inspired, based on CPG (Central Pattern Generators), these are specialised neurones that produce rhythms that control muscle activity in living beings. In the stationary state they act like fixed frequency oscillators which permits them to be substituted by a simplified model formed by sinusoidal generators. The advantage is that they are extremely simple to implement and require very few resources for their production. What is more they can be produced employing different technologies: software, digital circuits or even electro-analogical.

In this thesis a classification of the modular robots is established, according to their topology and type of connection and the hypothesis is presented to use sinusoidal generators as locomotion controllers for the apodal modular robots with one dimensional topology, of the groups pitch-pitch and pitch-yaw. The results show that this simplified model is viable and the movements obtained are very gentle and natural. The robots can move using at least five gaits. Some of them, such as rotation, are original, and as far as we know, have not been studied before nor implemented by other investigators.

Another problem that presents itself is that of the minimum configurations. To find the robots with the least number of modules possible that can move in one or two dimensions. Two minimum configurations capable of this and the relationship between their parameters have been found.

It has been shown that the answers found to the problem of co-ordination are valid for their use in real robots. They have been tested in four prototypes of apodal robots constructed on the basis of the union of Y1 modules, designed specifically for this thesis. The verifying of robots with a different number of modules has been carried out using the simulator developed for this purpose.

Finally the knowledge about the locomotion of apodal robots of the study groups has been resumed in 27 fundamental principals.

Contents

1	Introduction	3
1.1	Presentation	3
1.2	Aims of the thesis	6
1.3	Structure of the Document	8
2	The scientific-technological frame	11
2.1	Introduction	11
2.2	Locomotion	12
2.2.1	Levels of locomotion	12
2.2.2	Types of locomotion	12
2.2.3	Robot locomotion	12
2.2.4	Design of Mobile Robots	14
2.2.5	The problem of locomotion	15
2.3	Apodal robots	16
2.3.1	Tokyo Institute of technology: acm family	16
2.3.2	Shenyang Institute of Automation	18
2.3.3	Robotics Institute at Carnegie Mellon University	19

2.3.4	Bio-Inspired Robotics groups at EPFL	20
2.3.5	Others	21
2.4	Self-propelled apodal robots	22
2.4.1	Hirose Fukushima Robotics Lab (TiTech)	22
2.4.2	German National Research centre (GMD)	23
2.4.3	University of Michigan: OmniTread	24
2.4.4	EPFL Intelligent Systems Laboratory: Swarm-bot	24
2.4.5	Institute of Robotics at Beihang University (BUAA): JL-I	25
2.5	Modular robots and locomotion	25
2.5.1	A new approach to the problem of locomotion	25
2.5.2	Polypod	26
2.5.3	Polybot	26
2.5.4	Ckbot	30
2.5.5	M-TRAN	31
2.5.6	CONRO	32
2.5.7	SuperBot	33
2.5.8	Yamor	35
2.5.9	Molecube	36
2.6	Modular Robots and Structures	36
2.7	Classification of the modular robots	40
2.8	Co-ordination and locomotion	44
2.8.1	The problem of co-ordination	44
2.8.2	First approach: Manual solution	45

<i>CONTENTS</i>	xi
-----------------	----

2.8.3 Approach II: Inverse Kinematics	46
2.8.4 Approach III: Bio-inspired	46
2.8.5 Approach IV: sinusoidal generators	48
2.9 Modular robots applications	49
2.10 Conclusions	49

3 Models	53
-----------------	-----------

3.1 Introduction	53
3.2 Models of modules	53
3.2.1 Wired model	53
3.2.2 Hexahedral model	55
3.2.3 Real model: Y1 Module	57
3.3 Models of apodal robots	57
3.3.1 Parameters	57
3.3.2 Centre of mass	58
3.3.3 Types of connection	59
3.3.4 Blocks	60
3.3.5 Dimensions	63
3.4 Kinematic model	64
3.4.1 Definitions	64
3.4.2 Restrictions	64
3.4.3 Kinematic parameters	65
3.4.4 Specification of movements	66
3.5 Control model	66

3.5.1	Sinusoidal generators	67
3.5.2	Model for the pitch-pitch group	68
3.5.3	Model for the pitch-yaw group	70
3.5.4	Control spaces	72
3.5.5	Discussion about sinusoidal generators	73
3.5.6	Direct and inverse kinematics	74
3.6	Mathematical model	74
3.6.1	Introduction: Curves and waves	75
3.6.2	Serpenoid curve/wave	76
3.6.3	Discrete serpenoid curve/wave	83
3.6.4	3D serpenoid curve/wave	89
3.6.5	Circular curve/wave	93
3.7	Conclusions	96
4	Locomotion in 1D	99
4.1	Introduction	99
4.2	Continuous model	99
4.2.1	Wave propagation	100
4.2.2	Serpenoid Wave	101
4.2.3	Shape space h_1	102
4.2.4	The robot's dimensions	103
4.2.5	Stability principle	105
4.2.6	Step characterisation	110
4.3	Discrete model	113

4.3.1	Introduction	113
4.3.2	Differences to the continuous model	114
4.3.3	Discretization	121
4.3.4	Shape	123
4.3.5	Dimensions	125
4.3.6	Stability	129
4.3.7	Characterisation of the step	131
4.3.8	Hexahedral model	134
4.4	Kinematics	135
4.4.1	Introduction	135
4.4.2	Control space	135
4.4.3	Transformation of spaces	136
4.4.4	Locomotion region	137
4.4.5	Direct kinematics	139
4.4.6	Inverse kinematics	143
4.5	Case of study	148
4.5.1	Range of values of the parameters and constants	149
4.5.2	Shape space	149
4.5.3	Control space	149
4.5.4	Locomotion region	151
4.5.5	Working points	151
4.5.6	Locomotion	154
4.6	Principles of locomotion	156
4.7	Conclusions	157

5	Two-Dimensional Locomotion	159
5.1	Introduction	159
5.2	Problem of 2D locomotion	159
5.2.1	Approach	159
5.2.2	Outline	160
5.2.3	Methodology employed	161
5.2.4	Kinematics	163
5.3	Gaits	164
5.3.1	Solutions found	164
5.3.2	Classification according to waves	166
5.3.3	Characterisation of the subspaces g_i	166
5.3.4	Stability	168
5.4	Locomotion in a straight line	169
5.4.1	Description	169
5.4.2	Stability	169
5.5	Circular path	172
5.5.1	Description of the gait	172
5.5.2	Robot shape	172
5.5.3	Paths	173
5.5.4	Stability	174
5.5.5	Discrete robot	175
5.6	Rolling	177
5.6.1	Description of the gait	177

5.6.2	Robot shape	178
5.6.3	Mechanism of rolling	179
5.6.4	Robot's sections	180
5.6.5	Kinematics	181
5.6.6	Limitations from the geometry	188
5.6.7	Discrete model	192
5.6.8	Summary	193
5.7	Sideways movement	194
5.7.1	Introduction	194
5.7.2	Gait description	194
5.7.3	Robot shape	195
5.7.4	Stability	199
5.7.5	Wave types for the movement	200
5.7.6	Mechanism of movement	201
5.7.7	Kinematics	203
5.7.8	Inclined movement	206
5.7.9	Flapping movement	207
5.7.10	Discrete model	208
5.7.11	Summary	210
5.8	Rotation	211
5.8.1	Introduction	211
5.8.2	Gait description	211
5.8.3	The Robot's shape	212

5.8.4	Stability	213
5.8.5	Rotation mechanism	215
5.8.6	Kinematics	216
5.8.7	Rotation in 'U'	219
5.8.8	Discrete robot	220
5.9	Case study	223
5.9.1	Locomotion in a straight line	223
5.9.2	Circular path	227
5.9.3	Rolling	229
5.9.4	Sideways movement	230
5.9.5	Rotation	233
5.10	Principles of locomotion	233
5.11	Conclusions	234
6	Minimum configurations	237
6.1	Introduction	237
6.2	Modular robotics and minimum configurations	237
6.2.1	Atomic Unit of Movement (AUM)	238
6.2.2	Maximisation of energy efficiency	239
6.2.3	Analysis and synthesis of gaits	239
6.2.4	Design and testing of the modules	242
6.3	Problem to be resolved	243
6.3.1	Exposition	243
6.3.2	Scheme	243

6.3.3	Methodology	243
6.3.4	Kinematics	245
6.4	Configurations PP and PYP	246
6.4.1	Solutions found	246
6.4.2	Control models	246
6.4.3	Kinematic models	247
6.5	Gaits	252
6.5.1	Solutions found	252
6.5.2	Characterisation of the subspaces G_i	253
6.6	Locomotion in a straight line	254
6.6.1	Description of the movement	254
6.6.2	Study of the stages	254
6.6.3	Step	261
6.6.4	Dimensions	269
6.6.5	Summary	271
6.7	Rolling movement	271
6.7.1	Description of the movement	271
6.7.2	Kinematic model	273
6.7.3	Angle of rotation θ_1	276
6.7.4	Functions of stability	278
6.7.5	Conditions for rolling	283
6.7.6	Regions of movement	285
6.7.7	Step	287

6.7.8	Case study	287
6.7.9	Summary	288
6.8	Sideways movement	288
6.8.1	Description of the movement	288
6.8.2	Stability	290
6.8.3	Step	291
6.8.4	Direction of the movement	292
6.8.5	Summary	292
6.9	Rotation	294
6.9.1	Description of the movement	294
6.9.2	Step	294
6.9.3	Direction of turn	298
6.9.4	Summary	298
6.10	Principles of locomotion	299
6.11	Conclusions	300
7	Experiments	303
7.1	Introduction	303
7.2	Developed platform	303
7.2.1	Y1 Modules	303
7.2.2	Robots	306
7.2.3	Control scheme	306
7.2.4	Electronics	309
7.2.5	Software	310

7.3	Experiments of locomotion in 1D	313
7.3.1	The robot's shape	313
7.3.2	Stability	313
7.3.3	Displacement	317
7.3.4	Step	318
7.3.5	Step and phase difference $\Delta\phi$	325
7.4	Experiments of locomotion in 2D	329
7.4.1	3D serpenoid waves	329
7.4.2	Movement in a straight line	333
7.4.3	Sideways movement	337
7.4.4	Rotation	348
7.4.5	Rolling movement	358
7.4.6	Circular path	365
7.5	Experiments of the movement of the minimum configurations	373
7.5.1	Movement in a straight line	373
7.5.2	Rotation	382
7.5.3	Sideways movement	387
7.5.4	Rolling movement	390
7.5.5	Circular path	393
7.6	Conclusions	393

8	Conclusions	395
8.1	Main contributions	395
8.2	Other contributions	398
8.2.1	About methodologies	398
8.2.2	About movement in one dimension	399
8.2.3	About movement in a plane	399
8.2.4	About minimum configurations	400
8.2.5	About the robotic platform developed	401
8.3	Future lines of investigation	401
A	Demonstrations and developments	407
A.1	Centre of mass of an apodal robot	407
A.2	Supporting segments of the PP configuration	408
A.2.1	Supporting segment 1	408
A.2.2	Calculation of the supporting segment 2	409
A.3	Transitional phase of the PP configuration	411
A.4	Rotation angle of the PYP configuration	412
A.4.1	Stage 1	412
A.4.2	Stage 2	414
B	Genetic Algorithms	417
B.1	Description	417
B.2	Example	418
C	Y1 modules	419
C.1	Plans	419
C.2	Assembling	429

<i>CONTENTS</i>	1
D Simulation	431
D.1 ODE Parameters	431
D.2 Simulation of the Y1 modules	431
D.3 Examples of use	434

Chapter 1

Introduction

“My work is a game, but a serious game.”

– M.C. Escher.

In this introductory chapter the application environment for this thesis is presented, its aims and how the memory content has been organised. In the following chapter the context is described in more detail and the bibliography is given.

1.1 Presentation

This thesis deals with the locomotion of modular robots concentrating specifically on the study of configurations with one dimensional topology, what are called apodal robots. The problem faced is how to co-ordinate the movement of the articulations of these robots so that they can move as easily in one as in two dimensions.

Locomotion is the capability that permits living beings belonging to the animal kingdom to move from one place to another at will. There are two important aspects to have in mind: control and voluntariness. If the movement is to be considered locomotion the individual has to want to complete it and what is more be able to control it. In this way, the water lilies that rest on the surface of the water move driven by the currents or other animals, but it is not considered locomotion because it is neither voluntary or controlled. The robots that possess locomotive capacity are called mobile robots. The field of robotics that studies and designs robots capable of functioning for themselves in unknown environments is known as mobile robotics.

The study of locomotion is divided into two levels, called superior and inferior. The inferior level is in charge of the control and co-ordination of the actuators so that the robot can move from place

to place. It includes the different gaits that can be obtained (turns, moving in a straight line, side-ways movements, etc.). The questions to be resolved at this level are: How do I move? How do I co-ordinate the actuators to take a step? It is easy to resolve them if the robot has wheels or caterpillar tracts and the terrain is appropriate. It is sufficient to turn the motors to obtain the movement required. Nevertheless, when the robot has articulated feet or has to complete the manoeuvre using body motions, as is the case of apodal robots, resolving the difficulty is complicated. In these cases it is necessary to co-ordinate correctly all the articulations. The superior level is in charge of planning the routes, navigation and other higher level tasks. It is concerned with voluntariness. The questions that define this level are: Where do I want to go? How do I get there?

This thesis concentrates on the lower level of locomotion addressing the problem of the co-ordination to obtain different ways of movement for apodal robots.

One of the biggest challenges is to develop a robot that is as versatile as possible and is able to move from one place to another over various types of terrain, even the steepest and most broken. This is of special importance where the environment is unknown, such as the exploration of the surface of other planets, navigation in hostile environments or in search and rescue operations. Up to now the robots that have been made have less locomotive capacity than a mammal. Even when they are operated by remote control, where the superior level is carried out by a human, mobility is limited by the robot's design. To improve it raises the questions: What kind of elements are best: feet, wheels, caterpillar tracks, etc.? What configuration of feet must be used?

The traditional approach is to study *a priori* the characteristics of the terrain and design the most adequate structure of robot: whether it uses feet, wheels, or caterpillar tracks. This has the disadvantage that a wrong choice at this level will imply redesigning the robot. Also applications exist where the environment is changeable or unknown.

In 1994, Mark Yim, in his doctoral thesis, proposed a new approach. He proposed constructing robots employing simple modules, joined one to another to make up different configurations. Maximum versatility would be obtained if these modular robots were able to configure themselves. In this way the robots could change their form to enable them to move in the most efficient way, according to the terrain. To illustrate this idea, Yim proposed a setting in which a robot had to go from his laboratory in Stanford to a neighbouring building. To do this it had to cross the porch, pass underneath the railings, go down a step and cross broken ground. None of the robots known up to then could do it, even the remote controlled ones failed. Nevertheless a self configuring modular robot could adapt its form to cross the porch, following that it would become a worm to go underneath the railing and down the step. Finally it would transform itself into a quadruped to move across the broken ground. It is a robot that has used three different forms of locomotion. It has adapted to the terrain to move across it in the most efficient way possible.

A new area of investigation was born: modular robotics and locomotion. In this the basic modules are designed, and then based on them different configurations of robots are created. Each one will

have different locomotive characteristics. If also the modules are self configuring, the robots will be able to select at each moment the configuration best suited for each environment. The aim is to study the locomotive properties of all possible configurations. This is a titanic task, given that the quantity of potential configurations grows exponentially with the number of modules.

As a first step the modular robots can be classified according to their topological dimensions, of one, two or three dimensions. Each one of these groups has different characteristics and within each family sub-families appear with other properties.

This thesis studies modular robots with one dimensional topology. Within this family the way that the modules are connected between themselves defines three distinct groups. The groups that we will concentrated on are those with connection pitch-pitch and pitch-yaw.

This thesis studies the problem of the co-ordination needed so that apodal modular robots with one dimensional topology, of the groups pitch-pitch and pitch-yaw, can move in one or two dimensions respectively.

Another important aspect in the locomotion of the modular robots is the controller that is employed. Its mission is to calculate the positions of the articulations at each moment, in function of established parameters. The classical solution is to employ specific controllers that obtain the angles of the articulations by means of inverse kinematics. As an entrance the curves of the trajectory are used (either from the centre of the masses or from the extremes of the feet, if they have them) and the positions of the servos are obtained. This approach presents two problems when applied to modular robots. On one hand these controllers are too specific, which makes it difficult to re-use them in other configurations. Each configuration has its own kinematics and consequently its own equations, therefore each controller will be different. On the other hand, the calculating power necessary is high. Inverse kinematics demands many calculations that must be done quickly, which restricts the choice of microprocessor and its operational speed.

Another, different approach, is to use bio-inspired controllers. Millions of years ago nature resolved the problem of locomotion of living beings. Why not study how it has resolved it and find inspiration there. In the 60's biologists discovered that living beings possessed specialised neurones, called central pattern generators (CPGs). These centres produce rhythms that control muscular activity to carry out vital functions, such as breathing, bowel movements, chewing, locomotion, etc. The problem of co-ordination is resolved employing controllers that implement the mathematical models of these CPGs and finding the adequate values for their parameters. In contrast to the classic approach, the bio-inspired controllers are not based on the knowledge of where certain points are situated in space, but act directly on the articulations. They are, therefore, faster, generating movements that are more natural and, generally, demand less computing power.

Nevertheless, there exist a certain complexity in biological mechanisms, as well as a lot of redundancy. Perhaps these solutions are very specialised, being 'rich', supplying too much information

that may not be necessary for robotics locomotion. For this reason, the other approach for the control of movement, followed in this thesis, is to employ simplified models of CPGs. If the study of locomotion is made in permanent regime, a possible simplification is to substitute the CPGs for sinusoidal generators that directly control the position of the articulations of the robot. This is possible because CPGs act as fixed frequency oscillators once they have reached the stationary regime. What is more, the observation of animal locomotion shows that the frequencies of the rhythmic movements are equal and there is no evidence that oscillators of the dorsal spine use different frequencies.

The advantage of these controllers is that they are extremely simple to implement and require very few resources to realise. Also they can be formed using different technologies: software, digital circuits or even electronic analogue. By means of the use of FPGAs specific circuits can be designed that allow the robot to move “by hardware” in the same way that the tails of lizards move when they are severed. The problem of co-ordination is resolved by finding the amplitude values and the different phases of the generators that make the robot move.

The hypothesis of this thesis is the employment of sinusoidal generators as controllers for the locomotion of the modular apodal robots with one dimension topology, of the groups pitch-pitch and pitch-yaw.

1.2 Aims of the thesis

The main aim of this thesis is **to study the problem of locomotion of the modular apodal robots with one dimensional topology of the groups pitch-pitch and pitch-yaw; of any length, in one or two dimensions**. We want to know what gaits are possible and how to co-ordinate the robot’s articulations to obtain it.

The problem dealt with is very wide ranging and can be addressed from different viewpoints. The hypothesis examined is the use of a controller based on sinusoidal generators. Below the concrete **aims** are formulated, each one linked to a question:

1. To study the viability of the locomotion of the apodal robots of the mentioned groups of any length employing sinusoidal generators. (*Is robot movement achieved?*)
2. Discover different gaits. (*What types of movement can be performed?*)
3. Characterise the gaits using the minimum number of parameters. (*What is the minimum number of parameters needed to perform the movements?*)
4. Establish the lower limits of the number of modules that enables the robot to move. (*Which are the robots with the lowest number of modules capable of movement?*)

5. Discover the relationship between the parameters of the sinusoidal generators, the kinematics parameters of the robot and its shape. (*How does each parameter affect the movement controller and shape of the robot?*)
6. Sum up the results in a series of principals of locomotion that permit application engineers and other investigators to put into operation the apodal robots. (*What do I have to do so that this apodal robot of M modules moves in a certain way?*)

To address these questions this study presents the following **secondary aims**:

- Revise the state of the art in modular robots and apodal robots. Study the evolution of the robots created in the leading research centres, classify and identify the original contribution of this thesis.
- Creation of the mathematical models for robot groups: pitch-pitch and pitch-yaw.
- Develop a simulation software environment to evaluate the proposed solutions.
- Design a module for the construction of modular robots of the study groups.
- Construction of prototypes of modular robots to carry out the experiments and the verification of the solutions in real robots.

Finally, as a **personal aim** of the author of this thesis, the experimental platform created for the verification of the results, made up of hardware, software and mechanics, **has to be open and free**, and also designed, as far as possible, using **free development tools** that run in a free operating system. This aim will allow any investigator to reproduce the platform, verify the results of this thesis on it, and carry out improvements and continue with the investigation.

LIMITS

To make the study of the locomotion of apodal robots accessible, the following limits have been applied.

- The various movements of the apodal robots are studied in a permanent regime. This restriction permits the substitution of the CPGs for sinusoidal generators.
- The surface is homogeneous, without obstacles. The first step is to search for solutions to the problem of co-ordination for this kind of surface.

- Control in open loop. The articulations are positioned in open loop. The controller sends the desired positions, supposing that the servo¹ reaches them in a certain time. It does not wait to receive any type of notification. This supposition is reasonable given that the surface is homogeneous and without obstacles. There is no impediment to the movement of the servos.
- Modules without sensors. It is assumed that each module possesses only one actuator, and no sensor. On one hand they do not need sensors to read the position of the servos as the control is in open loop. On the other hand it is not necessary to obtain information of the environment at this level of locomotion. It will be necessary to add sensors to operate at the superior level.

Aims that DO NOT form part of the thesis

The realisation of a simulation software and the construction of prototypes of modular robots are planned to demonstrate the viability of the ideas proposed in the thesis. The aims that objectively do not form part of this thesis are the following:

- The construction of autonomous apodal robots. To verify the ideas proposed it is not necessary to construct prototypes that are autonomous. The controllers will be programmed in the computer and sent the positions of the servos to the robot by cable, by means of a serial connection. The power source will be external, situated outside the robot. Once the viability of the solutions is found, to make a robot that does not need any type of cable is purely a technological problem, and easily viable
- Superior levels of locomotion. It is not the aim of this thesis to programme behaviour in the robots or address other aspects related to the superior levels of locomotion, such as perceiving the environment, planning of routes, etc.

1.3 Structure of the Document

In the first chapter the context of the thesis has been introduced, without going into details and the aims have been presented. In the second chapter the progress in modular robotics and apodal robots will be described in greater detail and it will be shown more exactly where this thesis relates to it. In the third chapter the models used for the modules, apodal robots, the controller, the kinematics and the mathematical models will be presented.

The following three chapters form the major part of the thesis, each one is dedicated to a different problem. The study of locomotion has been divided into three parts. The first (chapter 4) the problem

¹Internally the servo closes the loop, using a potentiometer to confirm that it has reached the position, but this information is not supplied to the superior controller.

of one dimensional locomotion (in a straight line) of the apodal robots belonging to the pitch-pitch group is addressed. In the second (chapter 5) two dimensional locomotion of the pitch-yaw group is studied. In the third (chapter 6) the problem of the minimum configurations is dealt with and the answers found are given.

In the seventh chapter the developed robotic platform is described and the most relevant experiments are documented, both in simulations and real robots.

Finally, in the eighth chapter, the conclusions are expounded, with the future lines of investigation. At the end of each chapter the specific conclusions are given, in such a way that with reading the introduction and the conclusions of each chapter the reader will have a synthesis of the work done.

Chapter 2

The scientific-technological frame

“Naturally, we are only in the beginning of the beginning of the robotics revolution ”

– Isaac Asimov

2.1 Introduction

In this chapter the evolution of two types of robots, **the apodal and the modular**, will be studied. Emphasis will be placed on recently created prototypes and it will be seen, from a general perspective, how this thesis contributes to the studies. Many of the ideas and examples have already been presented in the introductory chapter, nevertheless they are included in this chapter as a self contained unit.

In the first place **the problem of locomotion** and some initial ideas will be introduced. This is followed by the evolution of apodal and self-propelled apodal state of the art robots that have been developed in the most prestigious research centres. Then the progress in a new branch of investigation of robotics, what is known as **modular robotics**, will be presented. At present the investigation concentrates not only on the locomotion of these robots, but also on their capabilities to form different structures. Finally **a classification** that includes modular and apodal robots **will be established**.

In the second part **the problem of co-ordination** and the different approaches of how to resolve it will be presented, concentrating on apodal modular robots.

2.2 Locomotion

2.2.1 Levels of locomotion

Locomotion is the capability that living beings belonging to the animal kingdom have, allowing them to decide to move from one place to another. This is one of the characteristics that distinguishes animals from plants. There are two important aspects to have in mind, **control** and **will**. To be accepted as locomotion the individual must want to do it and be able to control it.

The study of locomotion is divided into two levels, that are denominated the inferior level and the superior level. The **inferior level** is in charge of muscle control and co-ordination (or actuators in the case of robots) so that the individual can move. It also includes the different means of moving that can be obtained (turns, movement in a straight line, sideways movement, etc.). The questions to be resolved at this level are: How can I move? How can I co-ordinate all the muscles (actuators) to achieve the desired movement?

The **superior level** is in charge of path planning, navigation and other higher level tasks. It is related to the volition. The questions that define this level are: Where do I want to go? What route must I follow?

This thesis concentrates on the inferior level of locomotion, studying the mechanisms that enable apodal robots to move.

2.2.2 Types of locomotion

In nature the movement of animals has been adapted to the environment in which they live. It is possible to carry out a basic classification according to the environment in which they move. Therefore the locomotion can be: air borne, aquatic or terrestrial. This classification is not definitive. The land mammals are also able to move in water for short distances, for instance to cross a river. In this case they use a different way of walking, or gait, that permits them to swim.

Ground movement can be divided, in turn, into two categories, according to the organs that are employed to achieve movement: **locomotion by means of feet** (mammals, insects) or **by means of body motions** (snakes, caterpillars, worms).

2.2.3 Robot locomotion

One of the research areas in robotics is that of locomotion: giving the robots locomotive capabilities so that they can move from one place to another. These robots receive the generic name of **mobile**



Figure 2.1: Examples of robots with different effectors for terrestrial locomotion

robots. At the same time the study of locomotion is performed at the two levels mentioned above. Investigations of the superior level start with the supposition that robots can move, without taking into account the mechanisms that make it possible (feet, wheels...) and concentrates on the task of the superior level such as path planing, vision, collaboration, etc.

The same happens in animals, in the study of the inferior level of locomotion, robots can be classified according to the effectors employed to move them: **wheels, caterpillar tracks, feet** or the **body**. This category of **apodal robots** includes those robots, that like their counterparts in nature, achieve locomotion through body motions. These are the four classical categories for the study of locomotion, nevertheless the classification is not definitive. As Mark Yim has noted [163] in his doctoral thesis, new effectors can appear that do not fit in any of these categories. Such is the case of the *whegs*[116] and his version *mini-whegs*[103], created by Quinn et al. in the bio-robotics laboratory of the Case Western Reserve University. In them a wheel and a leg are mixed to produce some very interesting results. In the figure 2.1 there are some photos of robots that use different effectors to achieve movement: wheels, caterpillar tracks, whegs, body and four, six or eight feet.

The themes for investigation at the lower level of locomotion are the properties of the various effectors, how to achieve the co-ordination of the actuators, the different gaits, algorithms of control, etc. In the remainder of the chapter, when speaking of locomotion, it always refers to the inferior level.

2.2.4 Design of Mobile Robots

As in the animal kingdom, where locomotion of individuals is specifically adapted to the environment in which the animal normally functions, to design a mobile robot it is essential to know the terrain in which it is going to move. **The environment** is the key in deciding which effectors will be chosen and what gaits will be implemented. Therefore, for example, if the robot is going to move on flat surfaces where there is no need to overcome obstacles, wheels, or even caterpillar tracks, are sufficient.

The design process can be resumed in the following steps:

1. The study of the environment in which the robot is going to operate
2. The selection of effectors.
3. The implementation of the gaits.

These steps are very important. A wrong choice at this level will imply having to reconstruct the robot. For this reason investigations at this level are important: the better the properties of the effectors are known, the possible gaits, their efficiency, etc. greater will be the information available that enable the right design decisions to be made. Leger [83], in his doctoral thesis, addressed the problem of the automatic design of robots, using an evolutionary approach. His central idea is that the search for

solutions to locomotion is so wide ranging that it is necessary to create new software tools to explore the greatest possible number of solutions before taking a decision about which design to implement. At this level an error in the configuration of the robot is critical. For this reason he proposed using evolutionary algorithms to help the designers at this stage.

Nevertheless, applications exist where it is difficult to know a priori and in detail the ground, which leads to a lot of uncertainty in the initial stage of design. Such is the case when designing robots for **search and rescue operations** or **planetary exploration**. Due to this, the robot has to have the **maximum versatility** possible. Investigations concentrate on studying the most versatile effectors and all the different gaits possible.

2.2.5 The problem of locomotion

One of the biggest challenges in developing a robot is to make it able to move in all types of terrain, even the roughest and most broken. That is to say, a robot that is extremely versatile. This is of special importance in applications where the environment is insufficiently known or changeable, as in the exploration of the surfaces of other planets, hostile environments or search and rescue operations. What is it best to use, feet, wheels, caterpillar tracks...? How many feet? What type of movement? And if it has feet, how to configure them?.

The NASA has particular interest in this problem, financing projects destined to the building and evaluating of alternatives, so that the robots can move in rugged environments. Two of these projects in the initial stage (end of the 80's) were the CMU Ambler[77] and the Dante II[3]. They are examples that illustrate the design model described above: designs of specific structures based on the environmental specifications.

The Ambler is an autonomous robot for planetary exploration taking into account movement on the surface of Mars. Based on the specifications the robot was designed with 6 feet, 3.5 meters high and a weight of 2,500 kilos. The type of movement selected was by feet, in theory the most efficient mode[3]. Nevertheless this robot was never sent to Mars. The dimensions and weight of the robot were excessively large for the requirements and power consumption was very high.

The robot Dante II was also designed to explore broken ground and was tested in 1994 for the exploration of the mountain volcano Spurr, in Alaska. In this case the robot had 8 feet with a locomotion system called 'framewalker'. Despite knowing the specifications of the terrain, and that it had a cable maintaining it fixed to the summit and by which it descended, on the fifth day it tipped over and could not be recovered.

For exploring Mars, the NASA opted for using wheels[85] that up to now have given very good results. Nevertheless, wheels are very limited. They only allow the robot to move in controlled surroundings. This is one of the reasons why it is necessary to plan carefully and in advance the places

to which the robot will be sent, not only taking into account the importance of atmospheric conditions, the collection of scientific data, etc, but also permits the robot to move easily in its surroundings[38]. This is a big handicap.

Inspired by the marvellous locomotive abilities of animals with feet, Dirk Spennberg et al. of the University of Bremen developed the robot Scorpio[28], with 8 feet, able to move on sandy and rocky terrain, in places impossible for wheels. This project was financed by the DARPA and the robot was proposed as an alternative for the exploration of Mars. Motivated by the results, the development of the ARAMIES[137] was begun. This robot is a quadruped that can move on extremely adverse terrain and can, besides, carry on board scientific experiments. One of the aims is to explore the locomotive capabilities of quadruped robots in this type of surroundings.

2.3 Apodal robots

In contrast to terrestrial movement by means of feet, are the living beings that use corporal movements. The robots that use this kind of movement are known as **apodal robots**. The word apodal means “lacking feet”.

These robots possess characteristics that make them unique, the same as their counterparts: snakes, worms and maggots. On one hand is the ability to change their form. Compared with the rigid structures of the rest of the robots, the apodals can bend and adapt to the form of the terrain on which they move. On the other hand their section is very small compared to their size, which permits them to enter small tubes or orifices and get to places inaccessible to other robots.

This section analyses the apodal robots created in the most important research centres and their evolution up to now.

2.3.1 Tokyo Institute of technology: acm family

Hirose, of the Tokyo Institute of Technology pioneered studies of snake’s bio-mechanics for its application to robotics. It was implemented in 1976 the first snake robot called ACM-III (*Active Cord Mechanism*). In 1987 in the reference book "*Biologically Inspired Robots*"[51], the results of his investigation were collected and published.

One of Professor Hirose’s most important contributions to science was the discovery and formulation of the **serpenoid curve**[150], which is the form adopted by the snakes when moving. He proposed a model of vertebrae that moves by means of the action of two opposing muscles controlled by two springs that provoke a sinuous movement. Then he calculated the spinal column curve’s equation and finally compared it to the experimental results obtained from real snakes.



Figure 2.2: Evolution of the snake robots of the ACM family: (Active Cord Mechanism). Hirose-Fukushima Robotics Lab

In figure 2.2 the different prototypes developed up to the present are shown. The first one is the **ACM-III**¹ that measures 2 metres long and is made up of 20 articulations that move parallel to the ground (*yaw*), capable of moving at a speed of 40cm/s . Each module has some passive wheels that allow the robot to crawl along the ground. These wheels have the effect that the friction coefficient in a tangential direction is very low compared with the normal drag. It is this principal that allows the propulsion of the robot when the articulations are oscillated correctly. This mechanism has been baptised '*glide propulsion*' and is not only similar to that of snakes, but also to the movement of skaters.

The ACM-III prototype was about 20 years ahead of its time. This line of investigation was forgotten until, owing to the advent of modular robotics, prototypes of snake robots reappeared. Hirose and his collaborators renewed their interest in this system and they redesigned it with new technologies. In this way the **ACM-R1**[52] was born. It was a revised and modernised ACM-III. It included wireless communication with the robot to eliminate the need of cables. This prototype has 16 modules and can move at a speed of something like 50cm/s . The modules are smaller and better finished. Among the new experiments carried out the highlight is the trial of propulsion sliding on ice, using the same kind of blades that are used on ice skates [31].

The following prototype, **ACM-R2**, has greater freedom in each module allowing pitch as well as *yaw*[148] which permits the robot to adopt three dimensional forms. This prototype served principally

¹More information is obtainable on the web: http://www-robot.mes.titech.ac.jp/robot/snake_e.html

to study the viability of the robots with axes of pitch and yaw, and later evolved to the **ACM-R3**[101]. The functionality of the ACM-R3 is the same as the ACM-R2, nevertheless the design is completely new. Now each module has one degree of freedom. It is designed in such a way that when they are connected in chain the movements of pitch and yaw are alternated. The structure is more compact and lighter than its predecessor. One of the design novelties was to integrate some large sized wheels on either side of the module. This novel design permits the wheels to be always in contact with the surface, independently of the robots orientation, allowing it to be propelled in inclined positions. The prototype was used to investigate new ways of locomotion such as rolling, sinus-lifting or inclined movements[102].

With the idea of improving the model so as to be able to function in real situations, where there is dust, water, areas with difficult access, etc., the **ACM-R4**[160] was developed. It can be considered as an industrial version to be employed for inspection or search tasks in tubes or steep ground. Snake type propulsion requires many modules. With the idea of reducing the size, the wheels, that before were passive, are now active and can be moved by a motor. The ACM-R4 has only 9 modules. This characteristic has led to the appearance of new locomotive capabilities. It can be seen in one of the experiments how the robot advances along the ground, lifts up its body, supports itself on a chair, climbs onto it and finally gets off, showing how it can move in quite complicated terrain.

A characteristic of the snakes is that they can move as easily on the ground as in water. From ACM-R4 and an amphibious prototype, **Helix**[145] the version **ACM-R5**[159] was born. The robot can move along the ground using glide-propulsion, by means of some small passive wheels. Also each module has four fixed fins that in normal movement through water produce high resistance and low resistance for tangential movements.

2.3.2 Shenyang Institute of Automation

Hirose's work has served as inspiration for other investigators. One of them is Shugen Ma who repeated and enlarged Hirose's work in glide-propulsion and developed a simplified version of ACM-R1 with 12 less mechanically complicated modules and an improved system of control[87]. He also developed a software to simulate the real movement of the robot on different surfaces. The theory is that the robot moves along the serpenoid curve and that no normal slipping exists. Nevertheless, in practice this side slipping does appear, and produces loss of propulsive power. By means of the simulator it is possible to determine the values of the losses and find the optimum angle of the serpentine movement for each surface[88]. Lastly the locomotion of the robot on inclined terrain was studied[90]. Parallel to this, Professor Shugen Ma's group also started to study apodal robots with pitch and yaw connections[89]. A module that possessed a certain degree of freedom and activated by a servo was developed and with it configurations of robots were created to study different movements and their adaptations to the environment. Concretely a rolling movement to overcome obstacles was suggested[13], and in [12] the problem was studied in a more general way, suggesting other gaits depending on the environment.

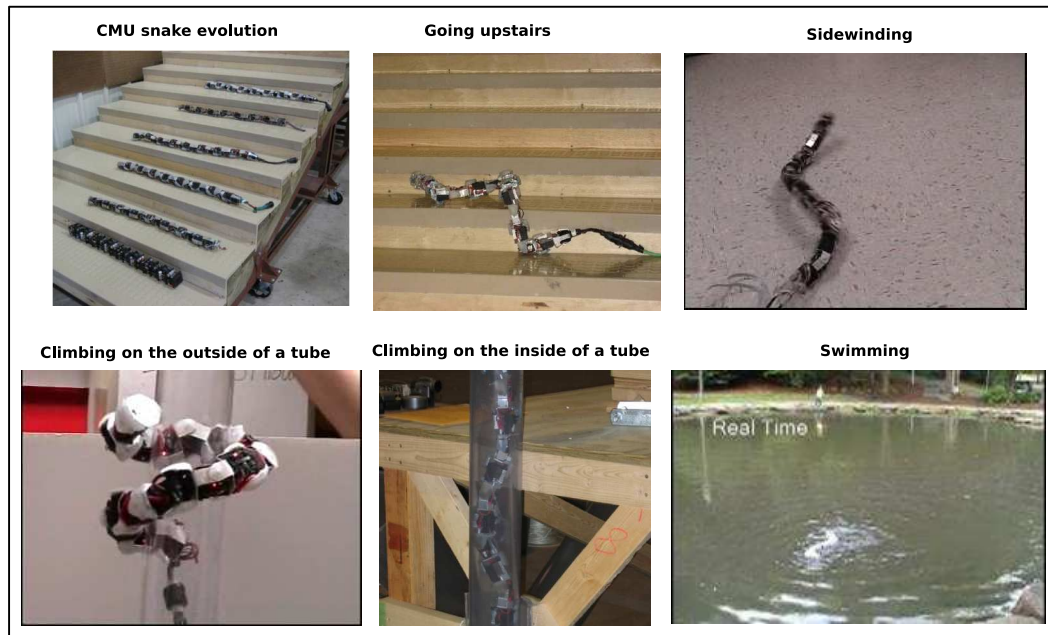


Figure 2.3: CMU's snake robot

2.3.3 Robotics Institute at Carnegie Mellon University

In CMU's (Carnegie Mellon University) Robotics Institute Kevin Downing studied apodal robots. In his doctoral thesis[29], financed by the NASA, developed a framework environment for the automatic gait generation for snake robots. He was one of the pioneers in applying genetic algorithms to find solutions for the locomotion of these robots.

Investigations on snake robots are being carried out in the bio-robotics laboratory² directed by Professor Howie Choset. The principal lines of investigation are mechanical and locomotion at both inferior and superior levels. In the area of mechanics new articulations are being developed[129] to attain snakes in 3D, as well as actuators that permit optimum climbing ability[26].

His investigations of the superior level have concentrated on planing movements, developing locomotive algorithms and positioning in what is known as hyper-redundants[18][17].

Some very interesting results are being obtained for the inferior level. The videos of the robots can be seen on *You Tube*³. The prototypes designed (see Figure 2.3) are based on Mark Yim's modules, described in more detail in the section 2.5. They use aluminium modules with a degree of freedom, activated by what is known as Super-servo. These are commercial servos that have been modified, adding their own electronics, sensors and communications bus [158]. Different types of 'skins' are

²<http://download.srv.cs.cmu.edu/~biorobotics/>

³Youtube channel: <http://www.youtube.com/user/CMUBiorobotics>



Figure 2.4: The prototypes Amphibot I and II of the EPFL bio-inspired group. The author of this thesis appears at the lower left, together with Alexander Crespi, author of Amphibot, when attending Clawar 2006 in Brussels.

used to cover the modules and allows the snake to move in all kinds of terrain, including aquatic environments.

The latest prototypes consist of 16 modules and can move in a straight line, sideways, climb on the inside or outside of a tube, swim and roll[86]. At this low level of locomotion the robots are tele-controlled by an operator, who constantly indicates the movements that the robot must carry out.

2.3.4 Bio-Inspired Robotics groups at EPFL

The bio-inspired robotics group at EPFL (*Ecole Polytechnique Fédérale de Lausanne*) has developed the amphibious robot **Amphibot**[23]⁴ that is capable of moving on ground and in water. It consists of 8 modules that move parallel to the ground and uses bio-inspired controls for locomotion, based on the CPGs (*Central Pattern Generators*) models of the lampreys, developed by Ijspeert[63].

The first prototype, **Amphibot-I**[24][22] could swim by means of undulations of the body, as well as move along the ground as snakes do, for which some passive wheels, similar to those of ACM, situated on the abdomen were included. In the second version, **AmphiBot II**[25], the modules were made more compact and feet were added. This robot could also move on the ground and swim like salamanders do, combining body and foot movement. For the control model the lamprey CPG models were used and demonstrated how the speed and direction of movement can be quickly adjusted, on the ground and in the water[62].

⁴More information is available on the web <http://birg.epfl.ch/page53468.html>



Figure 2.5: Left: Wormbot, designed by Conrad[21]. Right: S5, Miller[96]

2.3.5 Others

One of the most realistic snake robots obtained is the prototype **S5**⁵ developed by Miller[96]. It is made up of 64 articulations with the relationship between the length and width of the section nearing the proportions of real snakes. It is the fifth generation of snake robots.

The **WormBot**⁶ of Conrad et al.[21], developed by the University of Zurich's Neuroinformatics Institute, is a prototype of a snake robot that moves by means of undulations of its body and is based on the bio-inspired model of CPGs. It has implemented the lamprey CPGs[20]. The robot is autonomous and an operator can change the parameters of the couplings between oscillators.

A different approach is used in the robot **SES-1** y **SES-2** (Self Excited Snake Robots) developed by Ute et al[152] in the Tokyo Institute of Technology. In a prototype of 3 segments and 2 motors, movement is obtained through the principle of self-excitation. According to this principle springs are placed in parallel to the actuators. The torque of each motor depends on the angle of the adjacent motor, obtained by means of negative feedback. With this principle very quick and efficient movements are obtained. The first version SES-1 is formed exclusively of analogic circuits.

The figure 2.5 shows the Wormbot and S5 prototypes.

⁵More information on the web: <http://snakerobots.com>

⁶<http://www.ini.ethz.ch/~conradt/projects/WormBot/>

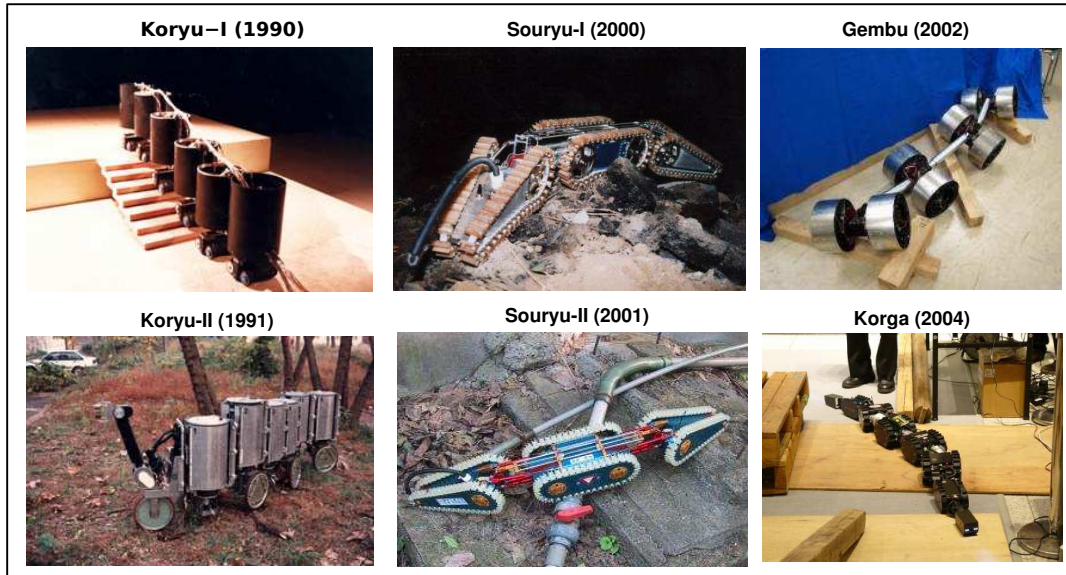


Figure 2.6: Self-propelled robots (serpentine robots) in the Hirose-Fukushima Robotics Lab

2.4 Self-propelled apodal robots

In contrast to the apodal robots that accomplish their locomotion by means of body motions, the self-propelled apodal robots displace themselves by means of active wheels or caterpillar tracks on the different parts that make up the robot. Though they have the form of a snake, they are not bio-inspired robots. This type of locomotion is not found in nature. Nevertheless it is included in this study because most of them are modular robots, formed by similar modules joined in a chain.

This kind of modular robots have also been named[47] as **serpentine robots**.

2.4.1 Hirose Fukushima Robotics Lab (TiTech)

Professor Hirose also pioneered this class of robot. From ACM-III structures were developed with self-propelled modules joined in a chain[55], these are known as **articulated bodies**⁷. Outstanding among the advantages of this type of robot is its ease of transport: the modules are separated one from the other and later joined together again, they can carry a load distributed on all the robot, they can move along narrow and twisting paths and the system is 'redundant', that is if one module fails another takes its place.

To explore the locomotive capabilities of their articulated bodies the **KORYU I** prototype[56] was developed, formed of 6 cylindrical bodies and propelled by caterpillar tracks. Each module has 3

⁷More information in the link: http://www-robot.mes.titech.ac.jp/robot/snake_e.html

degrees of freedom: vertical movement (axis z), turning movement (parallel to the plane xy) and wheels to propel it. It was noted that this robot could turn, climb obstacles and even stairs. The cylinders can also move vertically, which permits the robot to negotiate irregular surfaces. The second prototype, **KORYU-II**[57] uses, instead of caterpillar tracks, independent wheels which allows it to move with ease on sloping terrain. Experiments were carried out both in the city and the countryside.

The Japanese live in a seismic zone where earthquakes are frequent. Because of this the application of search and rescue are of special interest for them. After an earthquake people can be trapped in the rubble and they have to be rescued immediately. To develop a robot capable of manoeuvring in this type of environment, find the victims or survivors, using cameras and microphones, would be a great help.

The first prototype proposed was **Souryu-I**[144], made up of three segments. Each one is propelled by caterpillar tracks, but they are not independent, there is one motor that drives them all. The first one carries a camera and a microphone, and the rear one a radio receiver. The modules at the extremities can carry out pitch and yaw symmetrically. The robot has only three degrees of freedom. The following version **Souryu-II**[146] is similar but its modules are easily separated to facilitate transport and add special intermediate modules.

The **Genbu** (I, II y III)[71] generation of robots is formed by chains whose modules have two independent, active wheels and are joined by passive articulations. It has been developed to deal with fires. The motors are hydraulic and a hose-pipe can be fitted along the central axis of the robot to pump water and reach places inaccessible to the firemen.

Another robot is **Kogha**[65], developed for search and rescue operations. It has 8 modules connected in series with two caterpillar tracks, except the first and last ones. The connections between two modules dispose of two degrees of active freedom that allow them to climb obstacles and 3 degrees of passive freedom that allow them to adapt to the terrain.

Some of the prototypes are shown in the figure 2.6. In [53] a more detailed review of some of the robots developed by the Tokyo Institute of Technology can be found.

2.4.2 German National Research centre (GMD)

The GMD has developed two prototypes of self-propelled apodal robots. One is the **GMD-SNAKE**[73] (prototypes 1 & 2). This is made up of 12 driving wheels on each module. It has 6 modules, plus one at the head. The principal application for which it was designed is the inspection of tubes, though in [111] application to the inspection of buildings is being studied.

The other is the **Makro**[117] robot for inspecting drains of 30 to 60 cm diameter. It has 6 modules and the joints between them have 3 degrees of freedom. Each module has two wheels to drive it. At the head two cameras are fitted as infra-red sensors to detect obstacles. Though the robot is tele-directed, a software has been proposed to make it autonomous[141].



Figure 2.7: Different prototypes of self-propelled apodal robots (serpentine robots): GMD-snake Makro, Swarm-bot, OmniTread OT-8 y OT-4

2.4.3 University of Michigan: OmniTread

One of the most advanced self-propelled apodal robots is **OmniTread**⁸ developed by Granosik et al.[47] at the Laboratory of mobile robotics in the University of Michigan, for task of industrial surveillance. This robot is very robust and flexible. It uses pneumatic joints which gives it a lot of strength. The first version omnitread **OT-8** is composed of 5 hexahedral modules. Two caterpillar tracks have been placed on the four external faces of the robot. The inconvenience is that the air compressor is placed outside the robot, which necessitates a hose.

In the following version, **OT-4**[4] the robot has been reduced in size and electric micro-compressors have been added, thereby eliminating the need of a hose. It has an autonomy of around 75 minutes. (Figure 2.7).

2.4.4 EPFL Intelligent Systems Laboratory: Swarm-bot

The **Swarm-bot** robot⁹ has been developed at the EPFL Intelligent System Laboratory for the study of ‘the intelligent beehive’: colonies that are capable of self-organisation. The prototype developed[100] is formed by small mobile robots that have the capacity to assemble themselves to make bigger structures and therefore carry out other tasks. For example, if they have to cross a crevasse, they can organise themselves into a chain[99][48].

⁸More information in the web: http://www.engin.umich.edu/research/mrl/00MoRob_6.html

⁹More information <http://www.swarm-bots.org/>

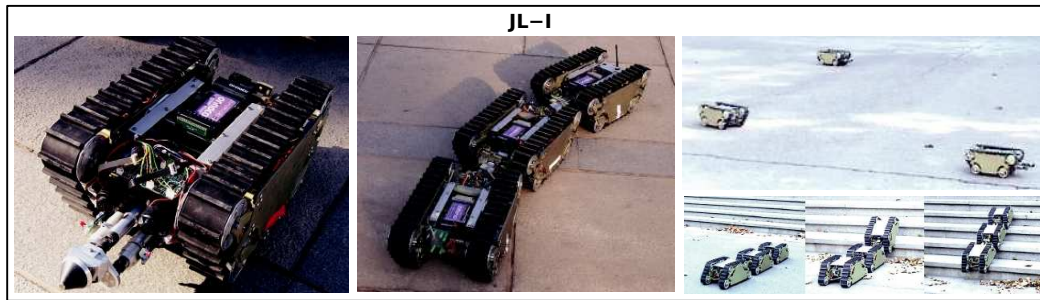


Figure 2.8: The robot JL-I

Each one of these modules is called **s-bot** and is totally autonomous. They use caterpillar tracks to move and are supplied with sensors (Figure 2.7).

2.4.5 Institute of Robotics at Beihang University (BUAA): JL-I

The Beihang University (Beijing China) Robotics Group started the design of this type of robot in 1999, with a two module design[153]. Each one has two caterpillars and an articulation with 2 degrees of freedom as well as a CCD camera and sensors. The articulations can also extend, allowing the robot to increase or shorten its length.

Based on this initial prototype, Houxiang et al designed the **robot JL-I**[181]. At present this is formed by 3 identical modules. It has 3 degree of freedom articulations, which gives it a vast capacity of movement. Not only can it climb obstacles, among other characteristics, but also stairs and recover itself if it turns over[178]. The robot is planned for military applications[185].

2.5 Modular robots and locomotion

2.5.1 A new approach to the problem of locomotion

In every discipline an investigator appears who revolutionises this area of knowledge, proposing new ideas and giving new insights. Such is the case with **Mark Yim**, who can be considered the father of **modular self-configuring robotics**. His work has inspired hundreds of investigators (Some of his articles have been referenced more than 250 times!).

In his 1995 doctoral thesis Mark Yim proposed a new approach to the locomotion problem[163]. The traditional solution, described in the section 2.2.3 is focused on designing a specific robot based on the analysis of a terrain's characteristics. What Yim proposed was using robots based on modules with the capability of re-assembling themselves into different forms. In this way, these new modular

robots could change their form adopting different configurations and gaits according to the terrain where they were operating at a particular moment.

To illustrate it, he proposed the scenario described in the introduction to this thesis. The question was asked what would the robot have to be like to be able to go from the Stanford Robotics Laboratory to a building on the other side of the street. The robot had to be capable of moving along level ground, cross the laboratory's porch, pass under a railing, go down some 60 cm steps and move across a rough piece of ground, covered in herbage.

To resolve the problem the best configurations for each type of terrain would have to be determined, using a self-reconfigurable modular robot. Initially, therefore, the robot would use a wheel type configuration to cross the porch (it was shown that this gait was the most efficient for level ground), next the "wheel" would open and the robot would transform itself into a worm that allowed it to pass under the railing and descend the steps. Finally it would change into a four footed spider, a configuration characterised by its greater stability, to cross the broken ground.

The advantage, therefore, of these self-configuring modular robots is their **great versatility**. What is more they can employ the most efficient configuration and gait for each class of terrain. That is to say, they combine the best features of apodal robots and robots with feet.

2.5.2 Polypod

This idea of self configuring robots would not have been such an innovation if Yim had not demonstrated their viability. It was not until some years later, after the publication of his thesis, that his idea took off and produced the boom in modular robots.

For the experiments of his thesis the first robot that was developed was **Polypod**. Though what was being proposed was the birth of self configuring modular robots, Polypod was manually self-reconfigurable, but it was used to implement distinct configurations and demonstrate the viability of his ideas. The Polypod's modules were mechanically complex and possessed two degrees of freedom. All the technical details are included in his thesis[163]. An amplified summary (in Spanish) can be found in [41].

2.5.3 Polybot

After finishing his doctoral thesis Mark Yim started to work as an investigator in the PARC (*Palo Alto Research Centre*) where he developed his famous robot **Polybot**[165]¹⁰. In reality it is not a robot, in the traditional meaning of the term, but the word covers various generations of modules from which modular robots can be created.

¹⁰Information about Polybot is available on <http://www2.parc.com/spl/projects/modrobots/chain/polybot/>

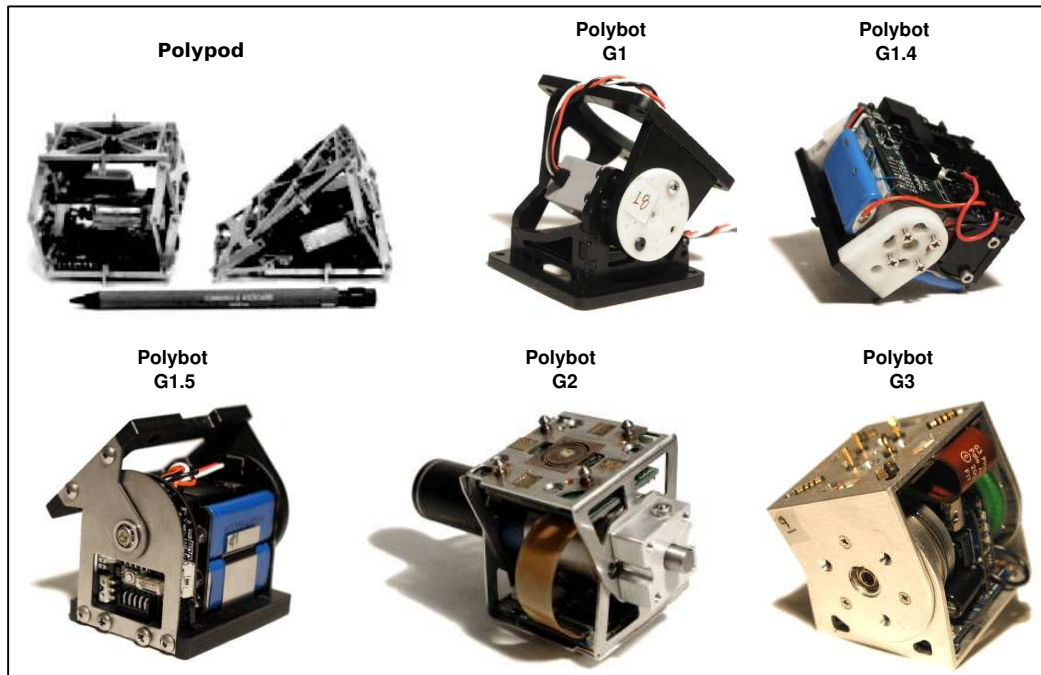


Figure 2.9: The modules of Polypod and Polybot

According to Yim the three promises of modular robotics[174] are versatility, reliability and low cost. **Versatility** is due to the fact that these robots can change their form and move in diverse kinds of terrain. **Reliability** lies in their self-repairing capacity. If one of the modules develops a fault it eliminates itself or is substituted by another. Finally the **low cost** is obtained by applying mass production of the modules. Large scale production leads to reduced costs.

Polybot is a platform for experimenting focused on the promise of versatility. Up to now five different types of modules have been created, grouped in three generations: G1, G2 and G3 (see figure 2.9). One of the aims of their design was simplicity, that is why they have all been given only one degree of freedom.

The **G1 generation** is not self-configuring, as the modules do not have the capacity to automatically join themselves together. Nevertheless it is possible to produce various manual configurations and test them. Three different modules have been designed. The first was made of plastic and employed a commercial servo as articulation. Mechanically it is much simpler than the modules developed for Polypod. A novel idea was introduced, that the base of each module should be square, enabling them to be connected one to the other, in different ways. In this way robots with joints that move on one plane, and others perpendicularly to them could be formed. Outstanding among the experiments is **the first example of simple re-configuration**, in which 12 modules adopt, initially, the form of a wheel. These move along a level surface until they arrive at some stairs. The robot opens up and converts itself into a worm that can descend the stairs. It was the first experiment in which a robot carried out



Figure 2.10: Polybot. Different configurations of Polybot G1

a re-configuration[166]. Besides this different locomotive configurations were experimented with a four footed spider and a worm configuration, movement through a tube and turns (Figure 2.10).

Having proved the viability of modules, sensors were introduced in the version **G1v4** to implement applications in closed loop. Experiments were carried out of climbing worms. Not only to climb walls and barriers (lineal configuration) but also to climb stairs (wheel configuration)[169][168]. One of the strangest experiments was imitating the human ‘undercarriage’ (hips and legs) making them move by pedalling a tricycle[174]. It is a further example of the versatility of modular robotics: configurations can be created that allow objects made for humans to be manipulated¹¹.

The G2 and G3 generations have the ability to join themselves together and separate[175], which permits the construction of authentically self-configuring robots. The **G3 generation** is a redesigned G2 to obtain a more compact module: Its dimensions allow it to fit in a 5 cm cube. This innovation was produced in the previous version. The first dynamic self-reconfiguration experiment was carried out successfully with the **G2 modules**[167]. The first part of the experiment demonstrates the simple re-configuration, in which Polybot adopts the form of a wheel with 12 modules. Following that it adopts a lineal configuration. In the second part the conversion from worm to a four legs spider is carried out. Both extremities fold inwards, parallel to the ground with the robot adopting the form of ∞ , coupled to both sides of the central module. The exterior modules separate so that the robot forms an X. Now the robot has 4 feet, each one formed by three modules. Finally the robot raises itself. The

¹¹It is interesting that – diverging from the theme – in his science fiction novels Isaac Asimov argue that the future of robotics lay with humanoid robots. All the tools that had been designed for humans could be used by robots, avoiding the need to redesign them.

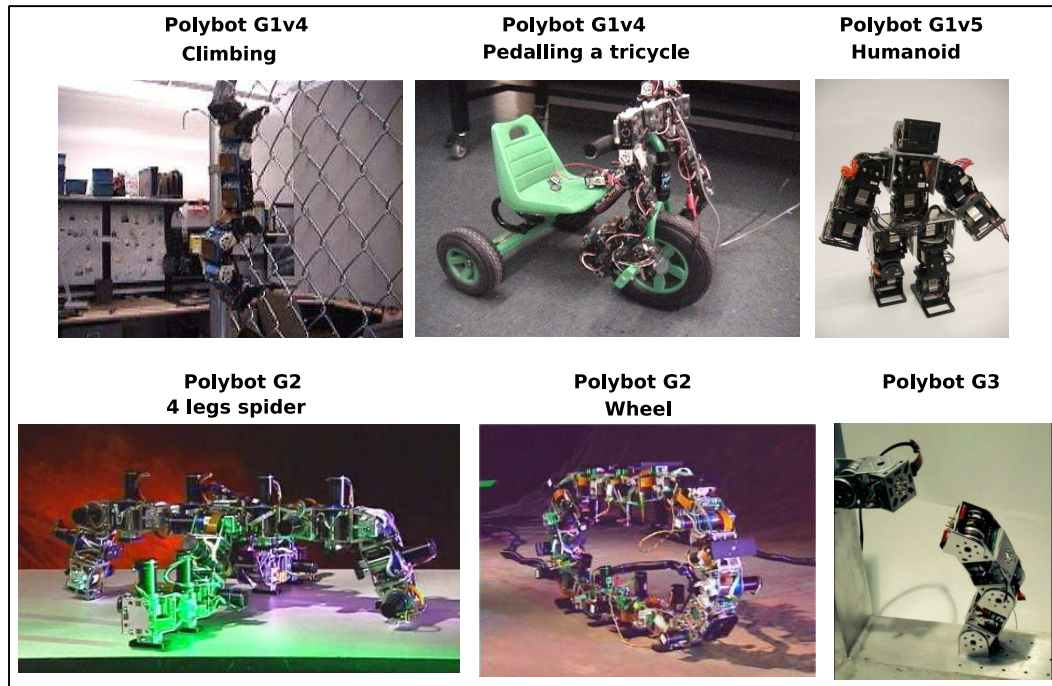


Figure 2.11: Different configurations of Polybot

great contribution obtained is the ability to automatically join modules using infrared rays as guides [118].

The **G1v5 modules** are the latest to be developed. They are not re-configurable, nevertheless they are designed using the lessons learned from all the previous modules. They are very robust and are prepared for commercialisation. The Polykinectis environment[39] has been developed to program and drive them. This includes programming in a scripting language to control the various configurations based on XML[182]. This environment was tested in a workshop given in the International Congress of Intelligent Robots and Systems in 2003 (IROS)¹². The experience was a success and the possibilities of modular robotics in the field of education was demonstrated.

The theoretic model for the programming of modular robots is known as phase automata[183][184]. It is based on the idea that principal movements are periodical. This periodicity is ruptured when certain events from the sensors occur. The other idea is that the signals that control the modules are the same, but with a time lag.

In the figure 2.11 the different configurations of the Polybot G1v4, G1v5, G2 y G3 generations are shown.

¹²The tutorial is available in the link: <http://www2.parc.com/spl/projects/modrobots/chain/polybot/parc/doc/tutorial/index.html>

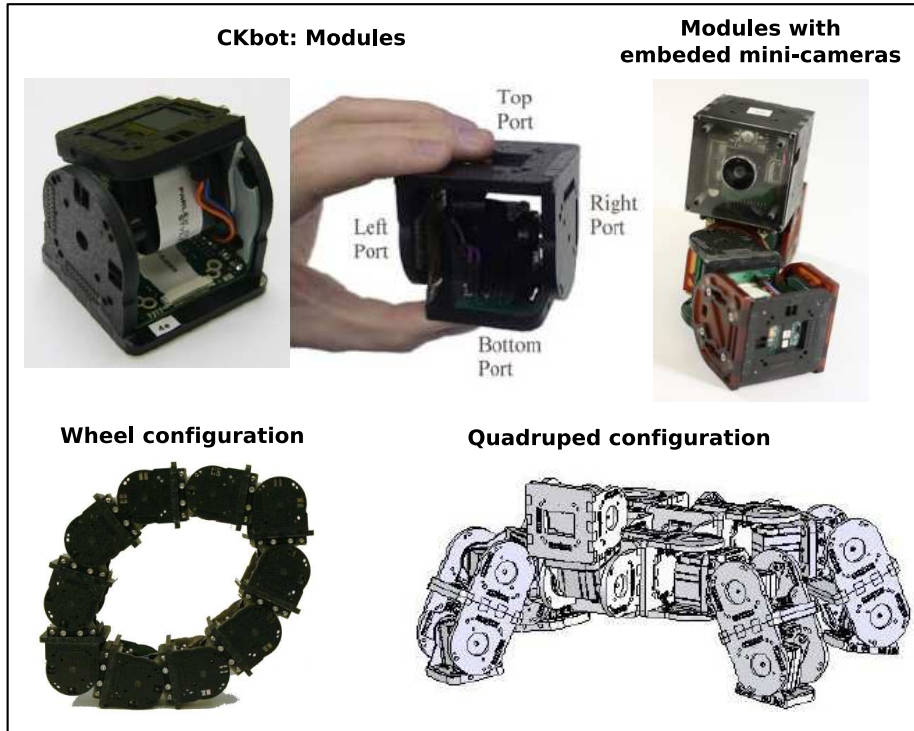


Figure 2.12: Modules and various configurations of Ckbot

2.5.4 Ckbot

In 2006 Mark Yim moved to the University of Pennsylvania where he founded the **ModLab**¹³, where investigations in the field of Modular robotics are carried out.

The modular robot **CKBOT** [113] (*Connector Kinetic roBot*) has been developed there to be used as a platform for his investigations. The modules of Ckbot have been inspired by the Polybot version G1v5: dynamically they are not reconfigurable, but they do permit the creation of different types of configuration to explore their locomotive capabilities. In the figure 2.12 the modules and some of the configurations that have been tested are shown.

Though Modlab is not very old, its contributions are very innovative. One of them is a new application baptised by Yim as ‘**self-reassembly after explosion**’ (SAE) [172][173]. The aim is to begin to explore the second of the modular robotics promises: **robustness** and **self repairing ability**. The following problem is still to be resolved: the starting point is a modular robot with a specific configuration. At a particular moment it suffers an impact and all its modules or parts of the robot are scattered over the immediate area. The robot must be able to put itself together again and continue with the task that it was doing.

¹³The web page is: <http://modlab.seas.upenn.edu/index.html> (Modular Robotic Lab)

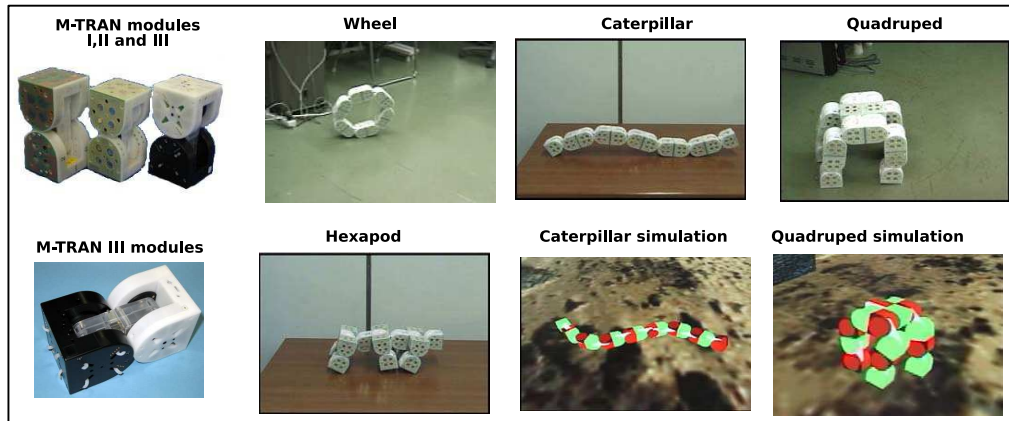


Figure 2.13: Modules and different configurations of the robot M-TRAN

To test the viability of the system, a configuration in the form of a humanoid robot has been created, made up of three groups of modules (known as *clusters*). Each cluster consists of 3 modules Ckbot and a module with a mini-camera[134]. The mechanical union between the three clusters is by means of permanent magnets, while the internal modules are joined by screws. In the experiment realised in [173], the humanoid configuration is walking. One of the investigators hits it and the three clusters are scattered across the ground. By means of the mini-cameras the different parts are capable of recognising each other and moving until they reconstruct the humanoid original and continue the task.

Besides this different gaits and configurations, for example a type of wheel movement[127] or the creation of a centipede robot from modules that add exterior feet[128], are continuing to be studied and analysed.

2.5.5 M-TRAN

One of the most advanced modular robots that exist at the moment is the **M-TRAN** (Modular TRANformer)[105]¹⁴ developed in the National Institute of Advanced Industrial Science and Technologies (AIST) in Japan. In the figure 2.13 the modules and different configurations of the robot are shown.

The present version has been the result of more than 10 years of investigation. It is a hybrid modular robot (see paragraph 2.7) that can configure itself to form chain topologies or lattices. Three generations of modules have been developed: M-TRAN I, II & III.

The project started in 1998, with **M-TRAN II**[110]. Faced with the search for simplicity in Polybot and Ckbot, the M-TRAN module has two degrees of freedom and a novel system of coupling between modules based on permanent magnets and SMA (*Shape Memory Alloy*) springs for separation. They

¹⁴More information is available in the link: <http://unit.aist.go.jp/is/dsysd/mtran3/>

are based on Profesor Hirose's principal of internally balanced magnetic units[54]. The modules are joined to each other by means of permanent magnets. The system's novelty is in the SMA springs that are activated by electric current to disconnect the modules. In the first experiments it was shown that the permanent magnets had sufficient force for one module to lift another. Also the viability of various configurations in movement was explored: wheel, worm, quadruped, and dynamic configuration [70]. As well as the mechanical and electronic design of the module, a powerful simulation system was developed[80] that was used to explore the modules' possibilities, causing a block of 12 modules to pass over obstacles and simulate different algorithms of planned movements[177] and simulations of self-reparation[109].

In 2002 the second generation: **M-TRAN-II**[108] was developed. The idea of the module is the same, improvements have been made in the mechanics and the hardware. The module was reduced in size by approximately 10%, and consumed less, which led to better autonomy, and the hardware allowed for wireless communication. The innovations that were introduced were in the field of the automatic generation of gaits, using CPGs and genetic algorithms [66]. Genetic algorithms are run in a PC and then the pattern of movements are down-loaded to the modules, either to the actual robot or to the simulation. More information can be found in [68]. Nevertheless, one of the most novel experiments that was done was the reconfiguration of a quadruped into a worm [78], something that had not been seen before. To achieve it, it is necessary to plan the steps that the modules have to follow to reach the goal [176]. Due to these experiments the M-TRAN became the most advanced modular robot.

The present generation, **M-TRAN III**[67] incorporate a new mechanical connecting mechanism, that replaces the permanent magnets. This has achieved improved energy efficiency and speed in connecting and disconnecting, though at the price of mechanical complexity. These modules, nevertheless, are no longer prototypes, but can be produced industrially. The electronics are much more powerful. Now each module has four microprocessors connected by a bus CAN (Controller Area Network). One is the master and the others slaves. The previous experiments of locomotion have been verified and amplified [81] and reconfigured [79]. One of the new possibilities of these modules is that of incorporating specialised modules, for example mini-cameras [104] to help in the implementation of the reconfiguration.

2.5.6 CONRO

The **CONRO** modules¹⁵ were developed by Castano et al.[10] at the University of South California's ISI (Information Science Institute) for the implementation of what are called **metamorphic systems**: robots that can change their shape. What Yim called self-configuring (the denomination that has prevailed). These modules have two degrees of freedom and self-coupling ability. In the initial experiments a snake and a hexapod were formed[9]. The coupling system was tested, though in the first version it has not been integrated into the modules yet.

¹⁵More information on the web: <http://www.isi.edu/robots/conro/>

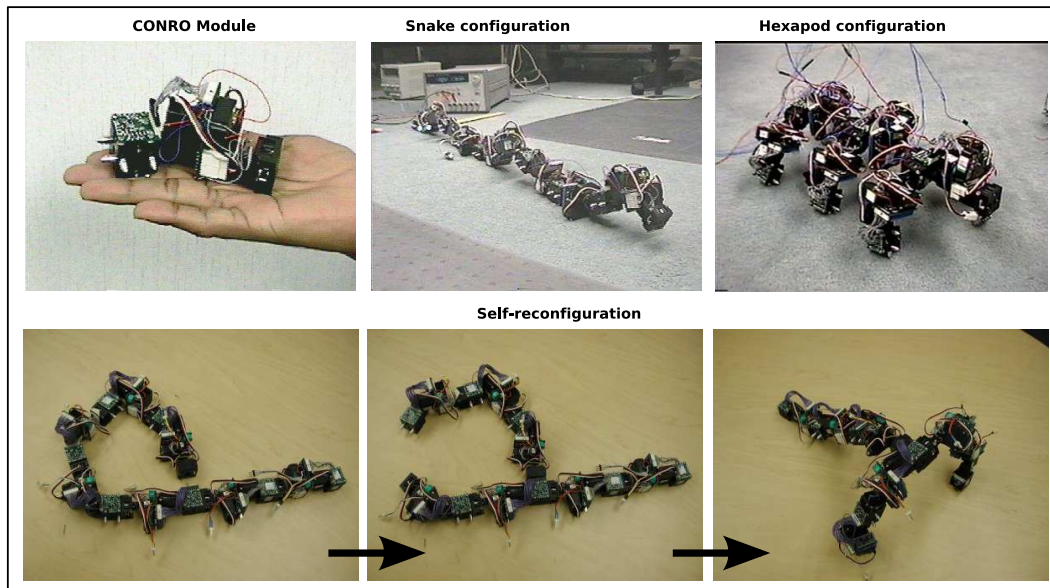


Figure 2.14: Conro module and different configurations

To represent the configuration of a re-configurable robot graphs are used to determine if two robots have the same configuration[11]. Also it is possible to locate special modules, for example a mini-camera [8].

In later studies a new bio-inspired system was proposed so that the modules could discover the changes in topography and could collaborate with other modules to carry out movement and self configuration. Two protocols based on the idea of hormones have been developed, one called Adaptive Communication (AC) and the other Adaptive Distributive Control (ADC)[132]. In [120] a system of autonomous coupling between modules is being studied.

The figure 2.14 shows what CONRO looks like as well as various configurations and one of the reconfiguring experiments that was carried out.

2.5.7 SuperBot

SuperBot¹⁶ is a modular robot created in the ISI Robotics Polymorphic Laboratory of the University of South California. The module designed is one of the most modern (2005) and is inspired in all the previous ones: Conro, Polybot, MTRAN y ATRON. It is a project financed by the NASA and the DARPA. and was developed, initially, to be used in space applications[130]. How to employ it as a mobile platform to move on another planet's surface and collect information is being studied[147]. Between 8-10 modules reconfigure to form the needed platform: such as wheel (for efficient movement), spider, snake, communication towers, etc. Another application is what the authors call MULE

¹⁶More information on: [web:http://www.isi.edu/robots/superbot.htm](http://www.isi.edu/robots/superbot.htm)

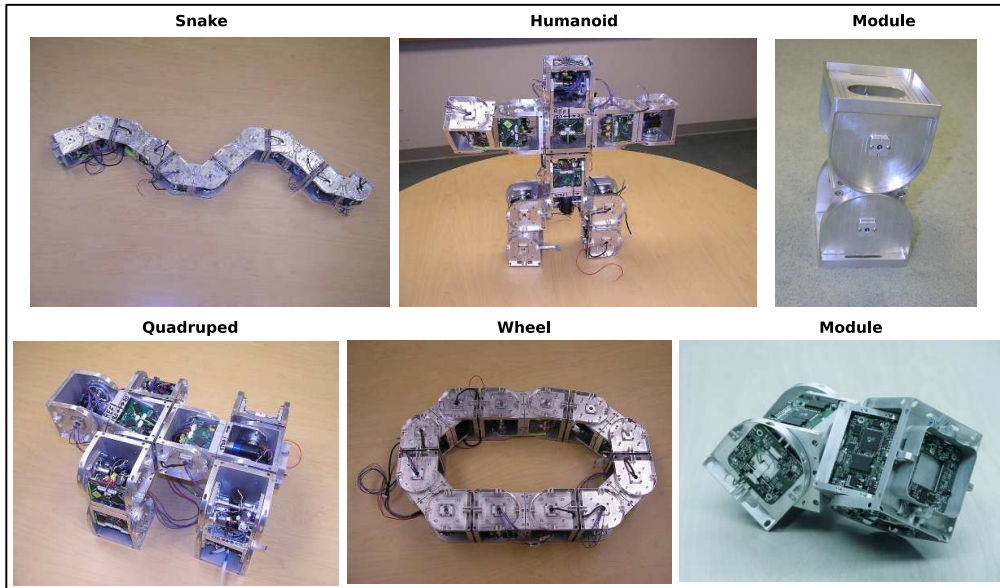


Figure 2.15: Different configurations of the SuperBot module

(*Multi-Use Lunar Explorer*) [84]. The idea is to place more than 100 modules on the chassis of a lunar vehicle and use them to carry out various geological tasks, with or without the help of the astronauts. Weight is very important on space missions. Instead of carrying different apparatus to make measurements, the modules can be reconfigured to form different structures according to need.

The latest application is that called OHMS (*Habitat Operations and Maintenance System*)[82] in which approximately 150 modules are used to obtain various tools: solar panels, cleaning and maintenance of the installations, monitoring and inspection in real time...

The mechanics of the Superbot modules are inspired in MTRAN, but includes an extra degree of freedom. The two extremities turn vertically (pitch) and rotate (roll) between themselves. It has, the same as MTRAN, a total of 6 contact surfaces where other modules can be joined, this allows not only the formation of chain type robots (see paragraph 2.7), but also solid 3D structures[131][124].

The re-configurable systems must resolve various challenges: 1) Distributed negotiation, in such a way that the modules agree on the global task they are to perform. 2) Distributed collaboration, that allows them to translate the global task into local tasks that each module can carry out. 3) Synchronisation, so that each local task is synchronised with the others.

These problems have already been addressed in the CONRO modules, but with the supposition that the topology did not vary while a task was being carried out. In [126] an algorithm is proposed to resolve these problems, allowing the topology to change. This is inspired in the concept of hormones[125].

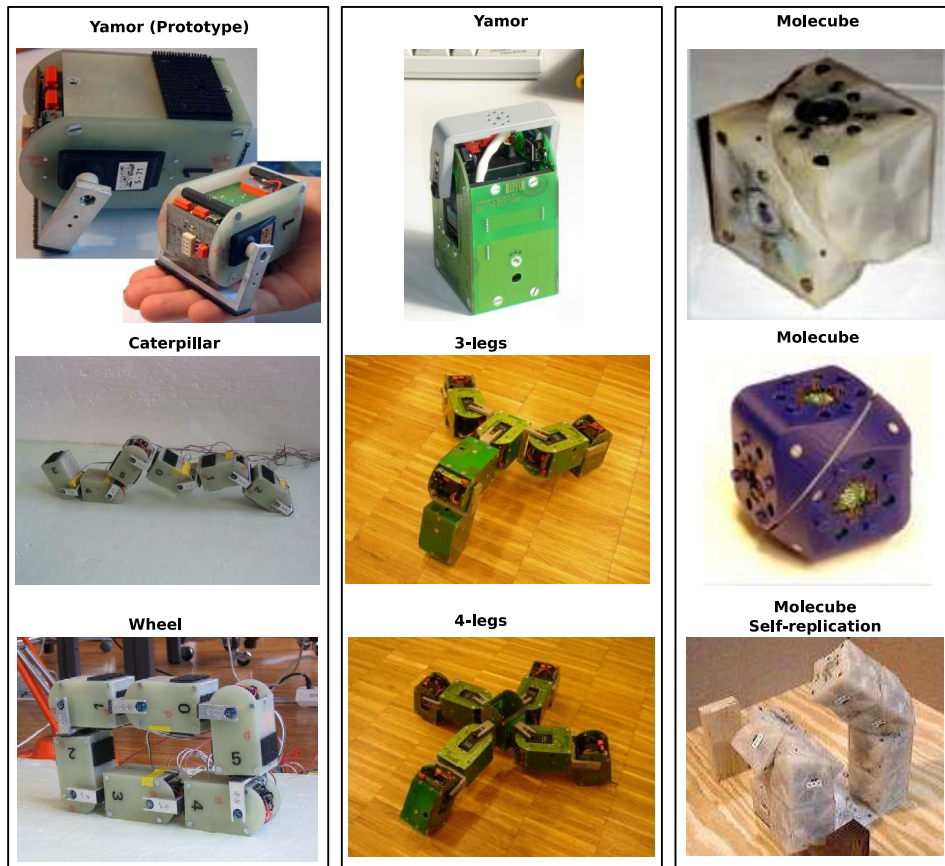


Figure 2.16: The modular robots Yamor and Molecube

2.5.8 Yamor

Yamor¹⁷ (*Yet Another Modular Robot*) is the modular robot developed in the bio-inspired robotics laboratory of EPFL, to study adaptive locomotion[98]. The developed module has one degree of freedom activated by a servo and the communication between modules, and the modules with the PC is by Bluetooth, which means that there are no wires. The control hardware includes FPGAs (Field Programmable Logic Arrays) which gives the system greater versatility for the implementation of specific controllers. The software developed allows the generation of movement functions using a GUI (Graphical User Interface), which is then down-loaded to the hardware[97].

Maye et al.[95] applied the CPG models to the movement of modular robots, carrying out experiments with Yamor, thereby validating the previous simulations. Worm, tripod and quadruped configurations were tested.

Yerly et al.[162] are working on the following generation of modules, adding accelerometers and improving the software.

¹⁷More information in <http://birg.epfl.ch/page53469.html/>

In the figure 2.16 the two versions produced of Yamor and the various configurations tested, are shown. In the central part are the following versions of modules and the tripod and quadrupe configurations.

2.5.9 Molecube

In the Cornell University CSL (Computational Synthesis Laboratory) the modules known as **Molecubes**¹⁸[186] have been developed. They have one level of liberty and form a cube. They differ from the rest in that they rotate on a diagonal axis, that unites two opposing points of the cube. When a 90 rotation is performed on this axis, another cube is obtained.

These modules are not adapted to resolve locomotive problems, though robots can be created with locomotive capacity. Their original purpose was to build **the first modular system capable of self replication**[187]. In the experiment that was performed, a tower composed of 4 molecubes, duplicated itself. For this another four modules were used as raw material for the duplication. The initial individual deposits its own modules in the places where the replica is to be created. Using the “raw material” supplied it self replicates. The final process ends after two and a half minutes. What is important is that the new copy can also duplicate itself. The new individual can create another, demonstrating that total self replication has been obtained (in behaviour as well as structure).

2.6 Modular Robots and Structures

Other area of investigation on the modular robots is **the capability to form structures that can be reconfigured**. In the figure 2.17 various of these prototypes are shown. The origins go back to 1988 with the proposal of Fukuda et al. **CEBOT**[34] (CELLular ROboT) developed at the Technology Institute of Tokyo. Each Cebot is treated as an autonomous cell that can move and join itself to others. Also the idea of a dynamically re-configurable robotics systems was developed[33]. This is a similar idea to the re-configurable robotics but it is applied to structures, instead of to locomotion. The system can be reorganised to carry out more complicated tasks. Each cell has its own knowledge (known as knowledge cells) and can use the knowledge of others. It is a system of distributed intelligence.

Chirikjian et al., of John Hopkins University PKL (*Protein Kinematics Lab.*) proposed the **metamorphic manipulators**[14]. It is a net of modules arranged in two dimensions that can move through a global structure because they have the ability to couple and uncouple with each other. Compared to CEBOT the modules can not move on their own, only being able to do so when connected to adjacent modules. The kinematics of these manipulators was studied[15] and their use was proposed for capturing satellites in space. Initially the manipulator has an undefined form, like an amoeba. By means

¹⁸The link for more information: <http://www.molecubes.org/>



Figure 2.17: Various lattice type modular robots

of the movement of some modules over others some tentacles appear that wrap round the object to be captured. Pamecha et al. implemented it in two modules, the robot was called **Metamorphic**[112]. Each module is of hexagonal shape and can warp by means of 3 actuators.

The idea of metamorphic manipulators was perfected by Murata et al., of the AIST, with the prototype **Fracta**[106]. The ‘cells’ are much simpler and do not have any actuators which means less consumption. To carry out the displacement and the coupling/uncoupling permanent magnets and electro-magnets are used. The same as Metamorphic, the structures that are formed are two dimensional.

The idea was enlarged with the building of three dimensional structures, and the designing of the robot **3D-Fracta**[107] with a cubic structure and six arms that join the centre with each one of the cube’s faces. A total of 6 actuators are used. These investigations together with Mark Yim’s idea of modular robotics were the seeds of the hybrid modular robot M-TRAN, that not only can move but also shape three dimensional structures.

Hamblin et al. created **Tetrobot**[49], formed by a tetrahedral module with spherical articulations. The system is reconfigured manually. Experiments have been done with arms and walking robots.

At the CMU’s Advanced Mechatronics Lab Unsal et al. developed the **I-CUBE** robot[58] formed by two elements: cubes (passive) and active segments. The segments have three degrees of freedom and are used as arms that hook onto the cubes. Different three dimensional structures can be built and they have the ability to modify themselves¹⁹.

In the PARC, Suh et al. developed the **Telecubes** robot[143]²⁰. It is a cube with 6 prismatic articulations that allows it to move all of its faces. What is more all of the faces have a coupling/uncoupling system by which modules can be connected one to another, and disconnected. With this system very compact 3D structures can be created and can re-configure themselves.

The distributed robotics laboratory of MIT²¹ is also interested in modular robots. Kotay et al. have created **Molecule**[76]. This robot imitates a two atom molecule, joined by a rigid segment. Each atom has 5 connectors to join it to other molecules and two degrees of liberty. The grouping of various molecules permits the creation of structures in two as well as three dimensions. In the first prototype only one molecule was implemented. Further work was done to improve the modules and a two molecule structure was implemented[74][75].

In the same laboratory, Rus et al. worked on **Crystal**[122], a configurable robot made up of atoms that can form two-dimensional structures. The atoms are four faced cubes that can expand. In contrast to other modular robots, where there is translation of the atoms, movement in this one is only obtained by expansion and compression [123].

¹⁹More information in <http://www.cs.cmu.edu/~unsal/research/ices/cubes/>

²⁰More information in <http://www2.parc.com/spl/projects/modrobots/lattice/telecube/index.html>

²¹More information: http://groups.csail.mit.edu/drl/wiki/index.php/Main_Page

The latest prototype developed in the MIT is **Miche**[36]. The idea is completely different to the rest of the modular robots. It starts from the idea of an amorphous structure, as if it was a marble block in the world of sculpture. The user specifies the 3D form he wants to “sculpture”. He makes the calculations and the system disconnects from the amorphous mass all the unnecessary modules. When the object is taken, the unused modules stay on the ground, leaving the created structure. The modules are cubes that only have the capacity to join themselves one with the other (they do not have any degrees of freedom). Among the experiments carried out a dog and a humanoid have been “sculptured”.

In Denmark, at the the Maersk Mc-Kinney Moller Institute for Production Technology, work is being done on **ATRON**[64]. Starting with the ideas of CONRO and M-TRAN a spherical module has been created that can rotate around its equator, dividing the module into two semi-spheres that rotate, one in relation to the other. The modules can link together in such a way that the rotation can be made on any one of the three axis: x, y, z. In the latest version 100 of these modules have been created and diverse simulations and experiments have been realised[19].

Goldstein et al., of CMU, are developing the idea of synthesising real structures in three dimensions from virtual modules, within the project **Claytronics**[37]²². The aim is the development of what is denominated a Claytronics: a computer generated synthetic object, but with a real physical structure. These systems are formed by atoms called **Catoms** (Claytronics Atoms) that can move in three dimensions in all the structure. By the re-combination of these atoms the Claytronic attains the desired shape. In the Miche prototype real structures are also synthesised, but the approach is that of a “sculpturer” that eliminates excess material. In the Claytronics’ approach it is its own atoms that reorganise to create the object.

In the first phase work is being done on Catoms restricted to two dimensions [72]. The movement of these catoms is obtained through the correct co-ordination of electro-magnets, in such a way that not one type of actuator is needed. The aim is to be able to miniaturise to achieve nano robots of this type that can be relocated to form the Claytronics.

In the Bio Inspired Robotics Laboratory (BIRG) and learning algorithms (LASA) of EPFL an innovative concept has been suggested. Use three dimensional structures for creating furniture that can be reconfigured. The prototype of the proposed module is **RoomBot**[2]²³ and is inspired in Yamor. In the figure 2.18 the shape of some of the furniture, made up of these modules, is shown. The desire is that the furniture forms part of the new centre that is being constructed. They are not only static, but also have the ability to move²⁴.

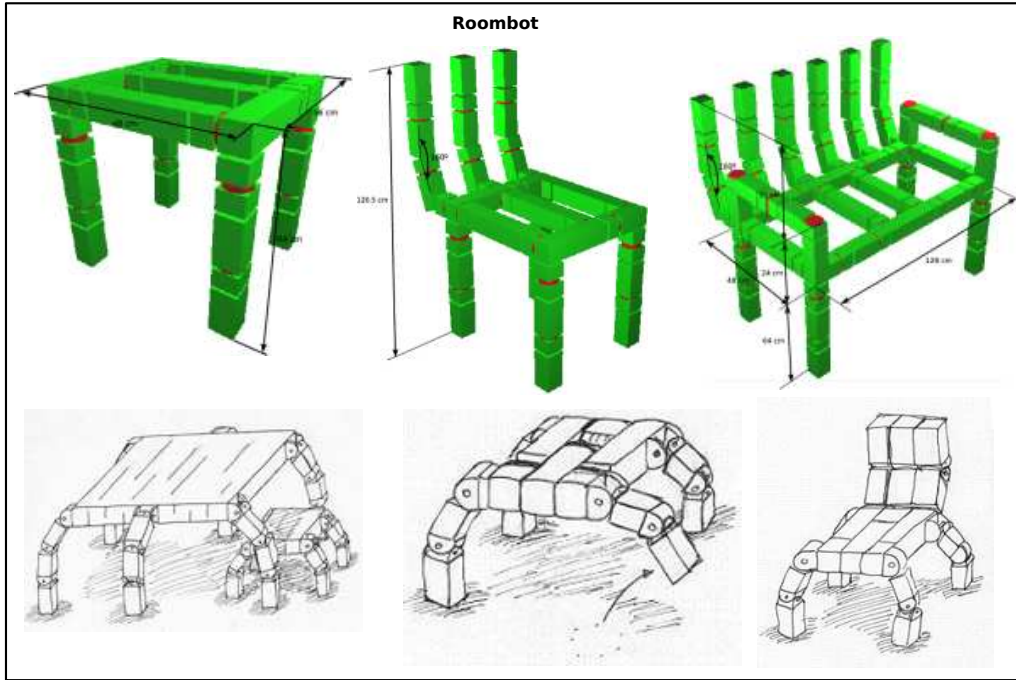


Figure 2.18: RoomBot prototype: a lattice modular robot designed to make re-configurable furniture

2.7 Classification of the modular robots

The figure 2.19 shows a classification of the modular robots according to their structure and connections, that will be explained below. All the robots presented previously are placed in different groups.

To study the modular robots' locomotive property configurations it is essential to classify them by groups that share the same characteristics. The proposed classification is based on the structure and the connections between the modules. One must emphasise that the re-configurable modular robots can belong to different groups, due to the fact that various configurations can be built with them. For example, with the Polybot modules an apodal robot with connections pitch-pitch can be created; that is included among the robots with one dimensional topology. But also a quadruped with two dimensional topology can be built.

Mark Yim[171] proposes a basic division of three groups: reticule (lattice), chains and hybrids. The **lattice type** modular robots connect with each other to form structures, in the same way that atoms join together to form complex or solid molecules. They are the robots that have been described in the section 2.6. The idea behind all of them is to make structures that can dynamically modify themselves. According to the type of structure, they can be grouped as 2D or 3D. Among the first are

²²More information in: <http://www.cs.cmu.edu/~claytronics/hardware/planar.html>

²³More information: <http://birg.epfl.ch/page65721.html>

²⁴Author's note: I am not very clear what use is this mobile furniture, nevertheless it seems to me an entertaining application. I would like to visit the centre to see the system in action ;-)

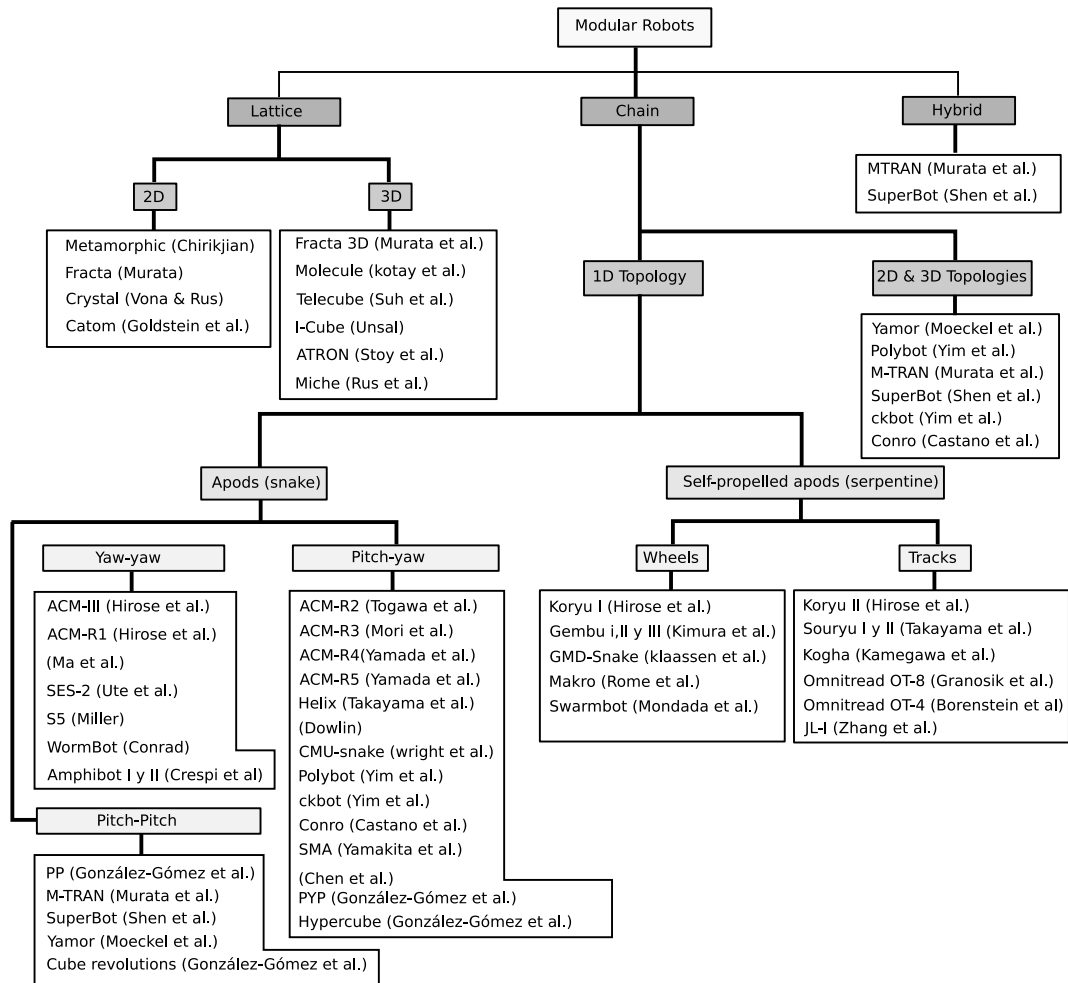


Figure 2.19: Classification of the modular robots

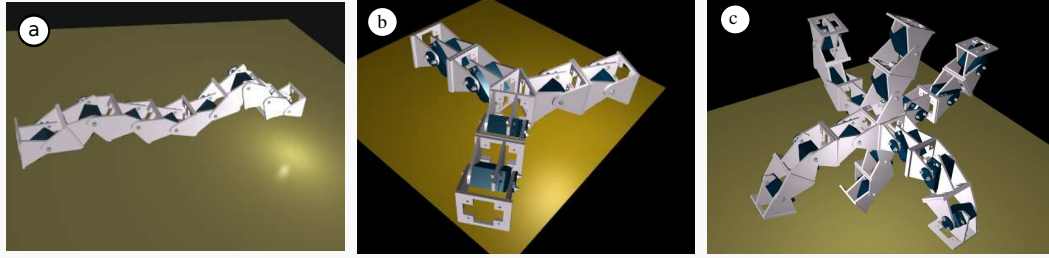


Figure 2.20: Example of the three sub-types of chain modular robots: a) 1D Topology; b) 2D Topology 2D; c) 3D Topology 3D

Metamorphic[14], **Fracta**[106], **Crystal**[123] and **Catom**[72]. Among the second **Fracta 3D**[107], **Molecule**[76], **Telecube**[143], **I-Cube**[151], **ATRON**[64] and **Miche**[36].

The **chain type** modular robots are formed by uniting different chains of modules. For example the structure of a quadruped robot can be seen as made up of five chains: a central one that acts as the spine and four more for the extremities. The robots of this group are better for locomotion because they reconstruct animal morphology. The chains of modules can act like feet, arms, spine, etc. The lattice type robots, though they can also move, are much slower, as they are based not on the global movement of the structures, but on module to module movement. The **hybrid modular robots** possess the characteristics of both these groups: surfaces can be built with them as well as chain like structures. Within this group are found the most advanced modular robots, **M-TRAN**[108] and **SuperBot**[130].

At the same time, according to their topology, **chain type robots** can be divided. They can have a 1D topology, such as worms and snakes, 2D topologies, quadrupeds, polygonal structures such as stars, pentagons, etc., or 3D topologies such as hedgehogs. In the figure 2.20 can be seen an example of the different topologies. Once more it must be emphasised that the re-configurable robots can have configurations with different topologies, for this reason they can be placed in various groups. The criterion followed in the diagram has been to place the robots according to the experiments that have been carried out with them. For example, with Polybot the experiments have been with the quadruped configuration, therefore it has been included in the 2D topologies group, but it has also been tested with a worm configuration, therefore it is in the 1D topology group.

The **1D topologies** can be worms, snakes, arms, legs, spines, etc. In general these structures are very flexible and can adopt different shapes. They can, for example, be introduced into tubes, intestines or in general tortuous routes. If they are sufficiently long, they can form loops and move like a wheel[69][142].

According to how the propulsion to move the robot is generated, we propose two categories. One is what we call **apodal robots**²⁵ that comprises all the robots that move by means of body motions.

²⁵Clarifying terminology: Granosik et al., proposed calling both groups of snake robots and serpentine robots. The first is what I baptised as apodal robots, and the second as self-propelled apodal robots

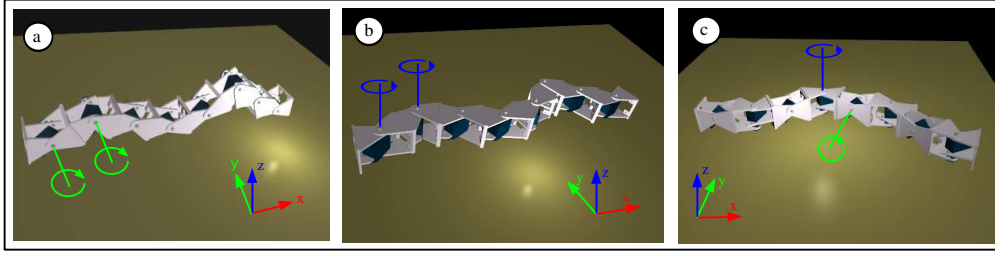


Figure 2.21: Different types of connections in the apodal robots a) Pitch-pitch. b) Yaw-yaw. c) Pitch-yaw.

The modules alone are unable to move, but when they are joined to form a chain and are adequately co-ordinated manage to do so. That would be the case of the biological worms and snakes. In another group are the robots that move by means of active wheels or caterpillar tracks. These are known as **self propelled apodal robots**. In these each module can move as an autonomous unit, using this system of propulsion. This group is employed in applications of search and rescue or inspection of tubes or bridges. Generally they are more industrial. As their mobility is by wheels or caterpillar tracks they can move across a wide variety of terrain. Being of 1D topology they possess the flexibility of this group and therefore can adapt their shape to the terrain, climb obstacles, go through tubes, etc.

Among the **apodal robots propelled by wheels** there is: **Koryu I**[56], **Gembu**[71], **GMD-Snake**[73], **Makro** [117] and **Swarmbot** [100]. Among the **apodal robots propelled by caterpillar tracks**: **KoryuII**[57], **Souryu I** [144], **Souryu II**[146], **Kogha** [65], **Omnitread OT-8** [47], **Omnitread OT-4**[4] and **JL-I**[181].

In the **apodal robots group**, we propose classifying them according to how the modules are connected one to the other. As can be seen in the figure 2.21, the connection can be of yaw-yaw type (that is to say the modules rotate parallel to the ground), or pitch-pitch (they do it perpendicularly) and pitch-yaw where the modules that rotate parallel to the ground alternate with those that turn perpendicularly to the ground.

The connectivity between modules is a very important characteristic and determines what sort of movement can be carried out. Therefore, the **yaw-yaw group** is that that includes all the robots that move like snakes. This type of movement requires that the friction coefficient in the tangent to the body axis is very small while the normal is infinite (or the greatest possible). The snakes obtain this thanks to their scaly skin. The snake robots use passive wheels to fulfil this requirement. For this reason, this group is special. Not only does it need body movement but also the passive wheels or skins. They are, therefore, specific robots. If one takes generic modules (for example the Polybot) and builds a robot of this group, one cannot obtain locomotion without adding external elements.

Within this group are found all the robots that are developed based on the gait of snakes on the level. They are: **ACM-III**[51], **ACM-R1**[52], **(Ma et. al)**[87], **SES-2**[152], **S5**[96], **WormBot**[21] and **Amphibot I & II**[23].

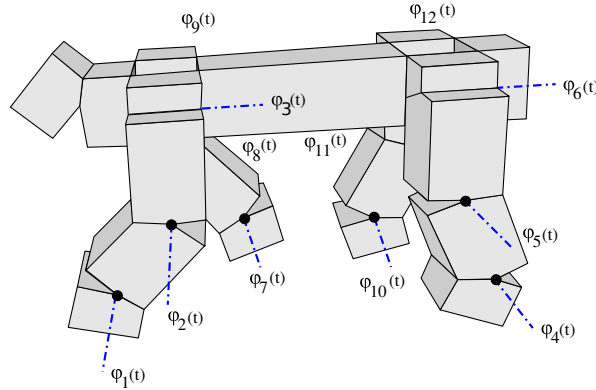


Figure 2.22: An example of the problem of co-ordination in a quadruped robot with 12 articulations. Finding the functions $\varphi_i(t)$ so that the robot can move

The **pitch-pitch group** only allows the robots to move in one dimension, forwards or backwards. It is a movement similar to the worms or caterpillars. They can also turn over on themselves to form a wheel. In this thesis this group of robots is used for a detailed study of one dimensional locomotion. The following robots have been subject to experiments with this type of connectivity: **M-TRAN**[108], **Polybot**[165], **Superbot**[130], **Yamor**[98], **PP**[43] and **Cube Revolutions**[42]. These last two carried out in this thesis.

The **pitch-yaw group** allows the robot to carry out many types of different movements, such as roll, side winding, climb, etc. Some of the robots already mentioned that have this type of connectivity are: **ACM-R2**[148], **ACM-R3**[102], **ACM-R4**[160], **ACM-R5**[148], **Helix**[145], **(Downlin)**[29], **CMU-snake**[158], **Polybot**[165], **Ckbot**[173], **Conro**[10], **SMA**[161], **(Chen et al.)**[13], **PYP**[43] and **Hypercube**[46]. These last two created by the author in this thesis.

2.8 Co-ordination and locomotion

We have presented the state of the art of apodal and modular robots, and have classified them according to their structure and connectivity. In this section their control will be analysed. We will see what alternatives exist to resolve problems of co-ordination and which is the one we have employed in this thesis.

2.8.1 The problem of co-ordination

When a mobile robot has wheels or tracks, the lower level of locomotion does not present any problems. One only has to make the motors turn to obtain the movement. The difficulties appear in the superior level tasks, such as the planning of routes and navigation.

Nevertheless, if the robot is articulated and it either has feet or it is an apodal robot, the problem of co-ordination arises, even if the movement is on a flat surface without obstacles. It is necessary that all movements of the articulations are synchronised so that the robot can travel. This problem can be stated in the following way:

Co-ordination problem: *Given that a robot with M articulations find the functions $\phi_i(t)$ that decide how it has to vary with time the angle of each articulation so that the robot manages to move.*

In the figure 2.22 an example of a quadruped modular robot can be seen, with two dimension topology and twelve articulations. The problem of the co-ordination will be solved if the functions $\phi_1(t), \dots, \phi_{12}(t)$ are found and the value of its parameters with which the quadruped is capable of travelling. The solution depends on the gait that one desires to obtain: movement in a straight line, sideways, turns, etc., and in general it will not be the only one.

In the following sections the different ways of addressing the problem are presented.

2.8.2 First approach: Manual solution

To implement easily the locomotion in modular robots, Mark Yim used, in Polypod, what he called ‘**gait control tables**’ [163]. The columns are vectors that contain an articulation’s discrete position for each moment. The positions are kept in the files momentarily. The controller revises the tables, sending at each moment the position to the actuators. When it arrives at the last line it starts from the beginning, carrying out a repetitive movement.

When the modular robots do not have many modules and the movements are simple, these tables can be created manually. It permits the definition of sequences of movement “frame by frame”, as if it were an animated film. This is the remedy adopted in the robot **Puchobot I**, developed by Prieto-Moreno [114]. Using a software with a graphic interface that runs in the PC, the user establishes the position of the articulations, that are recorded in the control table.

Another example is the hexapod robot **Melanie III** of Alonso-Puig [1]. The application that runs in the PC permits the manual generation of the sequences. The positioning of the articulations can be done either by the graphic interface itself (using sliders) or by using gestural programming, in such a way that the user places the robot’s feet in the desired positions and the application records them.

The manual solutions allows for the prototypes of the robots to be tested during their construction and to detect at an early stage of design any possible mechanical problems. Also it allows to explore very quickly possible solutions for the co-ordination. Nevertheless, they lack flexibility. To enable the robot to move in different ways a new control table has to be created. Also, if the robot possesses a lot of articulations, its creation can be tedious and complex.

2.8.3 Approach II: Inverse Kinematics

The classic approach is based on the idea of employing inverse kinematics. The idea is to apply the same techniques used for manipulators, but to the robot's feet. The functions $\varphi_i(t)$ are obtained from the functions of the trajectory of the supporting points. This method has been studied in detail in hexapods by Fligiolini[32] and has been implemented in the Alonso-Puig robot Melanie[1]. The trajectories of the feet's extremities are specified by means of sinusoidal functions. Using inverse kinematics the position of the angles $\varphi_i(t)$ are obtained.

The apodal robots can be considered as hyper hiper-redundant manipulators, formed by infinite articulations. Chirjkjian[16] employs functions to describe the form that the manipulator must adopt and gets the angular expressions. Gonzalez et al.[44] have also explored this type of solution, but using what is denominated the adjustment algorithm, in which it iterates on the articulations and goes finding the angles so that all of them are placed on a curve. With these algorithms the control tables have been automatically created and have successfully moved an eight articulation apodal robot. Spranklin[138], in his doctoral thesis, studies the kinematics and the dynamics of an apodal robot of the pitch-pitch group and proposes a solution using classic controllers.

The inconvenience of the classic approach based on inverse kinematics is that it requires greater computing power compared with the bio-inspired approach, that will be discussed next. Therefore the bio-inspired controllers generally need less powerful (and cheaper) microprocessors for their implementation.

2.8.4 Approach III: Bio-inspired

Another approach is to use nature as a source of ideas, and try to imitate it. Living beings in the animal kingdom just move. Their brains do not seem to be constantly reading the position of their extremities (x, y, z) , nor to use inverse kinematics to constantly contract their muscles.

In nature the vertebrates and invertebrates have special neurones called CPGs (*Central Pattern Generators*). These centres oscillate and produce rhythms that control muscle activity to carry out actions such as breathing, bowel movements, masticating, locomotion, etc. Based on biological studies mathematical models are constructed from these oscillators and they are applied to robots to control locomotion. In this bio-inspired approach the functions $\varphi_i(t)$ to be applied are obtained from the mathematical models of the CPGs. In contrast to the inverse kinematics approach, during the movement a bio-inspired controller does not know the position of its extremities. It only acts on the muscles to obtain locomotion. For this reason the computing power necessary is, in principal, less than that for approach II.



Figure 2.23: The lamprey used by the biologists to study its CPGs

2.8.4.1 CPGs and Biology

One of biology's investigation tasks is the physiology where, among other things, the mechanisms of living beings that carry out the basic functions, are studied, as for example walking. The existence of pattern generators was documented for the first time by Wilson[156] in his study on locust flight. In the experiment carried out by Shik et al. on de-cerebrated cats[133] in 1966, it was observed that a vertebrate's locomotion mechanism is situated in the spinal column, and was also based on pattern generators. The brain stimuli are not in charge of this movement, rather its "modulation". In 1980 Delcomyn[27] coined the term CPG to refer to this group of neurones that oscillate rhythmically.

Within this group of vertebrates, **the lamprey** (see figure 2.23) is the one that is most used to study CPGs, because its spinal column is transparent, contains few cells and lasts at least a week outside of the animal (in a saline solution) without deterioration. This allows the biologists to carry out experiments more easily[119].

Cohen proposed a **mathematical model for the lamprey's CPG**[20] and later Williams et al. carried out various experiments on the different phases observed[154], patterns generation[155] and the effects on the co-ordination[135].

2.8.4.2 CPGs and Robotics

The fusion of different fields of investigation always illuminates and permits addressing the problems from another perspective. This has occurred with robotics and biology. One of the pioneers in applying CPG models to robotics has been Ijspeert, of EPFL's Bio-inspired Robotics Laboratory. In his doctoral thesis[59] he proposed neuronal models for the implementation of CPGs for lamprey and salamander locomotion, thereby placing the foundations for its posterior implementation in a real robot. By means of evolutive algorithms parameters are obtained for an optimal locomotion. In later work he continued carrying out simulations of his models[63] and in 2004, together with Crespi, implemented the first prototype of **amphibot**[23] (see section 2.3.4), demonstrating the viability of his bio-inspired model for robot locomotion.

In later work the model was improved and the transition from one of the salamander's gaits to the other has been investigated. This animal's characteristics is that it can swim and also move on land. Both gaits have been modelled, simulated and implemented in amphibot[61]. In [60] the problem of how to make a smooth transition has been studied.

The CPGs model has not only demonstrated its value in specific robot designs, such as amphibot, but is also being successfully employed in the movement of generic modules. The EPFL is leader in these matters. Bourkin carried out simulations of locomotion of a modular robot with different morphologies such as: wheel, worm, quadruped. All of them used CPGs[5]. Further improvements in the simulations were made by Marbach et al.[91][92], and the validations in the robot Yamour were carried out by Sproewitz et al. [139][140] and [95].

The CPGs model has also been successfully applied in the modular robot M-tran. Kamimura et al. used Matsuoka's CPGs model[94] to implement the locomotion of a worm and a quadruped[68].

The CPGs bio-inspired model is not only being used in modular robots, but also in locomotion for quadruped robots [35][136], in the eight footed robot Scorpion[139], and even in humanoid robots [30].

In the neuro-computation group of the Autonomous University of Madrid's Politechnic School Herrero et al. have modelled and implemented CPGs based on Rulkov's model[121] to control an eight segment worm robot [50]. The experiments were carried out with the Cube Revolution robot, developed in this thesis.

2.8.5 Approach IV: sinusoidal generators

The problem of co-ordination has been resolved by nature. Therefore it is "only" necessary to imitate it to obtain robot locomotion. Nevertheless in the biological mechanisms there is certain complexity as well as a lot of redundancy. Perhaps the answers appear to be very specialised or too "rich" supplying too much information could be unnecessary for robot locomotion.

In the field of neuro-computing all the neurons and CPGs are modelled in detail, the mathematics equations are obtained and then simulated later. Moreover, it is possible to try these models in real robots, with the aim of confirming if they are correct, comparing the locomotion of the artificial animal robots with the real ones. The aim of these experiments, therefore, is to confirm the value of the models. The robot is only a medium towards this end. Nevertheless, from the robotics perspective what happens is the opposite. The aim is to have a robot that can move in the best way possible, with the least consumption of power and resources. The neuro-computing models are used as inspiration and the necessary simplifications are applied.

Due to this, another way of addressing the problem of the co-ordination is **to employ solutions based on the simplest of CPGs models possible**, in such a way that their implementation is simple

and needs the least resources. One possible simplification is **to substitute the CPGs by sinusoidal generators** that directly control the position of the robot's articulations, This simplification is workable for the study of robotics locomotion in a permanent regime, in that when the CPGs have reached the stationary regime, they behave like fixed frequency oscillators. What is more, observation of animal locomotion shows that the frequencies of the rhythmic movements are the same and there is no evidence that the different spinal oscillators use different frequencies[59][92].

One of the aims of this thesis is to explore the locomotion of apodal robots of the pith-pitch and pitch-yaw groups, using sinusoidal generators. This idea has been recently used for the movement of one dimensional topology robots to obtain smooth, natural, life like movements, as for example in the latest apodal robots of the CMU [86][158]. Chen et al. are using them to obtain movements that adapt to the surroundings [12]. Also the viability in two dimensional topology robots is being studied. Such is the case of the quadruped **PuchBot II**[115] in which Prieto-Moreno et al. have employed sinusoidal generators for movement in a straight line.

2.9 Modular robots applications

Modular robots have some characteristics that make them unique. Outstanding among them are movement flexibility, self repairing, self reproducing, self configuration and formation of solid structures.

Though these very advanced prototypes exist, as yet the possibility of their practical use is being explored. In the following section some of the references already given will be classified according to the three principal applications that are being evaluated.

- **Search and rescue:** [164][96][157][53][65][181].
- **Inspection of tubes and bridges:** [144][146][117][47][111]
- **Space exploration:** [170][137][130][82][84][147]

2.10 Conclusions

In this chapter we have seen the evolution of apodal modular robots and the latest prototypes that have been created in the most important international investigation centres. **The problem of locomotion** has been presented, and in contrast to the classical solutions using rigid structures with wheels, caterpillars or feet, the idea has arisen of using **self-configuring modular robots**, that are capable, at any moment, of changing their shape to be able to move in the most efficient way. Also modular robots have been developed that are orientated to the creation of two or three dimensional structures,

in a similar way to matter being formed by atoms and molecules. This will allow, in future, creation of solid objects that can change their shape.

From the view point of structure, in the last decade interest has grown in **apodal robots**. They have a one dimension topology that gives them a unique locomotive capability, such as the possibility of deforming the body to go through tubes or areas with many nooks and crannies. These robots move by means of body movement, in a way reminiscent of snakes and worms. **Self-propelled apodal robots** have been developed to be used in practical applications, they also have a one dimension topology, but movement is obtained by means of wheels or caterpillar tracks situated on each module and not by means of body movement.

To sum up, **a classification for all the mentioned robots has been established**, using as a yardstick the structures that they can form and the connection between modules. The groups in which this thesis is interested are the **apodal robots of pitch-pitch and pitch-yaw type**. The robot group with connection yaw-yaw, similar to real snakes, has been studied fully by other investigators. These robots need special conditions of friction between the body and the surface they travel on, which means that in the existing prototypes passive wheels or artificial skins have been added. Nevertheless, in the other groups locomotion is obtained solely by means of body motions. Their study will permit that any generic modular robot that adopt a one dimensional topology can move without having to use special modules or artificial skins.

When the inferior level of modular robot locomotion is studied **the problem of co-ordination** arises. This consists in calculating the functions and the parameters that must be applied to each of the articulations so that the robot can move. One way of solving the problem and which has led to very good results is the **bio-inspired approach** based on using the **mathematical model of animal CPGs** as control functions.

From the viewpoint of biology the CPGs are studied to understand their functioning and to know more about living organisms. To do this measurements on different animals are carried out, and mathematical equations are proposed to model these CPGs, simulations are made and are recently being implemented in animal robotics to confirm if they are correct, That is to say, **biological knowledge is used as an instrument to validate the robots**. Investigation concentrates on obtaining data and the modelling of the CPGs.

Nevertheless, from the robotics point of view the contrary happens. The aim is to have a robot that can move in the best way possible, with the least consumption of power and resources. The biological models are used as inspiration and the necessary simplifications are applied. The internal parameters of the CPGs and the biological significance does not have such importance. For this reason the other approach to robotics locomotion is that **the robots employ simplified CPGs models**. In this thesis we propose a model for locomotion of apodal robots based on **sinusoidal generators**.

Although other investigators have constructed prototypes of apodal robots of the groups pitch-pitch and pitch-yaw, up to now their locomotion has not been addressed from a general perspective. The

problems of direct and inverse kinematics have not been solved, neither has their locomotion been related to the number of the robot's modules. The following questions, therefore, are unanswered: *What is the minimum number of modules that a robot has to have to be able to move in one or two dimensions? What is the minimum number of control parameters necessary to obtain locomotion of the apodal robots, whatever the number of their modules? How to calculate the step that an apodal robot takes in function of the parameters employed in the sinusoidal generators? What amplitudes and differences of phase are to be applied to the modules' oscillations so that the robot fulfils the given restrictions?*

This thesis deals with, from a general perspective, the study of the apodal robot's locomotion, equally in one as in two dimensions. The relationship between the oscillators' parameters and the way in which they move the robot is established. A methodology is proposed to resolve the problems of inverse and direct kinematics and all the ideas are summed up in principals of locomotion. The **minimum configurations** are presented, that is the robots with the least number of modules that can move, with the movements they can make and the necessary control parameters' values. Finally experiments in simulation and with real modules have been carried out, that confirm the principles enunciated.

This thesis confirms the viability of using sinusoidal generators to control the permanent regime of the apodal robots locomotion. This allows the implementation of controllers using less resources than with the classical approaches and therefore they can be integrated into low range microprocessors, or directly as part of an FPGA's hardware.

Chapter 3

Models

“Science builds from approximations that gradually move nearer to the truth”

– *Isaac Asimov*

3.1 Introduction

In this chapter the models employed for the study of modular apodal robots are presented. In the first part models for the modules, the types of connection, the groups of robots and their parameters are introduced. In the second the three fundamental models: control, kinematics and mathematical models are described. Finally, the conclusion establishes the relationship between all these models and propose a solution to the problem of co-ordination.

3.2 Models of modules

To study the locomotion of modular robots three models are used: **wired**, **hexahedral** and **real**. The first is the most important and it is developed in the mathematical model. The hexahedral is used in the simulations and the last one for the construction of real robots, with which experiments are carried out.

3.2.1 Wired model

In this model the module is composed of two equal segments united by means of a joint. The segments are named left and right.

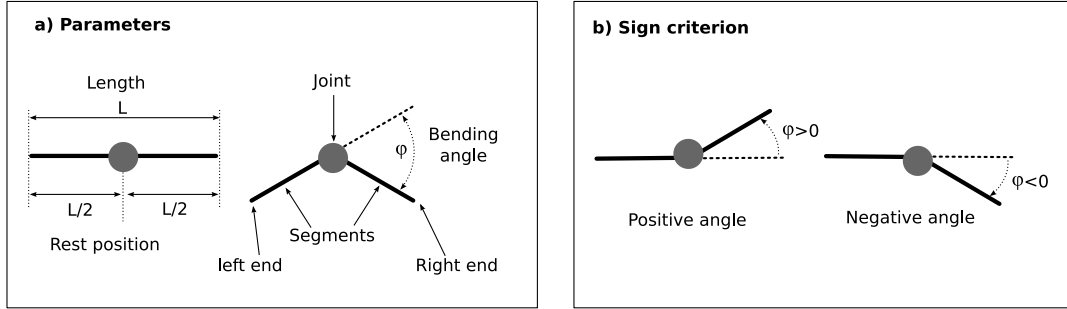


Figure 3.1: Wired model for the module. a) Parameters: Length and bending angle. b) Sign criterion for the bending angle

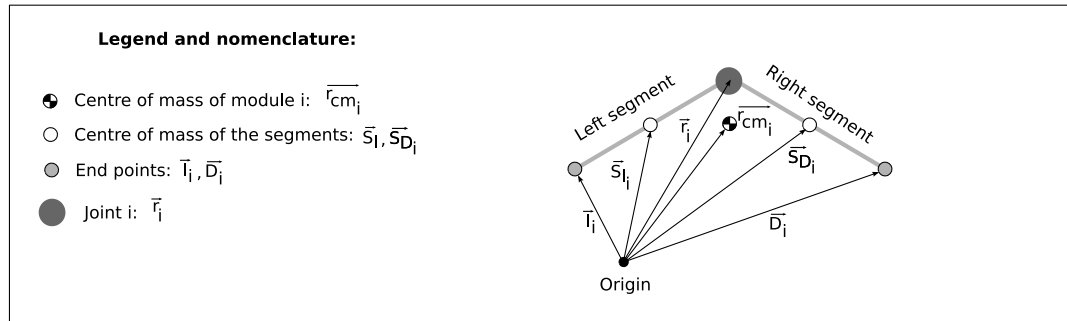


Figure 3.2: Position vectors and centre of mass of the module i

3.2.1.1 Parameters

The parameters of module i are (Fig. 3.1):

- **Bending angle (ϕ_i):** is the angle formed by the two segments. This is determined by the joint. Its value is restricted at interval $[-90, 90]$, which is typical of the commercial servos. The total range of turn is 180 degrees.
- **Length (L):** Total length of module when it is in the rest position. In this state the bending angle is zero degrees. Given that the segments are equal, each one will have a length of $L/2$.
- **Mass (m).** It is assumed that the mass is uniformly distributed between the two segments (and the joint does not have mass). Each segment will have a mass of $m/2$.
- **Position vector (\vec{r}_i):** Position of joint i
- **Position vector of the extremities:** \vec{l}_i, \vec{D}_i .

3.2.1.2 Centre of mass

The position vector of the centre of mass of the module i is denoted by \vec{r}_{cm_i} . It can be expressed in function of the position vectors of the joint \vec{r}_i , the left end \vec{T}_i and right end \vec{D}_i as indicated by the equation 3.1.

$$\vec{r}_{cm_i} = \frac{1}{4} (\vec{T}_i + 2\vec{r}_i + \vec{D}_i) \quad (3.1)$$

It is found by calculating the centres of mass of the left and right segments. From them, and assuming that the segments are equal, the expression of the centre of mass is obtained by means of the equation 3.2. The position vectors of the centre of mass of the segments can be expressed in function of the position vectors of the articulations and of the extremities, as indicated by the equation 3.3. Substituting these expressions in 3.2 the result is 3.1. In the figure 3.2 the module i with the different centres of mass and position vectors is shown.

$$\vec{r}_{cm_i} = \frac{1}{m_i} \left(\frac{m_i}{2} \vec{S}_{l_i} + \frac{m_i}{2} \vec{S}_{D_i} \right) = \frac{\vec{S}_{l_i} + \vec{S}_{D_i}}{2} \quad (3.2)$$

$$\vec{S}_{l_i} = \frac{\vec{T}_i + \vec{r}_i}{2}, \vec{S}_{D_i} = \frac{\vec{r}_i + \vec{D}_i}{2} \quad (3.3)$$

3.2.2 Hexahedral model

In the hexahedral model each module is represented by two hexahedrons joined by an axis (parallel to the y axis). Each hexahedron turns in relationship to the other on this common axis (fig. 3.3). The bending angle φ_i is that which forms the x axis of both bodies. The module's dimensions are $L \times W \times H$, where L is the length (x axis), W the width (y axis) and H the height (axis z). Each hexahedron has a mass of $m/2$ and a length of $L/2$.

In this model it is supposed that no collision exists between the two hexahedrons when they rotate, though they have the same measurements.

The position vector of the centre of mass is calculated using the same equation as in the case of the wired (eq. 3.1), taking into account the joints that are located in the module's centre and that the extremities \vec{T}_i y \vec{D}_i are the central points of the external faces of the left and the right hexahedron respectively.

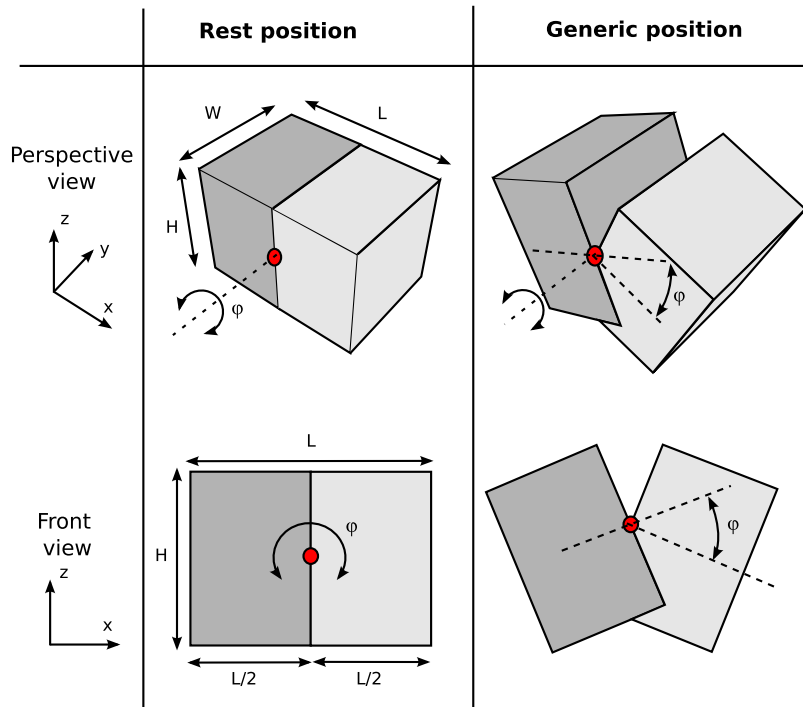


Figure 3.3: Parameters of the hexahedral model

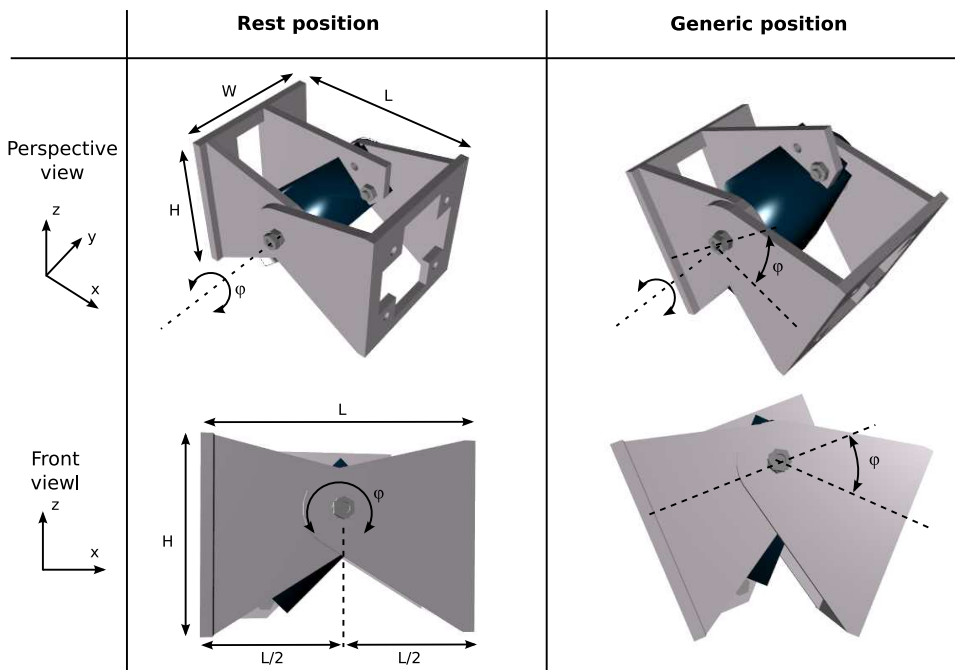


Figure 3.4: Y1 module, designed for building modular robots

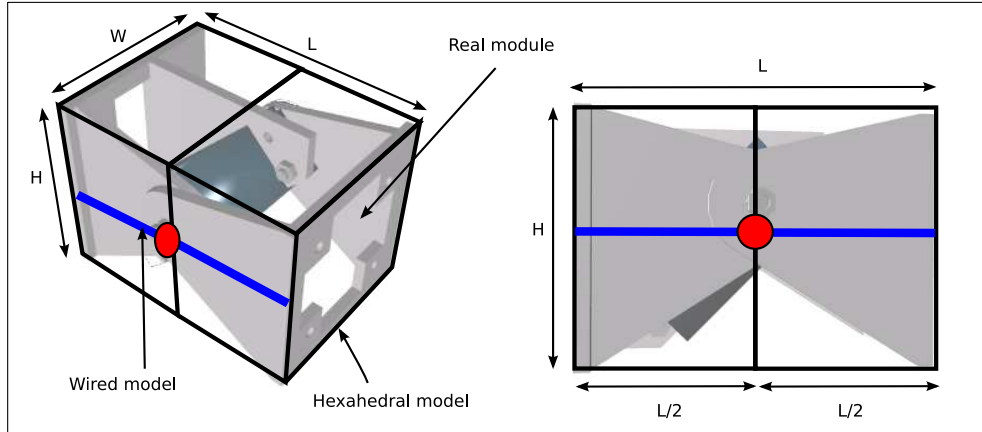


Figure 3.5: Models comparison: wired, hexahedral and real

3.2.3 Real model: Y1 Module

The **Y1 module** has been designed for carrying out experiments (section 7.2.1). Its aspect and parameters are seen in the figure 3.4, and the relationship to the wired and hexahedral models in 3.5. The hexahedral model has the same proportions as the Y1 module, so that it is the minimum hexahedron that contains in its interior the Y1 module. It must be noted that the hexahedral model is an approximation to the real module. Differences between them are: 1) The axis on which the Y1 module turns is not exactly in the centre. 2) When the bending angle is positive the points of contact with the ground are different.

3.3 Models of apodal robots

3.3.1 Parameters

Apodal robots that are studied in this thesis are uni-modular and therefore there is only one type of module. These are formed by means of equal M modules linked in a chain. The parameters defined are:

- **Number of modules (M).** Topologically this number is not bound at the upper limit. One can think of apodal robots of any number of modules. But in practise M will be limited by consumption, wiring, torque, etc. The inferior value to M is 2 (see chapter 6). Therefore , $M \geq 2$.
- **Robot length (l).** The robots being studied are made up of equal sized modules, all of them have the same length L . Therefore, $l = M.L$.

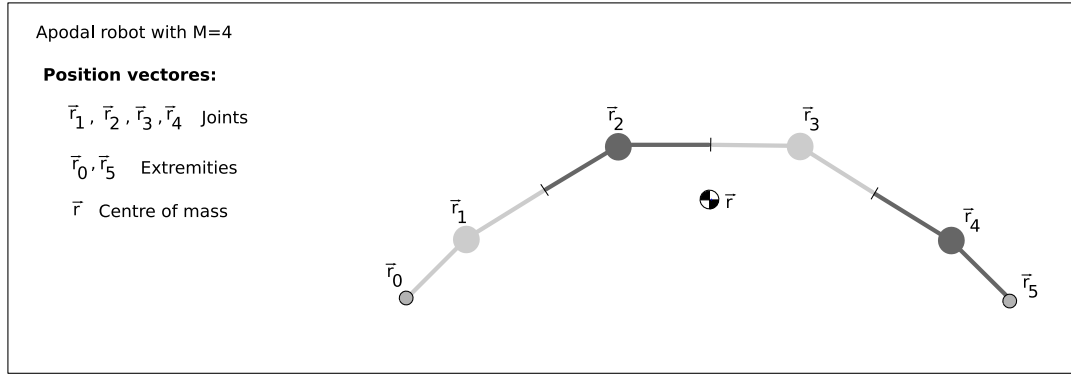


Figure 3.6: Centre of mass of an apodal modular robot made up of 4 modules

- **Total mass of robot (m_t).** As these modules are the same, the total mass of the robot will be $m_t = M.m$, where m is the module mass.
- **Position vector (\vec{r}):** determines the position of the centre of the robot's mass.

With the wired model a total of $M + 2$ points are used to describe apodal robots with M modules: corresponding to each joint plus the two extremities. Its position vectors are denominated by \vec{r}_i , with $i \in \{0 \dots M + 1\}$, where $\vec{r}_1 \dots \vec{r}_M$ are the position vectors of the module's joints and \vec{r}_0, \vec{r}_{M+1} are the left and right extremities, respectively.

3.3.2 Centre of mass

The centre of mass of an apodal robot made up of equal M modules is expressed in function of the position vectors of its points ($\vec{r}_0 \dots \vec{r}_{M+1}$) as indicated in the equation 3.4. This equation is generic for any apodal modular robot of M modules, regardless of the type of connection used. The figure 3.6 shows the centre of mass of an apodal robot of four modules and the different position vectors used for its calculation.

$$\vec{r} = \frac{1}{4M} \left(\vec{r}_0 + 3\vec{r}_1 + 4 \sum_{i=2}^{M-1} \vec{r}_i + 3\vec{r}_M + \vec{r}_{M+1} \right), M \geq 2 \quad (3.4)$$

To calculate this equation the formula for centre of mass of a system of M points, each of which has mass m , has been applied (eq. 3.5).

$$\vec{r} = \frac{1}{M} \sum_{i=1}^{i=M} \vec{r}_{cm_i} \quad (3.5)$$

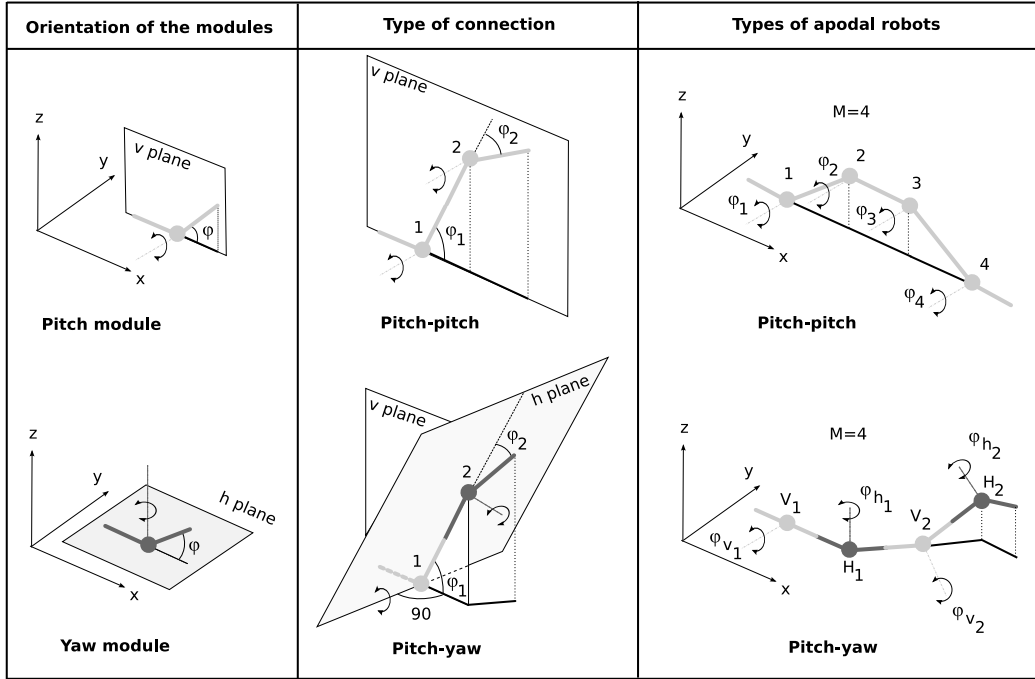


Figure 3.7: Module orientations, type of connections and configurations for the modular robots

Substituting \vec{r}_{cm_i} by its calculated value in 3.1 and rearranging it the result is 3.4. The detailed calculation can be seen in the section A.1.

3.3.3 Types of connection

The study of the robots is limited to the groups with pitch-pitch and pitch-yaw connections. In the figure 3.7 the wired model for these groups can be seen, as well as the two classes of connection between the modules.

3.3.3.1 Pitch-pitch connection

The pitch-pitch group is formed by all those robots in which the modules are connected with the same orientation, in such a way that all of them turn on the same vertical plane. This type of connection is denominated pitch-pitch. Because of mechanical limitations, these robots can only move in one dimension (forward or backward) and they are employed to study the locomotion in one dimension. The joints are numbered from 1 to M . The bending angles are expressed by means of φ_i , with $i \in \{1 \dots M\}$.

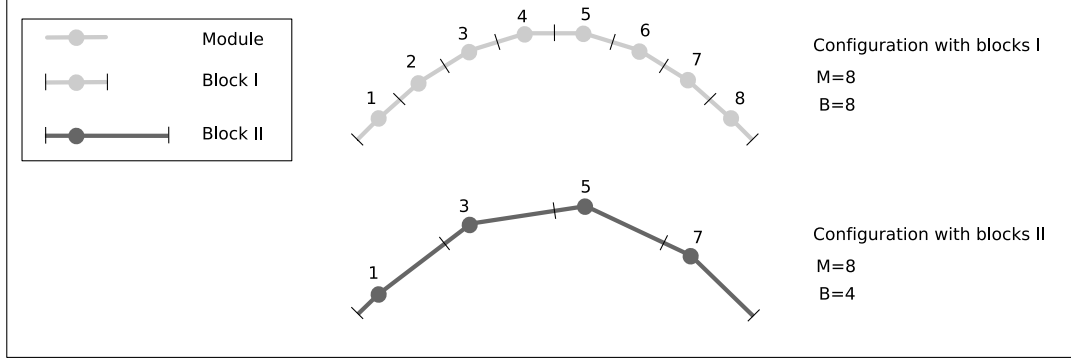


Figure 3.8: Example of the block concept. The same 8 module robot is shown but using two types of blocks. In the upper part it is composed of 8 blocks. In the lower it uses only 4

3.3.3.2 Pitch-yaw connection

This group is formed of robots that alternate the pitch and yaw orientated modules. The first ones are denominated verticals and the second horizontals. The number of vertical modules will be equal to the horizontal ones, which means that M will be an even number. For example, for a robot in this group with $M = 8$ there will be four horizontal modules and four vertical ones, placed alternatively.

The robots in this group can adopt different forms in 3D which means that their joints are not within the same plane, as in the case of the pitch-pitch group. They have the capability of moving on one plane and therefore will be those that are used in the chapter 5 for the study of 2D locomotion.

In this type of connection, two consecutive modules are rotated 90 degrees one in relation to the other, as can be seen in the central part of the figure 3.7. Module 1 will be used as reference, which will be by definition of a vertical type.

Two types of notation will be used to refer to these modules. On one hand, when it is not important to differentiate between the vertical and horizontal modules, the same notation will be used as for the pitch-pitch group, numbering the modules between 1 and M , using φ_i for their bending angles. On the other hand when it is necessary to distinguish between the two types of modules, V_i will be used for the verticals and H_i for the horizontals, taking $i \in \{1 \dots \frac{M}{2}\}$. The bending angles will be φ_{V_i} and φ_{H_i} respectively.

3.3.4 Blocks

3.3.4.1 Concept

The idea of blocks allows generalising the equations that describe the robot's shape (sections 3.6.3.2 and 3.6.4.5) and will be used in the chapters 4 and 5 to analyse locomotion. Blocks are a group

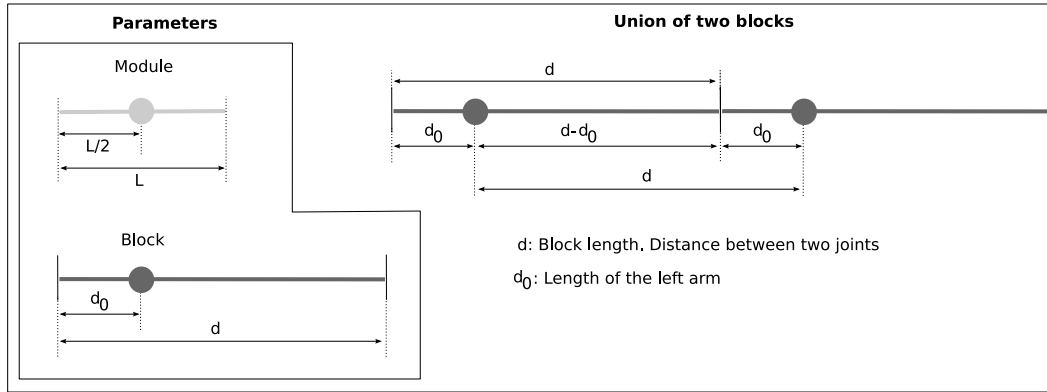


Figure 3.9: Parameters of the block

of connected modules. The construction of the robots is based on the repetition of these blocks. The configurations that will be studied are formed by the same type of blocks (the robots being homogeneous in their structure).

In the figure 3.8 an example of the use of blocks is shown. Given an eight module robot it can be considered as being made up of 8 blocks of one module. Nevertheless, if the even numbered articulations are fixed in their rest position (with a bending angle $\varphi_i = 0$) and only act on the odd numbered ones, the movement can be studied as if it were an equivalent robot composed of 4 equal blocks. The equations will be the same.

3.3.4.2 Parameters

To generalise the equations, instead of employing the module's parameters, those of the block are used, shown in figure 3.9. They are:

- **Length of the block (d).** This equals the parameter L of the module. Also d coincides with the distance between two articulations with the same orientation.
- **Length of left arm (d_0).** The blocks created can be asymmetric, so that the left segment is different to the right one. The parameter d_0 indicates the length of the left segment.

3.3.4.3 Type of blocks

The blocks employed in the study of the apodal robot's locomotion are four, shown in figure 3.10. They are:

- **Module block.** Made up of only one module with pitch orientation. This is the main block used in studying movement in a straight line.

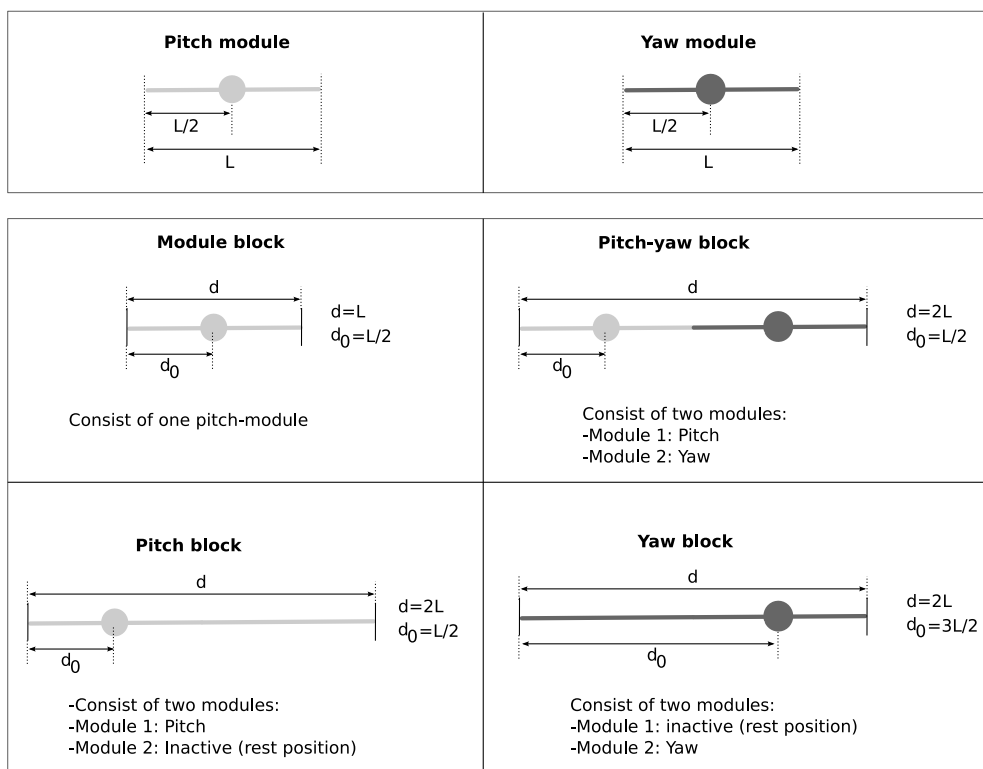


Figure 3.10: Parameters of the four types of blocks

Block type	d_0	\mathbf{d}	d_0/d
Module block	$L/2$	L	$1/2$
Pitch-yaw block	$L/2$	$2L$	$1/4$
Pitch block	$L/2$	$2L$	$1/4$
Yaw block	$3L/2$	$2L$	$3/4$

Table 3.1: Block types and the values of their parameters

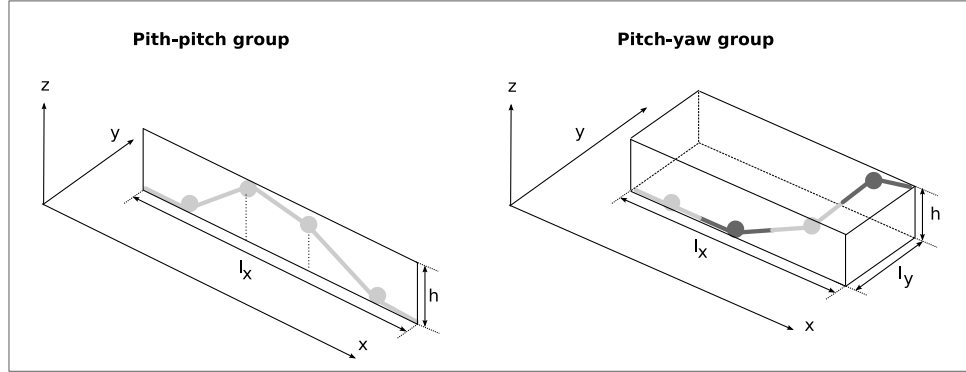


Figure 3.11: Dimensions of the pitch-pitch and pitch-yaw groups

- **Pitch-yaw block.** Formed by two modules, one pitch and one yaw. It is the basic block used to study movement in two dimensions.
- **Pitch block.** It has two modules, the first one is pitch and the second inactive in its rest position ($\varphi = 0$). It is used to study movement in a straight line of the pitch-yaw robots.
- **Yaw block.** Composed of two modules, of which the first one is inactive in the rest position, and the second is of the yaw type. This block allows the pitch-yaw robot's dimensions to be determined when they move in two dimensions and uses a plane wave.

The parameters of each block are expressed in function of the modules as the table 3.1 indicates.

3.3.5 Dimensions

The dimensions of an apodal robot with pitch-yaw connection are defined as the height (h), width (l_x) and (l_y) of the minimum hexahedron that contains the robot. In the case of the pitch-pitch group, the robot is contained in one plane, therefore the dimensions are defined as height (h) and l_x of the minimum rectangle that contains it. These ideas are shown in the figure 3.11.

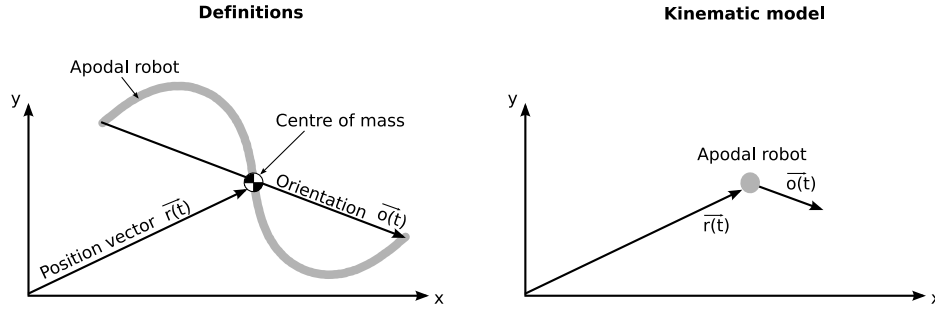


Figure 3.12: Kinematic model of apodal robots

3.4 Kinematic model

The study of the kinematics of apodal robots of the pitch-pitch and pitch-yaw groups is realised representing the robot by means of a point with orientation. Its movement and variations in the orientation are studied in the xy -plane.

3.4.1 Definitions

Given an apodal robot that rests on the plane $z = 0$ and has any shape, it is defined:

- **Position vector** $\vec{r}(t)$: Position of centre of mass. The equation 3.4 expresses the relation between $\vec{r}(t)$ and the position vectors of the joints and the extremities.
- **Orientation** $\vec{o}(t)$: Vector that joins the left extremity (tail) with the right (head). It allows the robot's orientation to be known instantly and with reference to an axis of reference.

In the figure 3.12 the vectors $\vec{r}(t)$ and $\vec{o}(t)$ are shown for a generic apodal robot, situated on the xy -plane. On the right its kinematics model is represented: a point in the position $\vec{r}(t)$ that points toward the direction given by $\vec{o}(t)$.

3.4.2 Restrictions

To make the study of apodal robot locomotion accessible the following restrictions are assumed.

1. **Level surfaces without obstacles.** The locomotion of apodal robots is studied on level surfaces where there are no obstacles. The movement plane will be $z = 0$.

2. **Movement in the steady state.** The study is limited to the stable condition, where the average speed of the robot remains constant and the gait is always the same. The problems of transition from one gait to another or changes in speed will not be addressed.
3. **Periodic movements.** It is assumed that the movements are recurring, with period T . In each cycle, the robot makes some basic, well co-ordinated movements that allows it to travel. The locomotion is obtained by repeating these elementary movements. Therefore it is only necessary to study the movement in one period. Modelling the movement with this limitation is in reality very natural, and very common in robotics. If the movements of animals on homogeneous and uniform surfaces is observed, they are cyclical. Mark Yim, with the robot Polybot[165] introduced the idea of representing these basic movements using some tables that specify in time the position of each module. The movement is obtained running them cyclically. The robots Scorpio[28] and Aramies[136] employ periodical movements that are modulated by reflex actions.

3.4.3 Kinematic parameters

The kinematic parameters that are employed for the study of apodal robots are:

- **Step:** $\vec{\Delta r}$. It is the distance covered by the robot during a cycle (eq. 3.6). At instants t and $t + T$ the robot will have the same shape. The step indicates the distance covered and in which direction.

$$\vec{\Delta r} = \vec{r(t+T)} - \vec{r(t)} \quad (3.6)$$

- **Angular step:** $\Delta\gamma$. This is the rotating angle around the z axis after a cycle. It is defined as the angle between the robot's orientation in t and $t + T$ (eq. 3.7)

$$\Delta\gamma = \widehat{o(t+T)o(t)} \quad (3.7)$$

In the figure 3.13 the geometric significance of the two parameters $\vec{\Delta r}$ and $\Delta\gamma$ are shown, when the robot has moved through a period T .

The average lineal speed of an apodal robot is calculated by means of the equation 3.8.

$$\vec{v} = \frac{\vec{\Delta r}}{T} = \vec{\Delta r} \cdot f \quad (3.8)$$

This speed is directly proportional to the product of the **step** taken and the **frequency**. Therefore the speed will increase either because of greater steps or because of shorter cycles.

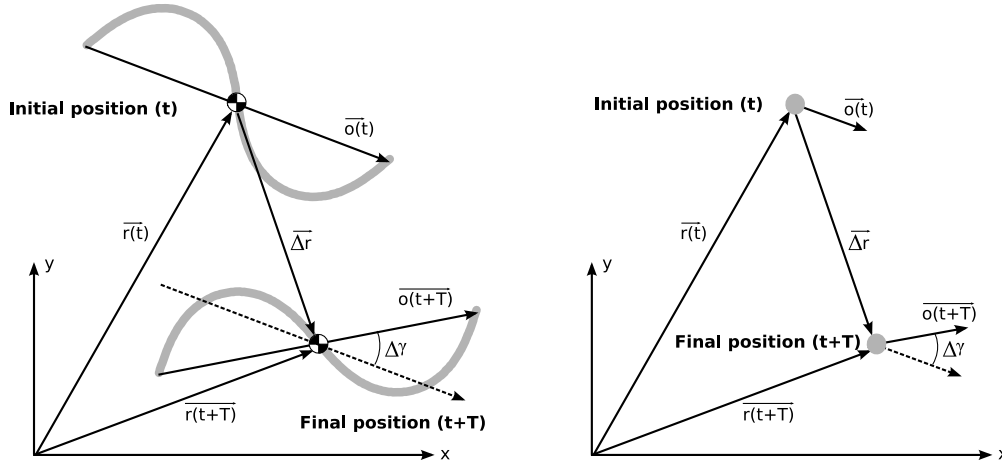


Figure 3.13: Kinematics parameters of interest

The **frequency** depends on the speed at which the joints move. A robot can take the same steps at a low frequency, as if it is moving in slow motion, or at a high frequency (the articulations move faster). In both cases the step $\vec{\Delta r}$ can remain constant. The maximum frequency is limited by the speed of the motors. Therefore it is a technological parameter.

Nevertheless, **the step** depends exclusively on the co-ordination between the articulations, with independence in relation to the speed at which they move. If the co-ordination is inadequate, the step will be very small, null or chaotic. On the other hand, in the well co-ordinated movements, this value will be constant and not null. What is more, the step can vary, from its maximum value (strides) to the smallest values (shuffles). Owing to the fact that a step is a parameter that does not depend on technology, but on the co-ordination between articulations, it is chosen to study locomotion.

3.4.4 Specification of movements

To specify the movement of an apodal robot **the kinematic parameters** step and angular step as defined in the earlier section are used. These will determine how the centre of mass moves. Nevertheless, it will also be necessary to establish **restrictions on the robot's dimensions**. For example, so that the robot is capable of moving in the interior of a tube, as well as specifying its gait, it must be ensured that its height will never exceed the tube's diameter.

3.5 Control model

The model employed for locomotion of the apodal robots is bio-inspired and is based on sinusoidal generators that position the joints in an independent way. The placing of the generators imitate a

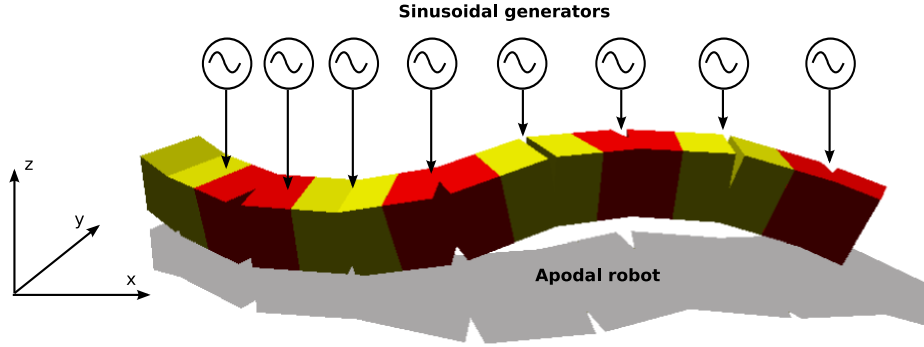


Figure 3.14: Bio-inspired control model based on sinusoidal generators that create oscillations on every module.

spine formed by CPGs connected in series. The general scheme is seen in the figure 3.14. Given an apodal robot of M modules, there will be M generators, each one associated to a module.

3.5.1 Sinusoidal generators

3.5.1.1 Equations

The bending angle of each joint in function of time is given by the expression 3.9.

$$\phi_i(t) = A_i \sin\left(\frac{2\pi}{T}t + \Psi_i\right) + O_i \quad i \in \{1 \dots M\} \quad (3.9)$$

Each generator i has the amplitude (A_i), phase (Ψ_i) and offset (O_i) parameters and all have the same period T . As was noted in the section 2.8.5, the oscillation frequency of the different CPGs that deal with the movement of animals are very similar[59]. Therefore, in this model, it is assumed that they oscillate with the same period T .

In the study of the co-ordination, the parameters for each cycle that are of interest are $\vec{\Delta r}$ and $\Delta\gamma$. We want to know how position and orientation of the robot varies in each cycle. The frequency does not affects the co-ordination, but the speed. Therefore the phase (ϕ) is used as variable instead of time and the position of the joints are studied in function of it. The equation 3.9 is re-written as:

$$\phi_i(\phi) = A_i \sin(\phi + \Psi_i) + O_i \quad i \in \{1 \dots M\} \quad (3.10)$$

For simulation and implementation of the movement it must be taken into account that the phase varies linearly with the time, according to the expression:

Symbol	Description	Range
φ_i	Bending angle of module i	$[-90, 90]$ Degrees
A_i	Amplitude of generator i	$[0, 90]$ Degrees
ϕ	Phase	$[0, 360]$ or $[-180, 180]$ degrees
T	Period	$T > 0$ seconds
ψ_i	Phase of generator i	$[-180, 180]$ degrees
O_i	Offset of generator i	$[-90, 90]$ degrees
M	Number of modules of the robot	$M \geq 2$

Table 3.2: Parameters for the sinusoidal generators employed

$$\phi(t) = \frac{2\pi}{T}t$$

3.5.1.2 Parameters

In the table 3.2 all the parameters, variables and constants employed are shown. The angle values are expressed in degrees. For the phase ϕ the interval $[0, 360]$ or $[-180, 180]$ is used, as convenient.

The bending angle of each module is situated in the range $\varphi_i \in [O_i - A_i, O_i + A_i]$. As the maximum range of movement of the modules is mechanically limited to 180 degrees, which is the typical value of the commercial servos, the following restriction must be observed:

$$|O_i| + A_i \leq 90 \quad (3.11)$$

3.5.1.3 The geometric meaning of the parameters

When the model of the sinusoidal generators is applied to the module's movement, these begin to oscillate. The total range of turn is given by the amplitude A . When the offset is 0, the oscillation is symmetric in relation to the rest position and the bending angle varies between the positions A and $-A$. When the offset is different to zero, the oscillation is not symmetric. The bending angle will be at a lesser distance to one of the extremities than to the other. In this case, φ will vary between the positions $A + O$ and $O - A$, as is graphically shown in the figure 3.15.

3.5.2 Model for the pitch-pitch group

The model of locomotion for the apodal, pitch-pitch robots is formed by M sinusoidal generators of amplitude A and with a phase difference between two consecutive modules ($\Delta\Phi$) fixed (figure 3.16). The equation that describes the oscillation of the module i is:

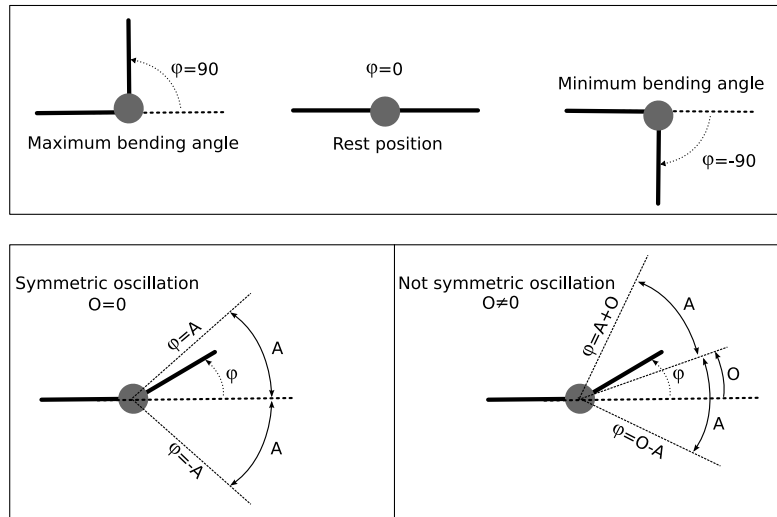
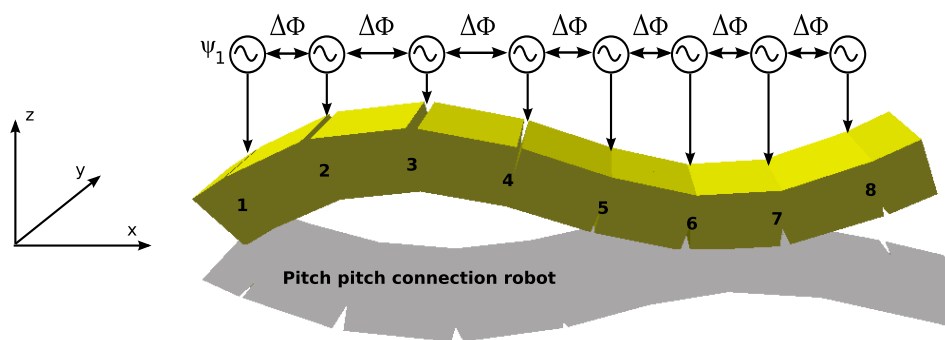
Figure 3.15: Geometric meaning of the parameters φ , A and O 

Figure 3.16: Control model for the pitch-pitch group

$$\varphi_i(\phi) = A \sin(\phi + (i-1)\Delta\phi + \psi_1), \quad i \in \{1 \dots M\} \quad (3.12)$$

The expression has been obtained based on the general equation of the sinusoidal generator (eq.. 3.10) applying the following limitations:

1. **All the generators have null offset** ($O_i = 0$). Therefore the oscillations are symmetric with respect to their rest positions.
2. **All the generators have the same amplitude** A . The angular sweep that they realise is the same for all the modules. This ensures that they all oscillate in the same way.
3. **Origin of phases in module 1**. The phases of the rest of the modules are expressed in function of module 1, to which the value ψ_1 is assigned. ψ_1 established the phase in the beginning. This will be important if it is desired that the robot begins its movements in a particular way. Nevertheless, the study has been restricted to the permanent regime, therefore the value of this initial phase is not important.
4. **Fixed difference phase between consecutive generators**. Taking as reference the biological models of the lamprey, where experiments have shown that the phase differences between consecutive CPGs remain fixed[154]. So, for the modules from 2 to M , the phase will be: $\psi_i = \psi_{i-1} + \Delta\Phi$. As the lag is the same for all, the previous equation can be written as $\psi_i = (i-1)\Delta\phi$ with $i \in \{1 \dots M\}$.

The limitation 4 guarantees the emergence of global waves that pass through the body of the robot making it move. The restrictions 1 and 2 homogenise all the generators, in such a way that no privileged generators exist, rather that all are equal. One consequence of this is that the robots present rotation symmetry. If they rotate 180 degrees in relation to their body axis (they place themselves face down) they will continue to move in the same way. The upper and inferior parts behave in the same way.

After applying all the limitations **this model needs only two parameters** ($A, \Delta\Phi$) to specify the generators and therefore the co-ordination, independent of the number of modules the robot has. For this reason, **the solution to the problem of the co-ordination are points in a two dimensional space**. This space is denominated **Homogeneous control space** and is indicated by H_1 .

The table 3.3 summarises the parameters of control of the pitch-pitch group.

3.5.3 Model for the pitch-yaw group

To control the locomotion of the robots belonging to the pitch-yaw group, the M generators are divided into two independent groups, one which acts on the pitch modules (verticals) and the other

Parameter	Description	Range
A	Amplitude of generators	$[0, 90]$ degrees
$\Delta\phi$	Phase difference between consecutive generators	$[-180, 180]$ degrees

Table 3.3: Control parameters for the pitch-pitch modular robots

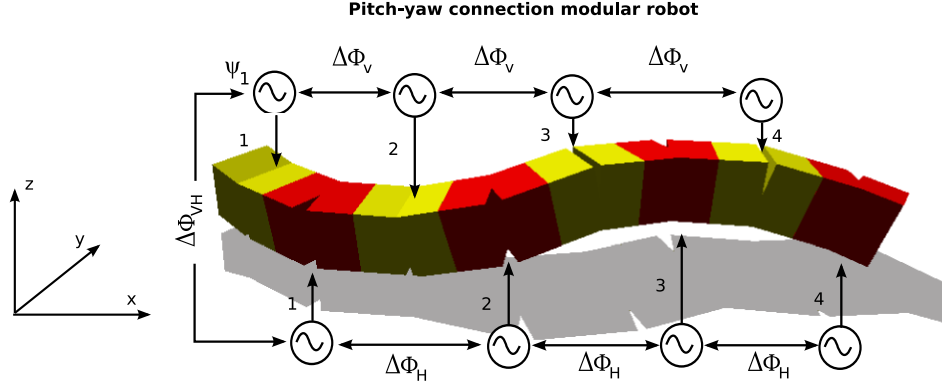


Figure 3.17: Control model for the pitch-yaw modular robot group

on the yaw modules (horizontal) (Figure 3.17). The oscillation equations for both groups, verticals (ϕ_{v_i}) and horizontal (ϕ_{h_i}) are:

$$\phi_{v_i}(\Phi) = A_v \sin(\Phi + (i-1)\Delta\phi_v), \quad i \in \left\{1 \dots \frac{M}{2}\right\}$$

$$\phi_{h_i}(\Phi) = A_h \sin(\Phi + (i-1)\Delta\phi_h + \Delta\phi_{vh}), \quad i \in \left\{1 \dots \frac{M}{2}\right\}$$

Both expressions have been obtained starting from the general equation of the sinusoidal generator (3.10) applying the following limitations:

1. **Division of the generators into two groups: horizontal and vertical.** They are independent groups, but within each one of them all the oscillators are equal, with the same parameters.
2. **Vertical homogeneous modules.** The same limitations as for the pitch-pitch group:
 - (a) The offset is void ($O_{v_i} = 0$) (symmetric oscillation)
 - (b) The amplitude is the same for all: A_v
 - (c) The phase difference between two consecutive vertical modules is the same ($\Delta\phi_v$), therefore $\psi_{v_i} = (i-1)\Delta\phi_v$
3. **Horizontal modules**

Notation	Description	Range (degrees)
A_v	Amplitude of the vertical generators	$[0, 90]$
A_h	Amplitude of the horizontal generators	$[0, 90]$
$\Delta\phi_v$	Phase difference between consecutive vertical generators	$[-180, 180]$
$\Delta\phi_h$	Phase difference between consecutive horizontal generators	$[-180, 180]$
$\Delta\phi_{vh}$	Phase difference between the vertical and horizontal generators	$[-180, 180]$

Table 3.4: Control parameters of the pitch-yaw modular robots

- (a) The offset is the same for all of them: (O_h). Values different to zero are necessary to carry out the circular turns. The rest of the movements is made with symmetric oscillation.
 - (b) The amplitude is the same for all of them: A_h
 - (c) The phase difference between two consecutive horizontal modules is the same ($\Delta\phi_h$), therefore $\psi_{h_i} = (i - 1)\Delta\phi_h + \psi_{h_1}$, where ψ_{h_1} is the phase of the horizontal module 1.
4. **Origin of phases in vertical module 1.** This will be the module taken as reference with a phase ψ_{v_1} .
5. **Fixed phase difference between vertical and horizontal modules ($\Delta\phi_{vh}$).** The co-ordination between verticals and horizontals is established by means of a fixed phase difference. As the vertical module 1 has been taken as reference, the value of the phase for the horizontal module 1 will be: $\psi_{h_1} = \Delta\phi_{vh} + \psi_{v_1}$.

The limitations are similar to those for the pitch-pitch group but applied to both the vertical and horizontal modules, each one with its own parameters. One difference is that the horizontal group does have a parameter O_h . Values of offset different to zero for the horizontal modules will allow the robot to move in circular paths. Nevertheless, if it dispenses with this movement, it can be assumed that $O_h = 0$ and eliminate this parameter from the control space.

The locomotion of the pitch-yaw group of robots in a plane is obtained by means of overlapping of the oscillations of the groups of horizontal and vertical modules. Both oscillations are linked by the parameter $\Delta\phi_{vh}$.

The vertical group is characterised by the parameters A_v and $\Delta\phi_v$, and the horizontal one by A_h , O_h , $\Delta\phi_h$ and $\Delta\phi_{vh}$. Six parameters in total. Therefore, **the solution to the problem of co-ordination for the pitch-yaw configurations are points in a six dimension space**. This space is known as **Homogeneous Control Space 2** and is denoted as H_2 .

The table 3.4 summarises the control parameters of the pitch-yaw group.

3.5.4 Control spaces

Using the sinusoidal generators, the problem of co-ordination of the pitch-pitch and pitch-yaw groups of robots is reduced to the search for solutions in the spaces H_1 and H_2 respectively. H_1 has two

dimensions and H_2 six. The kinematic and stability properties of the different movements can be studied by means of the relationships between the points of these spaces.

The control space of the sinusoidal generators, when limitations are not applied, is greater. According to what is expressed in the equation 3.9, for a robot of M modules, with Independence in its connectivity, M sinusoidal generators are used, each one of which has 3 independent parameters: A_i , O_i , ψ_i , which gives a total of $3M$ parameters. Therefore the general control space, G , has a dimension of $3M$.

All the solutions are found in this space. Greater the number of modules M , the greater will be the dimensions of G . This agrees with the intuitive idea that the more modules there are, the greater number of configurations of robots could be constructed and greater the variety of gaits that will appear.

Nevertheless, this thesis concentrates on the study of the **principle of locomotion that is common to all the one dimension topologies** with pitch-pitch and pitch-yaw connectivity, independent of the number of modules. That is to say, **the aim is to find the smallest sized sub-spaces of G that permit the locomotion of these robots in one or two dimensions**. They are the spaces H_1 and H_2 and their elements will be called **working points**.

3.5.5 Discussion about sinusoidal generators

The sinusoidal generator's model is bio-inspired and is obtained by approximation of the CPGs, when they reach the permanent regime.

Nevertheless, it is interesting to see the relation that these generators have with the problem of co-ordination, in which the generic functions $\varphi_i(t)$ to achieve robot movement using different gaits, want to be found.

If we start with the supposition that the functions $\varphi_i(t)$ are periodic (and as it is noted in the section 2.8.5 this fits in with the observations and experiments carried out by biologists), the breakdown will be in the Fourier series:

$$\varphi_i(t) = \frac{a_0}{2} + \sum_{n=1}^{\infty} (a_n \cos(\frac{2\pi n}{T}t) + b_n \sin(\frac{2\pi n}{T}t))$$

Approximating them by the first harmonic ($n=1$):

$$\varphi_i(t) \approx \frac{a_0}{2} + a_1 \cos(\frac{2\pi}{T}t) + b_1 \sin(\frac{2\pi}{T}t)$$

and carrying out the change of the variable $a_1 = A_i \sin \psi_i$, $b_1 = A_i \cos \psi_i$ and $O_i = \frac{a_0}{2}$, we arrive at:

$$\varphi_i(t) = O_i + A_i \sin \psi_i \cos\left(\frac{2\pi}{T}t\right) + A_i \cos \psi_i \sin\left(\frac{2\pi}{T}t\right)$$

and applying the definition of sine of the sum of two angles:

$$\varphi_i(t) = A_i \sin\left(\frac{2\pi}{T}t + \psi_i\right) + O_i$$

which is the general expression of the sinusoidal oscillators (eq. 3.9).

Therefore, when **the sinusoidal generators for fixed frequency are applied**, in reality what is being done is **to restrict the problem of co-ordination to those functions that have just one harmonic**.

3.5.6 Direct and inverse kinematics

The enunciation of the direct and inverse kinematics for the apodal robots belonging to the pitch-pitch and pitch-yaw groups are stated from the spaces H_1 and H_2 in the following way:

Direct kinematics Given a point p belonging to H_i ($i \in \{1, 2\}$), determine if locomotion exists, the type of movement, the value of its kinematic parameters $(\vec{\Delta r}, \Delta\gamma)$ and the size of the robot.

Inverse kinematics Starting from the kinematic parameters $\vec{\Delta r}$ and $\Delta\gamma$, the gait required and optionally restrictions of the dimensions, find the group of working points $\{p_i \in H_i\}$ that makes the robot move in this way (and with these dimensions).

To resolve these problems the relationship between the generator parameters and the kinematic parameters must be established. Firstly the mathematical model is developed to establish the relationship between the working points and the shape of the robot. In chapters 4 and 5 the relationship between these forms and locomotion are established.

3.6 Mathematical model

The mathematical model allows us to create parameters for the robot shape. As they are robots with a one dimension topology we can approximate them by curves. The curves used for the modelling of the pitch-pitch and pitch-yaw groups will be presented: serpenoid and 3D serpenoid curves. For each one of them we will study the continuous model first, supposing that the bending angle varies continuously for the length of the curve. Then they will be sampled to obtain the discrete model.

The equations obtained allow us to know the dimensions of the robot and what is the relationship to the control parameters of the sinusoidal generators.

	Pitch-pitch group	Pitch-yaw group
Type of curve/wave	Serpenoid	3D Serpenoid
Continuous bending angle	$\theta(s)/\theta(s, \phi)$	$\theta_v(s)/\theta_v(s, \phi)$ $\theta_h(s)/\theta_h(s, \phi)$
Discrete bending angle	$\varphi_i/\varphi_i(\phi)$	$\varphi_{v_i}/\varphi_{v_i}(\phi)$ $\varphi_{h_i}/\varphi_{h_i}(\phi)$
Parameters	α, k	$\alpha_v, \alpha_h, k_v, k_h, \Delta\phi_{vh}$

Table 3.5: Summary of the curves/waves and their parameters used for the mathematical modelling of the pitch-pitch and pitch-yaw modular robots

3.6.1 Introduction: Curves and waves

Apodal robots have a 1D topology, therefore their shape, at any moment, takes the form of a continuous curve. The robot's locomotion is produced by means of body movement. A corporal wave is defined as a continuous curve that varies its shape with the phase ϕ . So when we talk of a curve we refer to the shape for a fixed phase, while by wave we indicate its variation with ϕ .

To define the curves we will use the continuous variable s which represents the distance along the body's axis. A value of $s = 0$ is the point situated on the extreme left and $s = l$ is the extreme right, where l is the total robot length. Besides s , the waves will depend on ϕ .

We will define the curves by means of the bending angle. For the group of robots with pitch-pitch type of connection, the curve is contained on a plane and we will represent the bending angle (continuous) as a function of s . We will use the notation $\theta(s)$ to indicate that it is a bending angle of a continuous curve, facing φ_i when it is discrete. In the pitch-yaw group, the curve is in a three dimensional space and we will use two bending angles to describe it, indicated by $\theta_v(s)$ for the pitch and $\theta_h(s)$ for the yaw.

The wired model of the robot will be obtained sampling the curve at the points in which the joints are situated. To obtain equations that are more generic, the idea of block presented in the section 3.3.4 will be used, and the equations will be obtained in function of the parameters d and d_0 . The bending angle of the articulation i will be denoted by φ_i , that will be situated in the position $s = d_0 + (i - 1)d$. For the pitch-yaw group of robots φ_{v_i} and φ_{h_i} will be used. We will realise the sampling process as indicated in the expression 3.13.

$$\varphi_i = \theta(s)|_{s=d_0+(i-1)d} \quad (3.13)$$

The curves/waves employed for the pitch-pitch group are the serpenoids, and for the pitch-yaw group the 3D serpenoids. The information is summarised in the table 3.5. In the following sections these curves and their parameters will be studied.

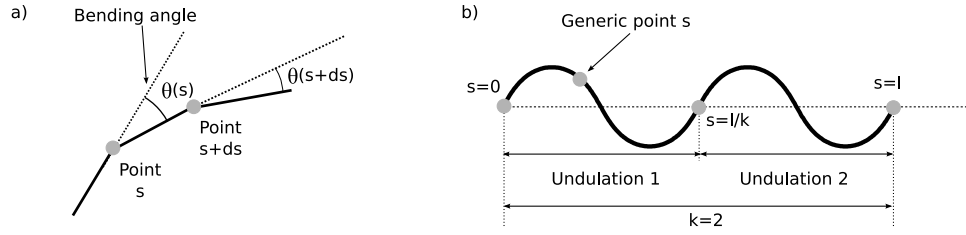


Figure 3.18: a) Bending angle of a continuous curve b) A Serpenoid curve

3.6.2 Serpenoid curve/wave

3.6.2.1 definitions

The **serpenoid curve** was discovered by Hirose[150] when he was studying the snake robots (yaw-yaw group). By definition it is a curve in which the bending angle varies sinusoidally for the length of the body axis (eq. 3.14)

$$\theta(s) = A \sin\left(\frac{2\pi k}{l}s\right) \quad (3.14)$$

The **bending angle** $\theta(s)$ is defined as that which forms the tangents to the curve that pass through two points separated by a distance ds (Figure 3.18a). The form of the serpenoid curve is shown in the figure 3.18b. It is a periodic curve formed by k undulations. The spatial period is l/k , where l is the total length. The section of the curve between $s = 0$ and $s = l/k$ is denominated **undulation**.

The **serpenoid wave** is defined as the serpenoid curve in which the bending angle depends also on the phase ϕ (eq. 3.15)

$$\theta(s, \phi) = A \sin\left(\phi + \frac{2\pi k}{l}s\right) \quad (3.15)$$

3.6.2.2 Formulation in Cartesian co-ordinates

The angle that the tangent to the curve for the point s makes with the x axis is denoted by α_s . Hirose[51] showed that the expression of α_s is given by the equation 3.16

$$\alpha_s = \alpha \cos\left(\frac{2\pi k}{l}s\right) \quad (3.16)$$

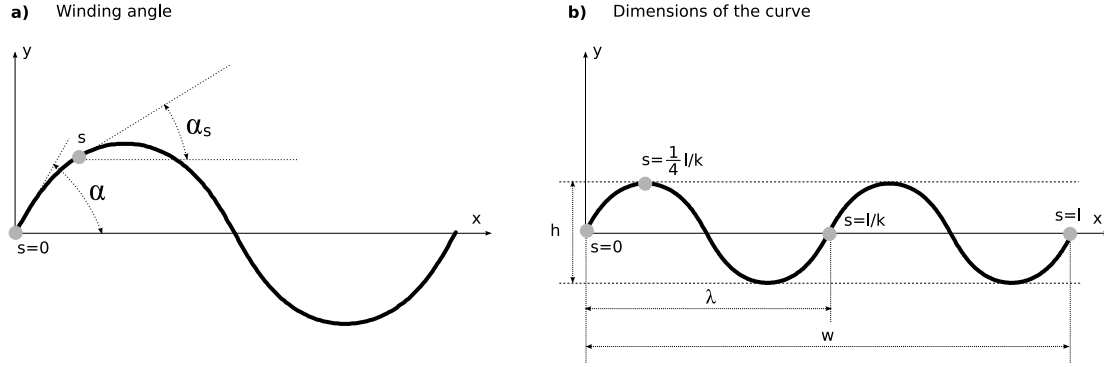


Figure 3.19: Continuous serpenoid curve: a) Definition of the winding angle α b) Dimensions.

where the parameter α is denominated the winding angle and is defined as the angle that forms the tangent that passes through the point of the curve $s = 0$. In the figure 3.19a) the definitions of α and α_s are shown.

The Cartesian co-ordinates x, y of the points of the curve are calculated by means of the integration of the cosines and sines respectively of α_s (eq. 3.17 and 3.18).

$$x(s) = \int_0^s \cos(\alpha_s) ds = \int_0^s \cos\left(\alpha \cos\left(\frac{2\pi k}{l}s\right)\right) ds \quad (3.17)$$

$$y(s) = \int_0^s \sin(\alpha_s) ds = \int_0^s \sin\left(\alpha \cos\left(\frac{2\pi k}{l}s\right)\right) ds \quad (3.18)$$

And for the serpenoid wave the co-ordinates are given by the equations 3.19 and 3.20.

$$x(s, \phi) = \int_0^s \cos\left(\alpha \cos\left(\phi + \frac{2\pi k}{l}s\right)\right) ds \quad (3.19)$$

$$y(s, \phi) = \int_0^s \sin\left(\alpha \cos\left(\phi + \frac{2\pi k}{l}s\right)\right) ds \quad (3.20)$$

These integrals have no analytical solution. They are resolved numerically.

3.6.2.3 Dimensions

The dimensions of the serpenoid curve are defined as height (h) and width (w) of the minimum rectangle that contains the curve. They are shown graphically in the figure 3.19b.

Given that the serpenoid curve is composed of k undulations, the dimensions are calculated considering only the first undulation. The width of an undulation is its wave length λ , and the total width is expressed as:

$$w = k\lambda \quad (3.21)$$

The highest point of the first undulation of the serpenoid is that in which the tangent is parallel to the x axis and its ordinate is positive. It will be the point s_h that fulfils this condition:

$$\alpha_s(s_h) = 0 \wedge y(s_h) > 0$$

is that which is found in $s_h = \frac{1}{4} \frac{l}{k}$. The height is calculated as the double of its ordinate, as the first undulation is an odd function in relation to its middle point, in such a way that the height of the crest is equal in absolute value to the trough (eq. 3.22)

$$h = 2y(s_h) = \int_0^{\frac{1}{4} \frac{l}{k}} \sin \left(\alpha \cos \left(\frac{2\pi k}{l} s \right) \right) ds \quad (3.22)$$

The wavelength λ is the abscissa of the point s_w situated at a distance equal to the spatial period, that is to say, $s_w = \frac{l}{k}$. Therefore, having in mind the equations 3.21 and 3.17 the total width is calculated:

$$w = kx(s_w) = k \int_0^{\frac{l}{k}} \cos \left(\alpha \cos \left(\frac{2\pi k}{l} s \right) \right) ds \quad (3.23)$$

The dimensions of the serpenoid wave are the same as those of the curve, because varying the phase ϕ what is obtained is a curve displaced to the right or the left. On being displaced neither the height or the width vary.

Restrictions for the calculation of dimensions The equations 3.22 and 3.23 for the calculation of the height and width are always valid while $k \geq 1$ and $\alpha \leq 90$.

The restriction $k \geq 1$ implies that the serpenoid has at least one complete undulation, and therefore at least a crest and a trough exist.

To simplify, for values of α greater than 90 degrees the width is calculated using the equation 3.23, though in reality it is an approximation. In these cases the initial and final extremes are not those that have the maximum and minimum values of abscissa.

3.6.2.4 Normalised dimensions

The **normalised serpenoid curve** is defined as that which has unit length ($l = 1$) and only one undulation ($k = 1$). Because of this, the curve is only characterised by the parameter α . The **normalised dimensions** of this curve are defined as height and width. Beginning with the equations 3.22 and 3.23 the following is obtained:

$$h_n(\alpha) = \int_0^{\frac{1}{4}} \sin(\alpha \cos(2\pi s)) ds \quad (3.24)$$

$$w_n(\alpha) = \int_0^1 \cos(\alpha \cos(2\pi s)) ds \quad (3.25)$$

The dimensions of the general serpenoid curve in function of the parameters α and k are calculated from the normalised dimensions:

$$h(k, \alpha) = \frac{l}{k} h_n(\alpha) \quad (3.26)$$

$$w(k, \alpha) = l \cdot w_n(\alpha) \quad (3.27)$$

These expressions are deduced from 3.22 and 3.23 making the change of variable $u = \frac{k}{l}s$.

In this way only the normalised dimensions are studied in function of α and from them the dimensions of any curve with length l and with k undulations can be obtained.

3.6.2.5 Parameters and the h_1 shape space

The serpenoid curve is characterised by the parameters: α , k and l . The apodal robots that are being analysed do not vary their length during movement, therefore l will be constant. The shape of the curve is characterised by α and k . The winding angle α determines the shape of each undulation and k the number of undulations.

The shape of a serpenoid curve, with $k = 1$, for different values of α are shown in the figure 3.20a). For $\alpha = 0$, the curve is converted into a segment of length l on the axis x . When $\alpha = 90$ the curve is tangent to the y axis at the origin. The value of α can continue increasing up to its maximum value of 120 degrees (figure 3.20b) in which two consecutive undulations are tangents at one point. Values

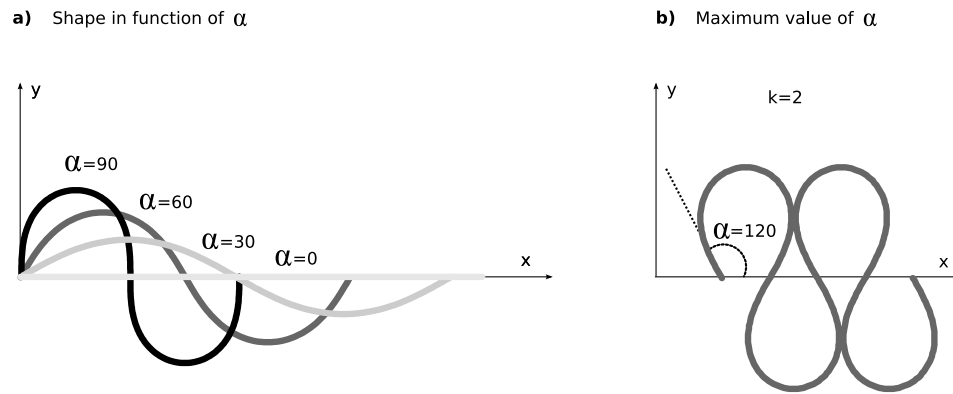


Figure 3.20: Serpenoid curve and winding angle α : a) Variation of the shape with α b) Maximum value of the winding angle α

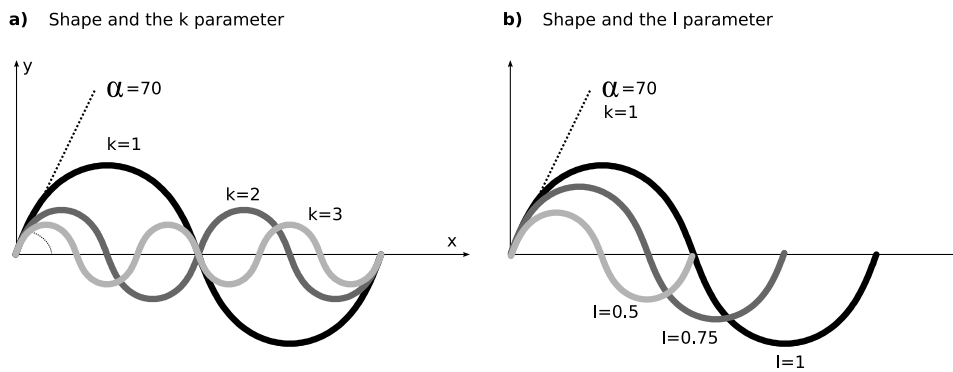


Figure 3.21: Serpenoid curve and the k y l parameters. a) Variation of the shape with con k , when l is constant. b) Variation of the shape with l , when $k = 1$

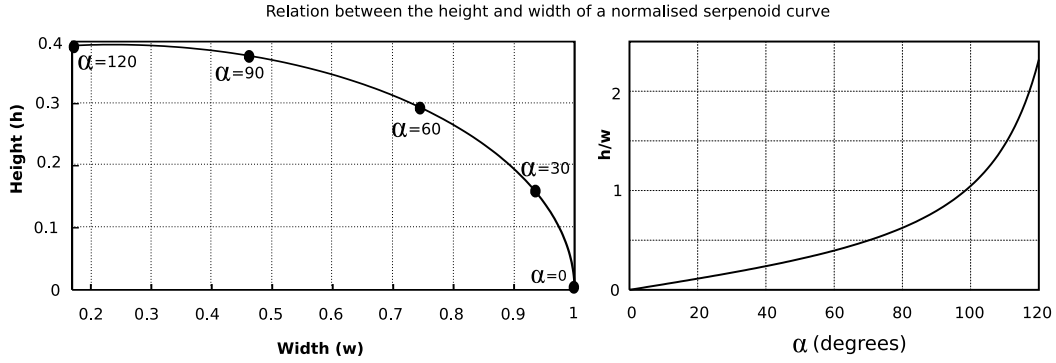


Figure 3.22: Relation between height and width of the serpenoid curve in function of α

greater than 120 degrees are not possible, as the robot's articulations would crash into each other. The range of values of α is, therefore, $[0, 120]$ degrees.

The parameter k determines the number of undulations (repetitions) that there are in a serpenoid curve (3.21a). The height of the curve is inversely proportional to k (eq. 3.26) which means that when the undulations increase it diminishes. In the continuous model k is not bound. If $k \rightarrow \infty$, the height will approach 0 and in the limit will be equal to a segment situated on the x axis. The width of the serpenoid, in the continuous model, does not vary with k (eq. 3.27).

The parameter l only influences in the scaling of the curve, but not in its shape, as is seen in the figure 3.21b). If α and k remain constant the curve will maintain the same proportions.

The shape of the serpenoid curve, therefore, is still characterised by the parameters (α, k) . The space h_1 is defined as that which has as elements the pairs (α, k) . This space will be used to define the robot's shape and we will call it the **shape space**.

3.6.2.6 The relation between height and width

The proportions of the serpenoid curve depend on the winding angle α . In the figure 3.22 the relation between height and width in function of α can be observed for a normalised serpenoid curve. When $\alpha = 0$, the curve is a straight line of unit length on the x axis. Its dimensions will be $h = 0$ and $w = 1$. When the winding angle is increased the width decreases while the height increases.

3.6.2.7 Serpenoid and sine curves

The lesser the winding angle value the greater is the similarity of a serpenoid curve to a sine curve. To compare them the **equivalent sine curve** is defined as being that which has the same dimensions h and w as a serpenoid curve. The formula is as follows:

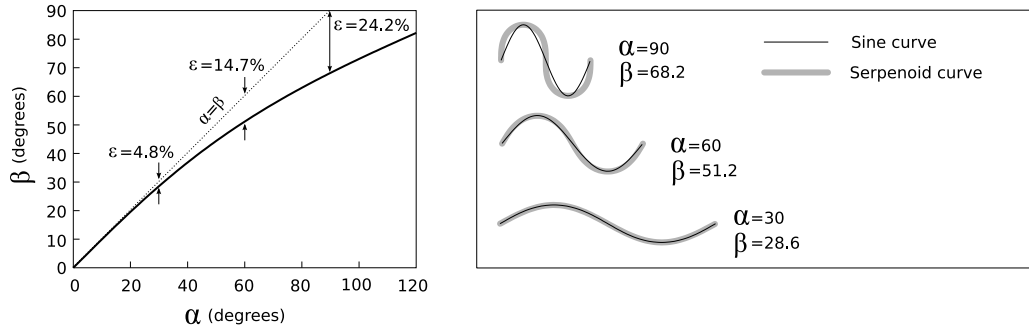


Figure 3.23: Comparison between the serpenoid and sine curves. Both with the same dimensions

Parameter	Description	Range
k	Parameter. Number of undulations	$k \geq 1$
α	Parameter. Winding angle	$\alpha \in [0, 120]$ (degrees)
ϕ	Variable. Phase	$\phi \in (-180, 180]$ (degrees)
l	Constant. Length	$l > 0$

Table 3.6: Parameters, variables and constants for the serpenoid wave

$$y = \frac{h}{2} \sin\left(\frac{2\pi k}{w}x\right), x \in [0, w]$$

Differentiating with respect to x and specifying for $x = 0$, the expression of the tangent at the origin are obtained, with which the gradient of the origin is calculated:

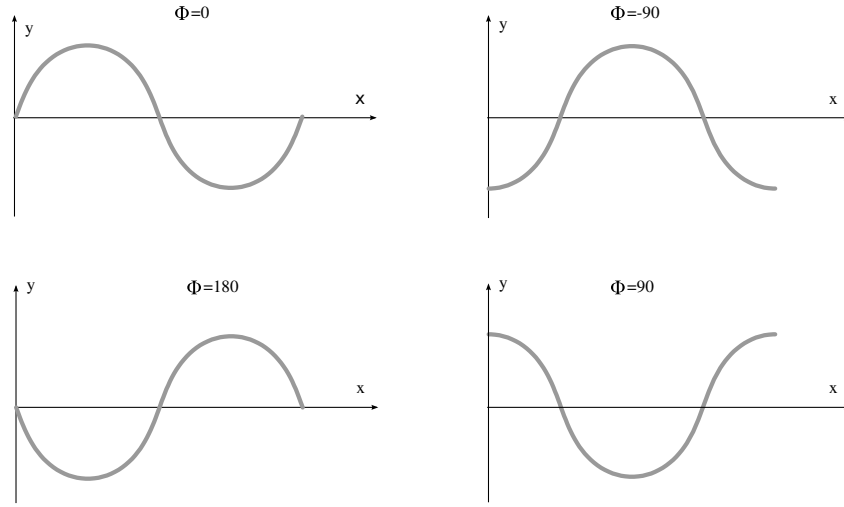
$$\beta = \arctan\left(\frac{h}{w}\pi\right)$$

β is the equivalent to parameter α , but for sine curves. The comparison between α and β is shown in the figure 3.23. For the values of α less than 46 degrees, the relative error is less than 10%.

3.6.2.8 Serpenoid wave

The serpenoid wave is characterised by the same parameters α and k of the serpenoid curve, but besides this the bending angles depend on the phase ϕ . Therefore, fixing α and k , the form of the wave changes with ϕ . In the figure 3.24 the shape in four different phases, is shown.

To sum up, in the table 3.6 the parameters, variables and constants of the serpenoid wave are listed.

Figure 3.24: The shape of the serpenoid wave for four values of the phase ϕ

3.6.3 Discrete serpenoid curve/wave

3.6.3.1 Definitions

The definition of a discrete serpenoid curve is the same as for the continuous case, but considering that the bending angle varies in discrete form with the variable i , instead of in the continuous way with s . The bending angle is expressed as the equation 3.28 indicates :

$$\varphi_i = A \sin(Bi) \quad (3.28)$$

The discrete variable i indicates the joint number and varies between 1 and M , M being the total number of modules. The winding angle α is defined as that which the left segment of the module 1 forms with the x axis. The total length l is calculated as $l = ML$, where L is the length of each module.

Given a continuous serpenoid curve with the parameters α , k and length l , its discrete serpenoid curve is defined as equivalent to M modules in the same way as that which has the same parameters α , k and the same length l .

The parameter α_i is defined as the angle that forms the left segment of the articulation i with the x axis. The winding angle α is, by definition, equal to α_1 .

In the figure 3.25a) is seen a discrete serpenoid curve with $\alpha = 60$, $k = 1$ and 8 modules. In the figure 3.25b) the continuous serpenoid of $\alpha = 60$ and $k = 1$ is compared with two discrete serpenoid curves of 4 and 8 modules.

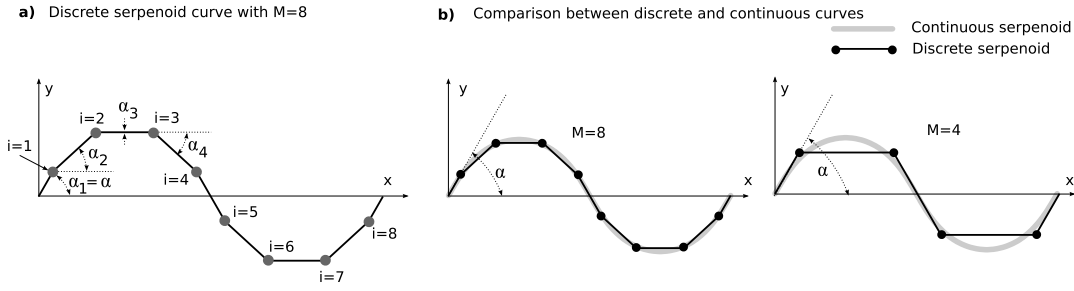


Figure 3.25: a) Discrete serpenoid curve with 8 modules ($M = 8$) b) Comparison between a continuous serpenoid curve with $\alpha = 60$ and $k = 1$, and two discrete serpenoid curves with 4 and 8 modules respectively.

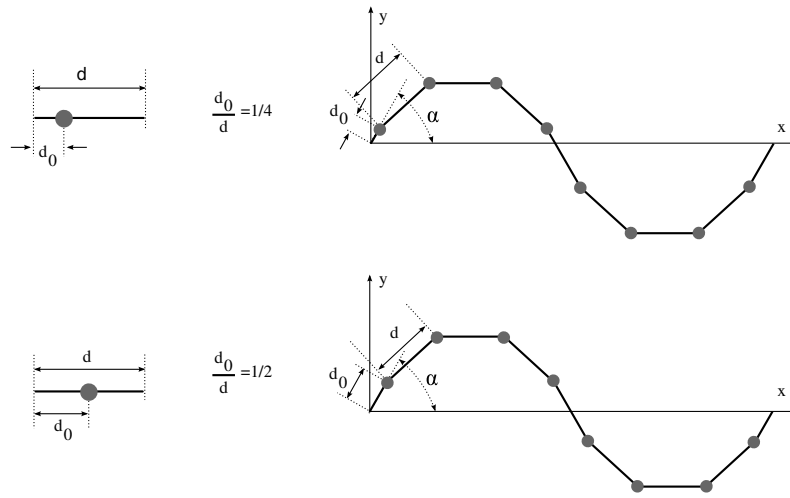


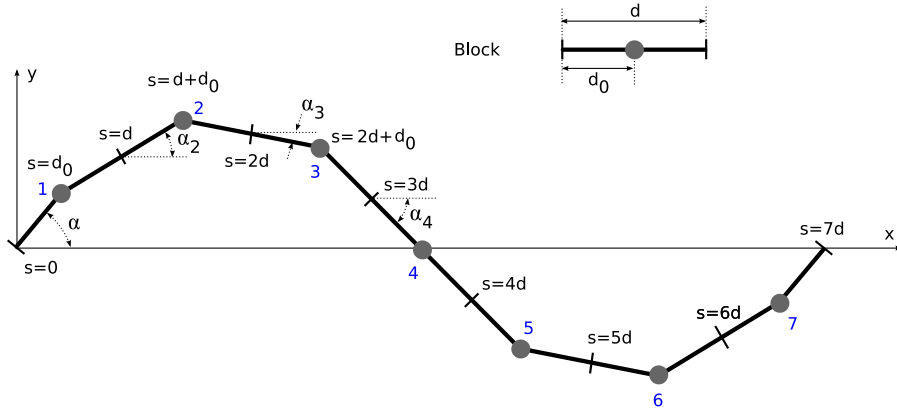
Figure 3.26: Two discrete serpenoid curves of 8 blocks, for different parameter values to d and d_0

In the discrete serpenoid wave the bending angle also depends on the phase ϕ :

$$\varphi_i(\phi) = A \sin(\phi + Bi)$$

3.6.3.2 blocks

The discrete serpenoid curve is formed of M equal modules. Nevertheless so that the equations be more generic and could be applied in more cases the concept of block, defined in the section 3.3.4 is used. The parameters of the blocks are d and d_0 . In the figure 3.26 two serpenoid curves of 8 blocks for different parameter values to d and d_0 are shown. The upper curve is employed to model movement in a straight line of the apodal robots of the pitch-yaw group. The lower curve describes the movement of the pitch-pitch group.

Figure 3.27: Notation employed for the discrete serpenoid curve. Example for $M=7$

3.6.3.3 Formulation

Beginning with a continuous serpenoid curve, the equations for the discrete curve are obtained specifying the variable s in the points of interest. Supposing that the block model is used, the joints are found at the points $s = d_0 + (i-1)d$ and the middle points of union between the blocks are in $s = (i-1)d$, with i between 1 and M (figure 3.27).

The angle that the segments of the curve form with the x axis (α_i), are obtained from the equation 3.16 making the change $s = (i-1)d$ and having in mind that $l = Md$:

$$\alpha_i = \alpha_s|_{s=(i-1)d} = \alpha \cos \left(\frac{2\pi k}{M} (i-1) \right), i \in \{1, M\}$$

For the discrete serpenoid wave, the angle with the x axis also depends on the phase:

$$\alpha_i(\phi) = \alpha \cos \left(\phi + \frac{2\pi k}{M} (i-1) \right), i \in \{1, M\}$$

The Cartesian co-ordinates (x, y) of each articulation referred to the left extremity is defined recursively:

$$x(i) = \begin{cases} d_0 \cos \alpha & i = 1 \\ x(i-1) + d \cos \alpha_i & i \in [2, M] \end{cases}$$

$$y(i) = \begin{cases} d_0 \sin \alpha & i = 1 \\ y(i-1) + d \sin \alpha_i & i \in [2, M] \end{cases}$$

Expanding the final expression is arrived at:

$$x(i) = d_0 \cos \alpha + d \sum_{\substack{j=2 \\ j \leq i}}^i \cos \alpha_j \quad (3.29)$$

$$y(i) = d_0 \sin \alpha + d \sum_{\substack{j=2 \\ j \leq i}}^i \sin \alpha_j \quad (3.30)$$

The bending angle is obtained from the expression 3.14 for values of $s = d_0 + (i-1)d$:

$$\varphi_i = \theta(s)|_{s=(i-1)d+d_0} = A \sin \left(\frac{2\pi k}{M} \left[(i-1) + \frac{d_0}{d} \right] \right)$$

And using the relation found by Ma[87] (eq. 3.39) between the amplitude A and the bending angle, the final expression of φ_i in function of the parameters α , k , d , d_0 and M is:

$$\varphi_i = 2\alpha \sin \left(\frac{\pi k}{M} \right) \sin \left(\frac{2\pi k}{M} \left[(i-1) + \frac{d_0}{d} \right] \right) \quad (3.31)$$

For the discrete serpenoid wave, the bending angle is:

$$\varphi_i(\phi) = 2\alpha \sin \left(\frac{\pi k}{M} \right) \sin \left(\phi + \frac{2\pi k}{M} \left[(i-1) + \frac{d_0}{d} \right] \right) \quad (3.32)$$

The Cartesian co-ordinates are:

$$x(i, \phi) = d_0 \cos \alpha + d \sum_{\substack{j=2 \\ j \leq i}}^i \cos \left(\alpha \cos \left(\phi + \frac{2\pi k}{M} (i-1) \right) \right) \quad (3.33)$$

$$y(i, \phi) = d_0 \sin \alpha + d \sum_{\substack{j=2 \\ j \leq i}}^i \sin \left(\alpha \cos \left(\phi + \frac{2\pi k}{M} (i-1) \right) \right) \quad (3.34)$$

3.6.3.4 Dimensions

In contrast to the continuous case, the dimensions of the discrete serpenoid wave depend on the phase ϕ . The height and width for a given phase is denoted respectively as $h(\phi)$ and $w(\phi)$. The dimensions (h, w) in a cycle are defined as the maximum value of $h(\phi)$ and $w(\phi)$:

$$h = \max \{h(\phi)\} \quad (3.35)$$

$$w = \max \{w(\phi)\} \quad (3.36)$$

Height For a given phase, the height is calculated with the expression:

$$h(\phi) = y_{\max}(i, \phi) - y_{\min}(i, \phi) = y(i_{\max}, \phi) - y(i_{\min}, \phi)$$

where $y_{\max}(i, \phi)$ and $y_{\min}(i, \phi)$ are the maximum and minimum values of the ordinate of the curve. These values are reached for the joints i_{\max} and i_{\min} . In a continuous serpenoid wave, the points s_{\max} and s_{\min} where the maximum and minimums are reached equalling α_S to zero. Resolving the following expressions are obtained:

$$s_{\max} = \frac{l}{2\pi k} \left(\frac{\pi}{2} - \phi \right), \quad s_{\min} = \frac{l}{2\pi k} \left(\frac{3\pi}{2} - \phi \right)$$

Changing the variable $s = (i - 1)d$ and retaining the integer part, i_{\max} and i_{\min} are obtained:

$$i_{\max} = E \left[\frac{M}{2\pi k} \left(\frac{\pi}{2} - \phi \right) + 1 \right], \quad i_{\min} = E \left[\frac{M}{2\pi k} \left(\frac{3\pi}{2} - \phi \right) + 1 \right]$$

With this, the expression to calculate the height of a serpenoid wave is:

$$h = \max \{y(i_{\max}, \phi) - y(i_{\min}, \phi)\} \quad (3.37)$$

where $y(i, \phi)$ is obtained with the equation 3.34.

Width The width will be equal to the abscissa of the extreme right. At the same time this is the abscissa of the articulation M plus the projection of the right segment of the last module. It is obtained with the expression:

$$w(\phi) = x(M, \phi) + (d - d_0) \cos(\alpha_{M+1}(\phi))$$

The total width will be the maximum value during the cycle:

$$w = \max \{x(M, \phi) + (d - d_0) \cos(\alpha_{M+1}(\phi))\} \quad (3.38)$$

3.6.3.5 The h_1 and H_1 spaces

The form of a serpenoid curve, be it continuous or discrete is characterised by the parameters (α, k) . Besides there are the constants l (length) and M (number of modules). The h_1 **shape space** is defined as that which has as elements the pairs (α, k) . This space is employed to define the robot's shape.

As is shown in the section 3.5.4, the parameters of the controller $(A, \Delta\phi)$ belong to the homogeneous control space H_1 and defines how each module moves and how it moves in relation to the previous one.

The relationship between both spaces is deduced from the comparison between the equations 3.12. They are presented in the equations 3.39 and 3.32:

$$A = 2\alpha \sin\left(\frac{\pi k}{M}\right) \quad (3.39)$$

$$|\Delta\phi| = \frac{2\pi k}{M} \quad (3.40)$$

In the control model, the phase difference $\Delta\phi$ can take various positive and negative values while in the mathematical model of the serpenoid curve only positive values have been used, for this reason in the equation 3.40 the absolute value of the phase difference is related to k and M .

The equations 3.40 and 3.39 allows the form of the robot to be known beginning with the local parameters of the controller, and vice-verse, starting from the shape discover what parameters of controller are to be established.

Parameter	Description	Range
k	Parameter. Number of undulations	$k \geq 1$
α	Parameter. Winding angle	$\alpha \in [0, 120]$
M	Constant. Number of articulations	$M \geq 2$
d	Constant. Distance between joints	$d > 0$
d_0	Constant. Left segment of the module	$d_0 > 0$
ϕ	Variable. Phase	$\phi \in (-180, 180]$
i	Variable. Joint number	$i \in \{1, M\}$

Table 3.7: Parameters, variables and constants for the discrete serpenoid curve/wave

3.6.3.6 Summary of parameters

The summary of all the parameters, constants and variables for the discrete serpenoid curve/wave are shown in the table 3.7.

3.6.4 3D serpenoid curve/wave

3.6.4.1 Definitions

Given a continuous curve within a three dimensional space, the parameters $\theta_v(s)$ and $\theta_h(s)$ are defined, respectively, as the vertical and horizontal bending angles from a point situated ins with respect to that which is in $s + ds$. The **3D serpenoid curve** is defined as that which the bending angles vary sinusoidally with s , according to the expressions:

$$\theta_v(s) = A_v \sin\left(\frac{2\pi k_v}{l}s + \psi_v\right)$$

$$\theta_h(s) = A_h \sin\left(\frac{2\pi k_h}{l}s + \psi_h\right)$$

It is a curve that is formed by the superposition of two serpenoid curves, one in the plane of pitch and the other in that of yaw. This means that each of these curves will have its own winding angle and number of undulations. The subscript v is used for the vertical articulations and h for the horizontal ones. Taking the point $s = 0$ as the origin of the phases, denoted by $\Delta\phi_{vh}$ the phase difference between the verticals and horizontals ($\psi_h - \psi_v$), and using the equation 3.39, the expression of the **3D serpenoid wave** can be expressed as:

$$\theta_v(s, \phi) = 2\alpha_v \sin\left(\frac{2\pi k_v}{M}\right) \sin\left(\phi + \frac{2\pi k_v}{l}s\right) \quad (3.41)$$

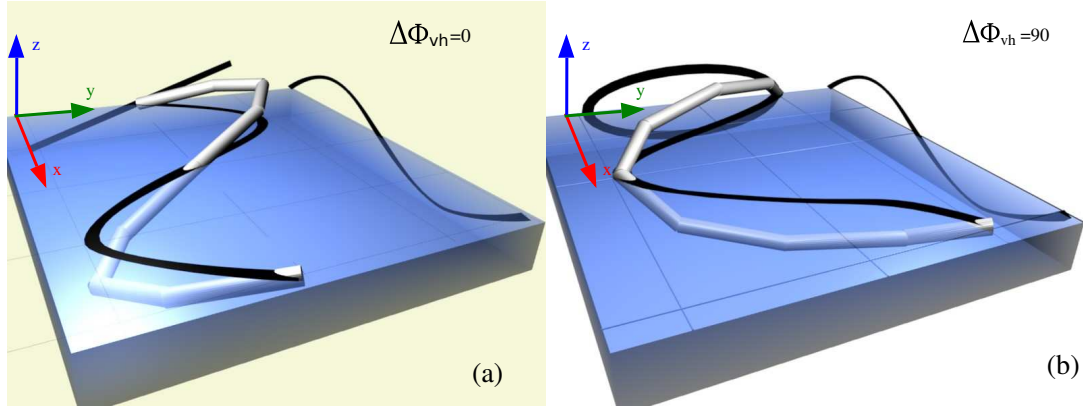


Figure 3.28: Different shapes of 3D serpenoid curve with $k_v = k_h = 1$. a) When $\Delta\Phi_{vh} = 0$. b) For $\Delta\Phi_{vh} = 90$

$$\theta_v(s, \phi) = 2\alpha_h \sin\left(\frac{2\pi k_h}{M}\right) \left(\phi + \frac{2\pi k_h}{l}s + \Delta\phi_{vh}\right) \quad (3.42)$$

3.6.4.2 Parameters and the h_2 shape space

The parameters to describe the 3D serpenoid are 5: α_v , k_v , α_h , k_h and $\Delta\Phi_{vh}$. The pairs (α_v, k_v) and (α_h, k_h) characterise respectively each one of the two vertical and horizontal serpenoids. $\Delta\Phi_{vh}$ is a new parameter that establishes the phase difference between the vertical and horizontal articulations.

This new parameter influences how the superposition of the two waves is effected. In the figure 3.28 an example of its effect is shown when $k_v = k_h = 1$. In the left hand figure (a), the 3D serpenoid curve is situated on the same plane, inclined at an angle in relation to the horizontal. Its projection on the plane zy is a straight line. To the right this projection is an ellipse.

We define the space h_2 as that which has as elements the tuples $(\alpha_v, k_v, \alpha_h, k_h, \Delta\Phi_{vh})$. The points of this space determine the shape of the curve and how the wave is propagated.

3.6.4.3 Family of 3D serpenoid curves/waves

The form of the 3D serpenoid wave determines the dimensions of the robot and the movements it carries out. A classification of the curves in function of their parameters will be established. They are summed up in the figure 3.29.

The waves will be divided into **isomorphous** and **non-isomorphous**. In the first the parameters k_v and k_h are equal which means that the variation of the vertical and horizontal bending angles is constant

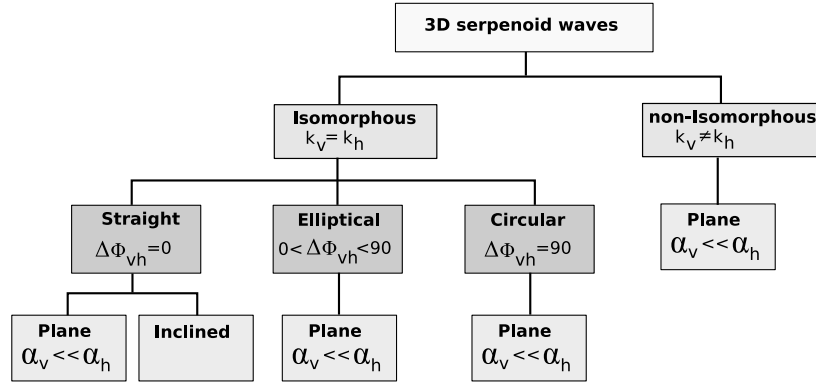
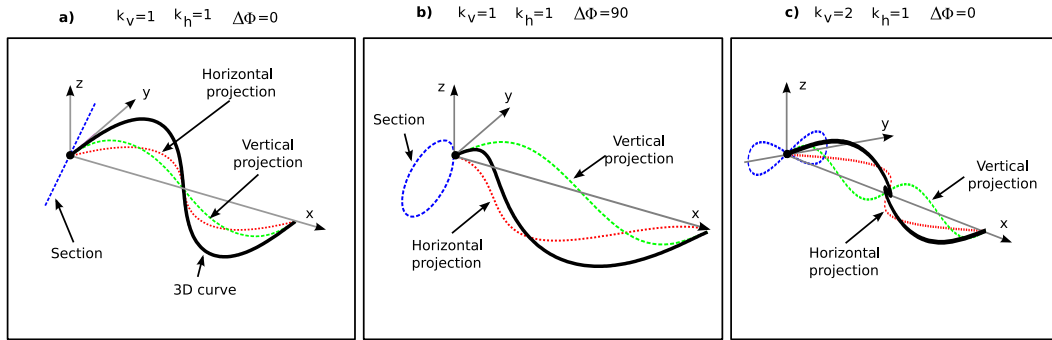


Figure 3.29: Classification of the 3D serpenoid curves

Figure 3.30: Examples of 3D serpenoid waves a) straight inclined isomorphous. b) Elliptical isomorphous c) Non-isomorphous with $k_v = 2k_h$

for all the points of the curve and a global wave appears that travels through the robot's body. In the non-isomorphous waves the shape of the wave is not constant and depends on the phase.

We call **plane waves** those in which the winding angle of the verticals is much less than that of the horizontal ($\alpha_v \ll \alpha_h$), so that in reality it can approximate to that of a 2D serpenoid wave on the plane $z = 0$.

The isomorphous waves are classified paying attention to the shape of their section, that is given by the parameter $\Delta\phi_{vh}$. By this means we will obtain the **straight**, the **elliptical** and **circular waves**. When $\Delta\phi_{vh} = 0$ the wave is propagated on a plane and its section therefore is a straight line that forms an angle with the y axis. The slant of the angle depends on the relation between α_v and α_h . For the plane waves the angle will be 0. Therefore the straight isomorphous waves will be divided into plane and inclined. When $\Delta\phi_{vh} = 90$ the section is circular and for $0 < \Delta\phi_{vh} < 90$ elliptical.

In the figure 3.30 three examples of 3D curves are shown. The one on the left is a straight inclined isomorphous curve. The middle one is an elliptical isomorphous curve and the one on the right a non-isomorphous curve, with $k_v = 2k_h$.

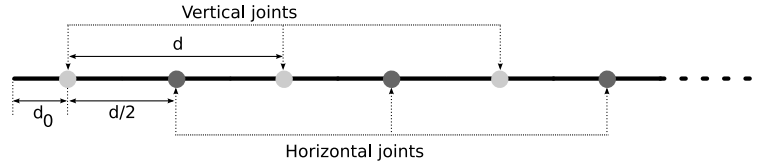


Figure 3.31: Model for the discrete 3D serpenoids

3.6.4.4 Dimensions

Of all the types of 3D serpenoid waves, those that will be used for locomotion on a surface will be the plane waves. In them the 3D serpenoid approximates to a serpenoid with the parameters α_h and k_h and its dimensions l_x and l_y can be calculated applying the equations 3.38 and 3.37 for the discrete model and 3.25 and 3.24 for the continuous.

The height is approximated by the equations 3.37(discrete) y 3.24(continuous) using the parameters α_v and k_v .

3.6.4.5 Discrete model

To model the discrete 3D serpenoid curve/wave blocks of the pitch-yaw type, made up of two joints, will be used (figure 3.31). In this model the vertical joints are placed on the points of the curve: $s = (i-1)d + d_0$ and the horizontal ones on $s = (i-1)d + d_0 + \frac{d}{2}$, where i is the joint number, contained between 1 and $M/2$.

The bending angles $\varphi_{v_i}(\phi)$ and $\varphi_{h_i}(\phi)$ are obtained specifying the equations 3.41 and 3.42 in the points s where the vertical and horizontal articulations are, respectively:

$$\varphi_{v_i}(\phi) = \theta_v(\phi)|_{s=(i-1)d+d_0} = 2\alpha_v \sin\left(\frac{2\pi k_v}{M}\right) \sin\left(\phi + \frac{4\pi k_v}{M} \left(i-1 + \frac{d_0}{d}\right)\right) \quad (3.43)$$

$$\varphi_{h_i}(\phi) = \theta_h(\phi)|_{s=(i-1)d+d_0+\frac{d}{2}} = 2\alpha_h \sin\left(\frac{2\pi k_h}{M}\right) \sin\left(\phi + \frac{4\pi k_h}{M} \left(i-1 + \frac{d_0}{d} + \frac{1}{2}\right) + \Delta\phi_{vh}\right) \quad (3.44)$$

3.6.4.6 Relation between the H_2 and h_2 spaces

The parameters of the H_2 space are expressed from those of h_2 by means of the following equations:

Notation	Description	Range
k_v	Parameter. Number of undulations in vertical joints	$k_v \geq 1$
k_h	Parameter. Number of undulation in horizontal joints	$k_h \geq 1$
α_v	Parameter. Winding angle for vertical joints	$\alpha_v \in [0, 120]$
α_h	Parameter. Winding angle for horizontal joints	$\alpha_h \in [0, 120]$
M	Constant. Number of joints	$M \geq 2$
d	Constant. Distance between joints	$d > 0$
d_0	Constant. Left segment of the block	$d_0 > 0$
ϕ	Variable. Phase	$\phi \in (-180, 180]$
i	Variable. Number of joints	$i \in \{1, M/2\}$

Table 3.8: Parameters, variables and constants of the discrete 3D serpenoid curve/wave

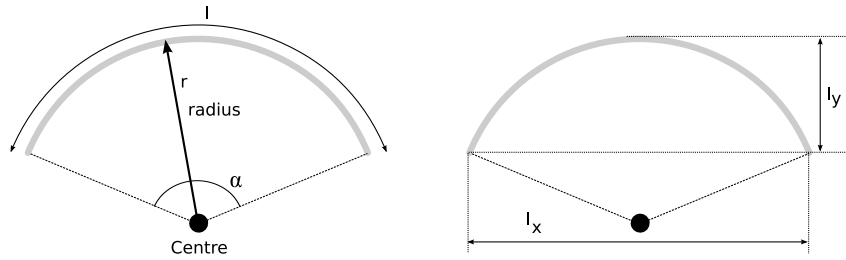


Figure 3.32: Parameters and dimensions of the circular curve

$$A_v = 2\alpha_v \sin \frac{2\pi k_v}{M}, \Delta\phi_v = \frac{4\pi k_v}{M} \quad (3.45)$$

$$A_h = 2\alpha_h \sin \frac{2\pi k_h}{M}, \Delta\phi_h = \frac{4\pi k_h}{M} \quad (3.46)$$

3.6.4.7 Summary of parameters

All the constant and variable parameters of the discrete 3D serpenoid curve/wave are given in the table 3.8.

3.6.5 Circular curve/wave

3.6.5.1 Continuous model

Definitions We define a **circular curve** as one in which the bending angle $\theta(s)$ is constant for the length of the curve. Therefore the curve will have the shape of a circular arc (Figure 3.32). The parameter α is defined as the angle of this arc.

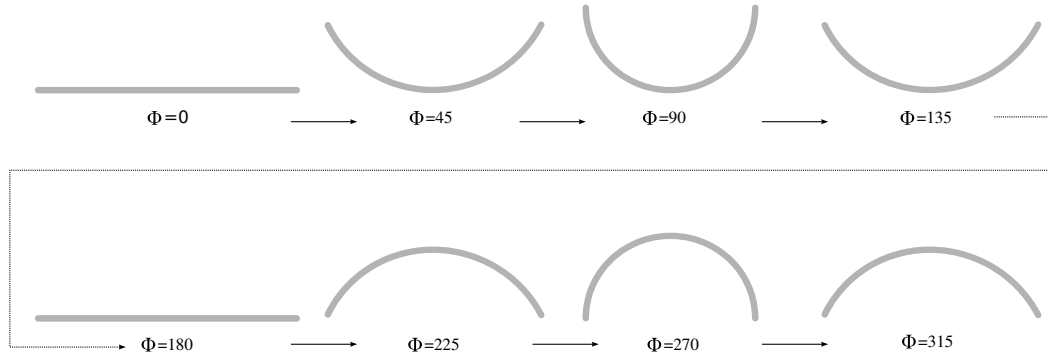


Figure 3.33: Example of a circular wave with $\alpha = 180$. Eight circular curves are shown for different values of the phase ϕ (and assuming an initial phase ϕ_0 equal to 0)

We define a circular wave as one in which α varies with the phase ϕ in a sinusoidal way, according to the expression:

$$\alpha(\phi) = \alpha \sin(\phi + \phi_0)$$

Where α is now the maximum angle of the arc and ϕ_0 the initial phase. As the length of the curve is l , the radius r is expressed as:

$$r = \frac{180l}{\alpha\pi} \quad (3.47)$$

where α is expressed in degrees.

Parameters The curve is characterised by the parameter α that has a value between 0 and 360 degrees. In the wave the angle of the arc is $\alpha(\phi)$ that varies with the phase. In the figure 3.33 the variation of the shape of a circular wave is shown with $\alpha = 180$ and $\phi_0 = 0$. Initially the curve is a straight resting on the x axis. When the phase is varied it adopts the shape of a circular arc, with angle $\alpha(\phi)$. The angle increases until it reaches its maximum α for $\phi = 90$. It then diminishes until it returns to being a straight ($\phi = 180$) and the operation is repeated but bending toward the opposite side. For a phase of $\phi = 220$ the curvature is maximum.

Dimensions The dimensions of a circular curve are l_x and l_y , as is shown in the figure 3.32. They depend on the parameter α and the length l of the curve. They are calculated by the equations:

$$l_x = \frac{2l}{\alpha} \sin\left(\frac{\alpha}{2}\right)$$

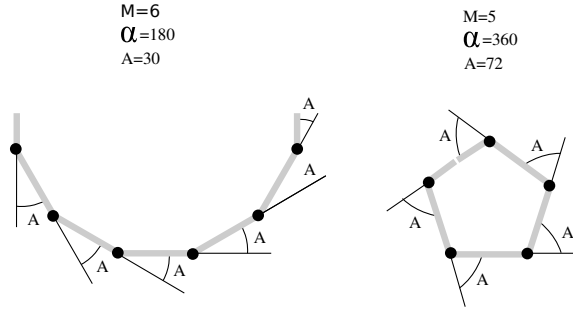


Figure 3.34: Example of two discrete circular curves

$$l_y = \frac{l}{\alpha} \left(1 - \cos \left(\frac{\alpha}{2} \right) \right)$$

Relation with the serpenoid curve The circular curve is obtained from a serpenoid curve/wave when the winding angle α is 0 and an offset different to zero is applied. What is obtained is a circular curve, that does not vary with ϕ . It will be used in chapter 5 to describe the robot turnings.

The circular wave is obtained from a serpenoid wave in which $k = 0$. Taking into account the equation 3.40, $k = 0$ implies that the phase difference $\Delta\phi$ between two consecutive articulations is 0, which means that all of them are in phase and their bending angle is the same. This angle varies with ϕ and makes the wave change shape (as, for example, in the figure 3.33).

3.6.5.2 Discrete model

The discrete circular curve is characterised because its M joints have the same bending angle A , that is equal to α/M :

$$\varphi_i = A = \frac{\alpha}{M} \quad (3.48)$$

and the discrete circular wave:

$$\varphi_i(\phi) = A \sin(\phi + \phi_0) = \frac{\alpha}{M} \sin(\phi + \phi_0)$$

The maximum value for A is 90 degrees, because of mechanical limitations in the implementation of the joints which means that it has to fulfil the following restriction:

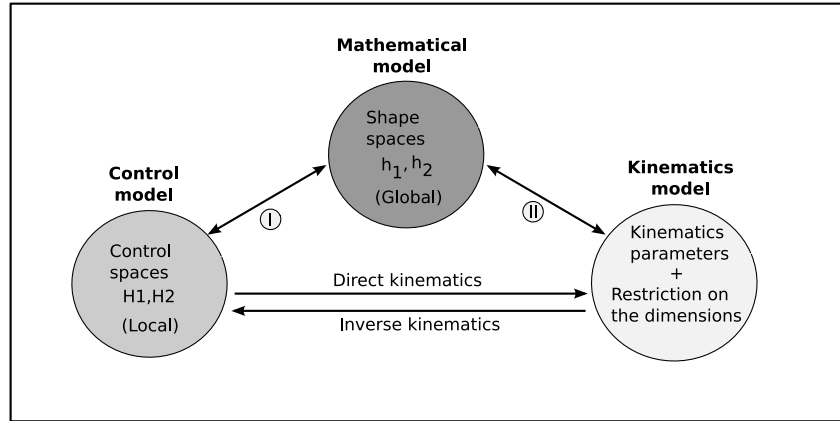


Figure 3.35: Relation between the different models

$$\frac{\alpha}{M} \leq 90$$

In the figure 3.34 two discrete circular curves are shown with different parameter values.

3.7 Conclusions

In this chapter the models have been presented that will be employed for the study of the locomotion of apodal robots of the **pitch-pitch** and **pitch-yaw groups**. With the first group one dimensional movement will be analysed and with the second bi-dimensional movement. All the robots are modelled as a series of **equal blocks** united between themselves. Each block formed by one or more **equal modules**, with pitch or yaw type connections. For the mathematical description the **wired model** is used, for the simulation the **hexahedral model** and for the experiments a **real model**.

To make the study of locomotion accessible it is assumed that the robots will be moving on a level surface without obstacles and be fixed to a permanent regime. It is supposed that the robot's movement is periodic with the cycle lasting T . Therefore, the movement from one place to another is due to the periodic repetition of some basic movements. The problem that has to be resolved is how to co-ordinate all the joints to generate these elementary movements in each cycle.

In this thesis this problem is approached from three different environments: kinematics, control and shape of robot (figure 3.35) and we will resolve it establishing quantitative and quality relationships between them, that are verified by means of experiments. In this chapter we propose the models and present the equations that relate the parameters of control to the shape of the robot.

The **kinematic model** is characterised by the **step** ($\vec{\Delta r}$) and **angular step** ($\Delta\gamma$) parameters, that indicates the movement and rotation of the centre of mass of the robot for each cycle. Also, the robot has certain dimensions that imposes some restrictions (such as, for example, movement inside a tube, where the height of the robot must be limited).

The **control model** proposed is bio-inspired and consists of sinusoidal generators that cause each and every one of the joints to oscillate independently. The **control spaces** are defined as H_1 and H_2 formed by tuples with the generator parameters. These spaces are those that have **the minimum dimension and allow the apodal robots with any number of modules to move**. There is no reason why these movements should be optimum. Adding more parameters, in principle, better solutions could be found.

From these models the problems of the direct and inverse kinematics, that establish relationships between the control model and locomotion, can be set forth with more precision. With **direct kinematics** the values applied to the controllers are the starting point and determine the kinematic parameters, the type of movement and the dimensions of the robot. With **inverse kinematics** the value of the control parameters are looked for, so that the robot moves with one type of movement and with given values of the kinematic parameters, as well as fulfilling certain restrictions in the dimensions.

To resolve the direct and inverse kinematics the **mathematical model** is developed with which parameters are obtained for the robot's shape and defines the **shape spaces** h_1 and h_2 . Each point of these spaces is associated to a shape of robot. The equations which related to the control spaces and that of the shapes have been presented. Apodal robots have a one-dimensional topology which means that their shape is described by means of curves and their movement by the waves that are propagated. Using a control model based on sinusoidal oscillations, the shape of the robots is described by means of **serpenoid curves and waves**. For the 3D serpenoids, a classification has been established in function of how they propagate and the shapes that they present. This will be used in chapter 5 to study locomotion on a plane. Each group of 3D serpenoids will have a different associated gait.

Chapter 4

Locomotion in 1D

“If I don’t know something, I will investigate”

– *Louis Pasteur*

4.1 Introduction

In this chapter we will study locomotion in a straight line of the pitch-pitch group of modular apodal robots when using the model of sinusoidal oscillators presented in the section 3.5.

Firstly locomotion using the continuous robotics model will be analysed. The basic principles of locomotion will be obtained, the shape space, the dimensions, the criteria of stability and an equation to calculate the step is proposed. Below we will itemise the previous ideas for the wired model of the discrete robot and present the methodology to resolve the problems of direct and inverse kinematics. Then a case study will be presented where we will apply all the previous concepts to an eight module robot. Data will be obtained that will then be contrasted with the experimental results in the chapter 7. Finally all the ideas will be summed up in 11 principles of locomotion.

4.2 Continuous model

Although the modular robots of the pitch-pitch group are by nature discrete, the understanding of the continuous model allows us to obtain the essential properties of one dimension locomotion that are common to all apodal robots, regardless of the number of modules. Displacement is only produced if movement of the robot’s modules are well co-ordinated. It will be seen that with the continuous model this co-ordination is satisfactorily explained.

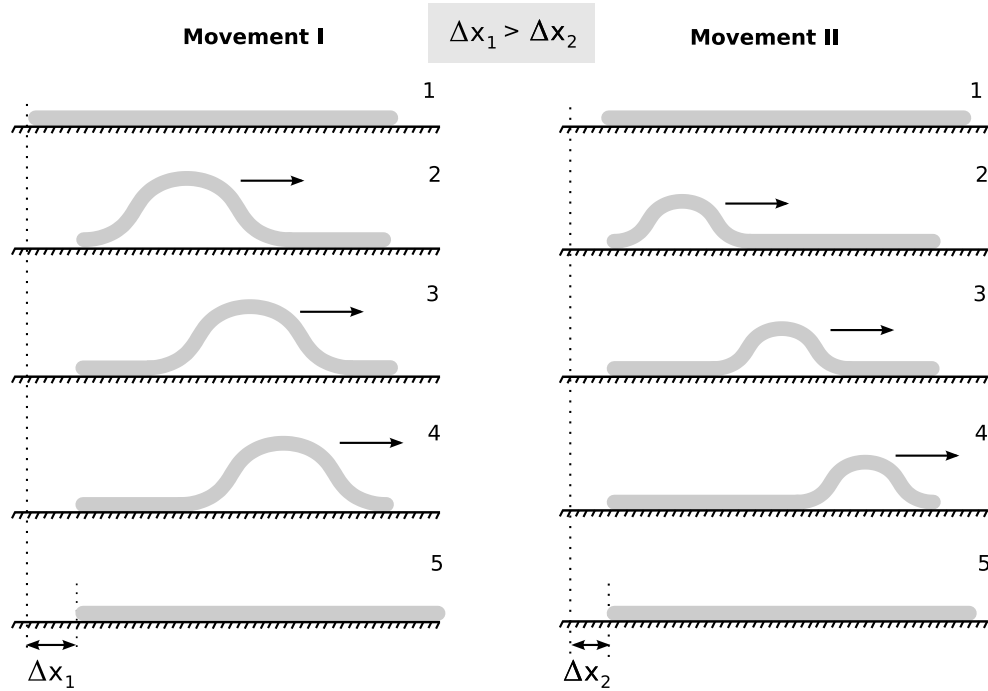


Figure 4.1: Locomotion by means of wave propagation in caterpillars when two different sizes of body waves are used

The mechanism of locomotion is due to the appearance of corporal waves that are propagated along the length of the robot.

4.2.1 Wave propagation

The mechanism of locomotion based on **wave propagation** is inspired by a caterpillar's movements. In it an undulation of the body appears that is propagated from its tail toward its head causing the animal to move a certain distance Δx , which is called **step**.

This mechanism of locomotion has the following properties:

- **The direction of the propagation of the wave determines if the robot moves forwards or backwards.** In the example 4.1 the waves are displaced toward the right, causing the robots to move in the same direction.
- **The step is determined by the dimensions of the body wave.** In the figure 4.1 the locomotion of a robot is shown when two different sizes of body waves are used. The movement I employs a higher wave which means that the step is bigger than the movement II ($\Delta x_1 > \Delta x_2$).

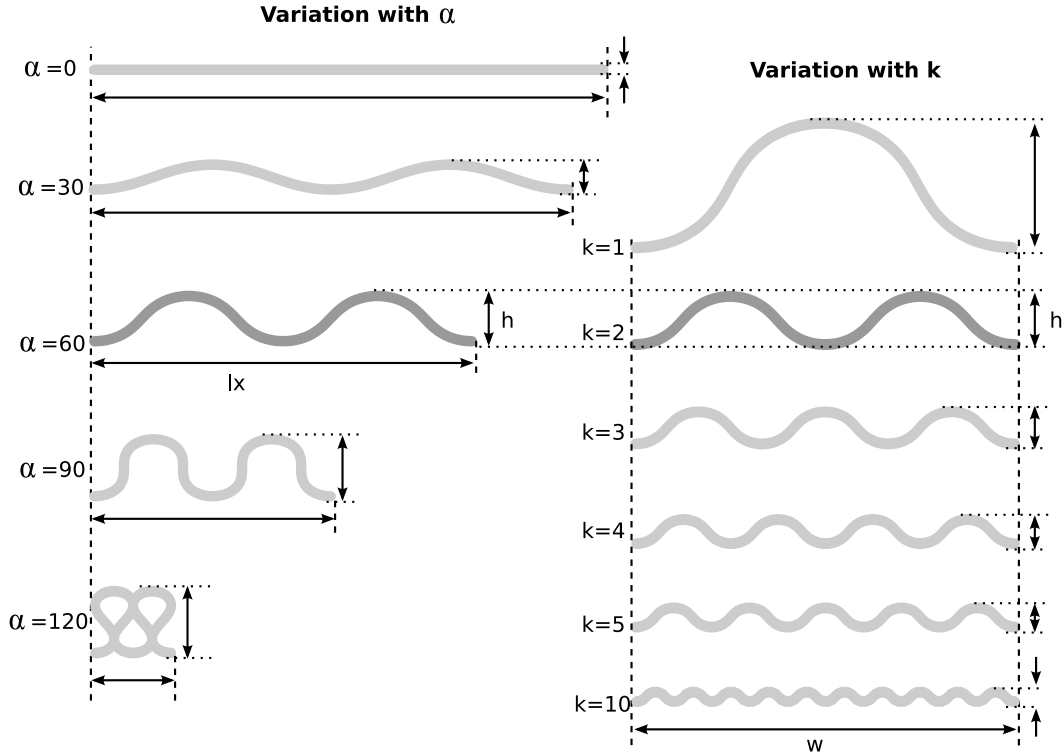


Figure 4.2: Variation of the robot shape with the α and k parameters, when $\phi = -90$

It is seen that it is the global properties of the wave that determine the robot's advance. This allows us to describe the kinematic model beginning with the characteristics of the waves that pass through the robot's body.

When the control model of sinusoidal generators (see section 3.5) is used the body wave that appears is a serpenoid type (section 3.6.2). In the following sections we will study this wave and its dimensions and we will deduce the criteria of stability and the step equation.

4.2.2 Serpenoid Wave

The parameters that characterise the serpenoid wave are summed up in the table 3.6. They are the winding angle α , the number of undulations k and the phase ϕ . The pair (k, α) determines the shape of the robot and its dimensions (height h and width w). We call this pair **working point**.

In the continuous model **the height and the width do not depend on the phase**, and they remain constant during the propagation of the wave. In the figure 4.2 the relationship between (k, α) and the shape, for a robot with length l and phase -90 , is shown graphically. In the central section the form of the robot, for $\alpha = 60$ and $k = 2$, has been drawn in a darker colour. On the left are the variations with the parameter α . The greater the value of α , greater is the height h but the width w is less. To the

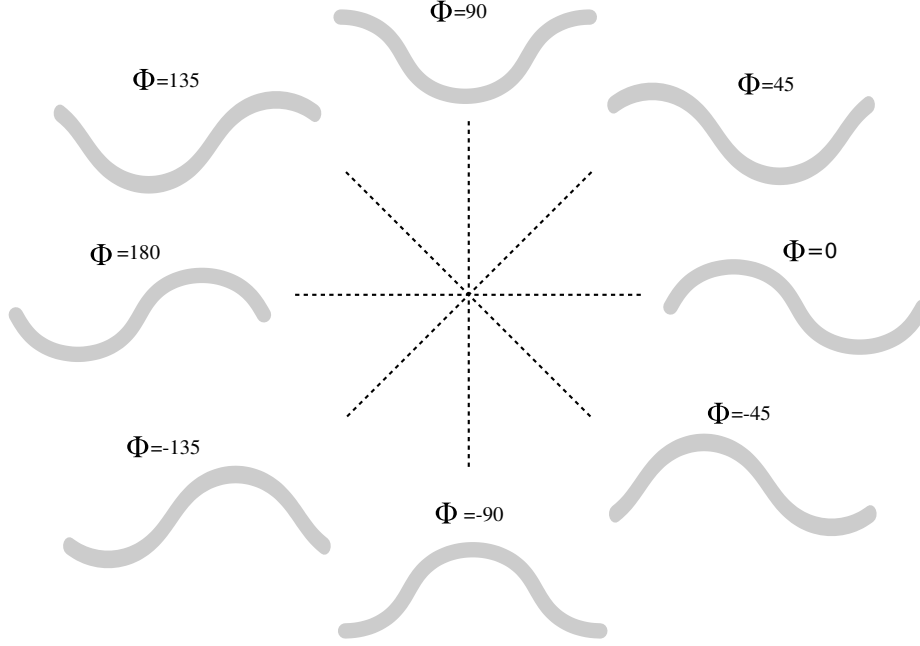


Figure 4.3: Variation of the shape with the phase, when $k = 1$ and $\alpha = 60$ degrees .

right the variation with k has been drawn. When the number of undulations are increased, the height diminishes but w remains constant.

The shape of the robot with the phase ϕ is shown in the figure 4.3. A positive increase of the phase causes the wave to move along the x axis negatively.

4.2.3 Shape space h_1

We call shape space h_1 being the total of all the working points (k, α) that are found in the region $\alpha \in [0, 120]$ and $k \geq 1$. Each one of these points determines the shape and dimensions of the robot for a given phase ϕ and length l . This space will be represented in a Cartesian system, whose abscissa are the number of undulations and the ordinates the winding angle, as is shown in the figure 4.4. In this example a phase of $\phi = -90$ is being used. For the points of the straight line $\alpha = 0$, the robot is a horizontal segment of length l . To see the variations of the shape the working point $(4, 60)$ is taken. A negative displacement in the ordinates makes the winding angle decrease and therefore the robot will “flatten out”: w increases and h diminishes (compare the points $(4, 60)$ and $(4, 30)$). A negative displacement of the abscissa causes a lessening in the number of undulations, increasing h while w remains constant (compare the points $(4, 60)$ and $(2, 60)$).

This representation of the shape space allows the restrictions of the robot’s dimensions to be expressed graphically. It is also useful to draw the graph of the dimensions and the step in relation to the working points.

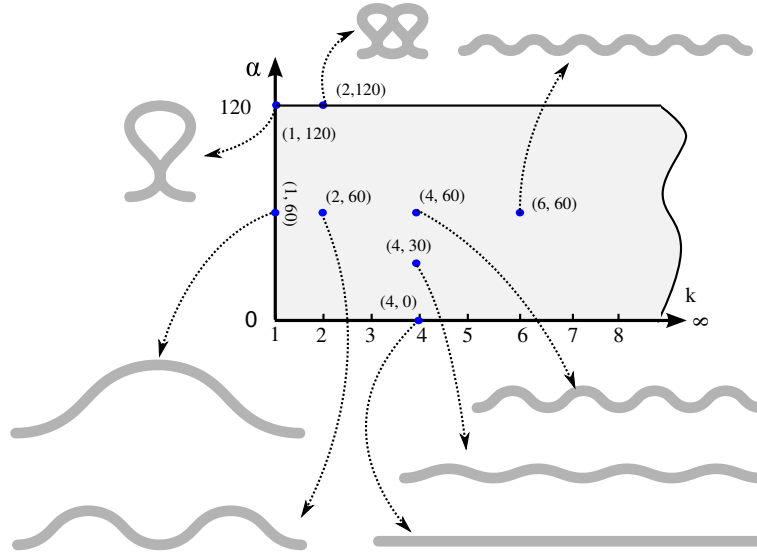


Figure 4.4: Graphical representation of the shape space h_1 . The robot shape are shown for different working points, when the phase is -90 degrees.

In the continuous model the value of k is not limited, which means that the axis x extends to infinity.

4.2.4 The robot's dimensions

Each point of a shape space corresponds to a robot of certain dimensions. The equations that link (k, α) to the normalized dimensions are 3.24 and 3.25. From them the height and width of the robots with a length l and number of waves k are calculated (equations 3.26 and 3.27).

In this section the variations in the dimensions of a continuous robot of length $l = 1$ are analysed as it moves in the shape space. The values h and w are represented as percentages in relation to the total length. Given that the parameter k is not limited, the region is limited to $k \leq 10$ to obtain a better graphical representation.

4.2.4.1 Height

The normalized height h_n is obtained from the point (k, α) by means of the equation 3.24. In the figure 4.5 it is shown graphically. The working point, where the robot is taller, is $(1, 120)$, which value is approximately 40% of its length. It is observed that it diminishes when k increases and α decreases.

In the figure 4.6 the height of the working point $(2, 60)$ and its variation in function of the parameters k (left) and α (right) are shown. The variation with α is quite linear between the values of approximately 0 and 60 degrees. The value of h is inversely proportional to k .

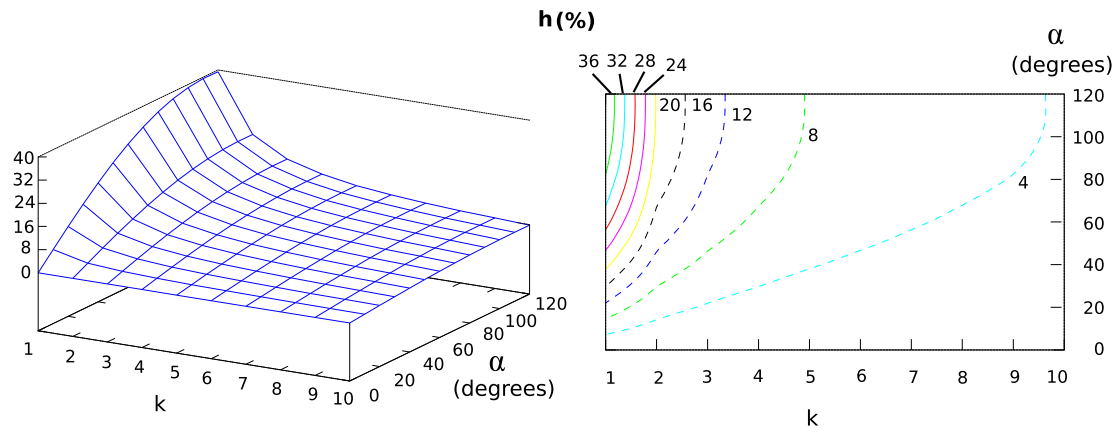


Figure 4.5: Normalized height of an apodal continuous robot in function of the working point (k, α)

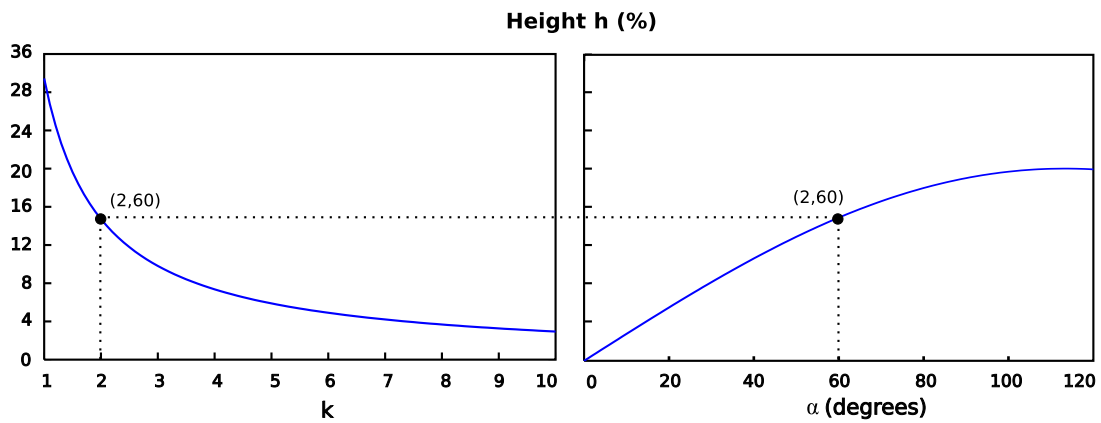
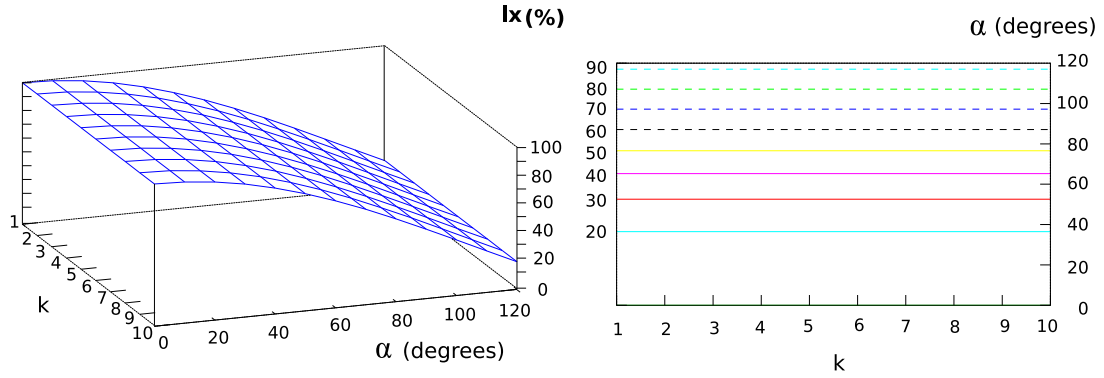
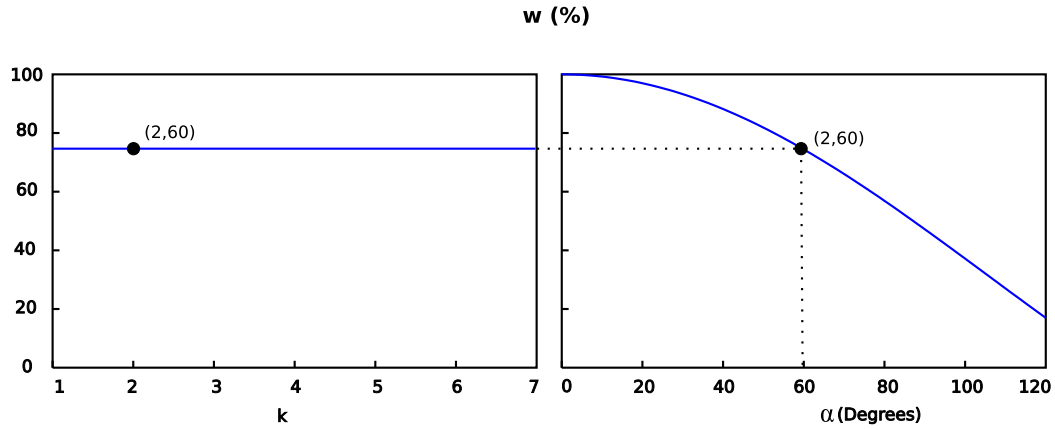


Figure 4.6: Normalized height for the working point $(2, 60)$ and its variations with k and α

Figure 4.7: Normalized width of an apodal continuous robot in function of the working point (k, α) Figure 4.8: Normalized Width of the working point $(2, 60)$ and its variations with k and α .

4.2.4.2 Width

The normalized width is obtained from the point (k, α) by means of the equation 3.25. The graph is shown in the figure 4.7. The width is maximum when $\alpha = 0$ and decreases with the increase of α . It remains constant with k .

In the figure 4.8 the working point $(2, 60)$ is shown and its variation with k and α . For values of α between 60 and 120 approximately, the variation of w is fairly linear.

4.2.5 Stability principle

The locomotion of the robot is determined by its shape and therefore by the position of the working point within the shape space. In some zones the movement will be statically stable, in others movement will not exist or will be very brusque. In this section a criterion is established to determine in which region of the shape space movement is statically stable.

We will say that **the robot is stable** for a phase ϕ if it is verified that at least two supporting points with the ground exist and that the centre of gravity falls within the segment that joins these two points.

Statically stable locomotion is defined as that in which the robot is stable for all phases. That is to say that the robot is stable during the propagation of the wave. It is verified also that when the locomotion is of this type the centre of gravity remains always at the same height and the movement is very smooth.

Principle of stability *If the number of undulations (k) is greater than or equal to two, then the robot's movement will be statically stable.*

What is more, within the region of stability, the greater the value of k , the greater will be the robot's stability. When k is increased the average of the supporting points will be greater and the height of the robot will decrease, improving the stability.

In the following paragraphs this principle will be studied in more detail.

4.2.5.1 Stability when $k \geq 2$

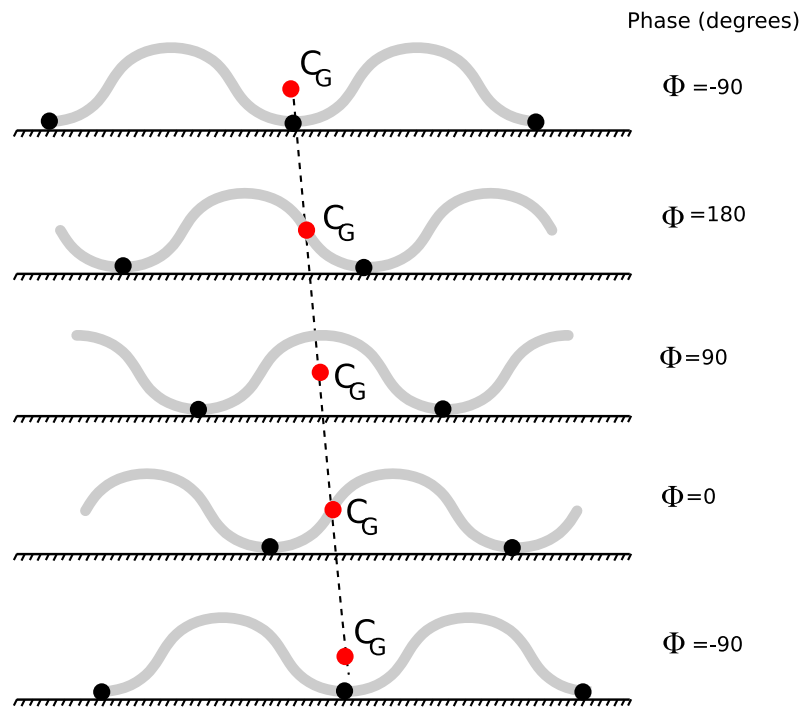
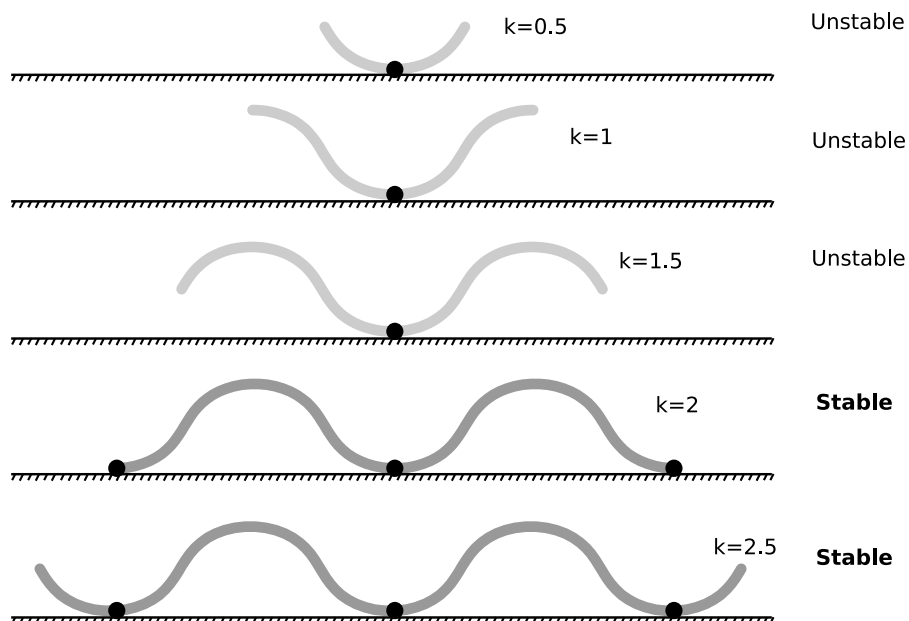
When the number of undulations is greater than or equal to 2, there will always be at least two supporting points with the ground and the robot will be stable. In the figure 4.9 five instants are shown during the movement of a robot with two undulations, with phases corresponding to -90 , 180 , 90 , 0 and -90 degrees. Initially three supporting points exist therefore the robot is stable. When the phase is varied the waves are propagated. For $\phi = 180$ there are only two supporting points, but as the projection of the centre of gravity (C_G) is within the segment that joins these two points, the robot is stable. This condition is verified for the other phases. Also the height of the centre of gravity remains constant.

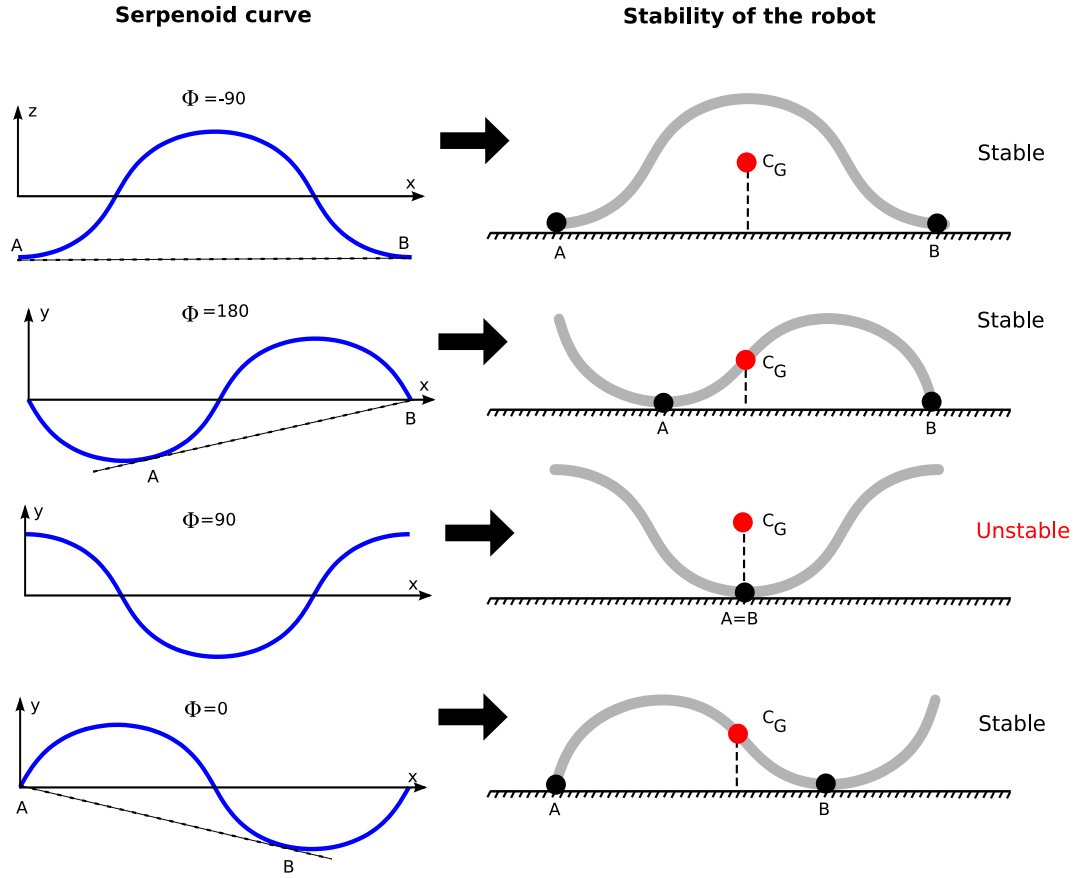
The situation is similar for $k \geq 2$ but with the difference that the average number of supporting points will increase.

4.2.5.2 Stability for $k < 2$

When $k < 2$ phases exist in which there is only one supporting point. In this situation the robot will incline forwards or backwards. During the movement, the average number of support points will be less than 2.

The worst situation is when there is only one supporting point. It occurs for the phases in which the robot has the shape of a "U" in its central part. In the figure 4.10 this situation is shown for different values of k . When $k = 2$ it passes from one to three supporting points.

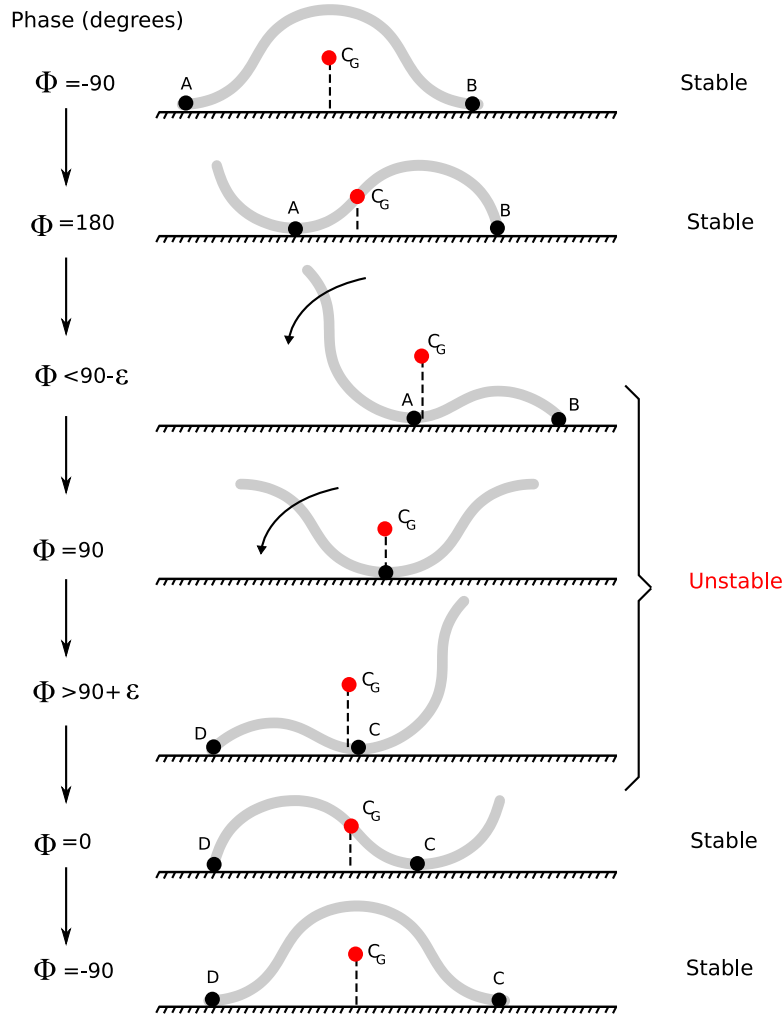
Figure 4.9: Robot locomotion when $k = 2$. It is statically stableFigure 4.10: Robot stability and the k parameter

Figure 4.11: Relationship between the phase and stability when $k = 1$

As an example of a movement that is not statically stable the case of $k = 1$ will be studied. First the relationship between the robot's phase and stability will be analysed. In the figure 4.11 on the left the shape of the wave is shown for different phases and on the right the actual orientation of the robot. The shapes are equal, but their inclinations vary. In the case of $\phi = -90$ both orientations are the same. The supporting points A and B are aligned. For $\phi = 180$, the initial supporting point is A. The robot must lean to the right so that point B also comes into contact with the ground. In this situation the robot is also stable. The same happens for $\phi = 0$ but it leans to the opposite side.

Nevertheless the worst case is produced for $\phi = 90$. There exists only one supporting point so the robot will lean towards the left or the right, or will wobble.

What the locomotion of the robot will be like can be obtained from this information. It has been drawn in the figure 4.12. It begins with a stable situation. As the phase increases the wave moves to the right. The robot begins to move in the same direction. When $\phi = 180$ the centre of gravity is nearer to point A and its height has decreased. When the phase is near to 90 degrees (the worst case), the projection of the centre of gravity is very near to A. As yet the robot leans to the right. When the situation is reached where the phase is near to 90 but greater than it ($90 + \epsilon$) the robot will lean toward

Figure 4.12: Stability of the robot when $k = 1$

the left with the supporting points A and B disappearing, while two new ones, C and D, will appear. This transition is not stable. It provokes a brusque movement in the robot. The wave continues being propagated and the movement continues stable until it reaches the initial phase $\phi = -90$, where the cycle ends.

The result is that for the case of $k = 1$ and in general for $k < 2$, the robot is not stable at every moment. There is an existing range of phases in which one extremity hits against the ground. This does not mean that movement cannot exist, rather that a transition, brusque in some of its phases, will appear. This effect can be controlled with the parameter α . For low values the robot will have little height and the inclination from one orientation to another will be smooth.

Also when the locomotion is not statically stable the height of the robot's centre of mass will not remain constant but will oscillate with the propagation of the wave.

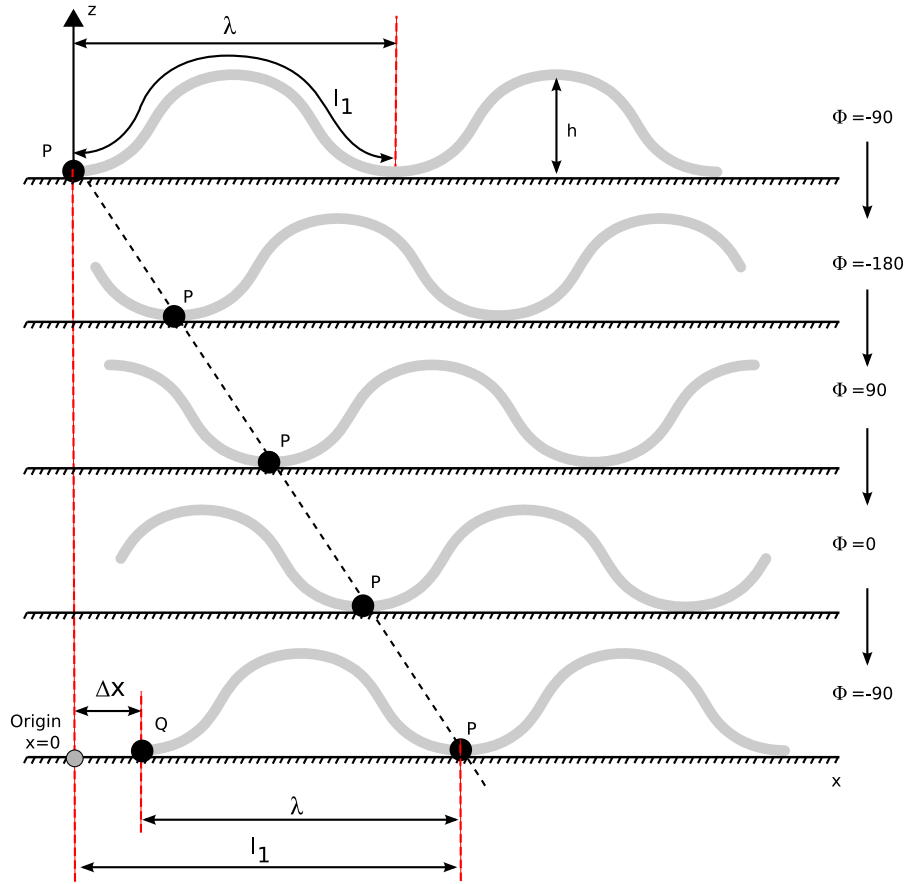


Figure 4.13: Step characterisation

4.2.6 Step characterisation

Of all the points of the shape space, only in those which fulfil the principle of stability the locomotion will be statically stable. This is the region where it could be known a priori which is the step that the robot takes in function of the parameters k and α .

4.2.6.1 Step equation

Step principle: *If the movement is statically stable and assuming that there is no slipping of the supporting points, the robot's step is calculated by means of the equation 4.1*

$$\Delta x = (l - w) \frac{1}{k} = \frac{l}{k} - \lambda = l_1 - \lambda \quad (4.1)$$

where l is the robot's length, w the width and k the number of undulations. The deduction is shown graphically in the figure 4.13 where the forward movement of the robot has been represented in five

different phases and with $k = 2$. The reasoning is the same when $k > 2$.

In the beginning there is a robot with an initial phase of -90 degrees. The parameter l_1 is the length of an undulation and is equal to l/k . The wavelength λ is the width of one undulation. It is equal to w/k (eq. 3.21). P is the point of contact with the ground that initially is on the extreme left. On varying the phase, this point moves towards the right.

Assuming that **there is no sliding**, on completing a cycle the point P will have moved a distance equal to the length of an undulation (l_1). A new support point, Q, appears on the left situated on the abscissa $l_1 - \lambda$. The distance that the left extremity of the robot has moved during a cycle is Δx , that is the abscissa of point Q, for which $\Delta x = l_1 - \lambda$. Placing l_1 and λ in function of l and k the final equation 4.1 is obtained.

4.2.6.2 Normalized step

The normalized step Δx_n is defined as the distance that a robot of unitary length advances. It is obtained from the equation 4.1 substituting l for 1:

$$\Delta x_n = \frac{1}{k} (1 - w_n) \quad (4.2)$$

where w_n is the normalized width. The calculation of the step for a robot of generic length is proportional to the normalized step:

$$\Delta x = l \Delta x_n$$

The equation 4.2 can be rewritten putting it exclusively in function of the working point as:

$$\Delta x_n = \frac{1}{k} \left(1 - \int_0^1 \cos(\alpha \cos(2\pi s)) ds \right) \quad (4.3)$$

4.2.6.3 Shape space and steps

The equation 4.3 associates a step to each one of the working points of the shape space. Given that we can only know a priori the step of the movements that are statically stable, the shape space is restricted to the points where the criterion of stability is established ($k \geq 2$).

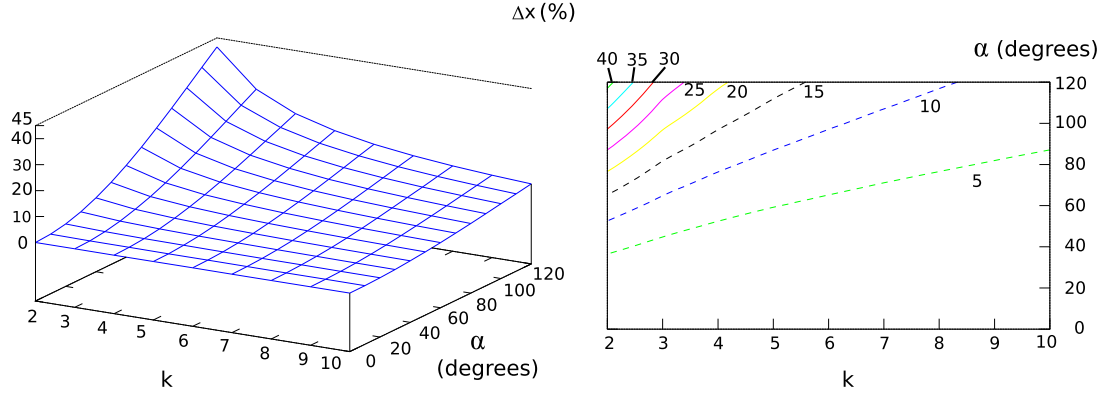


Figure 4.14: Normalized step of a continuous apodal robot in function of the working point (k, α)

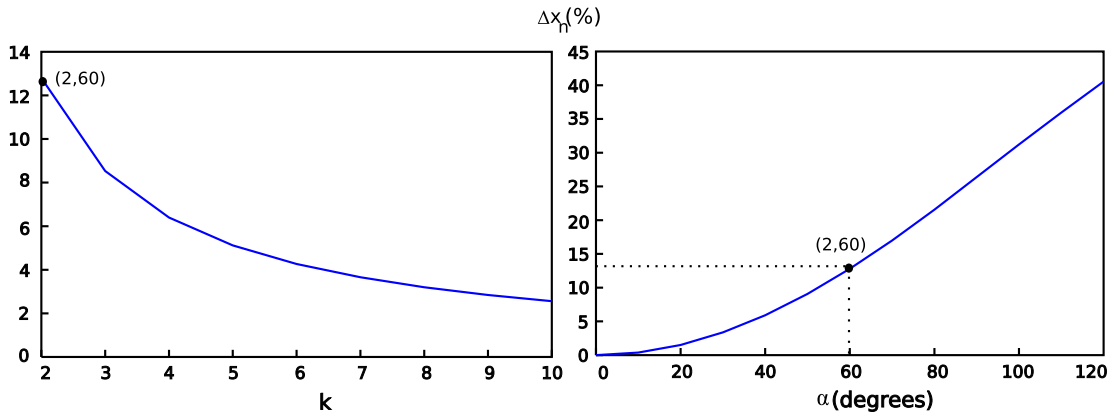


Figure 4.15: Normalized step in the working point $(2, 60)$ and their variation with k and α .

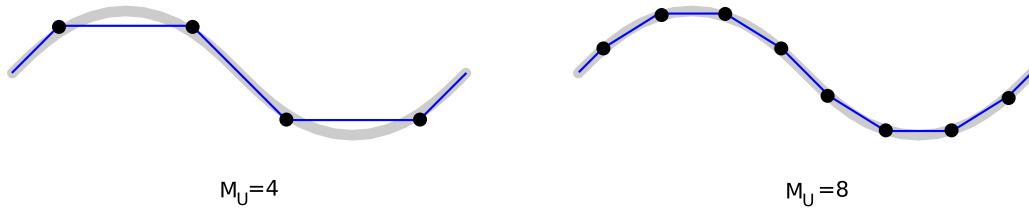


Figure 4.16: Comparison between a continuous serpenoid curve and two discrete serpenoid curves with 4 and 8 modules per undulation

The representation of the step for the points of the shape space with values $k \geq 2$ are shown in the figure 4.14. The maximum value of Δx is approximately 45% of the length and is obtained for the working point $(2, 120)$. That is to say that **the step will be bigger the greater that α is and the lesser that k is.**

In the figure 4.15 the working point $(2, 60)$ is shown and its variation with k and α . The variation of α between 60 and 120 is quite linear.

4.3 Discrete model

4.3.1 Introduction

The real apodal robots are by nature discrete. They are formed by the union of M modules. They are modelled using the same parameters as in the continuous case: winding angle α and number of undulations k . The mathematical model that is used is that of a discrete serpenoid curve/wave, introduced in the section 3.6.3.

In the continuous model, the joints are separated by an infinitesimal distance and an infinite number of them exists. Nevertheless, in the discrete model M modules exist, separated by a fixed distance d . The shape and properties of the robot depend, also, on the number of modules M that exist. To study the basic shapes a new parameter is defined, **the number of modules per undulation:**

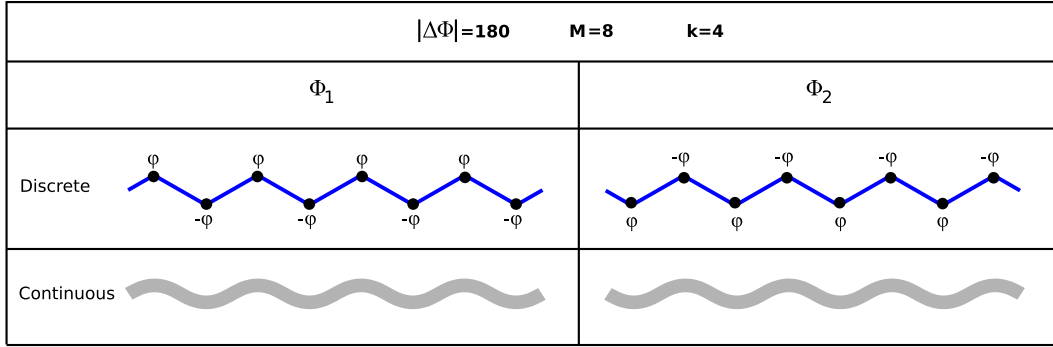
$$M_u = \frac{M}{k} \quad (4.4)$$

The parameter M_u is that which defines the shape of the undulations of the robot. So that the undulations of a robot with $M = 8$ and $k = 2$ will be the same as another with $M = 4$ and $k = 1$. Both with $M_u = 4$.

In the figure 4.16 a continuous serpenoid curve is shown on which two discrete serpenoids have been superimposed, one with four modules per undulation and the other with eight. The greater M_u , the more it will be like the discrete to continuous model.

Parameter	Description	Range
$\Delta\phi$	Phase difference	$\Delta\phi \in [-180, 180]$
M	Number of modules	$M \geq 2$
M_u	Modules per undulation	$M_u \in [2, M]$
k	Number of undulations	$k \in [1, M/2]$
A	Amplitude of the generators	$A \in [0, A_{max}]$, $A_{max} \leq 90$,
α	Winding angle	$\alpha \in [0, \alpha_{max}]$, $\alpha_{max} \leq 120$

Table 4.1: Parameters and their ranges for the discrete apodal robot model

Figure 4.17: Robot shape when $|\Delta\phi| = 180$ for the phases in which the bending angle is maximum

Due to this discretization process, limitations will appear in the values of α and k . Also, **the shape of the wave during the propagation will not be constant**, in contrast to the continuous case.

To study the properties of a discrete apodal robots' locomotion it is assumed that there are M blocks, each one with one pitch-joint (module blocks). The value of the pair of parameters d_0 and d will be therefore $L/2$ and L respectively (see table 3.1). For the study of the properties of locomotion in a straight line of the pitch-yaw group of robots, the results of this chapter can be applied directly, redoing the calculations using the corresponding values of d_0 and d .

The normalized discrete apodal robot is that which has $d = 1$. All the graphs of this section will be drawn considering normalized discrete robots.

4.3.2 Differences to the continuous model

In the discrete model limitations appear in the values of its parameters, that are summarised in the table 4.1. They will be analysed in the following sections.

4.3.2.1 Limitations on the phase difference ($\Delta\Phi$)

In the continuous model the joints are separated by an infinitesimal distance ds , and therefore the phase difference between the points s and $s + ds$ is also infinitesimal ($\Delta\phi \rightarrow 0$). Nevertheless, in

the discrete model this phase difference is given by the equation 3.40. It depends on the number of modules (M) and the undulations (k). If this equation is rewritten in function of the parameter M_u and the phase difference is expressed in degrees, it is:

$$|\Delta\phi| = \frac{360}{M_u} \quad (4.5)$$

By the definition of $\Delta\phi$, its range of values are found between -180 and 180 degrees. When $|\Delta\phi| = 180$, the consecutive joints are out of phase and therefore its bending angle fulfils $\phi_i = -\phi_{i+1}$. In the figure 4.17 the shape is shown that two discrete robots have when $|\Delta\phi| = 180$ for the phases where the bending angle is maximum. In these conditions all the joints have the same absolute value, but with contrary signs. The robot is formed of chained isosceles triangles. A robot of eight modules has been represented, with four undulations. In the lower part the equivalent continuous serpenoid curves have been drawn.

4.3.2.2 Limitations of M_u

Substituting the value $|\Delta\phi| = 180$ in the equation 4.5 gives the result that the minimum number of modules per undulation M_u is equal to 2. In this situation ($M_u = 2$) the robot has the shape shown in the figure 4.17 ($M_u = M/k = 8/4 = 2$).

The maximum value of M_u is equal to the number of modules. It is obtained for $k = 1$. In the theoretical model, there could be as many modules per undulation as desired, as M could be enlarged accordingly. Nevertheless, in practise the limitation will be given by the maximum torque of the servos employed in implementing the worm. A greater M_u , more modules will have to be raised, requiring a higher torque.

This thesis concentrates only on the kinematics and will not consider the torque of the motors, that we will suppose can be infinitely great. For this reason the range of values of the number of modules per undulation is $M_u \in [2, M]$, and M is an unbounded whole number.

4.3.2.3 Limitations of k

When the number of undulations are increased, the value of M_u decreases, as M is constant (eq. 4.4). Therefore, the maximum value of k is given by:

$$k_{max} = \frac{M}{M_{u_{min}}} = \frac{M}{2}$$

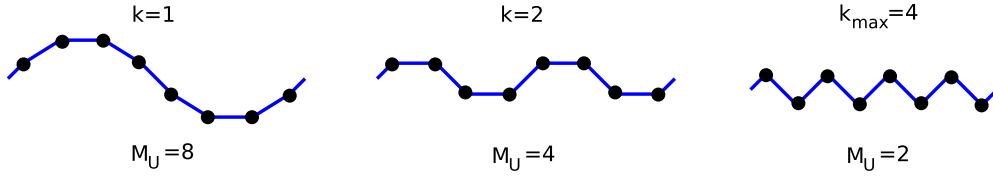


Figure 4.18: The shape of an M module discrete apodal robot when k is equal to one, two and four. It cannot have more than four undulations.

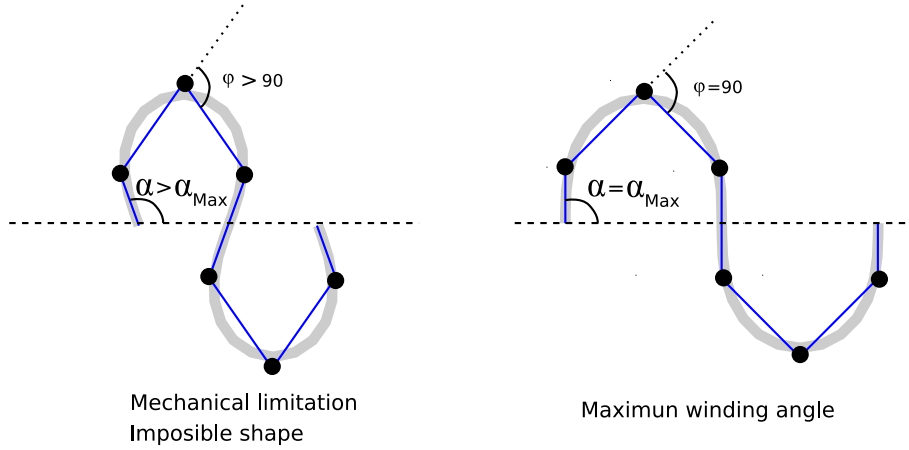


Figure 4.19: Limitation of the maximum value of the bending angle

In the figure 4.18 an eight module robot is shown with 1, 2 and 4 undulations. There cannot be more than 4 undulations.

As k and M_u are inversely proportional, the bigger that k is, the fewer number of modules there will be in each undulation and therefore the greater the error of the process of discretization. That is to say, the difference between the continuous serpenoid curve and the discrete one will be greater.

4.3.2.4 Mechanical limitations

In the continuous model, because of the serpenoid curve's geometry, the winding angle cannot be more than 120 degrees. Beyond this value there will be a collision between points of the same curve. In the discrete model, as well, there is a limitation of the maximum value of the bending angle, that cannot be greater than 90 degrees, due to the buffer on the servos used for its implementation. Therefore, the parameter A must always fulfil $A \leq 90$. There are, therefore, two limitations:

- **Servo limitation.** The bending angle of the servo can never be greater than its buffer ($A \leq 90$).
- **Geometrical limitation.** The winding angle α can never be greater than 120 degrees.

What is more, the parameters A and α are joined by the equation 3.39. The limitation of one parameter will affect the other and vice-versa. Therefore, in general in the discrete model there will be the following restrictions:

$$\alpha \leq \alpha_{max} \leq 120$$

$$A \leq A_{max} \leq 90$$

The figure 4.19 shows graphically a situation where there are limitations because of the servo. On the left it is drawn in a way that is NOT possible, in which $\alpha > \alpha_{max}$ and therefore violates the mechanical limitation of one of the joints and $\varphi > 90$, which is impossible. In the robot on the right, the value of A is 90, which means that there is at least one bending angle for a given phase in which φ will be 90. This limits the winding angle to a value inferior to its buffer of 120.

Therefore, not all the points of the control space H_1 and of the shape space h_1 are valid, only those that are found in the regions for which $A \in [0, A_{max}]$ and $\alpha \in [0, \alpha_{max}]$. For the rest of the points one or other of the previous limitations will be violated.

4.3.2.5 Regions of limitations

The parameters A_{max} and α_{max} depend on M_u and are given by the following equations:

$$\alpha_{max} = \begin{cases} \frac{45}{\sin(\frac{\pi}{M_u})} & M_u \leq M_{uL} \\ 120 & M_u > M_{uL} \end{cases} \quad (4.6)$$

$$A_{max} = \begin{cases} 90 & M_u \leq M_{uL} \\ 240 \sin\left(\frac{\pi}{M_u}\right) & M_u > M_{uL} \end{cases} \quad (4.7)$$

The constant M_{uL} divides the range of M_u into two regions, in each one of which appears a limitation. It is expressed as:

$$M_{uL} = \frac{\pi}{\arcsin\left(\frac{3}{8}\right)} \approx 8.2$$

When $M_u < M_{uL}$, the limitation is due to the servos. In this region $A_{max} = 90$ and α_{max} will always be less than 120 degrees. It is the example shown in the figure 4.19. The robot on the right has a joint

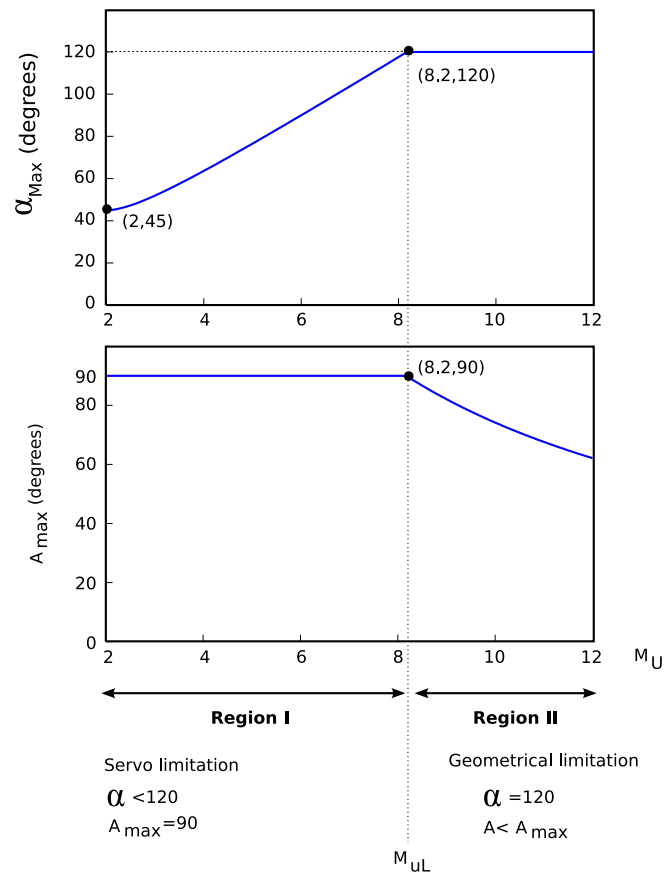


Figure 4.20: Graphical representation of α_{\max} and A_{\max} in function of M_u . The two regions of limitations are shown

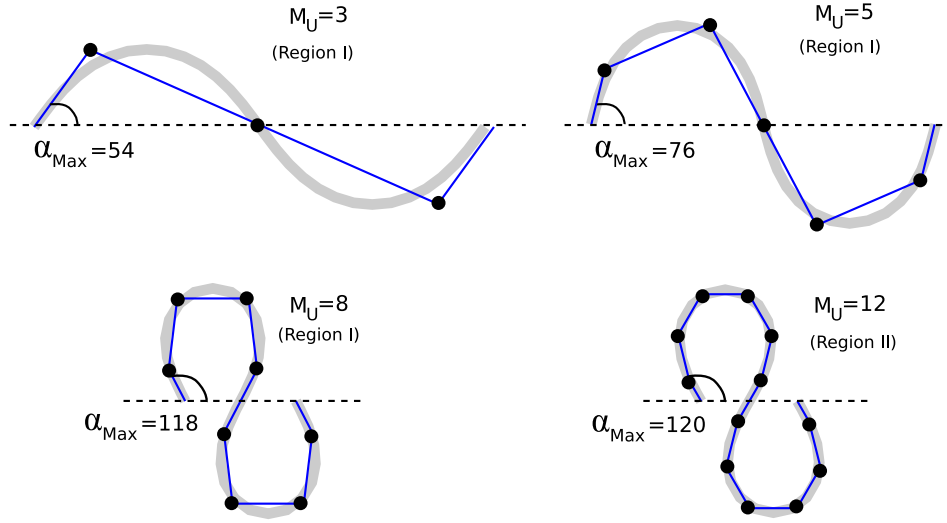


Figure 4.21: Graphical representation of the maximum winding angle for four different values of M_u .

with a bending angle equal to 90. This limits the maximum value of α . If α increases, this join will have an angle greater than 90, which is not possible because of the buffer.

In the region $M_u > M_{uL}$, the limitation is due to the geometry. In it $\alpha_{max} = 120$ and $A_{max} < 90$. If amplitudes greater than A_{max} are applied, parts of the robot will collide and the restriction $\alpha \leq 120$ will be violated.

In the figure 4.20 the graph of α_{max} and A_{max} is shown in function of M_u , as well as the two regions of limitation. In the figure 4.21 the shape of four robots have been graphically represented for values of M_u of 3, 5, 8 and 12. The first three are in the region I and the last in II.

Deduction of the expressions The equation 3.39 that relates the parameter A of a discrete serpenoid with the winding angle α can be rewritten in function of M_u as:

$$A = 2\alpha \sin\left(\frac{\pi}{M_u}\right) \quad (4.8)$$

Extracting the winding angle the result is:

$$\alpha = \frac{A}{2 \sin\left(\frac{\pi}{M_u}\right)}$$

A and α are directly proportional for which the maximum value of α is obtained for the maximum value of A , that is 90. What is more, it must always be less than or equal to 120 which gives the inequation:

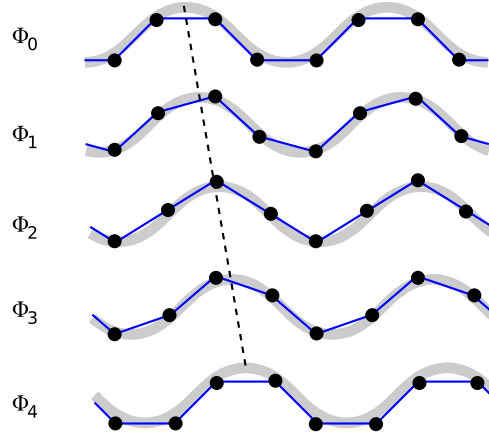


Figure 4.22: Variation of the shape of an apodal robot with the phase

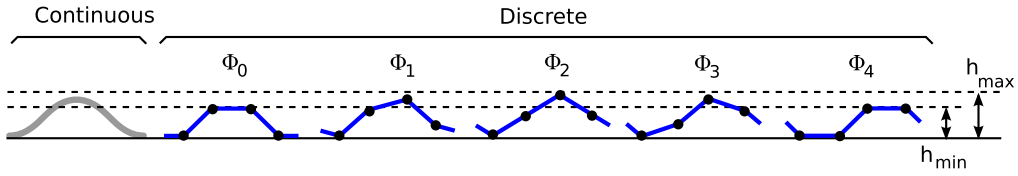


Figure 4.23: Variation of the dimensions with the phase

$$\alpha_{max} = \frac{45}{\sin\left(\frac{\pi}{M_u}\right)} \leq 120$$

Clearing M_u the value of M_{uL} , that delimits the two regions, is obtained:

$$M_{uL} = \frac{\pi}{\arcsin\left(\frac{3}{8}\right)} \approx 8.2$$

To obtain the expression of A_{max} the equation 4.8 is particularised for $\alpha = 120$. It will be valid in region II.

4.3.2.6 Behaviour with the phase

Another difference between the discrete and continuous models is the behaviour with the phase. In the continuous model the wave shape is the same, only it is displaced. Therefore the wave's dimensions of height and width remain constant with the phase. Nevertheless, in the discrete model the orientation of the segments changes with the phase. In the figure 4.22 the shape of a discrete apodal robot with 8

joints is shown for different phases. The continuous and discrete curves have been superimposed. In the phase ϕ_0 each undulation has the shape of a trapezium. Nevertheless, in the phase ϕ_2 the shape is triangular.

In the figure 4.23 the shape of an undulation of four articulations is shown for different phases and is compared with a continuous undulation. The height of the discrete undulation varies between a maximum and a minimum that are reached in the phases ϕ_0 and ϕ_2 respectively.

As is indicated in the section 3.6.3.4 the dimensions of a discrete serpenoid wave are defined as the maximum ones reached to vary ϕ . To speak of the height of an apodal robot as being 8 cm, for example, means that at least one phase will exist in which the height will have this value, though in all the other phases it could be less.

4.3.3 Discretization

In this section a criterion will be established to compare the continuous and discrete models. First the discretization error is defined and then the criteria are proposed that indicate when a continuous robot can be approximated to a discrete one and the error that is being made.

The comparison will be made supposing normalized discrete waves ($d = 1$) with only one undulation ($k = 1$).

4.3.3.1 Discretization error

Given a serpenoid wave with a winding angle α the discrete serpenoid wave is defined as the equivalent of M_u joints which has the same parameter α .

The comparison of the discrete and continuous waves will be made based in the worst case difference between the dimensions. We will calculate the relative error and will express it in terms of percentage. The normalized dimensions for the continuous and discrete model depend on the winding angle. The worst case is that in which the curvature is greatest, which is produced when the winding angle is the maximum possible ($\alpha = \alpha_{max}$).

The **error in height**, ε_h , is defined in the following way:

$$\varepsilon_h = \frac{h_c(\alpha_{max}) - h_d(\alpha_{max})}{h_c(\alpha_{max})}$$

where $h_c(\alpha_{max})$ is the normalized height of the continuous serpenoid wave for the maximum winding angle and $h_d(\alpha_{max})$ is the same but for the discrete wave. In a similar way the **error in width** is defined:

$$\varepsilon_w = \frac{w_c(\alpha_{max}) - w_d(\alpha_{max})}{w_c(\alpha_{max})}$$

From this **the discretization error** is defined as the maximum value of the errors in the dimensions:

$$\varepsilon_d = \max \{ \varepsilon_h, \varepsilon_w \}$$

With this definition, to speak of a 5% discretization error indicates that both the height and the width show a difference less than or equal to 5% in comparison to the continuous model's dimensions.

4.3.3.2 Discretization criteria

In this section three criteria are established to compare the discrete with the continuous model according to the different values of discretization error. They are:

- **Criteria of 15%:** If $M_u \geq 3$ then the discretization error is less than or equal to 15%.
- **Criteria of 10%:** If $M_u \geq 5$, then the discretization error is less than or equal to 10%.
- **Criteria of 5%:** If $M_u \geq 7$, then the discretization error is less than or equal to 5%.

The criteria that is employed in the rest of the sections will be that of 5%. Therefore the following affirmations can be made:

Principle of discretization: *The discrete robots that have a number of modules per undulation greater than or equal to 7 can be approximated for the continuous equations with an error less than 5% in their dimensions.*

Demonstration In the graph of figure 4.24 the discretization error is shown (ε_h and ε_w). From them are deduced the different discretization criteria. It is seen that the error in the width is always less than that of the height, therefore, it is ε_h which determines the discretization error. It is proved that for $M_u \geq 7$, the discretization error is less than or equal to 5%. The error in the width tends rapidly to reduce to 0 when M_u increases. The error in the height tends to diminishes more slowly and with oscillations.

In the graph at the right of the figure 4.24 the absolute error in the normalized height with respect to its length is represented. It can be seen how this error decreases with α and is a maximum when α is equal to α_{max} . If it is guaranteed that the error is below a threshold for α_{max} then it will be for any $\alpha < \alpha_{max}$.

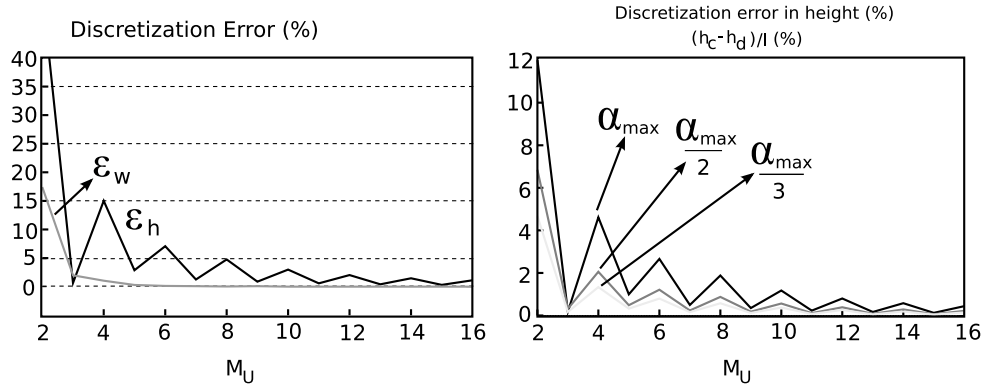


Figure 4.24: Left: Discretization error in function of M_u . Right: Absolute discretization error in height for different values of α .

4.3.4 Shape

4.3.4.1 Shape, phase and modules per undulation

The discrete apodal robots have different shapes according to the phase. When the wave is propagated its shape as well as its dimensions change. This variation with the phase can be represented in a diagram as is shown in the figure 4.25. On one hand, when M_u increases the shape increasingly becomes like that of the continuous model. According to the discretization criteria set forth in the section 4.3.3.2, when $M_u \geq 7$ the difference in the dimensions is less than 5%. In the case of the limit, $M_u = 2$, the variation of the phase makes the worm compress and expand. In this case a global wave is not propagated.

4.3.4.2 Shapes and winding angle

The variation of the shape with α is shown in the figure 4.26. As we show in the section 4.3.2.5, the maximum value of α increases with M_u until it reaches the highest value of 120 degrees where the geometric limitations appear. When α is increased maintaining the same M_u , the height increases and the width decreases.

4.3.4.3 Shape space

The same as in the continuous case, the shapes of the robot will be represented as points in the shape space. But in the discrete case, the points are the pairs (M_u, α) . With this we are representing the shape that one undulation has. Also, owing to the mechanical limitations it does not deal with a rectangular space, but the region that is between the axis M_u and the curves $\alpha = \alpha_{max}(M_u)$ and $\alpha = 120$ (eq. 4.6).

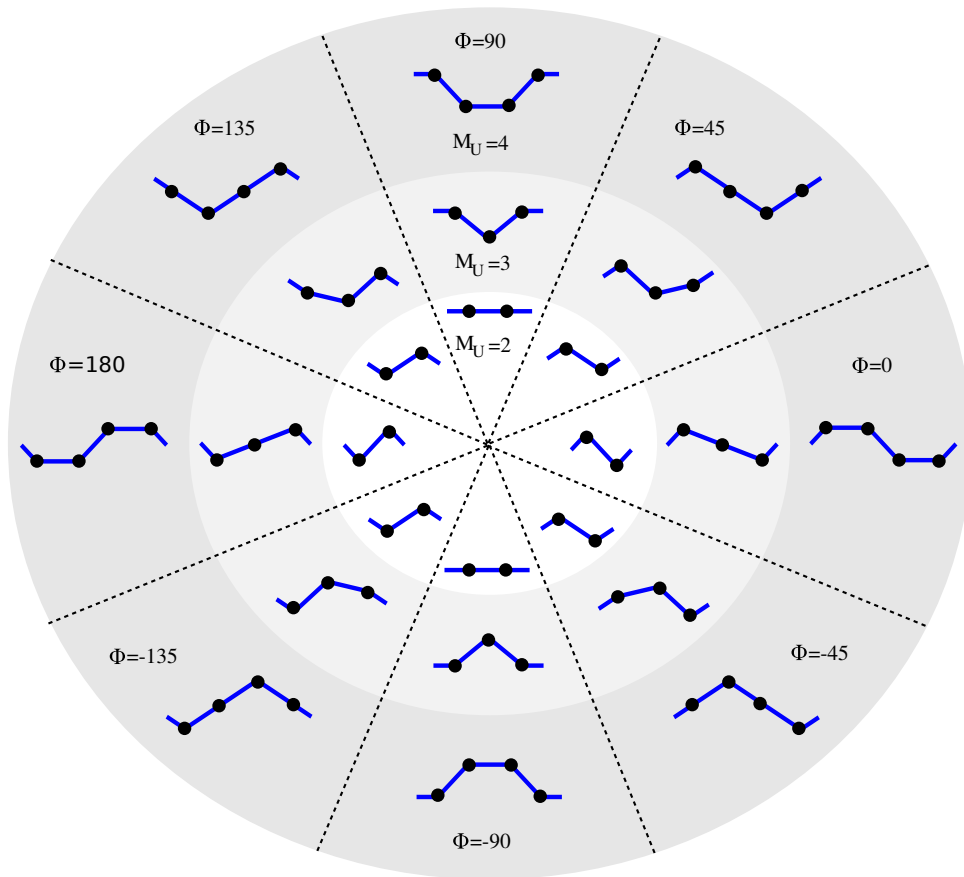
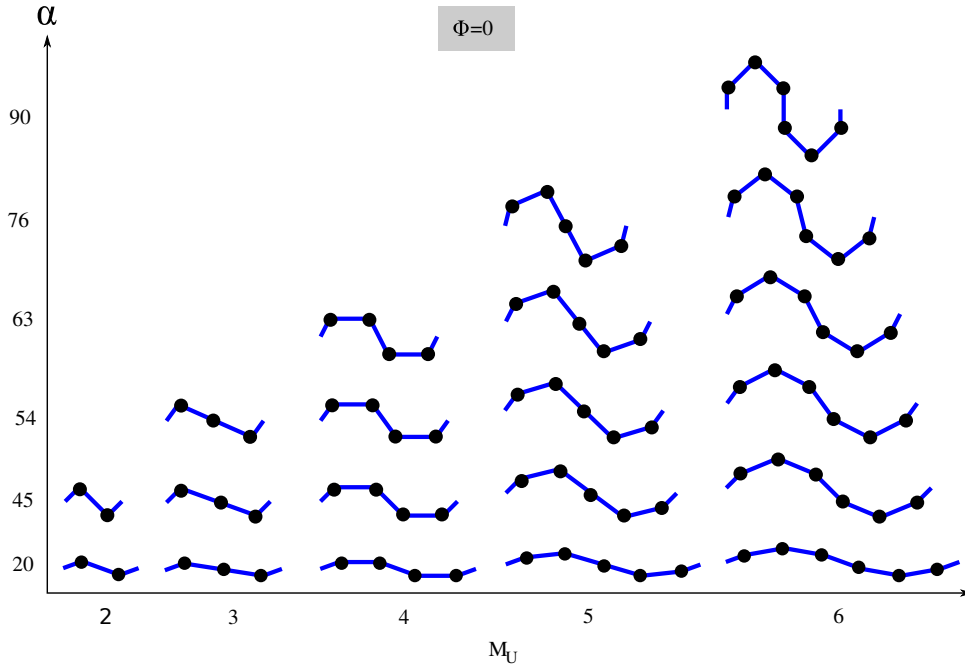


Figure 4.25: Variation of the robot's shape with M_U and the phase

Figure 4.26: Variation of the robot's shape with α and M_u

In the figure 4.27 a region of the shape space is shown and the aspect of the discrete apodal robots for different working points. The maximum value of M_u is M , that is obtained when $k = 1$ and the minimum is 2, corresponding to $k = M/2$.

4.3.5 Dimensions

In this section we will represent graphically the dimensions of the discrete robot for the different points in the shape space, together with the variation with the phase. The dimensions obtained are normalized in relation to the length of a block (d) and not so in relation to the total length (l) as in the continuous case. To obtain the dimensions of a generic robot they will have to be multiplied by the value of their parameter d .

4.3.5.1 Height

The normalized height of a discrete apodal robot is given by the equation 3.37 and it has been represented graphically in the figure 4.28. On one hand the height increases with M_u . This is logical. The greater the number of modules, greater will be the total length of a robot's undulation and therefore greater will be the height. It also increases with α , as in the continuous case.

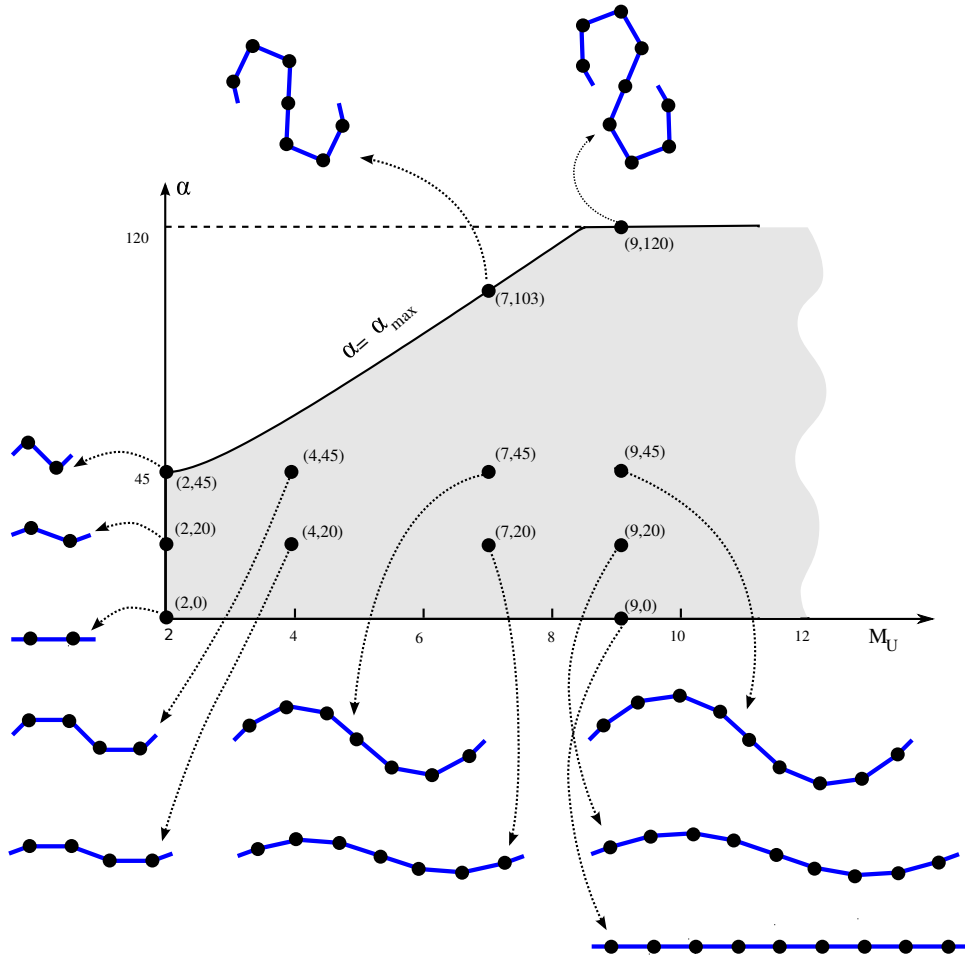
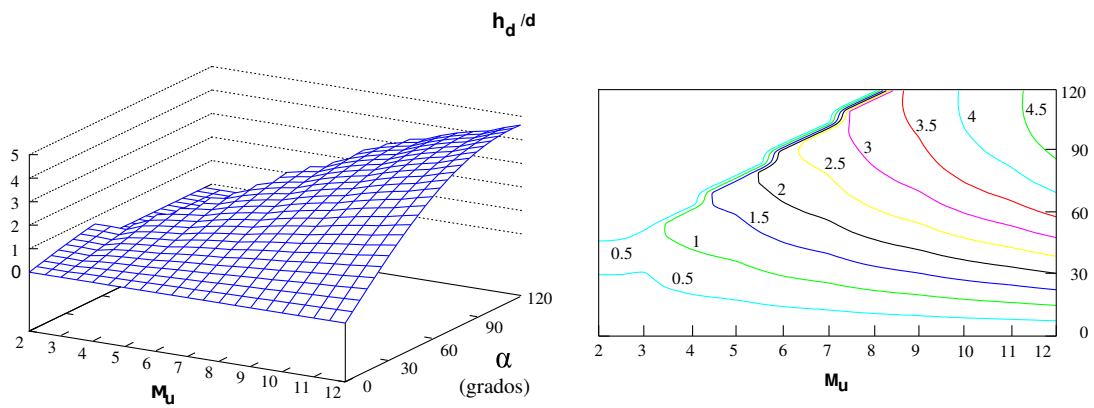


Figure 4.27: Shape space of the discrete apodal robots

Figure 4.28: Maximum normalized height of a discrete apodal robot (h_d) for every point in the shape space. The height is normalized in relation to the length of a block (d)

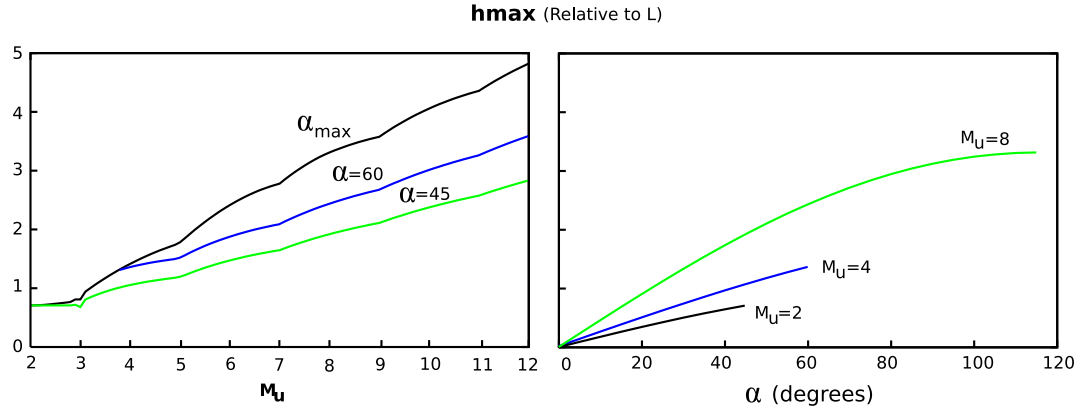


Figure 4.29: Variation of the height for different working points. **Left:** variation with M_u (shown for three different values of the winding angle). **Right:** Variation with α (shown for three different values of the M_u).

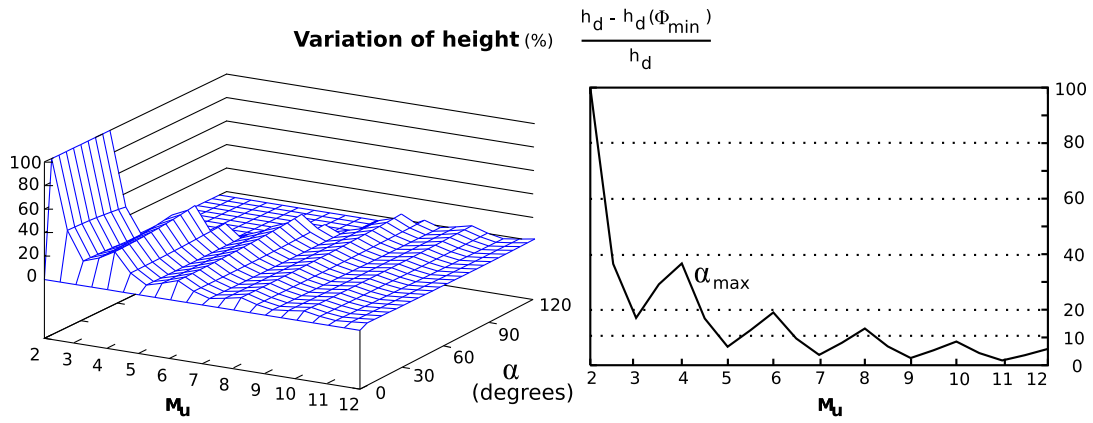


Figure 4.30: Variation of the height

In the figure 4.29 the variation for different working points is shown. On the left the variation with M_u has been drawn for different values of the winding angle. On the right is the variation with α , for robots with distinct number of modules per undulation.

The height varies also with the phase. By definition, the h_d is taken as the maximum value between phases (eq. 3.35). We denote the minimum value as $h_d(\phi_{min})$. So, the expression $h_d - h_d(\phi_{min})$ indicates the maximum variation of the height with the phase. This variation, relative to the maximum height, is represented graphically in the figure 4.30. When M_u increases the discrete robot becomes more like the continuous and therefore the variation in height will tend to zero. For values of M_u greater than 8, this variation is less than 10%.

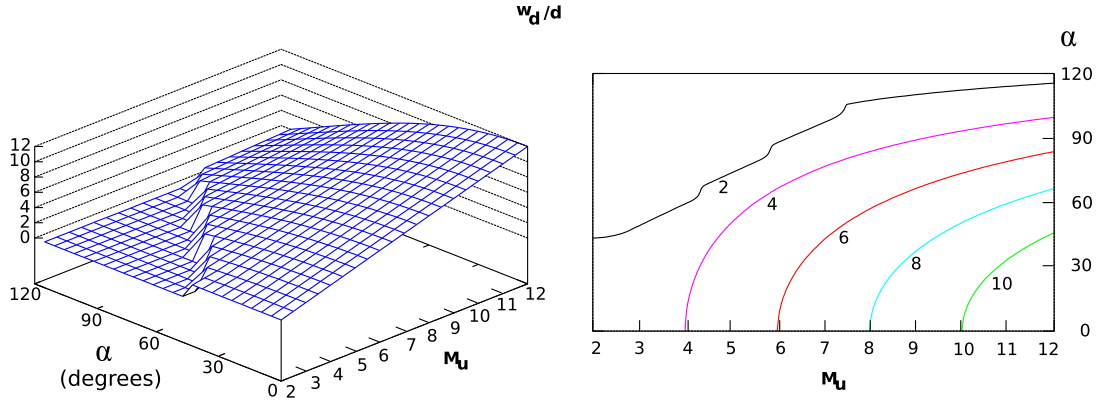


Figure 4.31: Maximum normalized width of the discrete apodal robot (w_d) for every point in the shape space. The width is normalized in relation to the length of the block (d)

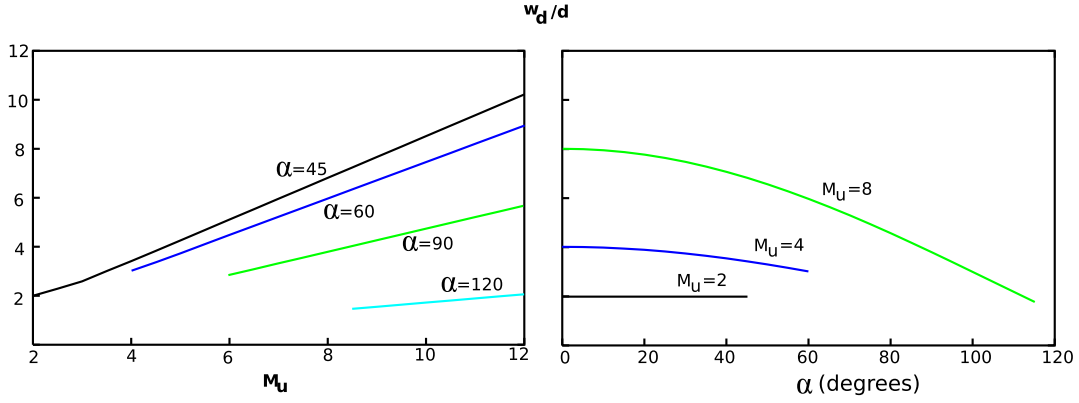


Figure 4.32: Variation of the width for different working points. **Left:** Variation with M_u . **Right:** Variation with α .

4.3.5.2 Width

We will study the width of the discrete apodal robots for an undulation (in this case the width will be equal to the wavelength). Its value is determined by the equation 3.38 and is shown graphically in the figure 4.31. The same as with the height, when M_u increases the width also increases. It also increases when α diminishes. When $\alpha = 0$, the robot is a straight line situated on the x axis and with a length equal to M_u .

In the figure 4.32 the width of different working points is shown. To the left the drawing shows the variation with M_u for robots with different values of α . To the right the variation with α is shown for three robots with values M_u of 2, 4 and 8 respectively.

The width also varies with the phase. We define the variation of the width by means of the expression $w_d - w_d(\phi_{min})$. It indicates the maximum variation of the width with the phase. It is represented graphically in the figure 4.33. It is observed that this variation falls very quickly with M_u and for

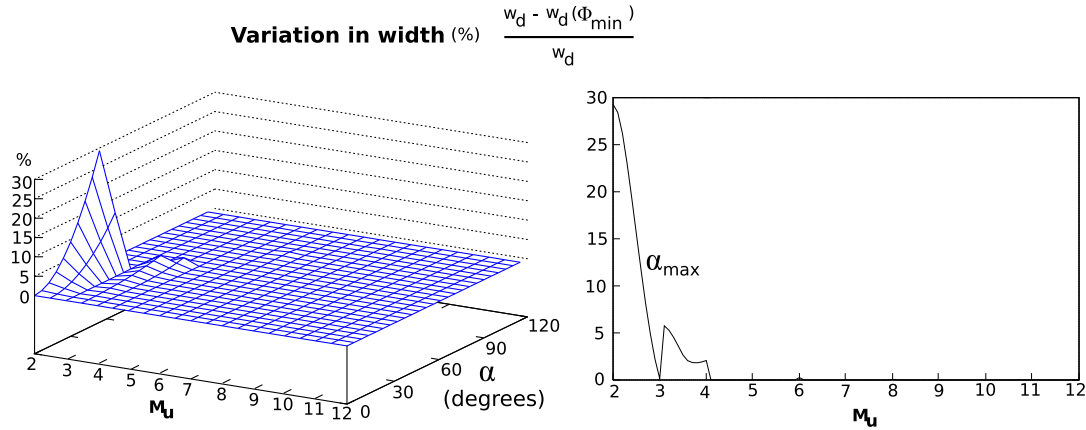


Figure 4.33: Variation of the wavelength

values above 3, the variation is below that of 5% (approximately). This implies that from $M_u \geq 3$ **the width remains practically constant during the propagation of the wave.**

4.3.6 Stability

The criterion for stability obtained for the continuous model (section 4.2.5) also applies for the discrete case. At every instance during the propagation of the wave there must exist at least two supporting points and the projection of the robot's centre of gravity must be situated between them. This is always guaranteed as long as $k \geq 2$. When this criterion is not fulfilled and $k < 2$ will exist a phase in which the robot will have only one supporting point, which means it will incline either forwards or backwards.

In the figure 4.34 the idea is shown applied to an apodal robot with $M_u = 3$. Two robots have been represented, one with $k = 1$ and the other with $k = 2$ for four different phases and they are compared to the shape of a discrete serpenoid wave.

In the case of $k = 2$, the robot has the same shape as a discrete curve, but "duplicated". There will always be at least two supporting points which means it is stable in all the phases. Unstable phases exist in the case of $k = 1$ in which the robot inclines. The worst case is produced for a 90 degree phase, where there is only one supporting point situated in the centre. The robot will incline forwards, backwards or oscillate.

That it does not fulfil the criterion of stability does not imply that locomotion is non-existent, only that it must be taken into account that some phases of transition are more abrupt. If the locomotion is carried out with high values of α , the transition will be very abrupt and the robot could suffer damage. Nevertheless, for small values it will be almost unperceived.

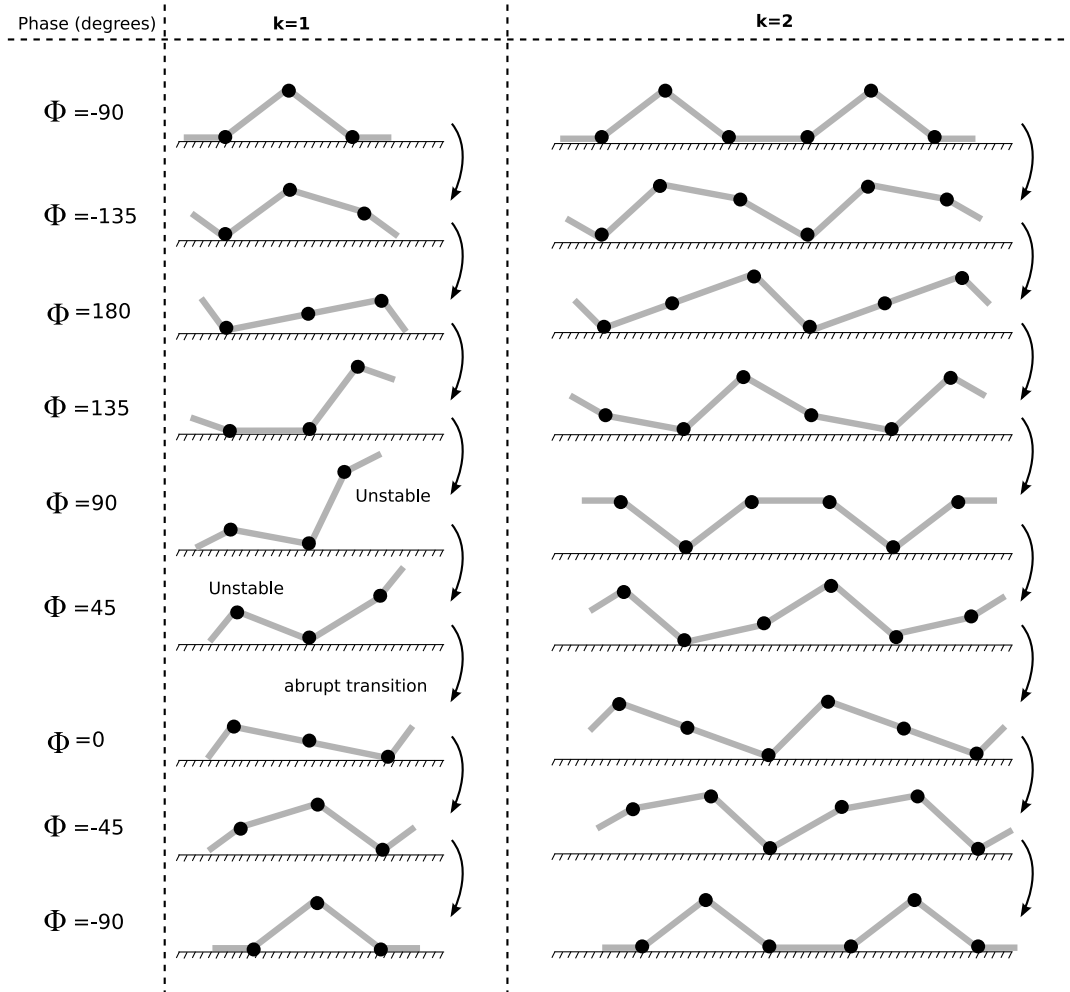


Figure 4.34: Stability of a discrete robot with $M_u = 3$ for values of k equal to 1 and 2

4.3.7 Characterisation of the step

4.3.7.1 Equation of the step

The way to calculate the step in the discrete apodal robots is similar to that in the continuous case. Supposing that no slipping of the supporting points exists and that the wavelength remains constant during its propagation, the step is calculated applying the equation of the continuous case (eq. 4.1). The figure 4.35 shows the movement of two discrete robots during a cycle, of 3 and 4 modules per undulation with $k = 2$.

Nevertheless, when dealing with a discrete robot **the width does not remain constant during the propagation**. For some phases the robot will have a greater width than others. This means that the distance between the two supporting points, the left one and the right one, will vary with the phase, causing, at the same time, that they slide on the surface. In the example of figure 4.35, during the first transition between the first two phases shown we have assumed that the two support points are situated at the same distance and that they remain immobile in respect to the ground. Nevertheless this generally does not happen. The geometry of the discrete curve implies that during the transition between these two phases this distance does not have to be equal. The left or right support point (or both) will have to move.

Principle of discrete robot's step : *If the movement is statically stable, the number of modules per undulation is greater than or equal to 3, and the ground is such that it does not allow the support points to slip, the robot's step is given by the equation 4.1.*

As we show in the section 4.3.5.2, the width of the discrete robot varies less than 5% when $Mu \geq 3$. This variation, besides, is practically non-existent for values greater than 4. In these cases, therefore, the step equation for the continuous robot can be applied to the discrete robot.

4.3.7.2 Shape space and step

The normalized discrete robot's step, for each one of the working points of the shape space is shown in the figure 4.36. It is observed that when the step increases with M_u : increasing the number of modules per undulation, greater will be the total length and width of the robot. Increasing the values of the winding angle, the width diminishes, therefore the step also increases.

In the figure 4.37 the step for different working points is shown. On the left are drawn the variations with M_u for robots with different values of α . On the right the variation is shown with α for three robots with values of M_u of 3, 4 and 8 respectively.

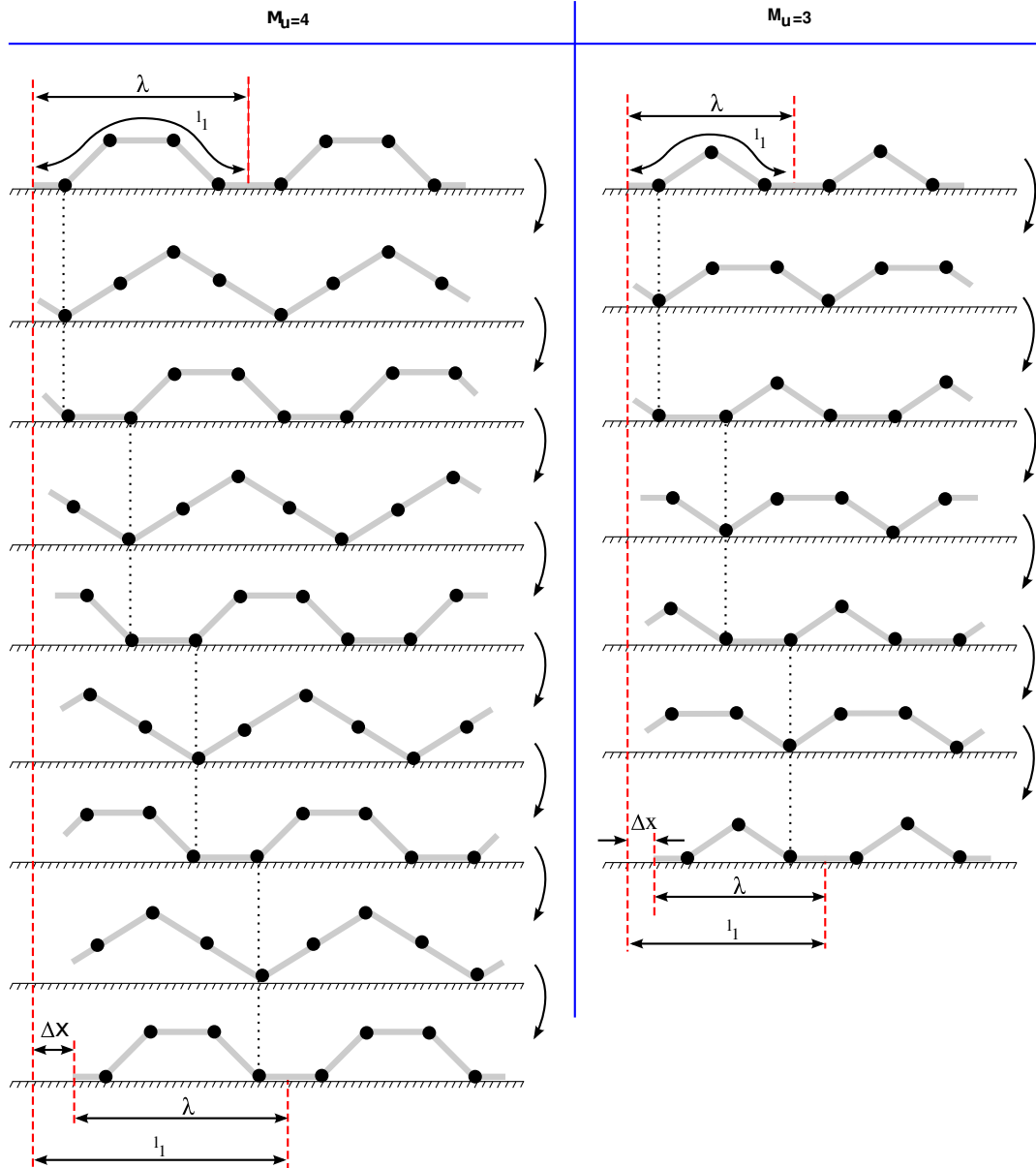


Figure 4.35: Step taken by two discrete robots with 3 and 4 modules per undulation

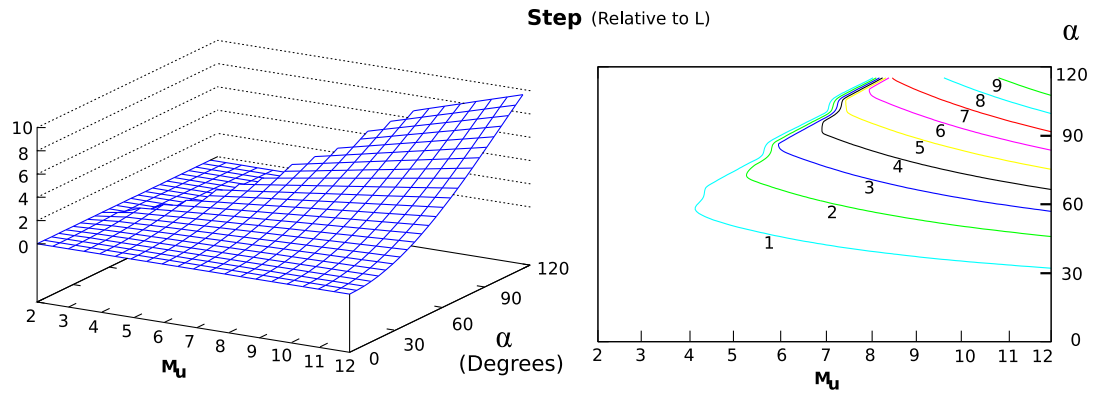


Figure 4.36: Normalized Step of the discrete apodal robot for every point of the shape space.

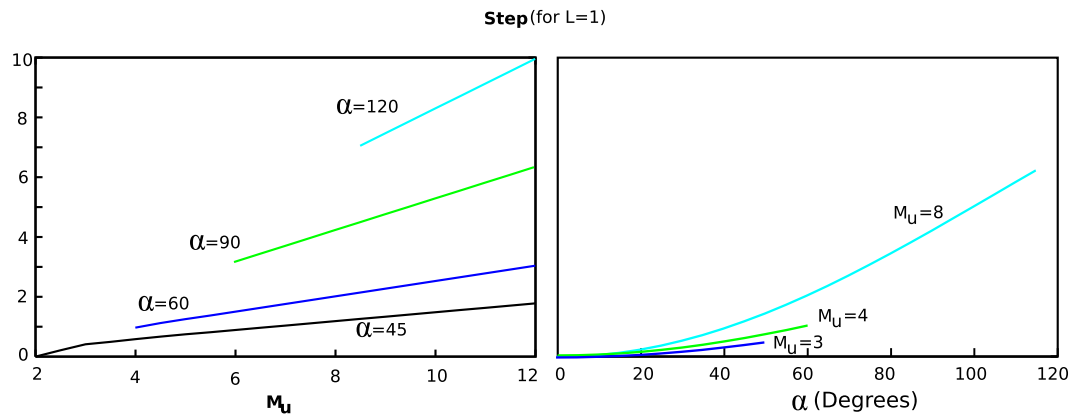


Figure 4.37: Locomotion of the discrete robot for different values of M_u and α

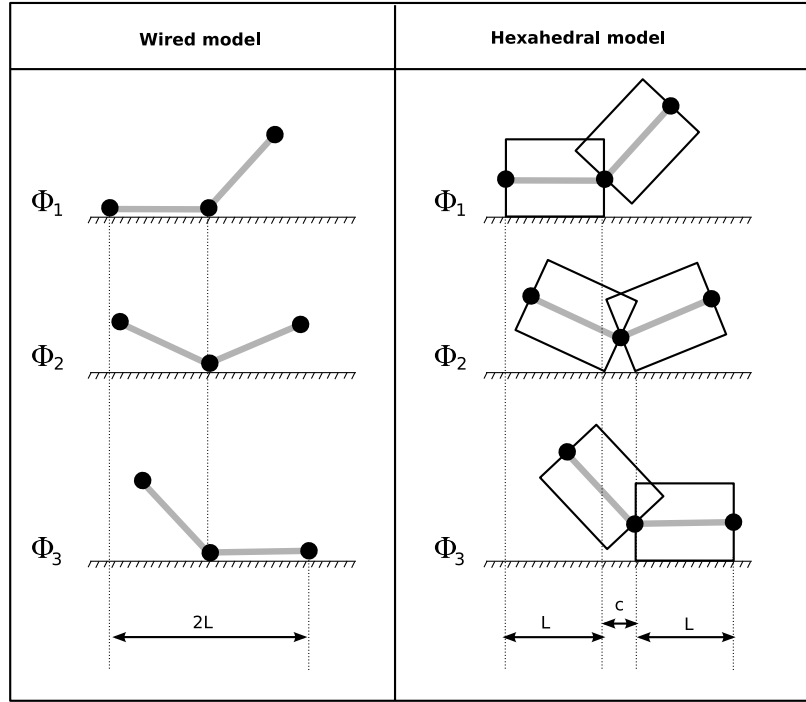


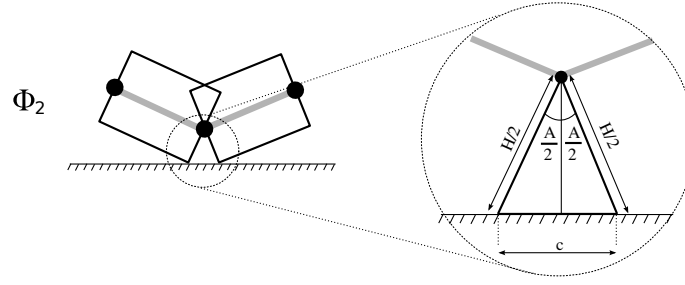
Figure 4.38: Differences between the locomotion of the wired and hexahedral models. Only the three joints on the lower part of the undulation are shown.

4.3.8 Hexahedral model

In this section we will see the relation that exists between wired and hexahedral models and how the equation to calculate the step can be applied.

In the figure 4.38 three articulations have been drawn in the phases ϕ_1 , ϕ_2 and ϕ_3 during the locomotion of an apodal robot of M modules. In these phases the joints shown are on the lower part of the undulation, in contact with the ground. The rest of them have not been drawn. In the wired model each joint is the supporting point on which the other articulations rotate. In the hexahedral model, nevertheless, two supporting points exist. On one the rotation is carried out during the transition from ϕ_1 and ϕ_2 , and on the other during the transition from ϕ_2 and ϕ_3 . Due to this, in each model, the distance between the left hand joint in ϕ_1 and the right hand one in ϕ_3 is different. In the first one it is equal to $2L$, and in the second it is $2L + c$. Therefore, to calculate the robot's step we can approximate the hexahedral model by an equivalent wired one in which case the length of the modules will be $L + c$. The equivalent length is $l_e = M(L + c) = ML + Mc = l + Mc$.

The value of the constant c depends on the dimensions of the hexahedral module. It is in the phase ϕ_2 that it is verified that the turning angle is maximum and has a value equal to the amplitude $\phi_i = A$. For this reason, the constant c is calculated as indicated in the figure 4.39, using the equation:

Figure 4.39: Calculating the c constant of the hexahedral model

$$c = H \sin\left(\frac{A}{2}\right)$$

The equation to calculate the step of the hexahedral model is obtained from the equation 4.1 substituting the length l for the equivalent length l_e :

$$\Delta x = \left(l + MH \sin\left(\frac{A}{2}\right) - w \right) \frac{1}{k} \quad (4.9)$$

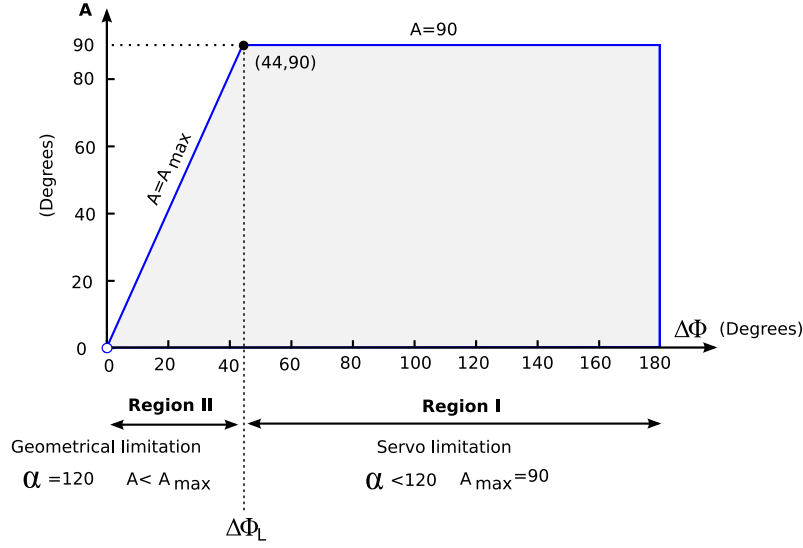
4.4 Kinematics

4.4.1 Introduction

In this section we will deal with the problems of direct and inverse kinematics and will propose a methodology to solve them. The parameters for the control and shape spaces will be established and we will introduce the idea of locomotion region. The proposed solution is based on realising a transformation between the spaces h_1 and H_1 .

4.4.2 Control space

The control space H_1 is formed by the pair of points $(\Delta\phi, A)$ that determine the values of the phase difference and amplitude that is applied to all the sinusoidal generators for the control of the robot. Due to the mechanical limitations described in the section 4.3.2.4, this space is divided into two limitation regions, I and II. From the equation 4.5 the phase difference that limits these two regions is obtained:

Figure 4.40: Graphical representation of the control space H_1

$$\Delta\phi_L = \frac{360}{M_{uL}} = 43.9 \approx 44 \quad (4.10)$$

When $\Delta\phi < \Delta\phi_L$, the limitation is due to the geometry and when $\Delta\phi > \Delta\phi_L$ it is due to the servo's buffer. The equation 4.7 to obtain A_{max} can be rewritten as:

$$A_{max} = \begin{cases} 240 \sin\left(\frac{\Delta\phi}{2}\right) & \Delta\phi < \Delta\phi_L \\ 90 & \Delta\phi \geq \Delta\phi_L \end{cases} \quad (4.11)$$

In the figure 4.40 the control space has been represented graphically together with the two regions of limitation.

4.4.3 Transformation of spaces

We propose to resolve the problems of direct and inverse kinematics by means of transformations between the control and shape spaces. In the case of direct kinematics, given a point P of the control space it has to be determined what is its equivalent point p in the shape space. From p the dimensions of the robot and step are calculated. For inverse kinematics, from the restrictions in the kinematic parameters and the dimensions, the regions in the shape space are obtained and these are transformed into their equivalents in the control space.

In the figure 4.41 both spaces are shown and the correspondence between the points $P_i \in H_1$ and $p_i \in h_1$. The points P_5 and p_5 are those that separate the two limitation regions: I and II and are fixed points that do not depend on M . Not so with the points P_4, P_3, p_4 and p_3 , that do depend on M .

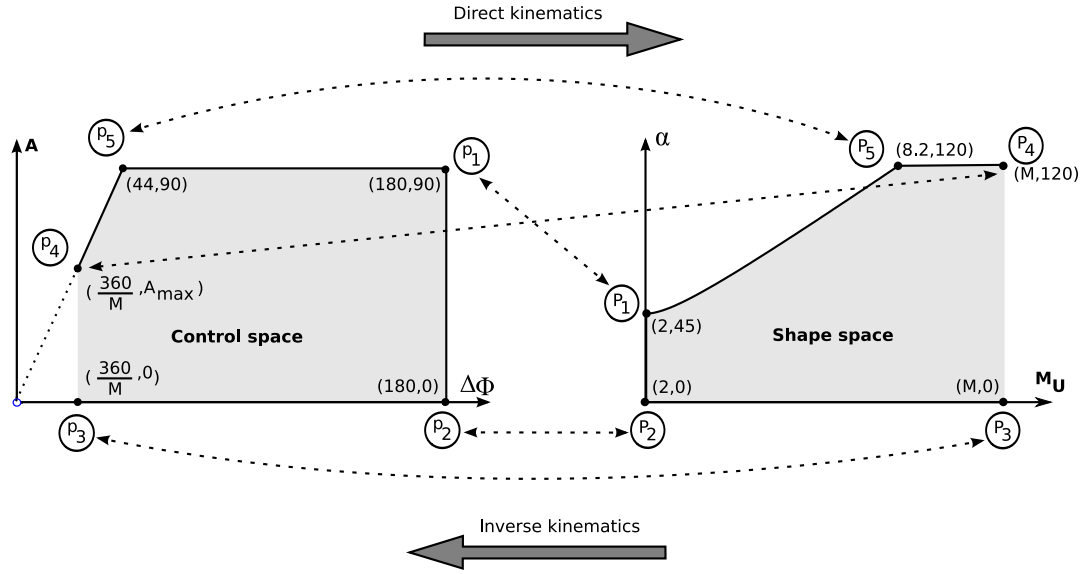


Figure 4.41: Transformation between the control and shape spaces

The equations to realise the transformations have already been presented in previous sections, there follows a summary:

$$A = 2\alpha \sin\left(\frac{\pi}{M_u}\right) \quad (4.12)$$

$$|\Delta\phi| = \frac{360}{M_u} \quad (4.13)$$

4.4.4 Locomotion region

We define the locomotion region as the interior region of the spaces H_1 or h_1 in which the robot is statically stable. By the criterion of stability explained in the section 4.2.5, the movement fulfils this property if it is verified that $k \geq 2$.

Both the step equation (eq. 4.1) and that for calculating the dimensions of the robot (eq. 3.37 and 3.38) are only applicable to the points situated in the locomotion region. The movement of the robot for the points situated outside of this region will not be uniform and will have to be studied using other methodologies.

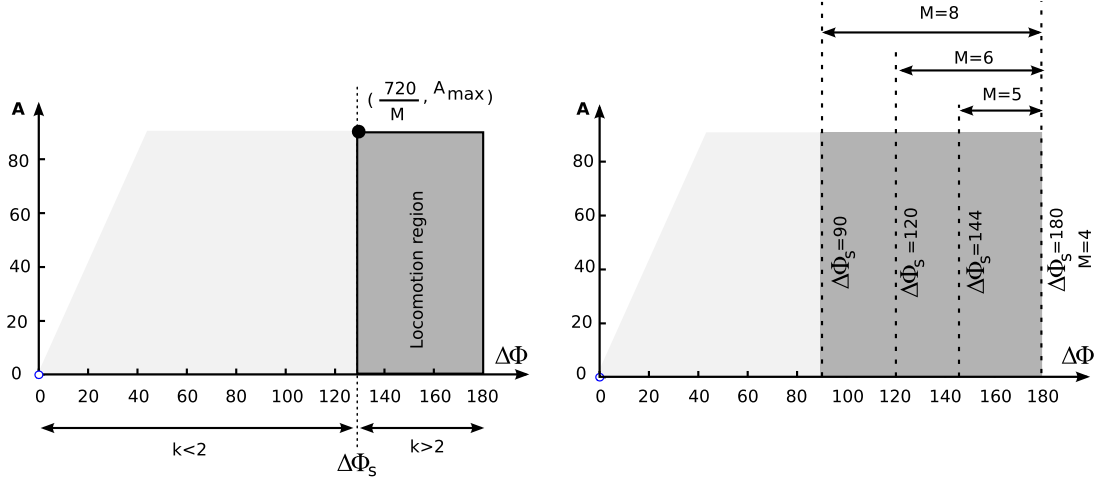


Figure 4.42: Locomotion region in the control space

4.4.4.1 Locomotion region in the control space

For $k = 2$, the number of modules per undulation is $M/2$ and substituting this value in the equation 4.13 the phase difference that determines the boundary between the locomotion region and the rest of the space H_1 is obtained:

$$\Delta\phi_s = \frac{720}{M} \quad (4.14)$$

All the points for which $\Delta\phi > \Delta\phi_s$ belong to the locomotion region and therefore the locomotion of the robot will be statically stable. To the left of the figure 4.42 the space H_1 and the locomotion region are shown. To the right the four locomotion regions that correspond to robots of 4, 5, 6 and 8 modules have been drawn. It can be seen how the region increases with M . If the robot has only 4 modules, this region is just a vertical line. If the number of modules were infinite, the locomotion region would be all of space H_1 .

4.4.4.2 Locomotion region in the shape space

The criteria for stability is fulfilled for all the points of h_1 in which $M_u < M/2$. In the figure 4.43 the locomotion region is shown graphically. Its value lies between M_u equal to 2 and $M/2$. As M increases, this zone increases and expands to the right. The space h_1 , as we saw in the section 4.3.2.4, is divided into two sub-regions of limitation, I and II. When $M/2 < M_{uL}$, the locomotion region is inside the limitation region I, that is to say, that there is a limitation because of the servos' buffer and the winding angle α will never exceed the maximum value of 120 degrees. When $M/2 > M_{uL}$ the locomotion region includes the complete region I and part of II.

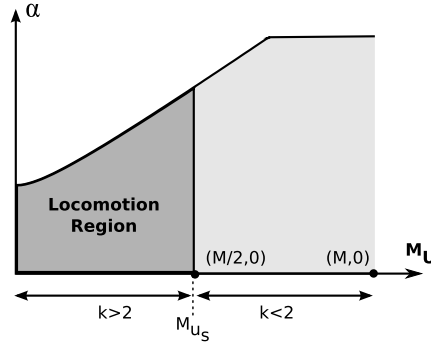


Figure 4.43: Locomotion region in the shape space

The value of M_u that separates the locomotion region from the region in which $k < 2$ is denoted by M_{us} and as we have seen is equal to $M/2$.

4.4.5 Direct kinematics

The problem of direct kinematics is to determine if displacement exists, the step Δx and the dimensions of the robot h and w when an amplitude A and a phase difference $\Delta\phi$ are applied to the sinusoidal generators. It is resolved analysing in which regions of the control space the selected working point is found. According to its location we will know if limitations exist because of the geometry or the servo, if it is an invalid point, if the locomotion is statically stable or not and which is the working point, in the shape space, that determines the dimensions of the robot and the step by which it moves. The stages to follow to resolve the direct kinematics are summed up in the proposed methodology.

4.4.5.1 Principle of symmetry of movement

The sign of the phase difference $\Delta\phi$ determines if the joint $i + 1$ moves a certain phase forwards or backwards in relation to the i . This causes the wave to move forwards or backwards. Therefore, it fixes the direction of the robot's movement, forwards or backwards. This sign only affects the direction of movement and not the robot's other parameters. With a fixed value for $\Delta\phi$, the dimensions and absolute value of the step will be the same for a robot that moves with $\Delta\phi$ as one that does it with $-\Delta\phi$.

Principle of symmetry: Given an apodal robot that is moving in a straight line and that is controlled by means of an amplitude A and a phase difference $\Delta\phi$, if the sign changes from $\Delta\phi$ the resulting movement will be equal to the initial one, but in the opposite direction, with the same absolute value of step and with the same dimensions.

Because of this principle of symmetry, we will only study the movement for positive values of $\Delta\phi$, drawing the control space for $\Delta\phi \in [0, 180]$.

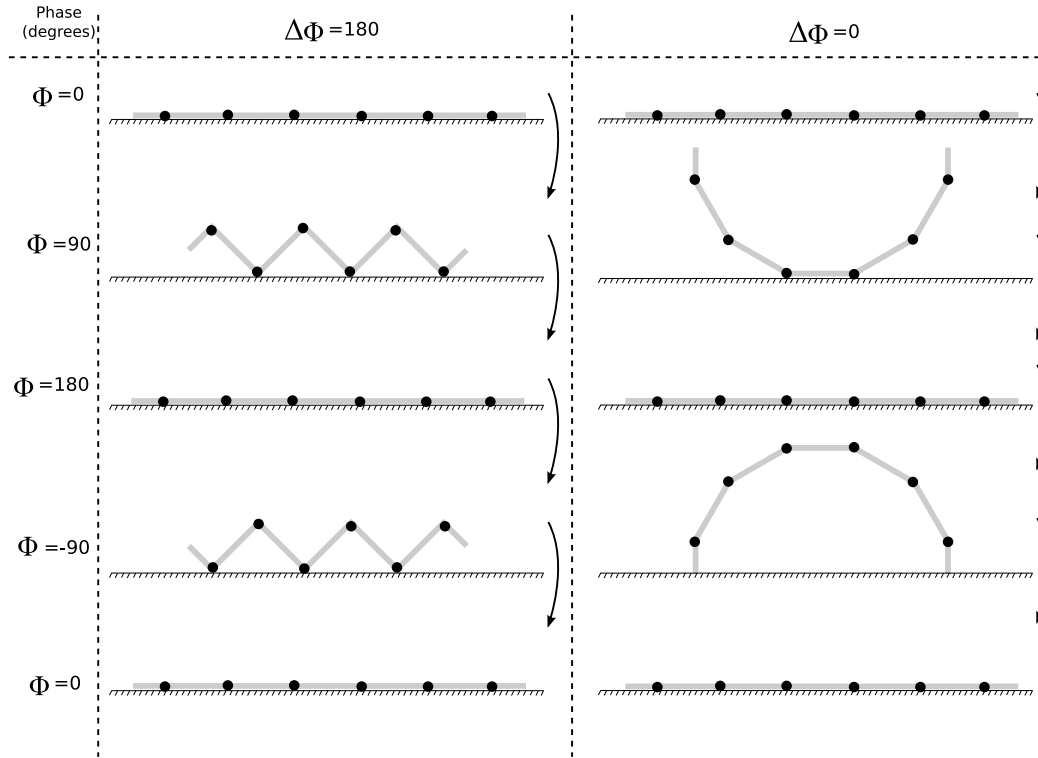


Figure 4.44: Evolution of the robot's shape when it is controlled with generators in phase (right) and out of phase (left)

4.4.5.2 Movements in phase and out of phase

When the phase difference is 180 degrees, the movement of two consecutive joints is in phase opposition. In this situation there is no propagation of waves, rather the ups and downs of the peaks and the valleys alternate. Therefore, there is no movement, neither forwards or backwards.

Principle of phase opposition: Given that an apodal robot to which the value of $\Delta\phi$ of 180 degrees is applied, it will not move. This happens for any value of amplitude of the generators.

The opposite case is when all the generators are in phase and therefore $\Delta\phi = 0$. Neither in this situation will a global wave that propagates appear and therefore movement will not exist. The shape of the robot is described by means of a discrete circular wave (section 3.6.5.2). To avoid collision between the head and the tail of the robot it is necessary to verify that the amplitude never exceeds the maximum value given by:

$$A_{max} = \begin{cases} 90 & M \leq 4 \\ \frac{360}{M} & M > 4 \end{cases}$$

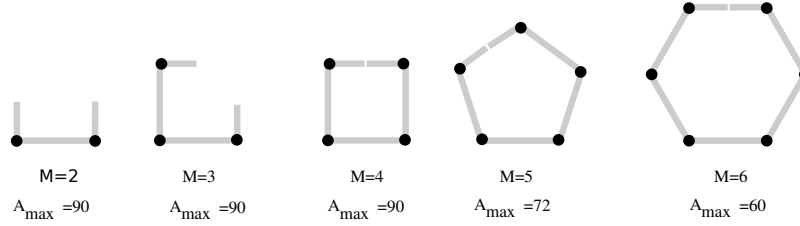


Figure 4.45: Robot's shape for $\phi = 90$ when the generators are in phase ($\Delta\phi = 0$) and the amplitude is maximum ($A = A_{max}$)

In the figure 4.45 the shapes of five robots with a number of modules between 2 and 6 are shown when the maximum amplitude is applied to them. When the phase is 90 degrees and for $M \geq 4$ they adopt the shape of regular polygons: square, pentagon, hexagon...

Principle of generators in phase: Given an apodal robot in which all its sinusoidal generators are in phase ($\Delta\phi = 0$), will not move. This happens independently of the value of the amplitude employed.

In the figure 4.44 the shapes that a 6 module robot adopts when moving with $\Delta\phi = 0$ and $\Delta\phi = 180$ are shown. When the joints are in phase opposition (left) the robot carries out contractions and expansions. When the generators are in phase, the robot folds up on itself and then opens. In the example shown it starts in an upright position supported on the ground, then it forms a U, then once more an upright, followed by an inverted U and then starts again. The amplitude value is that which determines the shape that the robot will assume. In none of the cases is there locomotion.

4.4.5.3 Minimum number of modules

Principle of minimum number of modules: So that an apodal robot moves in a straight line with a statically stable locomotion it must have at least 5 or more modules.

The region of locomotion, where the movement is statically stable is formed by the points whose phase difference is within the range $[\Delta\phi_s, 180]$, where $\Delta\phi_s$ is given by the equation 4.14. For values $M < 3$, $\Delta\phi_s$ is greater than 180 degrees, remaining outside the range. That is to say, in these cases, it is impossible that two undulations exist in the robot, because it is too short. For $M=4$, $\Delta\phi_s = 180$, and the region of locomotion is a straight line situated in $\Delta\phi = 180$. Now, yes, there are two undulations on the robot, but the generators are in phase opposition. By the principle of the opposition of phases, in this situation there is no locomotion. Therefore, M must be greater or equal to 5 modules.

This does not mean that robots with $M < 5$ cannot move. They can do so, nevertheless the movement is not uniform and there could exist abrupt transitions between phases. In this case a specific study of each robot has to be made.

4.4.5.4 Methodology for resolving direct kinematics

The methodology to address the problem of direct kinematics will be presented, as follows. Given that an apodal robot of M modules and in the working point P given for the pair $(\Delta\phi, A)$ we follow these steps:

1. Check that the values of A and $\Delta\phi$ are within its range of definition. $A \in [0, 90]$ and $|\Delta\phi| \in [0, 180]$. If that is not so, it is an invalid working point.
2. Check the validity of p and the region of limitation in which it is found.
 - (a) If $\Delta\phi \geq \Delta\phi_L$, where $\Delta\phi_L$ is calculated in the equation 4.10 and has an approximate value of 43.9 degrees, the working point p **is valid** and is found within the region of limitation I.
 - (b) If $\Delta\phi < \Delta\phi_L$, then:
 - i. Calculate A_{max} according to the equation 4.11.
 - ii. If $A \leq A_{max}$ it is a **valid point** situated in the region of limitation II.
 - iii. If $A > A_{max}$ it is an **invalid point**. It will cause the robot to adopt a shape that will collide with itself. There is a limitation in the geometry.
3. Check if p belongs to the locomotion region:
 - (a) If $\Delta\phi \leq \Delta\phi_s$, where $\Delta\phi_s$ is given for the equation 4.14, p does not belong to the locomotion region. Therefore the robot's movement will not be statically stable and the step equation cannot be applied.
 - (b) If $\Delta\phi \geq \Delta\phi_s$, p belongs to the locomotion region. Therefore the robot will have a statically stable movement. The sign of $\Delta\phi$ will determine the direction of the movement.
4. Obtain the point P (M_u, α) equivalent in the shape space:
 - (a) Obtain M_u by means of the equation 4.13.
 - (b) Obtain α from the equation 4.12.
5. Obtain the number of undulations k by means of the equation 4.1.
6. Calculate the dimensions h and w using the equations 3.37 and 3.38 respectively.
7. Calculate the step Δx with the equation 4.1.
 - (a) If $M_u < 3$ the theoretic step calculated will not be valid. In these circumstances the shape of the robot implies that the distance between the support points vary with the phase for which the step will depend on the surface and in general will be undetermined.

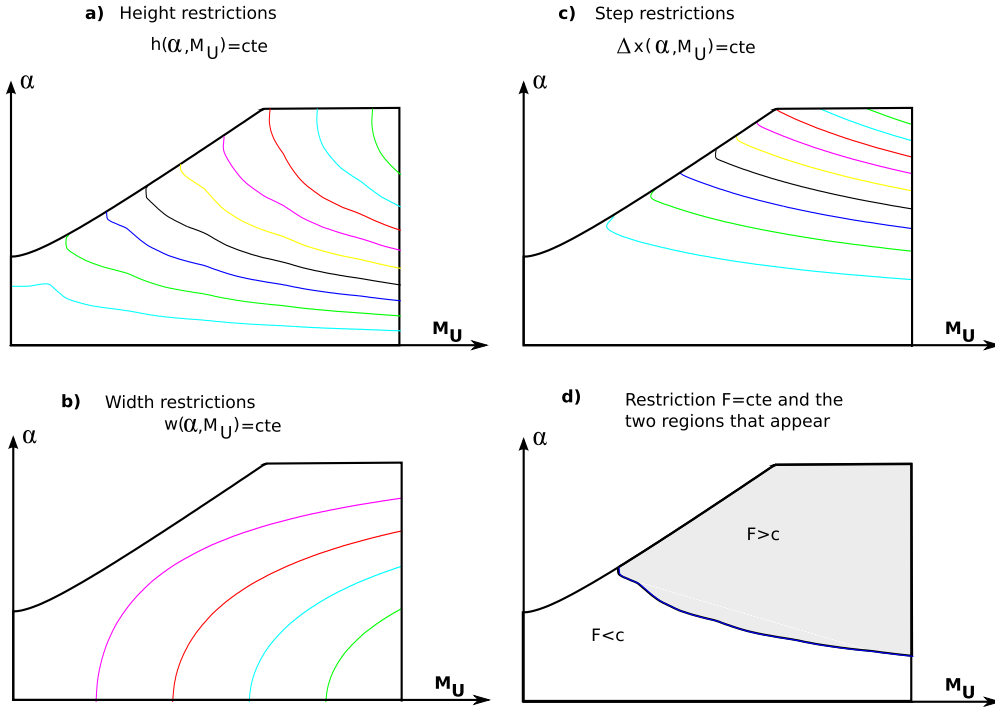


Figure 4.46: Restriction contour lines in the shape space a) Height b) Width c) Step d) The two regions that appear when the restriction $F = cte$ is applied

4.4.6 Inverse kinematics

The problem of inverse kinematics consists in calculating the working points in the control space so that the robot moves according to the specified restrictions. As well as the control parameters, the number of modules M that the robot must have to fulfil these restrictions can be calculated, if they are not given initially.

First we will see the types of restrictions and the partition into sub-regions that are generated in the shape space. Then we will analyse how to calculate the number of modules of the robot, we will formulate the proposed methodology to resolve the inverse kinematics and finally we will show how to apply this methodology using four problems as examples.

4.4.6.1 Restrictions

The restrictions employed are in the shape of $F = c$, where F can be any of the normalized functions of height (eq. 3.37), width (eq. 3.38) or step (eq. 4.1) and c is a real constant. In the shape space they are represented by means of contour lines. The points belonging to them assure that $F(M_u, A) = c$. Each line partitions the space h_1 into two regions: $F(M_u, A) < c$ and $F(M_u, A) > c$ (Figure 4.46d). It must be taken into account that these lines specify the restrictions for one undulation only and using

blocks with a distance between joints equal to 1, therefore before using them it will be necessary to normalize the value of the constant.

In the figure 4.46 the curves of the height, width and step restrictions are shown within the shape space. The 3 dimensional representations of the functions of height, width and step were presented in the figures 4.28, 4.31 and 4.36.

4.4.6.2 Number of modules M

The previous restrictions allow us to define the working regions formed by the points (M_u, α) . With problems of inverse kinematics M could be a fixed constant or it could have to be calculated. So the first case comes from an apodal robot constructed with M modules and where the control parameters need to be known so that it moves with the imposed restrictions. In the second case it is necessary to determine the number of modules M that has to have to satisfy these restrictions.

In both cases we will always use the criteria of stability to obtain M from M_u . For this reason, at least two undulations must exist ($k \geq 2$). Given that M is a whole number and M_u is real we will use the following expression:

$$M = \text{Round}(2M_u) \quad (4.15)$$

where $\text{Round}()$ is the function which rounds off the ratio to the next whole number.

When M is not specified, in general it is considered a value between M_{min} and a M_{max} . These values are obtained from $M_{u_{min}}$ and $M_{u_{max}}$ respectively using the equation 4.15.

The maximum and minimum number of modules per undulation will be the maximum and minimum abscissas of the points (M_u, α) of the working region. The value of $M_{u_{min}}$ can never be lower than 2.5, by the principle of minimum number of modules (section 4.4.5.3).

4.4.6.3 Methodology for resolving the inverse kinematics

The general methodology proposed for resolving inverse kinematics is:

1. Take the constant of the restrictions of the dimensions or the step (c) and normalise it: $c_n = c/L$. As we are using module type blocks the distance between joints is L (table 3.1). In the case that a width is specified as a restriction, this constant will be calculated as $c_n = c/kL$ where k is the minimum number of undulations. There will have to be at least two undulations ($k \geq 2$).

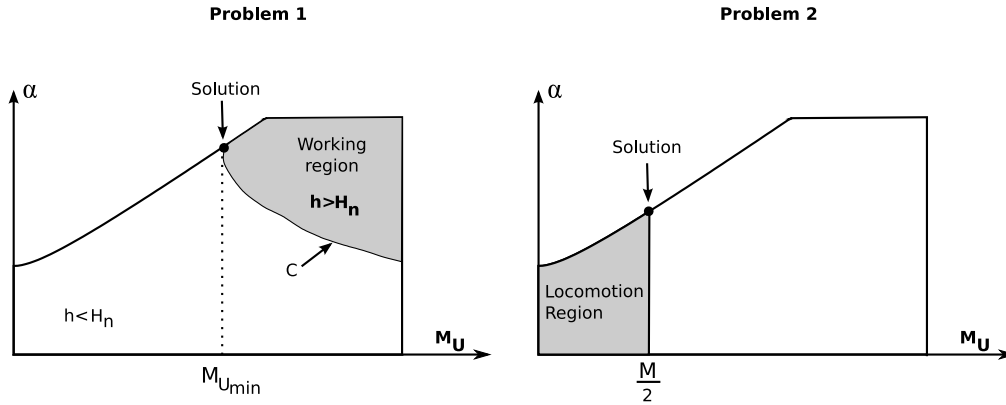


Figure 4.47: Shape spaces with the solutions of the problems 1 and 2

2. Obtain the curve of restriction given for $F = c_n$, where F is the function that gives the step, height or width. The shape space is partitioned into the two regions: $F > c_n$ and $F < c_n$. We call the working region the one which fulfils the restriction of the problem to be resolved.
3. Obtain the range of values of M . In general $M \in (M_{min}, M_{max})$ will be fulfilled. To calculate it the maximum and minimum abscissa of the work area: $M_{u_{min}}$ and $M_{u_{max}}$, and then the equation 4.15 must be applied to obtain M_{min} y M_{max} respectively.
4. Obtain the locomotion region. The maximum value of the abscissa, M_{us} , that borders this region is calculated as:
 - (a) If M is a known: then $M_{us} = M/2$.
 - (b) If it is desired to use the minimum number of modules, then $M_{us} = M_{min}$.
 - (c) If it is desired that the robot has the maximum number of modules then $M_{us} = M_{max}$.
5. Obtain the solution region as the intersection between the working and the locomotion regions. It will be the region of h_1 in which all the imposed restrictions are verified. This region could be: a point, a straight line or a surface.
6. Carry out the inverse transformation of the solution region. The points of the control space that belong to the transformed solution region will be the solutions looked for $(\Delta\phi, A)$ that fulfil all the restrictions. The inverse transformation of a point (M_u, α) in another $(\Delta\phi, A)$ of the control space will be carried out by means of the equations 4.13 and 4.12.

4.4.6.4 Example problem 1

Problem statement: *Decide the minimum number of modules for an apodal robot so that it moves with a height greater than or equal to H .*

Solution: A restriction in height ($h \geq H$) is being imposed and the value of M is not given, but it has to be the minimum. Applying the resolving process:

1. Calculate the normalized height: $H_n = H/L$.
2. Obtain the working region imposed by the restriction $h \geq H_n$. It is shown on the left side of the figure 4.47. All the points of this region make the robot move with a height greater than or equal to that specified.
3. While there does not exist a maximum value for the number of modules, there is a lower value for which $M \geq M_{min}$. The lesser abscissa of the points of the working region is $M_{u_{min}}$ (figure 4.47). From it M_{min} is obtained.
4. The locomotion region is given by $M_{us} = M_{u_{min}}$.
5. The intersection between the locomotion and the working regions is the solution point $(M_{u_{min}}, \alpha)$.
6. Applying the inverse transformation the solution point $(\Delta\phi, A)$ is obtained in the control space.

4.4.6.5 Example problem 2

Problem statement: *Given a robot of M modules, find the values of A and $\Delta\phi$ so that it moves with the maximum step.*

Solution: A restriction of the step is imposed (that is maximum) and the number of modules M is known.

1. There is no specified constant so nothing is done in this step.
2. It is known that the step is maximum for the maximum values of α (see figure 4.36) therefore the working region is the curve $\alpha = \alpha_{max}$ (eq. 4.6).
3. M is a given data, there is nothing to be done in this step.
4. The locomotion region is given by $M_{us} = M/2$.
5. The intersection between the locomotion and the working regions is the solution point $(M/2, \alpha)$. The value of α can be obtained as: $\alpha = \alpha_{max}(M/2)$.
6. Applying the inverse transformation the solution point $(\Delta\phi, A)$ is obtained in the control space.

4.4.6.6 Example problem 3

Problem statement: *Find the values A , $\Delta\phi$ and M so that the robot can move along the inside of a tube of diameter D*

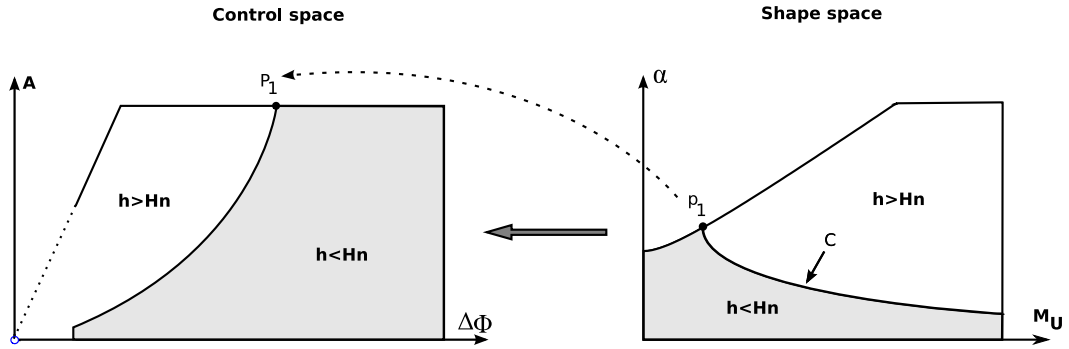


Figure 4.48: Shape and control spaces with the solutions to the problem 3

Solution: In this case the restriction is given by the condition that the robot's height must be less than the diameter of the tube: $h \leq D$. There are no restrictions on the number of modules. The stages to resolve the problem are as follows:

1. Calculate the normalized height: $H_n = D/L$
2. Obtain the region of the shape space where $h \leq D$ is fulfilled (Figure 4.48).
3. No maximum value exists for the number of modules, but there is a minimum one for which $M \geq M_{min}$. The minimum abscissa of the working region is in $M_u = 2$, but by the principle of the minimum number of modules we have to $M_{u_{min}} = 2.5$ and therefore $M \geq 5$
4. As no restriction is fixed for M , any value greater than or equal to 5 will be valid. In this case a generic locomotion region given for $M_{us} = M/2$ will be taken. If it is desired to calculate the robot with the least number of modules $M_{us} = 2.5$ be taken.
5. The intersection between the locomotion and the working region is the same working region. If in step 4 a minimum number of modules have been chosen for use then the solution is the point $(M_{u_{min}}, \alpha)$. Let's call it as point p_1 .
6. Realise the inverse transformation of the working region. The control region is obtained with the points $(\Delta\phi, A)$ that fulfil the initial established condition (Figure 4.48).

4.4.6.7 Example problem 4

Problem statement: Calculate the parameters A , $\Delta\phi$ and M so that the robot's step will be greater than or equal to S .

Solution: There is a restriction in the step: $\Delta x \geq S$. The stages are:

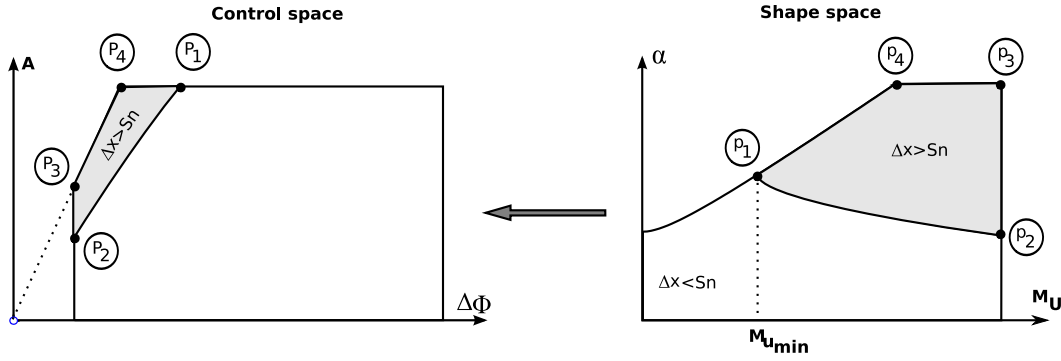


Figure 4.49: Shape and control spaces with the solution to the problem 4

1. Obtain the normalized step: $S_n = S/L$
2. Obtain the region of the shape space where $\Delta x \leq S_n$ (Figure 4.49).
3. The minimum number of modules is given for the point of the working region with the least abscissa. This allows us to calculate $M_{u_{min}}$ and M_{min} . Therefore the number of modules will have to fulfil $M \geq M_{min}$.
4. The same as in problem 3, the locomotion region for the generic case can be calculated, making $M_{us} = M/2$ or calculating it for the minimum number of modules, taking $M_{us} = M_{u_{min}}$.
5. The intersection between the locomotion region and the working region will be either the point, which is the solution point $(M_{u_{min}}, \alpha)$, or the same working area, according to the value of M_{us} chosen in stage 4.
6. Realise the inverse transformation of the working region. The control region is obtained with the point $(\Delta\phi, A)$ that fulfils the initial condition established (Figure 4.49). It will be the solution point P_1 or rather the complete transformation of the working region.

4.5 Case of study

In this section we are going to apply all the ideas developed in the chapter to study the wired model of an 8 module robot. The constants and the range of values of the parameters are calculated when $M = 8$, and the shape and control spaces are obtained as well as the locomotion region. As example three different working points are calculated and the shape and properties of the robot are shown in each one of them.

Parameter	Description	Range or value
M	Number of modules	$M = 8$
$ \Delta\phi $	Phase difference	$ \Delta\phi \in [45, 180]$
M_u	Number of modules per undulation	$M_u \in [2, 8]$
k	Number of undulations	$k \in [1, 4]$
A_{max}	Maximum amplitude of the generators	90
A	Generator's amplitude	$A \in [0, 90]$
α_{max}	Maximum winding angle	$\frac{45}{\sin(\frac{\pi}{M_u})} < 117.6$
α	Winding angle	$\alpha \in [0, \alpha_{max}]$
M_{us}	Border of the locomotion region in h_1	4
$\Delta\phi_s$	The limit of the locomotion region in H_1	$\Delta\phi_s = 90$.
L	Module length	7.2cm
d	block length	$d = L$
d_0	length of the Left arm of the block	$d_0 = L/2$

Table 4.2: The parameters and their range of values for the wired model of an 8 modules discrete apodal robot.

4.5.1 Range of values of the parameters and constants

In the table 4.2 the values of the calculated parameters and constants for this case study are shown. The values of M_u and k are obtained from the table 4.1 for $M = 8$.

4.5.2 Shape space

The shape space is shown in the figure 4.50. Also the aspect of the robots for some selected working points and for the phase $\phi = 0$ have been drawn.

Given that M_u is between 2 and 8, $M_u \leq M_{uL}$ is always verified, therefore in the shape space only the region of limitation I exists. There are no geometric limitations. From the equations 4.6 and 4.7 is obtained the maximum value 90 for the amplitude and for the winding angle:

$$\alpha_{max} = \frac{45}{\sin\left(\frac{\pi}{M_u}\right)}$$

that will always be strictly less than 120 degrees. The maximum value of this winding angle is had for $M_u = 8$ and its value is 117 degrees.

4.5.3 Control space

The control space is shown in the figure 4.51. It is a rectangle with the base situated between $\Delta\phi = 45$ and 180 degrees and the parameter A between 0 and 90.

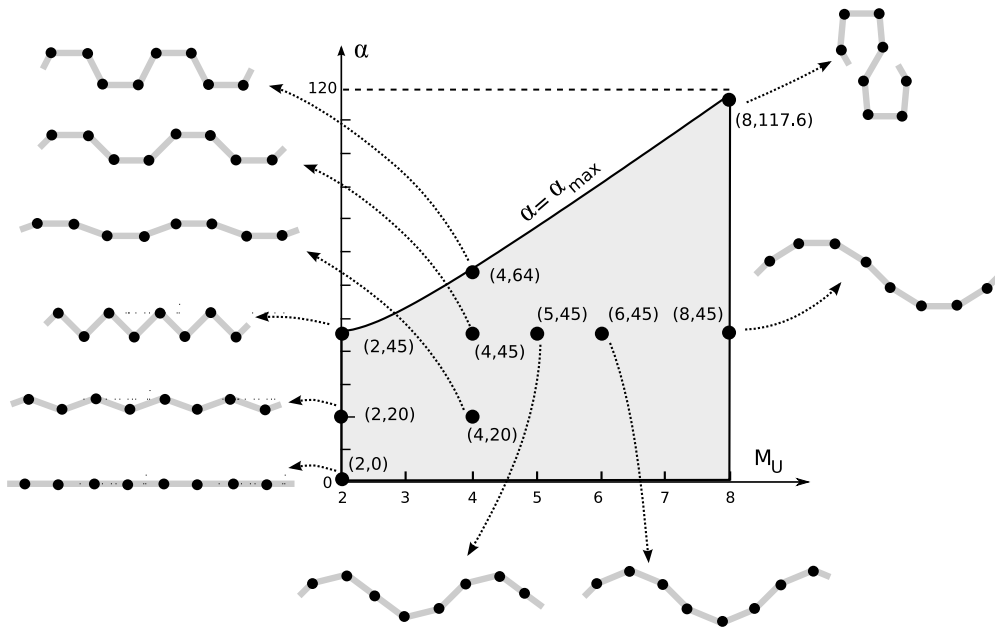


Figure 4.50: The Shape space of an 8 modules discrete apodal robot

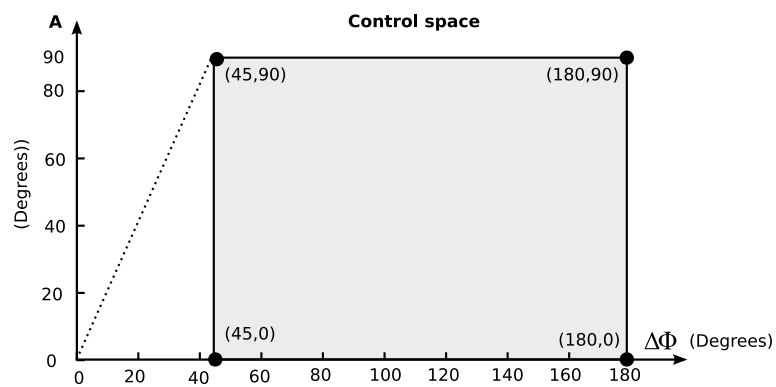


Figure 4.51: Control space of an 8 modules discrete apodal robot

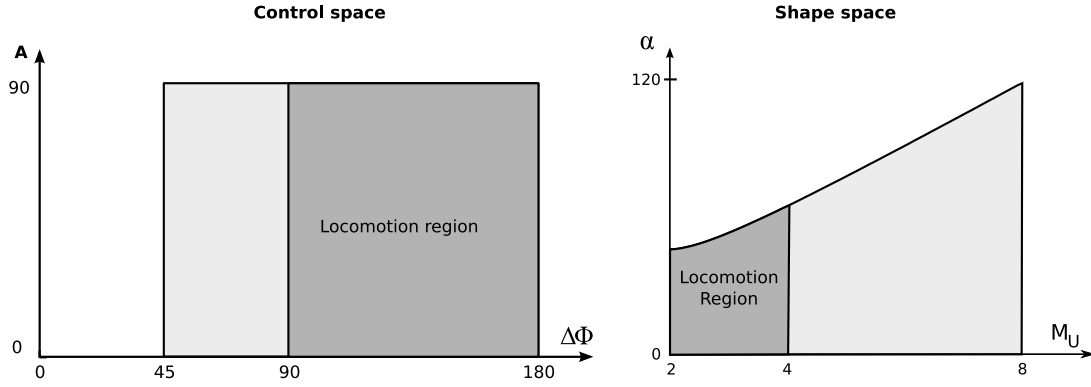


Figure 4.52: Locomotion region in the control and shape spaces of an 8 modules discrete apodal robot

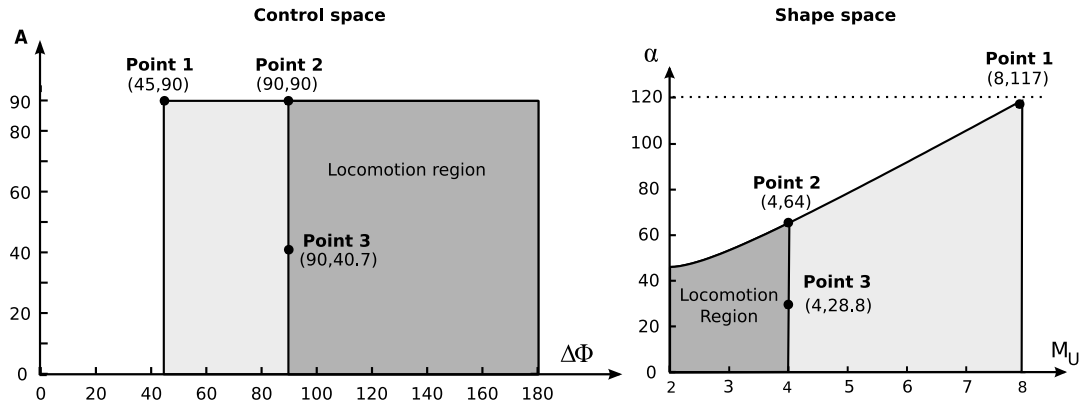


Figure 4.53: Situation of the selected working points in the shape and control spaces

The minimum value for $|\Delta\phi|$ is 45 degrees. It is calculated from the equation 3.40 specifying it for $k = 1$ and $M = 8$. If a smaller value is used, the robot will not have a complete undulation ($k < 1$) and the equations introduced in this chapter will not be valid.

4.5.4 Locomotion region

The locomotion region for the shape space is determined by $M_{us} = M/2 = 8/2 = 4$. For the control space, applying the equation 4.14 gives $\Delta\phi_s = 90$. The locomotion region of the spaces h_1 and H_1 have been drawn in the figure 4.52.

4.5.5 Working points

Three different working points have been selected. They are shown in the figure 4.53 and are summed up in the table 4.3. In point 1 the robot has a maximum height. This point is found outside the

Working point	(M_u, α)	$(\Delta\Phi, A)$	Height (cm)	Width (cm)	Step (cm)	Description
Point 1	(8, 117)	(45, 90)	[20.7, 23.8]	11.2	Unstable	Maximum height
Point 2	(4, 64)	(90, 90)	[6.5, 11.2]	[20.4, 20.8]	8.4	Maximum step
Point 3	(4, 28.8)	(90, 40.7)	[3.5, 5]	27	1.8	$h \leq 5\text{cm}$

Table 4.3: The three selected working points for an 8 modules discrete apodal robots

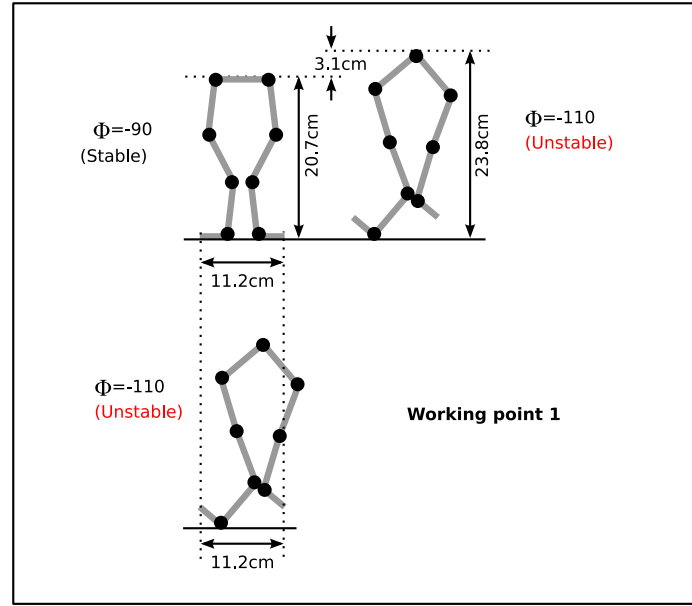


Figure 4.54: Dimensions of an 8 modules discrete apodal robot in the working point 1

locomotion region therefore it is an unstable configuration not valid for the movement. Point 2 in which the robot moves with the maximum step and in a stable mode. Finally, point 3 is calculated applying inverse kinematics so that it can move along the inside of a 5cm diameter tube and with the maximum step.

4.5.5.1 Point 1: Maximum height

The robot's shape and dimensions in working point 1 are shown in the figure 4.54, for the phases ϕ of -90 and -110 degrees. The height is maximum in the phase -110 degrees. As it deals with a discrete robot, the height varies with the phase. The maximum variation is of 3.1cm, that represents 13% of the maximum height. The width does not vary and has a value of 11.2cm for all the phases.

It is observed that for the phase -90 degrees the robot is stable. The projection of the centre of mass falls within the supporting segment and therefore the robot does not tip over. Nevertheless, in the phase of -110 degrees it is not stable and would overturn. At this point the criteria of stability is not being fulfilled.

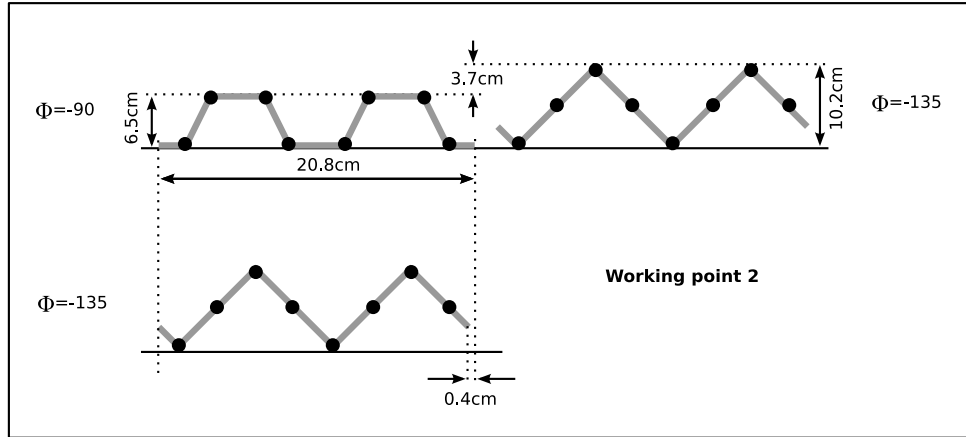


Figure 4.55: Dimensions of an 8 modules discrete apodal robot in the working point 2

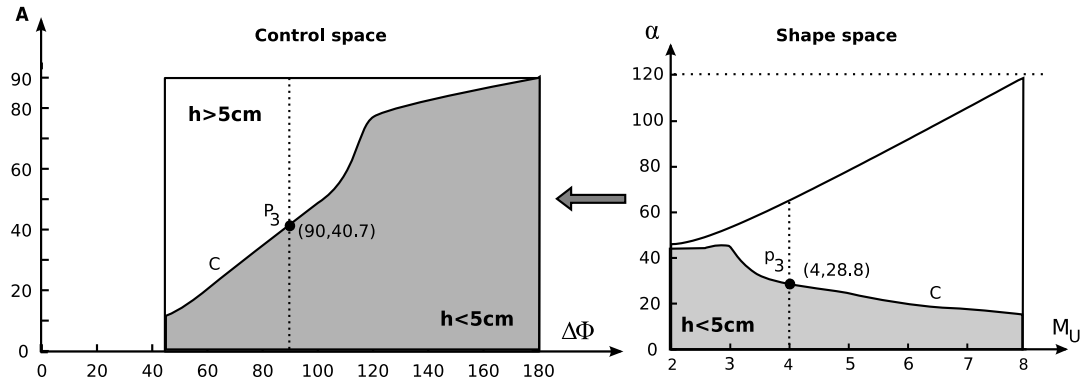


Figure 4.56: Application of the inverse kinematics for the calculation of the working point 3, in which an 8 modules discrete apodal robot is able to move through the inside of a 5cm diameter tube

4.5.5.2 Point 2: Maximum step

The work point 2 is calculated in such a way that the robot's step will be the maximum. The shape and dimensions are shown in the figure 4.55. The maximum height is reached for a phase of -135 degrees and the minimum in -90 degrees. The difference is of 3.7cm which represents 36% of the maximum height. The width hardly varies 0.4 cm (2% of the maximum width).

The robot's movement is statically stable as at every moment there are at least two supporting points.

4.5.5.3 Point 3: Movement through the inside of a tube

Point 3 is that which allows the robot to move along the inside of a tube of diameter $D = 5\text{cm}$ and at the same time the step will be the maximum. We will calculate it by applying the methodology proposed in the section 4.4.6.3:

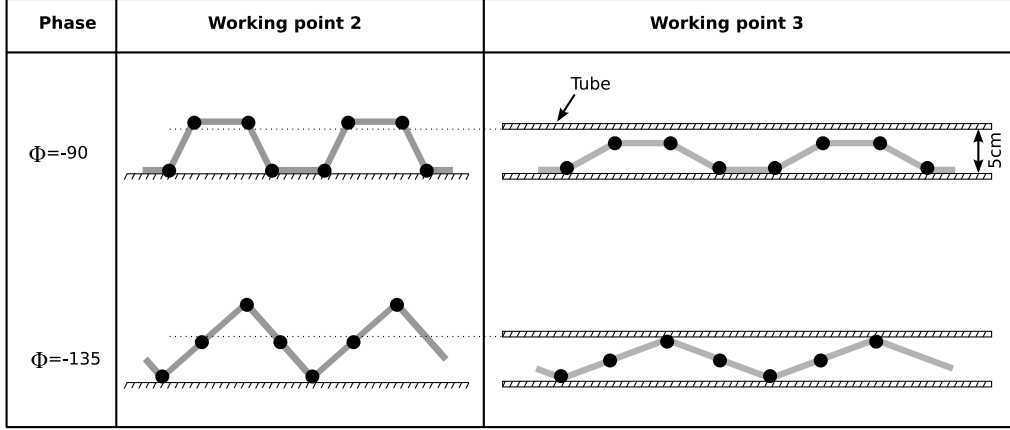


Figure 4.57: Comparison between the working points 2 and 3

1. Calculate the normalized height: $H_n = D/L = 5/7.2 = 0.69 \approx 0.7$
2. The region that satisfies the restriction $h < H_n$ is shown in the figure 4.56. The curve C is the limit of the working region.
3. $M = 8$ is a given data.
4. The locomotion region is that in which $M_{us} = M/2 = 8/2 = 4$.
5. The intersection between the working and the locomotion regions is a vertical line with abscissa $M_u = 4$. All the points of this straight line are solutions of the problem. As we want the solution in which the step is maximum, and the step for a fixed M_u increases with α , the solution is found in the intersection between the locomotion region and the curve C. It will be the point $(M_u, \alpha(M_u)) = (4, 28.8)$.
6. Carrying out the inverse transformation of this point the solution $P_3 = (90, 40.7)$ is obtained.

In the figure 4.57 the points 2 and 3 are compared. The shape is the same, as M_u is equal in both points. The difference is due to the point 3 where the winding angle is less which causes less height and a greater width. It can be observed that in the worst case, $\phi = -135$, the maximum height of the robot fulfils the restriction of being less than or equal to 5.

The step in point 2 is of 8.4 cm and in point 3 of 1.8 cm.

4.5.6 Locomotion

The locomotion of an 8 module discrete apodal robot for a cycle is shown in detail in the figure 4.58. Fifteen different phases have been represented. The different shapes of the undulations can be seen

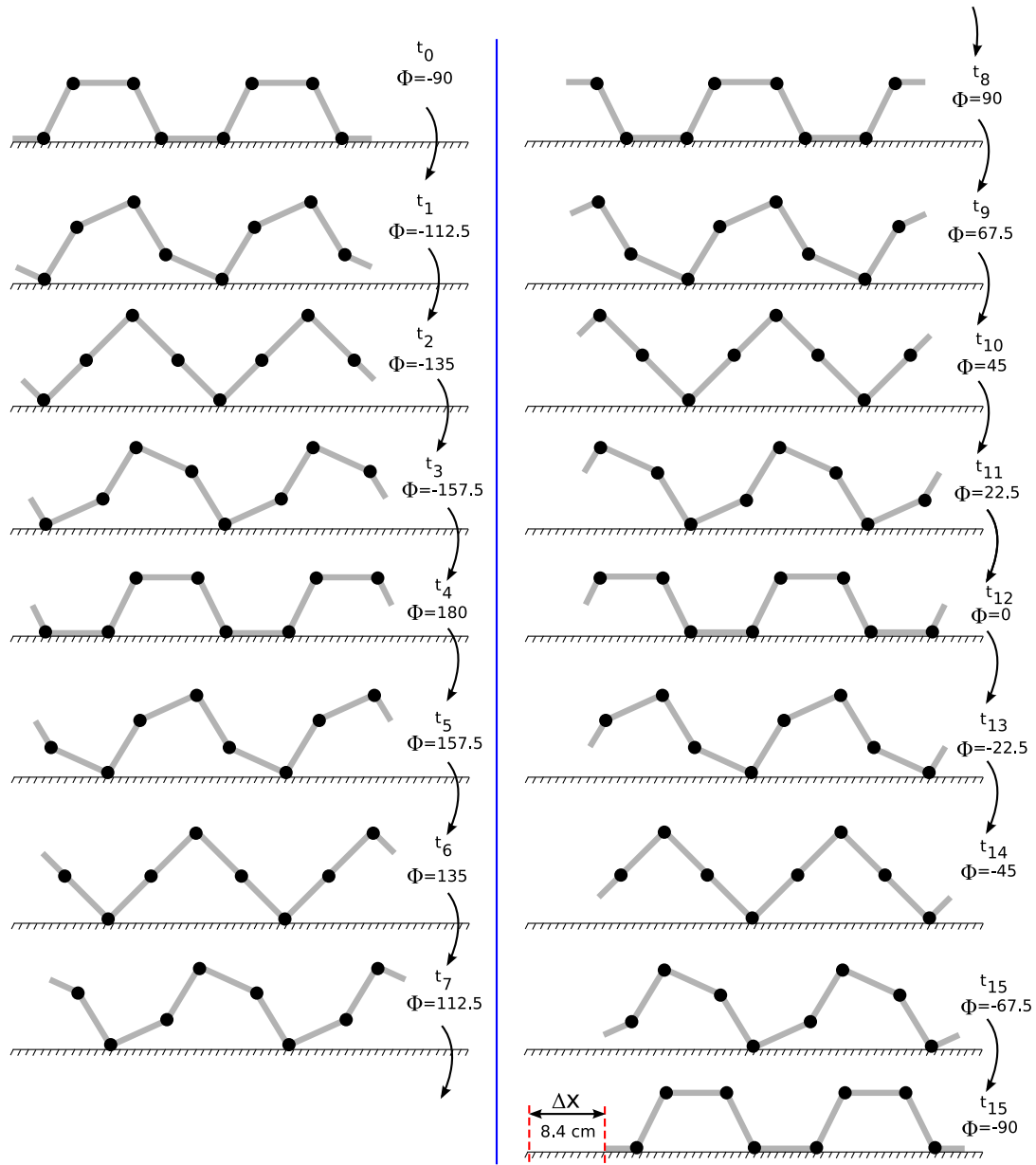


Figure 4.58: Locomotion of an 8 modules discrete apodal robot in the working point 2.

and in all of them there are always two supporting points that means that the locomotion is always statically stable. Also it can be seen that the robot's height varies while its width remains practically constant. At the end of the cycle the robot has advanced a distance equal to 8.4 cm that represents 40% of its width in this working point.

4.6 Principles of locomotion

The locomotion of the discrete apodal robot when sinusoidal generators are used have been summarised in the following 11 fundamental principles:

1. **Sinusoidal generators principle.** An apodal robot of M modules with pitch-pitch connections in which each one of the joints oscillate periodically using sinusoidal generators with an amplitude A and a phase difference $\Delta\phi$, is capable of moving in a straight line.
2. **body wave principle.** The mechanism of locomotion of an apodal robot controlled by sinusoidal generators is owing to the appearance of a body waves that travels along the robot.
3. **Direction of movement principle.** The direction of the displacement of the robot will be equal to that of the body wave. If the wave is propagated from the tail to the head, the robot will move forwards.
4. **Shape characterisation principle.** The body wave that appears during locomotion is of serpenoid type and is characterised by the parameters winding angle α and number of undulations k .
5. **Stability principle.** The locomotion of the robot is statically stable if there only exists at least two undulations that move through the robot, hence $k \geq 2$.
6. **Step principle.** The distance travelled by the robot during a cycle, called step, is directly proportional to the difference between the length of an undulation and its wavelength.
7. **Amplitude control principle.** The robot's height and step directly depends on the amplitude A of the generators. The greater the amplitude, greater will be the height and the step.
8. **Phase difference control principle.** The shape of an undulation and their number (k) depend on the phase difference $\Delta\phi$ of the generators.
9. **Symmetry principle.** The sign of the phase difference $\Delta\phi$ determines the robot's direction of displacement. Two movements with the same absolute value $|\Delta\phi|$ but of a different sign will be exactly equal, but realised in opposite directions.
10. **Generators in phase and opposition of phase principle.** If all the generators are in phase or in opposition of phase, wave propagation will not exist and therefore there will be no robot locomotion.

11. **Minimum number of modules principle.** The minimum number of modules required for an apodal robot to move in a statically stable way is five.

4.7 Conclusions

In this chapter the problem of **locomotion in one dimension** of apodal robots of the **pitch-pitch group** has been exhaustively studied.

The continuous model has been employed to understand the locomotion of these robots, independently of the number of modules. Therefore, **only by the parameters α and k the shapes the robots adopt when they move and their locomotion properties are specified**. The conditions that must be fulfilled so that the movement is statically stable have been stated and an equation proposed to calculate the step. With this the necessary relationship between the kinematic model and the mathematic one has been established.

From these concepts of the continuous model the discrete model has been analysed. The new parameters that appear have been identified, and their range of values and limitations. **Using the idea of shape space has been proposed to represent the robot's working points**, from the number of modules per undulation M_u and α . For each one of these points the robot will have a height, width and step.

We also propose **studying the kinematics of these robots by means of transformations between the control spaces and the shape spaces**. With this method not only is a compact representation obtained, but also the problems are simplified. The step and dimension restrictions are expressed by means of regions within the shape spaces.

The methodologies to resolve the direct and inverse kinematics by means of simple steps have been proposed. Examples of how to apply these methodologies to resolve such problems as the **maximisation of the robot's step** or to calculate its control parameters so that **it can move along the interior of a tube** have been presented.

The study of locomotion has been done generically for all the family of robots of the type pitch-pitch of M modules. As example of application, a **case study of an 8 modules robot** has been presented and numerically results obtained that are contrasted in the chapter on experiments with the measurements realised in the simulations and the real robot.

The model of apodal robot locomotion proposed allows us to understand the locomotion, establish parameters and carry out a priori calculations to predict how it will move to satisfy the restrictions imposed by the environment. What has been accomplished is **to explain the locomotion related to the displacement of a robot with the parameters of the generators**.

Finally, **all the ideas have been summed up in 11 fundamental principles** (section 4.6) that permit us to understand the apodal robots' locomotion controlled by sinusoidal generators.

Chapter 5

Two-Dimensional Locomotion

“The most exciting phrase that one can hear in science, that announces new discoveries, is not ‘Eureka!’ but

‘This is strange...’”

– *Isaac Asimov*

5.1 Introduction

In this chapter we study the locomotion of apodal robots of the pitch-yaw group when the model of sinusoidal oscillators presented in the section 3.5 are used as controllers.

We start by stating the problem of 2D locomotion and we propose, from a general viewpoint, a methodology to resolve it, with direct and inverse kinematics. Following this we describe the 8 gaits that have been found and we summarise the restrictions that characterise them. Then we study in detail each one of the methods of locomotion, analysing firstly the continuous then the discrete model. We apply all this to a case study of an 8 module robot that will be used in the chapter of experiments to confirm the validity of the models. Finally we sum up the most important ideas in 11 principles of locomotion.

5.2 Problem of 2D locomotion

5.2.1 Approach

The aim is to resolve **the problem of co-ordination** so that apodal robots can move over a two-dimensional homogeneous surface without obstacles, using the model of sinusoidal oscillators presented in the section 3.5.

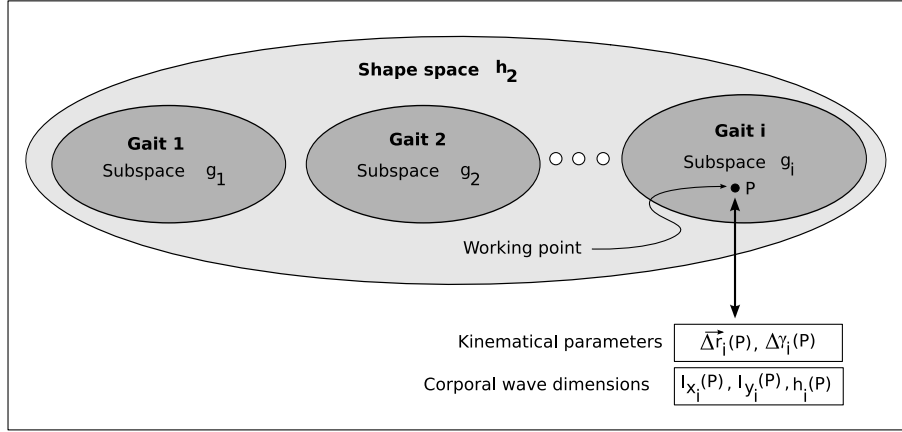


Figure 5.1: Scheme to address the two-dimensional locomotion problem

We will study it in a general way so that it is applicable to any apodal robot of M joints, where M is greater than an established minimum number. We model them as three-dimensional continuous curves that vary their shape with the phase, which we call corporal waves. These appear as superposition of the two waves that are applied to the vertical and horizontal joints. Therefore, they will be characterised by the parameters of shape space h_2 , of dimensions equal to 5. They are $\alpha_v, \alpha_h, k_v, k_h$ and $\Delta\phi_{vh}$ (section 3.6.4.2). Each point of h_2 represents a different corporal wave that is propagated when the phase ϕ varies. Of all of them, only some are valid and will cause the robot to move.

5.2.2 Outline

The scheme proposed to address the problem is that shown in the figure 5.1. Each gait of the robot is associated to a subspace g_i of h_2 , that will have a dimension less than or equal to 5 that we call **degrees of freedom** of the movement. The subspaces g_i are characterised by their parametric equations that establish relationships between their parameters and restrict their dimensions, determining their degrees of freedom.

In all the working points $p \in g_i$ the robot will move using the same gait i . The dimensions of the waves and the robot's kinematic parameters will depend on the point chosen. We will use the notation $l_{x_i}(p)$, $l_{y_i}(p)$, $h_i(p)$ to specify the dimensions of the corporal wave and $\Delta \vec{r}_i(p)$, $\Delta \gamma_i(p)$ for the kinematic parameters (variation of the position vector and its orientation in a cycle). Each gait i has its own subspace g_i and equations.

To illustrate these concepts we will take as an example the movement in a straight line, that was studied in chapter 4. It is associated to the subspace g_i . It is characterised by the restriction that horizontal waves do not exist therefore $\alpha_h = 0$. The parameters k_h and $\Delta\phi_{vh}$ are not used in this movement therefore we can also equal them to zero. Its dimension is, therefore, equal to 2 which

means it has two degrees of freedom. The points of g_i will be the pairs (α, k) , where α is the winding angle of the vertical wave and k its number of undulations.

5.2.3 Methodology employed

The methodology employed to solve the problem of locomotion in 2D is summed up by the following stages:

1. Find the gaits.
2. Characterise the subspaces g_i associated to the gaits found.
3. Confirm the simulated results with real robots.
4. Obtain the equations of the dimensions $l_{x_i}(p)$, $l_{y_i}(p)$, $h_i(p)$ for each subspace g_i .
5. Obtain the equations of the kinematic parameters $\overrightarrow{\Delta r_i}(p)$ and $\Delta \gamma_i(p)$ for each subspace g_i .
6. Resolve the problems of the direct and inverse kinematics, as proposed in the section 5.2.4.

5.2.3.1 Search for the gaits

What is required is to explore the control space to find different varieties of movement. For this, search techniques have to be employed. The solution adopted in this thesis has been to use **genetic algorithms**. The advantage they offer, compared to other techniques such as simulated annealing, is that as a result a population of individuals is obtained, and in it different types of movement can be found. We are not looking for best optimum movements that minimise a cost function, but to detect families of solutions.

The search space employed is H_2 , of 5 dimensions. As an evaluation function the step is used, rewarding the individuals that move with a bigger step, in the direction indicated. All the robots are initially situated at rest on the xy plane, with their longitudinal axis coinciding with the x axis. The evaluation functions employed have been the step in the x axis (Δx), in the y axis (Δy) and the rotation around the z axis ($\Delta \gamma$), for robots with a fixed length of 32 modules. More details can be found in the appendixB.

For the implementation a **simulator** has been developed (section 7.2.5), based on the *Open Dynamics Engine* (ODE). The evaluation functions take the initial position of the robot's centre of mass (angular or lineal position), waiting until two cycles of simulation have elapsed, the final position is obtained and the movement vector is calculated (or angular in the case of rotation). To ensure that the robot is in a stable situation, of permanent regime, the first two cycles are discarded, starting to measure from

the third. The robots which have a longer step during the following two cycles are rewarded. The frequency of the oscillators is fixed at the same value for all the individuals.

So, for example, to find the different gaits in the direction of y axis, the step Δy is calculated and the individuals that move furthest in this direction are rewarded. In the final population various families of individuals with different movements appear. Some with side-winding, others with an inclined sideways movement and others that roll.

For other types of movements, such as moving in a circular path, tests have been realised. From the movement in a straight line, whose parameters are known, it is assessed if the same movement is viable when the angle of the horizontal joints are changed.

5.2.3.2 Characterisation of the subspaces

Once the candidates for the gaits are found, they are transformed into shape space h_2 and the restrictions are looked for that meet the parameters so that the movement can be carried out. For some movements these relations are not obvious, for example in the case of an inclined sideways movement. The observations of the mathematical model of the wave must be combined to obtain conclusions.

Finally from this step the parametric equations are obtained that characterise the subspace.

5.2.3.3 Confirmation

The subspaces g_i obtained are confirmed by means of the simulation and are tested on real robots. It is necessary to prove that they are valid for robots with different number of modules (and not only for 32 that is the value employed in the searches) and that when the working point varies the movement continues to be of the same type but with other dimensions and kinematic parameters. If these criteria are not fulfilled, the movement is rejected. With this we ensure that the subspace really does characterise that type of movement, independently of the chosen number of modules and the working point chosen.

5.2.3.4 Obtaining the equations

Finally the equations are obtained to calculate the dimensions and the kinematic parameters of each one of the gaits. The dimensions of the three-dimensional wave are calculated from the mathematical model or by means of approximations such as the flat wave (section 5.3.4).

The calculation of the kinematic parameters depends on the gait. The equations can be obtained by means of geometrical methods, as was done in the section 4.2.6 when calculating the step of locomotion in a straight line or deriving them from the study of their dynamics.

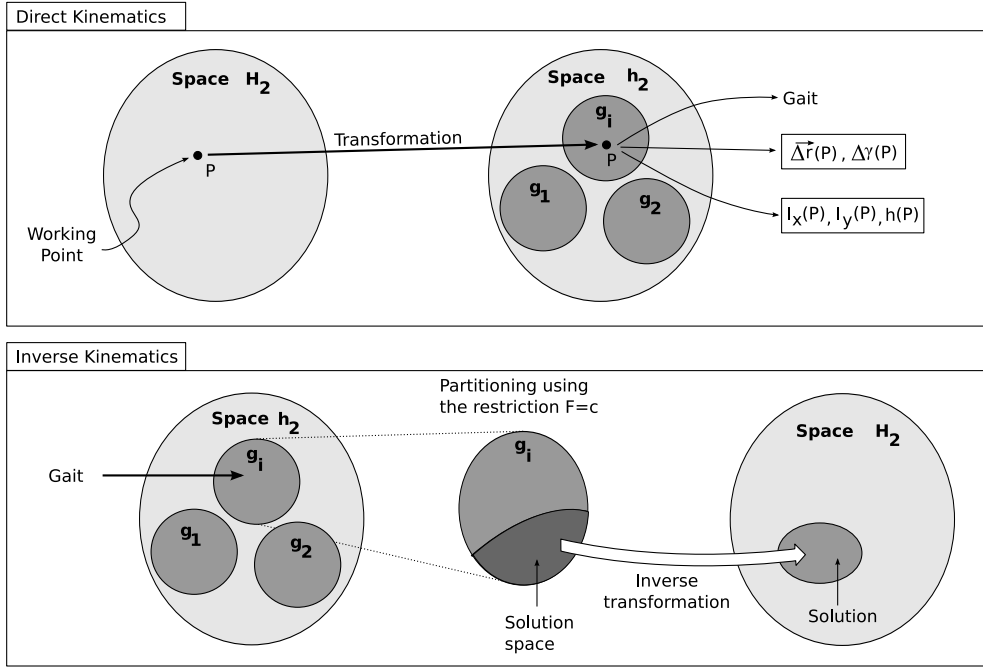


Figure 5.2: Inverse and direct kinematic scheme for the pitch-yaw robot group

5.2.4 Kinematics

The generic stages are proposed that have to be carried out to resolve the problems of the direct and inverse kinematics. The equations of characterisation of the subspaces g_i and the equations of the dimensions and of the kinematic parameters for each one of them are known. The outline is shown graphically in the figure 5.2.

Chapter 4 studied in detail how to resolve the kinematics for the subspace associated to the gait in a straight line. This section presents the stages in a general way, abstracting the degrees of freedom of the movement.

5.2.4.1 Direct kinematics

Problem statement Given a point P of the control space H_2 that determines the parameters of the sinusoidal generators ($A_v, A_h, \Delta\phi_v, \Delta\phi_h, \Delta\phi_{vh}$) determine the gait, its kinematic parameters and its dimensions.

We call space g to the union of all the subspaces g_i . The stages are:

1. Transform the point P of the control space to a shape space (point p), using the equations 3.45 and 3.46.

2. If p is NOT in g it is an invalid point. These parameter values are wrong and do not cause movement in any of the foreseen gaits.
3. If p belongs to g it will be a valid point. Establish the subspace g_i to which it belongs, testing to see if it fulfils the equations that characterise it. With this we will know the gait that the robot makes.
4. Apply the equations of the dimensions $l_{x_i}(p)$, $l_{y_i}(p)$, $h_i(p)$ and of the kinematic parameters $\vec{\Delta r}_i(p)$ and $\Delta \gamma_i(p)$.

5.2.4.2 Inverse kinematics

Problem statement Given some restrictions in the kinematic parameters and/or in the robot's dimensions, and with a known gait, find the parameters of the generators that must be applied.

The general stages are the following (figure 5.2):

1. Obtain the space g_i associated to the gait.
2. Apply the restrictions and partition to the subspace g_i . We will call the solution space as s .
3. Carry out the inverse transformation of the solution space s , with which we obtain the subspace S within the control space H_2 , which is the answer to the problem.

5.3 Gaits

5.3.1 Solutions found

Eight different gaits have been found, grouped into the following five categories: movement in a straight line, circular path, rolling, sideways movement and rotation (figure 5.3). The sideways movement can be carried out in three ways: normal, inclined and flapping (or rowing type). There are two rotations, as an “S” and as a “U”, according to the shape that the robot adopts during its movement.

Of all the movements found, **three of them are new and have not been previously studied or implemented by other researchers**, as far as we know. They are the movements of inclined sideways and the two kinds of rotation.

Movement in a straight line for the pitch-pitch type has been amply covered in chapter 4. The robots of the pitch-yaw group are equivalent to the former when the horizontal joints remain in their position

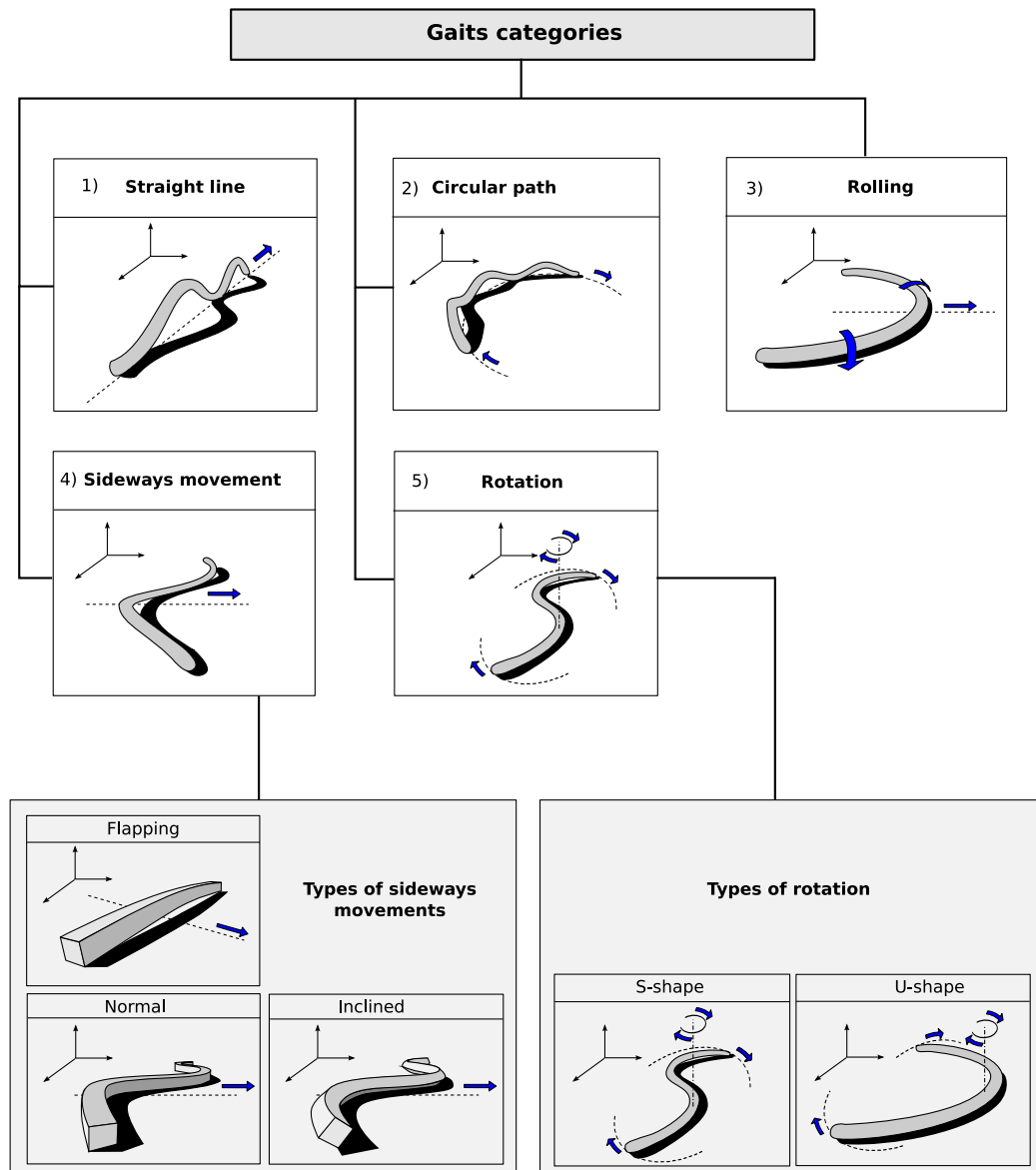


Figure 5.3: Locomotion gaits for the robots of the pith-yaw group

of rest. All the principles already studied are applied directly. For the calculations it is only necessary to have in mind that the blocks have some different parameters d and d_0 (section 5.4).

The movement in a circular path allows the robot to carry out turns of a defined radius. The mechanism of movement is similar to that of locomotion in a straight line but the turning angle of the horizontal joints remains fixed at a constant value different to zero so that it adopts the form of a circular arc (section 5.5).

The rolling movement means that all the modules rotate around a corporal axis moving the robot in a direction perpendicular to the longitudinal axis (section 5.6). The robot adopts the form of a “U” and rolls. This gait is very useful to recover the original orientation of the robot in case it overturns. For example, if it carries a camera in its head and overturns, it will recover the correct orientation by rolling.

With the **sideways movement** the robot moves toward one of its sides maintaining parallel its longitudinal axis (section 5.7). It encompasses three gaits. The **principal** one, in which the robot moves sideways undulating the body. It is similar to the movement made by some kinds of snakes when moving across sand, known by the term side-winding. The second is the **inclined** version. It is the same movement, but this time the modules are rotated an angle in relation to their body axis (section 5.7.8). The third is **flapping** in which the robot adopts the shape of a slightly curved “U” and the extremes perform circles. The supporting points of the extremes and middle alternate to produce movement (section 5.7.9).

The final category is made up of two **rotation movements**, that allow the robot to change the orientation of its longitudinal axis. One is rotation in the shape of an “S” (section 5.8), and is similar to the principal sideways movement, but rotating instead of moving. In the other the body adopts alternately the shapes “U” and inverted “U” (section 5.8.7).

5.3.2 Classification according to waves

The different gaits are generated by means of the superposition of the waves applied in the vertical and horizontal joints. They are of two types, serpenoid or circular. In the figure 5.4 the different gaits are shown in function of the waves used in the vertical and horizontal joints.

We denote the three-dimensional wave by the union of two letters, that correspond to the types of two-dimensional waves used. In total we have four types of waves: SS, SC, SR and CC.

5.3.3 Characterisation of the subspaces g_i

The gaits found together with the restrictions of their associated subspaces g_i , the parameters, the type of wave and the degrees of freedom have been summed up in the figure 5.5.

		Horizontal joints		
		Serpentoid (S)	Circular (C)	Rest (R)
Vertical joints	Serpentoid (S)	SS wave: Serpentoid 3D <ul style="list-style-type: none"> • Normal Sideways movement • Inclined Sideways movement • S-rotation 	SC wave <ul style="list-style-type: none"> • U-Rotation • Circular path 	SR wave <ul style="list-style-type: none"> • Straight line
	Circular (C)		CC wave: Circular 3D <ul style="list-style-type: none"> • Rolling • Flapping 	

Figure 5.4: Gait classification according to the waves applied in the vertical and horizontal joints

Locomotion gaits	Parameters	Degrees of freedom	Wave	Restrictions
Normal sideways movement	(α, k)	2	SS	$\alpha_h \approx \alpha$ $k_h = k_v = k$ $\alpha_v \rightarrow 0$ $ \Delta\Phi_{vh} = 90$
Inclined sideways movement	(α, k, β)	3	SS	$\alpha_h = \alpha \cos \beta$ $\alpha_v = \alpha \sin \beta$ $k_h = k_v = k$ $ \Delta\Phi_{vh} \rightarrow 0$
S-Shape rotation	(α, k)	2	SS	$\alpha_h = \alpha$ $k_h = k$ $\Delta\Phi_{vh} = 0$ $\alpha_v \rightarrow 0$ $k_v = 2k$
U-shape rotation	(α, k)	2	SC	$\alpha_h = \alpha$ $k_v = k$ $\alpha_v \rightarrow 0$ $ \Delta\Phi_{vh} = 90$
Circular path	$(\alpha_v, k_v, \alpha_h)$	3	SC	Curva circular
Straight line	(α, k)	2	SR	$\alpha_h = 0$
Rolling	α	1	CC	$\alpha_v = \alpha_h = \alpha$ $ \Delta\Phi_{vh} = 90$ $\alpha > \alpha_{\min}$
Flapping	α	1	CC	$\alpha_v = \alpha_h = \alpha$ $ \Delta\Phi_{vh} = 90$ $\alpha > \alpha_{\min}$

Figure 5.5: Summary of all the gaits with their parameters, type of wave, degrees of freedom and shape subspace restrictions

In all types of movement the three-dimensional wave is **flattened**, because it makes the parameter α_v much greater than the α_h or because the wave itself is flat. For this reason, the shape of the robot is approximated by a two-dimensional wave on the xy plane that in general needs two parameters for its description: α (that is its winding angle or the angle of the arc) and the number of undulations k . The dimensions of this wave are approximated by the horizontal wave, which is known. It will be a serpenoid or a circular wave.

The gaits of normal sideways movement, in a straight line and the two types of rotation have two degrees of freedom, denoted by the parameters α and k . According to the type of movement, the parameters will have different meaning. In the case of normal sideways movement α indicates the winding angle of the horizontal wave, that is to say, the shape that the robot's body has during the movement and k is the number of horizontal undulations. It is the same as in the case of rotation in "S". For the rotation in "U", α is the angle of the horizontal arc and k the number of vertical undulations.

The rolling and flapping gaits have only one degree of freedom given for α , that represents the angle of the arc that forms the body. As they are circular waves the parameters k_v and k_h are zero.

The movements with the greater degree of freedom are the circular path and the inclined sideways movement. In the first the winding angle and the number of undulations k are needed for the vertical wave, which, as in the one-dimensional movement, define the robot's step and shape. A third parameter is needed to specify the angle of the arc of the path. In the inclined sideways movement, as well as α and k it is necessary to specify the angle of inclination.

5.3.4 Stability

The stability of each one of the movements is studied in their corresponding sections, nevertheless, a criterion exists that is valid for all: **the application of a flat wave**.

If the component that is applied in the vertical joints has a parameter α very much smaller than that of the horizontals, then the centre of gravity remains very near to the ground and the movement will tend to be stable with independence of the number of supporting points on the ground.

When a flat wave is applied, the robot's shape approximates to that which it has due to its horizontal joints. What is more this allows the calculation of its dimensions from the horizontal wave.

Principle of the plain wave *In general the stability of all the movements is obtained making the parameter α of the vertical wave very small in comparison to that of the horizontal one. In this case, the three-dimensional wave is "flattened" and the robot's dimensions can be approximated by the horizontal wave.*

5.4 Locomotion in a straight line

5.4.1 Description

The apodal robots of the pitch-yaw group move in a straight line in a similar way to those of the pitch-pitch group. To obtain this movement, the horizontal joints must be in their positions of rest, with their angles of turn at zero ($\phi_{hi} = 0$) and a serpenoid wave is applied in the vertical joints.

All of the equations, principles and methodologies presented in chapter 4 for the pitch-pitch group of robots are valid also for the pitch-yaw group. For this it must be taken into account that these robots are formed by $M/2$ blocks of pitch type (section 3.3.4) and that the parameters d_0 and d are now $L/2$ and $2L$ respectively (see table 3.1).

The difference between both groups is in the geometry. Those of the pitch-yaw group are not symmetrical with respect to their geometrical centre neither are the blocks of the pitch type. In these the left arm has a length of $L/2$ and the right of $3L/2$. In the pitch-pitch group both arms have the same length ($L/2$).

5.4.2 Stability

The criterion of stability is the same as for the pitch-pitch group of robots. The movement will be statically stable if there are at least two undulations ($k_v \geq 2$). In the figure 5.6 the locomotion of a 20 module robot of the pitch-yaw group is shown. Only the vertical joints are represented. The horizontal modules have been drawn in another colour. In all the phases there are at least two supporting points for which the locomotion is statically stable.

In the figure 5.7 the locomotion of a 16 module robot has been drawn when k_v is less than 2. The robot advances, but during the transition between phases $\phi = 0$ and $\phi = -90$ there is only one supporting point which causes the robot to incline backwards.

The principle of minimum number of modules, in the case of the pitch-yaw group of robots has to be verified for the vertical joints. The robot will have to have at least 5 vertical modules. Therefore, these robots will have to have as a minimum 10 modules (5 vertical + 5 horizontal).

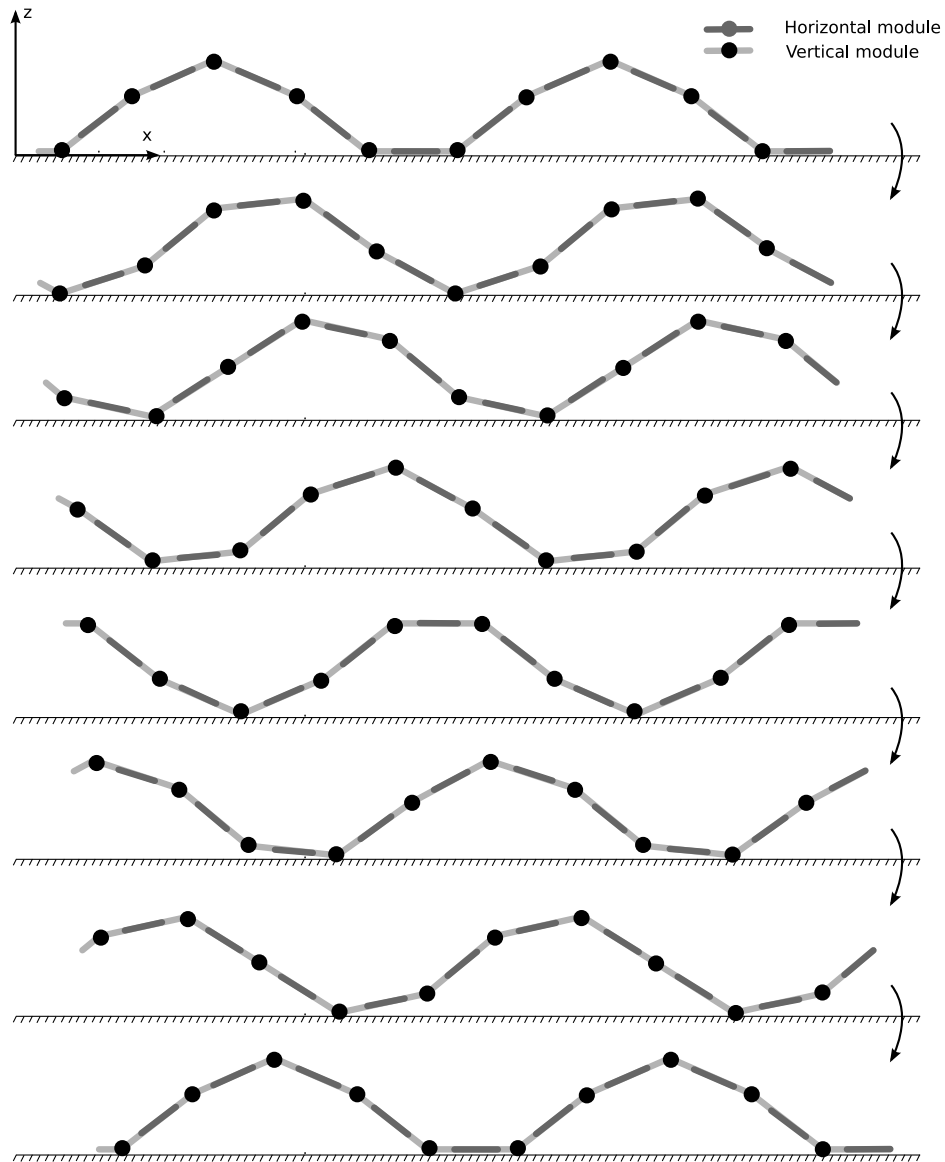


Figure 5.6: Statically stable locomotion of a twenty modules apodal robot of the pitch-yaw group

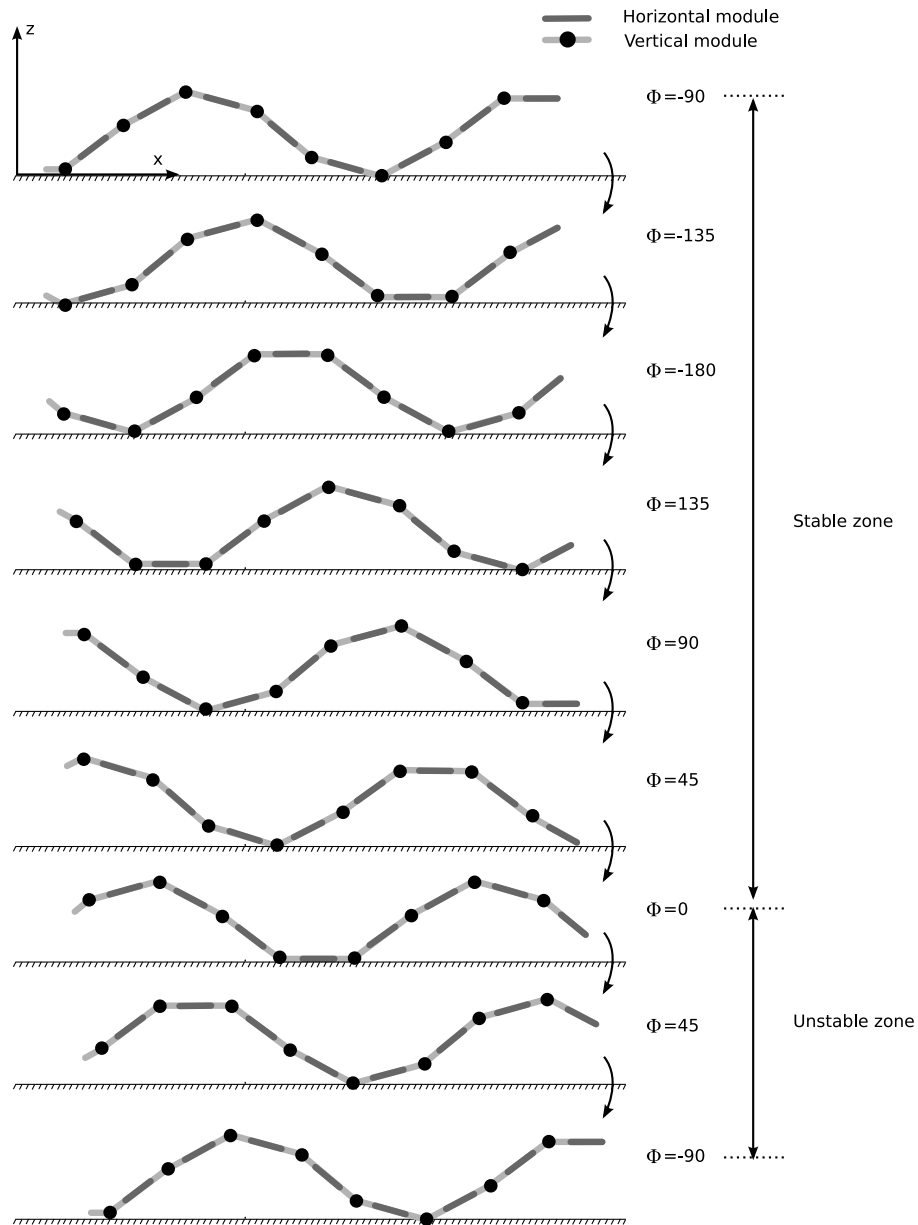


Figure 5.7: Not statically stable locomotion of a sixteen modules apodal robot of the pitch-yaw group

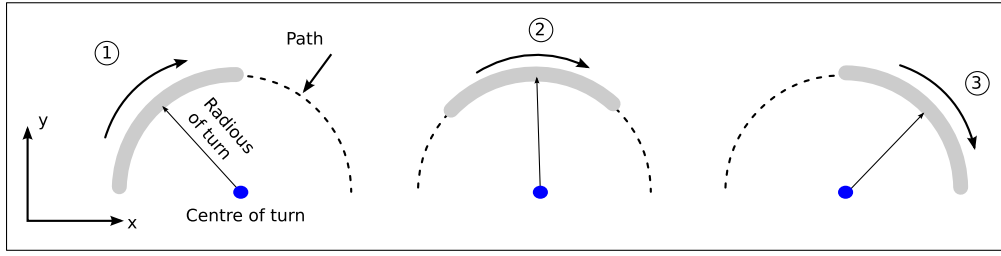


Figure 5.8: The robot moving along a circular path located on the xy plane

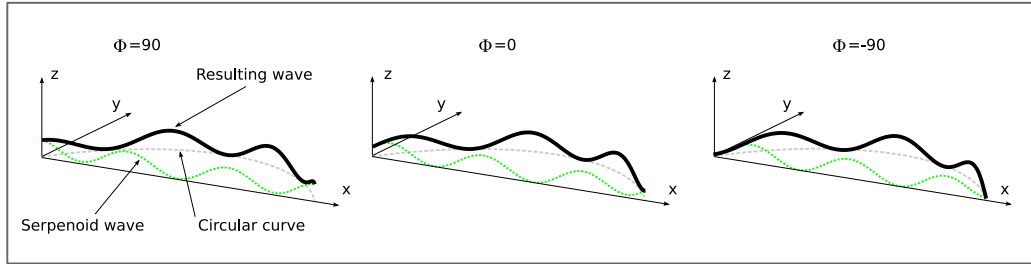


Figure 5.9: Robot shape when moving along a circular path: Superposition of a circular curve and a serpenoid wave

5.5 Circular path

5.5.1 Description of the gait

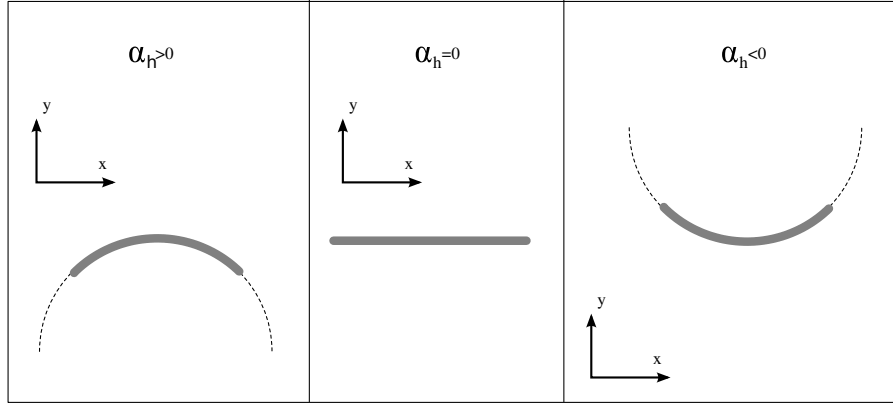
When a circular curve is superposed on the horizontal joints and a serpenoid wave in the vertical ones the robot moves following a path in a circular arc with a radius of turn r (figure 5.8). The circular curve in the horizontal forces the projection of the robot on the xy plane to be a circular arc. The propagation of the serpenoid wave for the verticals provokes the movement in one direction or another of the arc.

The movement has three degrees of freedom (α, k, α_h):

- α : Winding angle of the vertical serpenoid wave. $\alpha = \alpha_v \in [0, 120]$
- k : Number of undulations in the vertical serpenoid wave. $k = k_v \geq 1$
- α_h : Angle of the horizontal circular arc. $|\alpha_h| \in [0, 360]$

5.5.2 Robot shape

The robot's shape is a serpenoid wave that is "bent" in the form of a curve. In the figure 5.9 the circular curve is shown, the vertical serpenoid and the composition of both, for three different phases. The wave is propagated for the length of the circular path causing the robot's movement.

Figure 5.10: Path orientation according to the sign of α_h

5.5.3 Paths

The circular path that the robot follows is determined by the radius of the turn r . For a circular curve of length l , this radius is given by the equation 3.47. Given that in the vertical joints there is a serpenoid wave, its projection in the xy plane has a length equal to its width w . In addition his width, as well, as seen in section 4.2.4.2, does not depend on the number of undulations, but only on the winding angle. Therefore, the path that the apodal robot follows has a radius of turn r given by the equation:

$$|r| = \frac{w(\alpha_v)}{\alpha_h} \cdot \frac{180}{\pi} \quad (5.1)$$

where α_h is expressed in degrees and r in the same units as w .

The path depends only on the parameters α_v and α_h . The sign of α_h determines the orientation of the path (figure 5.10). When α_h is positive the curve has an orientation (concave or convex). If it is negative it has the opposite orientation. When it is zero the movement is in a straight line, as in the section 5.4.

Given an orientation, the radius of turn depends on the values of α_h and α_v . In the figure 5.11 the paths for different values of its parameters for an apodal robot of constant length l are shown. The radius of turn (eq. 5.1) is inversely proportional to α_h and directly proportional to the width of the serpenoid, which diminishes with the increase of α_v (section 4.2.4.2).

The minimum value of the radius is obtained for $\alpha_h = 360$ degrees and $\alpha_v = 0$. In this situation the robot has the shape of a circumference of radius $l/2\pi$. For $\alpha_v > 0$, the circumference does not get to close because its projection length will be w (that is less than l). In this ring configuration the centre of turn is the same as that of the circumference and the robot will turn around it.

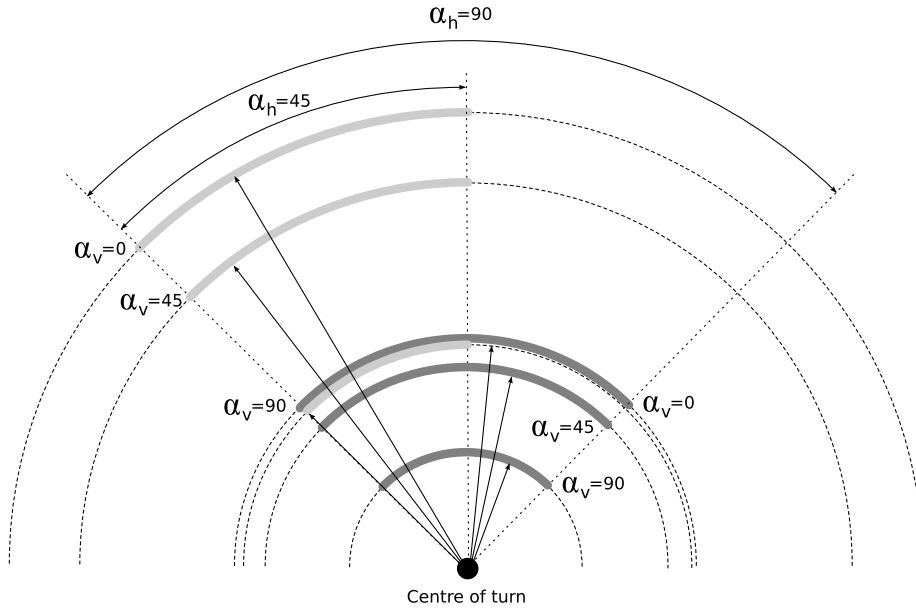


Figure 5.11: Three different paths for some values of the α_v and α_h parameters

5.5.4 Stability

5.5.4.1 Criterion of stability

For the analysis of stability we need to know the supporting points of the robot in function of the phase and of the parameters α_h , α_v and k_v . For the robot to be stable in all its phases it must be verified that there are at least three supporting points and the projection of the centre of mass lies within the polygon formed by these points.

Principle of stability *If the number of vertical undulations is greater than or equal to 3 ($k_v \geq 3$) then the movement of a continuous apodal robot in a circular path is statically stable.*

The demonstration of this principle has been made in numeric form for all the range of values of α_h and α_v with a resolution of one degree. For each pair of values (α_v, α_h) the co-ordinates of the supporting points and the centre of mass have been obtained, and it has been verified that the robot's centre of gravity fulfils the condition of stability.

In the figure 5.12 the projection of the robot's shape on the xy plane is shown, the polygon of supporting points and the centre of mass for different values of α_h and α_v in the three phases of -90 , 0 and 90 degrees. The most critical phase is $\phi = -90$. In it the centre of mass is very near to one of the lines of the support polygon. When the wave moves, the polygon varies, making sure that in all the phases the centre of gravity falls inside it.

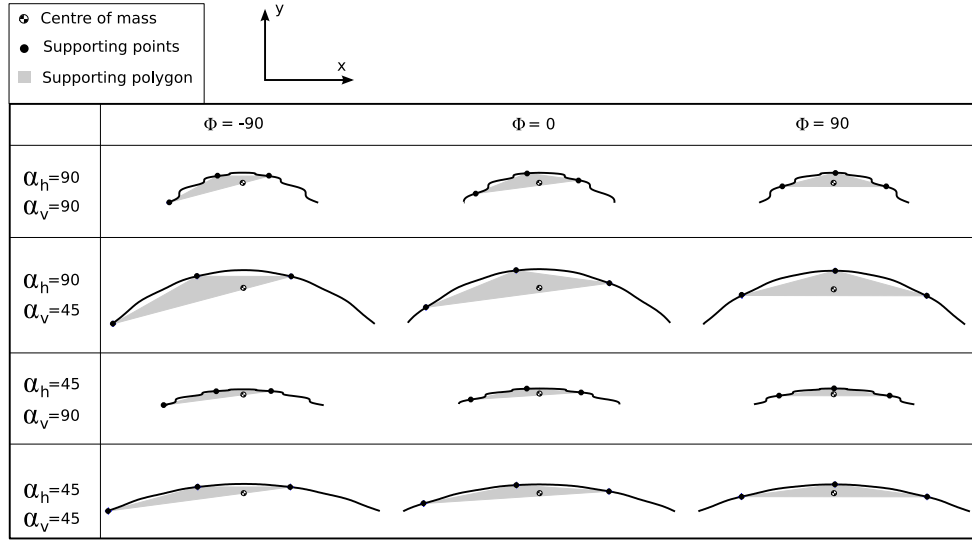


Figure 5.12: Supporting polygon and the centre of mass of an apodal robot with $k_v = 3$ for different values of the α_v and α_h parameters

5.5.4.2 Stability for $k_v < 3$

When the principle of stability is not fulfilled ($k_v < 3$), there are not always three supporting points, therefore the robot will incline to one side or the other. The parameters α_h , α_v and k determine the nature of the oscillation, with the possibility that the robot will fall over. In the figure 5.13 a robot with $\alpha_v = 45$ and $\alpha_h = 90$ with $k_v = 2$ has been represented. The phase $\phi = -90$ is stable. There are three supporting points and the centre of gravity falls within the supporting polygon. Nevertheless, when the wave is propagated there are only two supporting points. It happens for the phases $\phi = 0$ and $\phi = 90$. In these situations the robot will incline until there are one or more new supporting points. The supporting points in these phases are different. This means that the robot sways while it moves.

Therefore in the cases in which the principle of stability is not fulfilled ($k_v < 3$), the robot's movement in a circular path is possible, but not for all the values of α_v and α_h . There will always be oscillations in the movement that can be attenuated reducing the robot's height to achieve better stability. Nevertheless, when this is done the robot's step is reduced.

5.5.5 Discrete robot

In the discrete model limitations in the values of its parameters appear. We will calculate the minimum number of modules necessary to carry out the circular movement in a statically stable way and the limitations in the ranges of its parameters.

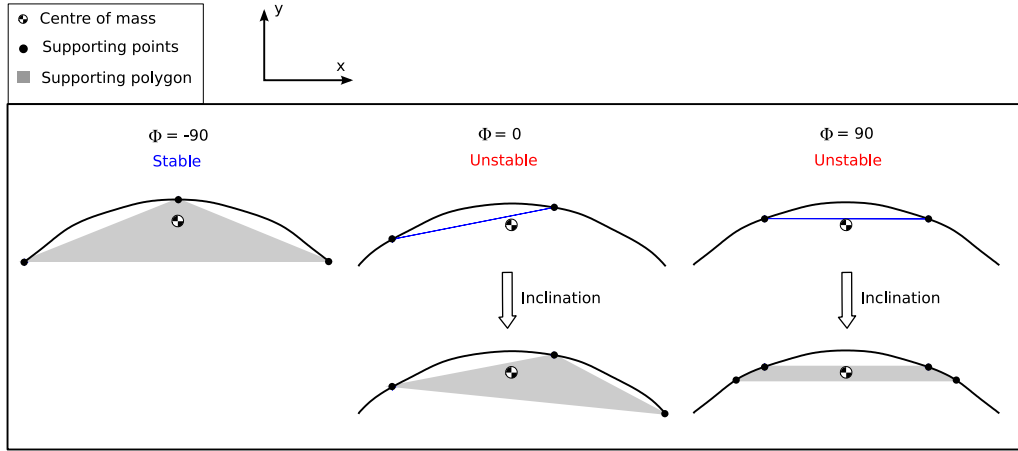


Figure 5.13: Supporting polygon and the centre of mass of an apodal robot with $k_v = 2$

5.5.5.1 Minimum number of modules

For a robot of the pitch-yaw group, the total number of modules M is related to the phase difference and the number of vertical undulations by the equation 3.45. M is directly proportional to k_v and inversely proportional to $\Delta\phi_v$ so the minimum will be obtained for k_v less ($k_v = 3$) and the $\Delta\phi_v$ maximum ($\Delta\phi_v = 180$):

$$M = \frac{4\pi k_v}{\Delta\phi_v} \geq \frac{12\pi}{\pi} = 12$$

This is the minimum value of M calculated mathematically. Nevertheless, owing to the principle of phase opposition, when the phase is 180 degrees, there is no locomotion. Therefore, it is necessary to add at least one more horizontal module and by definition the apodal robots of the pitch-yaw group have the same number of horizontal modules as vertical ones. Therefore the minimum number will be $M = 14$.

Principle of minimum number of modules *An apodal robot of the pitch-yaw group that has 14 or more modules, could move following a circular path in a statically stable way.*

5.5.5.2 Limitations

The parameters A_v and α_v have the same limitations as in the case of movement in a straight line (section 4.3.2.4): limitation by geometry and by the servo buffer. Therefore, in general, it is verified that: $\alpha_v \leq \alpha_{vmax} \leq 120$ and $A_v \leq A_{vmax} \leq 90$ where α_{vmax} and A_{vmax} are given by the equations 4.6 and 4.7 respectively.

For the horizontal joints the limitations are also by the geometry and the servo buffer. It is verified that: $\alpha_h \leq \alpha_{h_{max}} \leq 360$ and $A_h \leq A_{h_{max}} \leq 90$, where the maximum values are give by the equations:

$$\alpha_{h_{max}} = \begin{cases} 45M & M < 8 \\ 360 & M \geq 8 \end{cases} \quad (5.2)$$

$$A_{h_{max}} = \begin{cases} 90 & M \leq 8 \\ \frac{720}{M} & M > 8 \end{cases} \quad (5.3)$$

For its deductions we start with the equation 3.48 that relates the parameter α with the bending angle A of a circular curve and we particularise it for the pitch-yaw group in which there are $M/2$ horizontal modules:

$$A_h = \frac{\alpha_h}{\frac{M}{2}} = \frac{2\alpha_h}{M} \quad (5.4)$$

A_h is directly proportional to α_h therefore we will obtain its maximum value for the absolute maximum of α_h which is 360 degrees. Substituting this value in the equation 5.4 and applying the restriction $A_h \leq 90$:

$$A_{h_{max}} = \frac{720}{M} \leq 90$$

Clearing M we find that $M = 8$ is the value that defines the two areas of limitation. In one there will be geometric limitations and therefore $A_{max} < 90$. In the other the limitation will be the servo buffer and $A_{h_{max}} = 90$.

In a similar way for the parameter α_h we obtain:

$$\alpha_{h_{max}} = 45M < 360$$

For $M < 8$ the limitation will be due to the buffer and for $M \geq 8$ to the geometry.

5.6 Rolling

5.6.1 Description of the gait

In this movement the apodal robot rotates around its corporal axis and moves in a straight line along the y axis. It is composed of the superposition of two equal circular waves, one in the horizontal joints

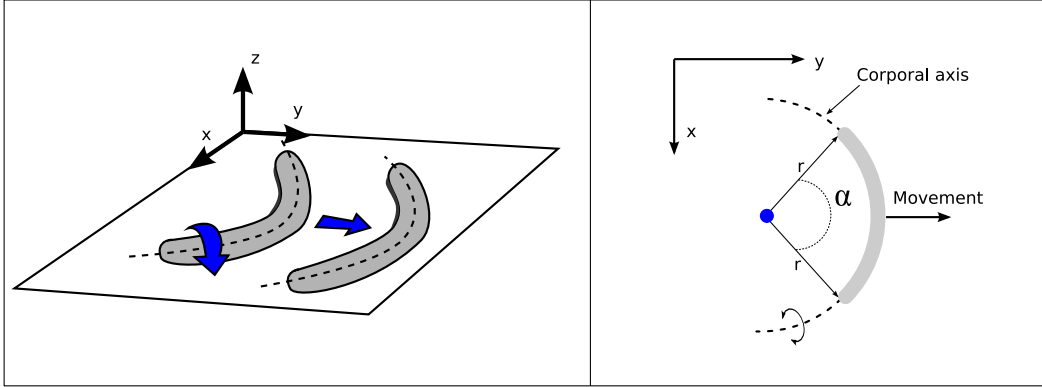


Figure 5.14: Description of the rolling movement

and the other in the vertical ones. The movement is characterised by the parameters α of the circular waves and the phase difference between them:

- α_v : Circular arc in vertical joints. $|\alpha_v| \in [0, 360]$.
- α_h : Circular arc in horizontal joints. $|\alpha_h| \in [0, 360]$
- $\Delta\phi_{vh}$: Phase difference between the vertical and horizontal waves.

Nevertheless, when $\alpha_v = \alpha_h$ and $\Delta\phi_{vh} = 90$ the shape of the robot is a circular arc that does not vary its radius of curvature with the phase. In these conditions the robot adopts the curved form and moves in a straight line, parallel to its corporal axis in a uniform, rectilinear movement (see figure 5.14).

Therefore, this movement is characterised by the parameter α that is the angle of the circular arc that it forms when it moves (It only has one degree of freedom).

5.6.2 Robot shape

When two equal circular waves are superposed, one in the vertical joints and the other in the horizontal ones, with the same value of α , the resulting shape is a circular arc that has an inclination with respect to the xy plane that varies with the phase ϕ . The bending angles between the vertical and horizontal joints are out of phase 90 degrees so that when some angles reach their maximum values the others will be 0 and vice-versa.

In the figure 5.15 the shape for the phases of 0, 45 and 90 degrees is shown (it is assumed that the initial phase ϕ_0 is zero). For $\phi = 0$, the horizontal joints form a circular curve of arc α , while the verticals are in their position of rest, with a bending angle of zero. The resultant arc is situated in the xy plane. For the phase $\phi = 90$ the opposite occurs. It is the verticals that have the shape of an arc

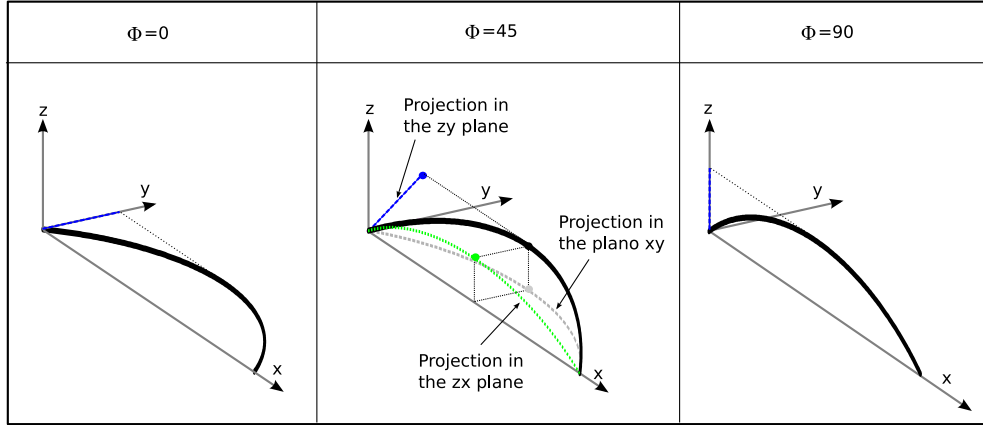


Figure 5.15: Shape of the corporal axis of the robot when rolling, for different phases

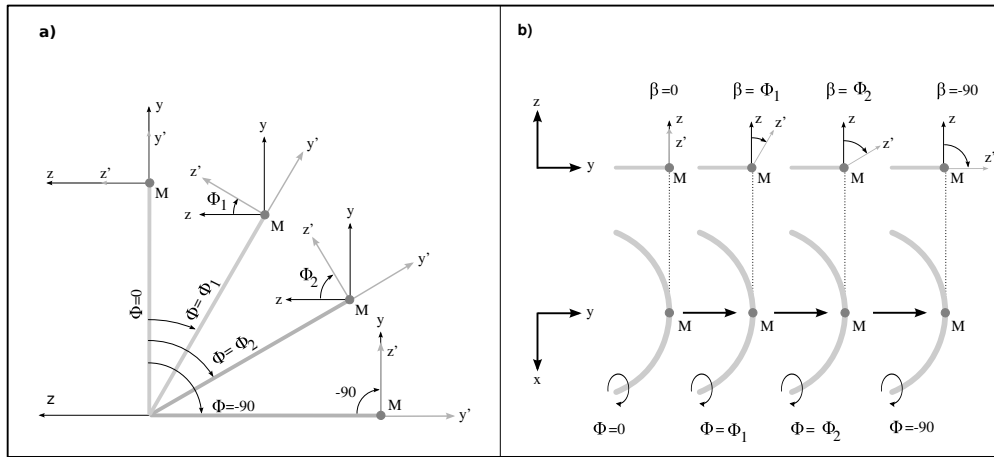


Figure 5.16: Mechanism of rolling

while the horizontals remain in their positions of rest which results in an arc situated in the xz plane. For a phase $\phi = 45$, the curve is an arc of α degrees that is inclined 45 degrees in relation to the xy plane.

The composition of two equal circular curves, with a phase difference of 90 degrees has the property that the angle formed with the xy plane is equal to the phase.

5.6.3 Mechanism of rolling

The curve that defines the robot's shape is rotated an angle equal to the phase. This means that the orientation of all its points also varies. In the figure 5.16 the shape of the curve for different values of the phase between 0 and -90 degrees is shown. Two reference systems are employed. One absolute xyz that is fixed to the ground and the other local, $x'y'z'$ situated at each point of the curve. In 5.16a)

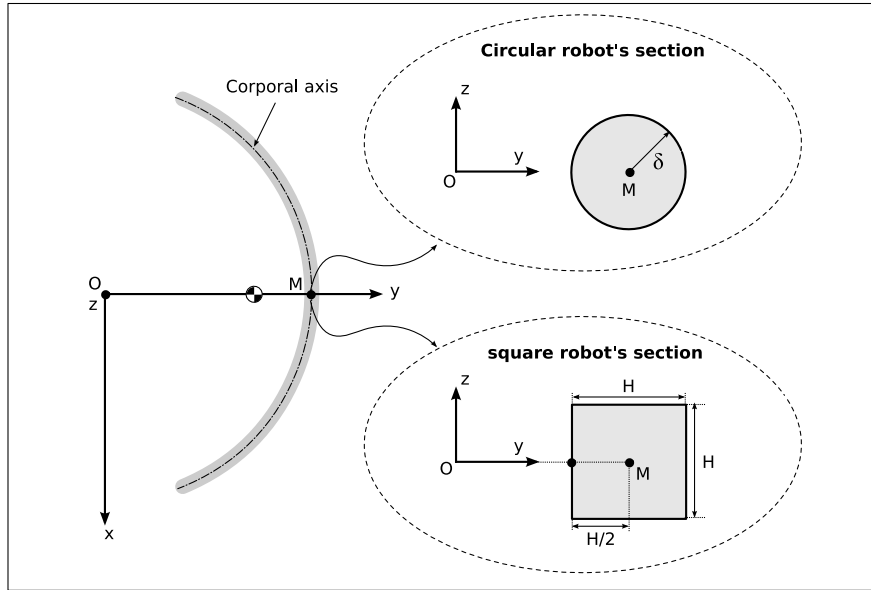


Figure 5.17: The two types of robot's section: circular and square

the projection of the curve in the zy plane has been represented and as an example the mid point of reference (M) has been taken. We define the orientation of the robot as the angle β that the z and z' axis of M form. This means that β is equal to the phase ϕ .

Due to the action of gravity, the curve is supported on the ground at all times. In the figure 5.16b) the projections in the zy and xy planes for different phases are shown. The shape of the curve does not vary with the phase and is always resting on the xy plane. But the orientation of its points does change, rotating around its local x' axis. The result is that all the points of the corporal axis of the robot rotate with an angular velocity: $w = 2\pi/T$ around x' , where T is the period of the oscillators.

5.6.4 Robot's sections

We will analyse the rolling movement taking into account two types of the robot's sections: circular and square. In the figure 5.17 both types and their parameters are shown, for a continuous robot situated on the xy plane. The point situated in the centre of the robot's axis ($s = l/2$) is denote by M , δ is the radius of the circle and H the side of the square.

To study the kinematics of the movement we will employ the model with a circular section. Given that the robot's corporal axis turns with angular velocity w , each one of the infinite sections behaves like a "wheel". We obtain the lineal speed of each one of them multiplying w by the radius δ . If the section were a point (wired model) there would be no movement.

The square section model allows us to study the real robot, that is formed by modules whose section

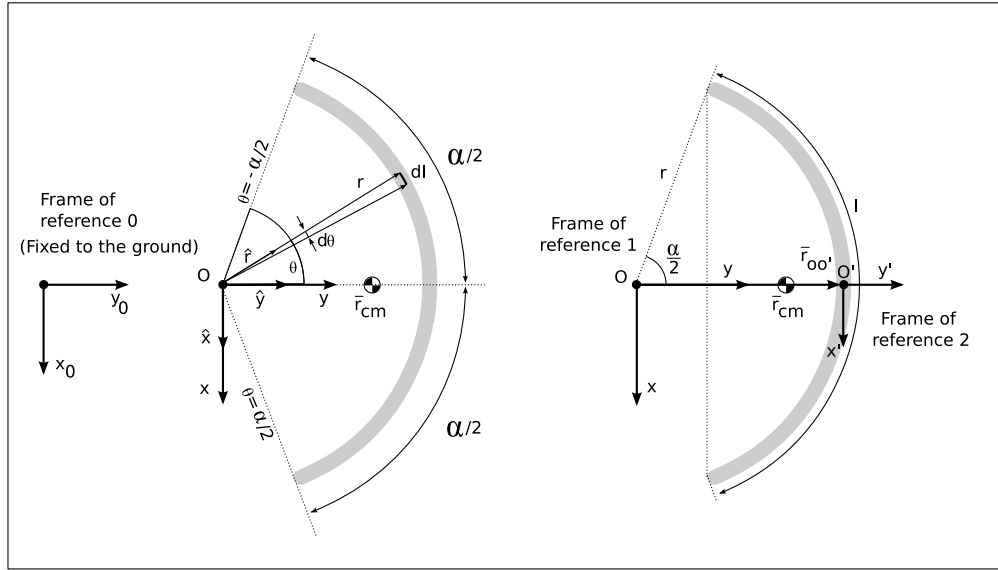


Figure 5.18: A circular arc with all its parameters and frames of reference

is of this type. We will see what restrictions appear when passing from the circular to the square model.

5.6.5 Kinematics

5.6.5.1 Fundamental notation and expressions

The notation employed and the explanatory drawings for studying the kinematics of the rolling movement are shown in the figure 5.18 and are summed up in the table 5.1.

Notation	Description
α	Angle of the circular arc
l	Length of the arc
θ	Integration variable
r	Radius of the arc
\hat{r}	Unitary radial vector
\hat{x}	Unitary vector of the x axis
\hat{y}	Unitary vector of the y axis
O	Origin of the frame of reference 1
O'	Origin of the frame of reference 2
\vec{r}_{cm}	Position vector of the centre of mass. Referred to frame 1
$\vec{r}_{oo'}$	Position vector of the frame of reference 2 in relation to 1

Table 5.1: Notation used for the description of the kinematics of the rolling gait

Three frames of reference are used. The 0 is fixed to the ground and its axis are x_o and y_o . It is employed to determine the speed and movement of the centre of mass of the robot. The frames 1 and 2 are local to the robot and move with it. The first has its origin in the centre of arc (O) and the second in the mid point of its body (O').

The radius vector \vec{r} that goes from the centre of the arc (O) towards one of its points is expressed as follows: $\vec{r} = r\hat{r}$ where r is the module of the radius and \hat{r} the unitary radial vector. The radius r is obtained from the parameters of the curve:

$$r = \frac{l}{\alpha} \quad (5.5)$$

The unitary radial vector is expressed in the frame 1 (with origin in O) as:

$$\hat{r} = \sin \theta \hat{x} + \cos \theta \hat{y} \quad (5.6)$$

The expression of the vector radius in function of the integration angle θ is:

$$\vec{r} = \frac{l}{\alpha} (\sin \theta \hat{x} + \cos \theta \hat{y}) \quad (5.7)$$

where \hat{x} and \hat{y} are the unitary vectors of the x axis and y respectively of the frame of reference 1.

The relation between the infinitesimals $d\theta$ and dl is:

$$dl = r d\theta = \frac{l}{\alpha} d\theta \quad (5.8)$$

The position vector of the origin of the frame 2 in relation to 1 is:

$$\vec{r}_{oo'} = \frac{l}{\alpha} \hat{y} \quad (5.9)$$

5.6.5.2 Centre of mass

The expression of the position of the centre of mass with respect to the frame 1 is:

$$\vec{r}_{cm} = \frac{2l}{\alpha^2} \sin\left(\frac{\alpha}{2}\right) \hat{y} \quad (5.10)$$

and with respect to the frame 2:

$$\vec{r}_{cm}' = \vec{r}_{cm} - \vec{r}_{oo'} = \frac{l}{\alpha} \left(\frac{2}{\alpha} \sin\left(\frac{\alpha}{2}\right) - 1 \right) \hat{y} \quad (5.11)$$

Proof: To calculate it we begin with the definition of the centre of mass:

$$\vec{r}_{cm} = \frac{1}{m_t} \int \vec{r} dm \quad (5.12)$$

where m_t is the total mass of the robot, \vec{r} the vector radius and dm the differential of mass. It is supposed that the mass is distributed uniformly along the length of the robot. The differential of mass is put in function of dl :

$$dm = \frac{m_t}{l} dl$$

And applying the equation 5.8 we obtain:

$$dm = \frac{m_t}{\alpha} d\theta \quad (5.13)$$

Substituting the expressions 5.8 and 5.7 in 5.12, we have:

$$\vec{r}_{cm} = \frac{l}{\alpha^2} \int_{-\frac{\alpha}{2}}^{\frac{\alpha}{2}} (\sin \theta \hat{x} + \cos \theta \hat{y}) d\theta$$

Given that the interval of integration is symmetric, the function sin is uneven and cos is even. The integral remains:

$$\vec{r}_{cm} = \frac{2l}{\alpha^2} \hat{y} \int_0^{\frac{\alpha}{2}} \cos \theta d\theta$$

and solving it we have the expression 5.10.

5.6.5.3 Path and speed

In this movement the body of the robot adopts the shape of a circular curve and rotates around its corporal axis at an angular velocity w . For the calculation it is supposed that the robot's section is circular, of radius δ . The position and the speed of the centre of mass is referred to by the frame 0, fixed to the ground.

In these conditions, the speed at which the robot's centre of mass displaces is given by the expression:

$$\vec{v}_{cm} = \frac{2w\delta}{\alpha} \sin\left(\frac{\alpha}{2}\right) \hat{y}_0 \quad (5.14)$$

It is a constant speed therefore it is a uniform rectilinear movement that is performed along the length of the y_0 axis, that passes through the robot's mid point (M). The speed depends on the parameter α . This means that it is the robot's shape that determines its speed. Therefore, when the robot's body is a complete circumference ($\alpha = 2\pi$), its speed is equal to 0. The robot does not move, though its points continue to rotate around its corporal axis at an angular velocity w .

The maximum value of the speed is obtained when $\alpha \rightarrow 0$, which corresponds to a robot's shape that tends to be a straight line. In these conditions the expression $\sin(\alpha/2)$ is approximated for $\alpha/2$ and we get:

$$v_{max} = \lim_{\alpha \rightarrow 0} V_{cm} = w\delta$$

The maximum speed is equal to the lineal speed of the points of its perimeter. Nevertheless, this is only correct for the values of α near to 0 in which the curve tends to be a straight line. For $\alpha = 0$ the equation 5.14 is not valid as in this case there are no circular waves and the bending angles of all the robot's articulations will be 0, therefore there will be no movement.

The space travelled by the robot with respect to the frame of reference 0 supposing that in the initial instant it is situated at the origin is obtained multiplying the equation 5.14 by the time t :

$$\vec{r}_{cm0} = \frac{2w\delta}{\alpha} \sin\left(\frac{\alpha}{2}\right) t \hat{y}_0 \quad (5.15)$$

Proof: We will deduce the equation 5.14. For this we will use the drawings shown in the figure 5.18.

It is supposed that the robot's section is circular of radius δ . Due to the rotation of its corporal axis with an angular velocity w , the lineal speed at each one of its points will be equal to $w\delta$. Consider each one of its infinite sections as "wheels" that move in a radial direction, with speed:

$$\vec{v} = w\delta\hat{r}$$

The speed of the centre of mass will be due to the contribution of each one of these differential “wheels” and is calculated by means of its integration along the length of the corporal axis of length l :

$$\vec{v}_{cm} = \frac{1}{l} \int_0^l \vec{v} dl = \frac{w\delta}{l} \int_0^l \hat{r} dl$$

Substituting \hat{r} and dl for their respective expressions 5.6 and 5.8 we obtain:

$$\vec{v}_{cm} = \frac{w\delta}{\alpha} \int_{-\frac{\alpha}{2}}^{\frac{\alpha}{2}} (\sin \theta \hat{x} + \cos \theta \hat{y}) d\theta$$

Having in mind that the interval of integration is symmetric, the function sin is odd, cos is even and the y axis is parallel to y_0 :

$$\vec{v}_{cm} = \frac{2w\delta}{\alpha} \hat{y}_0 \int_0^{\frac{\alpha}{2}} \cos \theta d\theta$$

And resolving we arrive at the expression 5.14.

5.6.5.4 Step

The robot’s step along the length of the y_0 axis is the distance covered by the robot during a time interval equal to T . It is calculated from the equation 3.6 substituting \vec{r} for the expression 5.15. Resolving this the step equation is obtained:

$$\vec{\Delta r} = \frac{4\pi\delta}{\alpha} \sin\left(\frac{\alpha}{2}\right) \hat{y}_0 \quad (5.16)$$

Its module is denoted by Δy . To study the variation of step with α , the normalised step is defined as:

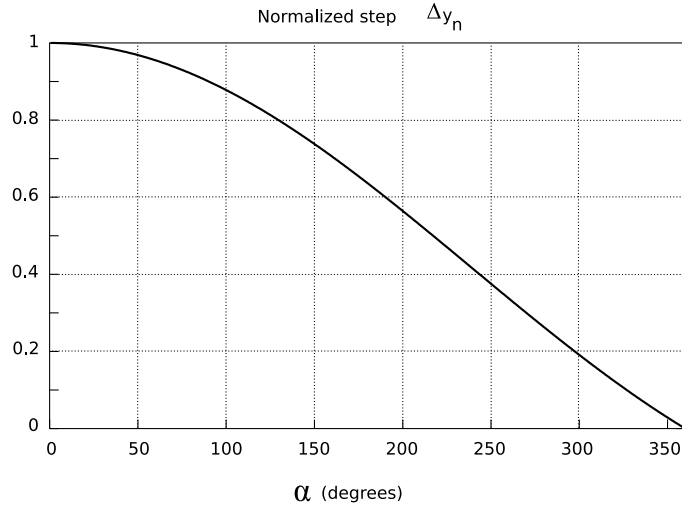


Figure 5.19: Graphical representation of the normalised step in function of α

$$\Delta y_n = \frac{2}{\alpha} \sin\left(\frac{\alpha}{2}\right)$$

with values in the range $[0, 1]$. This function depends only on α and not on the geometry of the module. In the figure 5.19 it is shown graphically and in the 5.20 the shape of the robot is shown for different values of α , together with the step.

For the case of a circular section, it is calculated from the normalised step multiplied by the perimeter of the circumference:

$$\Delta y = 2\pi\delta\Delta y_n = \frac{4\pi\delta}{\alpha} \sin\left(\frac{\alpha}{2}\right) \quad (5.17)$$

The step of the square section model The robot's step when the section is square is given by the expression:

$$\Delta y = 4H\Delta y_n = \frac{8H}{\alpha} \sin\left(\frac{\alpha}{2}\right) \quad (5.18)$$

The maximum value is equal to the perimeter of the section and is produced when α is near to zero. This situation is shown in the figure 5.21.

The robot's movement for both types of sections is essentially the same. After a cycle the distance travelled is equal to the product of its perimeter by the normalised step Δy_n , that does not depend on the type of section but on the angle of the arc (α).

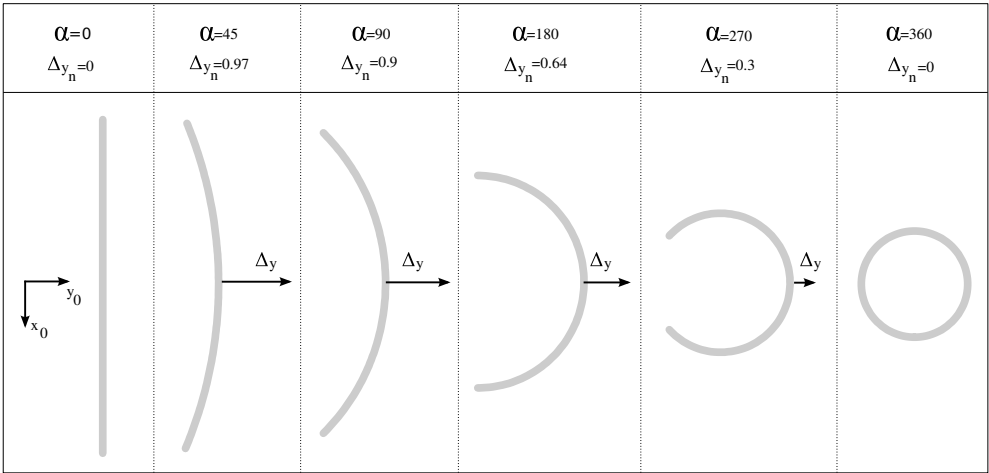


Figure 5.20: Relationship between the robot’s shape and the step

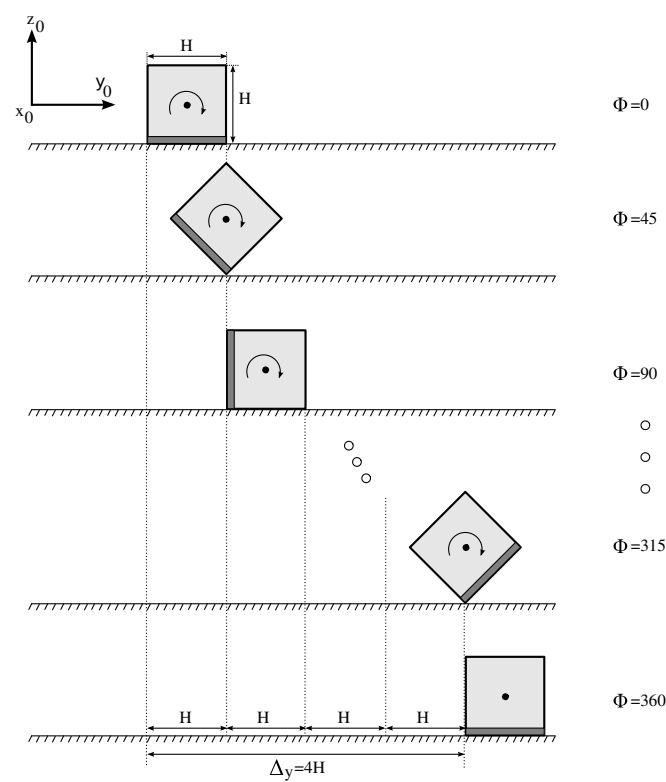


Figure 5.21: Step of the continuous robot with square section

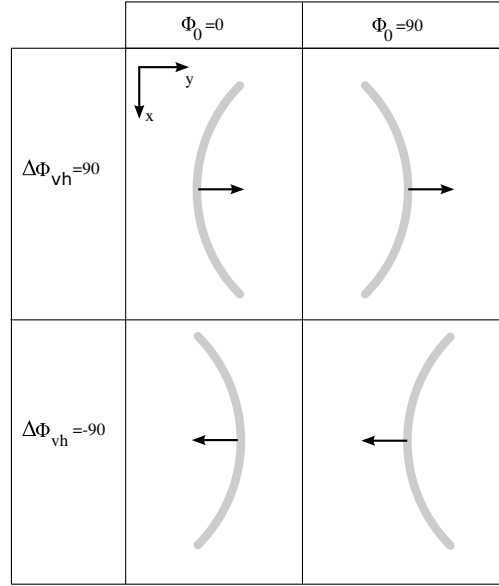


Figure 5.22: Direction of the movement and the robot's shape for different values of the $\Delta\phi_{vh}$ and ϕ_0 parameters

Nevertheless, the instantaneous position of the centre of mass is different. In the first case the height remains constant which means that the movement is smoother. In the second case, this height has oscillations and the movement is more abrupt. What is more, the square section imposes restrictions on the range of values of α . The movement is not made for all the values of α , but an α_{min} appears, below which value the robot does not roll (section 5.6.6).

5.6.5.5 Direction of movement

Chen et al. [12] studied the rolling movement and proposed it for overcoming obstacles. They showed that both the direction of movement and the shape of the robot when advancing are defined by the parameters $\Delta\phi_{vh}$ and the initial phase ϕ_0 . The results are summed up in the figure 5.22.

5.6.6 Limitations from the geometry

The type of section imposes restrictions on the values of α with which one can carry out the movement. When the section is circular, the robot will roll for any value of $\alpha \in (0, 360)$. Nevertheless, when the section is square this range is restricted to $\alpha \in [\alpha_{min}, 360)$. For $\alpha < \alpha_{min}$ the robot moves sideways without rolling (it carries out a flapping gait, described in the section 5.7.9).

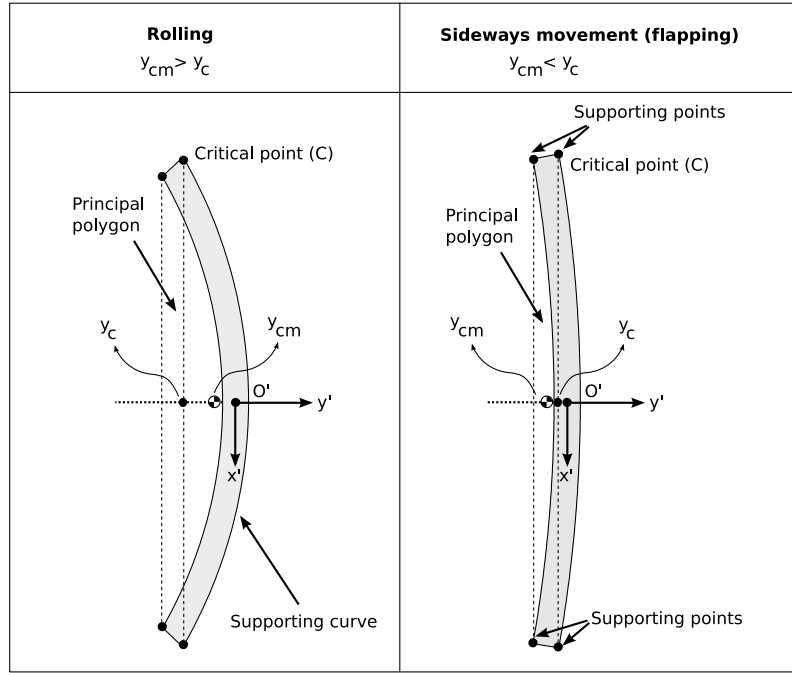


Figure 5.23: Rolling and sideways movement gaits according to the position of the centre of mass

5.6.6.1 Condition for rolling

The condition that must be fulfilled so that the square section robot carries out a rolling movement is that the ordinate of the centre of mass be greater than that of the critical point C :

$$y_{cm} > y_c \quad (5.19)$$

In the figure 5.23 a robot with a square section is shown with the centre of mass situated on both sides of the critical point C . The principal polygon is defined as that which forms the vertex of the tummy of the robot. When $y_{cm} < y_c$, the projection of the centre of mass is situated within the principal polygon which means that the robot remains in its normal orientation (it does not lean). A sideways type movement is produced.

When $y_{cm} > y_c$, the projection of the centre of gravity falls outside the principal polygon so that the robot leans on the supporting curve and it rolls.

The ordinate of the critical point can be expressed in the frame of reference 1:

$$y_c = \left(\frac{l}{\alpha} + \frac{H}{2} \right) \cos \frac{\alpha}{2}$$

and referred to 2 is:

$$y'_c = \left(\frac{l}{\alpha} + \frac{H}{2} \right) \cos \frac{\alpha}{2} - \frac{l}{\alpha} \quad (5.20)$$

5.6.6.2 Minimum angle α to roll

The rolling movement is realised when $\alpha \in (\alpha_{min}, 360)$ where the angle α minimum (in degrees) is given by the equation:

$$\alpha_{min} \approx \frac{120}{\pi} \left(\sqrt{\left(\frac{l}{H} \right)^2 + 18} - \frac{l}{H} \right) \quad (5.21)$$

When $\alpha < \alpha_{min}$ the movement will be flapping.

5.6.6.3 Proof

In this section, the deduction of the equation 5.21 is shown. From the expression 5.19 and substituting y_{cm} and y_c by their referred expressions from the frame 2 (eq. 5.11 and 5.20). We get the inequation:

$$\frac{l}{\alpha} \left(\frac{2}{\alpha} \sin \frac{\alpha}{2} - 1 \right) > \left(\frac{l}{\alpha} + \frac{H}{2} \right) \cos \frac{\alpha}{2} - \frac{l}{\alpha}$$

Grouping the terms we arrive at the expression:

$$\frac{2l}{\alpha^2} \sin \frac{\alpha}{2} - \left(\frac{l}{\alpha} + \frac{H}{2} \right) \cos \frac{\alpha}{2} > 0$$

The term on the left is denoted as $f(\alpha)$. The value α_{min} is obtained resolving the equation:

$$f(\alpha_{min}) = 0$$

This can be done by means of numeric methods. Nevertheless, the approach we have adopted is to approximate $f(\alpha)$ for another function $f_a(\alpha)$ that permits an analytical expression to be obtained.

Developing the function $\sin \frac{\alpha}{2}$ in a power series and retaining the first two terms:

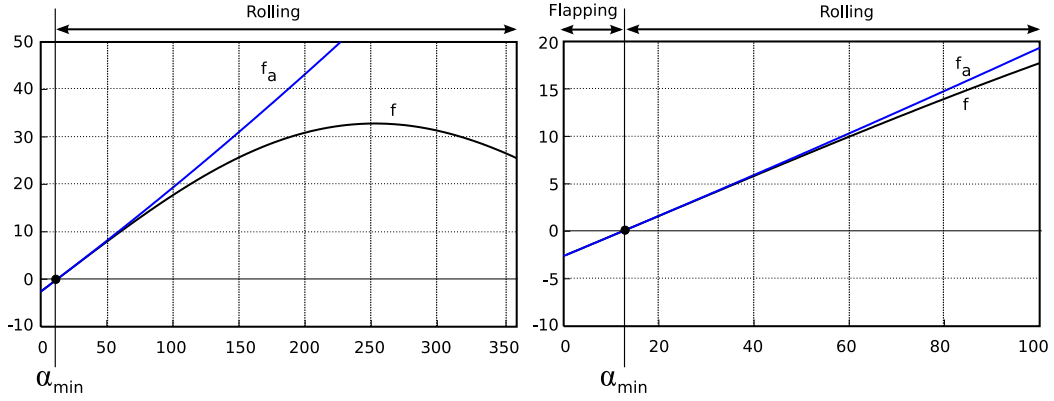


Figure 5.24: Graphical representation of the functions f and f_a for a ratio l/H of 10

$$\sin\left(\frac{\alpha}{2}\right) \approx \frac{\alpha}{2} - \frac{1}{3!}\left(\frac{\alpha}{2}\right)^3 = \frac{\alpha}{2} - \frac{\alpha^3}{48}$$

Doing the same with the function $\cos \frac{\alpha}{2}$:

$$\cos\left(\frac{\alpha}{2}\right) = 1 - \frac{\left(\frac{\alpha}{2}\right)^2}{2!} = 1 - \frac{\alpha^2}{8}$$

and substituting these expressions in the expression f , the approximated function is:

$$f_a(\alpha) = \frac{H}{16}\alpha^2 + \frac{l}{12}\alpha - \frac{H}{2}$$

Equating to zero and simplifying, the second degree equation is obtained:

$$\alpha^2 + \frac{4}{3}\frac{l}{H}\alpha - 8 = 0$$

Resolving the value looked for of α_{min} required (in radians) will be obtained as a solution to the equation:

$$\alpha_{min} = \frac{2}{3} \left(\sqrt{\left(\frac{l}{H}\right)^2 + 18} - \frac{l}{H} \right)$$

Passing it into degrees the equation 5.21 is arrived at.

The function f and its approximation f_a is shown in the figure 5.24, for a value of l/H equal to 10. It is observed that it is almost a lineal function for low values of α .

5.6.7 Discrete model

5.6.7.1 Equations

The equations for the bending angles are:

$$\varphi_v = A \sin(\phi + \phi_0)$$

$$\varphi_h = A \sin(\phi + \Delta\phi_{vh} + \phi_0)$$

where the amplitude A is given by the expression :

$$A = \frac{2\alpha}{M} \quad (5.22)$$

The values $\Delta\phi_{vh}$ and ϕ_0 determine the direction of movement in relation to the shape (section 5.6.5.5) and the amplitude A the arc of the corporal axis.

5.6.7.2 Shape

The shape of the robot is a discrete circular arc with an angle α formed by $M + 1$ segments. In the figure 5.25 the shape of an 8 module robot is shown and $\alpha = 180$ degrees for the phases of 0, 45 and 90 degrees. It can be seen that the robot is not symmetric with respect to the y axis (except for the phase of 45 degrees).

5.6.7.3 Minimum number of modules

The minimum number of modules for the robot to roll is 3 (1 yaw module between two pitch modules). This configuration is studied in more detail in the chapter 6.

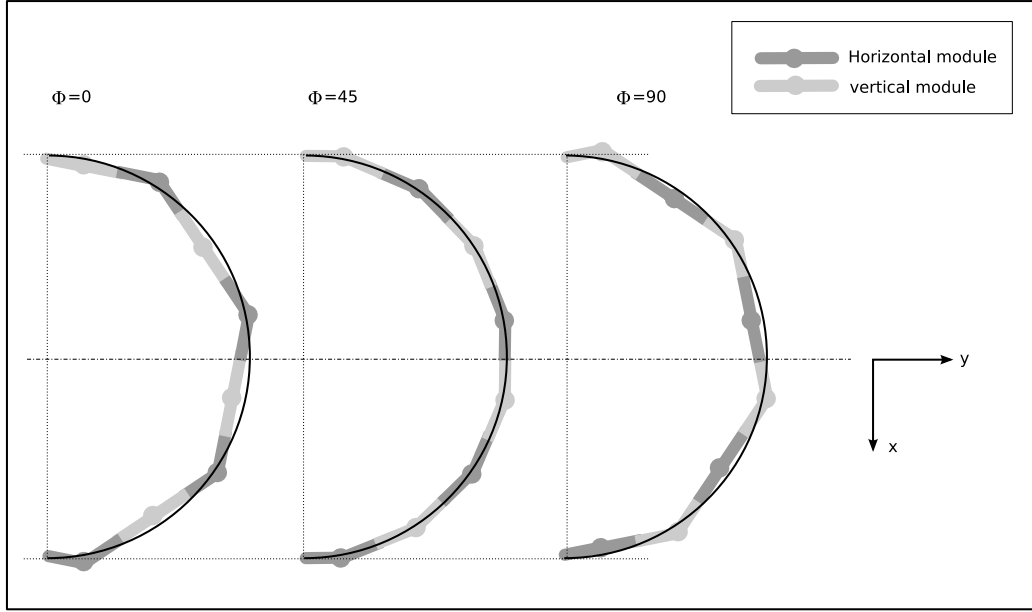


Figure 5.25: Comparison between the discrete and continuous models for three different phases. The robot has 8 modules and the parameter α is 180 degrees.

5.6.7.4 Limitations

In the discrete model the parameters α and A are limited in such a way that $\alpha \leq \alpha_{max} \leq 360$ and $A \leq A_{max} \leq 90$. The equations for α_{max} and A_{max} are 5.2 and 5.3 respectively, the same that the horizontal joints have in the case of a circular path movement (section 5.5).

5.6.8 Summary

A robot of the pitch-yaw type of M modules can roll when all the vertical and horizontal generators are in phase, the same amplitude A is applied to them and between the verticals and horizontals there is a phase difference of 90 degrees. In this situation the robot moves, adopting the shape of a circular arc of angle α . This angle is found between a maximum of 360 degrees and a minimum of α_{min} that depends on the type of the module's section and the relationship between the module's length (l) and width (H).

When $\alpha = 360$ there is no movement on the ground, but there does exist rotation of the corporal axis. This type of movement was simulated by Dowling[29] in his doctoral thesis. He proposed its utilisation for apodal robots' movement along the length of the outside of a tube, twining around its perimeter and rolling. Lipkin et al. [86] has used it in his latest prototypes.

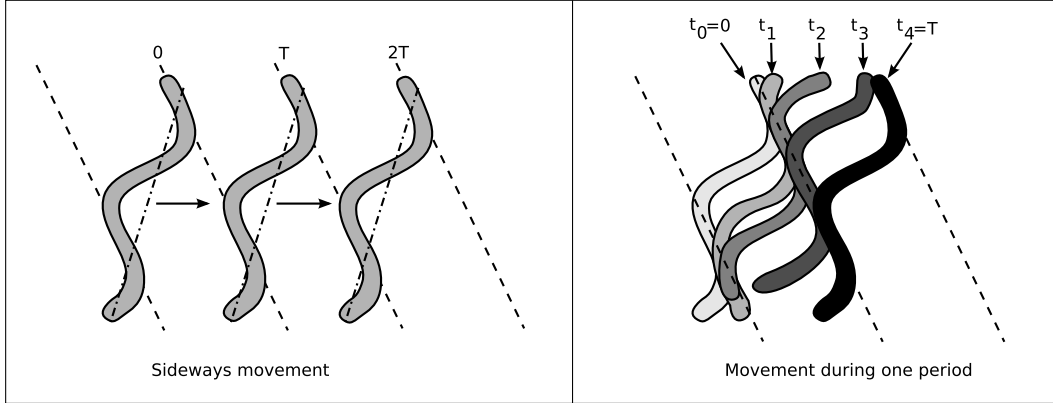


Figure 5.26: Sideways movement. Left: During two cycles. Right: Details of the movement during one cycle

5.7 Sideways movement

5.7.1 Introduction

The sideways movement category includes three different gaits. All of them allow the robot to move sideways maintaining its longitudinal axis with the same orientation. We will concentrate on the normal sideways movement. The other two types are the inclined sideways movement and flapping that are commented on in the sections 5.7.8 and 5.7.9 respectively.

5.7.2 Gait description

This movement allows the robot to move toward either side, without changing its orientation. The movement is known as *side-winding*. It is that which some types of snakes perform when they move along the sand. In the figure 5.26 the shape of the robot has been represented during its movement. The discontinuous lines join the points of the ground that have been in contact with its belly and correspond to the marks snakes would leave in the sand when they move in this way.

This type of sideways movement is obtained by means of the superposition of two serpenoid waves, one in the vertical joints and the other in the horizontal ones, with the same number of waves. The parameters that characterise the movement are 4:

- α_v : Winding angle of the vertical wave.
- α_h : Winding angle of the horizontal wave.
- k : Number of waves (the same for both verticals and horizontals).

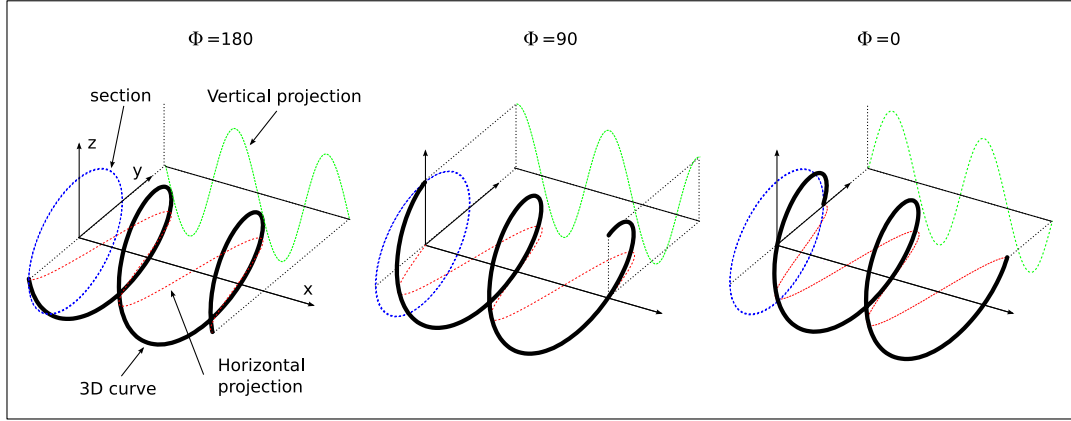


Figure 5.27: Graphical representation of a 3D isomorphous serpenoid wave for different phases and with $k = 2$, $\Delta\phi_{vh} = 90$ and $\alpha_v = \alpha_h$.

- $\Delta\phi_{vh}$: Phase difference between the vertical and horizontal waves.

The shape the robot's body adopts is that of a 3D serpenoid wave (section 3.6.4). If the condition of the flat wave is applied and the vertical winding angle becomes very small in comparison to the horizontal one this movement can be described by means of the parameters α , k that correspond with those of the horizontal wave. In the solutions obtained, the parameter $\Delta\phi_{vh}$ is 90 degrees.

5.7.3 Robot shape

In this section we will study the shape of the 3D serpenoid wave in relation to its four parameters.

5.7.3.1 Isomorphous waves

The composition of the two serpenoid waves with the same number of undulations (k) makes it appear a corporal three-dimensional wave that moves through the robot's longitudinal axis. The shape of this wave does not vary with the phase, it only moves. Therefore, the projection on the zy plane, that we will call section, is always the same for all the phases. We call this type of 3D serpenoid wave **isomorphous**.

In the figure 5.27 the propagation of an isomorphous wave is shown between the phases of 180 and 0 degrees, with $k = 2$. It is observed that the section is the same. For $\phi = 0$ the wave has displaced in a positive direction of the x axis.

The parameter k indicates the number of undulations that the three-dimensional wave has.

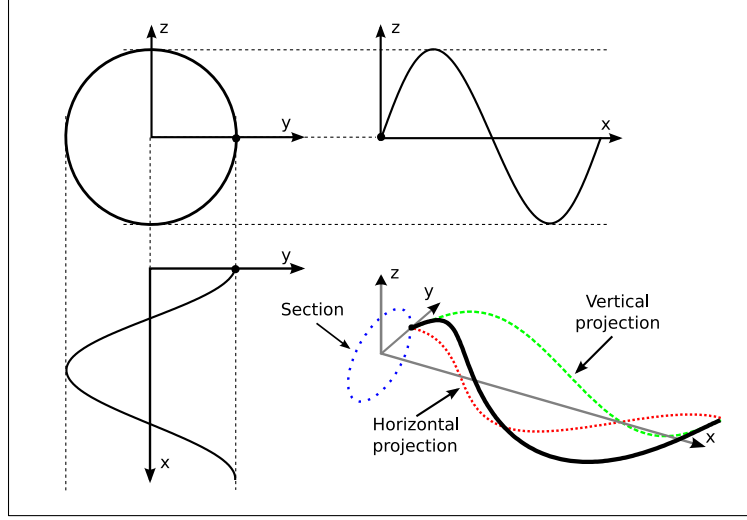


Figure 5.28: Circular isomorphous wave with con $k = 1$, $\alpha_v = \alpha_h$ and $\Delta\phi_{vh} = 90$ degrees

5.7.3.2 Parameter $\Delta\phi_{vh}$

The parameter $\Delta\phi_{vh}$ determines the shape of the wave's section, that can be:

- $\Delta\phi = 90$. **Circular isomorphous wave.** The projection in the zy plane is a circumference (figure 5.28). As we will see in the following section, the relation between the winding angles varies the scaling in the z axis.
- $\Delta\phi = 0$. **Linear isomorphous wave.** The section is a segment (figure 5.30). The robot shape is a serpenoid located on a plane perpendicular to the zy plane.
- $\Delta\phi \in (0, 90)$. **Elliptic isomorphous wave.** The section is an ellipse whose major axis is oblique to the y axis (figure 5.29). The minor axis varies with the phase difference being equal to the major for $\Delta\phi = 90$ and 0 for $\Delta\phi = 0$.

5.7.3.3 Relation α_v/α_h

The relation between the vertical and horizontal winding angles determines the scale of the z and y axis of the section. For a relation $\alpha_v/\alpha_h = 1$, the section has the same width as height. For $\alpha_v/\alpha_h = 0.5$ the height will be half the width.

Given the symmetry of the pitch-yaw group of robots, when carrying out a rotation of 90 degrees on its longitudinal axis, the modules that before were vertical now become horizontal and vice-versa. Therefore, if the relation α_v/α_h was equal to r , after the rotation of 90 degrees the shape of the

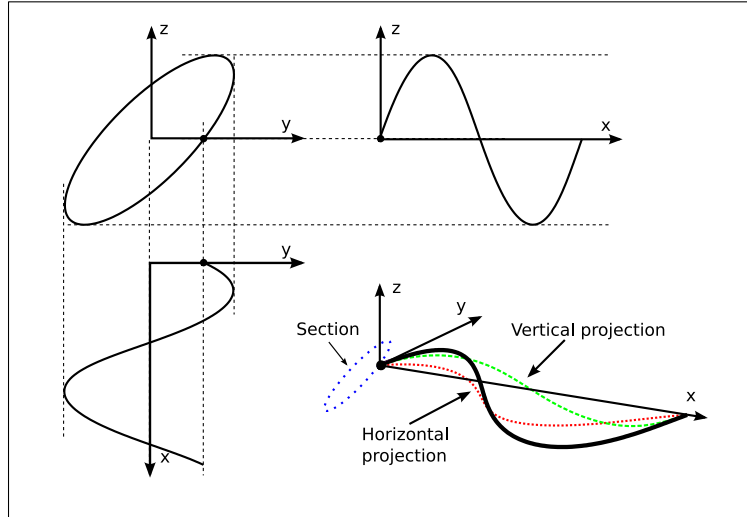


Figure 5.29: Isomorphous elliptic wave with $k = 1$, $\alpha_v = \alpha_h$ and $\Delta\phi_{vh} = 45$ degrees

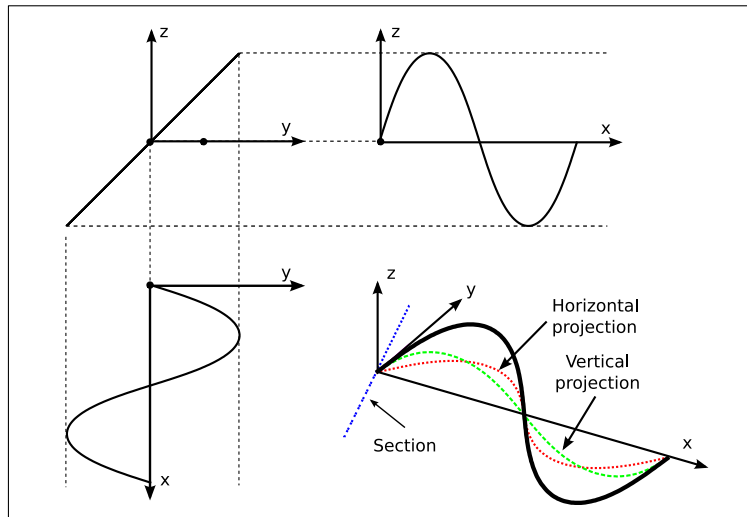


Figure 5.30: Linear isomorphous wave with $k = 1$, $\alpha_v = \alpha_h$ y $\Delta\phi_{vh} = 0$ degrees

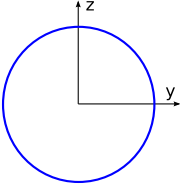
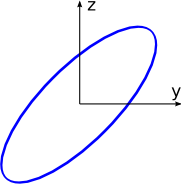
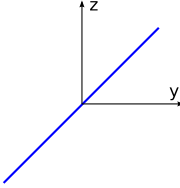
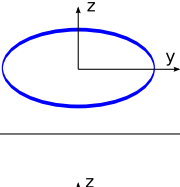
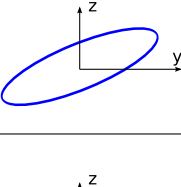
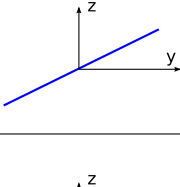
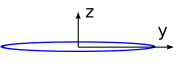
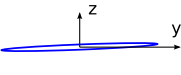
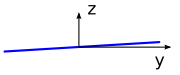
	Circular wave $\Delta\Phi_{vh}=90$	Elliptic wave $\Delta\Phi_{vh}=45$	Linear wave $\Delta\Phi_{vh}=0$
$\frac{\alpha_v}{\alpha_h}=1$			
$\frac{\alpha_v}{\alpha_h} = \frac{1}{2}$			
Flat waves $\frac{\alpha_v}{\alpha_h} \rightarrow 0$			

Figure 5.31: Type of waves according to the values of the parameters $\Delta\phi_{vh}$ and α_v/α_h

robot will be the same as if the relation $\alpha_v/\alpha_h = 1/r$ was applied. Because of this, only the values $\alpha_v/\alpha_h \in [0, 1]$ will be studied.

When the value of α_v is very small with respect to α_h the robot is “flattened”. We call this a **flat wave** (or plane wave) if it fulfils $\alpha_v/\alpha_h \rightarrow 0$. If $\alpha_v = 0$, there will not be a vertical wave, therefore the robot will have the shape of a serpenoid wave situated on the xy plane. The locomotion will have to be studied, as with the robots of the yaw-yaw group.

5.7.3.4 Linear isomorphous waves

The linear isomorphous wave has the shape of a serpenoid wave of parameters α and k that are found in a continuous plane that contains the x axis and is perpendicular to the xy plane. The value of the winding angle is given by the expression:

$$\alpha = \sqrt{\alpha_v^2 + \alpha_h^2} \quad (5.23)$$

The angle of inclination β that forms the plane of the wave with the y axis is:

$$\beta = \arctan\left(\frac{\alpha_v}{\alpha_h}\right) \quad (5.24)$$

This inclination is determined by the relation α_v/α_h . The maximum value is obtained for $\alpha_v/\alpha_h = 1$ and is of 45 degrees.

The values of the parameters α_h and α_v are obtained from the winding angle and the inclination by the expressions:

$$\alpha_v = \alpha \sin \beta, \quad \alpha_h = \alpha \cos \beta$$

The shape of the robot when isomorphous waves are used is characterised by the three parameters α , β and k . Within the category of the linear isomorphous waves we also include those in which the phase difference $\Delta\phi_{vh}$ is close to zero.

5.7.3.5 Flat isomorphous waves

The flat isomorphous waves have the shape of a serpenoid wave of parameters α and k situated on the horizontal (xy) plane. The winding angle is approximated by $\alpha \approx \alpha_h$.

The value of the parameter $\Delta\phi_{vh}$ is not important because as the wave is contained in the horizontal plane the circular, elliptic or straight shape are practically equal. Another characteristic is that the inclination of the isomorphous waves tend to be zero ($\beta \rightarrow 0$). Therefore, we only need the parameters α and k to characterise the robot's shape.

5.7.4 Stability

The stability of sideways movement is deduced from the shape of its section and therefore from the type of wave employed. For the movement to be statically stable it has to be ensured that the projection of the centre of gravity falls inside the support polygon. This polygon must have at least three unaligned points.

First we will analyse the stability in function of the parameter $\Delta\phi_{vh}$. According to its values we will have the circular, elliptic or linear waves. In the figure 5.32 the shape of its sections and the section of a real robot positioned on the ground are shown. The frame of reference formed by xyz is connected to the ground and the $x'y'z'$ are in the centre of the section and indicate to us its orientation.

In the case of a circular wave, all the supporting points are in the same straight line that passes through the point P and is parallel to the x axis. The robot is unstable. It will incline to the right, or the left or will oscillate. When the wave is elliptic the same thing happens. All the supporting points are on the straight line that passes through P and therefore it is unstable. Nevertheless, the stability is greater than in the previous case as the height of the centre of mass is lower.

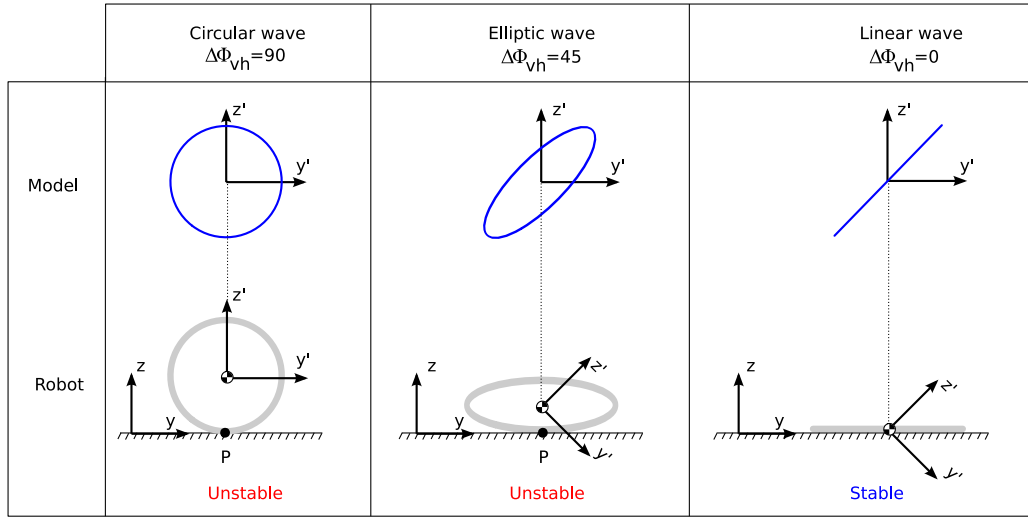


Figure 5.32: Robot stability according to the section of the wave

In the case of the linear wave, the robot is stable. The centre of mass is very near to the ground and will remain within the support polygon. If $\Delta\phi$ has a value near zero, the shape is not a straight line but a very deformed ellipse, with a very small lesser axis. The robot will not be statically stable as the section could incline toward one side or the other, but its oscillation will be negligible if $\Delta\phi$ is sufficiently small.

Principle of stability I *The linear isomorphous waves allow the robot's sideways movement to be stable.*

The analysis of the stability according to the values α_v/α_h is similar. The smaller the relation, the nearer will the centre of gravity be to the ground and the more stable will be the robot. But if it has a value of zero, then there will be only a horizontal serpenoid wave and no sideways movement. Therefore, the maximum stability is obtained when α_v/α_h is near to a zero but greater. That is to say, that when the vertical serpenoid wave is very small in relation to the horizontal one but with the winding angle sufficiently great to be able to lift the points from the ground and it can move.

Principle of stability II *The flat isomorphous waves permit the sideways movement of the robot to be stable.*

5.7.5 Wave types for the movement

Due to the principles of stability I and II, the sideways movement of the robot is characterised by the use of the **flat or linear isomorphous waves**. In both cases the shape of the robot will be that of a

Linea Isomorphous wave	Flat Isomorphous wave
α	α
k	k
α_v/α_h	$\alpha_v/\alpha_h \rightarrow 0$
$\Delta\phi_{vh} \rightarrow 0$	$\Delta\phi_{vh}$ does not matter

Table 5.2: Parameters for performing the sideways movement

serpenoid curve supported on the horizontal plane and characterised by the two parameters α and k . In the case of the linear wave α will be given by the equation 5.23 and for the plane wave it will be approximately by α_h .

What is more, for the linear waves the relation α_v/α_h allows the orientation β of the robot's points, to be changed, causing the robot to move in an inclined position (section 5.7.8). The information has been summarised in the table 5.2.

Therefore, the sideways movement is characterised by the same two parameters as in one-dimensional locomotion as in the case of the wired and continuous models the inclination of the points is indifferent.

5.7.6 Mechanism of movement

5.7.6.1 Framework of study

We will study the mechanisms to carry out the movement supposing that isomorphous plane waves are being employed and that the value of the parameter $\Delta\phi_h$ is 90 degrees. In this way we will make concrete explanatory drawings. Also we will suppose that $k > 2$ so that at all time at least two supporting points exist in the vertical projection.

From this we will analyse where the supporting points are situated, what happens in the transition between two close phases and finally what is the movement when a cycle has elapsed.

5.7.6.2 Supporting points

The supporting points are found in the part of the robot in which the co-ordinate z is minimum. That is to say, it is produced in the valleys of the vertical projection (zx plane) They have the following properties (see figure 5.33):

1. All the supporting points are found aligned according to the direction of the x axis. This is because there is only one contact point in the section of the robot (zy plane).

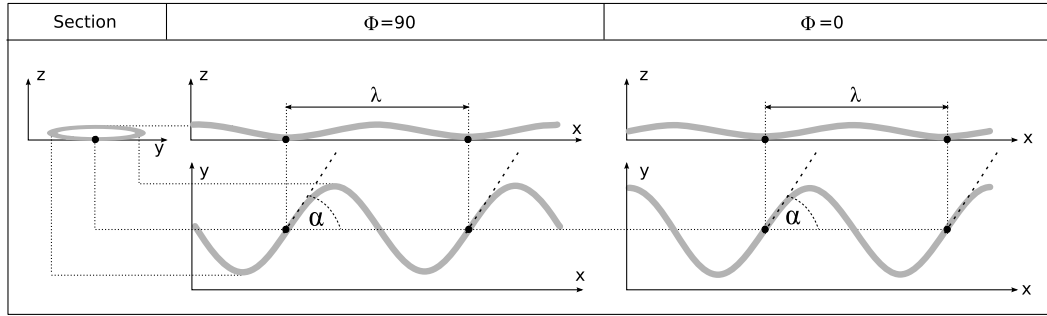


Figure 5.33: Supporting points for the phases 0 and 90 degrees

2. They are separated a distance equal to λ , which does not vary with the phase.
3. They are situated in the same point of the horizontal curve. As it is an isomorphous wave, the vertical and horizontal waves propagate with the same speed therefore the supporting points are always in the same position in relation to the horizontal curve.
4. As $\Delta\phi_{vh} = 90$ is taken, the supporting points are found in the points of the horizontal curve in which the slope is equal to the winding angle α .

In the figure 5.33 the vertical and horizontal projections, and the section for the phases of 90 and 0 are shown.

5.7.6.3 Movement between neighbouring phases

Initially the robot is in the phase Φ_1 , as is shown in the figure 5.34a), in which the supporting points are situated in the positions $s = s_i$ of the curve. When passing to the phase Φ_2 near to Φ_1 ($\Phi_2 = \Phi_1 + d\Phi$) the wave propagates and the new supporting points will be in $s_i + dl$, situated in the direction tangent to the curve at this point.

Therefore, when passing from the phase Φ_1 to Φ_2 the supporting points move following a straight line in the direction that forms an angle α with the x axis.

5.7.6.4 Movement during a cycle

At the end of a cycle, and supposing that there has been no sliding, the supporting points will have moved a distance equal to the length of an undulation of the curve ($l_u = l/k$), down the length of the straight lines that form an angle α with the x axis, as the figure 5.34b) shows.

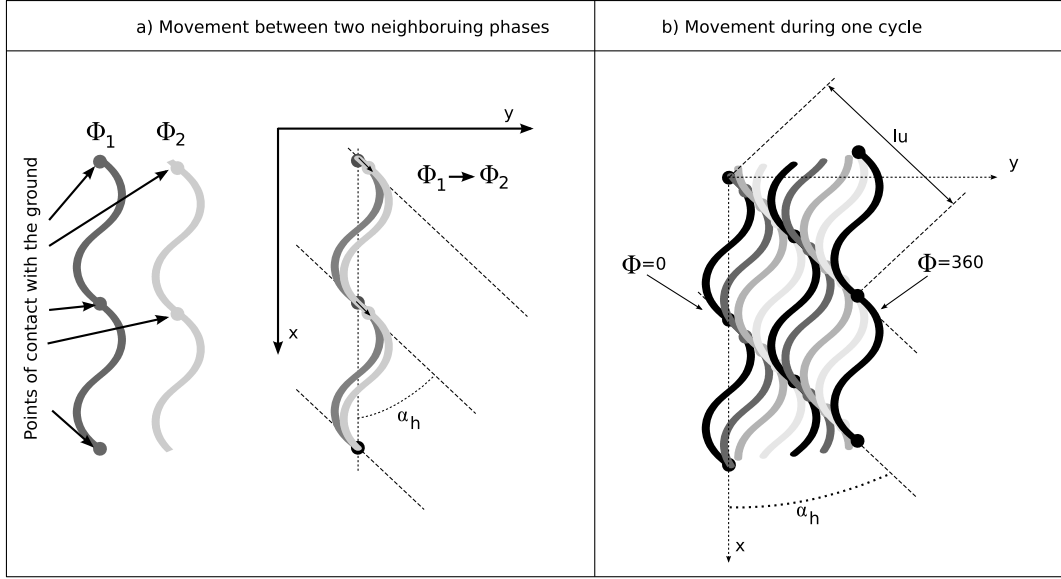


Figure 5.34: Sideways movement of the robot. a) Between neighbouring phases. b) During one cycle

5.7.7 Kinematics

5.7.7.1 Step equation

Given that there is no rotation, the kinematic parameter $\Delta\gamma$ is zero. The equation proposed to calculate the step is:

$$\vec{\Delta r} = \frac{l}{k} ((\cos \alpha - \lambda_n) \hat{x} + \sin \alpha \hat{y}) \quad (5.25)$$

where \hat{x} and \hat{y} are the unitary vectors in the x and y axis respectively and l is the robot's length. λ_n is the wavelength of a serpenoid of length 1 and number of waves equal to 1 that is calculated as $\lambda_n = x(1)$ where $x(s)$ is the function defined in 3.17.

The step module is:

$$|\vec{\Delta r}| = \frac{l}{k} \sqrt{1 + \lambda_n^2 - 2\lambda_n \cos \alpha} \quad (5.26)$$

and the direction of movement, defined as the angle γ that forms in relation to the y axis is:

$$\gamma = -\arctan \left(\frac{\cos \alpha - \lambda_n}{\sin \alpha} \right) \quad (5.27)$$

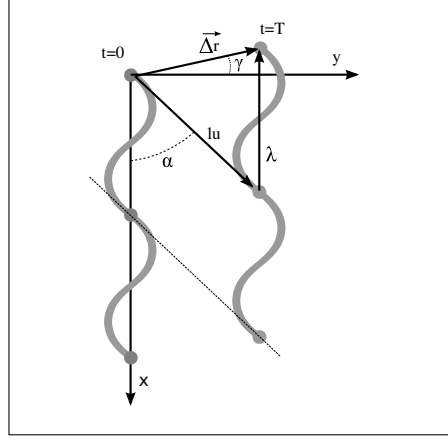


Figure 5.35: Deduction of the robot's step equation

5.7.7.2 Proof

The deduction of the equation 5.25 is obtained from the figure 5.35. The step is obtained by the following vector sum:

$$\vec{\Delta r} = \vec{l}_u + \vec{\lambda} \quad (5.28)$$

\vec{l}_u is a vector whose module is the length of an undulation and forms an angle α with the x axis. It is given, therefore, by the expression:

$$\vec{l}_u = \frac{l}{k} \cos \alpha \hat{x} + \frac{l}{k} \sin \alpha \hat{y}$$

The vector $\vec{\lambda}$ has as module the wavelength of the curve and is orientated toward the negative direction of the x axis:

$$\vec{\lambda} = -\lambda \hat{x}$$

Operating in 5.28 the following expression is arrived at:

$$\vec{\Delta r} = \frac{l}{k} \cos \alpha - \lambda \hat{x} + \frac{l}{k} \sin \alpha \hat{y} \quad (5.29)$$

The wavelength of a serpenoid curve can be expressed in function of the normalised serpenoid as:

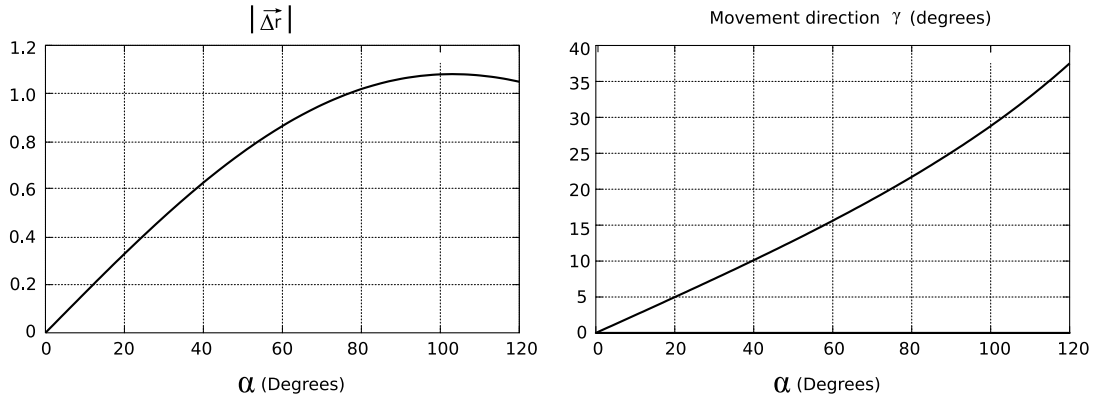


Figure 5.36: Variation of the step module and the direction in function of the α parameter

$$\lambda = \frac{l}{k} \lambda_n$$

Substituting in the equation 5.29 the final expression is arrived as required.

5.7.7.3 Variation with α

The variation of the step module and of the angle γ is shown in the figure 5.36 for a robot of unitary length and one undulation.

When the winding angle is increased, the robot's step increases and the path moves away from the direction of the y axis.

5.7.7.4 Direction of movement

For the same value of the parameter α the movement can be made in two different directions, and in each one of them in both directions, as is shown in the figure 5.37a).

The sign of $\Delta\phi_{vh}$ establishes in which of the two directions the robot will move, which will be defined by γ and $\gamma - 180$. In the figure 5.37b) the two families of supporting points are shown that there will be according to the sign of the phase difference. They will move along the straight lines that form α degrees with the x axis or for those that form $-\alpha$.

The direction of wave propagation decides the sign of the step. Therefore, if the step is given by $\vec{\Delta r}$, with a change of direction of propagation of the wave it becomes the opposite: $-\vec{\Delta r}$.

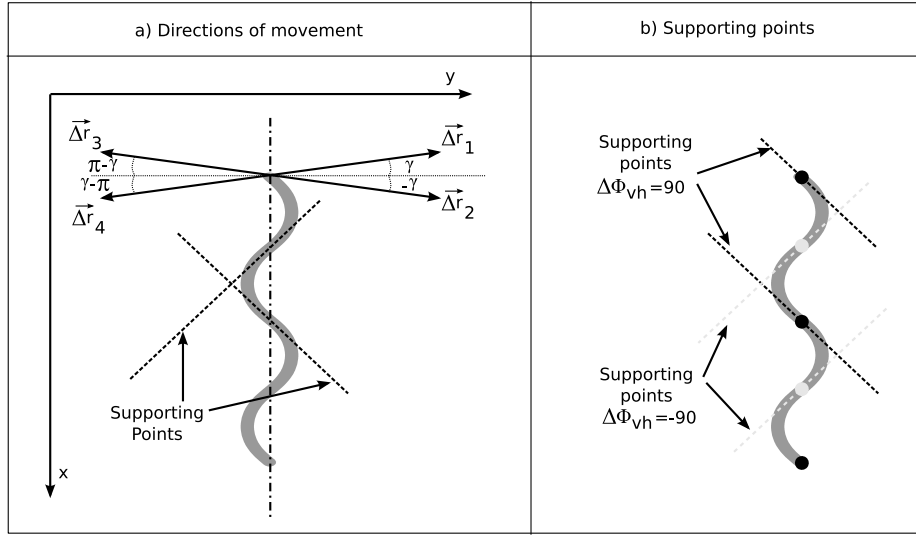


Figure 5.37: a) All the possible direction of movement for a robot with a given winding angle α . b) Position of the supporting points in function of the sign of the $\Delta\phi$ parameter

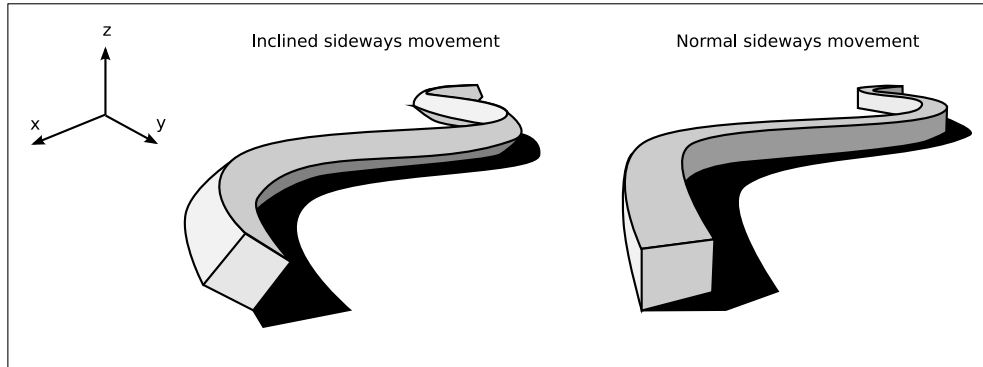


Figure 5.38: The two types of sideways movements: normal and inclined

5.7.8 Inclined movement

The sideways movement, as we saw in the section 5.7.5 is realised by flat or linear isomorphous waves. In both cases the parameters α and k allow us to determine the shape of the robot during this movement.

When linear waves are used it is also possible to control the robot's inclination, defined by the angle β that is calculated according to the equation 5.24. For the flat waves the inclination will always be zero degrees (or a value near to zero).

In the figure 5.38 two continuous robots with square sections have been drawn and that are moving using linear waves (left) and plane waves (right). Square sectioned robots have been chosen to be

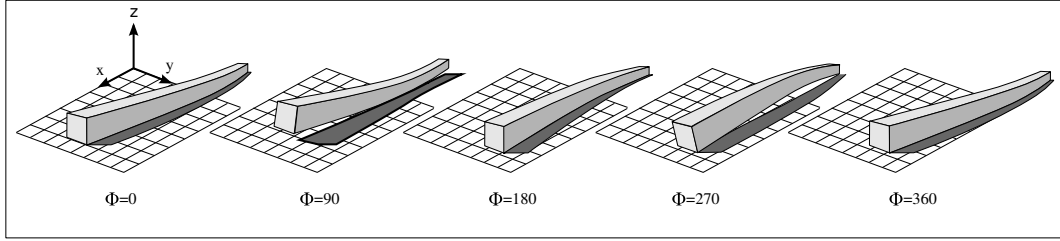


Figure 5.39: Flapping movement

able to appreciate the differences in the inclination. The robot on the left is inclined at a maximum angle β of 45 degrees.

One type of inclined movement was studied by Mori et al.[102] and implemented in the prototype ACM-R3. The movement achieved, described using the parameters and nomenclatures of this thesis, is based on linear isomorphous waves with $\Delta\phi_{vh} = 0$, so that all the points of the lower part of the robot are in contact with the ground. Because the ACM-R3 has passive wheels, when the serpenoid waves are propagated the robot is propelled forwards or backwards.

The movement that we have proposed allows the robot to carry out an inclined sideways movement. For this the parameter $\Delta\phi_{vh}$ has to be different to zero, but sufficiently small. This is, as far as we know, a new movement, previously not studied by other researchers.

5.7.9 Flapping movement

The flapping movement (or the rowing type movement) allows the robot to move sideways in a different way to that obtained by means of the flat or linear waves. In the figure 5.39 the movement of a square sectioned robot is shown, in five different phases. It is a similar movement to that of a rower in a boat, that moves the two oars at the same time to propel the boat. The robot's extremities follow a circular path. In the initial phase, $\phi = 0$, all the body is supported on the ground and is curved slightly backwards, the middle point being more advanced than the extremities. Then the extremities raise themselves and make a forward circular movement with the centre of the robot's tummy remaining in contact with the ground. In the phase $\phi = 180$ the situation is similar to the initial phase but with the body curved forwards, in such a way that now the central point is more retarded than the extremities. Finally the centre of the robot raises itself and moves forward supporting itself on the two extremities.

This movement is carried out applying the same circular waves as in the rolling movement (section 5.6). What differentiates one movement from the other is the curvature of the robot's body. For angles α less than an α_{min} (see section 5.6.6.2) a sideways movement is carried out and for greater angles the robot rolls.

This movement is known as flapping, and was first simulated by Dowling[29] in his doctoral thesis. Chen et al [13] implemented it and carried out experiments with a 10 module robot. Nevertheless

they did not propose an equation to define the α_{min} nor did they study the mechanisms why one or other type of movement is carried out.

The rowing type movement is slow, compared to the sideways movement (side-winding). Also the torque of the motors has to be greater as the length of the robot increases, so that the extremities can raise themselves. Nevertheless, it has the advantage that only three modules are necessary to carry it out, as is shown with the movement of the minimum configuration of pitch-yaw-pitch type presented in the chapter 6.

5.7.10 Discrete model

5.7.10.1 Equations

The equations for the bending angles of the vertical and horizontal joints are obtained from the general equations 3.43 and 3.44 applying the condition of isomorphous wave ($k_v = k_h$):

$$\varphi_{v_i} = 2\alpha_v \sin\left(\frac{2\pi k}{M}\right) \sin\left(\phi + \phi_0 + \frac{4\pi k}{M}(i-1)\right), i \in \left\{1 \dots \frac{M}{2}\right\}$$

$$\varphi_{h_i} = 2\alpha_h \sin\left(\frac{2\pi k}{M}\right) \sin\left(\phi + \phi_0 + \frac{4\pi k}{M}(i-1) + \frac{2\pi k}{M} + \Delta\phi_{vh}\right), i \in \left\{1 \dots \frac{M}{2}\right\}$$

The initial phase ϕ_0 determines the robot's shape in the initial moment and for the permanent movement regime it can be equalled to zero.

Expressed in function of the parameters of the oscillators and taking as initial phase $\phi_0 = 0$ the equations are:

$$\varphi_{v_i} = A_v \sin(\phi + \Delta\phi(i-1))$$

$$\varphi_{h_i} = A_h \sin\left(\phi + \Delta\phi(i-1) + \frac{\Delta\phi}{2} + \Delta\phi_{vh}\right)$$

5.7.10.2 The robot's shape

The shape the robot adopts when it moves using flat or linear isomorphous waves is that of a discrete serpenoid with parameters α and k . Therefore, the dimensions of the robot can be calculated applying

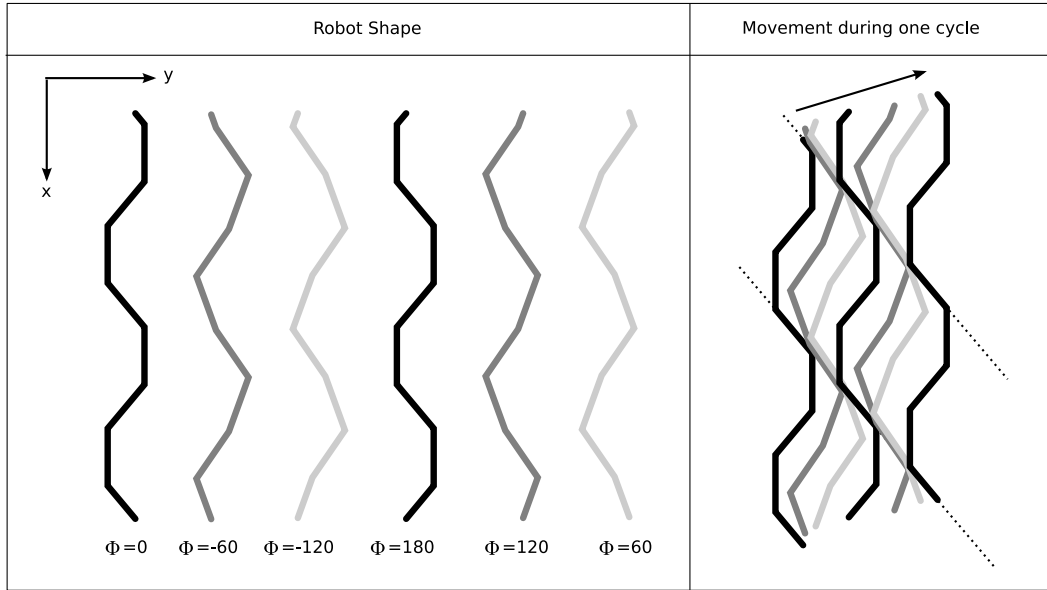


Figure 5.40: Sideways movement of a 16 modules apodal robot when using a flat isomorphous circular wave with $k = 2$ and $\alpha = 40$. a) The robot's shape in different phases. b) robot movement during one cycle

the same equations as in the case of one dimensional locomotion taking into account that the blocks are of the yaw type and the parameters d and d_0 are respectively $3L/2$ and $2L$ (see table 3.1).

In the figure 5.40 the movement of a 16 module apodal robot is shown. In the continuous case the robot's shape is always the same, only that it is displaced. The inclination of the points are always the same. In the discrete case the shape changes with the phase and therefore the inclination of the points also varies.

5.7.10.3 Minimum number of modules

The analysis of the minimum number of modules is realised in the same way as in the case of 1D locomotion. It has to be applied to a horizontal serpenoid wave and only taking into account the horizontal modules. On assigning a value of $\Delta\Phi$ equal to 180 degrees, there is no wave propagation therefore there is no robot movement. Also, to be able to use the equations of the robot's dimensions, there must be at least one undulation ($k \geq 1$).

Using the same criteria as for the 1D locomotion, if the number of horizontal modules is 2 ($k = 1$) there is a phase difference of 180 degrees, that does not allow for movement. Therefore there must be at least 3 horizontal modules, and as the configurations of pitch-yaw have the same number of horizontals as verticals, 6 is the minimum number of modules.

Parameter	Description	Range
M	Number of modules (vert+horiz)	$M > 6$
α	Winding angle	$\alpha \leq \alpha_{max} \leq 120$
$k = k_v = k_h$	Number of undulations (vert. y horiz)	$k \in [1, M/4]$
A	Horizontal generators amplitude	$A \leq A_{max} \leq 90$
$\Delta\phi$	Horizontal generators phase difference	$\Delta\phi \in (-180, 180)$

Table 5.3: Range of values for the different parameters for the sideways gait

For the flapping movement, nevertheless, the minimum number of modules is four. But a pitch-yaw-pitch type of configuration of only three modules can carry out this movement, as is shown in the chapter 6.

5.7.10.4 Limitations

The parameters A and α have the same limitations as in the case of the movement in a straight line (section 4.3.2.4): limited by geometry and by the servo buffer. Therefore, in general, it is verified that $\alpha \leq \alpha_{max} \leq 120$ and $A \leq A_{max} \leq 90$ where α_v and A_v are given by the equations 4.6 and 4.7 respectively. These equations have to be applied having in mind that the robot has $M/2$ horizontal modules.

The table 5.3 summarises the ranges of the parameter values.

When the inclined movement is employed, the limitation of α implies that the values of α_h and α_v meet with the restriction:

$$\sqrt{\alpha_v^2 + \alpha_h^2} \leq \alpha_{max}$$

For a maximum inclination of 45 degrees, where $\alpha_h = \alpha_v$, the value of α_h will always be less or equal to:

$$\alpha_h \leq \frac{120}{\sqrt{2}} = 84.85 \text{ grados}$$

5.7.11 Summary

A robot of M modules of the pitch-yaw type can move sideways when it uses flat or linear isomorphous waves. This is obtained by means of two superposed serpenoid waves, one in the horizontal joints and the other in the vertical ones, both with the same number of undulations.

There are three types of sideways movement according to the waves that are used.

1. **Main movement.** It is similar to that realised by some kinds of snakes when they move across sand (side-winding) and is obtained using flat waves, in which the winding angle of the vertical articulations is very small with respect to the horizontal ones.
2. **Inclined movement.** It is the same as the previous one, but the robot's body is rotated an angle β in relation to its corporal axis. It is obtained by means of the use of linear waves, with a value of $\Delta\phi_{vh}$ near to zero. The relation between the parameters α_v and α_h determines the angle of inclination. It is a movement that, as far as we know, has not been previously studied by other investigators.
3. **Flapping movement.** It is obtained applying two equal circular waves in which their parameter α is less than a limit angle α_{min} .

5.8 Rotation

5.8.1 Introduction

At least two gaits exist that allow the apodal robots of the pitch-yaw group to realise a rotation parallel to the ground, changing the orientation of their longitudinal axis. They are the rotation in “S” and in “U”. We will concentrate on the first that allows the rotation of robots of any length. The second is described in the section 5.8.7.

5.8.2 Gait description

By means of the rotating movement the robot turns parallel to the ground changing the orientation of its longitudinal axis an angle $\Delta\gamma$ in a clockwise or anti-clockwise direction. This allows the robot to change its orientation focusing the head toward the desired direction. It is a new way of movement that is not found in nature and has not been studied or implemented in any apodal type robot, as far as we know.

In the figure 5.41c) the initial and final positions of the robot after a cycle has been completed, are shown. The rotation is measured with respect to the longitudinal axis that passes through the centre of mass. In the figures 5.41a) and b) the robot's shape is shown during the rotation in the half-periods 1 and 2.

This movement is obtained by means of the superposition of two serpenoid waves, one in the vertical joints and the other in the horizontal, with a different number of waves. The parameters are:

- α_v : Winding angle of the vertical wave.

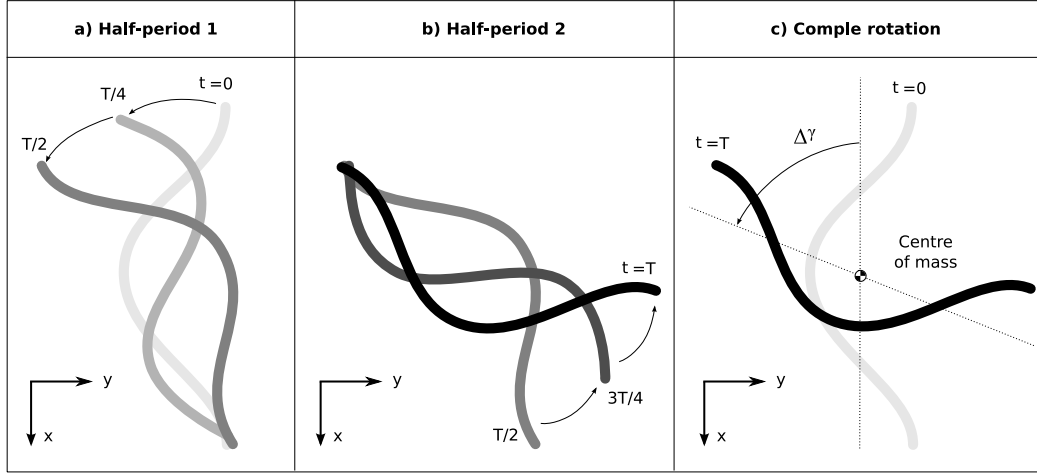


Figure 5.41: Rotation gait during one period, divided into two half-periods. a) Rotation during the first half-period. b) Second half-period. c) Initial and final positions.

- α_h : Winding angle of the horizontal wave.
- k_v : Number of the vertical waves.
- k_h : Number of the horizontal waves.
- $\Delta\phi_{vh}$: Phase difference between the vertical and horizontal waves.

The shape that the robot's body adopts is that of a 3D serpenoid wave (section 3.6.4). In the solutions found, the number of undulations of the vertical wave is double that of the horizontal ($k_v = 2k_h$) and $\Delta\phi_{vh} = 0$. What is more the wave is flat therefore $\alpha_v \ll \alpha_h$. The movement can be reduced to two degrees of freedom, defined by the parameters α and k , that correspond to the parameters of the horizontal wave.

5.8.3 The Robot's shape

5.8.3.1 Non isomorphous waves

When the superposed serpenoid waves have different numbers of waves ($k_v \neq k_h$) the shape of the 3D wave varies with the phase. Its projection in the zy plane will not be a constant curve, as in the case of the isomorphous waves, but it will go changing as it is propagated.

Having different values for k_v and k_h , the vertical wave is propagated at a different speed to the horizontal one, therefore the ground contact points are not in the same position in relation to the curve for all the phases, but they go moving. The interaction between the contact points with the

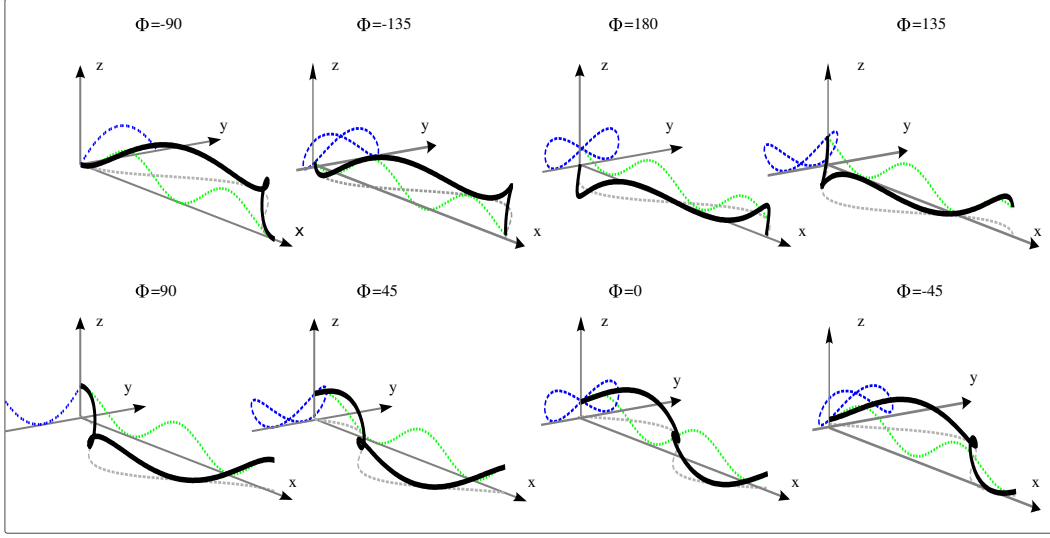


Figure 5.42: Robot's shape when two serpenoid waves are superposed, with $k_v = 2$ and $k_h = 1$, $\Delta\phi_{vh} = 0$

ground is not uniform. They will appear, in general, different forces for these points, therefore the robot will tend to turn. The relation k_v/k_h determines the supporting points that will appear in the robot and how these are moved by its body, determining the type of movement.

When $k_v/k_h \neq 1$ the wave is not isomorphous. The supporting points on the ground vary their relative distance one to the other and in general provoke a change in orientation. Nevertheless, the number of possible movements is infinite. The solution found is valid for robots with $M \geq 3$ number of modules. Among them $k_v/k_h = 2$ and $\Delta\phi_{vh} = 0$.

5.8.3.2 Wave with $k_v/k_h = 2$ and $\Delta\phi_{vh} = 0$

In the figure 5.44 the shape of a wave is shown when $k_v = 2$, $k_h = 1$ and $\Delta\phi_{vh} = 0$. Given that it is not isomorphous, the shape changes with the phase. The projection in the zy plane has different shapes according to the phase.

5.8.4 Stability

We will study the stability of the wave when $k_v/k_h = 2$ and $\Delta\phi_{vh} = 0$. In the figure 5.43 the projections in the yz planes (section), xz (vertical projection) and xy (horizontal projection) are shown together with the supporting points, when $k_h = 1$. In this situation there are only two supporting points, that guarantee the stability in the zx plane. Nevertheless, in the wired model it is unstable with respect to

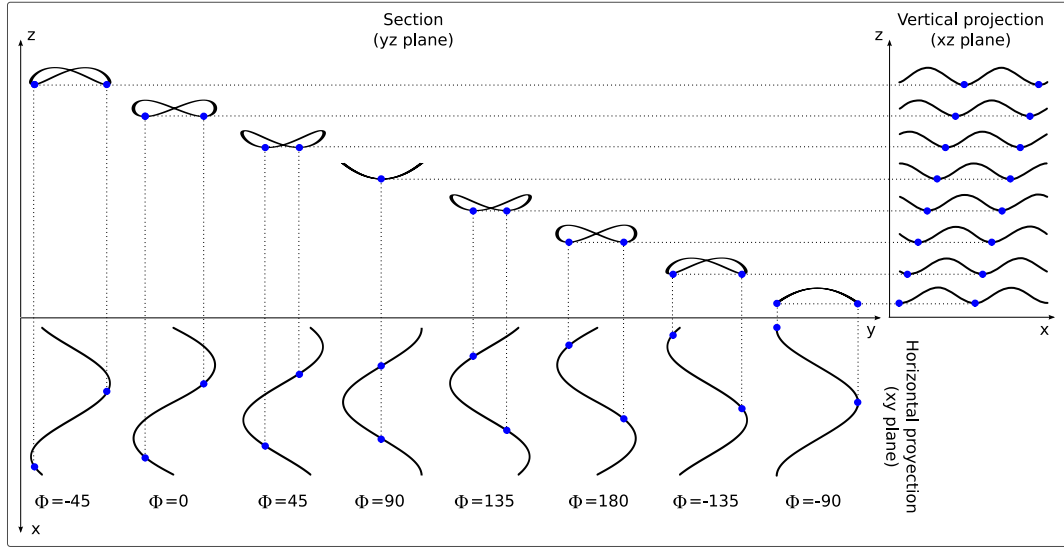


Figure 5.43: Robot's shape projections on the yz (upper), xz (right) and xy (lower) planes and the location of the supporting points

the x axis. It is necessary that there are at least three points of contact with the ground in the xy plane. The robot will rotate an angle around x until the third supporting point appears.

The supporting points go moving for the horizontal projection. Their relative position to the axis of symmetry goes changing. For the phase of 90 degrees they are in their furthest position. According as the phase changes, the points go nearing the axis until for a phase of -90 they are aligned with it. The relative movement of these points has two components: one parallel to the axis of symmetry and the other perpendicular to it. It is this movement perpendicular to the axis of moving toward or away from it that produces the rotation.

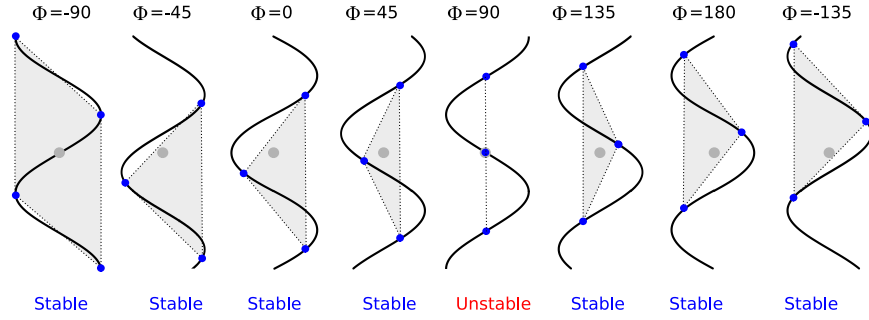
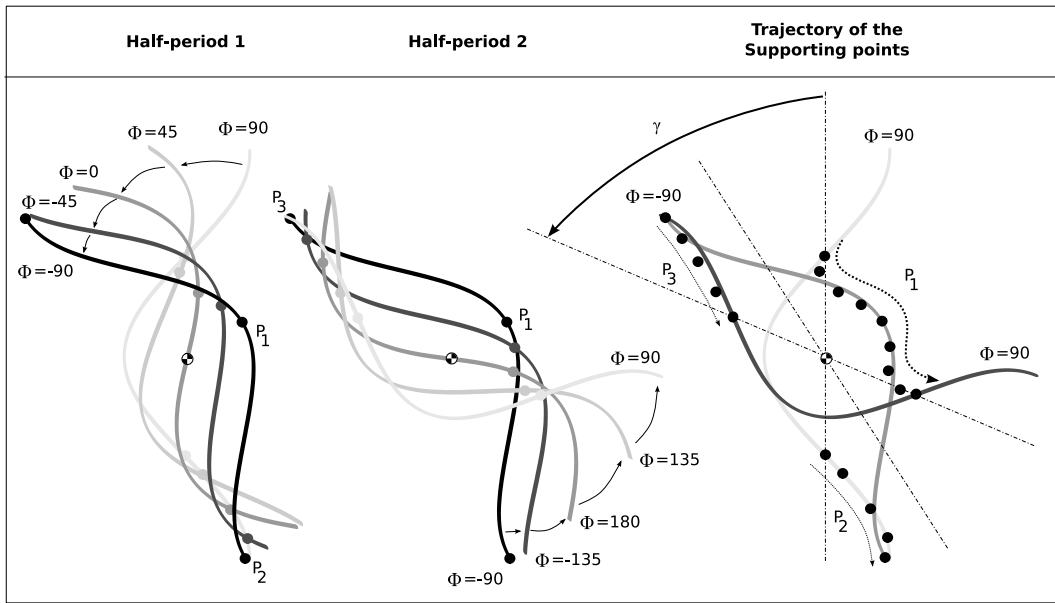
In general to obtain stability at least three support points will be necessary which means $k_h \geq 1.5$ must be fulfilled. In this situation the centre of gravity falls within the polygon formed by the three supporting points in all the phases except for $\phi = 90$, where the points are aligned and therefore the robot will fall over either to the right or the left, or will oscillate (figure 5.44).

Nevertheless, if instead of the wired model one with a square section is employed, this instability will disappear.

Another way to get stability is to use flat waves in which $\alpha_v/\alpha_h \rightarrow 0$. In this case, the same as with the side-winding, the robot's centre of gravity is very near to the ground and though there are not three supporting points at all times and the robot oscillates, these variations will be small.

Therefore there are two criteria for stability:

Stability Criteria I $k_h \geq 1.5$ and that the section is square.

Figure 5.44: Stability for $k_h = 1.5$ Figure 5.45: Rotation mechanism. Graphical representation of the supporting points with the ground during the rotation, when $k_v = 2$, $k_h = 1$ and $\Delta\phi_{vh} = 0$

Stability Criteria II *Flat waves, not isomorphous* $\alpha_v/\alpha_h \rightarrow 0$

5.8.5 Rotation mechanism

The rotation mechanism is due to the interaction of the supporting points with the ground. These points move through the length of the robot (figure 5.45). The rotation in a cycle can be divided into two stages: rotation during the first half-period (from $t = 0$ to $T/2$) and second (from $t = T/2$ to T). We take as the initial phase $\phi = 90$, where the supporting points are aligned with the robot's longitudinal axis. We will consider that the robot is made up of two parts of length $l/2$: the upper arm and the lower one. The supporting points will be P_1 and P_2 . The wave propagation is in the positive direction of the longitudinal axis ($x > 0$). P_1 and P_2 divides the curve into three parts that we will

call the upper, middle and lower extremities. Finally, the robot's extremities we will denominate the upper and lower extremities. Initially they are found in the points of the curve $s = l/4$ and $s = 3l/4$ respectively. According to the wave propagation, the P_1 moves toward the robot's central point $s = l/2$ and P_2 to the extremity $s = l$. As it advances, the upper arm becomes longer and the lower one shorter. The upper goes bending to the left in the measure that P_1 and P_2 move while the lower tends to remain in its position.

In the second half-period P_2 disappears and a new one appears, P_3 in $s = 0$. P_1 and P_3 move until they arrive at their positions situated in $s = 3l/4$ and $s = l/4$ respectively. The opposite occurs to the previous half-period. Now it is the right arm that is the longest, and which tends to bend toward the right while the left one tends to remain in its position.

When finalising the period, P_1 has travelled a distance equal to $l/2$ passing from $s = l/4$ to $3l/4$.

5.8.6 Kinematics

5.8.6.1 Rotation angle

To know the equation for obtaining the angle of turn in function of the parameters of the horizontal serpenoid curve, when flat waves are being employed, it is necessary to analyse the dynamic, obtain the components of force that act on the supporting points and the torque that they generate in relation to the centre of gravity. This analysis is outside the limits of this thesis and will be tackled in future studies.

Given the symmetry of movement in the two half-periods, during the discussion we will speak of the angle of rotation in a half-period γ_s . We will assume that the total rotation is: $\gamma = 2\gamma_s$.

5.8.6.2 Variation with α

The experiments carried out (chapter 7) prove that the angle rotated grows with the winding angle α_h .

5.8.6.3 Variation with k

The variation of the rotation angle with k is given by the expression:

$$\gamma = 4 \arcsin \left(\frac{\sin \left(\frac{\gamma_1}{4} \right)}{2k - 1} \right) \quad (5.30)$$

where γ_1 is the angle rotated when $k = 1$. In the graphic 5.46c the relationship is shown when γ_1 is of 30 degrees. It can be seen that when k increases the rotation angle diminishes. The figures 5.46a) and b) show the angle turned in a half-period for $k = 1$ and $k = 2$.

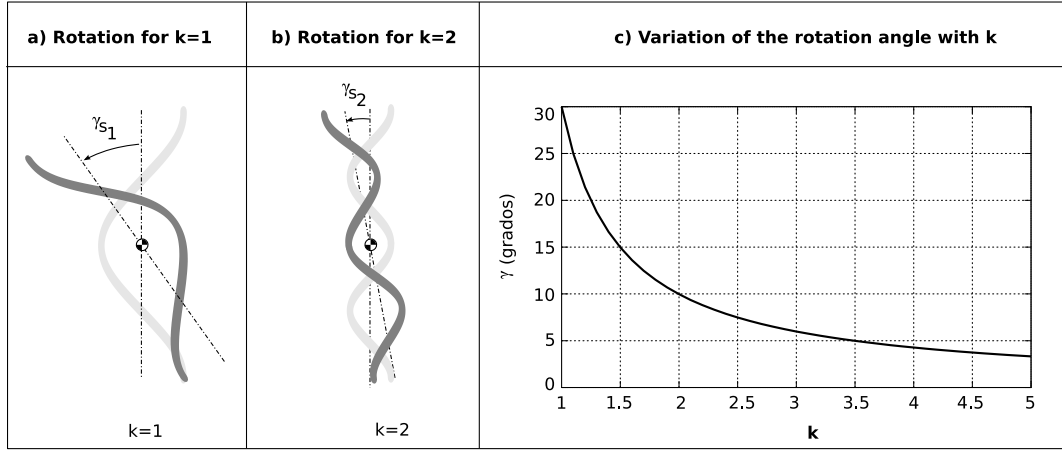


Figure 5.46: Rotation angle in function of k . a) Rotation with $k = 1$. b) Rotation with $k = 2$. c) Variation of the rotation angle with k

5.8.6.4 Demonstration

We will deduce the equation 5.30. We will study the variation of the rotation angle during a half-period. We call γ_{s1} the half-period angle 1 when $k = 1$ and γ_s for $k > 1$. The rotation angles in a period will be respectively:

$$\gamma_1 = 2\gamma_{s1}, \quad \gamma = 2\gamma_s \quad (5.31)$$

Starting with the initial phase $\phi = 90$ and we will take as reference the point P that is found at a distance of $\lambda/4$ from the centre of mass (figure 5.47a). When it has finished the half-period, the robot has rotated an angle γ_{s1} . The module of its vector movement is given by the expression:

$$\Delta r_1 = \frac{\lambda}{2} \sin\left(\frac{\gamma_{s1}}{2}\right)$$

When $k > 1$, the centre of mass is displaced a distance d in the positive direction of the axis as the figure 5.47b) shows. This distance can be expressed in function of k as:

$$d = \frac{\lambda}{2}(k - 1)$$

so that when $k = 1$, the centre of mass has not moved, for $k = 2$ it will be $\lambda/2$ displaced units. The movement of point P ($k > 1$) can be calculated as:

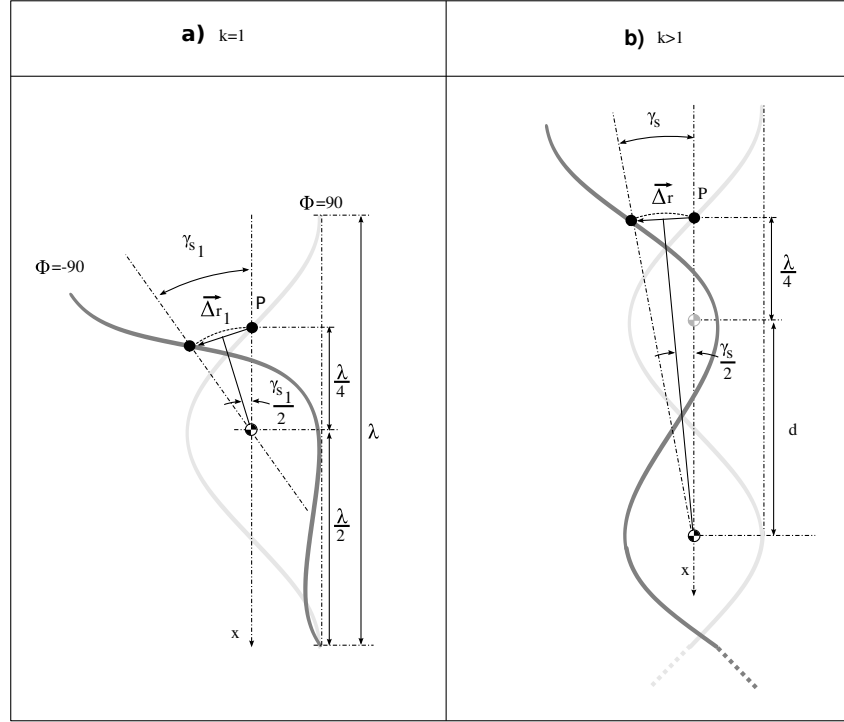


Figure 5.47: Movement of the point P during a half-period. a) For $k = 1$. b) For $k > 1$.

$$\Delta r = 2\left(\frac{\lambda}{4} + d\right) \sin\left(\frac{\gamma_s}{2}\right)$$

Substituting the expression of d :

$$\Delta r = \frac{\lambda}{2} (2k - 1) \sin\left(\frac{\gamma_s}{2}\right)$$

The segments Δr y Δr_1 are equal. When k increases the radius of turn has changed but this distance is the same. Equalling the two expressions $\Delta r = \Delta r_1$:

$$\sin\left(\frac{\gamma_s}{2}\right) = \frac{\sin\left(\frac{\gamma_{s1}}{2}\right)}{2k - 1}$$

And expressing γ_s and γ_{s1} in function of the angles in a cycle (eq. 5.31) we arrive at the final expression.

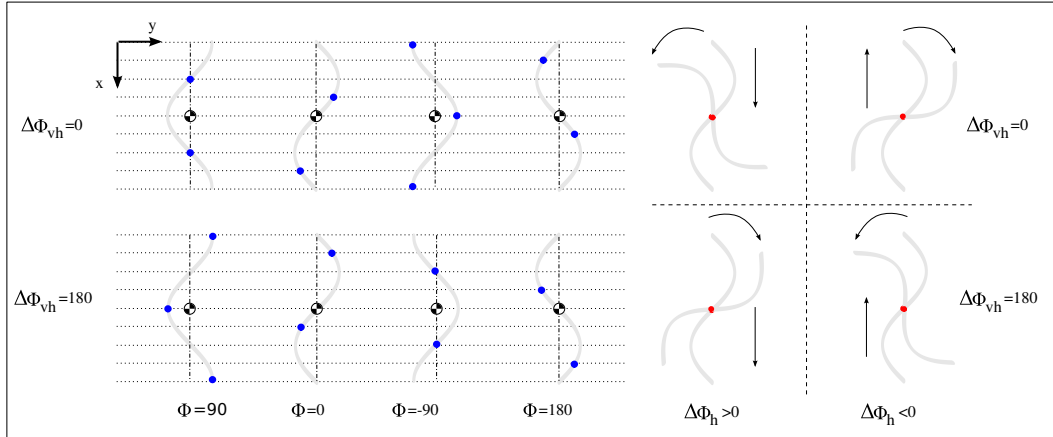


Figure 5.48: Direction of the rotation in function of the direction of propagation of the wave and the $\Delta\phi_{vh}$ parameter

5.8.6.5 Direction of rotation

There are four possibilities for the rotation, as is shown in the figure 5.48, according to the direction of propagation of the wave and the parameter $\Delta\phi_{vh}$. When changing the direction of the propagation of the wave, the direction of rotation changes. If $\Delta\phi_{vh} = 0$ and the wave is propagated in the positive direction of the longitudinal axis, it carries out an anti-clockwise rotation. If the direction of propagation changes the opposite will happen.

The parameter $\Delta\phi_{vh}$ determines the situation for the supporting points, as is shown in the figure 5.48. For $\Delta\phi_{vh} = 180$, its position relative to the curve is different from that for $\Delta\phi_{vh} = 0$. The direction of rotation will be the opposite if the direction of rotation remains the same.

Therefore the following options exist to change the direction of turn:

- Change the direction of the wave propagation (it will be necessary to change the signs of the parameters $\Delta\phi_v$ and $\Delta\phi_h$).
- Add 180 degrees to the parameter $\Delta\phi_{vh}$.

5.8.7 Rotation in 'U'

Besides the principal way of rotating, determined by the superposition of the two serpenoid waves, another means exists that we call rotation in "U". It is characterised by the superposition of a vertical serpenoid wave, with $k_v = 2$ and a circular horizontal ($k_h = 0$), with a value of $\Delta\phi_{vh} = 90$. The stability is obtained using flat waves, in which $\alpha_v/\alpha_h \rightarrow 0$.

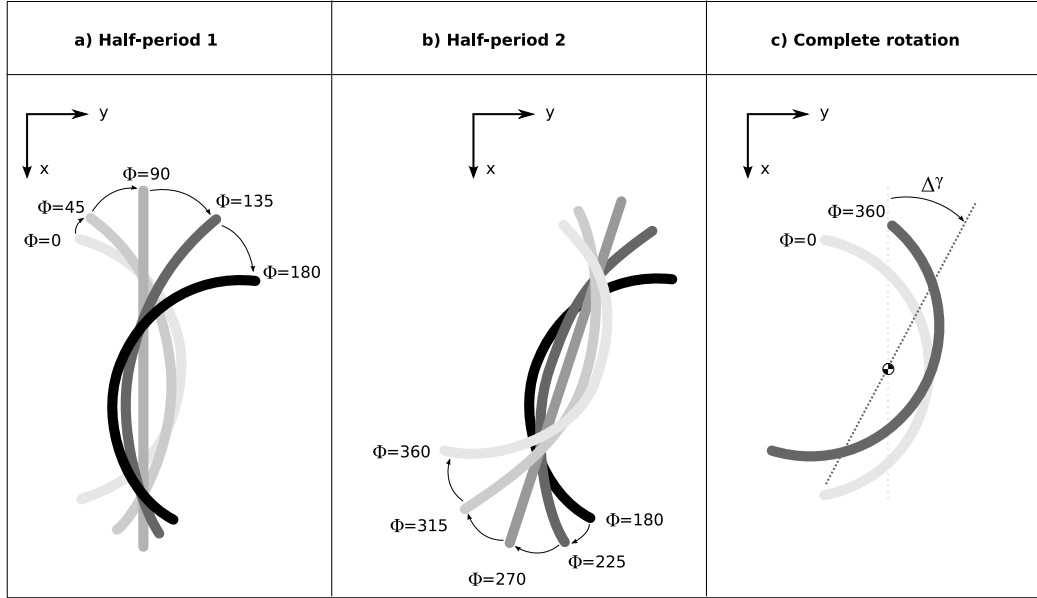


Figure 5.49: Rotation in “U”

The figure 5.49 shows how this rotation functions. In the horizontal joints there is a circular wave which means that the robot has the shape of a “U” that is converted into an inverted “U” and finally returns to a “U” (as shown in the figure 3.33 of the section 3.6.5).

The supporting points go moving for the length of the curve which means that they are found in different positions in the half-periods 1 and 2. In the half-period 1, the supporting points are nearer to the lower extremity therefore it tends to move less and the upper one turns more. In the half-period 2 the opposite occurs and now it is the upper one that tends to move less. The result is that during a cycle the robot realises a total rotation of a certain angle, around its centre of mass.

The advantage of this method of rotation is that it functions with discrete apodal robots with very few modules. In the chapter 6 this method is used for the rotation of the minimum configuration of just 3 modules.

5.8.8 Discrete robot

5.8.8.1 Equations

Main rotation movement This movement is obtained by means of the superposition of two serpenoid waves in which $k_v = 2k_h$ and $\Delta\phi_{vh} = 0$. We will denote the number of undulations of the horizontal serpenoid by k . Specifying in the general equations $k = k_h$ (3.43 and 3.44) we obtain (taking an initial phase $\phi_0 = 0$):

$$\varphi_{v_i} = 2\alpha_v \sin\left(\frac{4\pi k}{M}\right) \sin\left(\phi + \frac{8\pi k}{M}(i-1)\right), i \in \left\{1 \dots \frac{M}{2}\right\}$$

$$\varphi_{h_i} = 2\alpha_h \sin\left(\frac{2\pi k}{M}\right) \sin\left(\phi + \frac{4\pi k}{M}(i-1) + \frac{2\pi k}{M} + \Delta\phi_{vh}\right), i \in \left\{1 \dots \frac{M}{2}\right\}$$

If we denote by $\Delta\phi$ the phase difference between the horizontal generators and given that $k_v = 2k$, we have to $\Delta\phi_v = 2\Delta\phi$, the equations in function of the parameters of control remaining as:

$$\varphi_{v_i} = A_v \sin(\phi + 2\Delta\phi(i-1))$$

$$\varphi_{h_i} = A_h \sin\left(\phi + \Delta\phi(i-1) + \frac{\Delta\phi}{2}\right)$$

Rotation in “U” The vertical serpenoid is the same as in the principal case, taking $k_v = 2$. The horizontal is a circular wave with a phase difference of $\Delta\phi_{vh}$ degrees:

$$\varphi_{v_i} = 2\alpha_v \sin\left(\frac{4\pi}{M}\right) \sin\left(\phi + \frac{8\pi}{M}(i-1)\right), i \in \left\{1 \dots \frac{M}{2}\right\}$$

$$\varphi_{h_i} = \frac{2\alpha_h}{M} \sin(\phi + \Delta\phi_{vh}), i \in \left\{1 \dots \frac{M}{2}\right\}$$

In function of the control parameters:

$$\varphi_{v_i} = A_v \sin(\phi + 2\Delta\phi(i-1)), i \in \left\{1 \dots \frac{M}{2}\right\}$$

$$\varphi_{h_i} = A_h \sin(\phi + \Delta\phi_{vh}), i \in \left\{1 \dots \frac{M}{2}\right\}$$

Parameter	Description	Range
M	Number of modules (vert+horiz)	$M \geq 8$
α	Winding angle	$\alpha \leq \alpha_{max} \leq 120$
$k = k_h$	Number of undulations (horiz)	$k \in [1, M/8]$
A	Horizontal generators amplitude	$A \leq A_{max} \leq 90$
$\Delta\phi$	Horizontal generators phase difference	$\Delta\phi \in (-180, 180)$

Table 5.4: Range of values of the parameters of the main rotation gait for the discrete apodal robots

5.8.8.2 Minimum number of modules

Main movement Given that $k_v = 2k_h$, the limitation in the number of modules will be caused by the vertical serpenoid wave, in which it will reach the maximum value of $\Delta\phi_v = 180$ before it does in the horizontal. The relation between the vertical phase difference and the number of vertical undulations k_v is given by the equation 3.45. Putting it in function of k :

$$\Delta\phi_v = \frac{8\pi k}{M}$$

For the maximum value of $\Delta\phi_v = 180$ degrees, the minimum value of M/K is 8. The minimum number of modules will be for $k = 1$ (so that the equations for calculating the serpenoid dimensions are applicable k cannot be less than 1), which gives us a minimum value of 8 modules. That is to say that the 8 module apodal robot is that which has the least number of modules and that can rotate, using a principal type movement and with $k = 1$.

Rotation in “U” As is shown in chapter 6, the configuration pitch-yaw-pitch of three modules is capable of carrying out the rotation ($M = 3$). The value of k_v to apply is equal to 1. It is one of the advantages of this movement, that it permits the configurations of less than 8 modules to rotate. The value of k_v to obtain it must be less than 2.

5.8.8.3 Limitations

The parameters A and α have the same limitations as was the case of movement in a straight line (section 4.3.2.4): limitation by geometry and by the servo buffer. Because of this, in general it is verified that $\alpha \leq \alpha_{max} \leq 120$ and $A \leq A_{max} \leq 90$ where α_v and A_v are given for the equations 4.6 and 4.7. These equations have to be applied bearing in mind that there are $M/2$ horizontal modules.

In the table 5.4 there is a summary of the range of values of the parameters, for the principal movement of rotation.

For the case of secondary movement, the parameter α_h is found between 0 and 360.

5.8.8.4 Summary

A pitch-yaw type of robot of M modules can rotate parallel to the ground in both a clockwise and an anticlockwise direction. This movement is not found in nature and, as far as we know, has not previously been implemented by other investigators. Two types of rotation have been discovered:

1. **Rotation in “S”** (principal movement). It is obtained by means of the superposition of two serpenoid waves in which the vertical one has twice the number of undulations than the horizontal one and the two waves are in phase. The resulting wave is not isomorphic and to ensure stability it has to be of the plane type. It is valid for any robot with $M \geq 8$.
2. **Rotation in “U”**. It is obtained by means of the superposition of a serpenoid wave on the vertical articulations and a circular one on the horizontal articulations. It has the advantage of allowing the rotation of robots with few modules. It is valid for any robot with $M \geq 3$.

5.9 Case study

We will apply all the ideas developed to describe the five kinds of movement presented to the case of an 8 module robot of pitch-yaw type, of which 4 modules are horizontal and 4 vertical. We will calculate its movement at different working points that will be verified in the chapter on experiments.

5.9.1 Locomotion in a straight line

5.9.1.1 Range of values of the parameters

All the parameters are shown in the table 5.5. The values of M_{vu} and k_v are obtained from the table 4.1 substituting M for 4 (there are only 4 vertical joints).

5.9.1.2 Shape and control spaces

The shape and control spaces are shown in the figure 5.50. Also the robots' aspect has been drawn for the selected working points and for a phase $\phi = 0$.

It is always verified that $M_{vu} \leq M_{uL}$ therefore in the shape space there is only the region of limitation I. There are no geometric limitations. From the equations 4.6 and 5.3 it is found that the maximum value for the amplitude is 90 and for the winding angle:

Parameter	Description	Range
M	Number of modules	$M = 8$
$ \Delta\phi_v $	Vertical phase difference	$ \Delta\phi_v \in [90, 180]$
M_{vu}	Number of vertical modules per undulation	$M_{vu} \in [2, 4]$
k_v	Number of vertical undulations	$k_v \in [1, 2]$
A_{vmax}	Vertical generators Maximum amplitude	90
A_v	Vertical generators amplitude	$A_v \in [0, 90]$
α_{vmax}	Maximum vertical winding angle	$\frac{45}{\sin(\frac{\pi}{M_{vu}})} < 120$
α_v	Vertical winding angle	$\alpha_v \in [0, \alpha_{vmax}]$
M_{us}	Frontier of the locomotion region in h_1	2
$\Delta\phi_s$	Limit of the locomotion region in H_1	$\Delta\phi_s = 180$.
L	Module length	7.2cm
d	Block length	$2L$
d_0	Length of the block's left arm	$L/2$

Table 5.5: Parameters and their range of values for the wired model of an 8 modules pitch-yaw apodal robot when moving in a straight line.

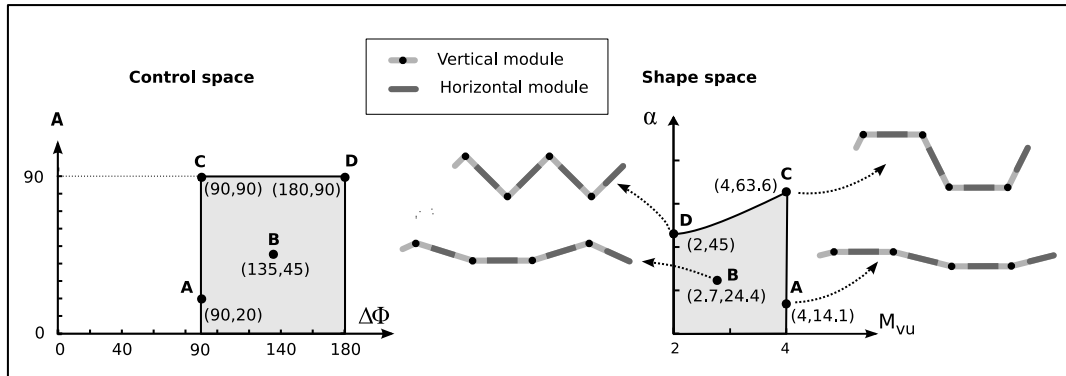


Figure 5.50: Shape and control spaces for the case study robot

Working point	α_v	k_v	M_{vu}	A_v	$\Delta\phi_v$	α_h	k_h	A_h
Point A	14.1	1	4	20	90	0	–	0
Point B	24.4	1.5	2.7	45	135	0	–	0
Point C	63.6	1	4	90	90	0	–	0
Point D	45	2	2	90	180	0	–	0

Table 5.6: Selected working points for the locomotion in a straight line of the case study apodal robot

$$\alpha_{h_{max}} = \frac{45}{\sin\left(\frac{\pi}{M_{vu}}\right)}$$

The maximum value for this winding angle is obtained for $M_{vu} = 4$ and is 63.6 degrees.

The minimum value for $\Delta\phi_v$ is calculated from the equation 3.45 itemising for $k_v = 1$ and $M = 8$. The range of variation is between 90 and 180. Lesser values than 90 will mean that $k_v < 1$ and the equations will not be valid.

The locomotion region is restricted to a straight line. But in it the phase difference of 180 degrees, therefore there is no locomotion. Therefore, the condition of stability is not fulfilled for any of the working points. To smooth the oscillations the parameter α_v must be sufficiently small.

5.9.1.3 Stability and locomotion

The robot does not move with a statically stable movement in any of the working points. In the figure 5.51 the wired model of a robot is shown moving when it uses the working point A ($k = 1, \alpha_v = 14.1$). From the phase $\phi = 90$ degrees the robot is unstable and will lean to the left. The effects of this inclination are in reality very small due to the fact that the parameter α_v has a low value. Despite this unstableness, the robot is capable of moving.

5.9.1.4 Selected working points

The selected points for carrying out the tests and experiments are shown in the table 5.6 and have been drawn in the shape and control spaces in the figure 5.50. The points A and B are used in the chapter of experiments for the simulation and locomotion of a real robot. Point C is where the robot reaches the maximum height and point D that which has the greatest height with the largest number of undulations. In this last point there is no locomotion.

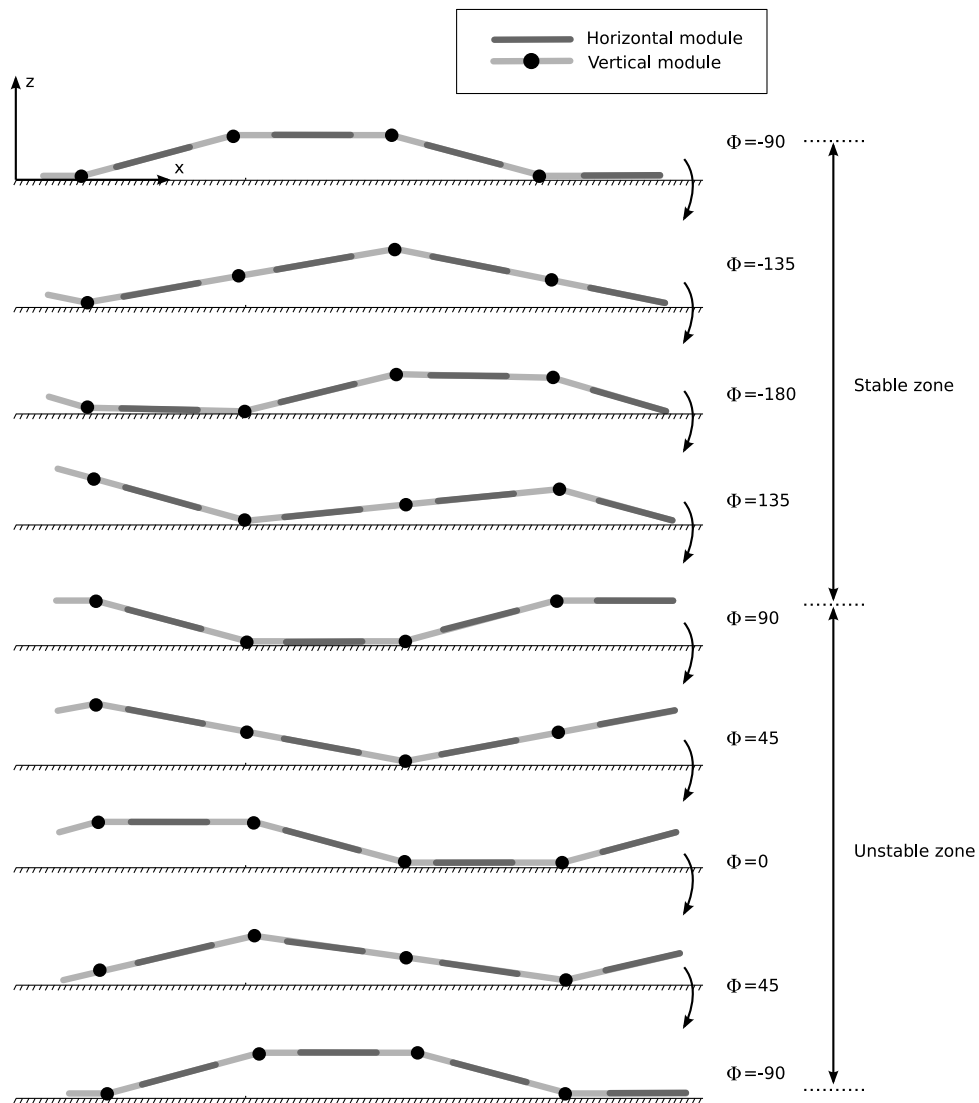


Figure 5.51: Locomotion in straight line of the case study robot in the working point A

Parameter	Description	Range
M	Number of modules	$M = 8$
$ \Delta\phi_v $	Vertical phase difference	$ \Delta\phi_v \in [90, 180]$
M_{vu}	Number of vertical modules per undulation	$M_{vu} \in [2, 4]$
k_v	Number of vertical undulations	$k_v \in [1, 2]$
$A_{v_{max}}$	Vertical generators maximum amplitude	90
A_v	Vertical generators amplitude	$A_v \in [0, 90]$
$\alpha_{v_{max}}$	Maximum vertical winding angle	$\frac{45}{\sin(\frac{\pi}{M_{vu}})} < 120$
α_v	Vertical winding angle	$\alpha_v \in [0, \alpha_{v_{max}}]$
$\alpha_{h_{max}}$	Maximum circular arc angle	$\alpha_{h_{max}} = 360$
α_h	Angle of the horizontal circular arc	$\alpha_h \in [0, \alpha_{h_{max}}]$
$A_{h_{max}}$	Horizontal generators maximum amplitude	90
A_h	Horizontal generators amplitude	$A_h \in [0, 90]$
L	Module length	7.2cm
d	Block length	$2L$
d_0	Length of the block's left arm	$L/2$

Table 5.7: Parameters and their range of values for the wired model of an 8 modules pitch-yaw apodal robot when moving in a circular path.

5.9.2 Circular path

5.9.2.1 Range of values of the parameters

All the parameters are shown in the table 5.8. Those that correspond to the vertical serpenoid are equal in the case of locomotion in a straight line. As $M = 8$ no geometric limitations are produced and from the equations 5.2 and 5.3 we have $\alpha_{h_{max}} = 360$ and $A_{h_{max}} = 90$.

5.9.2.2 Stability

Given that the number of modules of the robot in the case study is less than 14, *the principle of minimum number of modules* for the circular path is not fulfilled and the locomotion will not be statically stable. Oscillations will exist in the movement due to the fact that the supporting points change alternately. In these cases, to guarantee that a turn is realised correctly the vertical winding angle has to be small so that the height of the robot is very near to the ground and the oscillations are small. On the other hand, the smaller that α_v is, the smaller will be the step taken by the robot.

5.9.2.3 Working points

The selected working points are shown in the table 5.8 and the shape of the robot when they are applied is drawn in the figure 5.52. The vertical serpenoid wave is the same in all of them, with a low value α_v . The difference is in the radius of the curve. At point C it is the maximum possible. The robot adopts the shape of a square.

Working points	α_v	k_v	M_{vu}	A_v	$\Delta\phi_v$	α_h	A_h
Point A	12	1.3	3.1	20	120	90	22.5
Point B	12	1.3	3.1	20	120	180	45
Point C	12	1.3	3.1	20	120	360	90

Table 5.8: Selected working points for the locomotion in a circular path of the case study apodal robot

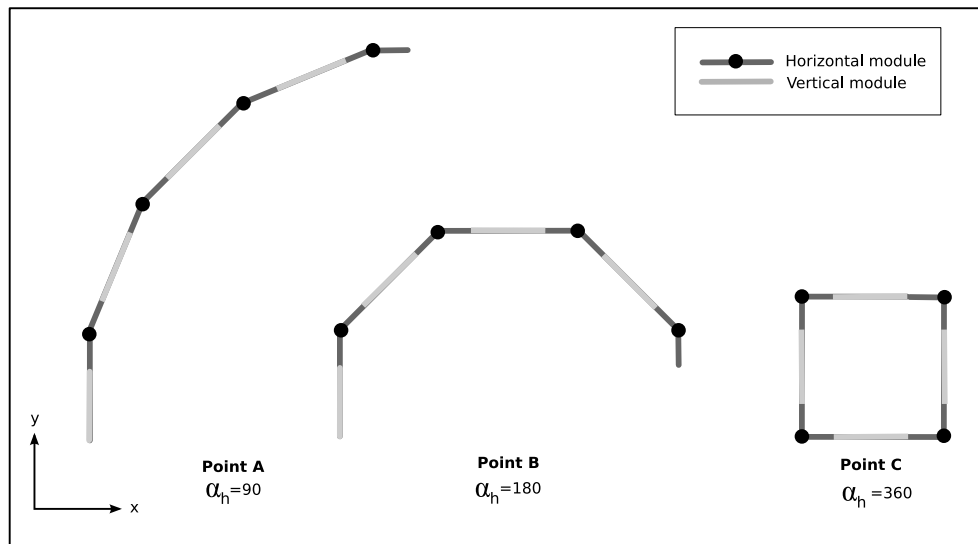


Figure 5.52: Case study robot shape for the selected working points

Parameter	Description	Range
M	Number of modules	$M = 8$
$\Delta\phi_v$	Vertical joints phase difference	$\Delta\phi_v = 0$
k_v	Number of vertical undulations	$k_v = 0$
$\Delta\phi_h$	Horizontal joints phase difference	$\Delta\phi_h = 0$
k_h	Number of horizontal undulations	$k_h = 0$
α_{max}	Maximum corporal axis arc angle	$\alpha_{max} = 360$
α_{min}	Minimum corporal axis arc angle	$\alpha_{min} = 30$
α	Corporal axis arc Angle	$\alpha \in [30, 360]$
A_{min}	Minimum amplitude	$A_{min} = 7.5$
A	Generators amplitude	$A \in [7.5, 90]$
l	Robot length	$57.6cm$
H	Module width	$5.2cm$
L	Module length	$7.2cm$
d	Block length	L
d_0	Length of the block's left arm	$L/2$

Table 5.9: Parameters and their range of values for the wired model of an 8 modules pitch-yaw apodal robot when rolling

Working points	α	A	$\Delta\phi_{vh}$	ϕ_0
Point A	120	30	90	90
Point B	180	45	90	90
Point C	240	60	90	90
Point D	360	90	90	90
Point E	32	8	90	90

Table 5.10: Selected working points for the rolling gait of the case study apodal robot

5.9.3 Rolling

5.9.3.1 Range of values of the parameters

All of the parameters are shown in the table 5.9. As $M = 8$ no geometric limitations are produced and from the equations 5.2 y 5.3 we have $\alpha_{max} = 360$ and $A_{max} = 90$.

Applying the equation 5.21 for the values $l = 57.6$ and $H = 5.2$ ensures that the minimum angle of the corporal axis, to produce the rolling movement, is of approximately 30 degrees. This gives a minimum amplitude for the generators of 7.5 (eq. 5.22).

5.9.3.2 Working points

The selected working points are shown in the table 5.10. The robot's shape when it moves according to the working point B is shown in the figure 5.53. The point D corresponds to the maximum possible

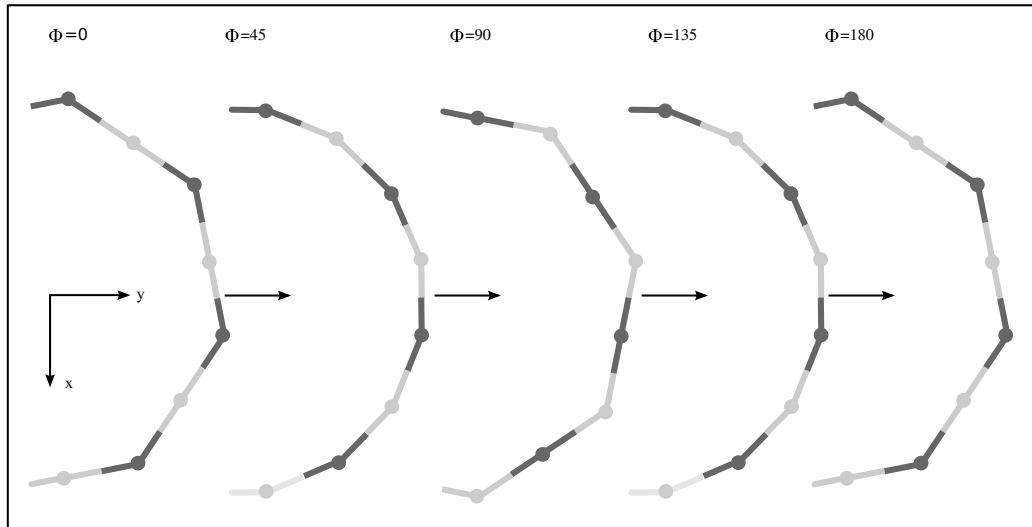


Figure 5.53: Robot Movement for the working point B

value of α . In this situation the robot's body goes alternating between a square and an octahedron. Rotation around the corporal axis exists, but there is no movement.

In the point E the robot rolls with the least angle possible. Lesser values will mean that it realises a sideways movement.

5.9.4 Sideways movement

5.9.4.1 Range of value of the parameters

All the ranges of the values for the different parameters so that the robot can move with the three types of sideways movement are summed up in the table 5.11.

5.9.4.2 Working points

The selected working points are shown in the table 5.12. The first two use the principal movement, with values of k of 1 and 1.5 respectively. The point C is an inclined movement with $k = 1$ and a winding angle of 60 degrees (approximately) The last is a flapping type movement.

Parameter	Description	Range
M	Number of modules	$M = 8$
L	Module length	$7.2cm$
H	Module width	$5.2cm$
Main sideways movement		
wave	Plane isomorphous	$k = k_h = k_v$
k	Number of undulations	$k \in [1, 2]$
$\frac{\alpha_v}{\alpha_h}$	Serpenoid coefficients ratio	$\frac{\alpha_v}{\alpha_h} \rightarrow 0$
M_{uh}	Horizontal modules per undulation	$M_{uh} \in [2, 4]$
α_{max}	Maximum winding angle	$\alpha_{Max} = \frac{45}{\sin(\frac{\pi}{M_{uh}})} \leq 63.6$
α	Winding angle. $\alpha \simeq \alpha_h$	$\alpha \in [0, \alpha_{max}]$
$\Delta\phi_{vh}$	Phase difference between the vert. and horiz. waves	$ \Delta\phi_{vh} \in [0, 90]$
$\Delta\phi$	Phase difference	$ \Delta\phi \in [0, 180]$
A_{max}	Horizontal generators maximum amplitude	$A_{max} = 90$
A	Horizontal generators amplitude	$A \in [0, 90]$
Inclined sideways movement		
wave	Linear isomorphous	$k = k_h = k_v$
$\Delta\phi_{vh}$	Phase difference between the vert. and horiz. waves	$ \Delta\phi_{vh} \rightarrow 0$
k	Number of undulations	$k \in [1, 2]$
α_{max}	Maximum winding angle	$\alpha_{Max} = \frac{45}{\sin(\frac{\pi}{M})} \leq 117.6$
α	Winding angle. $\alpha = \sqrt{\alpha_h^2 + \alpha_v^2}$	$\alpha \in [0, \alpha_{max}]$
β	Inclination angle	$\beta \in [0, 45]$
Flapping		
wave	Superposition of equal circular waves	$k = k_h = k_v, \alpha = \alpha_v = \alpha_h$
k	Number of undulations	$k = 0$
α_{max}	Maximum Corporal axis' arc angle	$\alpha_{max} = 30$
α	Corporal axis' arc angle	$\alpha \in [0, 30]$
$\Delta\phi$	Phase difference between the vert. and horiz. waves	$\Delta\phi = 0$
A_{max}	Generators maximum amplitude	$A_{max} = 7.5$
A	Generators amplitude	$A \in [0, 7.5]$

Table 5.11: Parameters and their range of values for the wired model of an 8 modules pitch-yaw apodal robot when performing sideways movements

Points	α_v	α_h	k_v	k_h	$\Delta\phi_{vh}$	A_v	A_h	$\Delta\phi_v$	$\Delta\phi_h$	Description
Point A	14.1	28.3	1	1	90	20	40	90	90	Main movement
Point B	10.8	21.6	1.5	1.5	90	20	40	135	135	Main movement
Point C	42.4	42.4	1	1	30	60	60	90	90	Inclined movement
Point D	28	28	0	0	90	7	7	0	0	Flapping

Table 5.12: Selected working points for the sideways movements of the case study apodal robot

Parameter	Description	Range
M	Number of module	$M = 8$
L	Module length	$7.2cm$
H	Module width	$5.2cm$
Main rotating gait		
wave	Non-isomorphous plane	$k_v = 2k_h$
k	Number of horizontal undulations	$k = 1$
k_v	Number of vertical undulations	$k_v = 2$
$\frac{\alpha_v}{\alpha_h}$	Serpenoid coefficients ratio	$\frac{\alpha_v}{\alpha_h} \rightarrow 0$
M_{uh}	Horizontal modules per undulation	$M_{uh} = 4$
α_{max}	Maximum winding angle	$\alpha_{Max} \leq 63.6$
α	Winding angle. $\alpha \simeq \alpha_h$	$\alpha \in [0, \alpha_{max}]$
$\Delta\phi_{vh}$	Phase difference between the vert. and horiz. waves.	$ \Delta\phi_{vh} \in [0, 90]$
$\Delta\phi$	Horizontal generators phase difference	$ \Delta\phi = 90$
$\Delta\phi_v$	Vertical generators phase difference	$ \Delta\phi = 180$
A_{max}	Horizontal generators maximum amplitude	$A_{max} = 90$
A	Horizontal generators amplitude	$A \in [0, 90]$
Rotation in “U”		
wave	superposition: serpenoid + circular	—
$\Delta\phi_{vh}$	Phase difference between the vert. and horiz. waves	$ \Delta\phi_{vh} = 90$
k	Number of horizontal undulations	$k = 0$
k_v	Number of vertical undulations	$k_v \leq 2$
α_{max}	circular arc maximum angle	$\alpha_{Max} = 360$
α	Circular arc angle	$\alpha \in [0, \alpha_{max}]$
A	Horizontal generators amplitude	$A \in [0, 90]$
$\Delta\phi_v$	Vertical generators phase difference.	$ \Delta\phi_v = 180$

Table 5.13: Parameters and their range of values for the wired model of an 8 modules pitch-yaw apodal robot when rotating

Points	α_v	α_h	k_v	k_h	$\Delta\phi_{vh}$	A_v	A_h	$\Delta\phi_v$	$\Delta\phi_h$	Description
Point A	15	28.3	2	1	0	30	40	180	90	Main movement
Point B	5.3	34	1.6	0.8	0	10	40	140	70	Main movement
Point C	10	160	2	0	90	20	40	180	90	Rotation in “U”

Table 5.14: Selected working points for the rotating gait of the case study apodal robot

5.9.5 Rotation

5.9.5.1 Range of values of the parameters

All the range of values for the different parameters so that the robot can move with the three types of sideways movement are summed up in the table 5.13.

5.9.5.2 Working points

The selected working points are shown in the table 5.14. The first two correspond to the inclined movement, with values of k of 1 and 0.8 respectively. The point C is of secondary type.

5.10 Principles of locomotion

We sum up the locomotion of the discrete apodal robots of the pitch-yaw group when sinusoidal generators are used in 11 fundamental principles of locomotion.

1. **Principle of the sinusoidal generators.** An apodal robot of M modules, with pitch-yaw type connection in which the vertical and horizontal joints are made to oscillate periodically using sinusoidal generators is capable of carrying out at least five families of movement: straight line, circular path, rolling, sideways movement and rotation.
2. **Principle of the superposition of waves.** The movements within the different families are obtained by means of the superposition of two dimensional waves in the vertical and horizontal joints, that are propagated in the same direction. A three dimensional wave appears that passes through the robot's body making it move.
3. **Principle of movement direction.** The direction of movement is determined by the direction of the propagation of the corporal three-dimensional wave, which at the same time depends on the phase difference between the horizontal and vertical waves.

4. **Principle of shape characterisation.** The shape of the robot when it moves is characterised by the three-dimensional wave that appears as the result of the superposition of the two dimensional waves, that can be serpenoid or circular waves. The corporal wave is defined by the parameters of the two dimensional waves plus the phase difference between them. The serpenoid waves have two parameters, the winding angle and the number of undulations; and the circular ones only the angle of the arc.
5. **Principle of the flat wave.** In general the stability of all the movements is obtained by making sure that, compared to the horizontal, the vertical wave's parameter α is as small as possible. In this case the three dimensional wave is "flattened" and the robot's dimensions can be approximated to those of the horizontal wave.
6. **Principle of movement in a straight line.** If the vertical wave is serpenoid and the horizontal joints remain in their positions of rest, with a turning angle of zero degrees, the robot's locomotion will be in a straight line and all the principles of one dimensional locomotion will apply.
7. **Principle of the circular path.** If the vertical wave is serpenoid and the horizontal one is a circular curve (whose bending angles do not depend on the phase) the robot will perform a movement in a circular path of an angle equal to the parameter α of the circular curve.
8. **Principle of rolling movement.** If two circular waves with a 90 degree gap between them and with the same parameter α are superposed, the robot will turn around its corporal axis and roll along the ground. The value of α must be greater than a given threshold.
9. **Principle of sideways movement.** Generally sideways movement is obtained by means of the superposition of two serpenoid waves that have the same number of undulations. What is more, for robots with a square section two types of movement appear: inclined and rowing.
10. **Principle of rotation.** Generally rotation is obtained by means of the superposition of two serpenoid waves in which the number of vertical undulations is double that of the horizontal ones. What is more rotation can be in the shape of a "U" if the horizontal wave is of the circular type.
11. **Principle of parameter α .** The increase of the parameter α means that the step of the different gaits increases, except in the rolling movement, where it decreases.

5.11 Conclusions

In this chapter the problem of the apodal robots' locomotion on a level homogeneous surface, free of obstacles, controlled by sinusoidal generators, has been addressed.

We propose a **methodology** to resolve this problem, based on finding gaits by using **genetic algorithms** and characterised by the subspace of h_2 . The steps to follow **to resolve the direct and inverse kinematics** from these subspaces are also presented and the equations that join their working points with the robot's dimensions and the kinematic parameters.

The gaits are characterised by the equations of their associated subspaces, that establish the relationships between the five parameters α_v , α_h , k_v , k_h , $\Delta\phi_{vh}$. The number of free parameters we call **degrees of freedom** of movement.

The mechanism that allows the robot's locomotion is the emergence of a **three-dimensional corporal wave** that is the resultant of the **superposition of the two-dimensional waves** that are applied to the vertical and horizontal joints. Studying the corporal waves allows us to discover, during the movement, the robot's dimensions and support points where the robot makes contact with the ground that give it stability, and also to deduce the equations of the kinematic parameters.

Applying the methodology proposed **8 different gaits have been found** grouped in five categories: straight line, circular path, rolling, sideways movement and rotation. The equations of characterisation have also been obtained. **All the movements have been confirmed by means of simulations and their application to real robots.**

Three new gaits have been discovered that, as far as we know and understand, have not been studied previously nor implemented by other investigators. They are the sideways inclined movement and two types of rotation. These last mentioned are very important as they allow the robot to change the orientation of its longitudinal axis, and be able to face in any direction.

The **control model based on simplified CPGs** of sinusoidal type generators is not only valid for one-dimensional movements, but is also **viable for two-dimensional locomotion of pitch-yaw type modular robots**, with a number of modules equal to or greater than a minimum value. What is more, it is not only viable, but it also allows a variety of movements sufficiently large enough that the superior level of control can direct the robot to any point of the surface, with whichever orientation and employing different paths.

The straight line and sideways movements allow the robot to reach whichever point (x,y) of the ground. By means of rotation, also, they can point in any direction. The rolling movement guarantees that the robot can recover its initial position if it turns over, in the same way that caterpillars can right themselves if you turn them upside down. The robot will be able, also, to move in circular paths that allow it to rotate, go round obstacles or, using them in combination with other movements, to complete more complex paths.

From the shape of the three-dimensional wave the gaits discovered have been studied in detail. They have between 1 and 3 degrees of freedom. The **movement in a circular path** is obtained by the superposition of a serpenoid wave on the vertical articulations and a circular curve on the horizontal

ones. It has three degrees of freedom, the angle of the arc of the path and the parameters α and k of the vertical serpenoid.

The **rolling movement** is characterised by the superposition of two equal circular waves and a gap between them of 90 degrees. It has only one degree of freedom, α to specify the angle of the body's arc. If the robot has a square section, the threshold value α_{min} appears, that allows it to fulfil the movement for greater values of α . If they are less what is obtained is the **flapping sideways movement**. An expression for the step has been obtained that shows that it decreases with the increase of α .

The **normal sideways movement** is that which is known as side-winding. This is characterised by the superposition of two serpenoid waves with the same number of undulations. The three-dimensional wave is of the isomorphous type as it does not vary its shape during the propagation. This causes the contact points with the ground to always be in the same relative position to the wave, and two points will always be separated the same distance λ . It has two degrees of freedom α and k that correspond to those of the horizontal wave. This movement can be implemented in its **inclined version** in which a new parameter, β , appears to specify this inclination. In both movements the robot's step increases with α .

The **rotating movement** allows the robot to change the orientation of its longitudinal axis, Two variations exist, the rotation in S and in U. The first is characterised by the superposition of two serpenoid waves and the second one by that of a serpenoid and a circular one. Both have two degrees of freedom and the rotated angle increases with the parameter α .

Finally, the same as in the case of locomotion in one dimension, all the principal ideas have been summed up in some **principles of locomotion** (section 5.10).

Chapter 6

Minimum configurations

”The bottom line is that us scientist are lucky: we can play at what we love all our lives.”

– Lee Smolin. *Theoretical physicist and cosmologist*

6.1 Introduction

In this chapter we present and resolve the problem of the minimum configurations: *to find the modular robots with the least possible number of modules that are capable of movement in one and two dimensions, and to decide what values are to be applied to their parameters to achieve the different gaits.*

We begin by introducing the previous ideas and why the minimum configurations are so important. Next we present the problem and propose a methodology to resolve it. Then we describe the two minimum configurations found and the different gaits that can be executed. Each one of them is studied in detail, proposing equations to obtain the step. Finally the ideas are summed up in 5 principles of locomotion.

6.2 Modular robotics and minimum configurations

The study of the minimum configurations was presented for the first time by the author of this thesis [43] in 2005. It is a new idea that, as far as we know, had not previously been implemented nor studied by other researchers. In the following sections we describe the reasons why the minimum configurations are important and some of their applications.

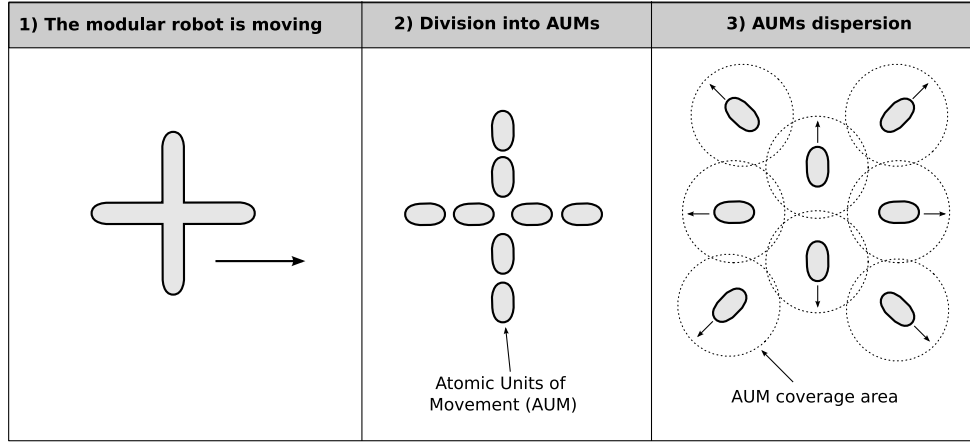


Figure 6.1: Application of a self-reconfigurable modular robot for maximising the coverage area

6.2.1 Atomic Unit of Movement (AUM)

In the field of modular robot locomotion the minimum configurations constitute an Atomic Unit of Movement (AUM). They are the robots with the least number of modules and that can move in one or two dimensions.

The self-configuring modular robots are those that have the capacity to change their form by means of connecting and disconnecting their modules. These robots can divide themselves into smaller sub-robots. The division can continue while their parts are greater than or equal to the AUM. If one of the modules of an AUM separates, it will not be able to move, thereby losing its autonomy of movement.

If the minimum configurations are known *a priori* the maximum number of autonomous sub-robots (N) that can be obtained from a modular robot of M modules are known. It will be given by the relation:

$$N = \frac{M}{M_{min}} \quad (6.1)$$

where M_{min} is the number of modules of the AUM.

The maximisation of the number of robot parts is important in the applications where it is necessary to maximise a certain coverage area. In them, each AUM will have sensors or communication systems that have a range or coverage. By means of the dispersal of all the AUM this range is increased. In the figure 6.1 an example of this idea is shown of a self-configuring modular robot of M modules that is initially placed in the zone and can move through it until it reaches its goal. It has been represented by means of a star to indicate that it could adopt any shape for the locomotion, as for example a quadruped, that would allow it to overcome the obstacles more easily. Once the arrival

point is reached, the robot divides into N atomic units, each one of them would be of a minimum configuration. In this way, the number N will be maximum (eq. 6.1). Following this each one of the AUM disperses over the zone increasing the area of coverage. Once the mission is finalised, they join together again forming the initial robot and abandoning the work zone.

6.2.2 Maximisation of energy efficiency

Mark Yin in his doctoral thesis [163] defined movement efficiency of modular robots as the energy necessary to move a unit of distance. He proposed an equation¹ to measure the efficiency of the different gaits and to be able to decide which is the best. In this formula the efficiency is inversely proportional to the number of modules. Because of this, the fewer the number of modules, the more efficient will be the movement.

Given that the minimum configurations are those that have the least possible number of modules, they will be therefore **the modular robots with the greatest energy efficiency**. They can move the maximum distance consuming the minimum of energy. This is of special interest in the space exploration applications, where modular robots are wanted for exploring other planets [170][130][84].

6.2.3 Analysis and synthesis of gaits

The knowledge of the minimum configurations and the co-ordination to achieve their movement can be applied to the study of the movement of other modular robots, for their analysis or their synthesis. We propose the idea of identifying parts of the study robots with the minimum configurations and thereby being able to analyse their movements using the knowledge gained from them.

As is shown in the section 6.4, the minimum configuration to move in one dimension is constituted by the union of two pitch joints. Any modular robot in which a similar structure is identified, can be object of study from the perspective of the minimum configuration. In the figure 6.2 an example applied to the robots JL-I [181] and M-TRAN III[105] is shown. The first is a self-propelled modular apodal robot, in which its modules are mobile units that are propelled by means of caterpillar tracks (see section 2.4.5). When three of its modules join together forming a chain, its structure is identified as that of a minimum configuration: three segments united by two pitch type joints. Therefore, applying the co-ordination studied for it, it becomes possible for JL-I to move by means of corporal movements, without using the caterpillars. This gait had not previously been foreseen by its creators [178].

The modules of the M-TRAN robot has two degrees of freedom and again can be identified with the minimum configuration of type Pitch-Pitch. Because of this, these modules are on their own an

¹The equation can be found on page 96 of his thesis

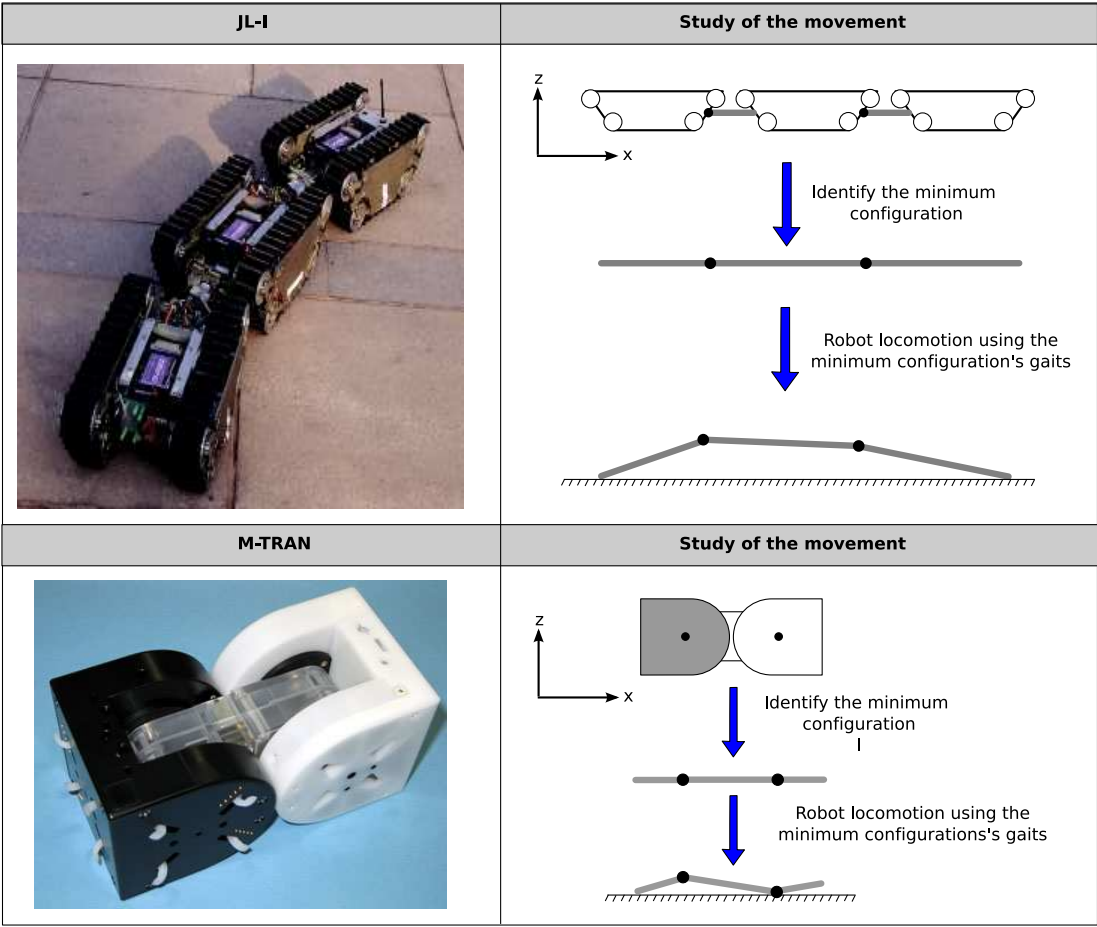


Figure 6.2: Example of the analysis of the movement of the JL-I and M-TRAN robots using the minimum configurations

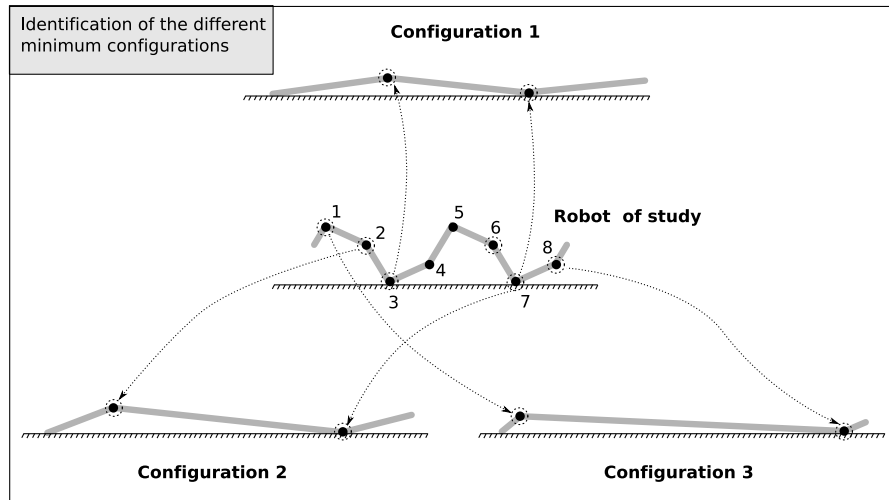


Figure 6.3: Studying the locomotion of an 8 module apodal robot using the minimum configurations

AUM. In the papers that describe these modules there are no mention of this property and neither have experiments of locomotion using only one module been carried out. They are designed with two degrees of freedom so that there are 6 surfaces of inter-connection with adjacent modules to be able to form solid structures. Nevertheless, using the technique of analysis proposed it has been deduced that they are an AUM.

Another example of the use of this technique can be applied to the locomotion of the pitch-pitch group of robots, as is shown in the figure 6.3. An 8 module robot can move as explained in detail in the chapter 4, using waves that are propagated through its body. Nevertheless, different minimum configurations can be identified. If the joints 3 and 7 are taken as reference and the rest remain in the state of rest (with a bending angle of zero degrees) the configuration 1 is obtained. The robot is now equivalent to a minimum configuration where the propulsion is obtained only by means of two joints. Two other configurations are also shown, that of the 2 and the 3 are obtained by taking as reference the modules 2 and 7 for one and 1 and 8 for the other respectively.

What is more, this technique is very useful in being able to rapidly identify if a specific configuration of a modular robot can move. In the figure 6.4 a modular robot is shown with two-dimensional topology and in the form of a cross. All the joints are pitch type. It would be right to ask is if this configuration can move. To discover its movements the technique of genetic algorithms could be applied, the same as has been used to discover the gaits of apodal robots of the pitch-yaw group. But a rapid analysis can also be made obtaining the wired model and identifying the minimum configurations. It is seen that the robot is made up of two of them, one orientated on the x axis and the other on the y axis. Therefore, it seems that this robot can move independently for each one of its axis applying the co-ordination found for the PP configuration. What is more, it seems logical to think that if the two movements are superimposed at the same time, the robot will move in a diagonal direction. These “intuitive” ideas allow mechanisms of co-ordination to be obtained: candidates for their future trial

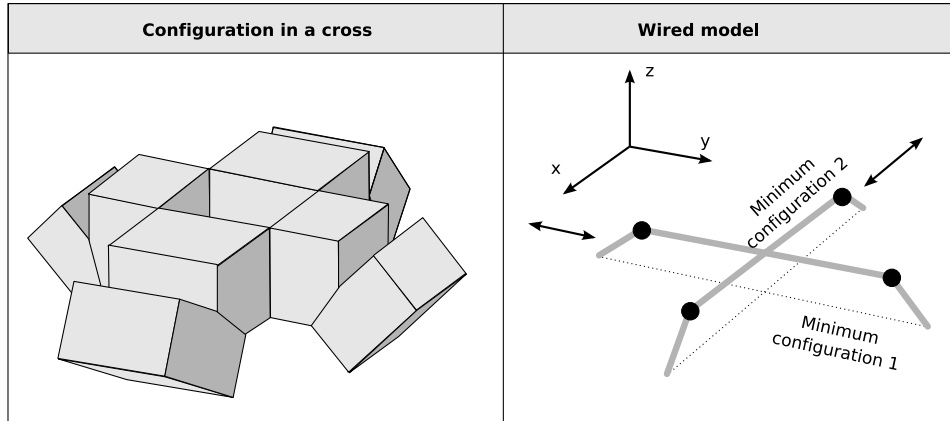


Figure 6.4: Studying the locomotion of a 4 module configuration in a cross, using the analysis of minimum configurations

in experiments with simulators or real robots. As in the case of the cross configuration.

6.2.4 Design and testing of the modules

In modular robotics the design is centred on the modules and the robots are constructed from them. During the design phase and testing at least M_{min} prototypes of modules will be constructed and with them a minimum configuration created and tested to see if it moves correctly. This means that only the prototypes needed for the tests will be constructed, keeping down the design costs. The same occurs in the simulation tests, in which it will have to be proved that, at the very least, the minimum configuration can move.

When designing modular robots for certain applications, the minimum configurations can be used as design criterion. For example, as in the case of the M-TRAN robot, if the module is designed with two pitch-pitch joints, it will be in and of itself an AUM.

In the applications of self assembling after an explosion [173] proposed recently by Mark Yim and his team (more information in the section 2.5.4), the minimum configurations must be taken into account. There are two alternatives. One is to construct the AUM from the existing modules, with strong unions between them (using bolts, for example). Between the different AUM the unions should be reversible, in such a way that on receiving an impact they can separate without suffering damage (using permanent magnets, for example). The other option is to construct modules that of themselves form the AUM and therefore can move. A module will be constructed equivalent to a minimum configuration.

6.3 Problem to be resolved

6.3.1 Exposition

The problem is to find the configurations of apodal robots with the smallest number of modules that can move in one or two dimensions. Therefore the minimum possible number of modules necessary M_{min} must be found and then the problem of co-ordination be resolved to achieve movement.

The solution for the co-ordination does not have to be valid now for the general case of M modules, but only for the configurations of M_{min} modules. This is why they are not described using global waves nor characteristics related to the shape of the robot (shape space) but we will go directly to the control parameters of the spaces H_1 and H_2 . These solutions will be points within these spaces. H_1 for the configuration PP and H_2 for the PYP.

6.3.2 Scheme

The scheme to approach the problem is similar to that proposed to resolve the locomotion of apodal robots in two dimensions (section 5.2), excepting that now a control space is employed (H_2) instead of a shape space (h_2). The scheme of the presentation for the locomotion in two dimensions suggested in the figure 5.1 is equally applicable to this case. Each gait is associated to a control subspace that we will call G_i . These are characterised by some parametric equations that establish the relations between their parameters, determining the degrees of freedom of the gait.

The dimensions of the robot during the movement as well as the kinematic step parameters and the angular step will depend on the chosen working point p . They will be defined by the functions $lx_i(p)$, $ly_i(p)$, $h_i(p)$, $\Delta\gamma_i$ and $\vec{\Delta r_i}(p)$, that depend on the space G_i .

6.3.3 Methodology

The methodology is similar to that presented in the section 5.2.3. The only difference is that when discovering the gaits it has to be done on the configurations with different quantities of modules, beginning with $M = 1$.

1. Discover the gaits of the configuration with M_i modules
 - (a) Iterate M_i from 1 until the solution is found
 - (b) Find the gaits of the configuration of M_i modules.

- (c) If the solutions are found, M_i is the minimum configuration. If not increase M_i and return to point (b).
- 2. Characterise the control subspaces G_j
- 3. Validate the results in simulation and with real robots.
- 4. Obtain the equations of the robot's dimensions ($lx_j(p), ly_j(p), h_j(p)$), for each subspace G_j
- 5. Obtain the equations of the kinematic parameters ($\Delta\gamma_j$ and $\overrightarrow{\Delta r_j}(p)$) of each subspace.
- 6. Resolve the problems of the direct and inverse kinematics.

6.3.3.1 Search for solutions

The control space H_2 has to be explored to find the different gaits for each one of the configurations of M_i modules. To do this, start from the configuration of $M = 1$ and then go increasing the number of modules. This process is carried out until the first configuration is reached that is able to execute various gaits.

The way to carry out the search for a configuration of M_i modules is by means of genetic algorithms, in a similar way as was indicated in the section 5.2.3.1.

Another way of approaching the problem would be to use the genetic algorithms in which the genotype contains the information on the number of modules M_i , which would allow, at the same time, the investigation of robots with different numbers of modules, instead of having to iterate on M_i , searching for solutions for each one of them. The second solution has been chosen because it is known *a priori* that M is going to be a small value.

In the case of movement in a straight line it is known that the minimum number of modules that enables the robot to move in a stable way, by means of global waves is $M = 5$ (4.4.5.3). For this reason, it is only needful at the worst to test a maximum of 4 configurations to find one that can move in a straight line. The same happens for the sideways movement, where it is guaranteed that for $M \geq 6$ the robot can move (5.7.10.3). In the case of rotation the movement is guaranteed for $M \geq 8$.

Therefore, in the worst of situations, to find the minimum robot that can move in all these gaits, a maximum of 7 configurations would have to be tested. We have chosen the iterative algorithm as being the simplest to implement and allow, even to carry out the iterations, executing sequentially the search program manually: first with $M = 1$, then with $M = 2$, etc. or executing the 7 program in parallel.

If it were not known *a priori* what the number of M is, then the option of codifying the number of modules in the genotype would be more efficient than a sequential search.

6.3.4 Kinematics

The steps to resolve the problems of the direct and inverse kinematics are similar to those employed for the case of the locomotion of apodal robots of M modules (section 5.2.4), but without the need to execute transformations between the space h_2 and H_2 . Given that the search space is directly the control space H_2 , the steps become simplified.

6.3.4.1 Direct kinematics

Proposition *Given a point P of the control space H_2 that determines the parameters of the sinusoidal generators $(A_v, A_h, \Delta\phi_v, \Delta\phi_h, \Delta\phi_{vh})$ define the type of movement, its kinematic parameters and its dimensions.*

We will denominate the space G to the union of all the subspaces G_i . The steps to follow are:

1. If P is NOT in G it is an invalid point. These parameter values are incorrect and will not cause movement in any of the foreseen gaits.
2. If P belongs to G it will be a valid point. Determine the subspace G_i to which it belongs, testing to see if it fulfils the equations that characterise it. With this we will know the type of movement that the robot will carry out.
3. Apply the equations of the dimensions $l_{x_i}(P)$, $l_{y_i}(P)$, $h_i(P)$ and of the kinematic parameters $\vec{\Delta r}_i(P)$ and $\Delta\gamma_i(P)$.

6.3.4.2 Inverse kinematics

Proposition *Given some restrictions in the kinematic parameters and/or the dimensions of the robot, and knowing the type of gait, find the parameters of the generators that have to be applied.*

The general steps are as follows:

1. Obtain the space G_i associated to the gait.
2. Apply the restrictions and partition the subspace G_i . One of these partitions will be the space solution.

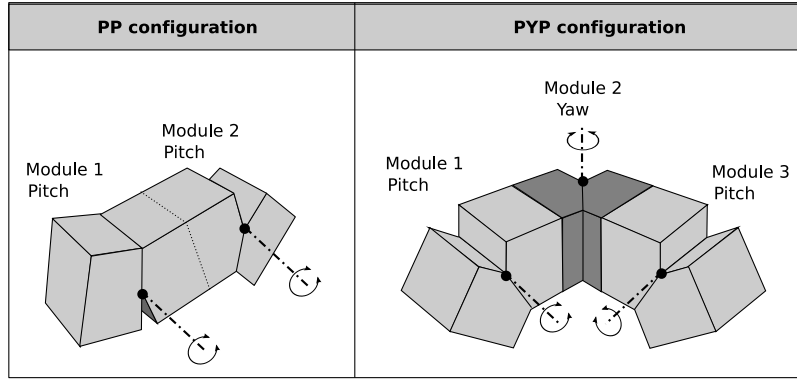


Figure 6.5: The minimum configurations PP and PYP

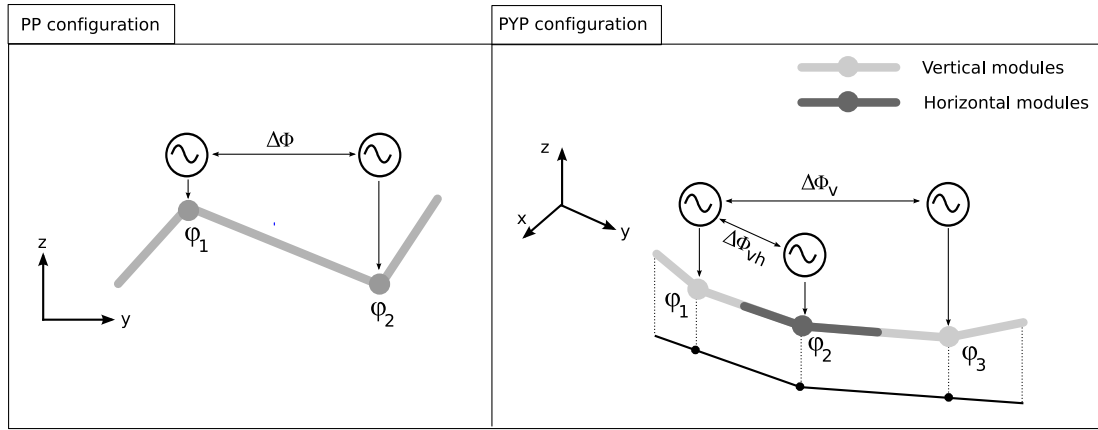


Figure 6.6: Control model for the PP and PYP minimum configurations

6.4 Configurations PP and PYP

6.4.1 Solutions found

Following the methodology described in the section 6.3.3 the minimum configurations are the two shown in the figure 6.5. We call them configuration PP and PYP (pitch-pitch and pitch-yaw-pitch). The first is made up of two pitch type modules. It can move in a straight line, forwards and backwards. The second is formed by three modules. Those at each end are pitch type modules and the one in the middle is yaw. It can move with at least five different gaits (section 6.3.3).

6.4.2 Control models

The control model is based on the sinusoidal generators introduced in the section 3.5, particularised for the configurations of two or three modules. The general scheme of control is shown in the figure

6.7.

6.4.2.1 Configuration PP

Two generators are used. The bending angles are described by means of the equations:

$$\begin{aligned}\varphi_1 &= A \sin(\phi) \\ \varphi_2 &= A \sin(\phi + \Delta\phi)\end{aligned}\tag{6.2}$$

The control space H_1 has two dimensions, the same as in the case of the apodal robots with a greater number of modules. The points are the pairs $(A, \Delta\phi)$.

6.4.2.2 Configuration PYP

Three generators are employed. Two of them for the control of the vertical joints and one for the horizontal ones. The bending angles vary following the equations:

$$\begin{aligned}\varphi_1 &= A_v \sin(\phi) \\ \varphi_2 &= A_h \sin(\phi + \Delta\phi_{vh}) \\ \varphi_3 &= A_v \sin(\phi + \Delta\phi_v)\end{aligned}$$

The control space H_2 is formed by 4 parameters: $A_v, A_h, \Delta\phi_v$ and $\Delta\phi_{vh}$. The parameter $\Delta\phi_h$ makes no sense, as it only exists one horizontal module. This space has therefore one dimension less than in the general case of the robots' movement of the pitch-yaw group of M modules.

6.4.3 Kinematic models

6.4.3.1 Configuration PP

Geometry

The geometric and kinematic models of the PP configuration are shown in the figure 6.7. This configuration is formed by the union in chain of two modules of pitch type. It has two joints, with bending angles φ_1 and φ_2 , and three rigid segments of lengths $L/2$, L and $L/2$. We define the angle φ_0 as the one that the left segment forms with the horizontal and determines the orientation of the robot.

For kinematics study we are interested in four points: the two extremes (left and right) and the two joints. We will use the nomenclature P_0, P_1, P_2 and P_3 to refer to them. Their position vectors with respect to the frame of reference G are denoted by $\vec{r}_0, \vec{r}_1, \vec{r}_2$ and \vec{r}_3 .

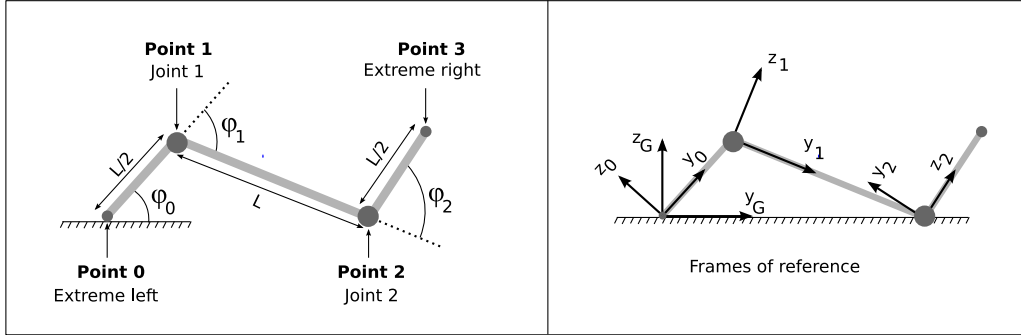


Figure 6.7: Geometric and kinematic models of the PP configuration

Frames of reference

We will employ four different frames of references that are shown in the figure 6.7. The frame R_G is situated on P_0 and its y_G axis is parallel to the ground. The frame R_0 is on P_0 with its y_0 axis along the length of the left segment of the robot. It is rotated an angle φ_0 with respect to R_G . R_1 and R_2 are on the points P_1 and P_2 respectively. The first is rotated an angle φ_1 with respect to R_0 and the second φ_2 on R_1 .

Position vectors and principal points

The position vectors expressed in the frame of reference R_G are calculated in the following way:

$$\begin{aligned}
 \vec{r}_0 &= \vec{r}_G^0 = 0 \\
 \vec{r}_1 &= \vec{r}_G^1 = H_G^0 \vec{r}_0^1 \\
 \vec{r}_2 &= \vec{r}_G^2 = H_G^0 H_1^1 \vec{r}_1^2 \\
 \vec{r}_3 &= \vec{r}_G^3 = H_G^0 H_1^1 H_2^2 \vec{r}_2^3
 \end{aligned} \tag{6.3}$$

Where H_b^a represents the homogeneous transformation of the frame of reference a to b . They are matrices that are given by the rotations of the x axis and the movements in the y axis. They are expressed with the notation:

$$R_x(\varphi) = \begin{pmatrix} 1 & 0 & 0 & 0 \\ 0 & \cos \varphi & -\sin \varphi & 0 \\ 0 & \sin \varphi & \cos \varphi & 0 \\ 0 & 0 & 0 & 1 \end{pmatrix}, \quad T_y(y) = \begin{pmatrix} 1 & 0 & 0 & 0 \\ 0 & 1 & 0 & y \\ 0 & 0 & 1 & 0 \\ 0 & 0 & 0 & 1 \end{pmatrix}$$

The matrices H_b^a are calculated as follows:

$$H_G^0 = R_x(\varphi_0), H_0^1 = T_y\left(\frac{L}{2}\right) R_x(\varphi_1), H_1^2 = T_y(L) R_x(\varphi_2) \quad (6.4)$$

The vectors \vec{r}_b^a indicate the position of point a , referred to the frame b . They are:

$$\vec{r}_0^1 = \frac{L}{2}\hat{y}_0, \vec{r}_1^2 = L\hat{y}_1, \vec{r}_2^3 = \frac{L}{2}\hat{y}_2 \quad (6.5)$$

Substituting the expressions 6.5 and 6.4 in 6.3 the position vectors are obtained of all the points referred to the frame R_G .

Centre of mass

The expression for the centre of mass is obtained applying the position vectors 6.3 previously calculated in the general expression of centre of mass of an apodal robot 3.4. Specifying for $M = 2$ we obtain its expression:

$$\vec{r}_{cm} = \frac{1}{8} (3\vec{r}_1^1 + 3\vec{r}_2^2 + \vec{r}_3^3)$$

Representation by means of complex numbers

The geometry of the configuration PP can be expressed by means of complex numbers. We will take the zy plane as the complex plane. The three segments that form the configuration we denote by means of the complex numbers z_0, z_1 and z_2 . Its modules represent the length and its arguments the angles that are formed with the y axis. Its expressions are:

$$\begin{aligned} z_0 &= \frac{L}{2}e^{j\varphi_0} \\ z_1 &= Le^{j(\varphi_0+\varphi_1)} \\ z_2 &= \frac{L}{2}e^{j(\varphi_0+\varphi_1+\varphi_2)} \end{aligned}$$

The angle that forms the right segment with the y axis is the argument of the complex z_2 and is equal to the sum of the φ_i :

$$\arg(z_2) = \varphi_0 + \varphi_1 + \varphi_2 \quad (6.6)$$

The points can be expressed by means of the addition of these complexes:

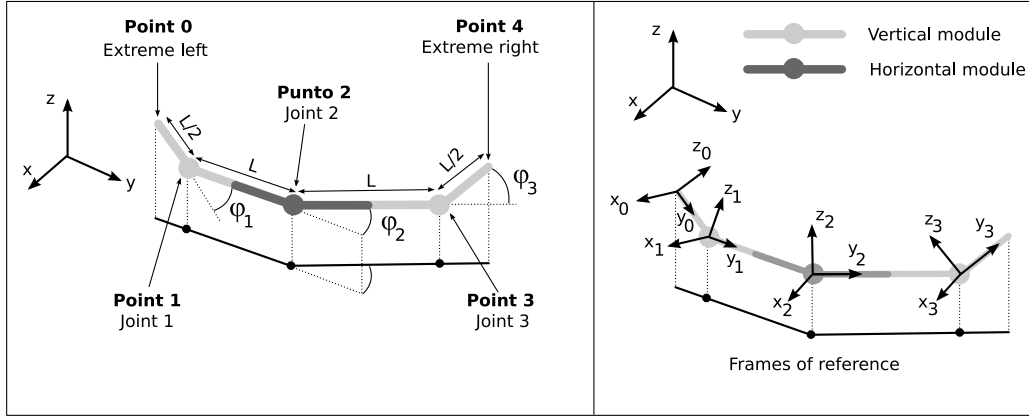


Figure 6.8: Geometric and kinematic models of the PYP configuration

$$\begin{aligned}
 P_0 &= 0 \\
 P_1 &= z_0 \\
 P_2 &= z_0 + z_1 \\
 P_3 &= z_0 + z_1 + z_2
 \end{aligned}$$

6.4.3.2 Configuration PYP

Geometry

The geometric and kinematic models of the PYP configuration are shown in the figure 6.8. This configuration is formed by the union in chain of two pitch type modules and one of yaw type situated in the middle. It has, therefore, three joints, with bending angles ϕ_1 , ϕ_2 , and ϕ_3 , and four rigid segments of lengths $L/2, L, L$ and $L/2$.

The principal points are five: the three joints plus the two extremes. We will use the nomenclature P_0 , P_1 , P_2 , P_3 and P_4 to refer to them. Their position vectors with respect to the frame of reference R_0 we denote by \vec{r}_0 , \vec{r}_1 , \vec{r}_2 , \vec{r}_3 and \vec{r}_4 .

Frames of reference

We will use four frames of reference, situated at the points P_0 , P_1 , P_2 , P_3 and P_4 that we will call R_0 , R_1 , R_2 , R_3 and R_4 . Also a frame of reference connected to the ground R_G is needed that allows the orientation of the robot to be specified.

Position vectors of the points

The position vectors expressed in the frame of reference R_0 are calculated:

$$\begin{aligned}
 \vec{r}_0 &= 0 \\
 \vec{r}_1 &= \vec{r}_0^1 \\
 \vec{r}_2 &= \vec{r}_0^2 = H_0^1 \vec{r}_1^2 \\
 \vec{r}_3 &= \vec{r}_0^3 = H_0^1 H_1^2 \vec{r}_2^3 \\
 \vec{r}_4 &= \vec{r}_0^4 = H_0^1 H_1^2 H_2^3 \vec{r}_3^4
 \end{aligned} \tag{6.7}$$

Where H_b^a represents the homogeneous transformation of the frame of reference a to b . They are given for the rotations around the x and y axis, and the movements in the axis. We will use the notation:

$$R_x(\varphi) = \begin{pmatrix} 1 & 0 & 0 & 0 \\ 0 & \cos \varphi & -\sin \varphi & 0 \\ 0 & \sin \varphi & \cos \varphi & 0 \\ 0 & 0 & 0 & 1 \end{pmatrix}, \quad R_z(\varphi) = \begin{pmatrix} \cos \varphi & -\sin \varphi & 0 & 0 \\ \sin \varphi & \cos \varphi & 0 & 0 \\ 0 & 0 & 0 & 0 \\ 0 & 0 & 0 & 1 \end{pmatrix}, \quad T_y(y) = \begin{pmatrix} 1 & 0 & 0 & 0 \\ 0 & 1 & 0 & y \\ 0 & 0 & 1 & 0 \\ 0 & 0 & 0 & 1 \end{pmatrix}$$

The matrices H_b^a are calculated as follows:

$$H_0^1 = T_y\left(\frac{L}{2}\right) R_x(\varphi_1), \quad H_1^2 = T_y(L) R_z(\varphi_2), \quad H_2^3 = T_y(L) R_x(\varphi_3) \tag{6.8}$$

The vectors \vec{r}_b^a indicate the position of the point a referred to the frame b . They are:

$$\vec{r}_0^1 = \frac{L}{2} \hat{y}_0, \quad \vec{r}_1^2 = L \hat{y}_1, \quad \vec{r}_2^3 = L \hat{y}_2, \quad \vec{r}_3^4 = \frac{L}{2} \hat{y}_3 \tag{6.9}$$

Substituting the expressions 6.9 and 6.8 in 6.7 the position vectors are obtained for all the points referred to the frame R_G .

Centre of mass

The expression for the centre of mass is obtained applying the position vectors 6.7 previously calculated in the general expression of the centre of mass of an apodal robot 3.4. Specifying for $M = 3$ the expression is:

$$\vec{r}_{cm} = \frac{1}{12} (3\vec{r}_1 + 4\vec{r}_2 + 3\vec{r}_3 + \vec{r}_4)$$

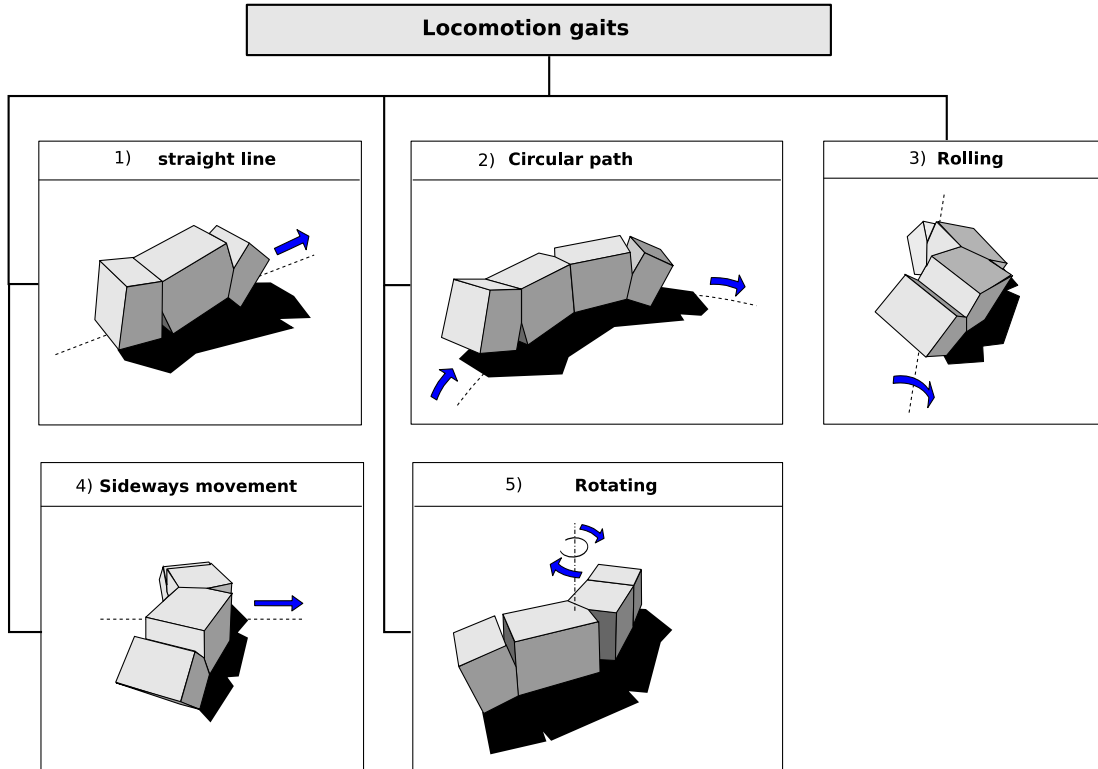


Figure 6.9: Locomotion gaits for the minimum configurations

6.5 Gaits

6.5.1 Solutions found

Five gaits have been discovered for the configuration PYP: straight line, circular path, sideways movement, rolling and rotation (figure 6.9). All of them are totally new and had not been implemented nor studied previously because the subject of the minimum configurations had not been dealt with until now.

In the **straight line movement** the central module remains in the home position ($\varphi_2 = 0$) and only the vertical joints move. Therefore the PYP configuration behaves as if it were a PP in which the central segment has a greater length. In the section 6.6 the straight line movement for the PP configuration will be studied in detail. All the ideas will be applicable to the PYP only re-calculating with a different value for the length of the central segment.

The **circular path movement** is obtained making it move in a straight line but fixing the position of the central module to an angle φ_2 distinct to 0, in a similar way to how it is done in the case of the same type of movement for the apodal robots of M modules.

Gait	Parameters	Degree of freedom	Characterisation
Straight line	$(A, \Delta\phi)$	2	$A = A_v, \Delta\Phi = \Delta\phi_v, A_h = 0, \Delta\phi_{vh} = 0$
Circular path	$(A_v, A_h, \Delta\phi_v)$	3	$\Delta\phi_{vh} = 0$. Central module does not oscillate
Rolling	A	1	$A = A_v = A_h, \Delta\phi_v = 0, \Delta\phi_{vh} = 90, A > A_{min}$
Sideways	A	1	$A = A_h, A_v \rightarrow 0, \Delta\phi_v = 0, \Delta\phi_{vh} = 90, A < A_{hL}$
Rotating	A	1	$A = A_h, A_v \rightarrow 0, \Delta\phi_v = 180, \Delta\phi_{vh} = 90$

Table 6.1: Summary of movements with their parameters, degrees of freedom and the characterisation of the control subspaces

The PYP configuration, despite having only three modules, is capable of **rolling**. This movement is studied in detail in the section 6.7. The co-ordination is the same as the general case. The vertical joints are in phase and the horizontal is out of phase 90 degrees.

The **sideways movement** is of the flapping or “rowing” type. It allows the robot to move sideways, maintaining the same orientation. The co-ordination is the same as in the rolling movement. The value of the amplitude A determines if this movement is executed or that of rolling (section 6.8).

The **rotating movement** permits the robot to change its body orientation to point the head in any direction (section 6.9).

6.5.2 Characterisation of the subspaces G_i

In the table 6.1 all the gaits found for the minimum configuration of PYP are summed up together with their parameters, degrees of freedom and the characterisation of the control subspaces G_i .

The movement in a straight line has two degrees of freedom. One is the amplitude A that decides the step and the other the phase difference $\Delta\phi_v$ that establishes the co-ordination between the segments so that it carries out the movement. The central module remains fixed in its home position $A_h = 0$ and the parameter $\Delta\phi_{vh}$ is not used therefore is set to zero.

The movement with most degrees of freedom is that of the circular path. It is the same as in a straight line but with one more parameter that specifies the arc angle of the path. The central module does not oscillate, it remains in its fixed position at a concrete value different from zero.

The remaining movements all have one degree of freedom. The rolling movement has the characteristic that the two amplitudes A_v and A_h are equal, the vertical modules are in phase and the central one out of phase 90 degrees. The parameter A defines the arc angle that the robot adopts during its movement. So that it can carry out this movement, A has to be greater than the minimum value A_{min} (section 6.7.6).

The sideways movement is characterised by the same values for the differences of phase as in the rolling movement. The two vertical modules oscillate in phase and the horizontal is out of phase 90

degrees. The parameter A determines the robot's step during this movement. The vertical amplitude A_v does not influence in the movement, therefore we use a value near to 0 but different. If $A_v = 0$ there is no movement.

Finally, the rotation movement is characterised by the vertical joints being in opposition of phase ($\Delta\phi_v = 180$) and the horizontal out of phase 90 degrees. The parameter A decides the angle of rotation and the same as in the previous case, A_v does not affect it therefore it has to be greater than 0 but the nearest possible to it so that the movement is the most stable and efficient possible.

6.6 Locomotion in a straight line

6.6.1 Description of the movement

Movement in a straight line of the PP configuration is shown in the figure 6.10. The left and right segments function as “feet”. The co-ordination between them is that which determines what the movement is like. In general we study it dividing it into four stages. During stage 1 the robot carries out a **contraction** resulting in the joint 1 being more elevated. A mini-wave appears that is **propagated** during stage 2 and reaches the right side of the robot. Now it is the joint 2 that is higher. In stage 3 the robot **expands** and the mini-wave disappears. Finally in the fourth stage the robot **recovers** its original shape.

During each stage the movement is stable. The projection of the centre of mass remains at every instant within the supporting segment. Nevertheless the movement is not uniform as in the general case with $k = 2$. As is shown in the chapter of experiments, the movement of the centre of mass does not vary with time linearly.

6.6.2 Study of the stages

6.6.2.1 Supporting points

In all the stages the robot always has two supporting points, which means that the robot is stable for all its phases. In the figure 6.11 the stages and the supporting points are shown. During stage 1 the points in contact with the ground are P_0 and P_2 . The robot contracts until the right segment touches the ground and the new supporting points become P_0 and P_3 , situated in the left and right extremities respectively. The mini-wave is propagated until in stage 3 the point P_0 is substituted by P_1 . Then the robot expands, causing the mini-wave to disappear. In the final stage the two supporting points are P_1 and P_2 .

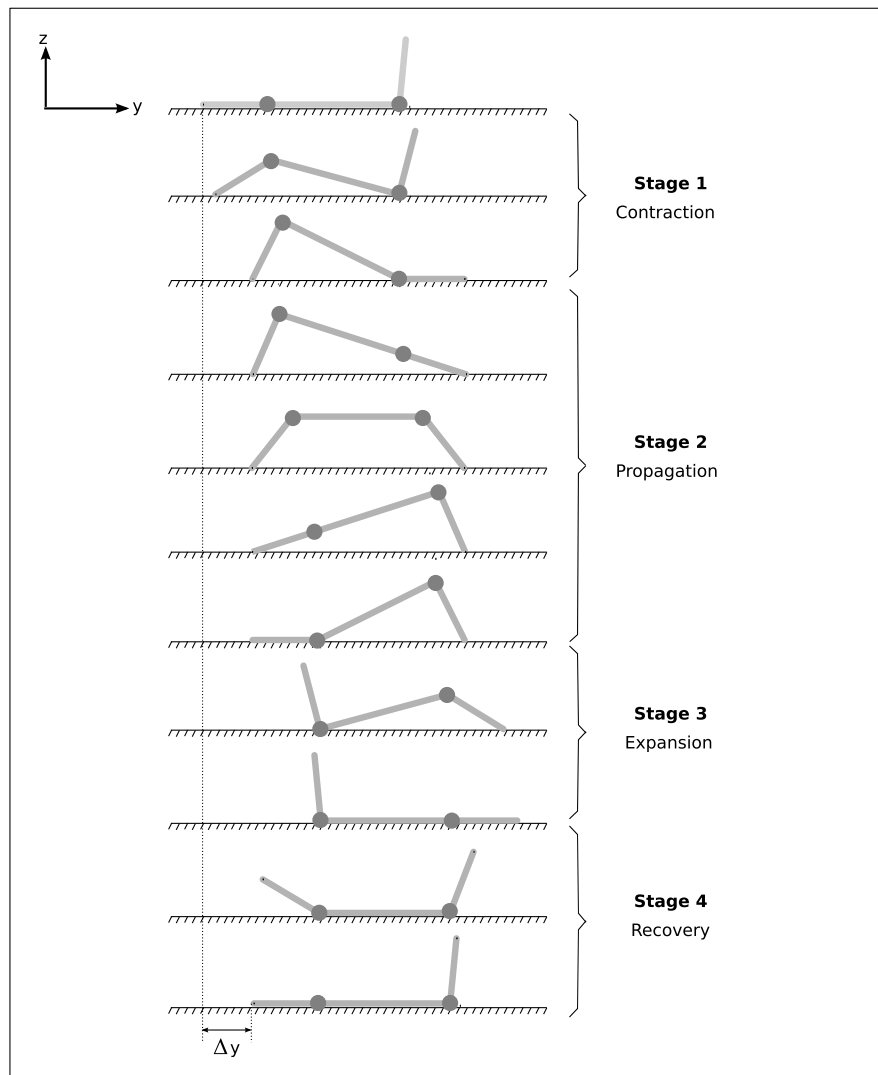


Figure 6.10: Locomotion of the PP configuration and its stages

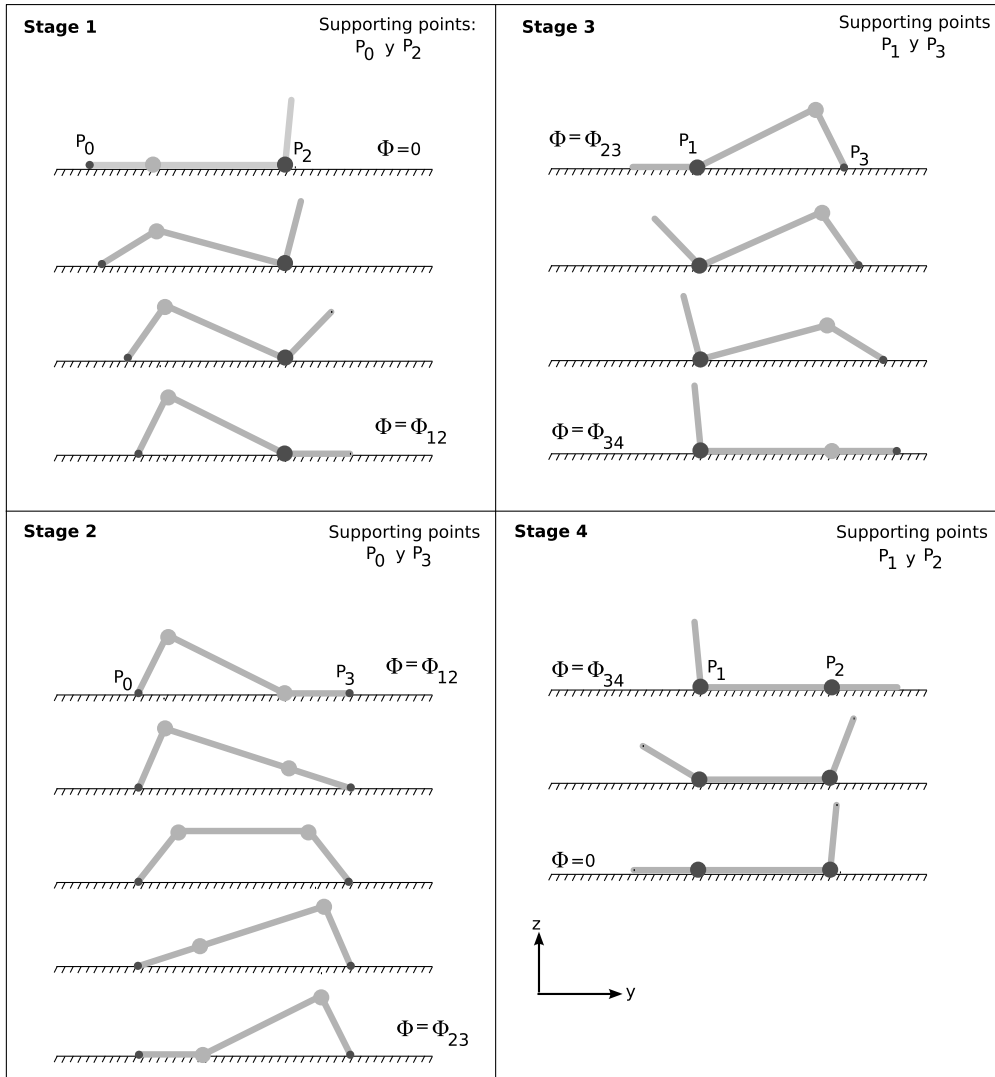


Figure 6.11: Stages and the supporting points during the locomotion of the PP configuration in a straight line

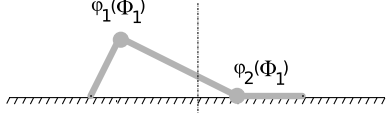
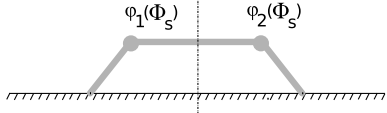
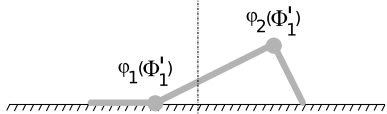
Phase	Robot shape	Symetries
$\Phi = \Phi_1$		$\varphi_1(\Phi_1) = \varphi_2(\Phi_1')$ $\varphi_2(\Phi_1) = \varphi_1(\Phi_1')$
$\Phi = \Phi_s$		$\varphi_1(\Phi_s) = \varphi_2(\Phi_s)$
$\Phi = \Phi_1'$		$\varphi_1(\Phi_1') = \varphi_2(\Phi_1)$ $\varphi_2(\Phi_1') = \varphi_1(\Phi_1)$

Figure 6.12: Symmetry of the robot shape with respect to the phase ϕ_s

6.6.2.2 Symmetries

The shape of the robot during stages 1,2 and 3 is symmetric with respect to the phase ϕ_s . In the figure 6.12 the shape of the robot is shown in ϕ_s , ϕ_1 and ϕ_1' . The robots in ϕ_1 and ϕ_1' are symmetric. If the values of the bending angles in ϕ_1 are known, the corresponding ones in ϕ_1' are also known, given by the expression:

$$\begin{aligned}\varphi_1(\phi_1') &= \varphi_2(\phi_1) \\ \varphi_2(\phi_1') &= \varphi_1(\phi_1)\end{aligned}\tag{6.10}$$

The phase of symmetry ϕ_s is given by the expression:

$$\Phi_s = -\left(90 + \frac{\Delta\Phi}{2}\right)$$

The equation that associates the symmetric phases ϕ_1 and ϕ_1' is:

$$\phi_1' = -(\phi_1 + \Delta\phi + 180)\tag{6.11}$$

Demonstrations

From the expressions of the bending angles 6.2 it is proved that $\varphi_1(\phi_s) = \varphi_2(\phi_s)$:

$$\varphi_1(\phi_s) = A \sin \phi_s = A \sin \left(-90 - \frac{\Delta\Phi}{2} \right) = A \sin \left(90 + \frac{\Delta\Phi}{2} \right) = A \cos \left(\frac{\Delta\Phi}{2} \right)$$

$$\varphi_2(\phi_s) = A \sin(\phi_s + \Delta\Phi) = A \sin \left(-90 - \frac{\Delta\Phi}{2} + \Delta\Phi \right) = A \cos \left(\frac{\Delta\Phi}{2} \right)$$

The expressions 6.10 are also verified:

$$\varphi_1(\phi_1') = A \sin(\phi_1') = A \sin(-(\phi_1 + \Delta\phi + 180)) = -A \sin(\phi_1 + \Delta\phi + 180) = A \sin(\phi_1 + \Delta\phi) = \varphi_2(\phi_1)$$

$$\varphi_2(\phi_1') = A \sin(\phi_1' + \Delta\phi) = A \sin(-(\phi_1 + \Delta\phi + 180) + \Delta\phi) = A \sin(-(\phi_1 + 180)) = A \sin(\phi_1) = \varphi_1(\phi_1)$$

6.6.2.3 Supporting segments

We call supporting segments those which join the supporting points and are denoted by Sa_i where the sub-index i indicates the stage. Each stage has a supporting segment. We will use the notation of complex numbers to obtain its expressions. An important property of these segments is that they rest on the ground (y axis) and therefore **their argument will always be 0**. This is the condition that we will employ to calculate the orientation angle φ_0 in the section 6.6.2.4.

$$\arg(Sa_i) = 0, \forall i \in \{1..4\} \quad (6.12)$$

The expressions of Sa_i in function of the geometry of the robot and of the angles φ_i are shown next, together with its modules and arguments. The calculations are developed in the appendix A.2.

Stage 1

$$Sa_1 = z_0 + z_1 = Le^{j\varphi_0} \left(\frac{1}{2} + e^{j\varphi_1} \right)$$

$$\|Sa_1\| = L\sqrt{\frac{5}{4} + \cos(\varphi_1)} \quad (6.13)$$

$$\arg(Sa_1) = \varphi_0 + \arctan \left(\frac{\sin(\varphi_1)}{\frac{1}{2} + \cos(\varphi_1)} \right)$$

Stage 2

$$Sa_2 = z_0 + z_1 + z_2 = Le^{j\varphi_0} \left(\frac{1}{2} + e^{j\varphi_1} + \frac{1}{2}e^{j(\varphi_1+\varphi_2)} \right)$$

$$\|Sa_2\| = L\sqrt{\frac{3}{2} + \cos(\varphi_1) + \cos(\varphi_2) + \frac{1}{2}\cos(\varphi_1 + \varphi_2)} \quad (6.14)$$

$$\arg(Sa_2) = \varphi_0 + \arctan\left(\frac{\sin\varphi_1 + \frac{1}{2}\sin(\varphi_1 + \varphi_2)}{\frac{1}{2} + \cos\varphi_1 + \frac{1}{2}\cos(\varphi_1 + \varphi_2)}\right)$$

Stage 3

$$Sa_3 = z_1 + z_2 = Le^{j(\varphi_0+\varphi_1)} \left(1 + \frac{1}{2}e^{j\varphi_2} \right)$$

$$\|Sa_3\| = L\sqrt{\frac{5}{4} + \cos(\varphi_2)}$$

$$\arg(Sa_3) = \varphi_0 + \varphi_1 + \arctan\left(\frac{\sin(\varphi_2)}{2 + \cos(\varphi_2)}\right)$$

Stage 4

$$Sa_4 = z_1 = Le^{j(\varphi_0+\varphi_1)}$$

$$\|Sa_4\| = L$$

$$\arg(Sa_4) = \varphi_0 + \varphi_1$$

6.6.2.4 Orientation angle φ_0

The orientation angle φ_0 is that which the robot's left segment forms with the horizontal. It is necessary to know it to be able to determine the position vectors of the robot's points and of its centre of

mass. This angle depends on the stage in which the robot is found during the movement. We will use the notation $\varphi_0^i(\phi)$ to represent its value in the stage i . For a given phase ϕ the expressions are:

$$\varphi_0^1(\phi) = -\arctan\left(\frac{\sin \varphi_1(\phi)}{\frac{1}{2} + \cos \varphi_1(\phi)}\right), \phi \in [0, \phi_{12}] \quad (6.15)$$

$$\varphi_0^2(\phi) = -\arctan\left(\frac{\sin \varphi_1(\phi) + \frac{1}{2} \sin(\varphi_1(\phi) + \varphi_2(\phi))}{\frac{1}{2} + \cos \varphi_1(\phi) + \frac{1}{2} \cos(\varphi_1(\phi) + \varphi_2(\phi))}\right), \phi \in [\phi_{12}, \phi_{23}]$$

$$\varphi_0^3(\phi) = -\varphi_1 - \arctan\left(\frac{\sin \varphi_2}{2 + \cos \varphi_2}\right), \phi \in [\phi_{23}, \phi_{34}]$$

$$\varphi_0^4(\phi) = -\varphi_1(\phi), \phi \in [\phi_{34}, 360]$$

Where ϕ_{12} , ϕ_{23} and ϕ_{34} represent the values of the phase that separate one phase from another (section 6.6.2.5).

Demonstrations

The expressions for calculating φ_0 are obtained applying the condition 6.12 that establish that the argument of all the supporting segments is zero. With this it forces the robot's orientation to be determined by the condition that its supporting points are aligned and in a horizontal position.

Making $\arg(Sa_i) = 0$ and clearing φ_0 the equations of φ_0^i are obtained.

6.6.2.5 Transition between stages

The values of the phases that separate one stage from the other are denoted by ϕ_{12} , ϕ_{23} and ϕ_{34} . They are given by the expressions:

$$\Phi_{12} = -\arctan\left(\frac{\sin \Delta\Phi}{\left(1 - \frac{A_0}{A}\right) + \cos \Delta\Phi}\right), A_0 = \arctan\left(\frac{\sin A}{\frac{1}{2} + \cos A}\right)$$

$$\Phi_{23} = -\Phi_{12} - 180 - \Delta\Phi$$

$$\Phi_{34} = -180 - \Delta\Phi$$

Demonstrations

First we will calculate ϕ_{12} . The condition that determines whether it is in stage 1 or 2, is that the right segment is resting on the y axis. That is to say, that $\arg(z_2) = 0$ is fulfilled. This implies that:

$$\varphi_0^1 + \varphi_1 + \varphi_2 = 0$$

Substituting φ_0 by the expression 6.15, the bending angles for those given in 6.2 and clearing the phase the equation of ϕ_{12} is obtained. The steps to follow are detailed in the appendix A.3.

The calculation of Φ_{23} and Φ_{34} is made applying the condition of symmetry 6.11 and bearing in mind that they are symmetric with respect to the phases ϕ_{12} and $\phi = 0$ respectively.

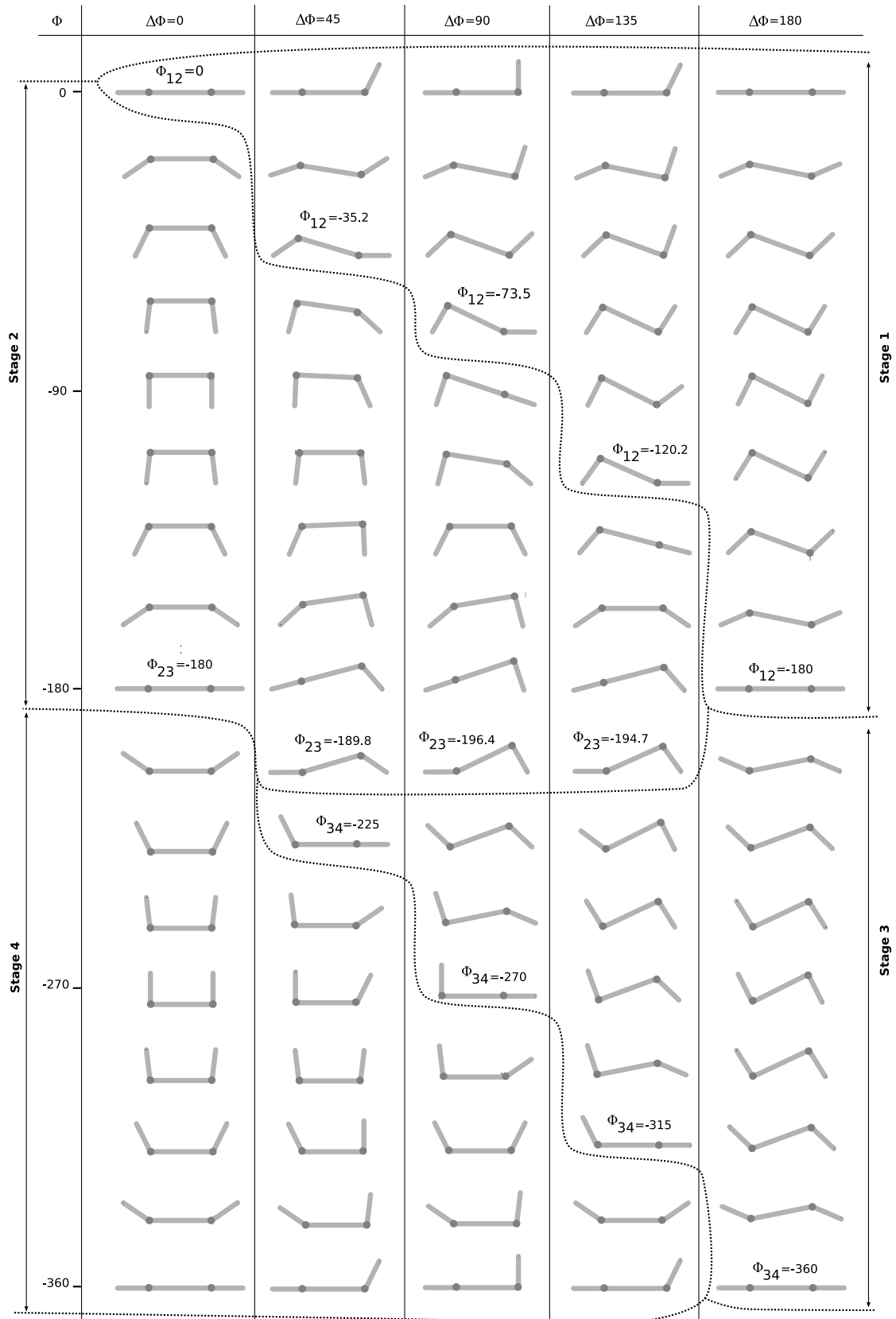
6.6.3 Step

6.6.3.1 Co-ordination

The straight line movement is controlled by the parameters A and $\Delta\phi$. The first is related to the size of the step and the dimensions of the robot. The second is that which determines the co-ordination of the segments and that the robot can move.

In the figure 6.13 the robot's movement for different values of $\Delta\phi$ are shown and how they vary with the phase ϕ . When the two joints are in phase ($\Delta\phi = 0$) the left and right segments move exactly equally causing the robot to sprawl on the ground, having the shape \square , then again sprawled, with the shape \sqcup and starting again. There is no displacement. The movement has only two stages, the second and fourth.

When the joints are in opposition of phase ($\Delta\phi = 180$) the robot contracts and expands, but without displacement. The movement has only two stages, the first and the third. Therefore, with the movement of apodal robots of one dimension, the same principle of generators in phase and in opposition of phase is fulfilled.

Figure 6.13: Co-ordination of the locomotion in a straight line in function of the phase difference $\Delta\phi$

For the rest of the values of $\Delta\phi$ there does exist displacement. In general the movement will depend on the interaction with the ground of the supporting points. To realise a detailed analysis it is necessary to study the dynamics of the system. Nevertheless, analysing only the geometry we will obtain conclusions on how the co-ordination must be carried out.

6.6.3.2 Co-ordination criterion

To be able to obtain the values of A and $\Delta\phi$ that allow a well co-ordinated movement, it is necessary to establish first a criterion to measure how good the co-ordination is.

Of the four stages, the fundamental one so that the movement is accomplished correctly is the second, where the mini-wave that has appeared is propagated from the tail to the head. If the co-ordination is wrong, the propagation will not exist and therefore there will be no movement. In this stage, the supporting points are the two extremes. We will reckon that the movement is better co-ordinated when there is the least interaction with the ground, thereby less energy loss through friction. So that, if during this stage the co-ordination is such that the supporting points always remain equidistant one from the other, there will be no relative movement between them and no loss through friction will be produced. What is more, the movement will be independent of the environment, behaving in a similar way as the independence of the value of the coefficient of friction. Contrariwise, if the joints are forced to vary this distance during the propagation, an undesirable friction will appear which will produce energy loss as well as introducing uncertainty into the movement. The movement will be very dependant upon the type of surface.

The criterion proposed is the following:

Criterion of co-ordination: *It is said that the configuration PP is moving with a good co-ordination if the distance between the supporting points P_0 and P_3 remains constant during stage 2 or its variation is minimum.*

This criterion allows us to compare the movement at different working points. Observing the movement when $\Delta\phi = 0$ of the figure 6.13, it is seen that the variation of the distance between the supporting points in stage 2 is very great. There will be a lot of interaction with the ground. If the coefficient of friction is very high, it could happen that the robot will not even be able to pass from the initial position to the shape of \square . For $\Delta\phi = 45$, the variation of the distance is less which leads to a decrease in the interaction with the ground. For $\Delta\phi = 135$ this distance varies very little. It is a better co-ordinated movement than in the previous cases. When they are in opposition of phase ($\Delta\phi = 180$) the propagation stage does not exist and therefore there is no movement.

The questions that arise are: *What values of A and $\Delta\phi$ lead to the best co-ordinated movement? Which is the equation that relates the step with these parameters?*

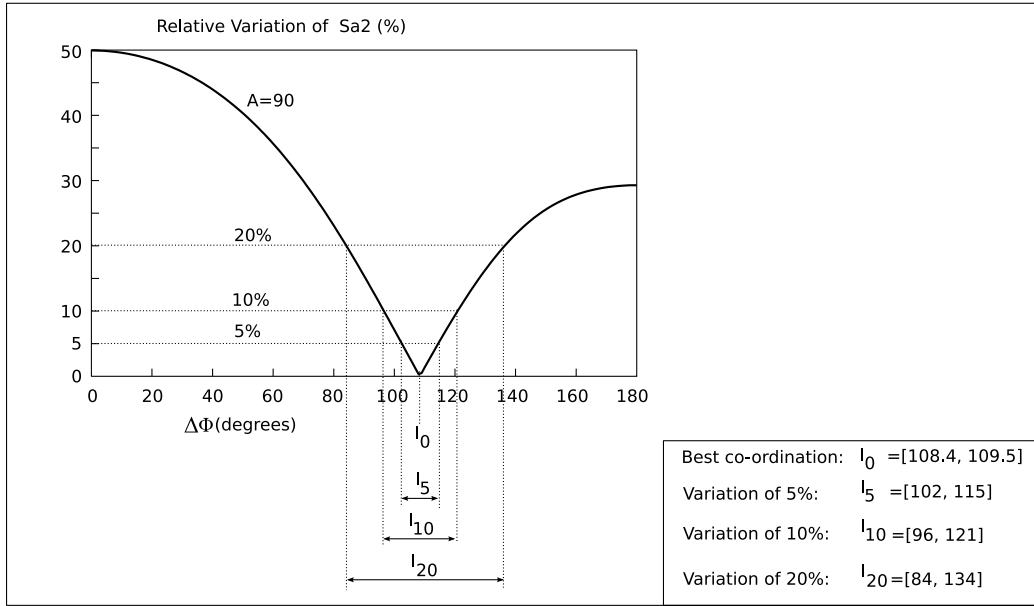


Figure 6.14: Relative variation of the supporting segment 2 in function of the phase difference $\Delta\phi$ for an amplitude A of 90 degrees

6.6.3.3 The best co-ordinated movement

Applying the previous criterion of co-ordination the results obtained are:

1. *The **best co-ordinated movement** is obtained for values of $\Delta\phi$ within the interval $[108.4, 109.5]$, with independence of the amplitude of A used. For them it is verified that the variation of the supporting segment during stage 2 is practically nil.*
2. *For a given value of $\Delta\phi$, the co-ordination improves with the decrease of the amplitude. The smaller A is, the smaller will be the variation of the supporting segment of stage 2.*

In the figure 6.14 the relative variation of the supporting segment 2 is shown in function of the parameter $\Delta\phi$ for the case of maximum amplitude, where the co-ordination is the worst. From it more flexible criterion can be established:

- $\forall A$, if $\Delta\phi \in [84, 134]$, the variation will be less than or equal to 20%.
- $\forall A$, if $\Delta\phi \in [96, 121]$, the variation will be less than or equal to 10%.
- $\forall A$, if $\Delta\phi \in [102, 115]$, the variation will be less than or equal to 5%.

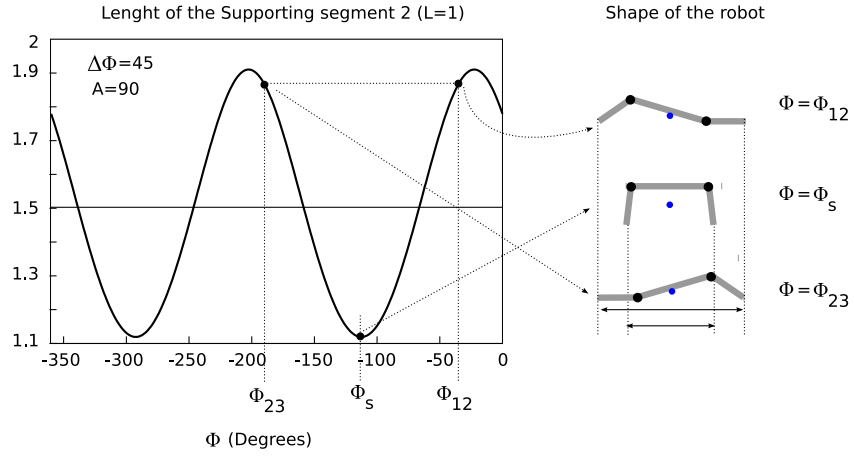


Figure 6.15: Variation of the supporting segment 2 in function of the phase for $A = 90$ y $\Delta\phi = 45$

6.6.3.4 Study of the supporting segment 2

To demonstrate the earlier conclusions it is necessary to study what happens to the supporting segment 2 during the propagation stage. Its length is given by the equation 6.14. If it is expanded employing the expressions of the bending angles in 6.2 the following is obtained:

$$\|Sa_2\| = L \sqrt{\frac{3}{2} + \cos(A \sin(\phi)) + \cos(A \sin(\phi + \Delta\Phi)) + \frac{1}{2} \cos(A \sin(\phi) + A \sin(\phi + \Delta\Phi))} \quad (6.16)$$

This expression is only valid for the phases included in the interval $[\phi_{12}, \phi_{23}]$. In the figure 6.15 the variation with ϕ for $A = 90$ and $\Delta\phi = 45$ has been represented graphically. It varies in a periodic way. For $\phi = \phi_{12}$ and $\phi = \phi_{23}$ the length is maximum and for $\phi = \phi_s$ it is minimum. On the right of the figure the shape of the robots for different working points has been drawn. This allows to visualise graphically the variation of the distance in the supporting points. The minimum is always in ϕ_s and the maximum in ϕ_{12} and ϕ_{23} .

The figure 6.16 shows the graphic restricted to the interval $[\phi_{12}, \phi_{23}]$ for the values of $\Delta\phi$ of 0, 45, 90 and 109, together with the shapes of the robot in ϕ_{12} and ϕ_s , where the length is maximum and minimum respectively. For $\Delta\phi = 0$ the variation is the maximum. Increasing its value the variation decrease until it reaches the value of $\Delta\phi = 109$ where it is minimum and the length remains almost constant with the phase.

To obtain the values of $\Delta\phi$ that minimise the variation in length of the supporting segment 2 we approximate the expression 6.16 for its development in Fourier series and keep the first harmonic:

$$|Sa_2| \approx c_0 + c_2 e^{j2\phi} + c_{-2} e^{-j2\phi} = c_0 + 2|c_2| \cos(2\phi + \Delta\Phi)$$

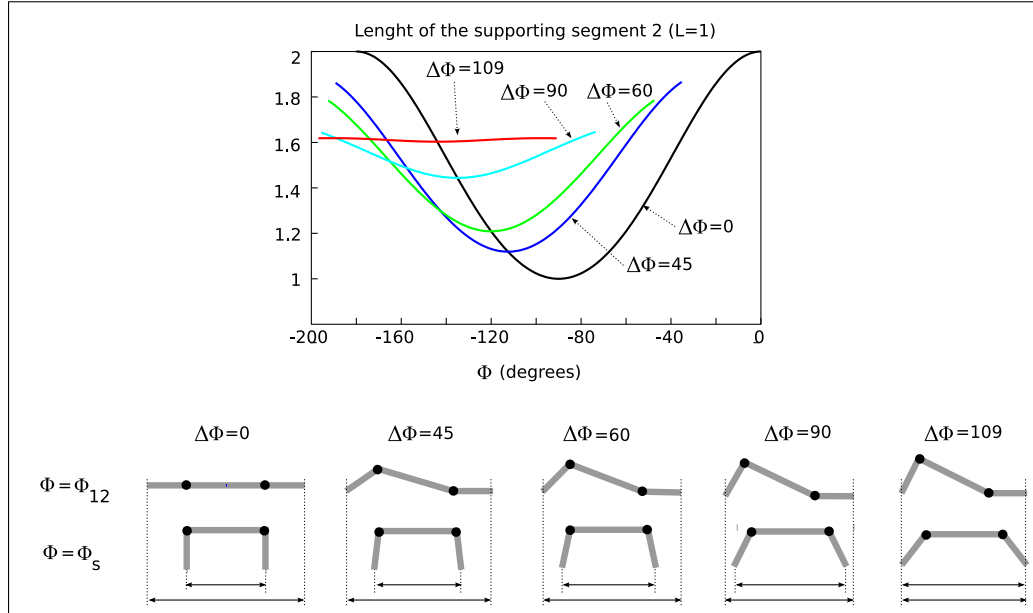


Figure 6.16: Graphical representation of the variation of Sa_2 in function of ϕ for different values of $\Delta\phi$

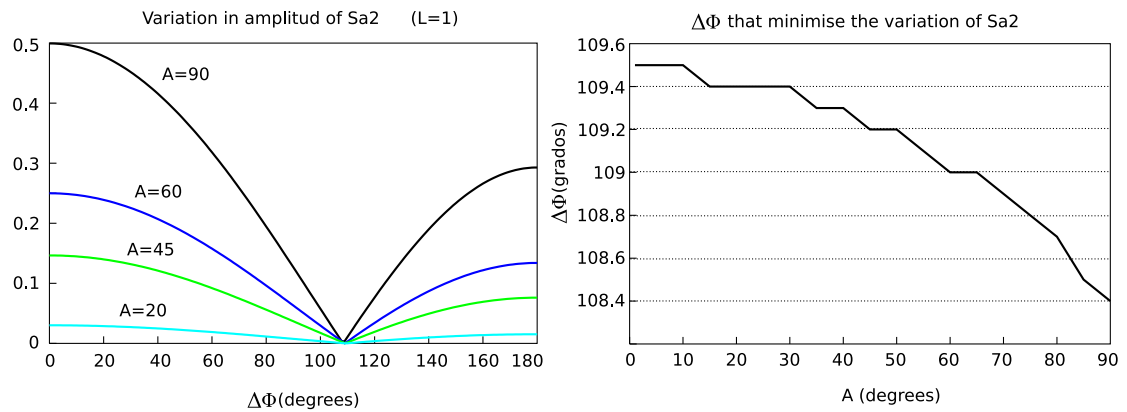


Figure 6.17: **Left:** Variation of the oscillation amplitude of Sa_2 in function of $\Delta\phi$ for different values of A . **Right:** Variation of $\Delta\phi$ that minimise the amplitude of Sa_2 in function of A .

The Fourier coefficients c_i are calculated numerically because they cannot be expressed in an analytical way. The term $2|c_2|$ represents the amplitude of the oscillation. In the figure 6.17 this term has been represented in function of $\Delta\phi$ and for different values of A . It is observed that:

- The variation decreases with the decrease of A . Therefore, in the worst case, where the variation is maximum it is produced for $A = 90$.
- The variation is minimum (tends to zero) for a phase difference in the range $[108, 110]$. It is in this interval where, with independence of the amplitude of A employed, the length of the supporting segment remains constant.

6.6.3.5 Step equation

To study how the parameters A and $\Delta\phi$ affect the step it is necessary to realise an analysis of the dynamics, taking into account the coefficients of friction with the ground. Nevertheless, we propose an equation that allows us to know the step if the movement is well co-ordinated.

For its calculation we will suppose the following:

- During the contraction (1st stage) the joint 2 does not slide on the ground.
- During the propagation the supporting points do not slide.
- While expanding (3rd stage) the joint 1 does not slide.

With these assumptions **the robot's step is equal to the contraction**. That is to say, that the contraction that is produced during stage 1 and that causes the appearance of a mini-wave that is propagated is that which determines the robot's step.

The value of this contraction is established, therefore, during stage 1 and will be equal to the length of the supporting segment 1 in the phase $\phi = \phi_{12}$. Itemising the equation 6.13 the step equation is obtained:

$$\Delta y = |Sa_1|_{\phi=\phi_{12}} = L \sqrt{\frac{5}{4} + \cos(A \sin \phi_{12})} \quad (6.17)$$

6.6.3.6 Step variation with A and $\Delta\phi$

The figure 6.18 represents the step in function of A and $\Delta\phi$. It is observed that it increases with A . In the central zone, where $\Delta\phi = [90, 110]$ its value is high. The maximum value is found in $\Delta\phi = 107$ degrees. It is verified that the point where the step is maximum is very nearer to the point where the co-ordination is the best.

In the figure 6.19 the working point (109.90) is shown and its variation with A and $\Delta\phi$.

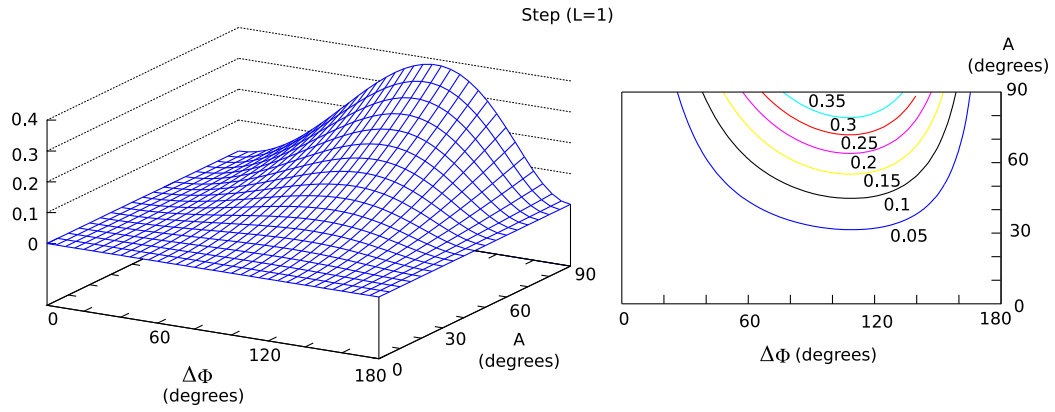


Figure 6.18: Graphical representation of the step given by the locomotion in a straight line of the PP configuration in function of A and $\Delta\phi$

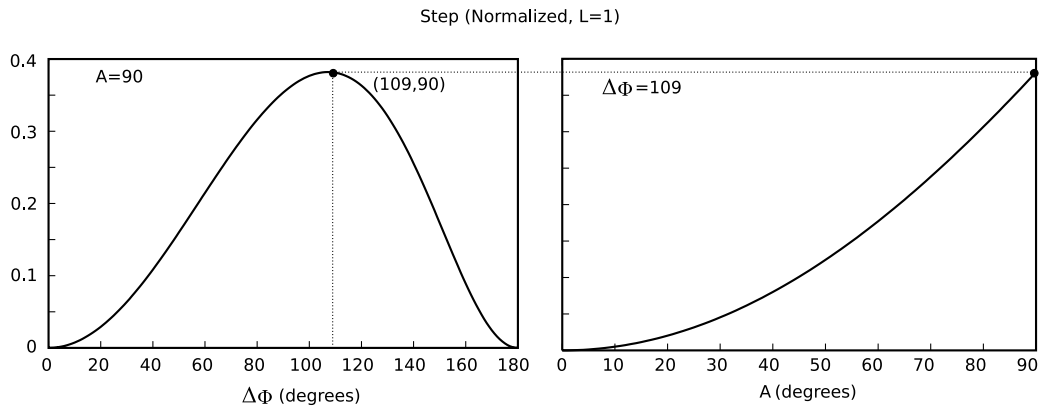
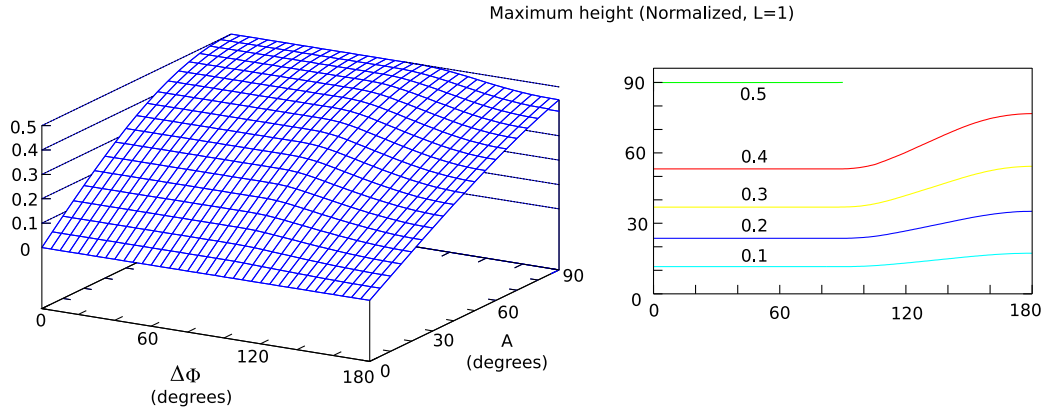


Figure 6.19: Working point $(109, 90)$ and its variation with A and $\Delta\phi$

Figure 6.20: Height of the PP configuration in function of A and $\Delta\phi$

6.6.3.7 Direction of movement

The direction of movement is controlled with the variation of ϕ and the sign of $\Delta\phi$. The combinations are:

- ϕ varying between $[0, -360]$
 - ◇ $\Delta\phi > 0$, movement in a positive direction of y axis
 - ◇ $\Delta\phi < 0$, movement in a negative direction of y axis
- ϕ varying between $[0, 360]$
 - ◇ $\Delta\phi < 0$, movement in positive direction of y axis
 - ◇ $\Delta\phi > 0$, movement in direction negative of y axis

6.6.4 Dimensions

6.6.4.1 Height

In the figure 6.20 the height of the configuration PP and its variation with the parameters A and $\Delta\phi$ is shown when the length of the segments is $L = 1$. The maximum height of the configuration is $L/2$ that is obtained for $A = 90$ and $\Delta\phi = 0$. The variation with $\Delta\phi$ is small. For $\Delta\phi > 90$ the value remains constant and diminishes for $\Delta\phi < 90$. The influence of the amplitude is greatest. It is possible to get the robot to have a height from 0 to the maximum.

In the figure 6.21 the variation of the height of the working point $(90, 90)$ is shown.

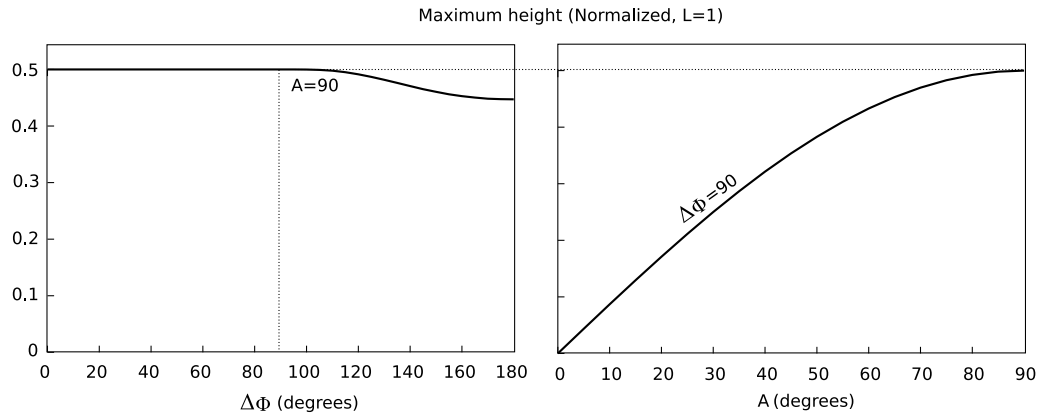


Figure 6.21: **Left:** Variation of the height with $\Delta\phi$ for $A = 90$. **Right:** Variation of the height with A for $\Delta\phi=90$

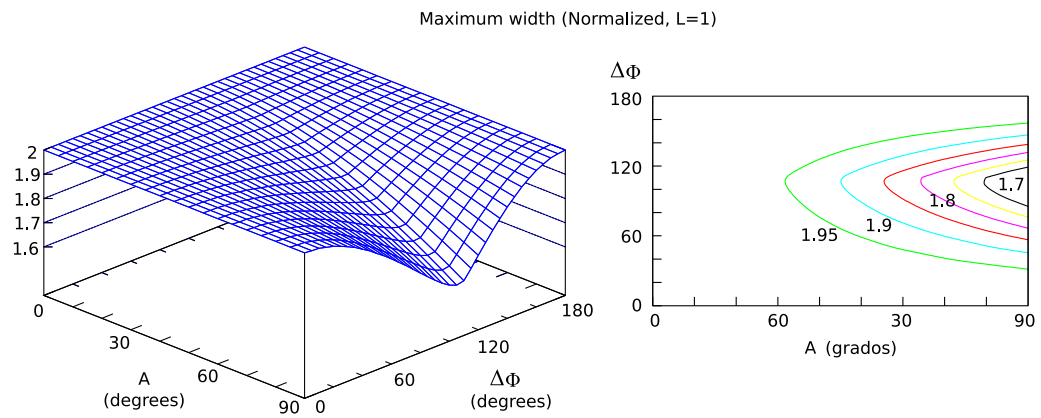


Figure 6.22: Width of the PP configuration in function of A and $\Delta\phi$

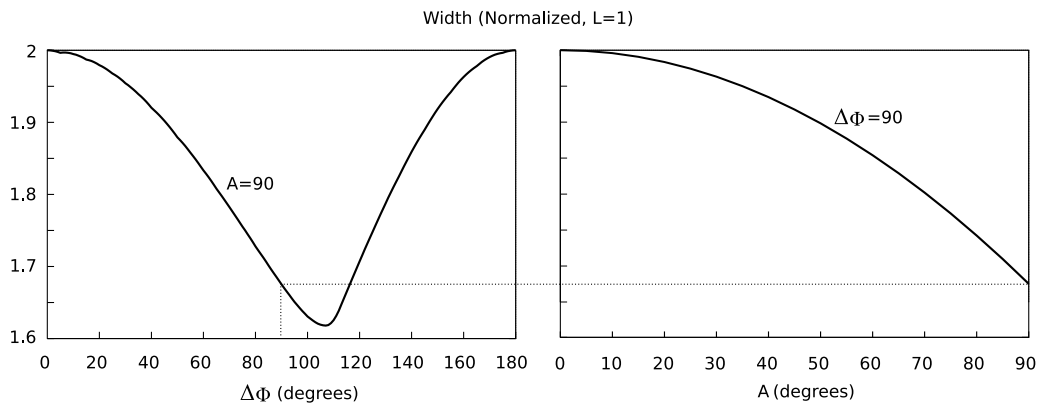


Figure 6.23: Variation of the width. **Left:** With $\Delta\phi$ for $A = 90$. **Right:** with A for $\Delta\phi = 90$

6.6.4.2 Width

The figure 6.22 shows the width and its variation with A and $\Delta\phi$. It decreases when A increases. The variation with $\Delta\phi$ present the maximum in 0 and 180 and the minimum is in the interval $[107, 109]$.

In the figure 6.23 the variation of the width has been represented for the working point $(90, 90)$.

6.6.5 Summary

The study of the movement of the configuration PP has been divided into **four stages**. In each one of them there are different supporting points. The **orientation angle** ϕ_0 has been calculated for all of them, which allows the position vectors of all the joints to be obtained.

To study the co-ordination a **criterion of good co-ordination** has been defined based on the relative distance between the supporting point of stage 2, which is where the mini-wave of movement is propagated. If this distance is constant or small, there will be no losses in the propagation of the wave.

An **equation** has been proposed **to calculate the step**, based on the premise that it is equal to the initial contraction. Its value increases with the amplitude A and is maximum for a difference of phase of $\Delta\phi = 107$ degrees, very near to the interval where the co-ordination is the best.

As a conclusion to this movement, for the wired model **the best co-ordination is produced in the interval** $[108, 110]$ and if the amplitude is of 90 degrees, the step will be practically the same as the maximum.

6.7 Rolling movement

6.7.1 Description of the movement

The rolling movement allows the configuration PYP to rotate its modules around its corporal axis causing movement. In the solution found the restrictions that have to be applied to produce it are: $\Delta\phi_{vh} = 90$, $\Delta\phi_v = 0$ y $A_v = A_h = A$. This movement, therefore, has one degree of freedom, A , that determines the shape of the robot when it rolls.

In the figure 6.24 the wired model of the configuration PYP is shown rolling during half a cycle. Each cycle is divided into two semi-periods, within the phases $\phi \in [0, 180]$ and $\phi \in [180, 360]$, in which the movement is the same. In each one of them the robot rotates 180 degrees. Each one of these semi-periods is also divided into 2 stages. In the figure 6.24 the two stages of semi-period 1 are

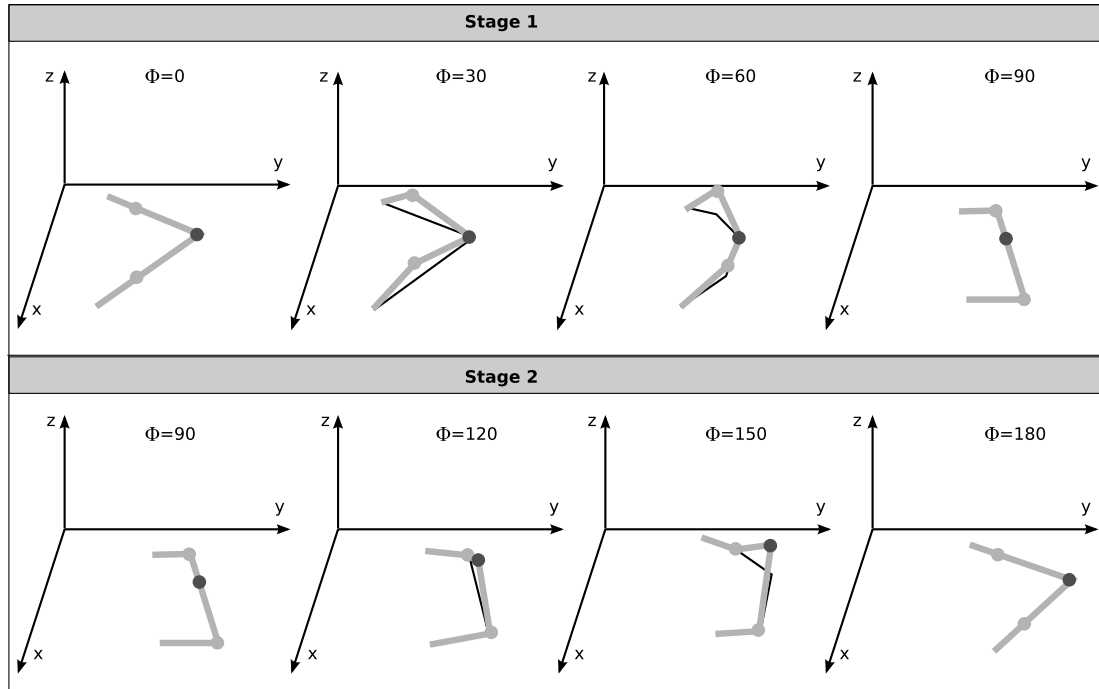


Figure 6.24: Rolling movement of the PYP configuration wired model

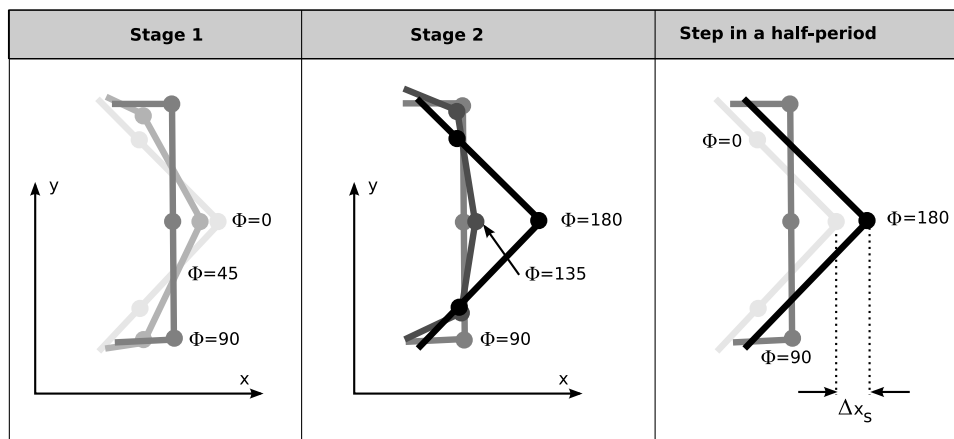


Figure 6.25: Top view of the wired model of the PYP configuration when rolling

represented, within the phases $\phi \in [0, 90]$ and $\phi \in [90, 180]$. In each one the robot rotates 90 degrees. In the figure 6.25 the projection in the horizontal xy plane is shown in which the step Δx that the robot takes at the end of a cycle can be seen. It is observed that the supporting points vary their position with respect to the ground therefore to find the exact step equation of the wired model the dynamics will have to be studied. In general its value will depend on the type of surface.

The mechanism of rotation is different in the two stages. At the beginning of stage 1 the joints have the orientations of pitch-yaw-pitch (PYP) and at the end, as each one of them has rotated 90 degrees, the new orientation will be yaw-pitch-yaw (YPY). Stage 2 begins with this orientation and on rotating 90 degrees it ends up with the original orientation, PYP. In reality it is a rolling movement of two different configurations, the PYP and the YPY. Because of this, in the study, we will differentiate between the parameters A_h and A_v . The equations that we will use are:

$$\begin{aligned}\varphi_1 &= \varphi_3 = A_v \sin \phi \\ \varphi_2 &= A_h \sin \left(\phi + \frac{\pi}{2} \right) = -A_h \cos \phi\end{aligned}\tag{6.18}$$

This allows us to determine the corresponding values of A_v and A_h that have to be applied separately in each stage to obtain the movement. In the section 6.7.8 it will be applied to the case in which $A_v = A_h = A$ and with the dimensions of the Y1 modules designed in this thesis.

In the remaining sections we will study the movement assuming that the modules are hexahedrons with dimensions $L \times W \times H$. Nevertheless, this is not a necessary requirement. That the robot rolls is an intrinsic characteristic of the wired model. A minimum configuration PYP with null values of width and height can roll. When the modules are hexahedrons restrictions appear in the amplitudes in such a way that movement will be produced for values of A_h and A_v greater than a certain minimum value. This is analysed in detail in the section 6.7.5.

6.7.2 Kinematic model

To study the movement we will employ the kinematic model shown in the figure 6.26. Instead of using the general model of the configuration PYP shown in the section 6.4.3.2, we take advantage of the symmetry of this movement to simplify the equations. We will take as origin the central joint (number 2). The frames of reference employed are R_0 , R_1 , R_2 and R_3 . The frames R_2 and R_3 are situated on the joints 2 and 3 respectively, as in the general case. R_1 is also found on the joint 2. Its x_1 axis is orientated in the direction of the axis of symmetry. R_2 is rotated an angle θ_2 with respect to R_1 . Because of the symmetry, this angle is equal to $\varphi_2/2$.

The frame of reference R_0 is also situated on the joint 2 and its plane x_0y_0 is parallel to the ground. We use it as reference to know the angle θ_1 that has rotated the robot with respect to the y_0 axis.

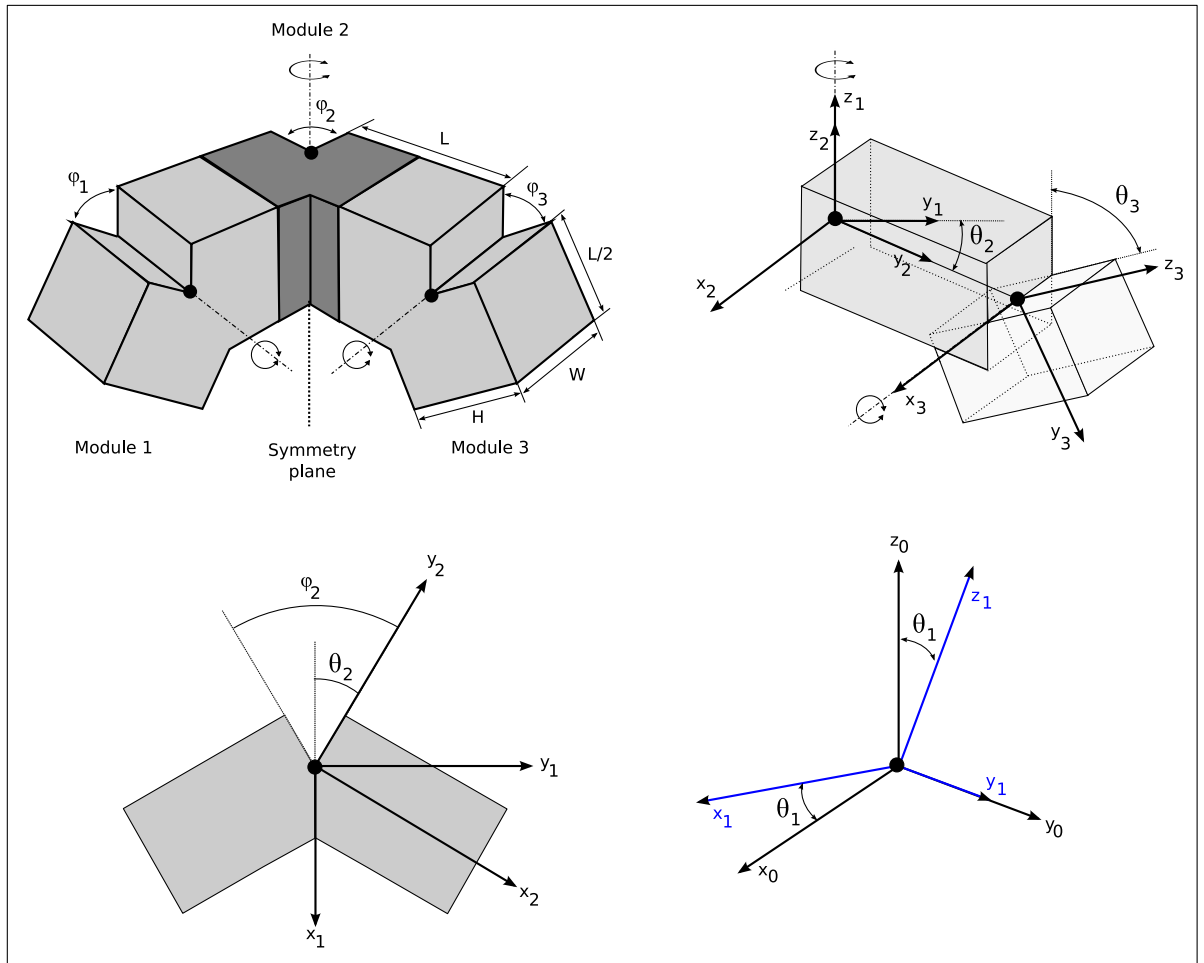


Figure 6.26: The kinematic model employed for the study of the rolling gaits of the PYP configuration

Therefore the movement is described by means of three angles θ_1, θ_2 and θ_3 . By the criterion of signs employed, we have:

$$\begin{aligned}\theta_2 &= -\frac{\varphi_2}{2} \\ \theta_3 &= -\varphi_3\end{aligned}\tag{6.19}$$

The robot's angle of rotation, θ_1 is obtained as a function of θ_2 and θ_3 and its expression depends on the stage of movement. It is calculated in the section 6.7.3.

The homogeneous transformations that define the model, using the same notation defined in the section 6.4.3.2, are:

- Transformation between the frames R_3 and R_2 : Rotation of an angle θ_3 around x_3 and move it a distance L along y_2 :

$$H_2^3 = T_y(L) R_x(\theta_3) = \begin{pmatrix} 1 & 0 & 0 & 0 \\ 0 & \cos \theta_3 & -\sin \theta_3 & L \\ 0 & \sin \theta_3 & \cos \theta_3 & 0 \\ 0 & 0 & 0 & 1 \end{pmatrix}$$

- Transformation between the frames R_2 and R_1 : Rotation of an angle θ_2 around z_2 :

$$H_1^2 = R_z(\theta_2) = \begin{pmatrix} \cos \theta_2 & -\sin \theta_2 & 0 & 0 \\ \sin \theta_2 & \cos \theta_2 & 0 & 0 \\ 0 & 0 & 1 & 0 \\ 0 & 0 & 0 & 1 \end{pmatrix}$$

- Transformation between the frames R_1 and R_0 : Rotation of an angle θ_1 around the y_1 axis

$$H_0^1 = R_y(\theta_1) = \begin{pmatrix} \cos \theta_1 & 0 & \sin \theta_1 & 0 \\ 0 & 1 & 0 & 0 \\ -\sin \theta_1 & 0 & \cos \theta_1 & 0 \\ 0 & 0 & 0 & 1 \end{pmatrix}$$

- Rotation of -90 degrees with respect to the x_0 axis to define the initial state of the frame of reference R_0 at the beginning of stage 2:

$$H_{-90} = \begin{pmatrix} 0 & 0 & -1 & 0 \\ 0 & 1 & 0 & 0 \\ 1 & 0 & 0 & 0 \\ 0 & 0 & 0 & 1 \end{pmatrix}$$

6.7.3 Angle of rotation θ_1

6.7.3.1 Stage 1

The rotation angle θ_1 is given by the following expression:

$$\theta_1 = \arctan \left(-\frac{\sin(A_v \sin \phi)}{(2 + \cos(A_v \sin \phi)) \sin\left(\frac{A_h}{2} \cos \phi\right)} \right) \quad (6.20)$$

At the beginning of stage 1, when $\phi = 0$, the robot has not rotated and the result is that $\theta_1 = 0$. When the stage finishes ($\phi = 90$) the robot has rotated an angle $\theta_1 = -90$.

Demonstration

During stage 1, the supporting points are the two extremities (points P_0 and P_4) and the central joint (Point P_2) (see figure 6.24). To calculate θ_1 the condition is imposed that P_4 is in contact with the ground and therefore its co-ordinate z referred to in the frame R_0 must be 0 for all the phases. That is to say, the following are fulfilled:

$$\vec{r}_4 \cdot \hat{z}_0 = 0$$

Applying the equation 6.3 results in:

$$\left(H_0^1 H_1^2 H_2^3 \vec{r}_3^4 \right) \cdot \hat{z}_0 = 0$$

Substituting \vec{r}_3^4 for its value (equation 6.5), operating and clearing θ_1 the expression is obtained (the details can be found in the appendix A.4.1):

$$\tan \theta_1 = -\frac{\sin \theta_3}{(2 + \cos \theta_3) \sin \theta_2}$$

Putting θ_2 and θ_3 in function of the bending angles (equation 6.19):

$$\tan \theta_1 = -\frac{\sin(A_v \sin \phi)}{(2 + \cos(A_v \sin \phi)) \sin\left(\frac{A_h}{2} \cos \phi\right)}$$

Substituting the bending angles for their values for the rolling movement (eq. 6.18) the final expression 6.20 is obtained.

6.7.3.2 Stage 2

The angle of rotation θ_1 is given by the following expression:

$$\theta_1 = -90 + \arctan\left(\frac{\sin\left(\frac{A_h}{2} \cos \phi\right)}{\tan(A_v \sin \phi)}\right) \quad (6.21)$$

Stage 2 begins in the phase $\phi = 90$, in which the robot has rotated an angle of $\theta_1 = -90$. Finalising in $\phi = 180$, obtaining a value of $\theta_1 = -180$.

Demonstration

In stage 2 the left and right segments remain in contact with the ground, supported on the plane $z_0 = 0$. To calculate θ_1 this condition is imposed on the right segment. It must fulfil:

$$\vec{d}_4 \cdot \hat{z}_0 = 0$$

Where \vec{d}_4 represents the orientation of the right segment. If this vector is referred to the frame R_3 and is denoted by \vec{d}_3^4 , the expression is:

$$\left(H_{-90}H_0^1H_1^2H_2^3\vec{d}_3^4\right) \cdot \hat{z}_0 = 0 \quad (6.22)$$

The right segment is that which goes from the joint 2 to the point P_4 . Its expression referred to the frame R_3 is therefore:

$$\vec{d}_3^4 = \frac{\hat{L}}{2} y_3$$

Substituting in the equation 6.22, operating and clearing the expression θ_1 is obtained (the details are in the appendix A.4.2):

$$\tan \theta_1 = \frac{\sin \theta_2 \cos \theta_3}{\sin \theta_3}$$

Expressing the angle θ_1 taking as reference stage 1:

$$\theta_1 = -90 - \arctan \left(\frac{\sin \theta_2}{\tan \theta_3} \right)$$

Putting θ_2 and θ_3 as a function of the bending angles (equation 6.19):

$$\theta_1 = -90 - \arctan \left(\frac{\sin \frac{\varphi_2}{2}}{\tan \varphi_3} \right)$$

Substituting the bending angles by their values for the rolling movement (eq. 6.18) the final expression is obtained 6.7.3.

6.7.4 Functions of stability

6.7.4.1 Exposition

The wired model of the configuration PYP always rolls, independently of the length of the modules. Nevertheless, in the hexahedric model this movement is not always carried out. It depends on the position of the centre of mass that is a function of the geometric parameters of the robot and of its bending angles. In this section we will study the conditions that must be fulfilled to produce the movement.

In the figure 6.27 the two possible movements are shown: rolling and sideways gaits for each one of the stages. That one or other is realised depends on the position of the critical point C with respect to the centre of mass (C_m). If C has an abscissa less than C_m then the supporting polygon is such that

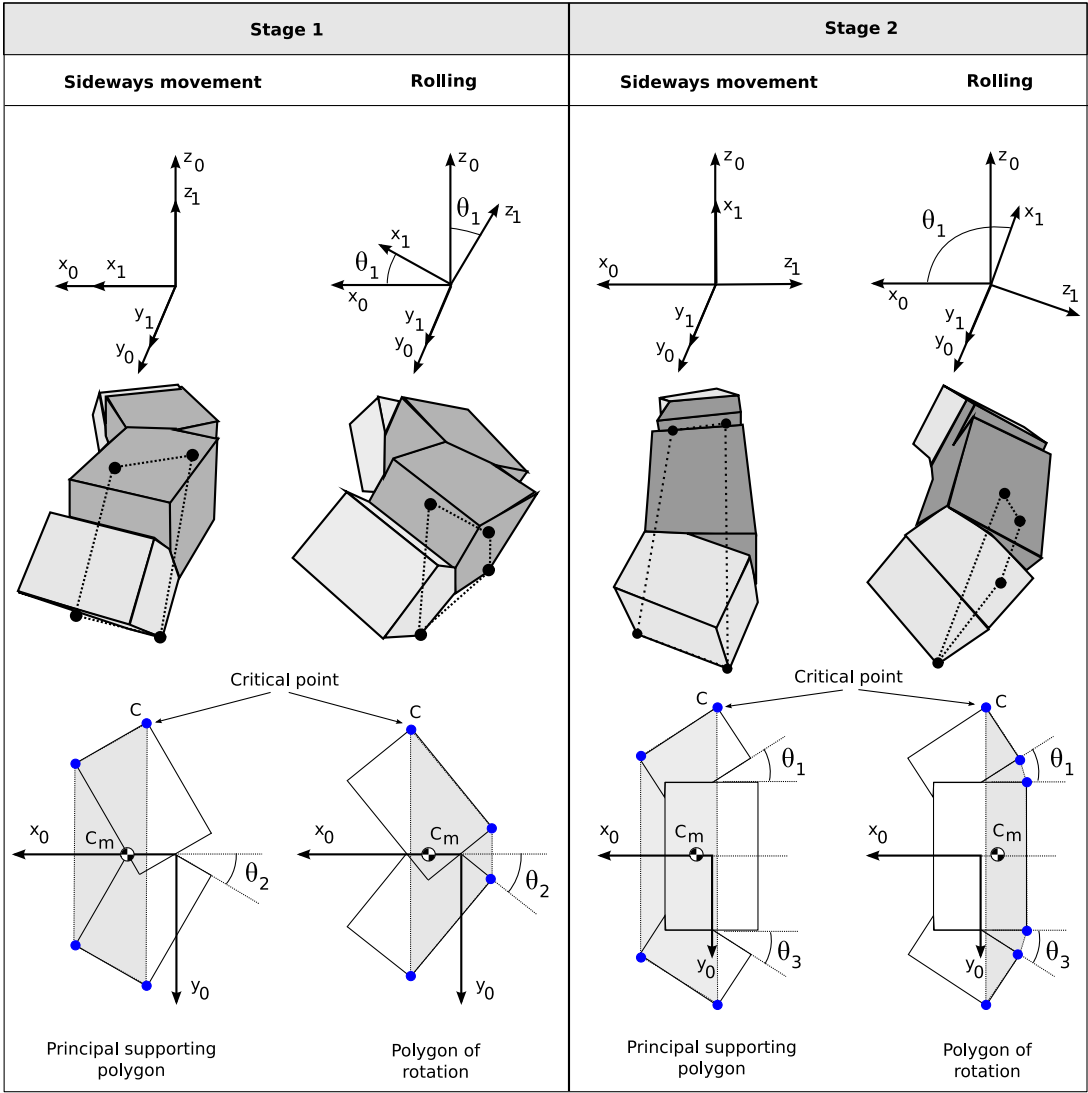


Figure 6.27: Rolling and sideways movements of the PYP configuration as a function of the position of the centre of mass

the robot's orientation is parallel to the plane x_0y_0 ($\theta_1 = 0$ in stage 1 or $\theta_1 = 90$ in the stage 2). We call it the **principal supporting polygon**.

Otherwise, if the abscissa of C is greater than that of C_m , the supporting polygon is denominated **polygon of rotation** and the orientation of the robot changes. Now $\theta_1 > 0$ in stage 1 and $\theta_1 > 90$ in stage 2.

6.7.4.2 Expressions

The function of stability is defined as the difference between the abscissa of the critical point C and that of the centre of mass, referring to the frame R_0 . Its general expression is:

$$e(\phi) = \vec{C}_0 \cdot \hat{x}_0 - \vec{C}_{m_0} \cdot \hat{x}_0 \quad (6.23)$$

Particularising for the two stages, the final expressions are obtained:

- **Function of stability for stage 1:**

$$e(\phi) = \left(\frac{W}{2} \cos \frac{\varphi_2}{2} - \sin \frac{\varphi_2}{2} \left(\frac{5}{12} L \cos \varphi_3 - \frac{H}{2} \sin \varphi_3 + \frac{L}{3} \right) \right) \cos \theta_1 + \left(H \cos \varphi_3 + \frac{5}{6} L \sin \varphi_3 \right) \frac{\sin \theta_1}{2} \quad (6.24)$$

- **Function of stability for stage 2:**

$$e(\phi) = \left(\frac{W}{2} \cos \frac{\varphi_2}{2} - \sin \frac{\varphi_2}{2} \left(\frac{5}{12} L \cos \varphi_3 + \frac{H}{2} \sin \varphi_3 + \frac{L}{3} \right) \right) \cos \theta_1 - \left(H \cos \varphi_3 - \frac{5}{6} L \sin \varphi_3 \right) \frac{\sin \theta_1}{2} \quad (6.25)$$

6.7.4.3 Deductions

Stage 1

For the equation 6.23 we substitute the values of \vec{C}_0 and \vec{C}_{m_0} for stage 1. In the figure 6.28 the situation of the critical point referred to the frame R_3 and the notation employed is shown.

The centre of mass is calculated from the centres of mass of each one of the two bodies. Their position vectors are denoted by \vec{E}_0 and \vec{D}_0 , referred to the frame R_0 . The robot can be seen as constituted of three equal blocks of mass M . Applying the formula of the centre of mass, supposing that the mass is uniformly distributed:

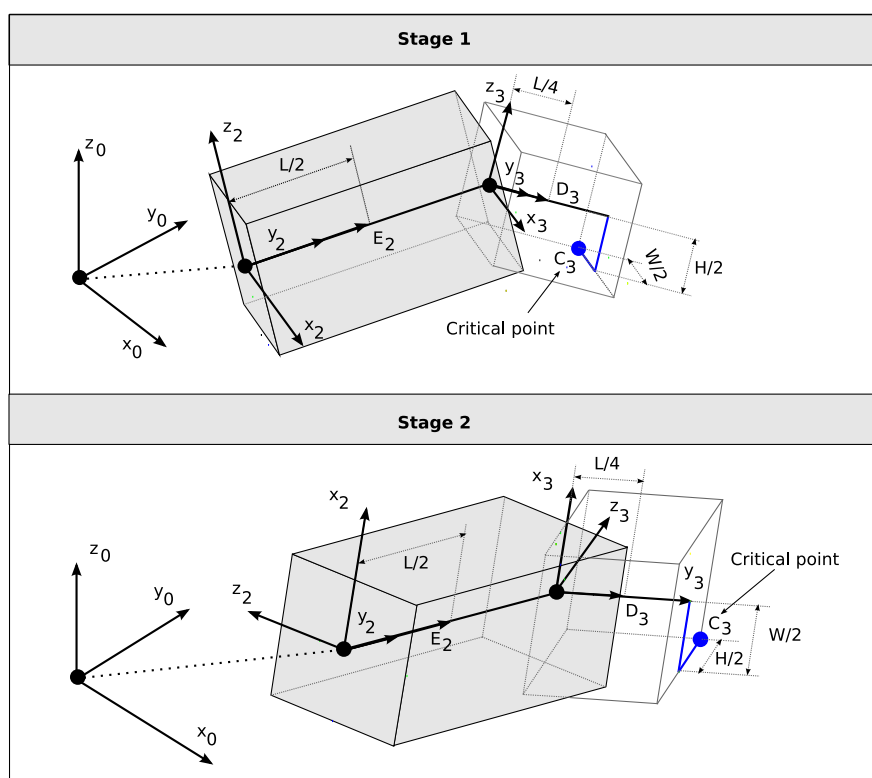


Figure 6.28: The critical point C in the two stages

$$\overrightarrow{Cm_0} = \frac{1}{M_T} \sum_{i=1}^n M_i \overrightarrow{r_i} = \frac{1}{3M} (2M\overrightarrow{E_0} + M\overrightarrow{D_0}) = \frac{1}{3} (2\overrightarrow{E_0} + \overrightarrow{D_0}) \quad (6.26)$$

The vectors $\overrightarrow{E_0}$ and $\overrightarrow{D_0}$ expressed with respect to the reference frame R_2 and R_3 are:

$$\begin{aligned} \overrightarrow{E_0} &= H_0^1 H_1^2 \overrightarrow{E_2} \\ \overrightarrow{D_0} &= H_0^1 H_1^2 H_2^3 \overrightarrow{D_3} \end{aligned}$$

Substituting in the equation 6.26 we obtain:

$$\overrightarrow{Cm_0} = \frac{1}{3} (2H_0^1 H_1^2 \overrightarrow{E_2} + H_0^1 H_1^2 H_2^3 \overrightarrow{D_3}) = \frac{1}{3} H_0^1 H_1^2 (\overrightarrow{E_2} + H_2^3 \overrightarrow{D_3}) \quad (6.27)$$

The critical point $\overrightarrow{C_0}$ as a function of the frame R_3 is:

$$\overrightarrow{C_0} = H_0^1 H_1^2 H_2^3 \overrightarrow{C_3} \quad (6.28)$$

Substituting 6.27 and 6.26 in 6.23:

$$e(\phi) = \overrightarrow{C_0} \cdot \hat{x}_0 - \overrightarrow{Cm_0} \cdot \hat{x}_0 = \left(H_0^1 H_1^2 H_2^3 \overrightarrow{C_3} - \frac{1}{3} H_0^1 H_1^2 (\overrightarrow{E_2} + H_2^3 \overrightarrow{D_3}) \right) \cdot \hat{x}_0$$

Operating we arrive at:

$$e(\phi) = \left(H_0^1 H_1^2 \left(\frac{2}{3} \overrightarrow{E_2} + H_2^3 \left(\frac{\overrightarrow{D_3}}{3} - \overrightarrow{C_3} \right) \right) \right) \cdot \hat{x}_0 \quad (6.29)$$

The values of E_2 , D_3 and C_3 are obtained from the figure 6.28:

$$\begin{aligned} \overrightarrow{C_3} &= \frac{L}{2} \hat{y}_3 - \frac{W}{2} \hat{x}_3 - \frac{H}{2} \hat{z}_3 \\ \overrightarrow{E_2} &= \frac{L}{2} \hat{y}_2 \\ \overrightarrow{D_3} &= \frac{L}{4} \hat{y}_3 \end{aligned} \quad (6.30)$$

Substituting 6.30 in 6.29:

$$e(\phi) = \left(\frac{W}{2} \cos \theta_2 + \sin \theta_2 \left(\frac{5}{12} L \cos \theta_3 + \frac{H}{2} \sin \theta_3 + \frac{L}{3} \right) \right) \cos \theta_1 + \left(H \cos \theta_3 - \frac{5}{6} L \sin \theta_3 \right) \frac{\sin \theta_1}{2}$$

Placing it in function of the bending angles (eq. 6.19) the final expression 6.24 is arrived at.

Stage 2

The reasoning is the same as for stage 1, the only changes are the co-ordinates of the critical point that are now (see figure 6.28):

$$\vec{C}_3 = \frac{L}{2}\hat{y}_3 - \frac{W}{2}\hat{x}_3 + \frac{H}{2}\hat{z}_3$$

Substituting in the equation 6.29 gives:

$$e(\phi) = \left(\frac{W}{2} \cos \theta_2 + \sin \theta_2 \left(\frac{5}{12}L \cos \theta_3 - \frac{H}{2} \sin \theta_3 + \frac{L}{3} \right) \right) \cos \theta_1 - \left(H \cos \theta_3 + \frac{5}{6}L \sin \theta_3 \right) \frac{\sin \theta_1}{2}$$

Placing it in function of the bending angles (eq. 6.19) the final expression 6.25 is arrived at.

6.7.5 Conditions for rolling**6.7.5.1 General conditions**

The general conditions for carrying out both movements are given in the following:

Condition for the sideways movement: *If for the initial phase $\phi = 0$ it is verified that $e(0) > 0$, then the movement will be sideways in all the phases.*

The sideways movement can only be realised when the robot is in stage 1 (in which the configuration is PYP), therefore the condition is only valid in this stage. When the supporting polygon is the principal, the function of stability only depends on the bending angle of the central joint φ_2 . The joints φ_1 and φ_3 only makes the centre of mass rise or descend, but do not modify its abscissa. What is more, when $\phi = 0$, the absolute value of the bending angle φ_2 is maximum (it is equal to A_h by the equation 6.18). This is the worst case, where the abscissa of the centre of mass is nearer to the critical point. For values of ϕ greater than ϕ_0 , the distance increases. Therefore, if it is guaranteed that for $\phi = \phi_0$ the supporting polygon is the principal, it will continue to be so for all the phases.

Condition for rolling: So that the robot rolls two conditions must be verified:

1. That initially the supporting polygon be that of rotation: $e(\phi_0) < 0$

2. That the projection of the centre of mass remains within the rotation polygon for all the phases. That is to say that $e(\phi) < 0$ for all ϕ . This condition is verified if $\max(e(\phi)) < 0$.

The first condition does not guarantee that the rolling movement will be carried out. It implies that initially the supporting polygon will be that of rotation, but the phase varying the supporting polygon could become the principal, changing the robot's orientation. If this occurs, the resulting movement is unstable. The robot constantly changes its orientation and therefore is incapable of moving sideways or rolling.

These conditions will be analysed in the two stages.

6.7.5.2 Conditions in stage 1

- **Condition of sideways movement:** If $A_h < A_{hL}$, the movement will be a sideways one, where A_{hL} is given by:

$$A_{hL} = 2 \arctan \left(\frac{2}{3} \frac{W}{L} \right) \quad (6.31)$$

- **Condition for rolling:** If $A_h > A_{hL}$ and $e_{\max}(A_v, A_h, L, W, H) < 0$ are true the movement will be a rolling one where e_{\max} is the maximum value of the function of stability: $e_{\max} = \max(e(\phi))$.

The expression of e_{\max} can be resolved numerically. Given a value $A_h > A_{hL}$, iterations are carried out in the values of A_v (between 0 and 90) to find the point where the condition $e_{\max} = 0$ is fulfilled. In the section 6.7.8 it has been resolved for the hexahedric model with the dimensions of the Y1 modules.

Demonstration

To deduce the equation 6.31 the restriction $e(0) = 0$ is imposed, where $e(\phi)$ is the function of stability of stage 1 (equation 6.24). Operating:

$$e(0) = -\frac{3}{4}L \sin \frac{\varphi_2}{2} + \frac{W}{2} \cos \varphi_2 = 0$$

Clearing φ_2 :

$$\tan \frac{\varphi_2}{2} = \frac{2}{3} \frac{W}{L} \Rightarrow \varphi_2 = 2 \arctan \left(\frac{2}{3} \frac{W}{L} \right)$$

The bending angle φ_2 in the phase $\phi = 0$ is equal to $-A_h$ (eq. 6.18). Taking the absolute value the final expression is obtained 6.31.

6.7.5.3 Conditions in stage 2

- **Condition for rolling.** If $A_v > A_{vL}$ and $e_{max}(A_v, A_h, L, W, H) < 0$ is met the movement will be rolling. A_{vL} is given by the expression:

$$A_{vL} = \arctan\left(\frac{6}{5} \frac{H}{L}\right) \quad (6.32)$$

Demonstration

Imposing the restriction $e(90) = 0$, where $e(\phi)$ is the function of stability of stage 2 (equation 6.25). Operating, the following is obtained:

$$H \cos \varphi_3 - \frac{5}{6} L \sin \varphi_3 = 0$$

Clearing φ_3 :

$$\tan \varphi_3 = \frac{6}{5} \frac{H}{L} \Rightarrow \varphi_3 = \arctan\left(\frac{6}{5} \frac{H}{L}\right)$$

The bending angle φ_3 in the phase $\phi = 90$ is equal to A_v (eq. 6.18), the final expression 6.32 is obtained.

6.7.6 Regions of movement

Employing hexahedron modules of dimensions $L \times W \times H$, the rolling movement is only carried out for certain values of the vertical and horizontal amplitudes that form the region of movement. In the figure 6.29 the generic aspect of this region is shown. In the interior points of this region the robot will roll.

The solutions found in the rolling movement have equal amplitudes. If $A_v = A_h = A$, the minimum amplitude, A_{min} , is defined as:

$$A_{min} = \max\{A_{vL}, A_{hL}\}$$

So, the condition for rolling is expressed in this way:

Condition for rolling if $A > A_{min}$ then the robot will roll.

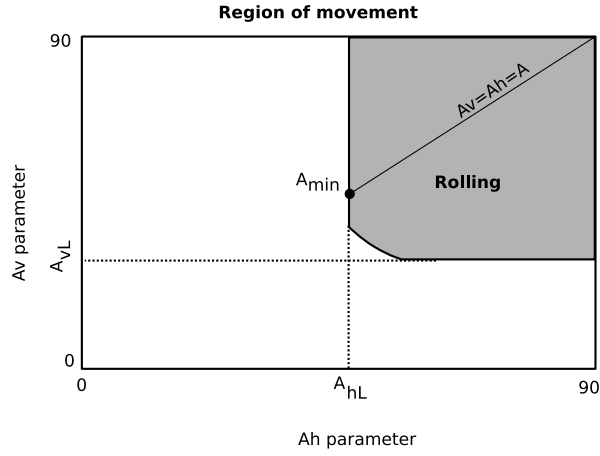


Figure 6.29: Region of movement for the PYP configuration to roll, in function of the A_h and A_v parameters

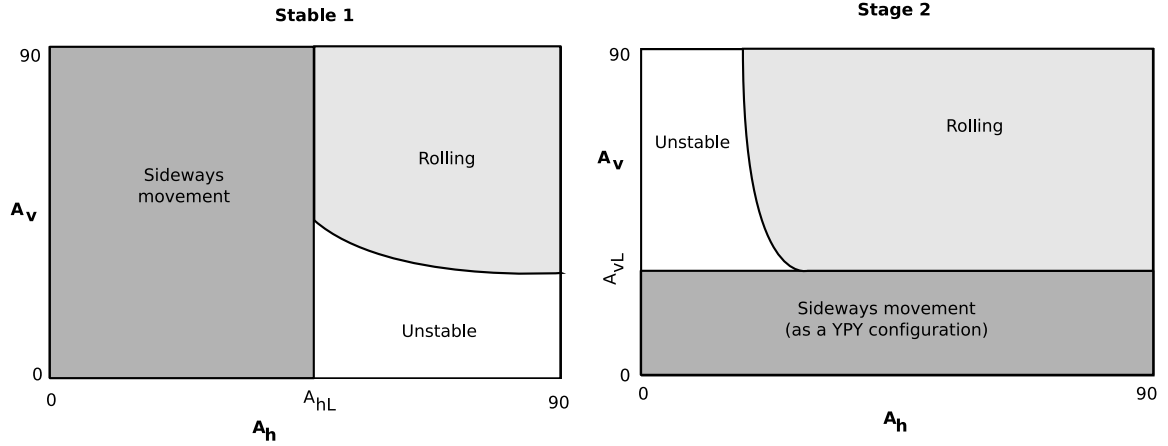


Figure 6.30: Regions of movements for the stages 1 and 2

6.7.6.1 Obtaining the region

We will study how the region of movement has been obtained. For this we will analyse the region in stages 1 and 2. So that the rolling movement is carried out in a continuous way, the working point (A_h, A_v) employed must belong to the region of roll of the two stages. The solution region will be obtained as the intersection of the regions of stage 1 and 2. In the figure 6.30 the regions are shown separately.

Stage 1

If $A_h < A_{hL}$ the movement will be sideways, independently the of value of A_v . When $A_h > A_{hL}$, two sub-regions exist depending on the value of A_v . In one of them, the supporting polygon is always that

of rolling and therefore the robot will roll. In the other, the two polygons will alternate therefore it will be an unstable zone. The curve that separates both sub-regions is calculated numerically from the condition $emax = 0$, where $emax$ is the maximum value of the function of stability in stage 1.

Stage 2

For stage 2 the same thing happens. When $A_v < A_{vL}$ the movement will be sideways, but in the position YPY. When $A_v > A_{vL}$, once again there are two sub-regions, one in which the rolling movement is produced and the other in which the supporting polygons alternate.

6.7.7 Step

Supposing that a hexahedric model is being employed with the generic dimensions $L \times W \times H$ and that the values of the amplitudes A_v and A_h are near to the frontier of the region of movement, the step approximation is given in each stage by the parameters W and H . Therefore:

- Step in stage 1: $\Delta x_1 \approx W$
- Step in stage 2: $\Delta x_2 \approx H$

Therefore, in these conditions, the total step is given by:

$$\Delta x \approx 2(W + H)$$

If the module's section is square ($H = W$), then the step is:

$$\Delta x \simeq 4H \tag{6.33}$$

6.7.8 Case study

In this section numerical values will be obtained when the modules' dimensions correspond to those of the Y1 modules, employed in the experiments. In the figure 6.31 the regions of movement have been represented and in the table 6.2 the values of all of the parameters are summed up.

The values of A_{vL} and A_{hL} are calculated from the equations 6.32 and 6.31 respectively. The value of A_{min} will be the maximum of the two, that is 51.4. The regions have been obtained resolving numerically the implicit equations $emax(A_v, A_h) = 0$ of both stages.

Finally, from the equation 6.33 the approximate step is obtained, when the amplitude A is greater than A_{min} but close to it.

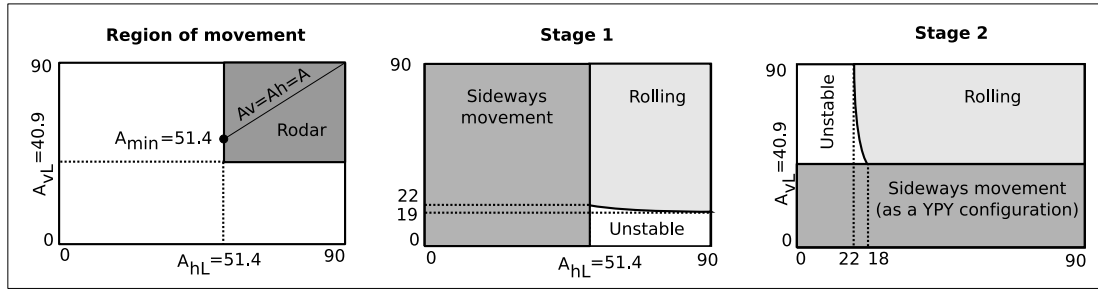


Figure 6.31: Regions of movement for the case study: Stage 1, 2 and final

Parameter	Description	Value
H	Module height	5.2 cm
W	Module width	5.2 cm
L	Module length	7.2 cm
A_{hL}	Horizontal limit amplitude	51.4 degrees
A_{vL}	Vertical limit amplitude	40.9 degrees
A_{min}	Minimum amplitude for rolling	51.4 degrees
Δx	Step	20.8 cm

Table 6.2: Parameters for the case study

6.7.9 Summary

The study of the rolling movement is divided into **two stages**. In the first the robot passes from the configuration PYP to YPY and in the second from YPY to PYP. For each one of them the **rotating angle** θ_1 has been calculated in function of the phase, and the **stability function**, that determines which is the supporting polygon. From this function **the conditions** have been stated that must be fulfilled so that either the sideways or the rolling movement is carried out. The expressions of the vertical and horizontal limit amplitudes that differentiate these gaits have been obtained. Their graphic representation divides the space into regions of movement. Finally the values of the different parameters for robots constructed with the Y1 modules have been calculated.

6.8 Sideways movement

6.8.1 Description of the movement

The sideways movement allows the configuration PYP to move towards the sides without varying the orientation of its corporal axis. It is a flapping or ‘rowing’ type movement, the same as that presented in the section 5.7.9, but for a three module robot. The restrictions to be applied to be able to carry out this movement are the same as in the case of the rolling movement: $\Delta\phi_{vh} = 90$ and $\Delta\phi = 0$. It has

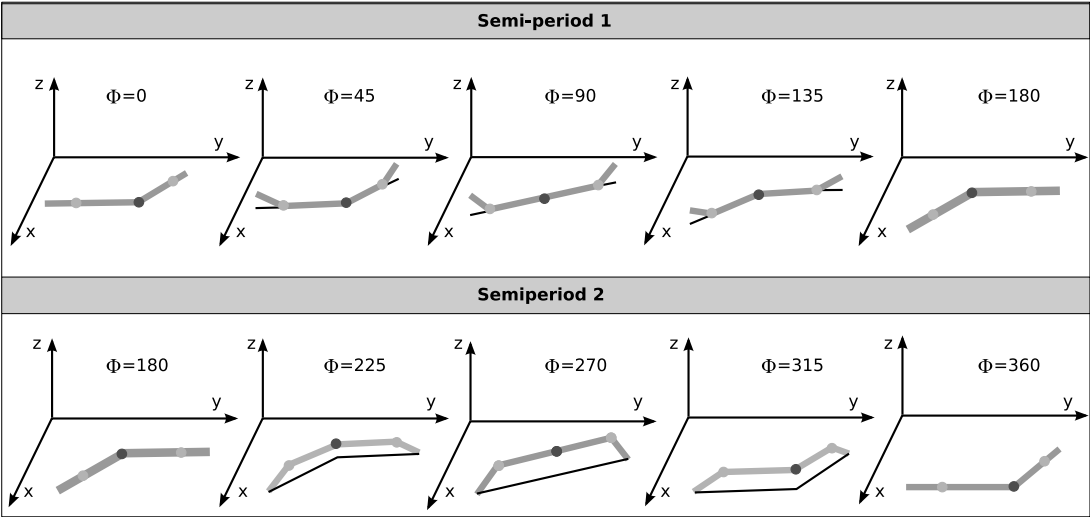


Figure 6.32: Wired model of the PYP configuration when performing the sideways movement

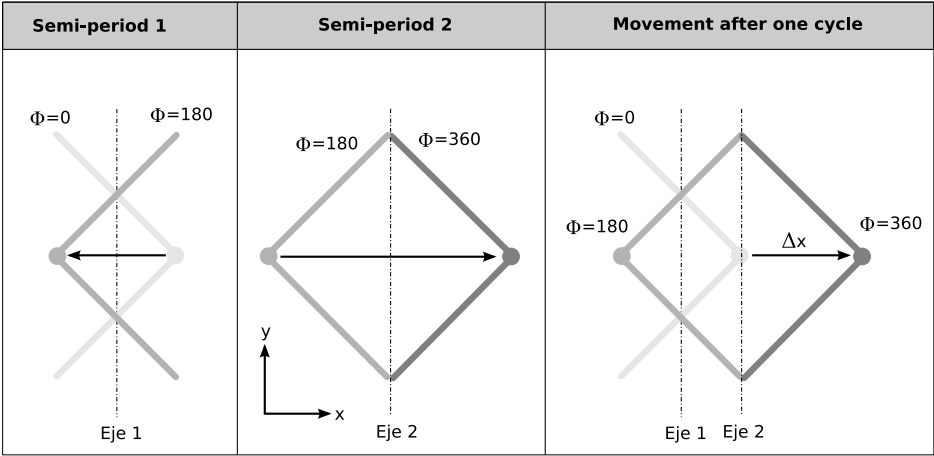


Figure 6.33: Top view of the PYP configuration when performing the sideways movement

only one degree of freedom, A_h , that determines the robot's step. The parameter A_v can be the same as A_h or near to 0 so that the height of the centre of mass be less and more stability is achieved.

In the figure 6.32 the movement of the wired model is shown. In reality this model is not stable. Phases exist in which there are only two supporting points, as for example in $\phi = 225$ so that the robot would roll. Nevertheless it has been drawn so as to better understand its mechanism of movement. For the movement to be stable it is necessary to verify that the parameter A_h be less than A_{hL} which is obtained by means of the equation 6.31.

The movement is divided into **two semi-periods** contained in the phases $\phi \in [0, 180]$ and $\phi \in [180, 360]$. During the first one, it is the vertical modules that move forward while the horizontal is at rest in contact with the ground. The two arms of the robot, left and right move in such a way that at the end of the semi-period they are advanced. During semi-period 2 the real movement is carried out. The robot's extremes are used as supporting points that remain fixed to the ground. The horizontal module moves in such a way that it goes forward and the cycle then commences once more.

In the figure 6.33 the horizontal projection of the robot in the phases 0, 180 y 360 is shown. During semi-period 1 the horizontal joint rotates and the robot changes shape symmetrically to the axis 1. There is no movement. During semi-period 2 the extremes make contact with the ground and on rotating the horizontal joint the robot moves a distance. At the end of the cycle, the robot has taken a step Δx . The equations for the bending angles are:

$$\begin{aligned}\varphi_1 &= \varphi_3 = A_v \sin \phi \\ \varphi_2 &= A_h \sin \left(\phi + \frac{\pi}{2} \right) = -A_h \cos \phi\end{aligned}\tag{6.34}$$

6.8.2 Stability

The stability is studied in section 6.7.5. So that it can carry out the movement the hexahedric model must be employed and the modules have to have the dimensions $L \times W \times H$. The condition that enables the robot to move sideways is:

Condition of movement: *If $A_h < A_{hL}$, the movement will be a sideways one*

The type of movement is determined by the working point (A_h, A_v) of stage 1's region of movement, described in the section 6.7.6.1. The parameter A_{hL} is given by the equation 6.31. Within the zone where the movement is stable, the value of A_v can be any within the range $[0, 90]$.

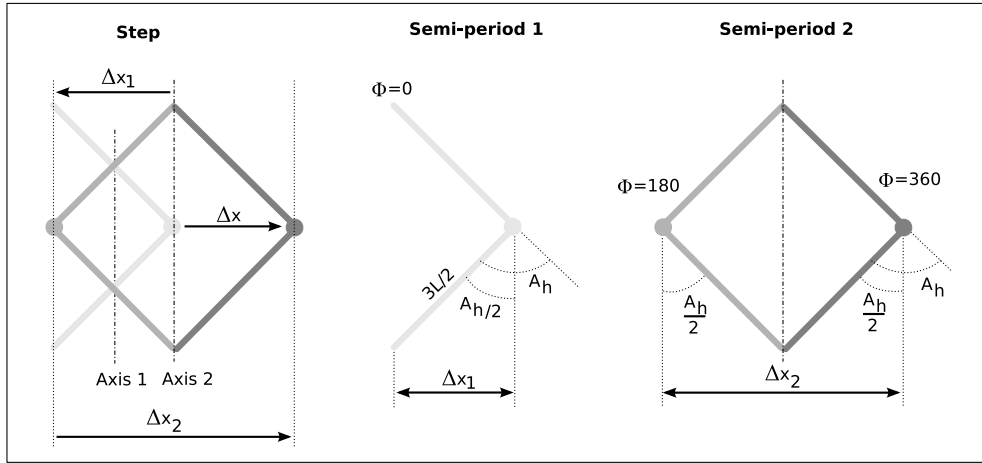


Figure 6.34: Calculating the step of the sideways movement from the geometry

6.8.3 Step

We will approximate the step by means of the equations obtained from geometry. Assuming the following:

- During semi-period 1 there is no absolute movement. The centre of mass is in the same position in the phases $\phi = 0$ and $\phi = 180$.
- During semi-period 2 the extremities remain in contact with the ground and DO NOT slide.

With these assumptions, the equation proposed for the step is:

$$\Delta x = \frac{3L}{2} \sin\left(\frac{Ah}{2}\right) \quad (6.35)$$

The greater the amplitude value of the horizontal joint the greater the step.

6.8.3.1 Deduction

The total step will be equal to the sum of the steps given in each one of the semi-periods. We will calculate the step that the central point takes. The total step will be:

$$\Delta x = \Delta x_2 - \Delta x_1$$

From the figure 6.34 the steps for both semi-periods are obtained.

- Step in semi-period 1:

$$\Delta x_1 = \frac{3L}{2} \sin\left(\frac{A_h}{2}\right)$$

- Step in semi-period 2:

$$\Delta x_2 = 2 \frac{3L}{2} \sin\left(\frac{A_h}{2}\right) = 3L \sin\left(\frac{A_h}{2}\right)$$

With which the total step arrives at the equation 6.35

6.8.4 Direction of the movement

The direction of the movement can be changed in the following ways:

- If the phase varies between 0 and 360 degrees
 - ◇ $\Delta\phi_h > 0$, movement in positive direction of the x axis
 - ◇ $\Delta\phi_h < 0$, movement in negative direction of the x axis
- If the phase varies between 0 and -360
 - ◇ $\Delta\phi_h > 0$, movement in negative direction of the x axis
 - ◇ $\Delta\phi_h < 0$, movement in positive direction of the x axis

6.8.5 Summary

The sideways movement is divided into **two semi-periods**. One in which the central module moves forward and the other in which the extremes move forward. The co-ordination is the same as in the case of the rolling movement. If the amplitude is **less than a certain threshold** A_{hL} then the robot will move sideways.

The wired model is unstable. The movement will only be realised if the modules have a thickness. For this case **an equation for the step** has been proposed, deduced from geometry.

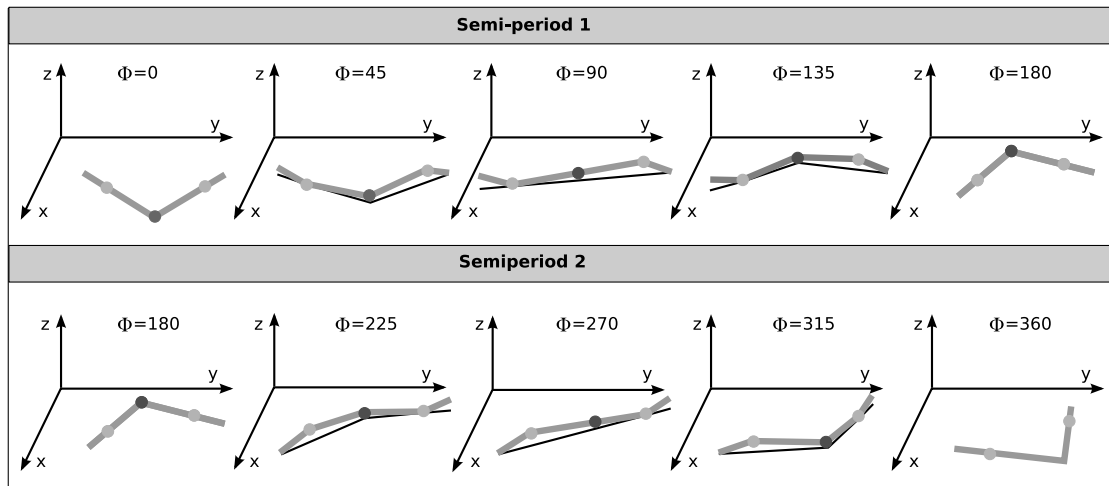


Figure 6.35: Wired model of the PYP configuration while rotating

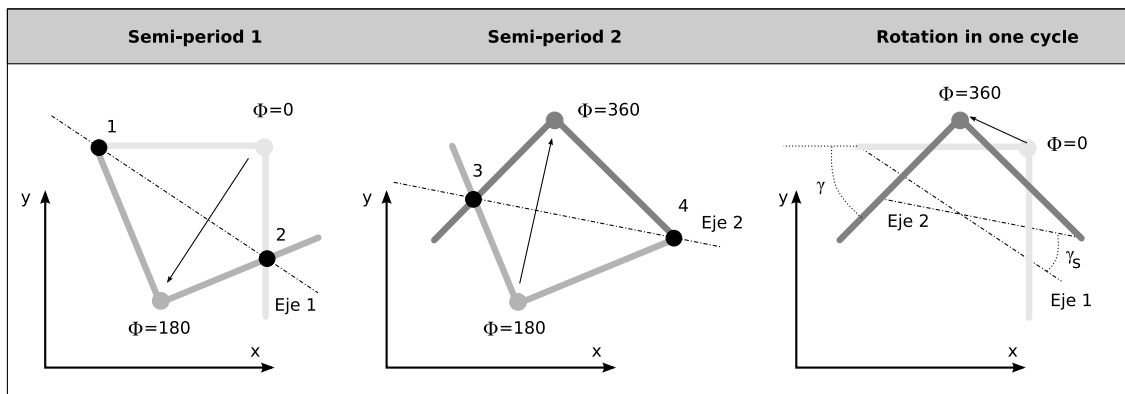


Figure 6.36: Top view of the rotation gait

6.9 Rotation

6.9.1 Description of the movement

The rotation allows the PYP configuration to change the orientation of its longitudinal axis. The restrictions that apply to realise the movement possible are $\Delta\phi_v = 180$ and $\Delta\phi_{v/h} = 90$. It has only one degree of freedom A_h , that decides the angular step. The parameter A_v can have any value between 0 and 90.

In the figure 6.35 the movement of the wired model is shown. It is divided into **two semi-periods** included between the phases $\phi \in [0, 180]$ the first one and $\phi \in [180, 360]$ the second. In each semi-period the robot moves symmetrically with respect to an axis. When the initial phase is 0, the vertical joints have the bending angles at 0 therefore the robot stands on the ground. The vertical joints begin to move, one upwards and the other downwards, two supporting points appearing. At the same time the horizontal joint goes rotating. For $\phi = 180$ the horizontal joint has moved and the robot has a symmetric shape with $\phi = 0$.

In semi-period 2 the process is repeated but now the horizontal joint moves with respect to another axis of symmetry. The supporting points on the ground are different in relation to the previous semi-period.

In the figure 6.36 the first and second semi-periods are shown and the final rotation, in the xy plane. During semi-period 1, the supporting points are 1 and 2, contained in the axis of symmetry. When semi-period 2 commences, the supporting points change to 2 and 4 and therefore the axis of symmetry changes (axis 2) and when the rotation finishes the shape of the robot will be that of $\phi = 360$. On the right the robot is shown in its initial positions ($\phi = 0$) and its final positions ($\phi = 360$). The angle that has rotated is γ and the which it makes with the axis of symmetry is γ_s .

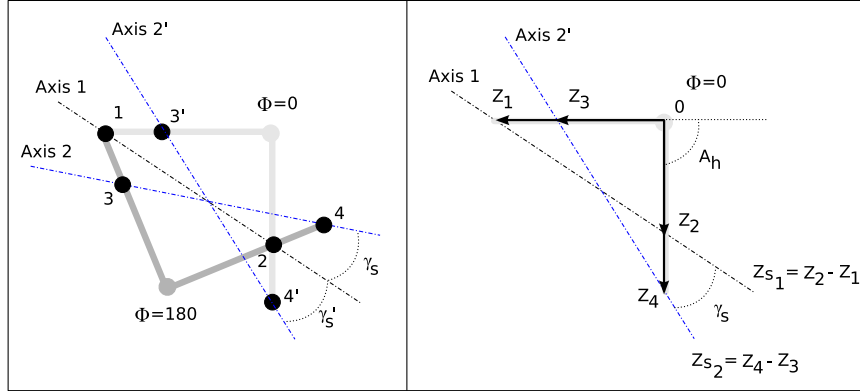
The equations for the bending angles are:

$$\begin{aligned}\varphi_1 &= A_v \sin \phi \\ \varphi_2 &= A_h \sin \left(\phi + \frac{\pi}{2} \right) = -A_h \cos \phi \\ \varphi_3 &= -A_v \sin \phi\end{aligned}\tag{6.36}$$

6.9.2 Step

6.9.2.1 Expression

The equation for calculating the angular step is:

Figure 6.37: Geometrical model used for the calculation of γ_s

$$\gamma = 2 \arctan \frac{\sin A_h}{\frac{3}{2} + \cos A_h} - 2 \arctan \left(\frac{3}{2} \frac{\sin A_h}{1 + \frac{3}{2} \cos A_h} \right) \quad (6.37)$$

The rotation angle only depends on the parameter A_h . It is also verified that it is equal to the double of the rotation angle of each semi-period: $\gamma = 2\gamma_s$ in the wireless model.

Deduction of γ_s The angle γ_s is that formed by the two axis of symmetry of the rotation. The axis 1 passes through the points 1 and 2 and the axis 2 through the points 3 and 4. The axis 2 is the one that passes through the points 3 and 4 when $\phi = 180$. To calculate γ_s it is simpler to use the axis 2' which is that which passes through the points 3' and 4' which are the points 3 and 4 when the phase is 0. Both axis are symmetric with respect to axis 1 and it is verified that $\gamma_s = \gamma'$ (see figure 6.37 left).

In the figure on the right the elements for its calculation are shown. For $\phi = 0$, we have:

$$\varphi_1 = A_v \sin \phi = 0$$

$$\varphi_3 = A_v \sin (\phi + \pi) = 0$$

$$\varphi_3 = A_h \sin \left(\phi + \frac{\pi}{2} \right) = A_h$$

Taking advantage of the previous symmetry, it has to be:

$$\gamma_s = \gamma'_s = \arg(Zs_2) - \arg(Zs_1)$$

where Zs_1 and Zs_2 are two complexes that have the same direction as the axis 1 and 2' respectively. The axis 1 can be obtained as:

$$Zs_1 = Z_2 - Z_1 = Le^{-jA_h} + \frac{3}{2}L = L \left(e^{-jA_h} + \frac{3}{2} \right)$$

$$Zs_2 = Z_4 - Z_3 = \frac{3}{2}Le^{-jA_h} + L = L \left(\frac{3}{2}e^{-jA_h} + 1 \right)$$

where the complexes z_1, z_2, z_3 and z_4 expressed in relation to the origin are:

$$\begin{aligned} Z_1 &= -\frac{3}{2}L \\ Z_2 &= Le^{-jA_h} \\ Z_3 &= -L \\ Z_4 &= \frac{3}{2}Le^{-jA_h} \end{aligned}$$

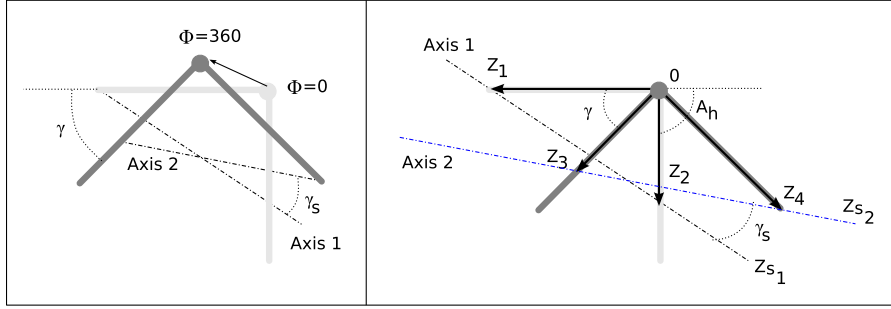
To obtain γ_s the arguments of Zs_1 and Zs_2 are calculated:

$$\arg(Zs_2) = \arctan \frac{\text{im}(Zs_2)}{\text{Re}(Zs_2)} = \arctan \frac{-\frac{3}{2}\sin A_h}{1 + \frac{3}{2}\cos A_h}$$

$$\arg(Zs_1) = \frac{\text{im}(Zs_1)}{\text{Re}(Zs_1)} = \arctan \frac{-\sin A_h}{\frac{3}{2} + \cos A_h}$$

Deduction of γ Now starting with the robot in the initial positions ($\phi = 0$) and the final positions ($\phi = 360$). The following complexes are defined:

$$\begin{aligned} Z_1 &= -\frac{3}{2}L \\ Z_2 &= Le^{-jA_h} \\ Z_3 &= Le^{j(\gamma-\pi)} \\ Z_4 &= \frac{3}{2}Le^{j(\gamma-A_h)} \end{aligned}$$

Figure 6.38: Geometrical model used for the calculation of γ

On one hand the complex Z_{s2} can be expressed as:

$$Z_{s2} = Z_{s1} e^{j\gamma_s} = L e^{j\gamma_s} \left(\frac{3}{2} + e^{-jA_h} \right)$$

because $Z_{s1} = Z_2 - Z_1 = L \left(\frac{3}{2} + e^{-jA_h} \right)$. On the other hand it can be expressed as:

$$Z_{s2} = Z_4 - Z_3 = L e^{j\gamma} \left(\frac{3}{2} e^{-jA_h} + 1 \right)$$

Taking the arguments of both expressions and equalling:

$$\text{Arg}(Z_{s2}) = \gamma_s + \arctan \left(\frac{-\sin A_h}{\frac{3}{2} + \cos A_h} \right) = \gamma + \arctan \left(-\frac{\frac{3}{2} \sin A_h}{1 + \frac{3}{2} \cos A_h} \right)$$

From where, clearing γ results in:

$$\gamma = \gamma_s - \arctan \left(\frac{\sin A_h}{\frac{3}{2} + \cos A_h} \right) + \arctan \left(\frac{\frac{3}{2} \sin A_h}{1 + \frac{3}{2} \cos A_h} \right)$$

And for the expression of γ_s we have to $\gamma = 2\gamma_s$

6.9.2.2 Variation of γ with A_h

In the figure 6.39 the relation of the angle of rotation γ with the parameter A_h is shown graphically. It is practically lineal.

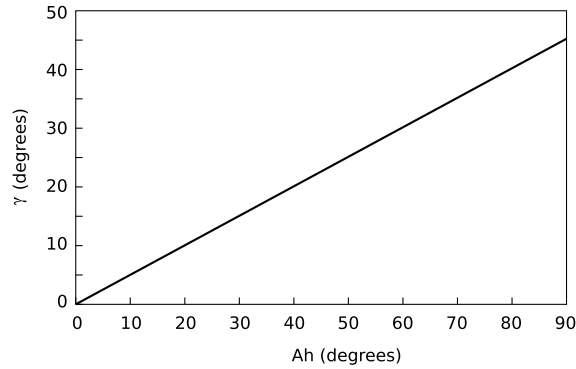


Figure 6.39: Variation of the rotation angle γ with the A_h

6.9.3 Direction of turn

The direction of movement is controlled with $\Delta\phi_h$. The combinations are:

- ϕ varying between 0 and 360
 - ◊ $\Delta\phi > 0$. Anti-clockwise rotation
 - ◊ $\Delta\phi < 0$. Clockwise rotation
- ϕ varying between 0 and -360
 - ◊ $\Delta\phi > 0$. Clockwise rotation
 - ◊ $\Delta\phi < 0$. Anti-clockwise rotation

6.9.4 Summary

The rotating movement is divided into **two semi-periods**. In each one of them the longitudinal axis has changed its orientation. The co-ordination is obtained causing the extremities to oscillate in opposition of phase and the central one out of phase 90 degrees. The movement is stable for all the amplitudes.

An equation has been proposed for the **angular step**, obtained from the geometry of the movement. The relation between the step and the amplitude of the horizontal module is very linear. Greater the amplitude greater will be the angle of rotation.

6.10 Principles of locomotion

The locomotion of the minimum configurations can be summed up in 5 principles of locomotion:

1. **Principle of the PP configuration.** A robot made up of a chain of two modules of pitch type that are controlled by means of sinusoidal generators is capable of moving forwards or backwards in a straight line.
2. **Principle of the configuration PYP.** A robot made up of a chain of three modules, with the two extremities being pitch type and the middle one yaw type, controlled by means of sinusoidal generators is capable of moving across a two dimensional surface using at least five different types of gait: straight line, circular path, sideways movement, rolling and rotation.
3. **Principle of the control parameters.** The control space of the minimum configurations has four dimensions and their points are of the shape $(A_h, A_v, \Delta\phi_v, \Delta\phi_{vh})$, where A_v and A_h are the amplitudes of the vertical and horizontal generators, $\Delta\phi_v$ is the phase difference between the verticals and $\Delta\phi_{vh}$ is phase difference between the verticals and the horizontal.
4. **Principle of the co-ordination.** The phase differences between the generators, $\Delta\phi_v$ and $\Delta\phi_{vh}$, are the parameters that determine the co-ordination of the movement, the gait and in which direction it is carried out.
5. **Principle of the step.** The amplitudes of the generators, A_v and A_h , determine the robot's step (linear or angular). When these parameters increase, the step will be greater, except in the rolling movement, where it decreases.

6.11 Conclusions

In this chapter **the problem of locomotion of the minimum configurations** on a flat, homogeneous surface without obstacles has been addressed, when sinusoidal generators are used to control them.

It deals with a **new problem** that has not previously been raised or studied by other investigators. We propose **a methodology to resolve it**, based on exploring the gaits and the candidate configurations employing genetic algorithms.

Two minimum configurations have been found that move in one and two dimensions. The **PP configuration** is made up of two pitch modules and the **PYP** of three, two pitch and the central one yaw. The first one moves, forwards or backwards in a straight line, and the second one can carry out five different gaits: straight line, circular path, sideways movement, rolling and rotating.

The minimum configurations are **atomic units of movement (AUM)** as they contain the smallest possible number of modules to be able to move. With them **is maximised the number of sub-robots** into which a self-configuration modular robot can be divided to resolve problems such as the maximisation of the area covered. Also the minimum configurations are **the most efficient** in relation to the energy needed for movement. The PYP configuration, considered as an atomic unit of movement, can reach any point (x,y) of the ground, and can be orientated in any direction and can recover its original position in case of overturning, thanks to the rolling movement.

A technique of analysis and synthesis of movements has been proposed based on identifying the minimum configurations in the wired model of other robots. This allows new gaits to be found as well as how to deduce the viability of the movement of certain configurations that *a priori* it would not be known if they could move.

The control model based on simplified CPG of sinusoidal generator types is also valid for the locomotion of minimum configurations. Therefore it can be applied to one dimensional movement in any apodal robot with more than 1 module, and in the case of movement in two dimensions any robot of the pitch-yaw group of more than two modules.

All the gaits are characterised by the equations of their subspaces of control that establish relations between the four parameters $A_v, A_h, \Delta\phi_v$ and $\Delta\phi_{vh}$. The free parameters are the degrees of freedom of the movement. The kinematics of all the movements have been studied and the equations to calculate the step in function of its control parameters proposed.

The movement in a straight line has two degrees of freedom, A and $\Delta\phi$. A criterion has been proposed to establish the working point with the best co-ordination. It has been demonstrated that with the wired model, the best co-ordination is obtained in the range of $\Delta\phi$ between 108° and 110° .

The **circular path movement** is similar to the straight line adding a parameter that determines the radius of turn. Therefore it has three degrees of freedom.

The **rolling movement** has been studied in detail and the value of the minimum amplitude that has to be applied so that it can carry it out calculated, in function of the modules' dimensions. It has only one degree of freedom, A , that defines the shape that the robot adopts during the movement. To carry it out the two vertical joints are in phase and the horizontal one out of phase 90 degrees.

The **sideways movement** allows the robot to move sideways maintaining the same orientation of its body. The co-ordination is exactly the same as in the case of rolling. According to the chosen amplitude one or other movement is obtained.

The **rotating movement** allows the robot to change its corporal orientation. It has one degree of freedom, A , that determines the angular step and rotation. The two vertical joints are in opposition of phase, and the horizontal one out of phase 90 degrees.

Finally all the principal ideas are summed up in five principles of locomotion (section 6.10).

Chapter 7

Experiments

“They are vain and plagued with errors the sciences that have not been born of experiments, mother of all certainty.”

– *Leonardo Da Vinci*

7.1 Introduction

This chapter describes some of the experiments that have been carried out to validate the solutions found to the problem of the co-ordination of the apodal robots.

In the first part the platform developed to carry out the experiments is presented, made up of the mechanics, electronics and the software, and the four prototypes of the apodal robots constructed are described: *Cube Revolutions*, *Hypercube*, *Minicube-I* and *Mincube-II*.

In the second part some of the experiments carried out are documented. They have been divided into three groups: locomotion in 1D, locomotion in 2D and minimum configurations, that correspond to the chapters 4, 5 and 6.

7.2 Developed platform

7.2.1 Y1 Modules

The modules designed to implement the modular robots are the **Y1 modules**, shown in the figure 7.1. Their inspiration came from the first generation of the Polybot modules, created by Mark Yim. The

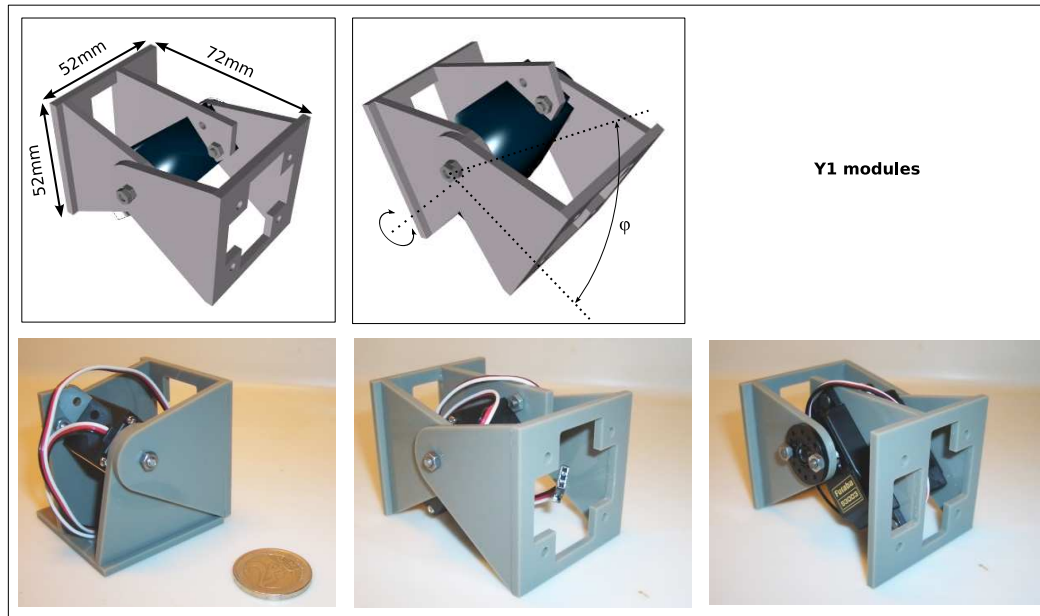


Figure 7.1: The Y1 modules, designed for building modular robots

Dimensions:	$52 \times 52 \times 72 \text{ mm}^3$ (height x width x length)
Weight:	50gr
Material:	3mm thick methacrylate
Section:	square (52x52)
Degrees of freedom	1
Servo:	Futaba 3003
Torque:	$3.2 \text{ Kg.cm} / 0.314 \text{ N.m}$
Speed:	260 degrees/sec.
Bending angle range:	180 degrees
Control signals:	Pulse Width Modulation (PWM)
Union between modules:	By means of screws

Table 7.1: Characteristics of the Y1 modules

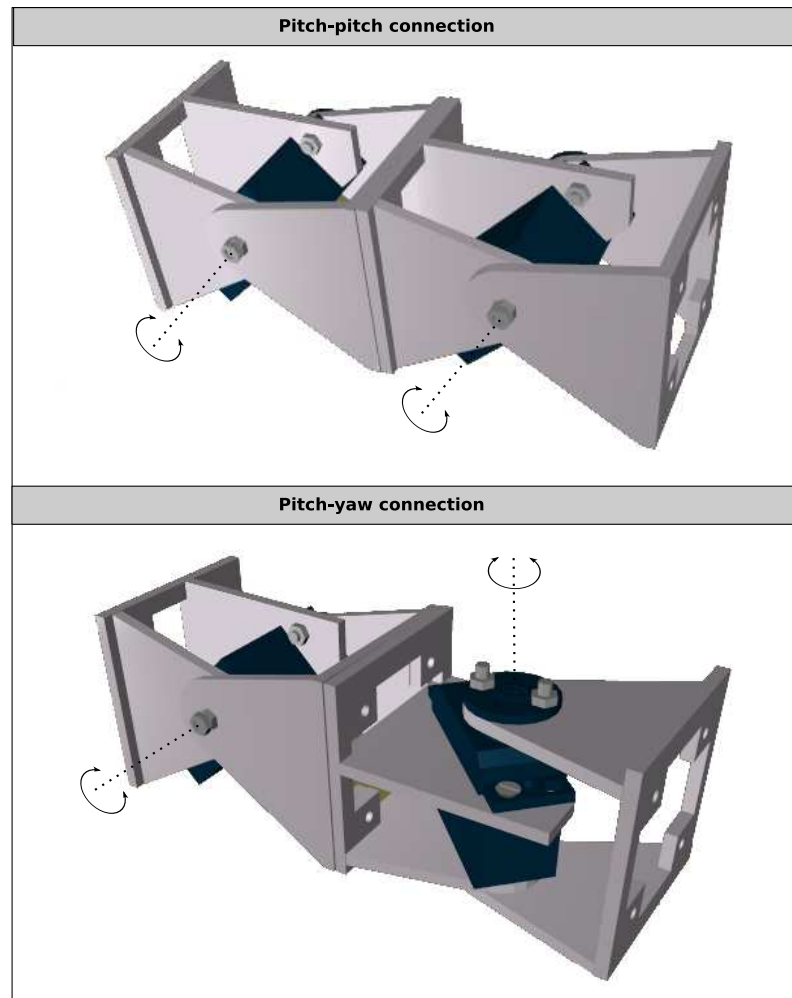


Figure 7.2: Two Y1 modules with pitch-pitch and pitch-yaw type connections

idea of the Y1 modules was that they should be easy to build, and have been designed for the Futaba 3003 servos or compatibles, that are cheap and can be obtained in any model air plane store.

The characteristics are summed up in the table 7.1. They are constructed in 3 mm thick methacrylate. The pieces have been cut by laser and have been joined by means of a contact adhesive. The consumption and torque depend on the characteristics of the servo employed.

The section is square, which allows the union of the modules to be of the pitch-pitch type, or pitch-yaw (figure 7.2). This union is fixed by means of screws that join both modules. All the robots described in this thesis have been constructed with this module.

All the information needful for their construction is available on line¹. The plans and instructions for assembling them are found in the appendix C.

¹http://www.learobotics.com/wiki/index.php?title=M%C3%B3dulos_Y1

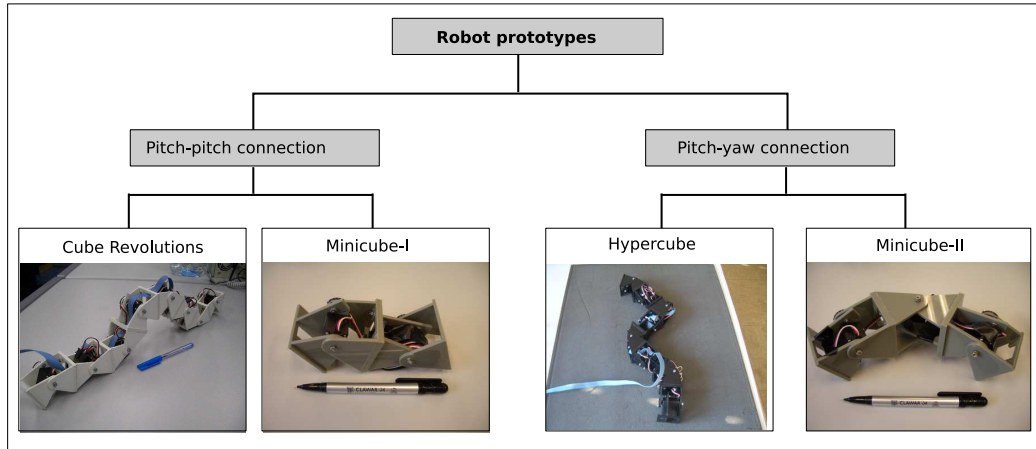


Figure 7.3: The four prototypes of apodal robots that have been constructed to carry out the experiments

7.2.2 Robots

Four prototypes of apodal robots, shown in figure 7.3 have been constructed to carry out the experiments. All of them are made up of various Y1 modules in a chain. They are divided into two groups, the robots with pitch-pitch connection and those with pitch-yaw connection. For each group two prototypes have been created, one with 8 modules and the other with the minimum number of modules.

Therefore, within the group of apodal robots with pitch-pitch connection the two robots are **Cube Revolutions**² and **Minicube I**³ that are shown in the figure 7.4 and 7.5 respectively. The first is composed of 8 modules. The second one corresponds to the minimum configuration *PP*.

For the pitch-yaw group the robots are **Hypercube**⁴ and **Minicube-II** (figure 7.4 and 7.5), of 8 and 3 modules respectively. Minicube II is the minimum configuration *PYP*.

7.2.3 Control scheme

The control scheme of the robots is shown in the figure 7.6. The algorithms of locomotion are executed in a computer, with the *GNU/Linux Debian Sarge* operating system. The positions of each servo are sent by serial communication (protocol *RS-232*) to the micro controller Skypic board [45], based on the *PIC16F876A*. This is connected by means of a cable to the modular robot being controlled. It generates the PWM signals for positioning the servos.

²http://www.learobotics.com/wiki/index.php?title=Cube_Revolutions

³<http://www.learobotics.com/wiki/index.php?title=MiniCube>

⁴<http://www.learobotics.com/wiki/index.php?title=Hypercube>

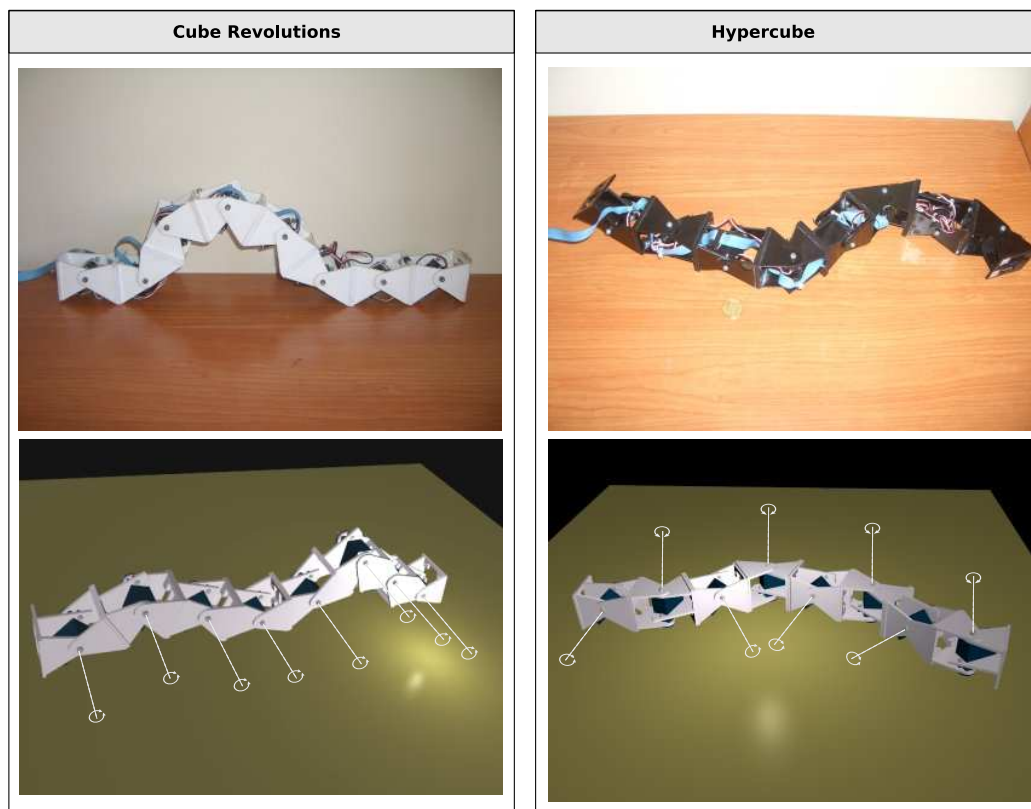


Figure 7.4: The Cube Revolutions and Hypercube Robots

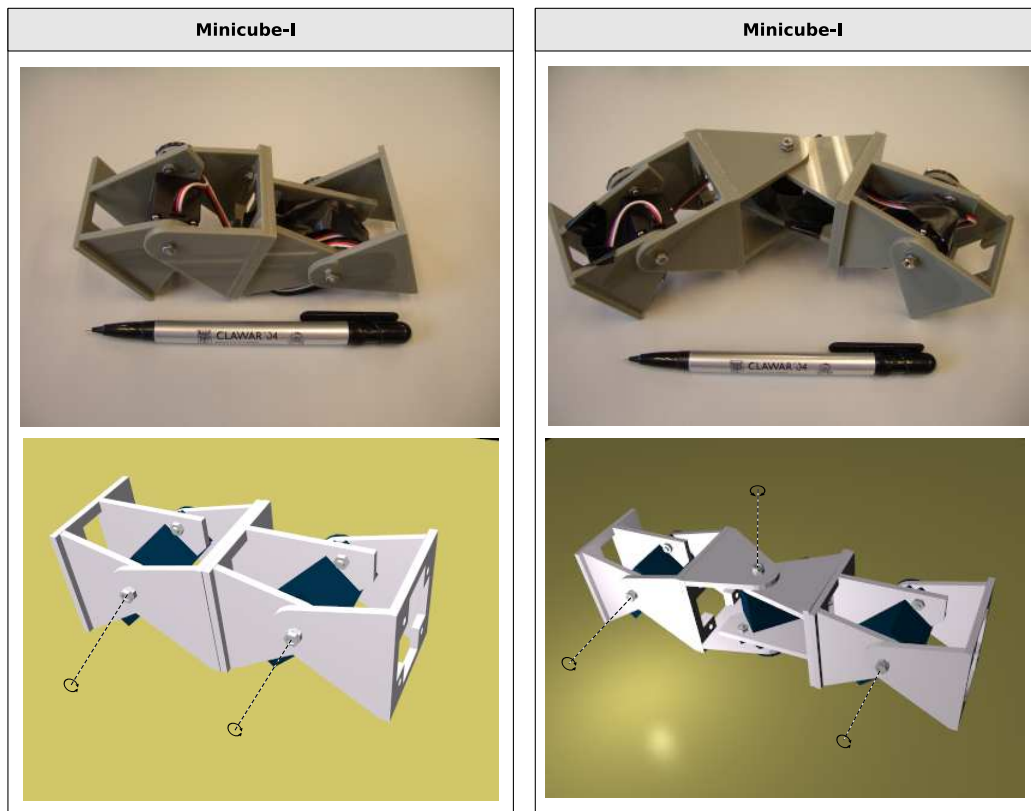


Figure 7.5: The Minicube I and II Robots. They are the minimum configurations

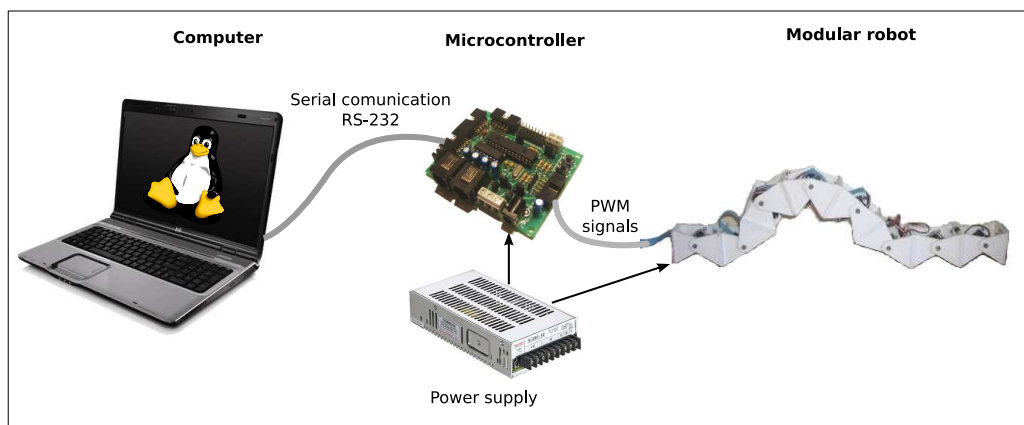


Figure 7.6: Control scheme of the modular robots

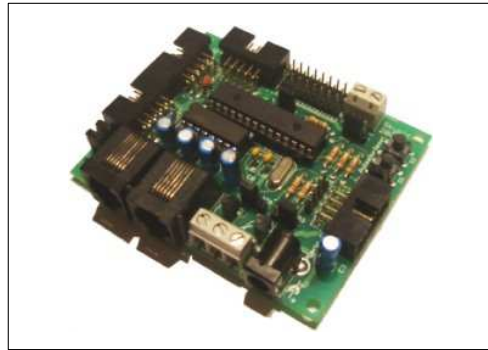


Figure 7.7: The Skypic board for controlling the modular robots

Microprocessor:	PIC16F876A
Clock frequency:	20Mhz
Processor architecture:	RISC. 8-bit data. 14-bit instructions
Power supply:	Between 4.5 and 6 volts
I/O pins:	22
A/D channels:	8. Resolution: 10 bits
Flash memory:	8Kb
SRAM memory:	368 bytes
EEprom memory:	256 bytes
Timers	3 (8 and 16 bits)
Communications:	Asynchronous (<i>RS-232</i>). Synchronous: <i>I2C</i> and <i>SSP</i>
Other:	Two capture, compare and PWM units

Table 7.2: Skypic board features

Both the electronics and the power source are situated outside the robots. The aim of the experiments is to test the locomotion in real robots, to later make them autonomous. With the proposed scheme the tests are simpler, quicker and cheaper. Nevertheless, once the viability of the sinusoidal controllers and the validity of the equations have been demonstrated, it is proposed that in future work a more advanced module, integrating the electronics and batteries, will be built.

7.2.4 Electronics

The **Skypic board** has been used as the electronic controller⁵. It has been designed by Andrés Prieto-Moreno and the author of this thesis [45]. This is published under a free hardware licence [40]. The technical characteristics are shown in the table 7.2.

⁵<http://www.iearobotics.com/wiki/index.php?title=Skypic>

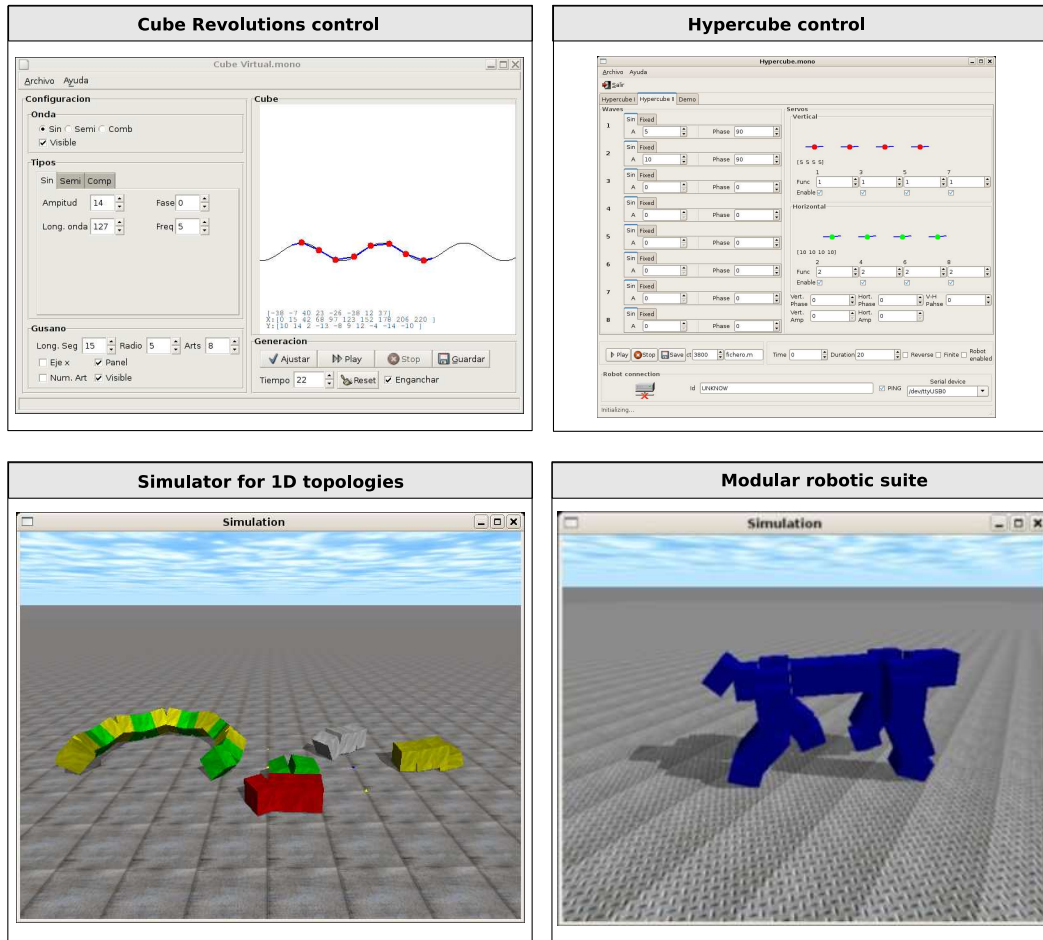


Figure 7.8: Screenshots of some of the software applications developed

7.2.5 Software

7.2.5.1 Mathematical models

The mathematical models presented in this thesis have been implemented in **Octave** (version 2.1.73). From them the shape of the robots has been drawn, both for the continuous and the discrete types of the pitch-pitch and pitch-yaw groups, and the graphs have been obtained.

7.2.5.2 Simulation

To simulate the locomotion of the apodal robots a set of libraries and programmes that use the **open-source physical engine ODE**⁶ (Open Dynamics Engine, version 0.5) have been created. They have

⁶<http://www.ode.org/>

been programmed in **C language** and allow the definition of the type of connection of the robot, the specifying of the parameters of the sinusoidal generators and the carrying out of the simulations. The simulations can be done visually or on the console, dumping on files the details requested, such as the position of the centre of mass, speed, rotation, etc.

To employ the **genetic algorithms** applications have been created based on *pgapack*⁷ (version 1.0), that, using the previous simulation libraries evaluate each one of the individuals of the population to determine the fitness function.

This software has been made specifically to work with 1D topologies of modular robots. Nevertheless, Rafael Treviño has implemented the **MRSuite environment** for his bachelors thesis[149], directed by the author of this dissertation. This software allows working with topologies of one or two dimensions. It is programmed in **Python**, and allows the visual design of modular robots adding the control functions of the joints and the execution of simulations.

In the figure 7.8 some screenshots of the applications implemented are shown.

7.2.5.3 Control

To control the real robots the previous applications of simulation can be used, that allow the position of the servos to be sent by the serial port to the electronics. This means that the operator can decide to see the simulation on the computer or connect the real robot to analyse its actual movements.

Also two specific applications have been created for the *Cube Revolutions* and *Hypercube* robots (see the screenshots in figure 7.8) that allow to visually specify the values of the parameters of the generators and make tests. They are programmed in the **C# language**, using the open-source virtual machine of the Mono project⁸.

For the movement of the servos a firmware for the Skypic board has been implemented. The applications that run in the PC send information to this programme that then generates the PWM control signals for the servos. It is called *Servos*⁹.

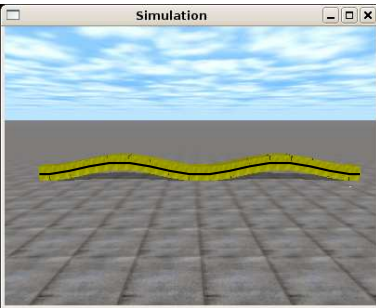
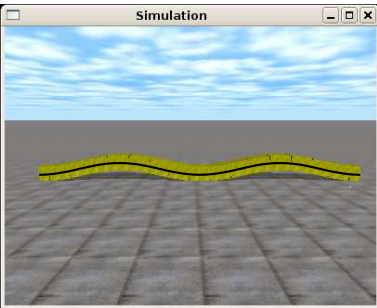
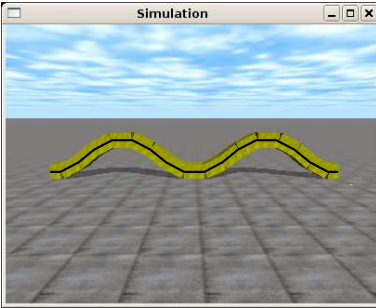
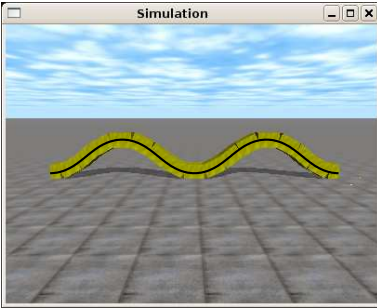
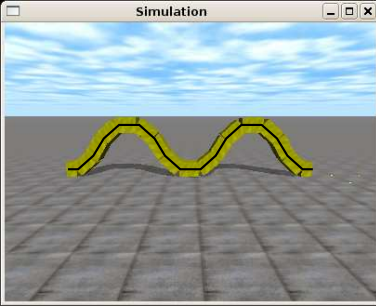
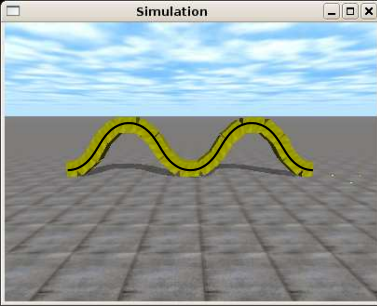
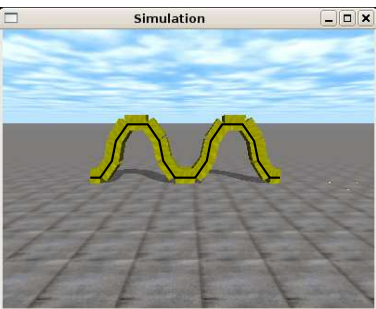
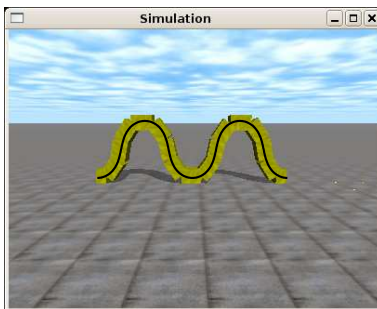
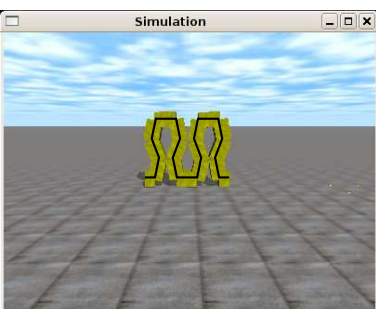
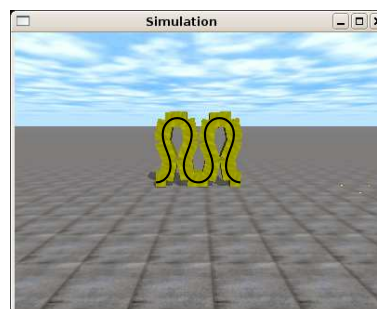
Parameters	discrete curve	Continuous curve
$A=10$ (degrees) $\alpha=13.1$ (degrees) $\Phi=-90$ (degrees) $M=16$ $k=2$ $Mu=8$		
$A=30$ (degrees) $\alpha=39.2$ (degrees) $\Phi=-90$ (degrees) $M=16$ $k=2$ $Mu=8$		
$A=45$ (degrees) $\alpha=58.8$ (degrees) $\Phi=-90$ (degrees) $M=16$ $k=2$ $Mu=8$		
$A=60$ (degrees) $\alpha=78.4$ (degrees) $\Phi=-90$ (degrees) $M=16$ $k=2$ $Mu=8$		
$A=85$ (degrees) $\alpha=111.1$ (degrees) $\Phi=-90$ (degrees) $M=16$ $k=2$ $Mu=8$		

Figure 7.9: Experiment 1: comparison between the shape of a 16 module apodal robot and the discrete and continuous serpenoid curves

7.3 Experiments of locomotion in 1D

7.3.1 The robot's shape

7.3.1.1 Experiment 1: Comparison between the shape of the robot and the theoretical curves

In this experiment the shape of a 16 module apodal robot is compared with the continuous and discrete curves obtained by the equations 3.19, 3.20 and 3.33, 3.34 respectively. The comparison is made at different working points. The results are shown in the figure 7.9.

The continuous and discrete curves have been generated from the scripts in Octave and have been superimposed on the simulator's screenshots. They have been increased in size to facilitate their comparison.

In this experiment it is shown that the continuous curve and the discrete are very similar. Two undulations are employed therefore there are 8 modules per undulation ($M_u = 8$). According to the criterion of discretization presented in the section 4.3.3.2, given that M_u is greater than 7 the error in the dimensions will always be less than 5%.

This experiment also allows the validation of the simulator, showing that the virtual robot generated has the shape of a serpenoid wave.

7.3.1.2 Experiment 2: Comparison between the shape of the Cube Revolutions and the theoretical curves

The shape of an 8 module virtual robot is compared to the discrete serpenoid curve and with the robot Cube Revolutions (figure 7.10). It is demonstrated that the real robot adopts the serpenoid shape.

7.3.2 Stability

7.3.2.1 Experiment 3: Stability for different values of k

We will analyse what happens to a 16 module robot with different values of the parameter k . To do this the height of the centre of mass and that of the mid point have been represented in the figure 7.11. The height of the centre of mass when k is 1 oscillates. After reaching its maximum point it falls abruptly.

⁷http://www-fp.mcs.anl.gov/CCST/research/reports_pre1998/comp_bio/stalk/pgapack.html

⁸http://www.mono-project.com/Main_Page

⁹<http://www.learobotics.com/proyectos/stargate/servidores/sg-servos8/sg-servos8.html>

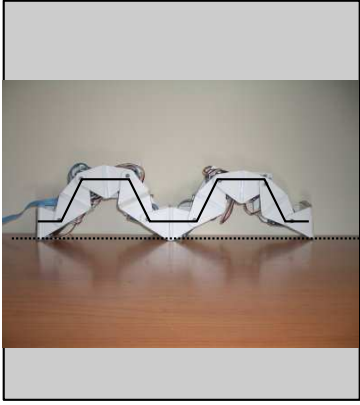
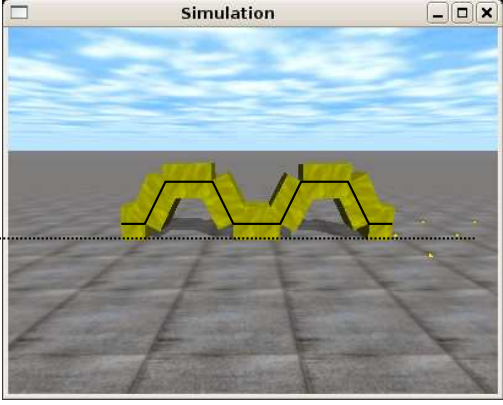
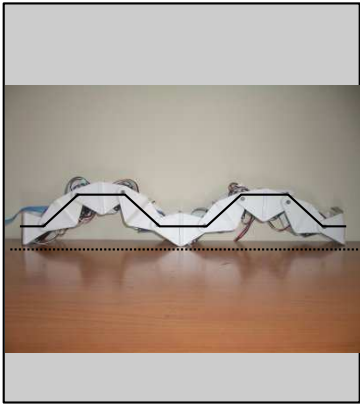
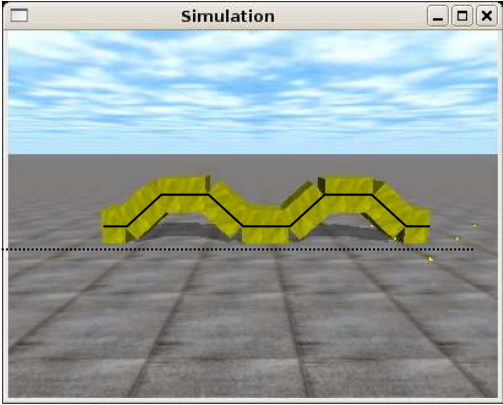
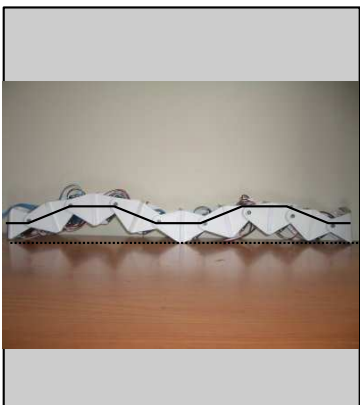
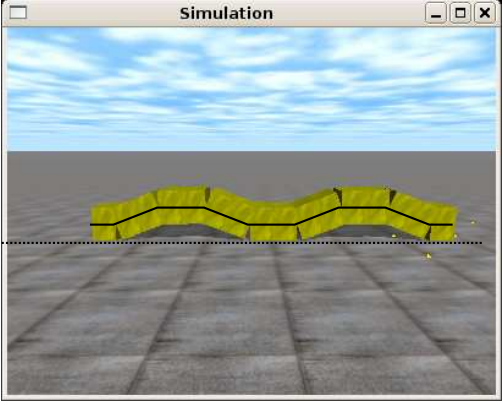
Parameters	Real robot	Virtual robot
$A=90$ (degrees) $\alpha=63.4$ (degrees) $\Phi=-90$ (degrees) $M=8$ $k=2$ $Mu=4$		
$A=60$ (degrees) $\alpha=42.4$ (degrees) $\Phi=-90$ (degrees) $M=8$ $k=2$ $Mu=4$		
$A=30$ (degrees) $\alpha=21.2$ (degrees) $\Phi=-90$ (degrees) $M=8$ $k=2$ $Mu=4$		

Figure 7.10: Experiment 2: Comparison between the shape of an 8 module virtual robot with the discrete serpenoid curve and the Cube Revolutions robot

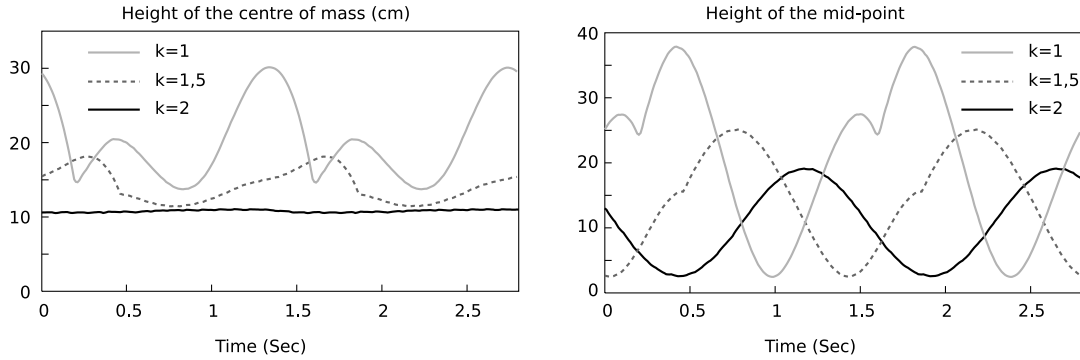


Figure 7.11: Experiment 3: Stability of a 16 module apodal robot in function of k

When k increases, the stability is greater. For $k = 1.5$, the maximum height that it reaches has decreased and though there are still oscillations these are smoother and of less amplitude.

Finally, when $k = 2$, fulfilling the principle of stability expounded in the section 4.2.5, the centre of mass stays at a constant height and the movement is uniform and smooth.

In the graph at the right the height of the mid point of the robot is shown. It varies between a minimum (when it is contact with the ground) and a maximum when it is at its highest. When $k = 1$ it is observed that the height oscillates, but points appear where the smooth movement is lost (the function cannot be differentiated). At a certain moment the robot falls to one side or the other due to having only one support point which provokes the loss of smoothness. When $k = 1.5$, this effect continues to exist, but is less marked. Also it is observed that the maximum height of the point is lower. Finally, in the stable case ($k = 2$) the oscillation of the height is a sinusoidal wave.

7.3.2.2 Experiment 4: Stability of Cube Revolutions for different values of k

In this experiment we analyse the stability of an 8 module apodal robot. In the figure 7.12 the shapes and positions of two robots have been shown, one simulated and the other real, in phases near to instability for different values of k . The behaviour is as described in the section 4.2.5. When k is equal to 1, the system is unstable. Both robots, the simulated and the real behave as described in the section 4.2.5.1 and as drawn in the figure 4.12. As the phase nears the zone of instability, the robot leans to the right causing the left extremity to be raised. The moment comes when stability is lost and the robot inclines to the left with the extremity hitting the ground. Now it is the module of the right which is in the most elevated position. The robot does not actually fall over, nevertheless it is a very abrupt movement.

When $k = 1.5$, the same happens but in a smoother way. Now it is the left extremity that does not reach so high but the movement is not uniform, but has a transition zone between one inclination and another. Finally, when $k = 2$ the robots move smoothly.

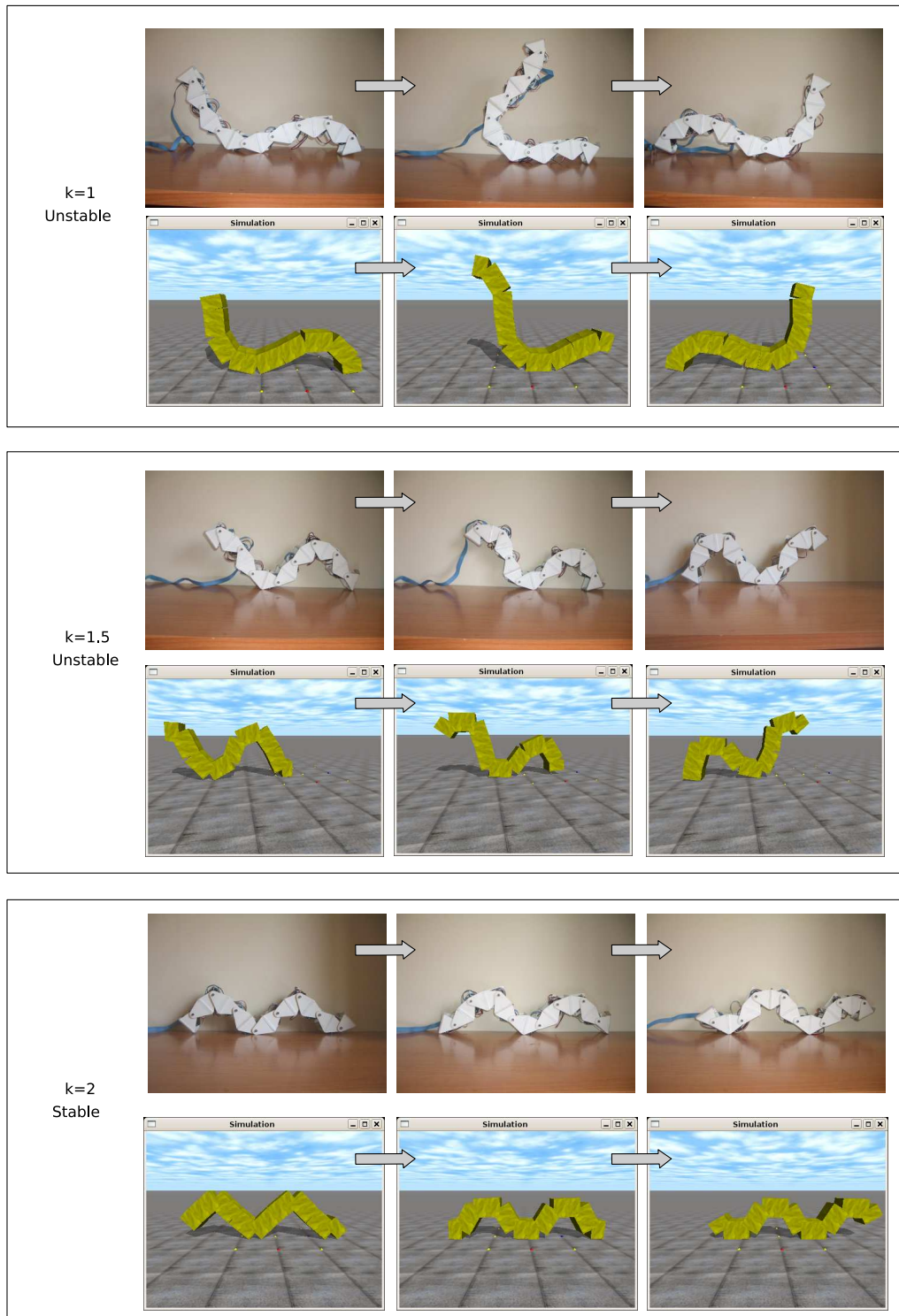


Figure 7.12: Experiment 4: Stability of an 8 module apodal robot in function of k . Then Shape and position of both the real and virtual robot are shown

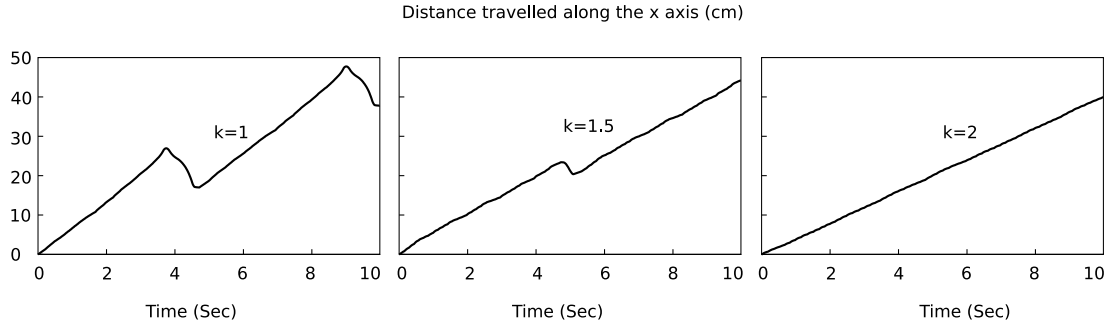


Figure 7.13: Experiment 4: Stability of an 8 module apodal robot in function of k . Space travelled by the robot

Working points	α	k	M	A	$\Delta\Phi$
Point A	42.4	2	8	60	90
Point B	32.4	3	8	60	135

Table 7.3: Chosen working points for the movement in a straight line of an 8 module apodal robot

In the figure 7.13 the space travelled by the robot in the direction of the x axis is shown in function of the time. It can be seen that it is a movement that is NOT uniform when $k < 2$. Intervals appear in which the distance varies abruptly. Nevertheless, for $k = 2$, the movement is uniform. The speed in this case will be constant and equal to $\Delta x/T$, where Δx is the step and T the period. The space travelled is calculated by means of the equation:

$$x = \frac{\Delta x}{T} t$$

7.3.3 Displacement

These experiments show how qualitatively an 8 module apodal robot moves, both in simulation and in reality. To do this two working points have been chosen, A and B, shown in the table 7.3. In both points the robot is stable, with values of k equal to 2 and 3 respectively.

7.3.3.1 Experiment 5: Simulation

In the figure 7.14 the distance travelled by the robot as a function of time, during the simulation, is shown. Given that for both working points the locomotion is statically stable, these graphs are very linear. They are rectilinear and uniform movements.

It is also proved that when the sign of the parameter $\Delta\phi$ is changed the displacement of the robot is the same, but in the opposite direction, as indicated by the principle of symmetry (section 4.4.5.1).

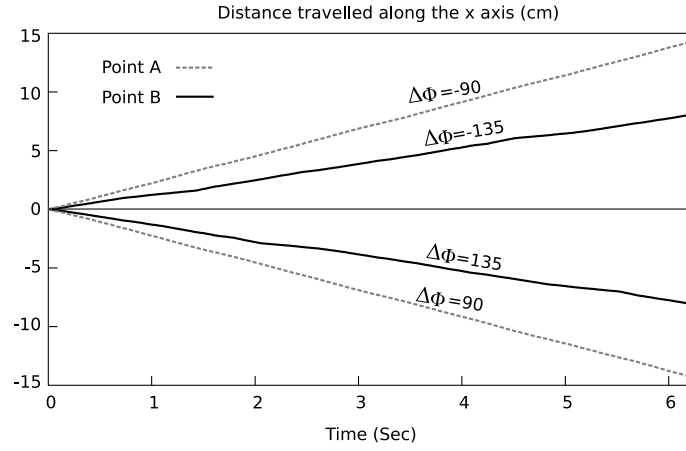


Figure 7.14: Experiment 5: Distance travelled by an 8 modules virtual apodal robot for the working points A and B, in both directions

In the figures 7.15 and 7.16 9 shots of the robot's movements in the points A and B respectively are shown. The initial and final positions are also compared and the step of the robots is shown. The aim is to show qualitatively what the movement is like. It is verified that the movement is carried out and that for different working points, both the co-ordination and the step are distinct.

7.3.3.2 Experiment 6: Locomotion of Cube Revolutions

In the figures 7.17 and 7.18 the locomotion of Cube Revolutions in the working points A and B respectively are shown, in the same instants as in the case of the simulation of experiment 5. It is observed that the shape of the robot in these instants is very similar to that of the simulation despite the fact that the simulation is with hexahedral shaped models and the real robot has a different geometry.

With this experiment it is demonstrated that the real robots can move and they do so in a similar way to the results of the simulation.

7.3.4 Step

In this group of experiments the theoretical equations proposed are contrasted to enable the calculation of the step with the information obtained from the simulations and the movement of the real robot. The experiments are carried out with the three models of module: the wired, the hexahedral and the real.

For the wired and hexahedral models, the graphs of the variation in step is compared with the parameter α for robots with different number of modules per undulation (M_u). All the experiments have been carried out with $k = 2$.

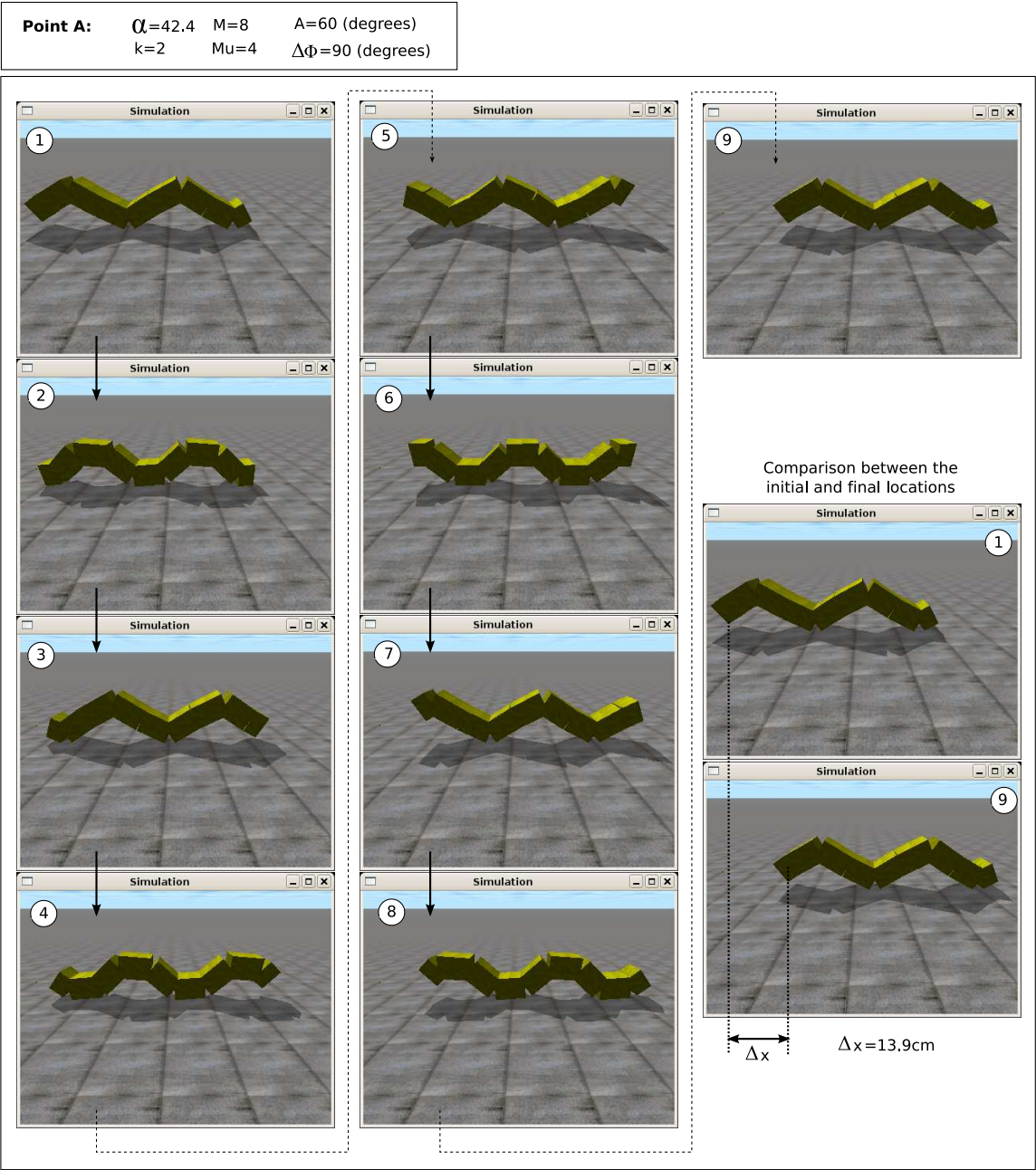


Figure 7.15: Experiment 5: Simulation of the locomotion in a straight line of an 8 module apodal robot for the working point A

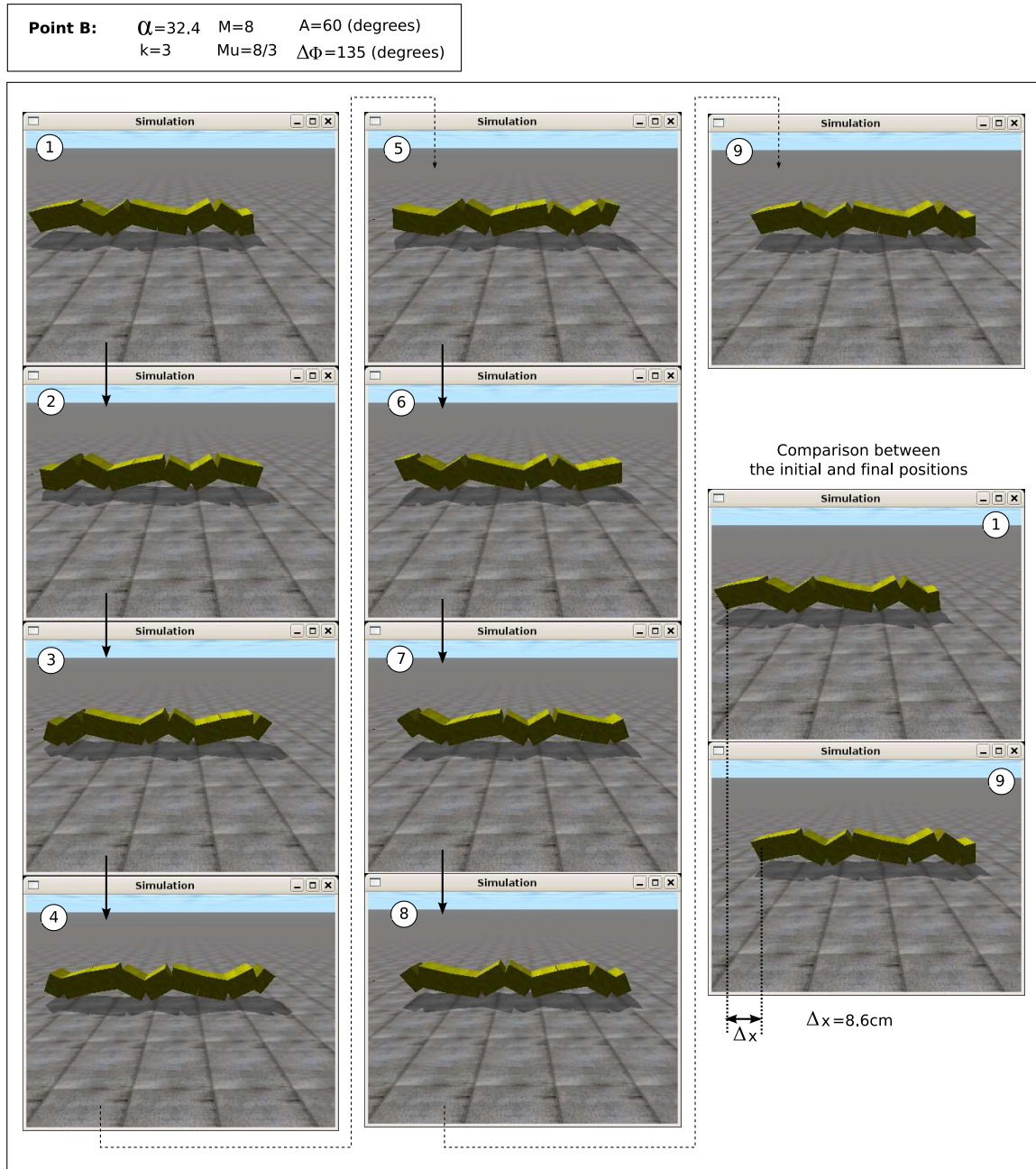


Figure 7.16: Experiment 5: Simulation of the locomotion in a straight line of an 8 module apodal robot for the working point B

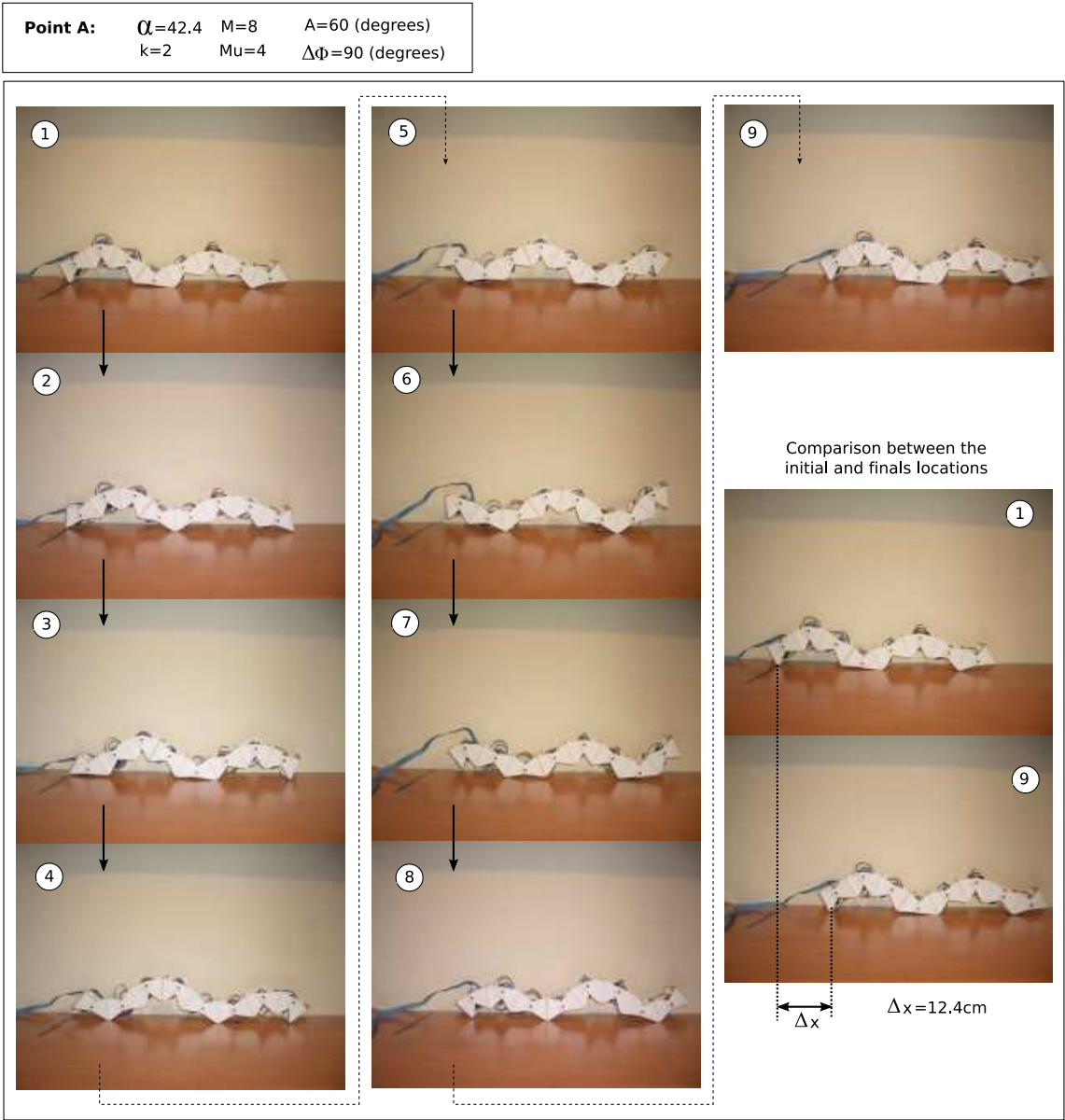


Figure 7.17: Experiment 6: Locomotion of the Cube Revolution robot in a straight line, for the working point A

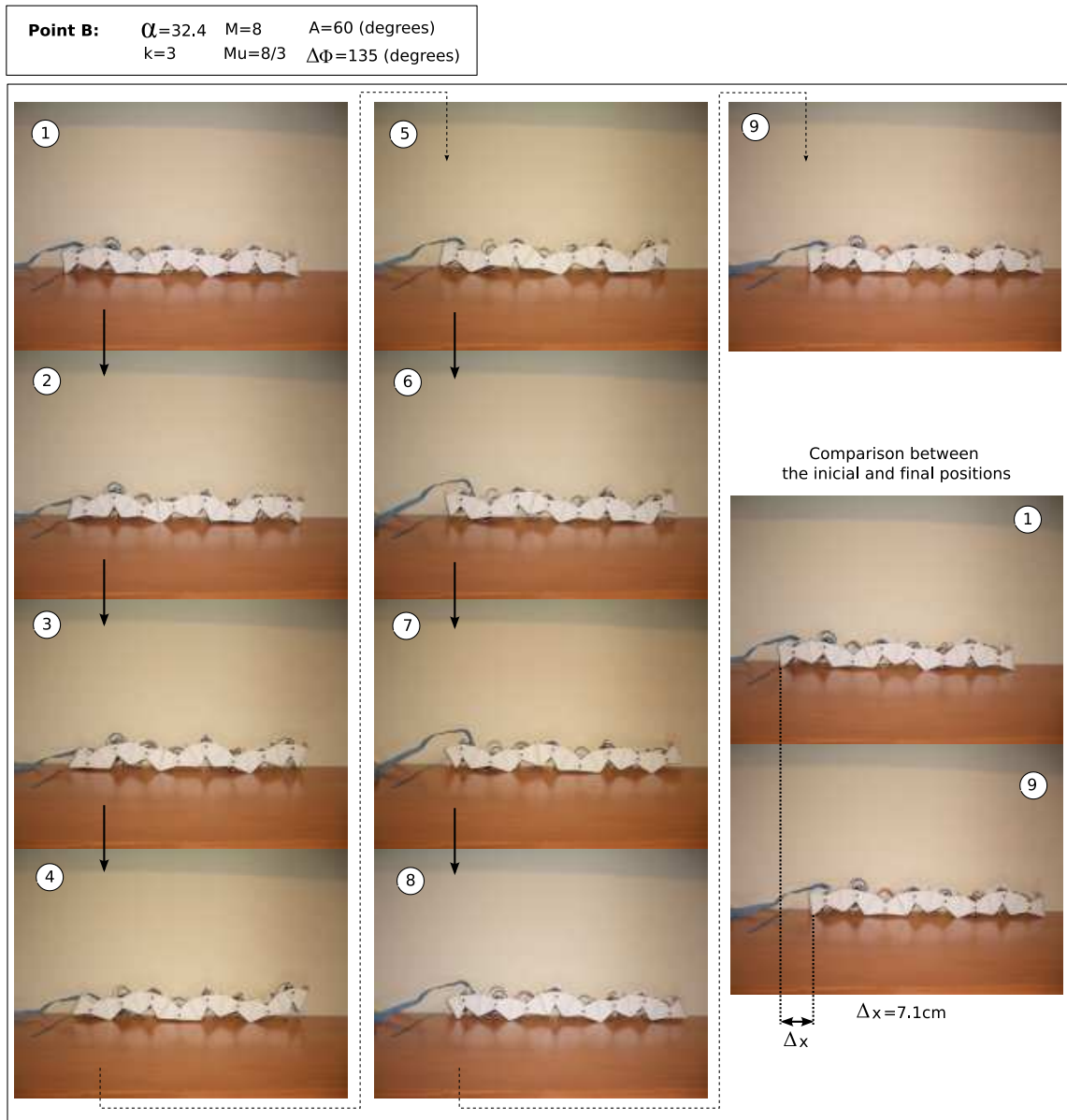


Figure 7.18: Experiment 6: Locomotion of the Cube Revolution robot in a straight line, for the working point B

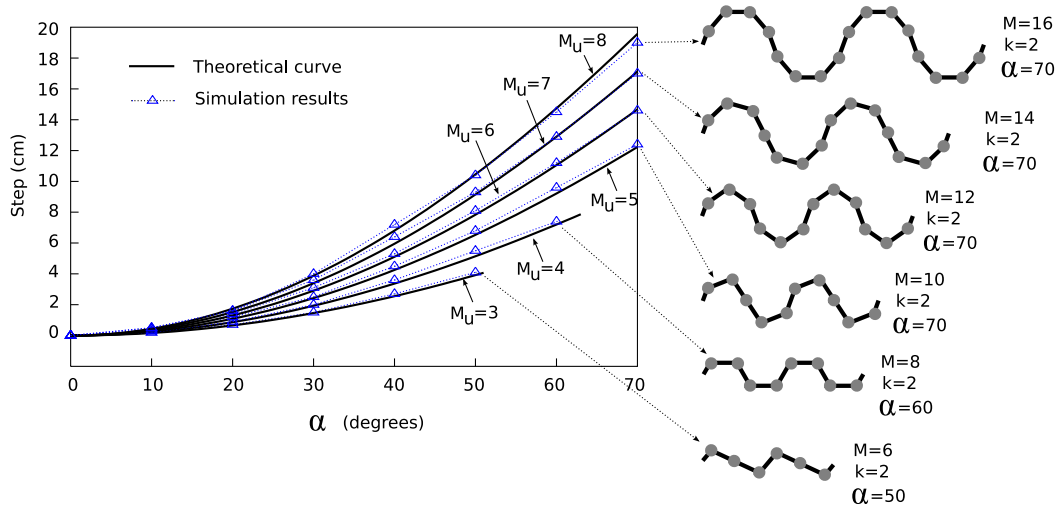


Figure 7.19: Experiment 7: Comparison between the theoretical and simulated steps for an apodal robot with different modules per undulation. Wired model

7.3.4.1 Experiment 7: Wired model's step

In the figure 7.19 the results obtained in the simulation of movement in a straight line of six apodal robots are shown, with the modules per undulation between 3 and 8. The variation in relation to the parameter α is shown. These values are contrasted with those predicted for the theoretical equation 4.1 and it is observed that they are very similar.

For the simulation of the wired model a robot with flattened modules of a length L and a width W , but a negligible height, has been used.

It can also be seen that the step increases with the winding angle α .

7.3.4.2 Experiment 8: Hexahedric model's step

The figure 7.20 shows the results of the simulation of the movement in a straight line of apodal robots in which the model of module is hexahedric of length L and height H . They are compared with the theoretical results obtained by the proposed equation 4.9 and it is observed that they are similar. The value in the simulation is always a little below the theoretical one. In the theoretical model it has been assumed that there is no movement of the supporting points. In the simulation this is not the case therefore what happens is slightly inferior to the prediction. In the worst case the relative error is less than 8%.

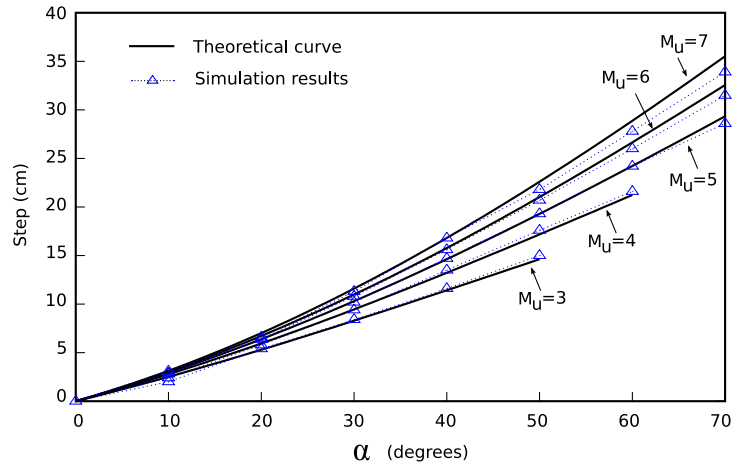


Figure 7.20: Experiment 8: Comparison between the theoretical and simulated steps for an apodal robot with different number of modules per undulation. Hexahedral model

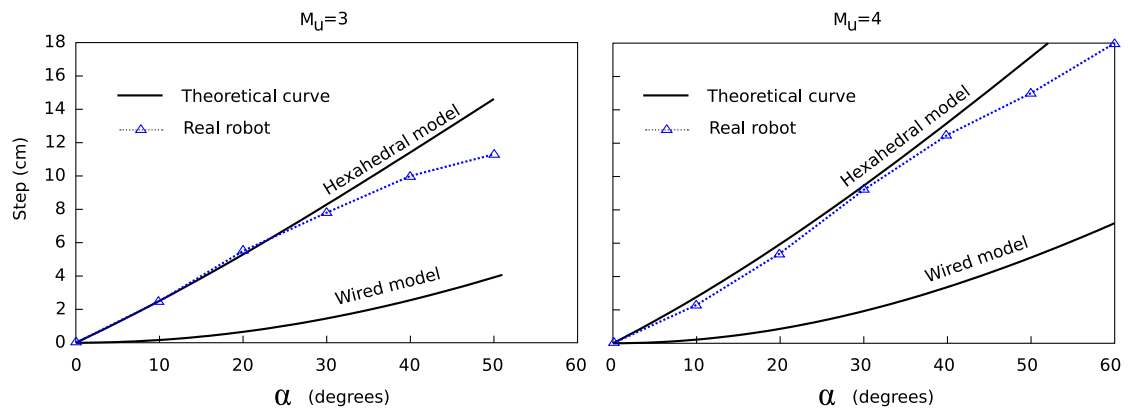
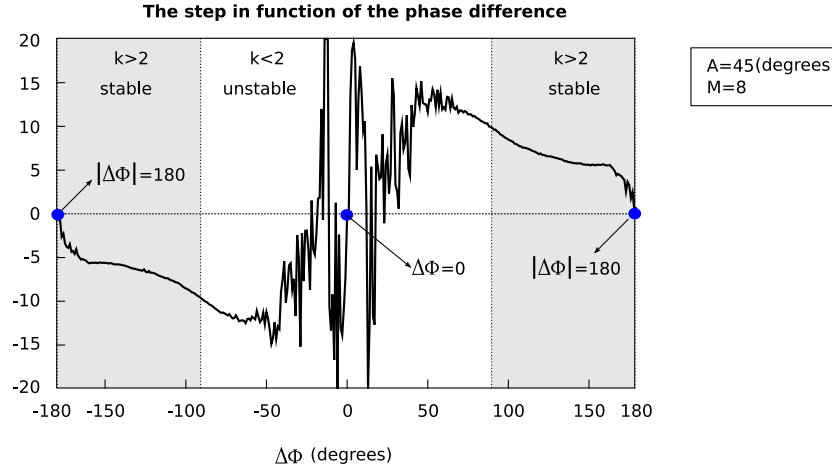


Figure 7.21: Experiment 9: Comparison between the step given by Cube Revolution and the theoretical models (wired and hexahedral)

$\alpha(\text{degrees})$	0	10	20	30	40	50	60
$\Delta x_3(\text{cm})$	0	2.5	5.5	7.8	10	11.3	—
$\Delta x_4(\text{cm})$	0	2.3	5.4	9.2	12.5	15	18

Table 7.4: Experiment 9: Measurements of the robot's step for different values of α and M_u Figure 7.22: Experiment 10: The step of an 8 module virtual robot in function of $\Delta\phi$

7.3.4.3 Experiment 9: Step of the Cube Revolutions robot

In the figure 7.21 the results obtained in the movement in a straight line of Cube Revolutions with the predictions for the wired and hexahedric models are compared. Experiments have been carried out for the values of M_u equal to 3 and 4 that correspond with $k = 2.6$ and $k = 2$ respectively. It is observed that the equation that most approximates to the robot's step is that of the hexahedric model. Nevertheless, when the values of α become near to the maximum, they begin to differ from the theoretical ones.

In the table 7.4 the numerical values that have been measured in the real robot are shown. In these experiments the robot has moved during a period and the distance covered has been measured with a ruler, repeating it various times to avoid erroneous results. The symbols Δx_3 and Δx_4 denote the step taken by the robots with parameters $M_u = 3$ and 4 respectively.

7.3.5 Step and phase difference $\Delta\phi$

7.3.5.1 Experiment 10: influence of $\Delta\phi$

In the figure 7.22 the robot's step has been shown in function of the phase difference for an 8 module virtual apodal robot. The amplitude applied to the generators has been fixed at $A = 45$ degrees.

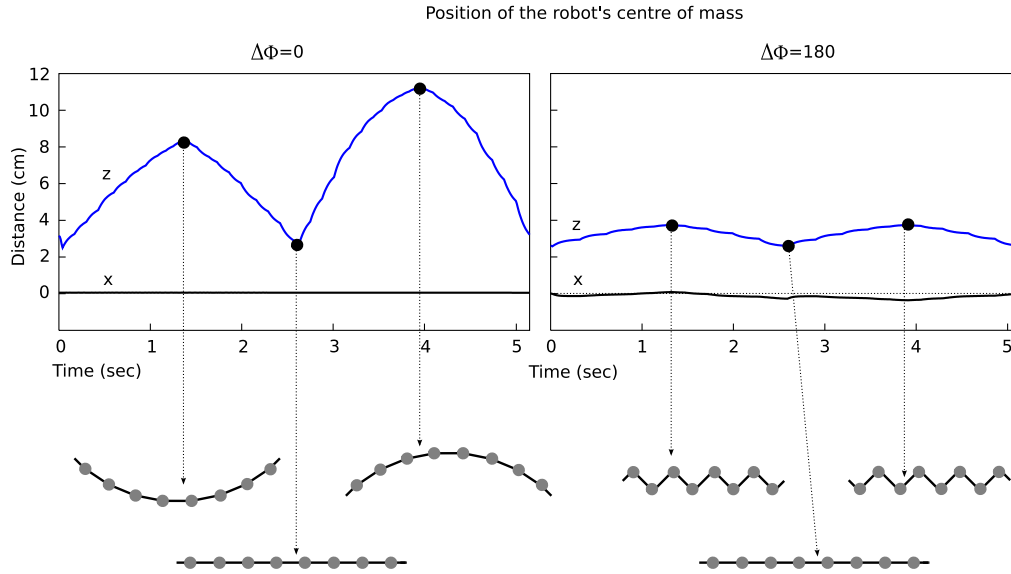


Figure 7.23: Experiment 11: Simulation of the movement of an 8 module robot when the generators are in phase and 180 degrees out of phase

It is observed that the graph is odd. This is due to the symmetry principle (section 4.4.5.1). If the sign of $\Delta\phi$ is changed the movement is made with the same step but in the opposite direction.

In the points where $\Delta\phi$ is 0 and 180 degrees, the step is nil, as established by the principle of generators in phase and opposition of phase (section 4.4.5.2).

In the region that is blank, the value k is less than 2, therefore the robot is unstable. What is more the movement is chaotic. A small variation in $\Delta\phi$ means that the step passes abruptly from a maximum value to a minimum. Within the stable zone, the step is inversely proportional to $\Delta\phi$ until it reaches a value in the region of 165 degrees where the effect of the phase opposition dominates and the step falls off quickly to zero.

7.3.5.2 Experiment 11: Generators in phase and opposition of phase

This experiment is the confirmation of the phase and the opposition of phase principle for which the robot does not move in these conditions. In the figure 7.23 the x and z co-ordinates of the centre of mass of the robot in function of time when the generators are in phase ($\Delta\phi = 0$) and in opposition of phase ($\Delta\phi = 180$). Also the shape the robot adopts at different points has been drawn. In both cases the z co-ordinate oscillates, causing the height of the robot to rise and fall. Movement in x does not exist, though there is a slight oscillation in the case of opposition of phase.

In the figure 7.24 the shape the virtual robot and Cube Revolutions adopt in the situations in which $\Delta\phi = 0$ and $\Delta\phi = 180$ are shown. For Cube Revolutions only the movement in opposition of phase

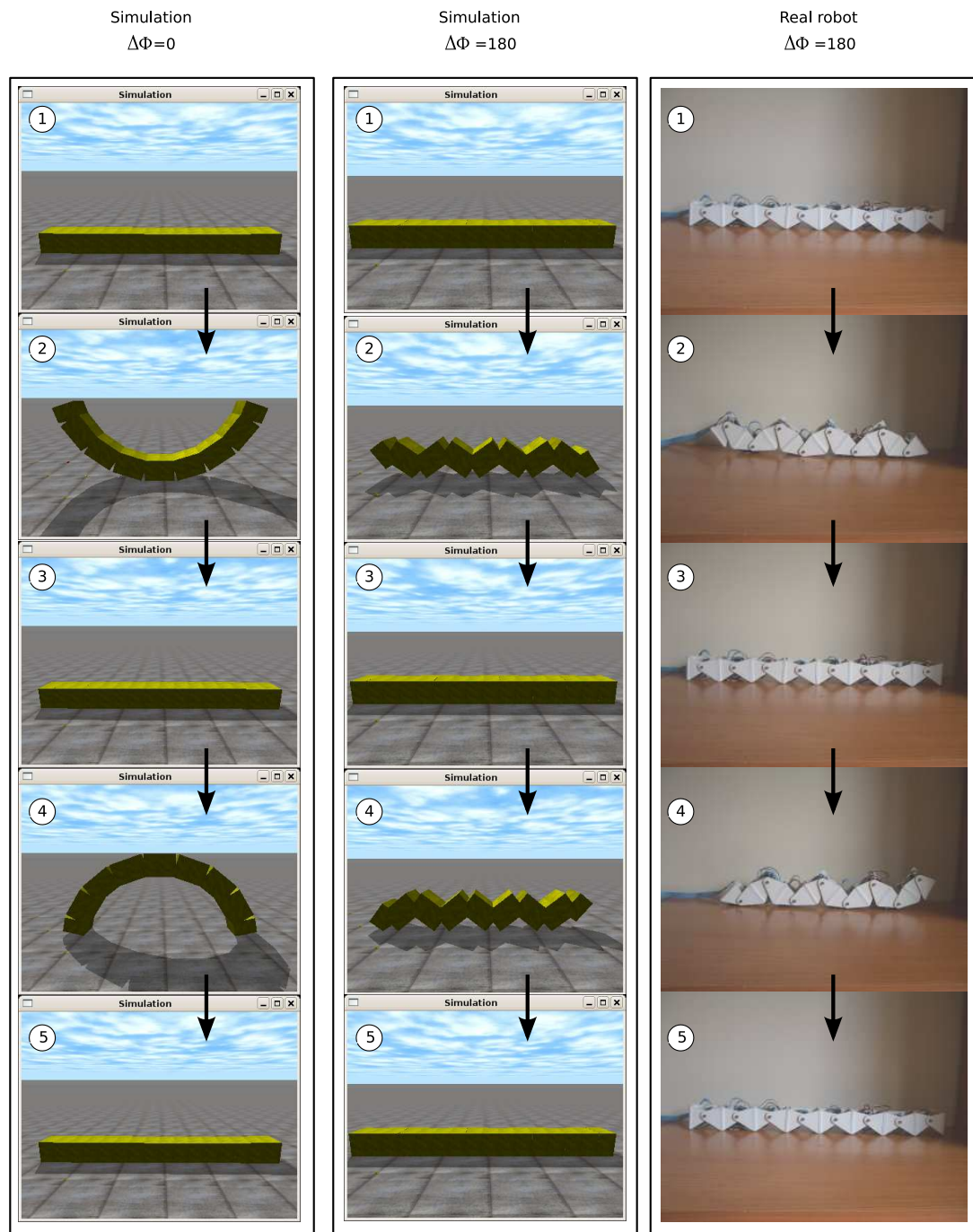


Figure 7.24: Experiment 11: Shapes of the virtual and real robots when the generators are in phase and 180 out of phase

has been presented, as the servos do not have sufficient power to adopt the shapes that are produced when the generators are in phase. It is the confirmation in practise of the figure 4.44 obtained from the theoretical equations.

7.4 Experiments of locomotion in 2D

7.4.1 3D serpenoid waves

These experiments show some of the shapes that the body of the pitch-yaw group of 32 module robots adopt, when two serpenoid waves are superimposed, one in the vertical joints and the other in the horizontal ones, forming a 3D serpenoid wave. The classification of these waves is shown in the section 3.6.4.3.

7.4.1.1 Experiment 12: straight isomorphic waves

The isomorphic waves have the characteristic that their projection in the zy plane is a fixed figure, that does not vary with the propagation of the wave. We denominate the straight isomorphic waves as those whose projection in this plane is a straight line. In this experiment two types of straight isomorphic waves are shown, the flat and the inclined and their projection on the xy plane is compared with a serpenoid curve calculated by means of the theoretical equation (see figure 7.25). It is observed that for both types of waves, the shape adopted is that of a serpenoid curve. In the case of the straight inclined isomorphic wave the resulting angle of the winding of the curve is calculated by the equation 5.23 and for the two examples their values are of 72.4 and 92.3 degrees. Two screenshots for each curve, one showing its shape in the xy plane and the other in perspective to be able to appreciate the incline.

7.4.1.2 Experiment 13: Elliptical and circular isomorphic waves

In this experiment the elliptical and circular isomorphic waves are shown in an apodal robot with 32 modules. The results are shown in the figure 7.26. Each type of wave is shown for different values of the parameters α and k . Also the flat versions of the curves have been included, in which α_h is of an order of magnitude greater than α_v . For this reason the shape of the robot is “flattened” and can approximate to a serpenoid curve.

7.4.1.3 Experiment 14: Non isomorphic waves

In this experiment the shape of a 32 module robot is shown when non isomorphic waves are used. In the upper figure 7.27 the screenshots have been realised in different phases to be able to see that the shape changes with the phase. In the second example, where $k_h = 1$ it can be seen that for $\phi = \phi_1$ the section of the robot is an ellipsoid and for $\phi = \phi_2$ it has the shape of ∞ .

The robots in the lower part of the figure correspond to those that have two flat non isomorphic waves. They can be approximated by two serpenoids on the xy plane.

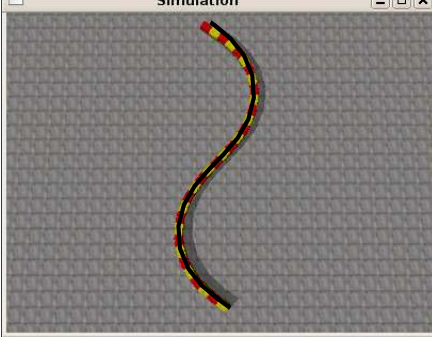
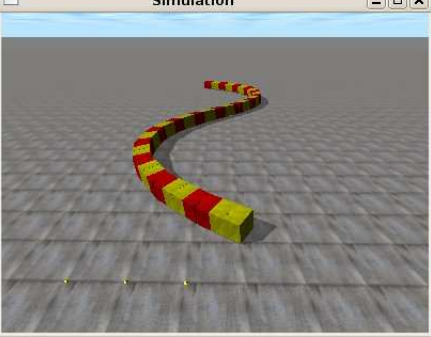
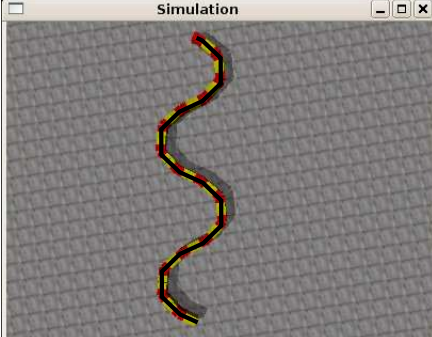

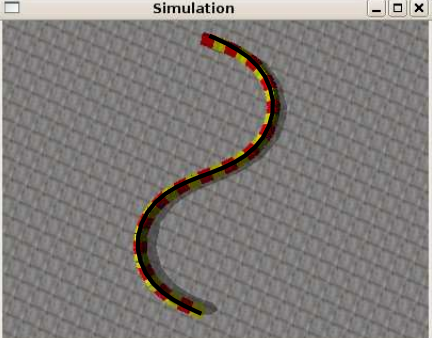

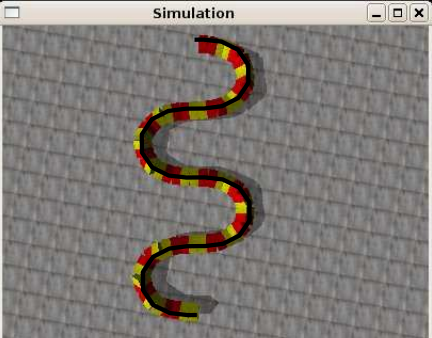

3D wave	Parameters	Top View	Perspective view
Flat straight Isomorphous	$M=32$ $k_h=k_v=1$ $\alpha_v=7.7$ $\alpha_h=51.2$ $\Delta\Phi_{vh}=0$		
	$M=32$ $k_h=k_v=2$ $\alpha_v=6.5$ $\alpha_h=65.3$ $\Delta\Phi_{vh}=0$		
Inclined straight Isomorphous	$M=32$ $k_h=k_v=1$ $\alpha_v=51.2$ $\alpha_h=51.2$ $\alpha=72.4$ $\Delta\Phi_{vh}=0$		
	$M=32$ $k_h=k_v=2$ $\alpha_h=65.3$ $\alpha_v=65.3$ $\alpha=92.3$ $\Delta\Phi_{vh}=0$		

Figure 7.25: Experiment 12: Straight isomorphous waves







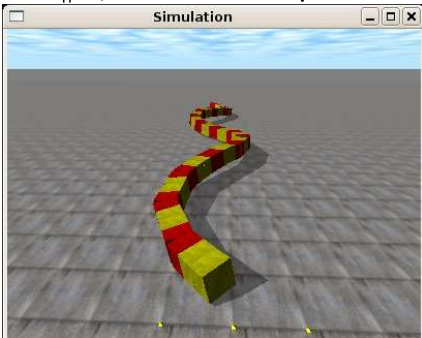
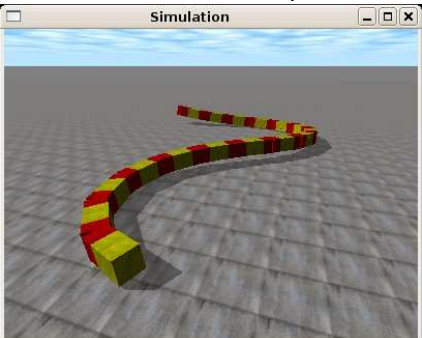
<p>Elliptic isomorphous</p> <p>$\Delta\Phi_{vh}=45$ $M=32$</p>	<p>$k_h=k_v=2 \quad \alpha_v=\alpha_h=39.2$</p> 	<p>$k_h=k_v=1 \quad \alpha_v=\alpha_h=51.3$</p> 
<p>Flat elliptic isomorphous</p> <p>$\Delta\Phi_{vh}=45$ $M=32$</p>	<p>$k_h=k_v=2 \quad \alpha_h=39.2 \quad \alpha_v=6.5$</p> 	<p>$k_h=k_v=1 \quad \alpha_h=76.9 \quad \alpha_v=5.1$</p> 
<p>Flat circular isomorphous</p> <p>$\Delta\Phi_{vh}=90$ $M=32$</p>	<p>$k_h=k_v=2 \quad \alpha_v=\alpha_h=39.2$</p> 	<p>$k_h=k_v=1 \quad \alpha_v=\alpha_h=76.9$</p> 
<p>Flat circular isomorphous</p> <p>$M=32$ $\Delta\Phi_{vh}=90$</p>	<p>$k_h=k_v=2 \quad \alpha_h=39.2 \quad \alpha_v=2.6$</p> 	<p>$k_h=k_v=1 \quad \alpha_h=76.9 \quad \alpha_v=5.1$</p> 

Figure 7.26: Experiment 13: Elliptic and circular Isomorphous wave


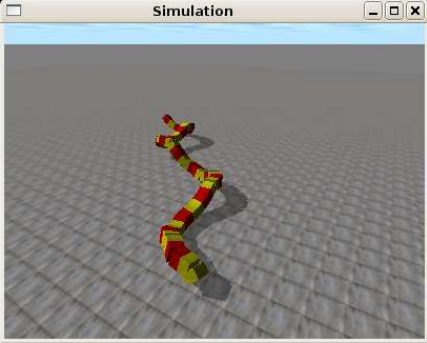

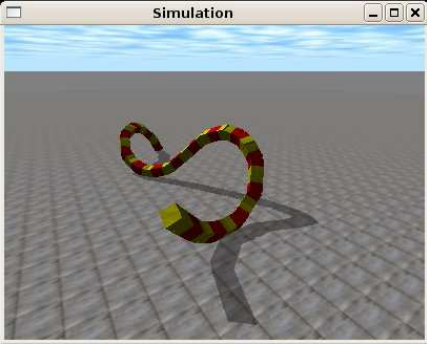
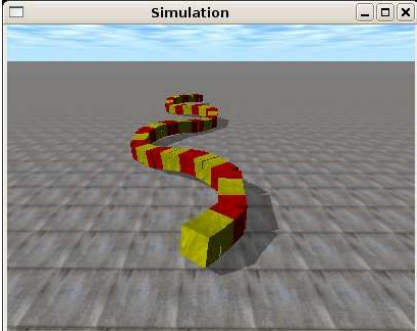
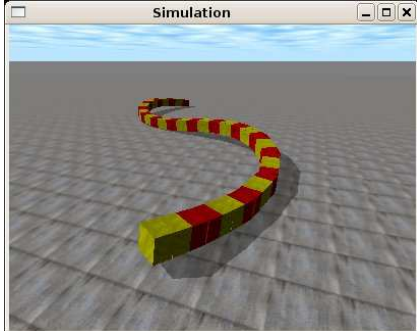
3D wave	Parameters	$\Phi = \Phi_1$	$\Phi = \Phi_2$
NON isomorphous	$M=32$ $k_h=2$ $k_v=4$ $\alpha_v=28.3$ $\alpha_h=52.3$ $\Delta\Phi_{vh}=0$		
	$M=32$ $k_h=1$ $k_v=2$ $\alpha_v=39.2$ $\alpha_h=76.9$ $\Delta\Phi_{vh}=0$		
Flat NON isomorphous	$k_v=4$ $\alpha_v=7.1$ $M=32$ $k_h=2$ $\alpha_h=52.3$ $\Delta\Phi_{vh}=0$		
	$k_v=2$ $\alpha_v=6.5$ $M=32$ $k_h=1$ $\alpha_h=51.3$ $\Delta\Phi_{vh}=0$		

Figure 7.27: Experiment 14: Non isomorphous waves

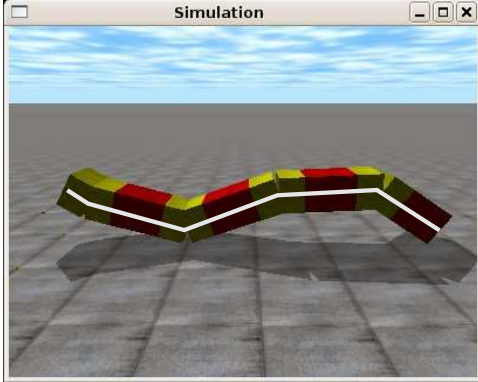
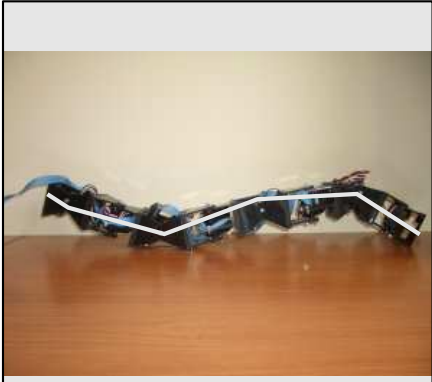
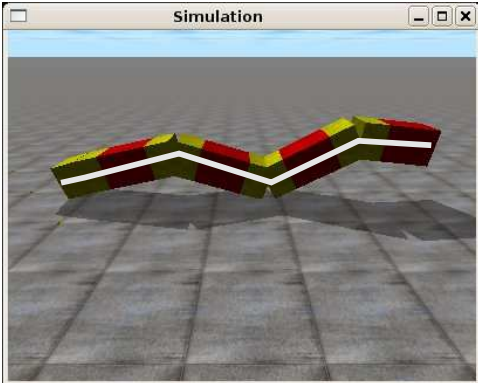

Parameters	Virtual robot	Real robot
$A=40$ $\alpha=28.3$ $\Phi=161$ $M=8$ $k=1$		
$A=45$ $\alpha=24.4$ $\Phi=-70$ $M=8$ $k=1.5$		

Figure 7.28: Experiment 15: Comparison between the real and virtual robots with the theoretical curve

7.4.2 Movement in a straight line

7.4.2.1 Experiment 15: Shape of the robot

In the figure 7.28 the shape of an 8 module robot with pitch-yaw connection, is compared — both simulated and real — with the shape obtained by means of the theoretical equations 3.29 and 3.30. Compared to the robots of the pitch-pitch group, the blocks that are now employed are of pitch-yaw type and the parameters d and d_0 have the values $L/2$ and $2L$ respectively (section 3.3.4.3). It is observed that the theoretical curve and the shape of the two robots are similar.

7.4.2.2 Experiment 16: Simulation of movement of Hypercube in a straight line

In this experiment the movements in a straight line of the Hypercube robot are simulated, when the working points A and B, shown in the table 7.5 are used. In the figure 7.29 the graph of the distance

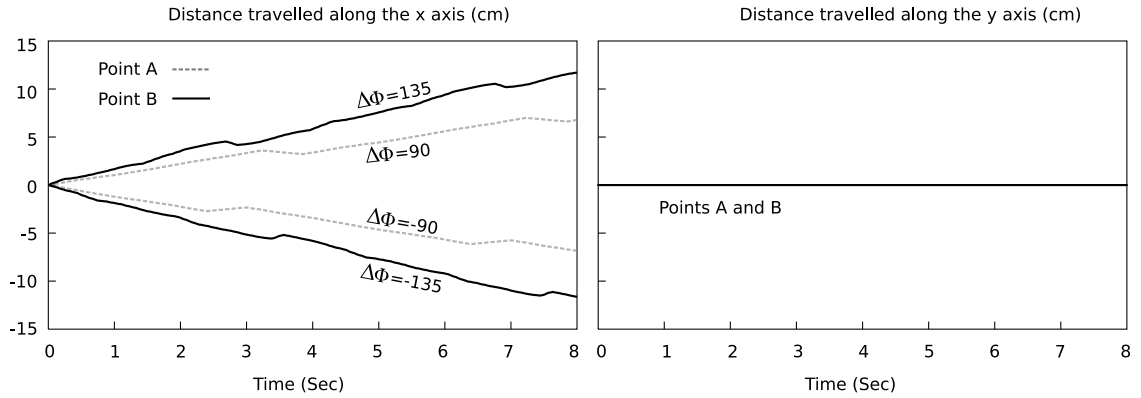


Figure 7.29: Experiment 16: Distance travelled by the robot in function of time (during two cycles)

Working points	α_v	k_v	A_v	$\Delta\phi_v$	α_h	k_h	A_h
Point A	14,1	1	20	90	0	—	0
Point B	24.4	1.5	45	135	0	—	0

Table 7.5: Working points used for the experiments on the locomotion in a straight line

travelled along the x axis in function of the time is shown, during two cycles, for the two working points. It is seen that they are not straight lines. The movement is not uniform rectilinear. This is due to the fact that the established criterion of stability is not fulfilled and in both cases k is less than 2. Given that the robot has only 4 vertical modules, this criterion is never fulfilled. Nevertheless, the robot's movement is carried out. What is more, changing the sign of the parameter $\Delta\phi$, the movement is realised in the opposite direction.

Also shown is the value of the movement on the y axis, demonstrating that it is non-existent. The robot only moves in a straight line.

The figure 7.30 shows the screenshots of the simulated movement in a straight line that corresponds to 8 moments in time, when the working point B is used.

7.4.2.3 Experiment 17: Hypercube's movement in a straight line

This experiment demonstrates that the robot Hypercube is capable of moving in a straight line. In the figure 7.31 the photos taken during the movement are shown, corresponding to the same moments as in the simulation shown in the figure 7.30.

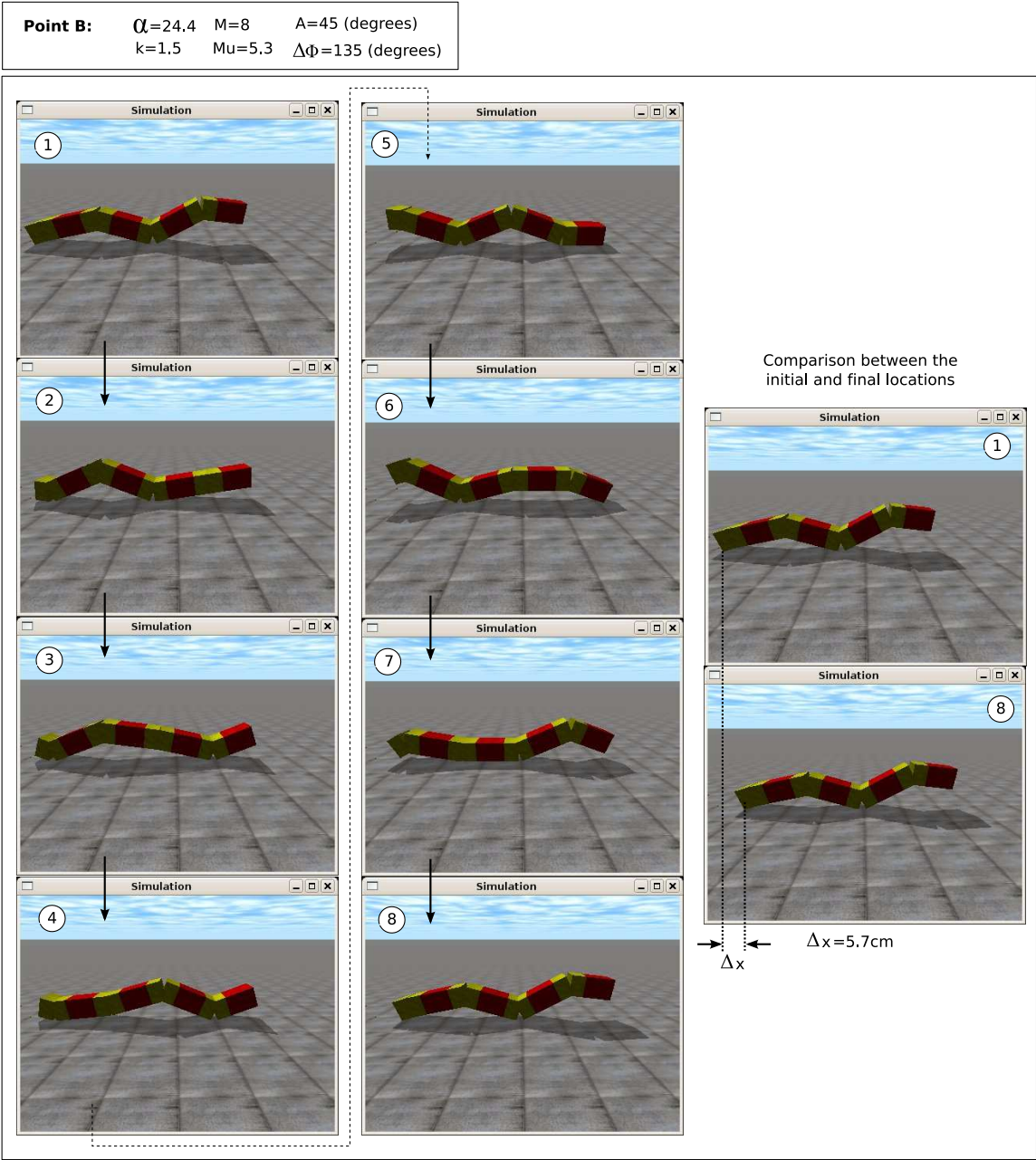


Figure 7.30: Experiment 16: Screenshots of the locomotion of the virtual Hypercube robot in a straight line

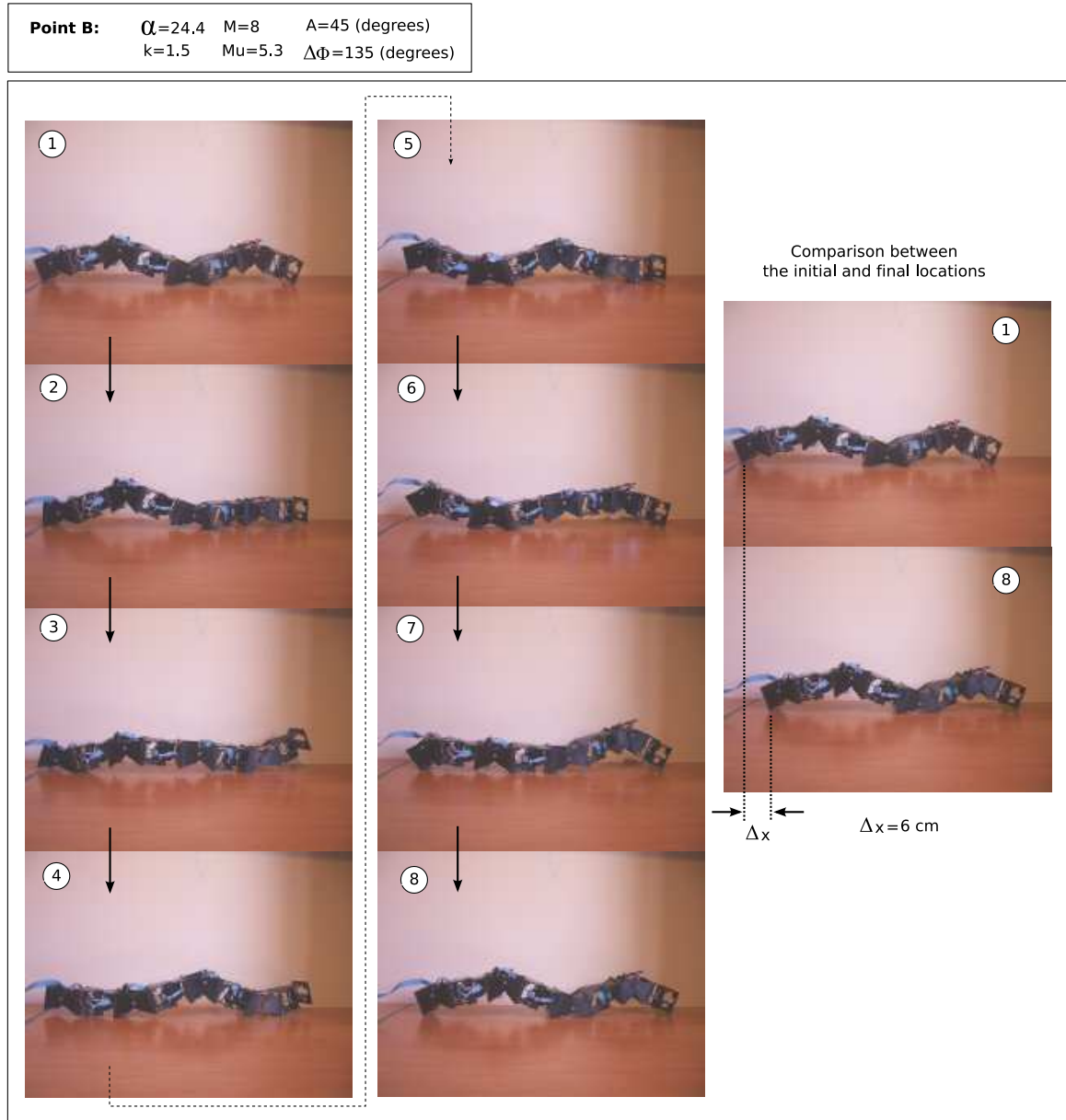


Figure 7.31: Experiment 17: Locomotion of the Hypercube robot in a straight line

Working points	M	α_v	k_v	A_v	$\Delta\phi_v$	α_h	k_h	A_h	$\Delta\phi_h$	$\Delta\phi_{vh}$
Point A	32	6.5	2	5	45	52.3	2	40	45	90
Point B	32	5.1	1	2	22.5	51.2	1	20	22.5	90
Point C	8	14.1	1	20	90	28.3	1	40	90	90
Point D	8	10.8	1.5	20	135	21.6	1.5	40	135	90
Point E	8	42.4	1	60	90	42.4	1	60	90	30

Table 7.6: Working points used for the experiments on sideways movement

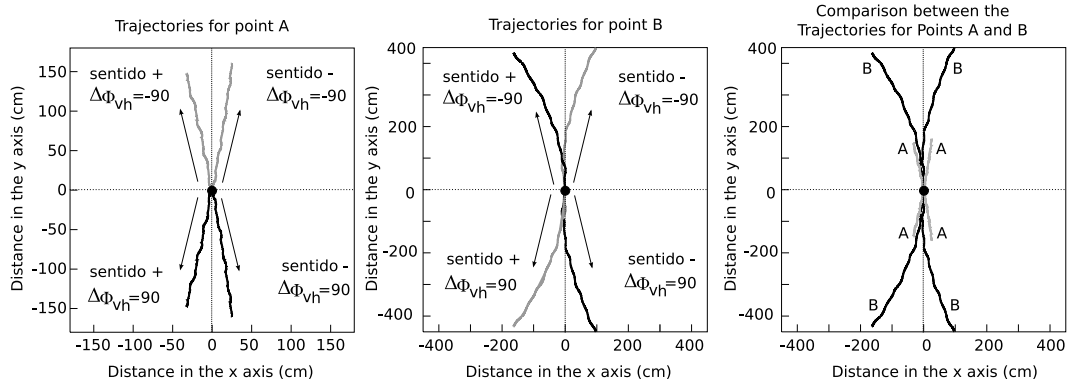


Figure 7.32: Trajectories of centre of gravity of a 32 module apodal robot for the working points A and B

7.4.3 Sideways movement

7.4.3.1 Working points

All the working points employed in the sideways movement experiments are shown in the table 7.6. The points A and B are for the simulation of a 32 module apodal robot and the rest for an 8 module one.

7.4.3.2 Experiment 18: Movement of the continuous model

In this experiment the path travelled by a 32 module apodal robot are calculated when its sideways movement is simulated. The working points employed are A and B. The results are shown in the graphs of the figure 7.32. The duration of the simulation is of four periods. For each point 4 paths have been represented in function of the sign of $\Delta\phi_{vh}$ and in the direction of the propagation of the corporal wave (section 5.7.7.4).

It is observed that the robot follows a rectilinear path in the point A, but in B it starts to bend. That is to say, besides a sideways movement there is a small change in the orientation.

In comparing both paths it is seen that the robot has advanced further in point B than in A.

In the figures 7.33 and 7.34 the screenshots during the movement of the robots are shown, in points A and B respectively, for one cycle.

7.4.3.3 Experiment 19: Step of the sideways movement

In this experiment the steps given by the robots in the points A and B in the simulation are compared with the theoretical equations of the module (eq. 5.26) and the orientation (eq. 5.26). It is seen that

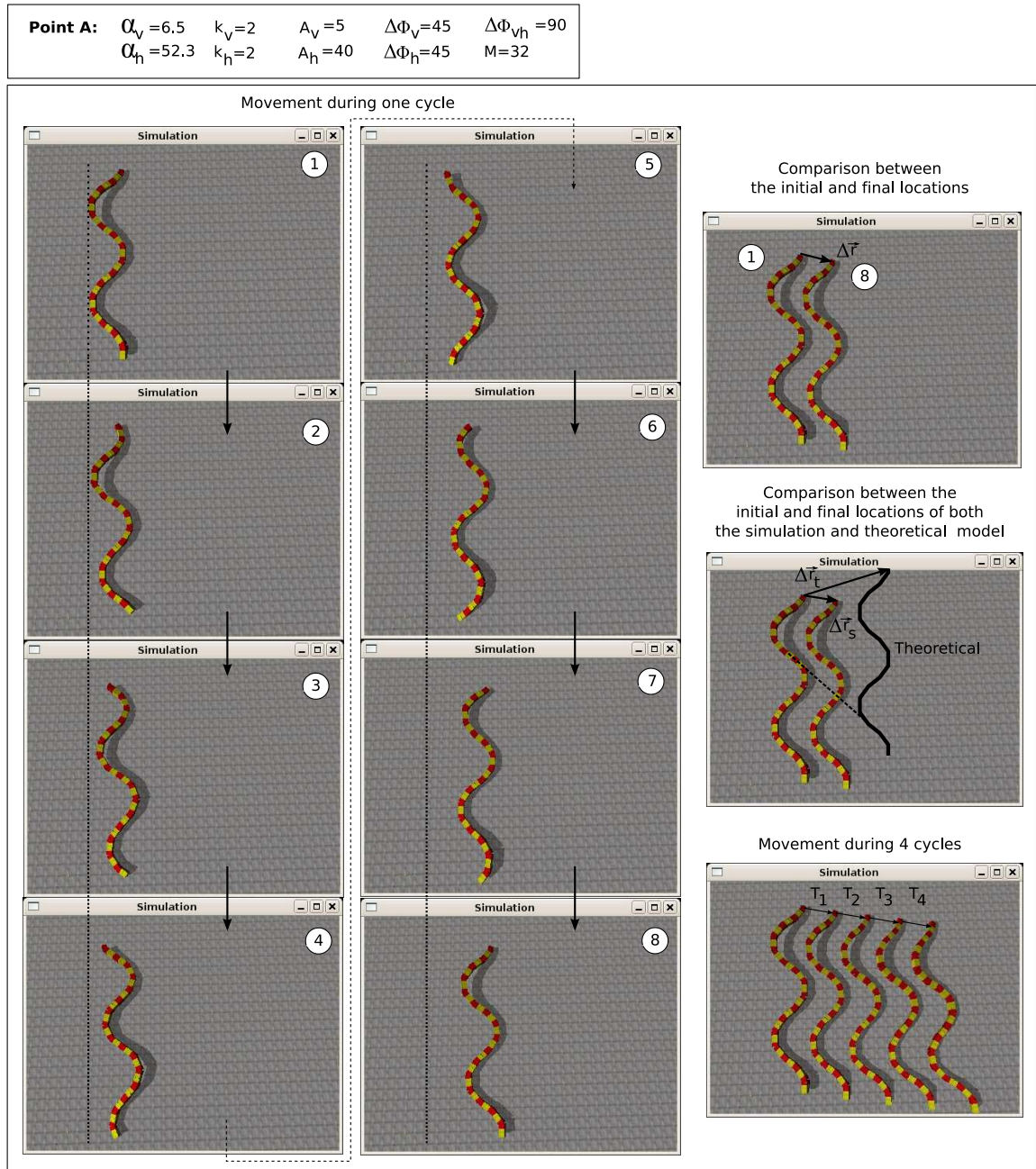


Figure 7.33: Experiment 18: Screenshots of the simulation of the sideways movement for the working point A

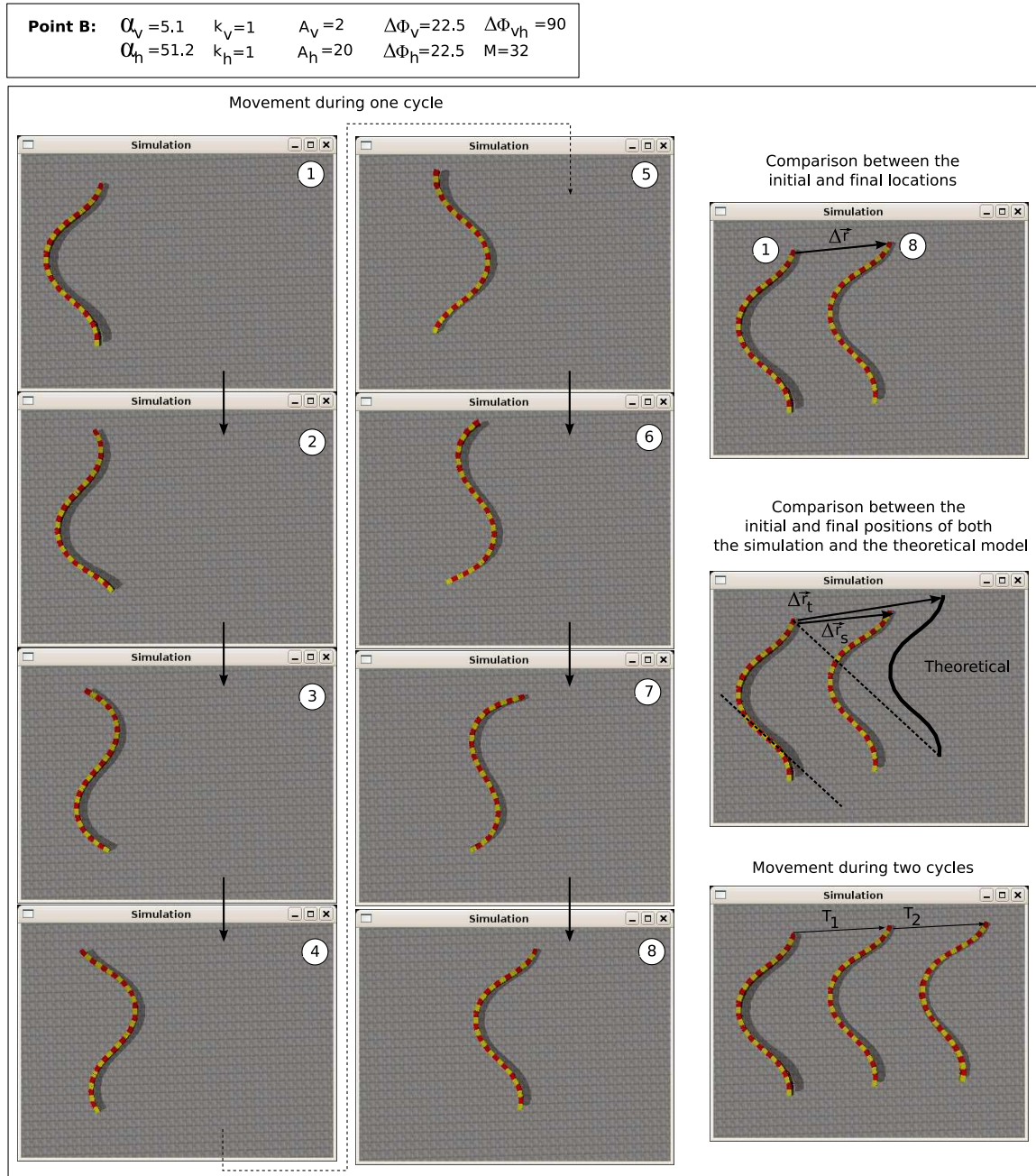


Figure 7.34: Experiment 18: Screenshot of the simulation of the sideways movement for the working point B

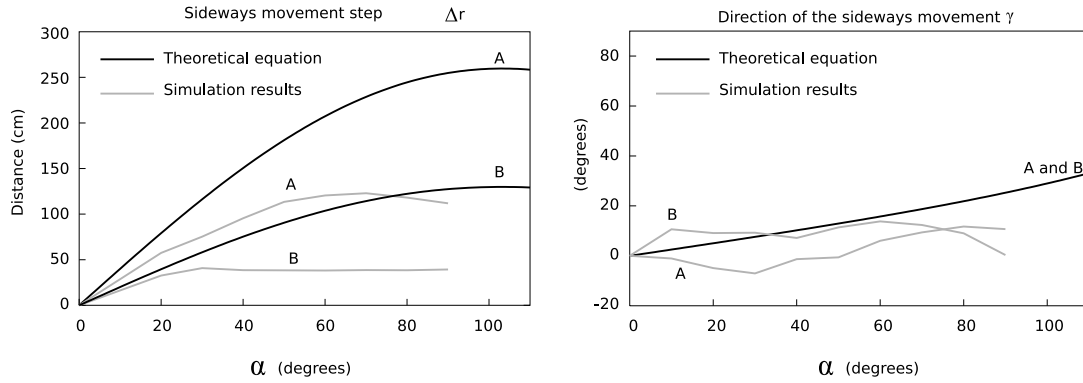


Figure 7.35: Experiment 19: Comparison between the step for the working points A and B

the values of the simulation are below the theoretical ones. The theoretical equation is calculated for the wired model and supposing that the supporting points remain fixed to the ground, nevertheless in the simulation of the hexahedric model this does not happen. The points slide.

7.4.3.4 Experiment 20: Simulation of Hypercube in the points C and D

The simulation of the sideways movement of an 8 module apodal robot in the working points C and D are shown in the figures 7.36 and 7.37.

7.4.3.5 Experiment 21: Movement of Hypercube in the points C and D

The sideways movement of the Hypercube robot in the working points C and D are shown in the figures 7.38 and 7.39.

7.4.3.6 Experiment 22: Comparison between simulation and a real robot

In this experiment the curves of the real robot's step are compared with the simulation for points C and D and they are compared with the theoretical curves. The results are shown in the figure 7.40.

7.4.3.7 Experiment 23: Inclined sideways movement

The simulation and real movement of the robot when the movement is of an inclined sideways type (point E) is shown in the figures 7.41 and 7.42.

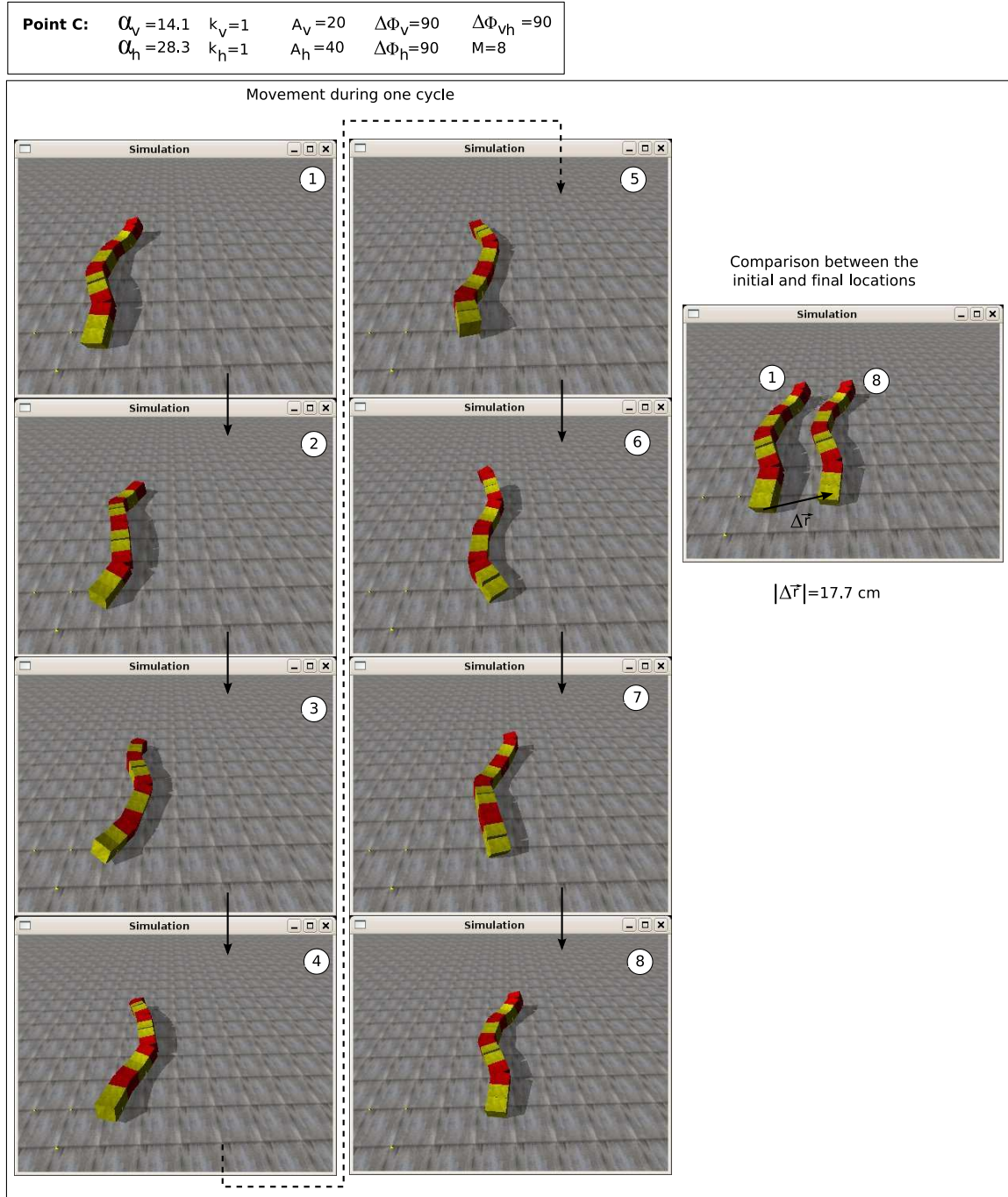


Figure 7.36: Experiment 20: Simulation of the sideways movement of the Hypercube robot for the working point C

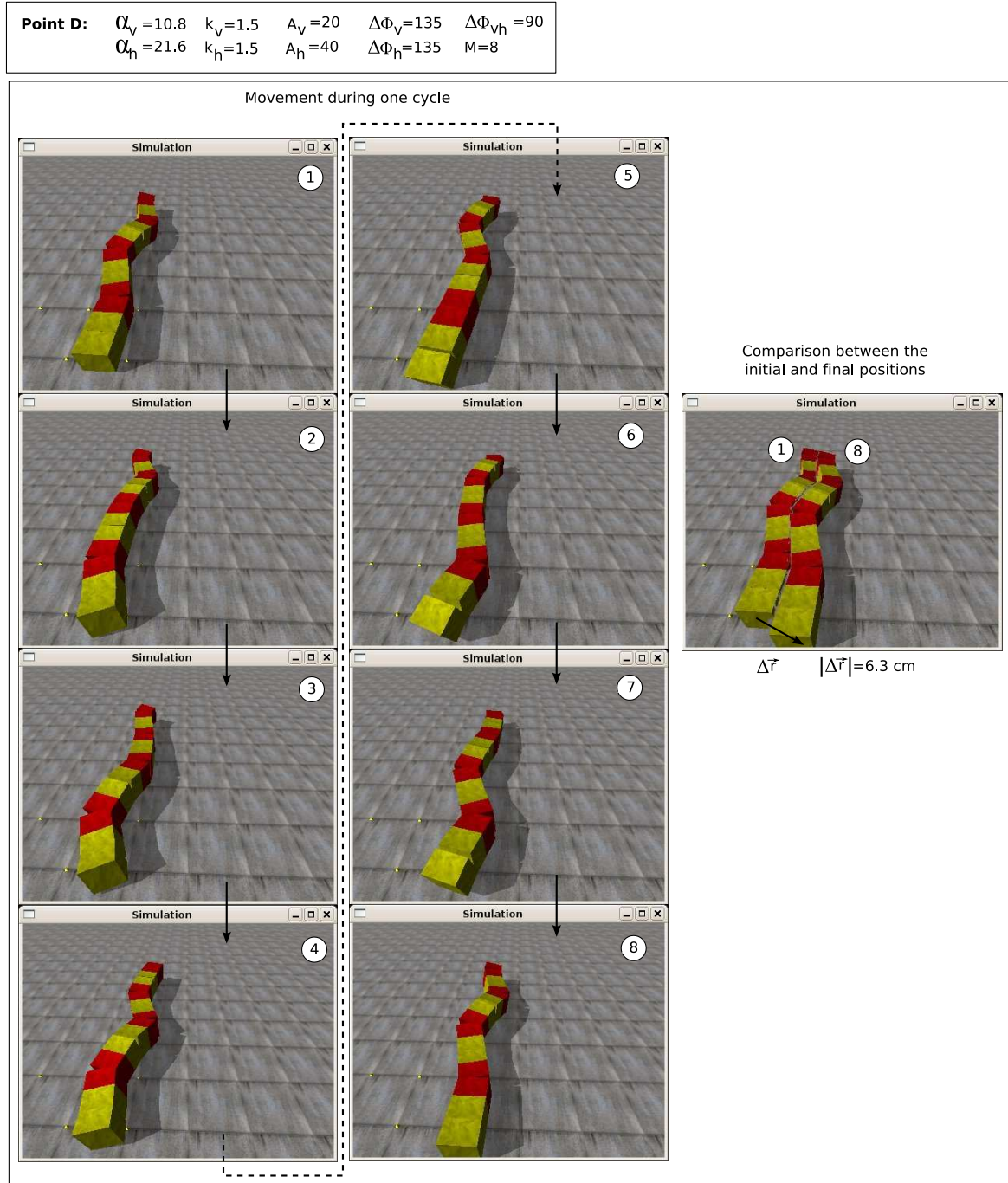


Figure 7.37: Experiment 20: Simulation of the sideways movement of the Hypercube robot for the working point D

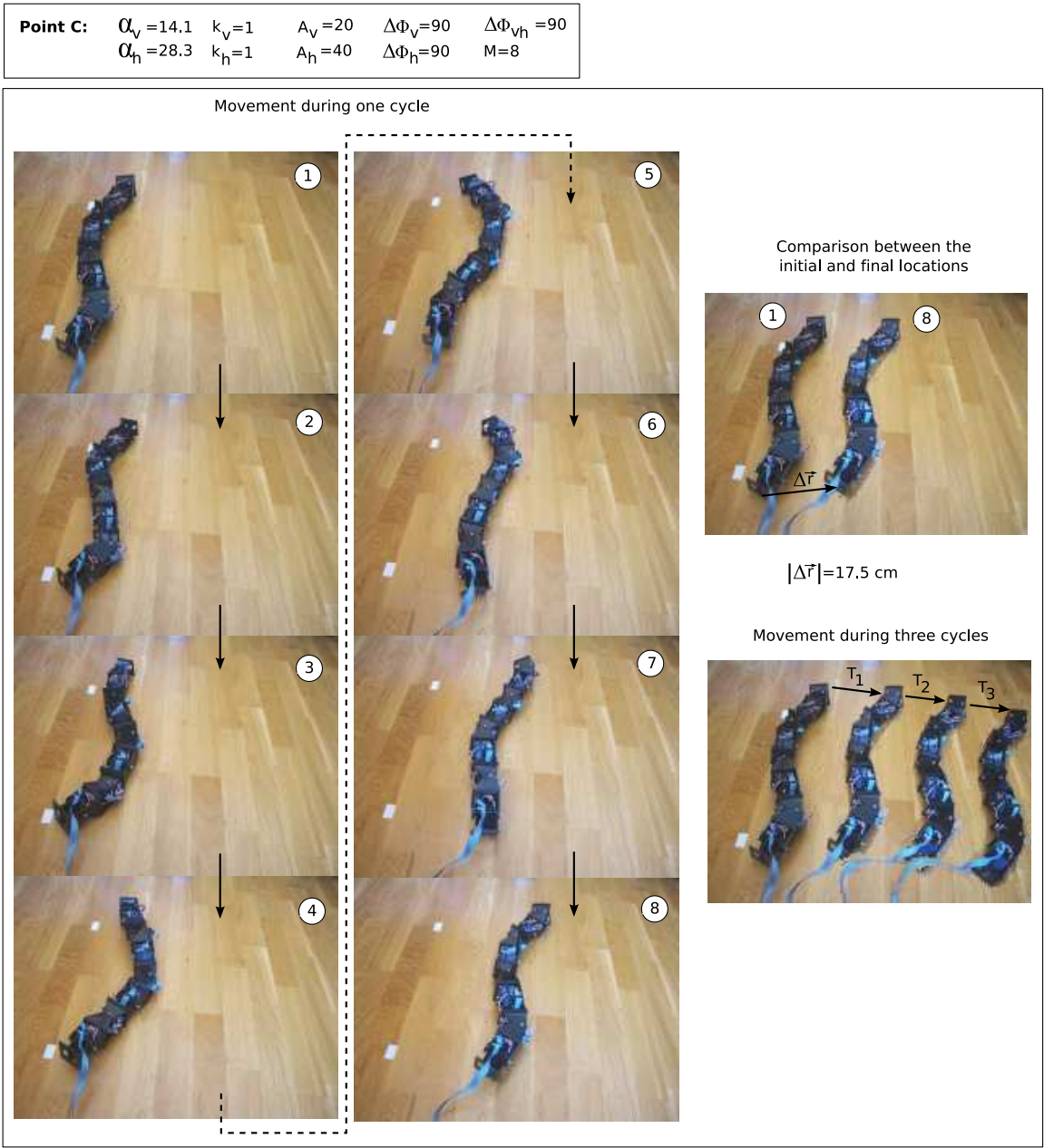


Figure 7.38: Experiment 21: Sideways movement of the Hypercube robot for the working point C

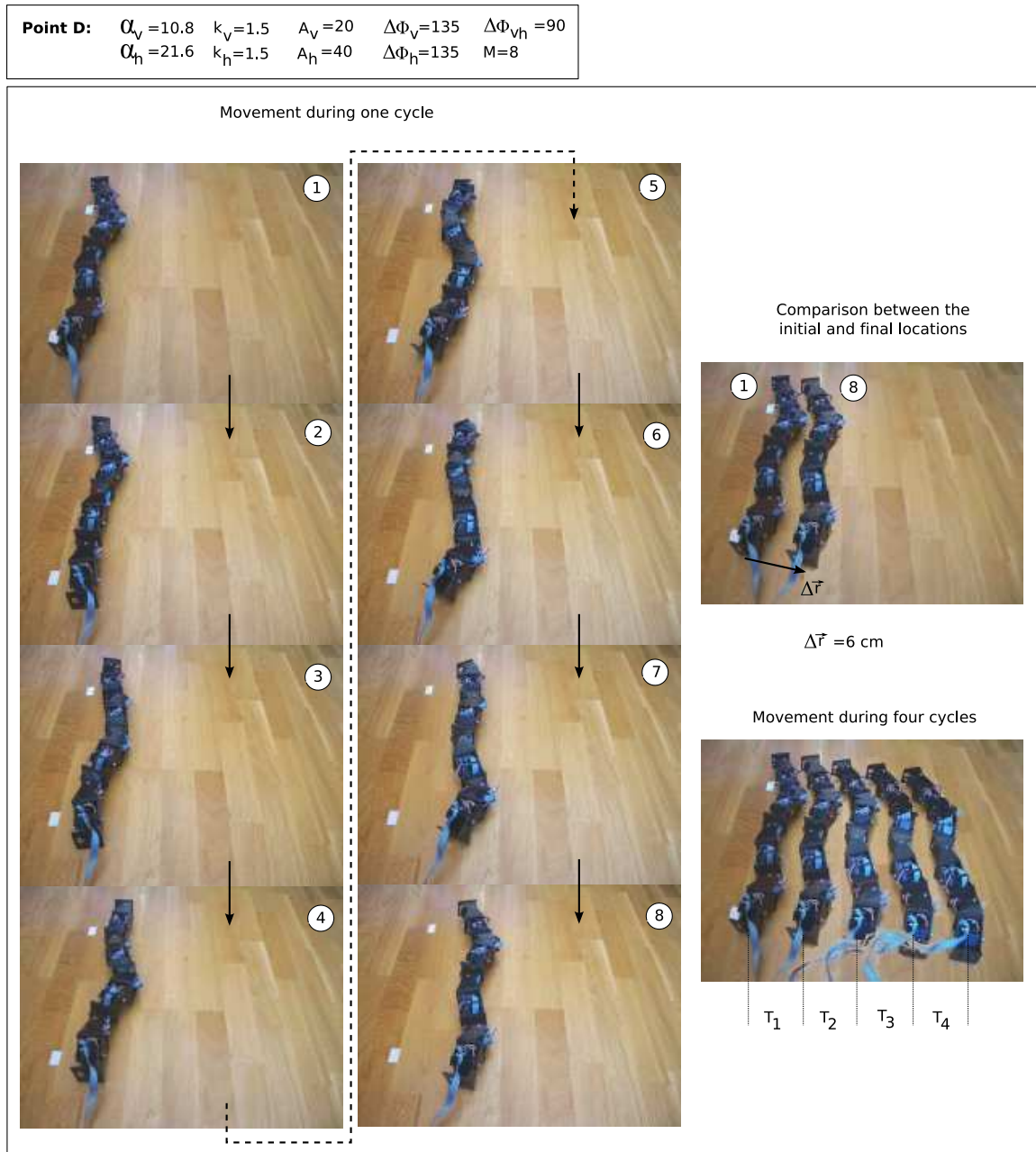


Figure 7.39: Experiment 21: Sideways movement of the Hypercube robot for the working point D

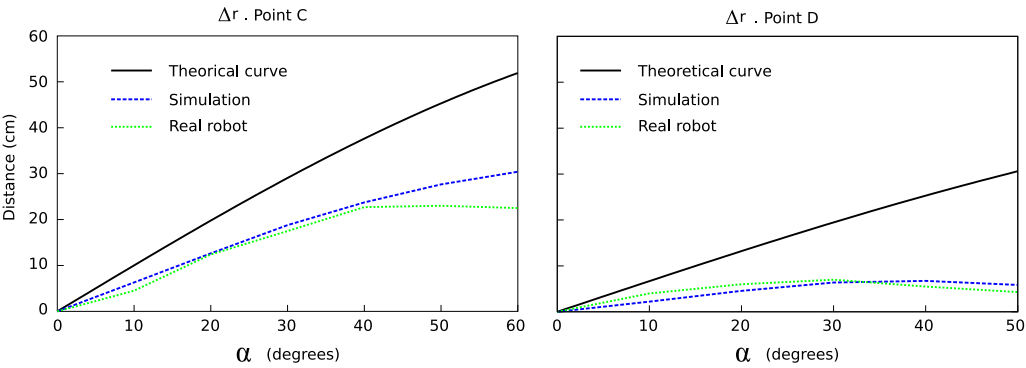


Figure 7.40: Experiment 22: Comparison between the simulation and locomotion of Hypercube

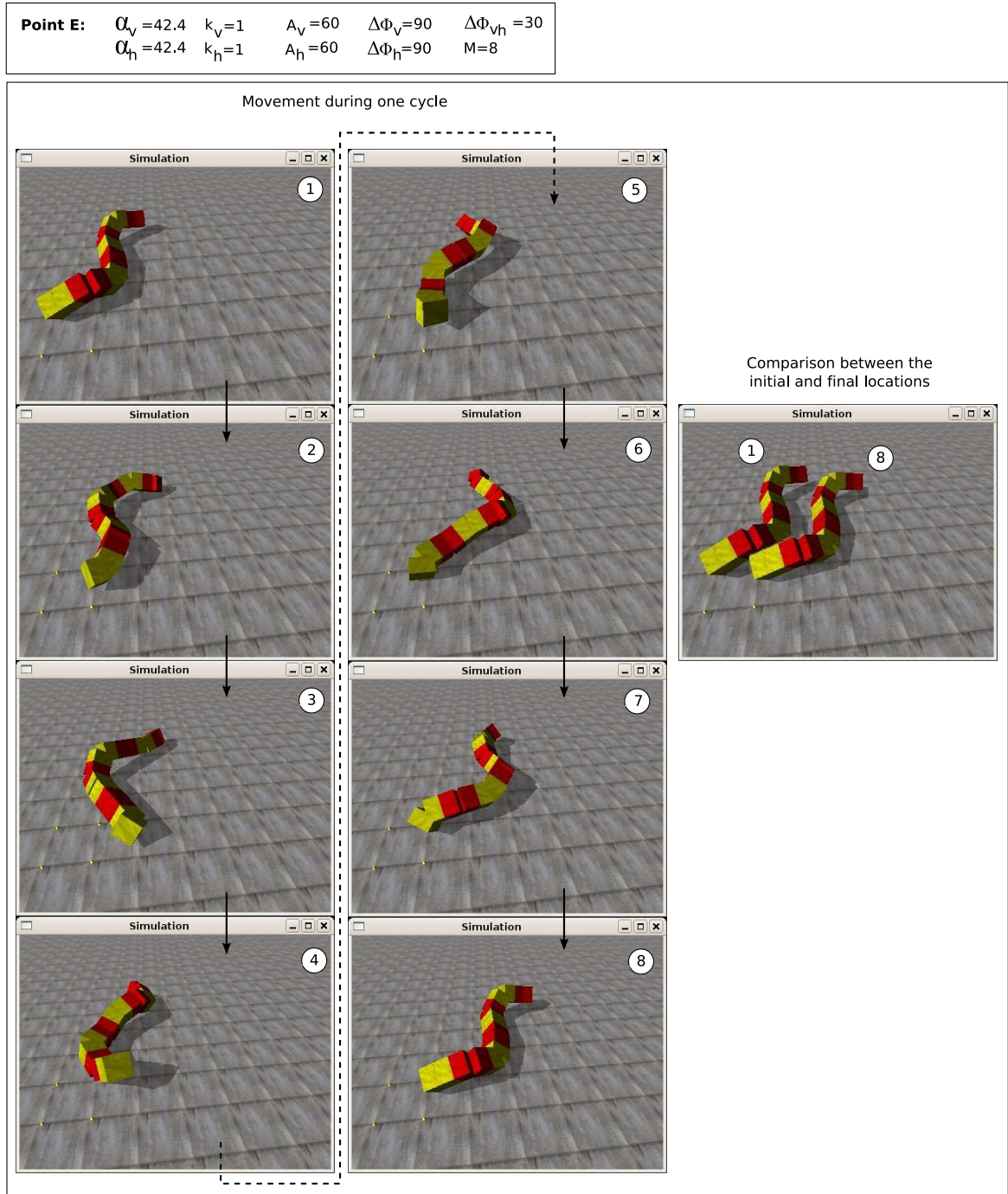


Figure 7.41: Experiment 33: Simulation of the inclined sideways movement of Hypercube for the working point E

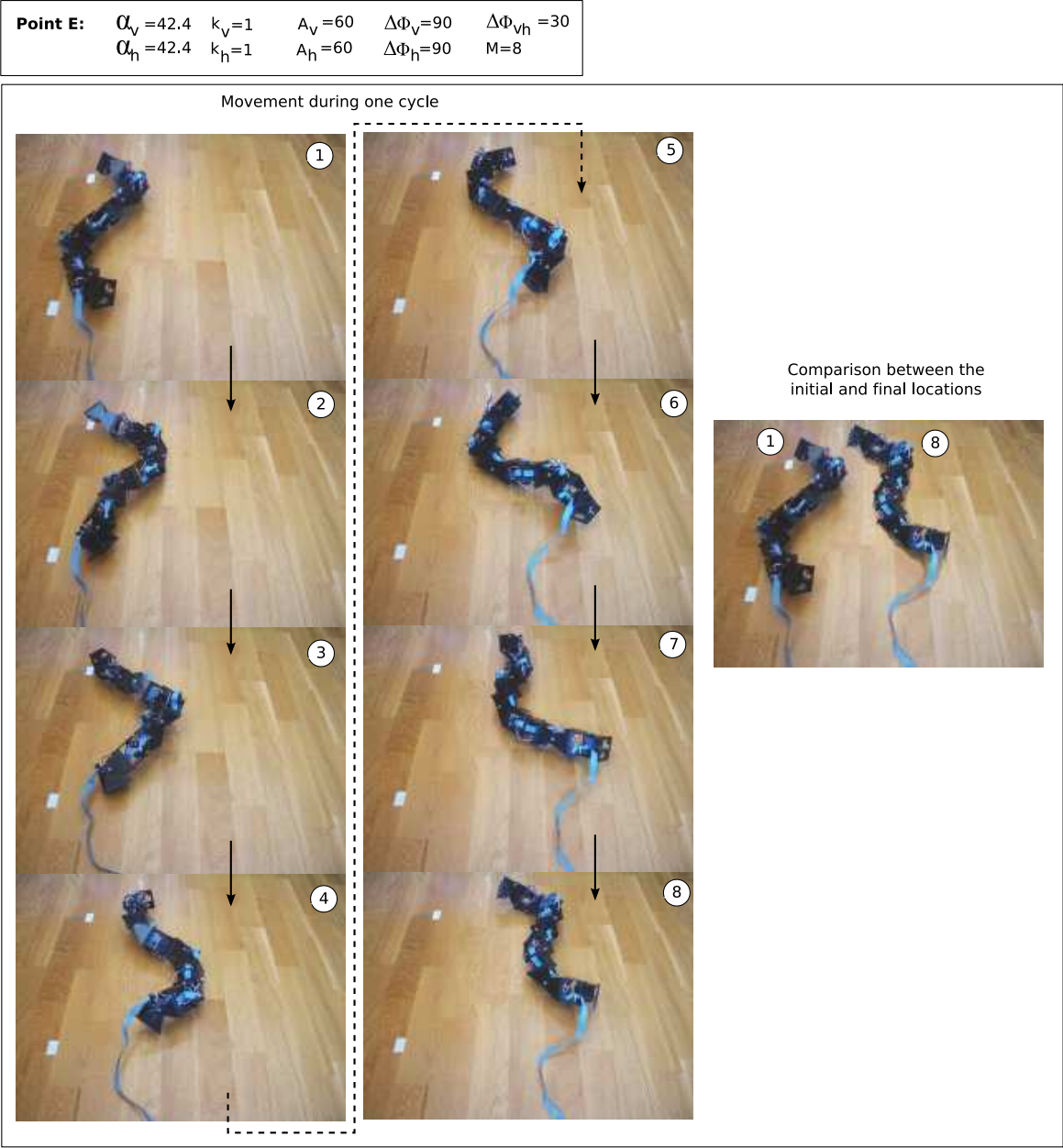


Figure 7.42: Experiment 23: Sideways movement of Hypercube for the working point E

Working point	M	α_v	k_v	A_v	$\Delta\phi_v$	α_h	k_h	A_h	$\Delta\phi_h$	$\Delta\phi_{vh}$
Point A	32	13.1	4	10	90	52.3	2	40	45	0
Point B	32	12.8	2	5	45	51.3	1	20	22.5	0
Point C	8	15	2	30	180	20	1	40	90	0
Point D	8	5.3	1.6	10	140	34	0.8	40	70	0

Table 7.7: Working points used for the experiments on rotation

7.4.4 Rotation

7.4.4.1 Working points

All the working points used in the experiments of sideways movement are shown in the table 7.7. The points A and B are for simulation of a 32 module apodal robot and B and C for one of 8 modules.

7.4.4.2 Experiment 24: Path of movement in the points A and B

The paths of the centre of mass of a 32 module apodal robot in the xy plane when it rotates in the working points A and B are shown in the figure 7.43, for four periods. For each point two paths have been shown corresponding to the two directions of the propagation of the corporal wave. It can be seen that when the direction of propagation is changed the rotations are made in the opposite direction.

Also the angle of orientation of the central module has been shown. Initially 0 degrees is taken as reference. This orientation oscillates, due to the yaw movement of the central module, but the average value increases with each cycle due to the rotation.

The movement in point B has a greater angular step. At the end of four periods the robot has rotated practically 360 degrees and the position of the centre of mass is very near to the initial position.

In the figures 7.44 and 7.45 8 instants are shown during the rotation in a cycle of the apodal robots, at the points A and B respectively.

7.4.4.3 Experiment 25: Variation of the angle of rotation with α

In the figure 7.46 the graph that relates the angular step rotated by the apodal robot to the winding angle α is represented. The data has been obtained from the simulation of a 32 module apodal robot, for the working points A and B. The tendency is for the angle of rotation to increase with α .

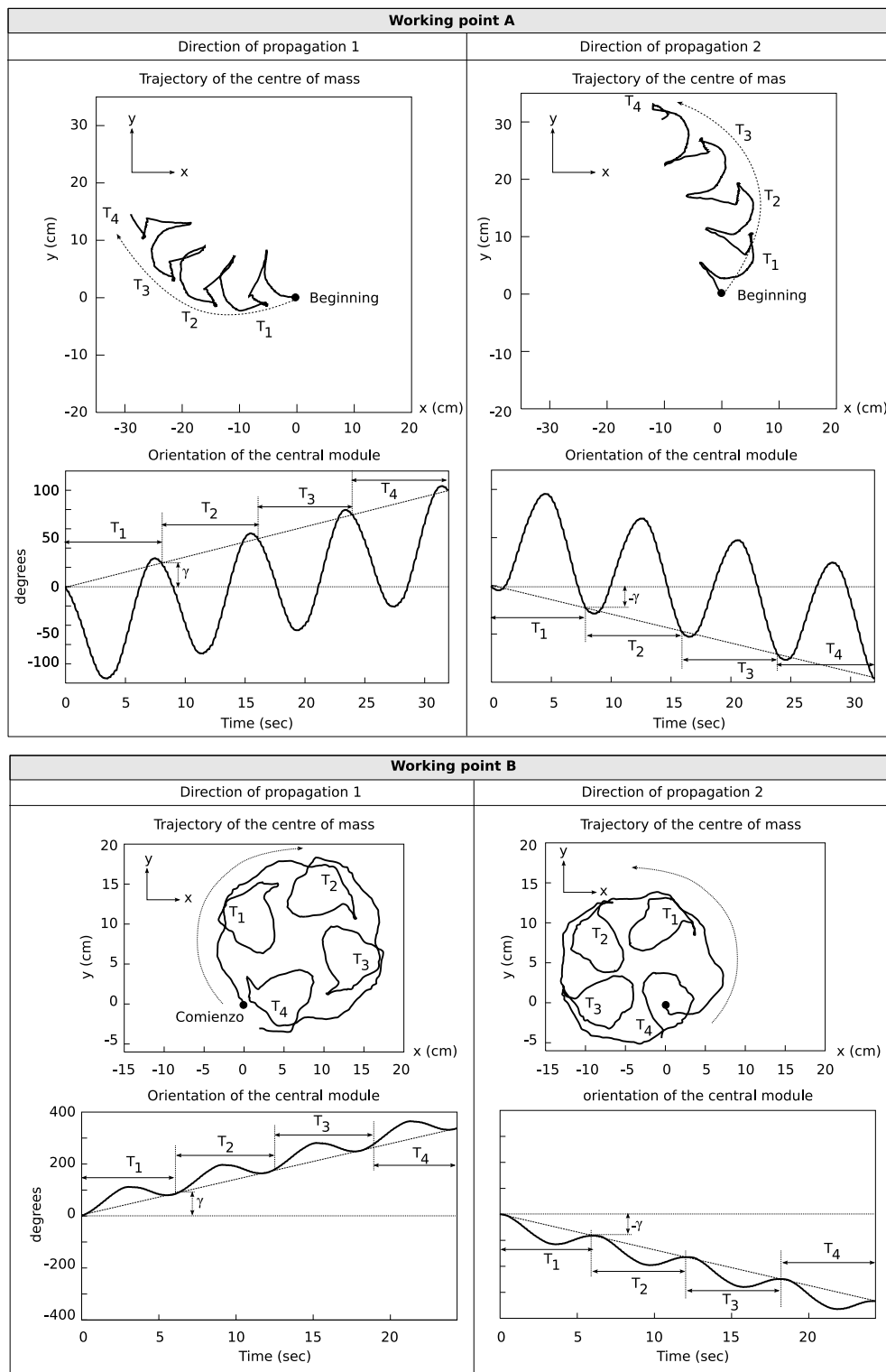


Figure 7.43: Experiment 24: Rotation of a 32 module apodal robot for the working points A and B

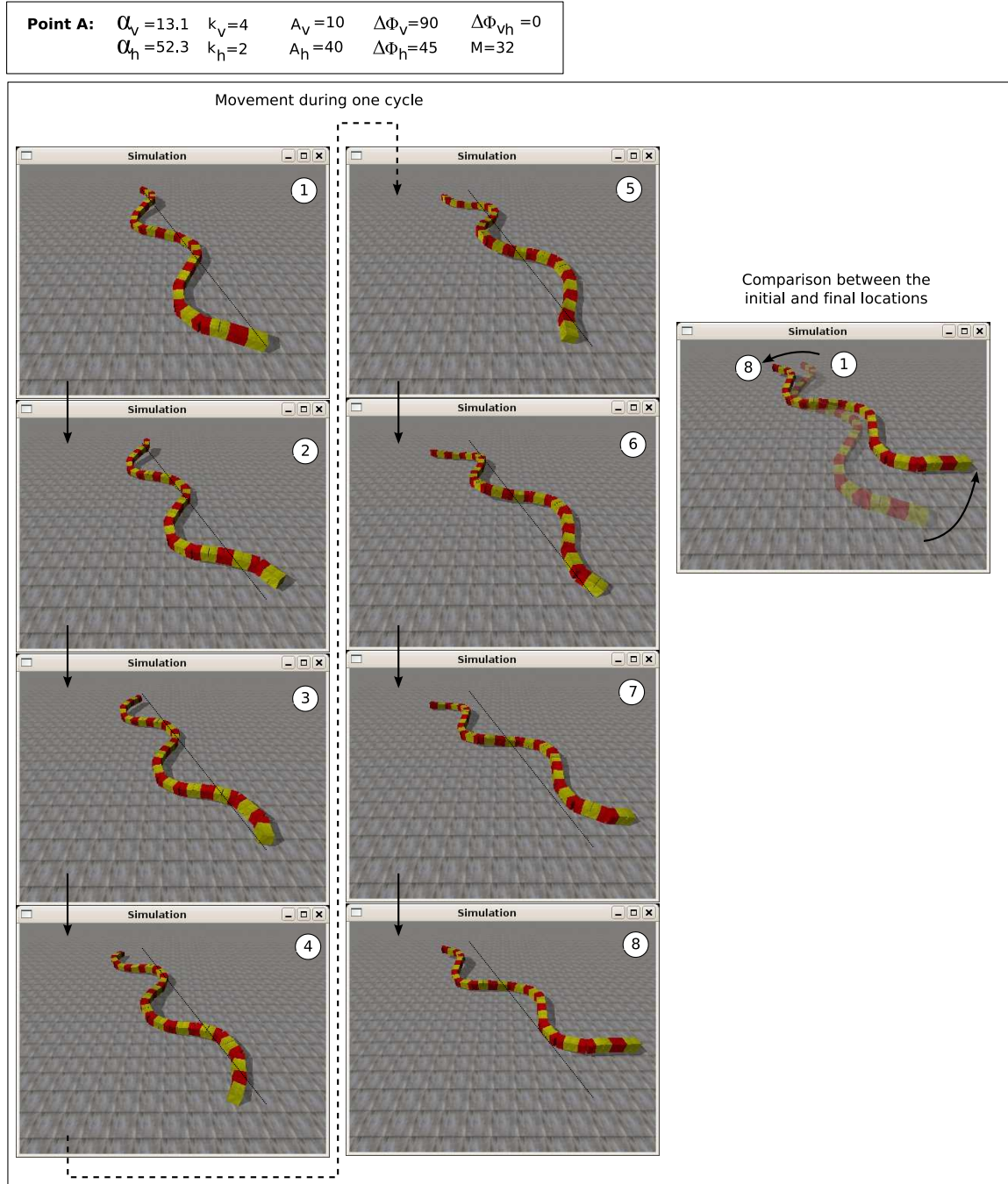


Figure 7.44: Experiment 24: Simulation of the rotation gait of a 32 apodal robot for the working point A

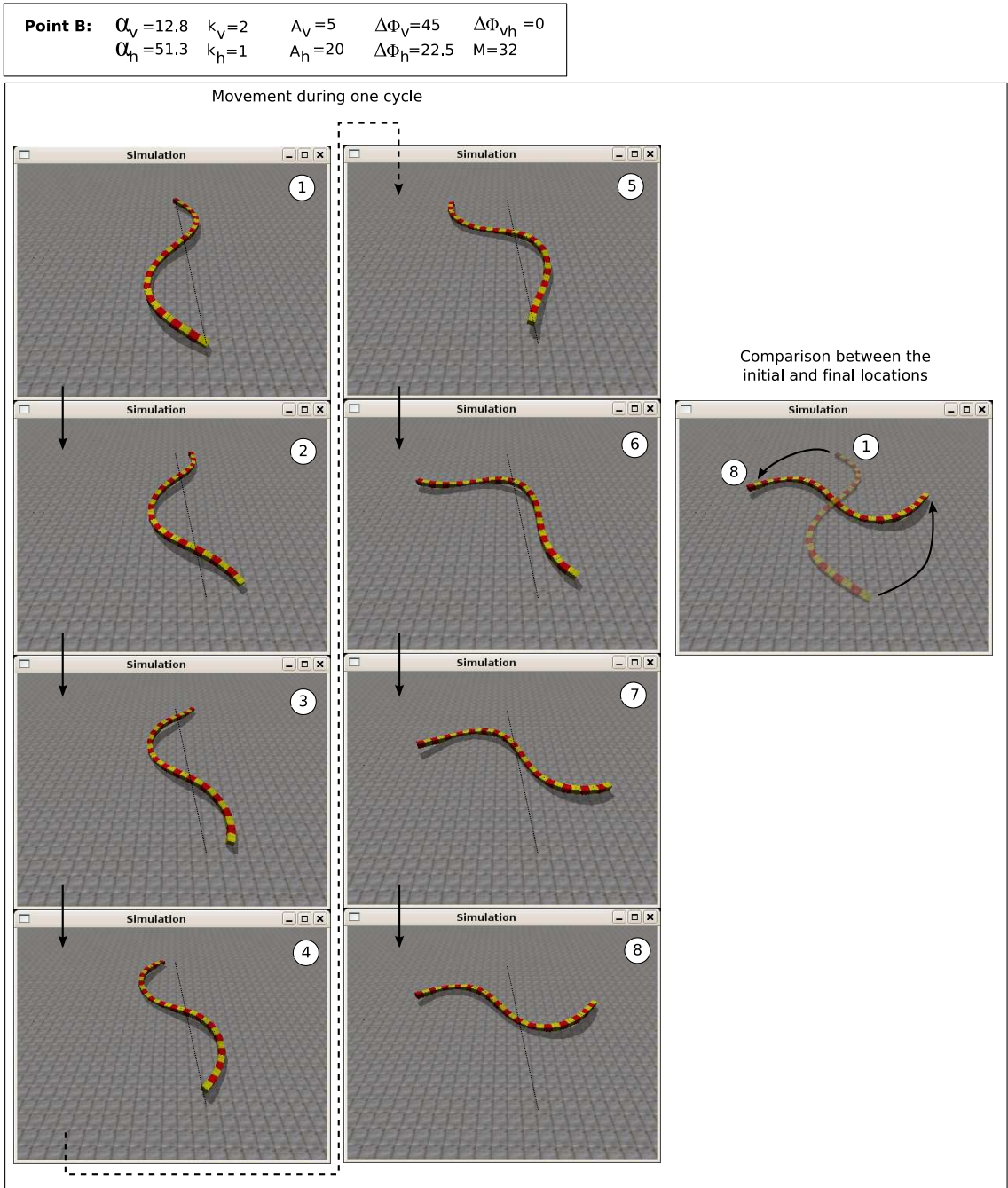


Figure 7.45: Experiment 24: Simulation of the rotation gait of a 32 apodal robot for the working point B

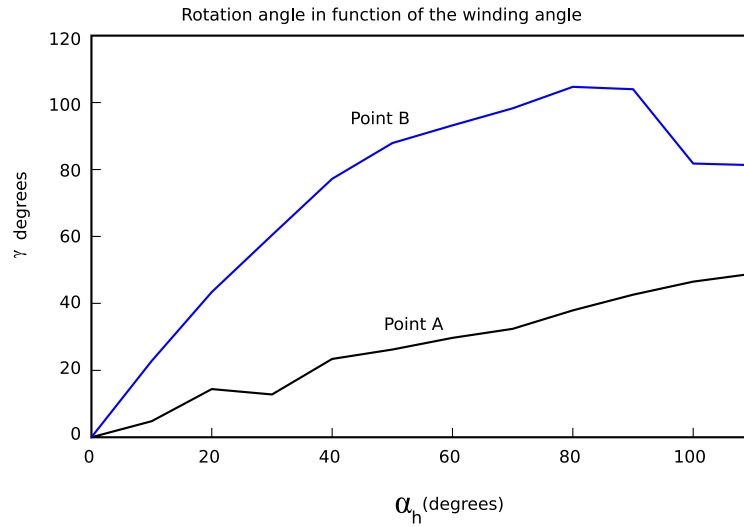


Figure 7.46: Experiment 25: Rotation angle in function of α

7.4.4.4 Experiment 26: Simulation of Hypercube

The simulation of the sideways movement of an 8 module apodal robot in the working points C and D is shown in the figures 7.47 and 7.48 respectively.

7.4.4.5 Experiment 27: Rotation of Hypercube

The rotation of the Hypercube robot in the points C and D is shown in the figures 7.49 and 7.50 respectively.

7.4.4.6 Experiment 28: Comparison between the simulation and the real movement of Hypercube

In the figure 7.51 the comparison of the results obtained of the simulation and the real movement of Hypercube in the working points C and D respectively are shown. In both the tendency is for angular step to increase when the winding angle is increased.

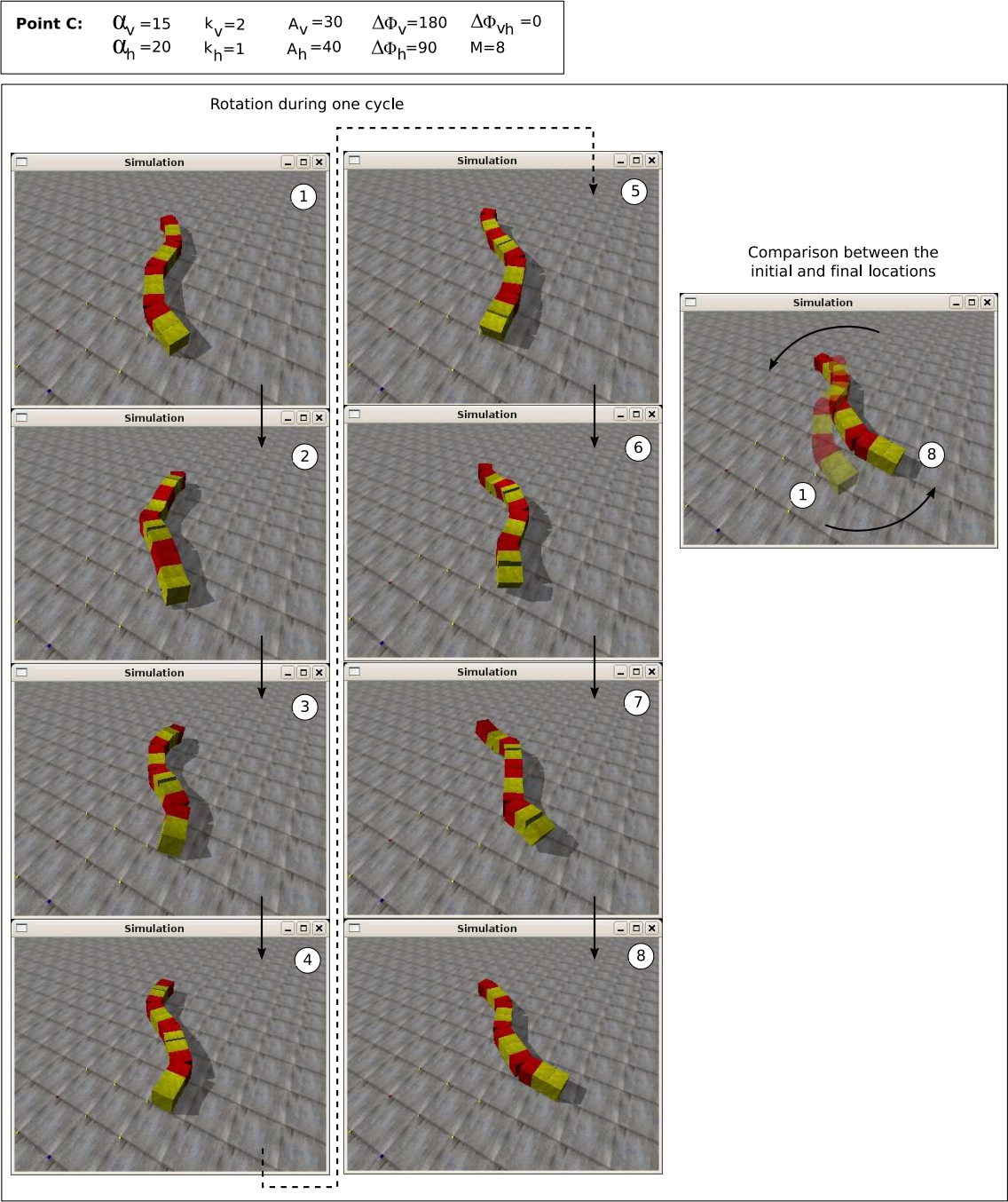


Figure 7.47: Experiment 26: Simulation of Hypercube in the working point C

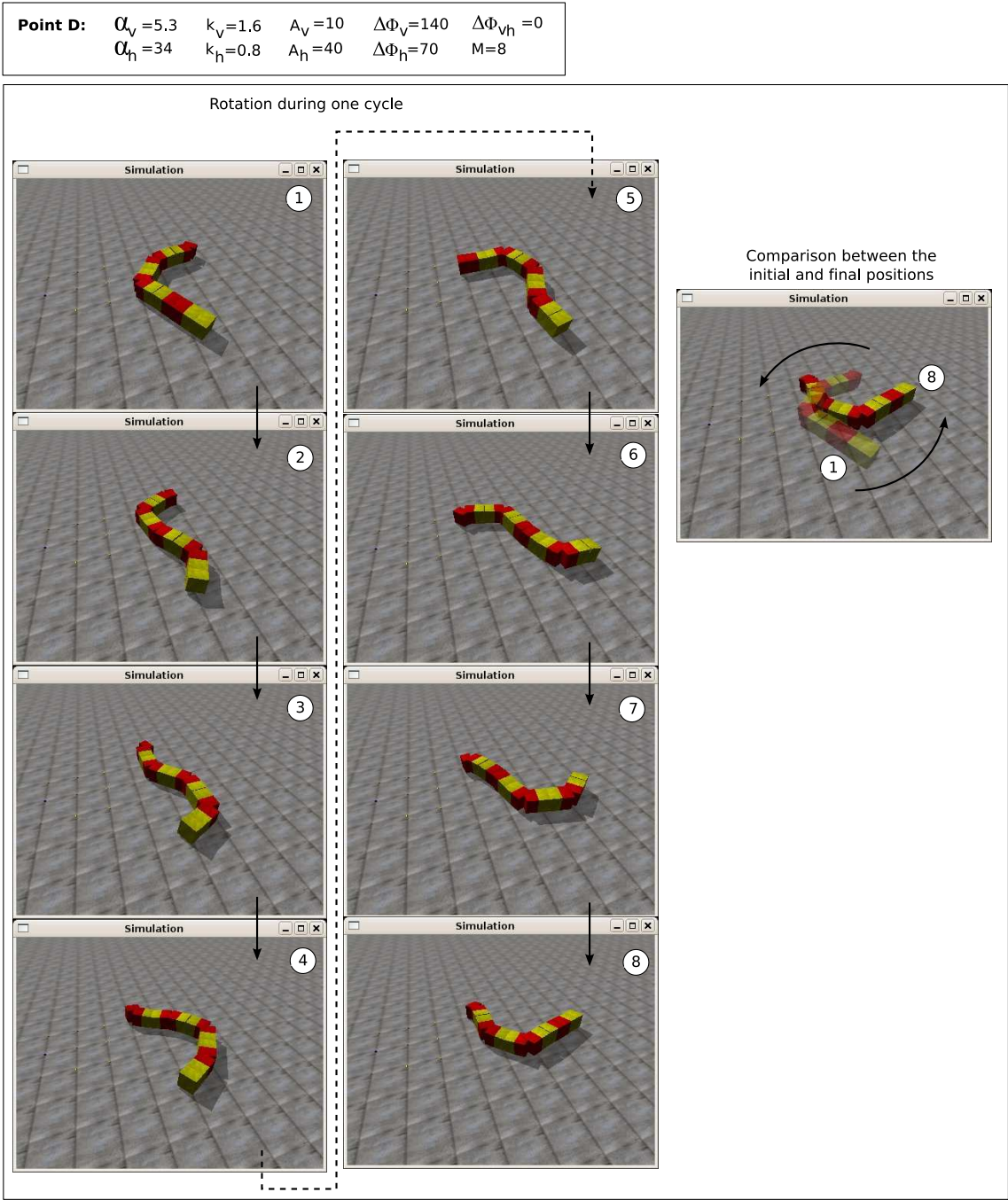


Figure 7.48: Experiment 26: Simulation of the rotation of Hypercube in the working point D

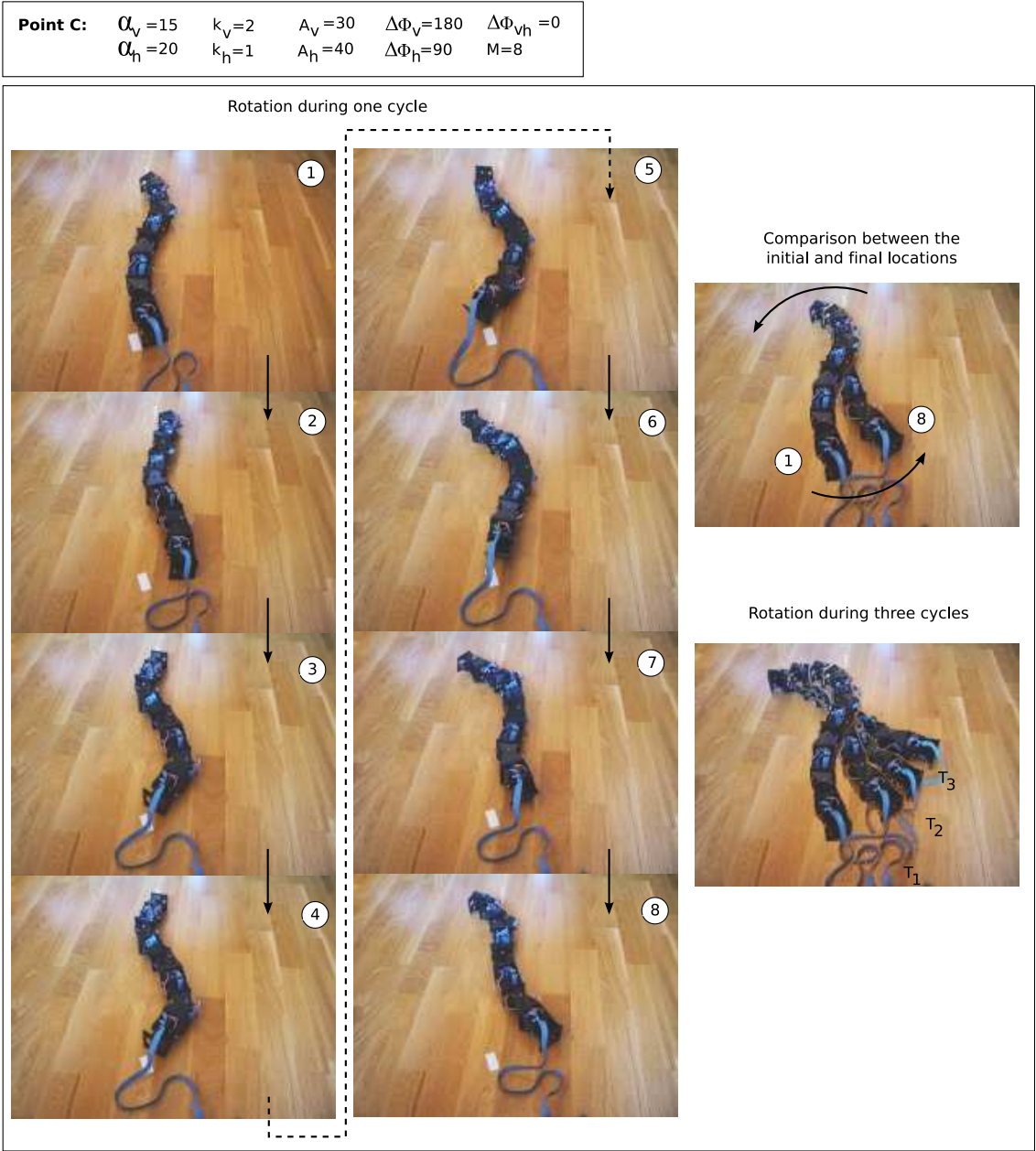


Figure 7.49: Experiment 27: Rotation of Hypercube in the working point C

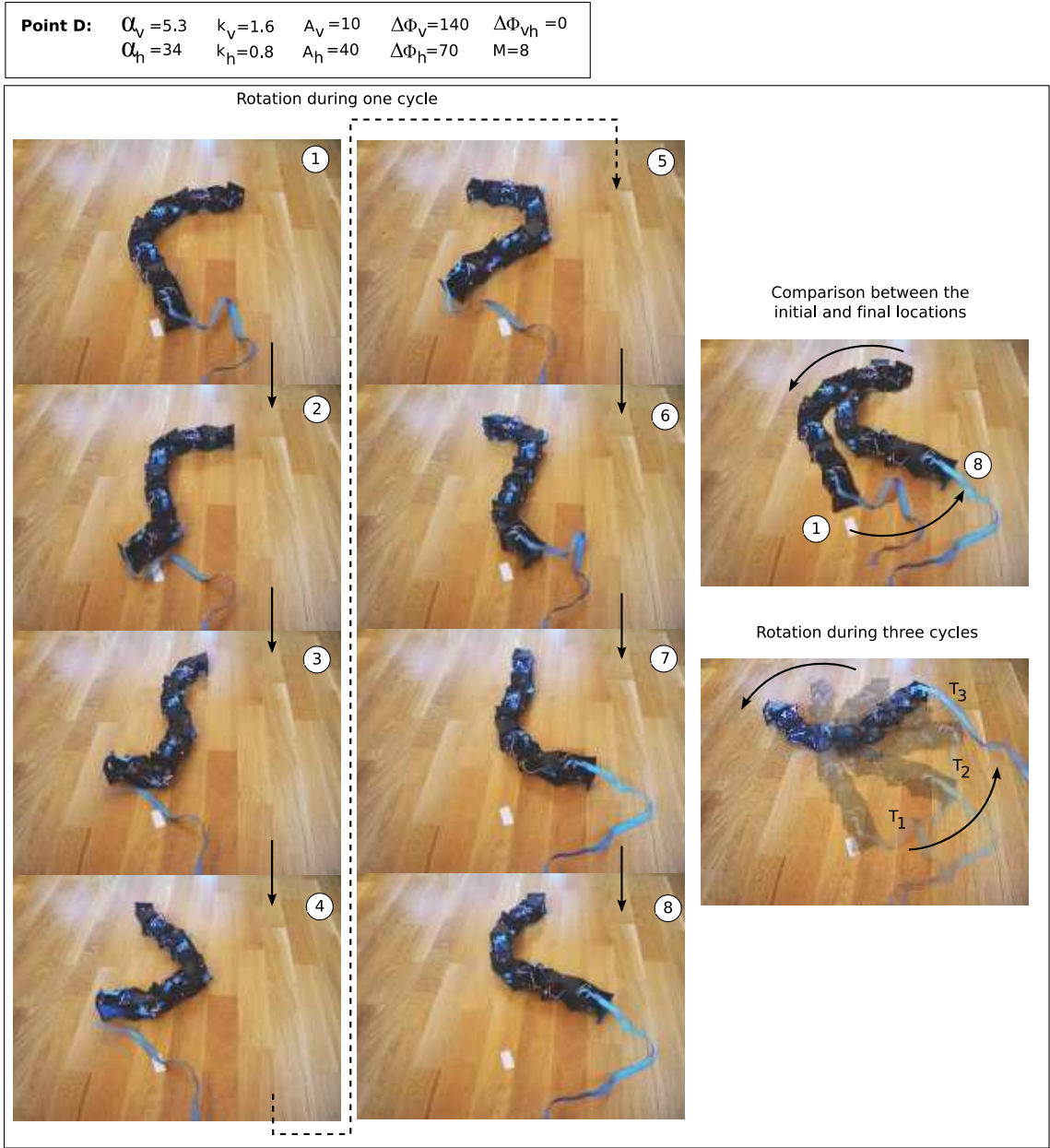


Figure 7.50: Experiment 27: Rotation of Hypercube in the working point D

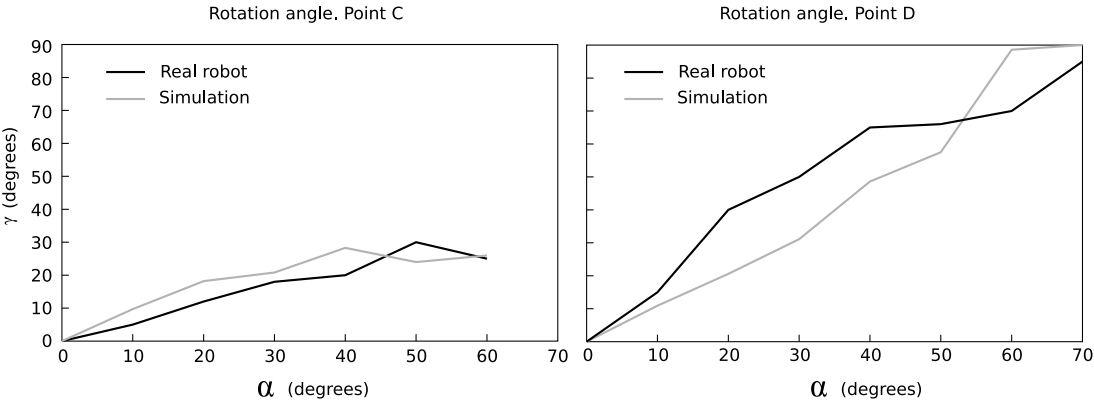


Figure 7.51: Experiment 28: Comparison between the simulated and real rotation gaits

Working points	M	α	A	$\Delta\phi_v$	$\Delta\phi_h$	$\Delta\phi_{vh}$
Point A	20	40	4	0	0	90
Point B	20	180	18	0	0	90
Point C	20	270	27	0	0	90
Point D	20	360	36	0	0	90
Point E	8	120	30	0	0	90
Point F	8	240	60	0	0	90

Table 7.8: Working points used for the experiments on rolling

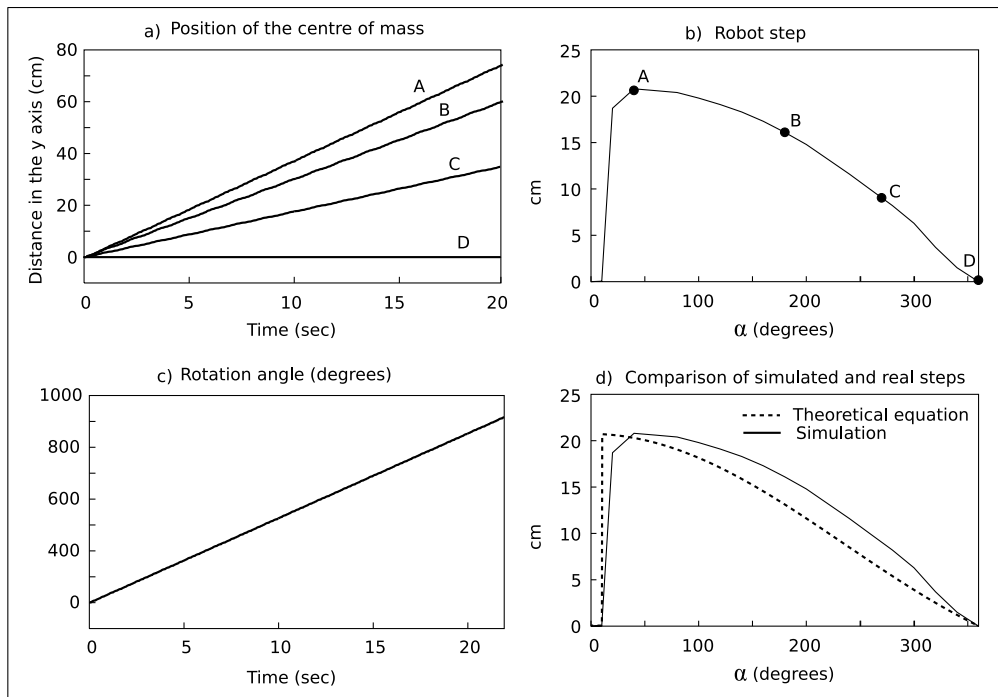


Figure 7.52: Experiment 29: Results of the simulation of a 20 modules apodal robot when rolling in the working points A,B,C and D

7.4.5 Rolling movement

7.4.5.1 Working points

The working points employed in the experiments of the rolling movement are shown in the table 7.8. The first four are for the simulation of a 20 module apodal robot and the E and the F for the movement and simulation of an 8 module Hypercube.

7.4.5.2 Experiment 29: Kinematics of the movement

In this experiment the rolling movement of a 20 module robot has been simulated in the working points A, B, C, and D. The results obtained are shown in the four graphs of the figure 7.52.

In the graph *a)* the distance travelled along the y axis and for the centre of mass of the robot in function of time, can be seen. It is observed that it deals with a uniform rectilinear movement, as had been obtained in the section 5.6.5.3. What is more, the speed of the movement varies with the parameter α . The point A is that which has an α less and is that which moves with greater speed. On the other hand, in the point D, α has a maximum value of 360 and there is no movement.

The robot rolls with a constant angular velocity. Given that the period in all the working points is the same, the angular velocity of gyration is the same for all. The angle that it rotates around its corporal axis in function of time is shown in the graph *c)*. It is the same for all the working points. In the point D, the robot rolls, but it does not advance.

The variation of the robot's step with α is shown in *b)*. On the curve the steps given in the selected working points have been represented. In the lower graph (*d*) these experimental values are compared with those obtained by the step equation (eq. 5.16).

Given that the simulated robot has a square section, the movement is only realised when α is greater than α_{min} , where this minimum value is given by the equation 5.21. For the robot of the experiment, of 20 modules, the square section of the side $H = 5.2cm$ and length of the module $L = 7.2cm$, the α_{min} has a value of 12.3 degrees. The experiments confirm that for lower values the robot does not roll.

In the figures 7.53 and 7.54 the screenshots of the movement in the different working points are shown.

7.4.5.3 Experiment 30: Simulation and movement of Hypercube

In the figures 7.55 and 7.56 Hypercube is shown at different moments during the rolling gait, for the working points E and F respectively. Both the simulations and the real movement of the robot have been carried out.

7.4.5.4 Experiment 31: Comparison between the real movement and the simulation of Hypercube

In the figure 7.57 the comparison of the robot's step in function of α with the simulation and the theoretical equation is shown. First it is noted that the value of α_{min} of the simulation and the theory

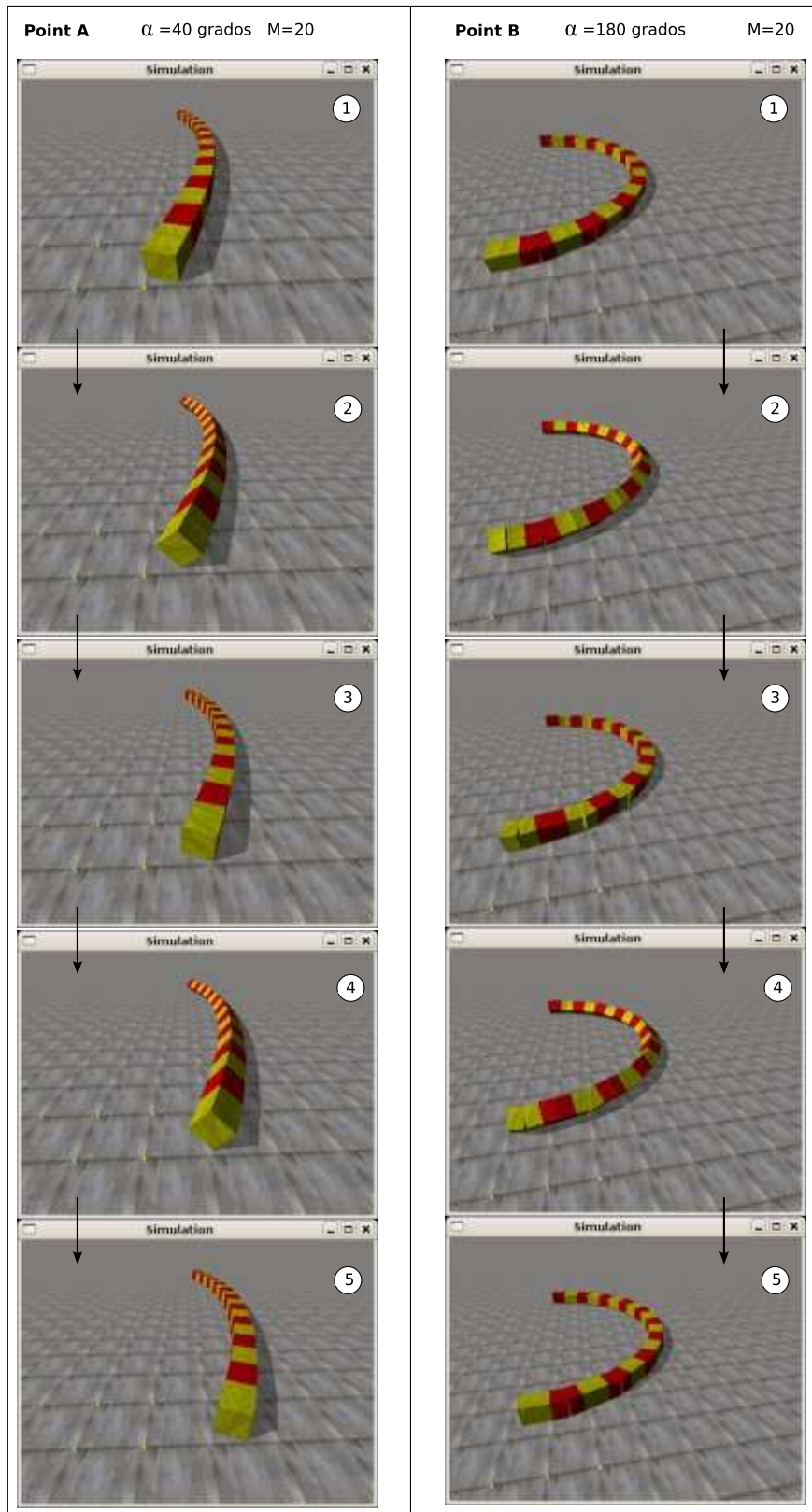


Figure 7.53: Experiment 29: Rolling gait of a 20 modules apodal robot for the working points A and B

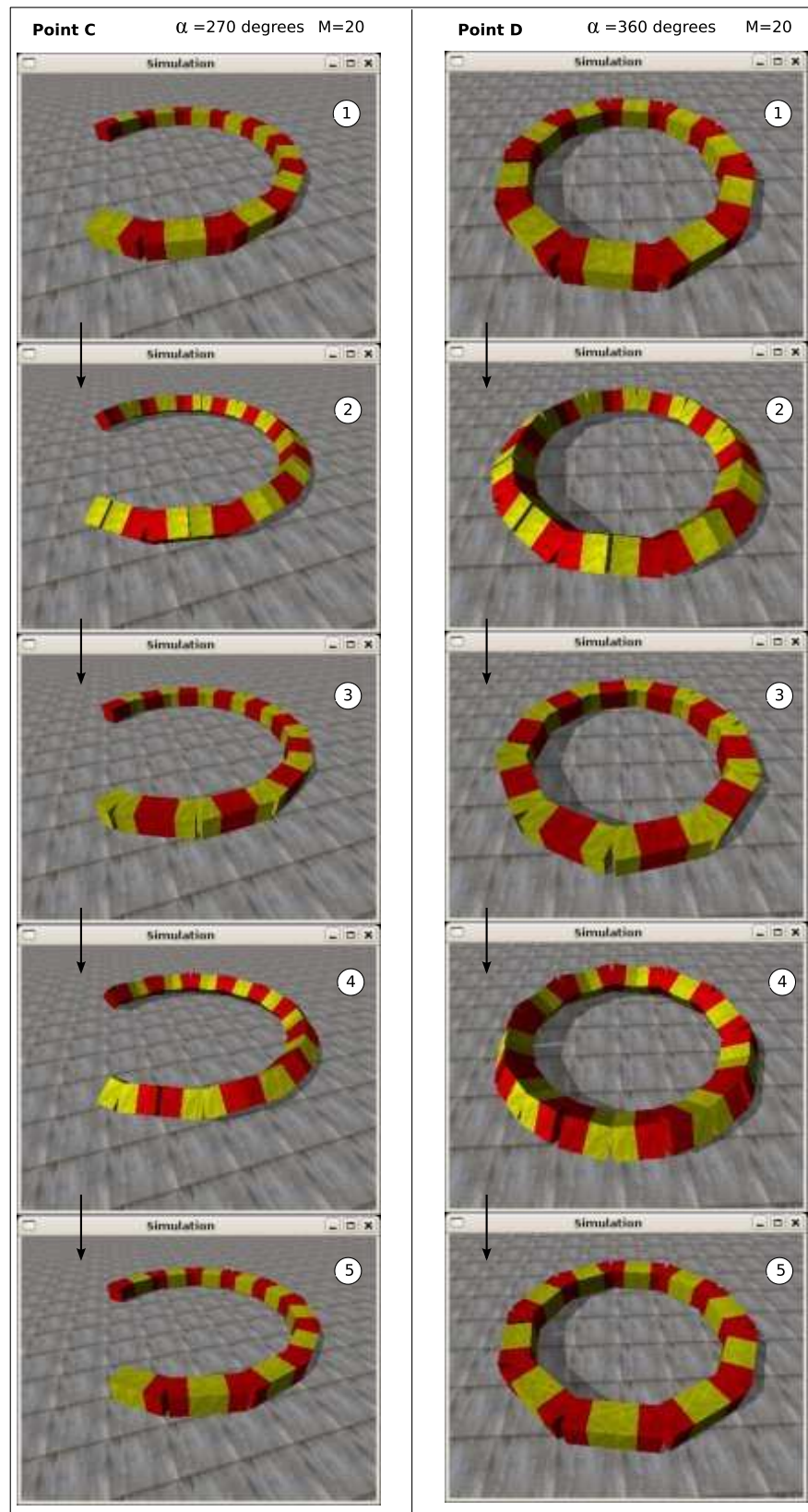


Figure 7.54: Experiment 29: Rolling gait of a 20 modules apodal robot for the working points C and D

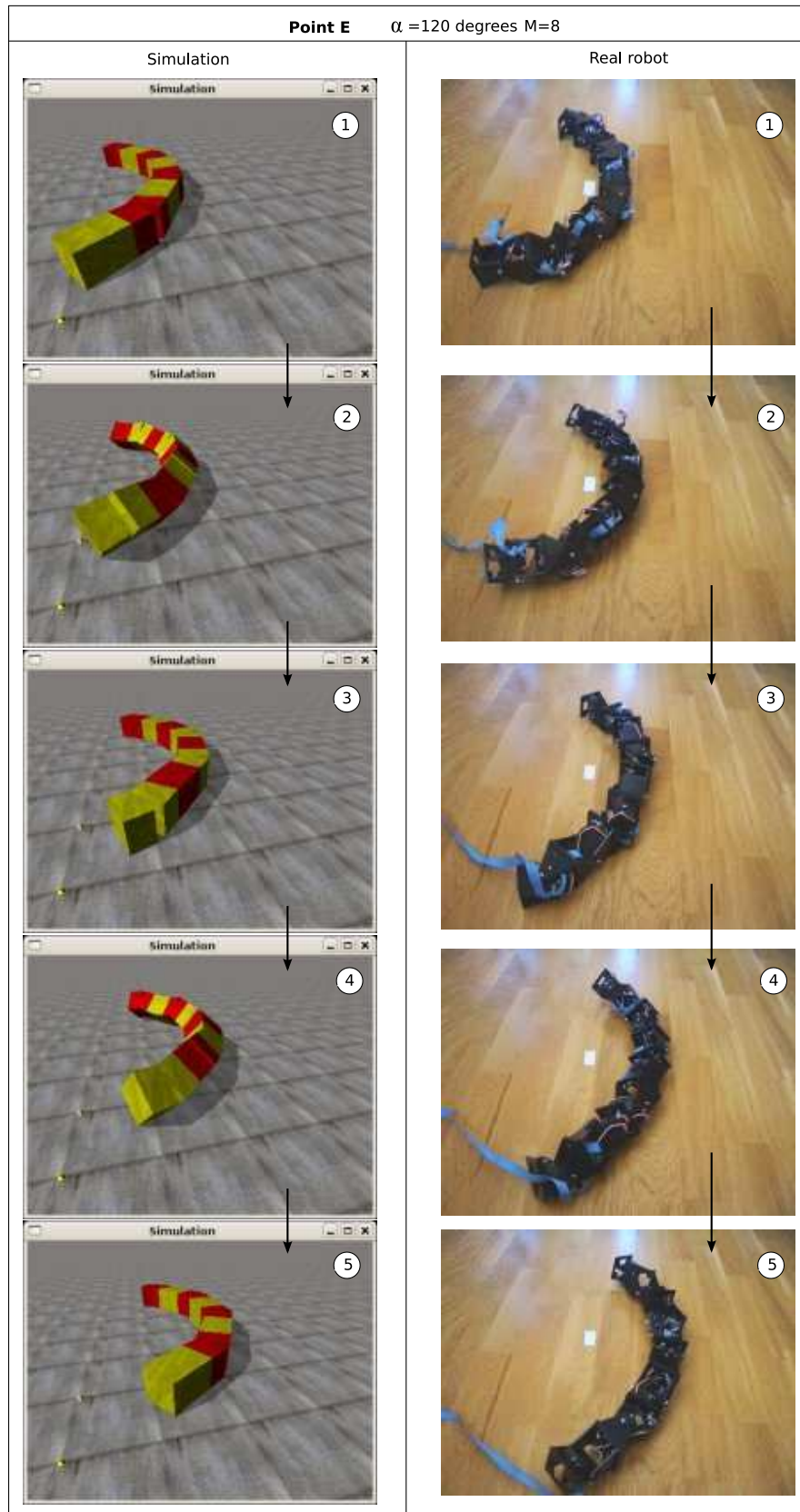


Figure 7.55: Experiment 30: Rolling gait and its simulation in Hypercube, for the working point E

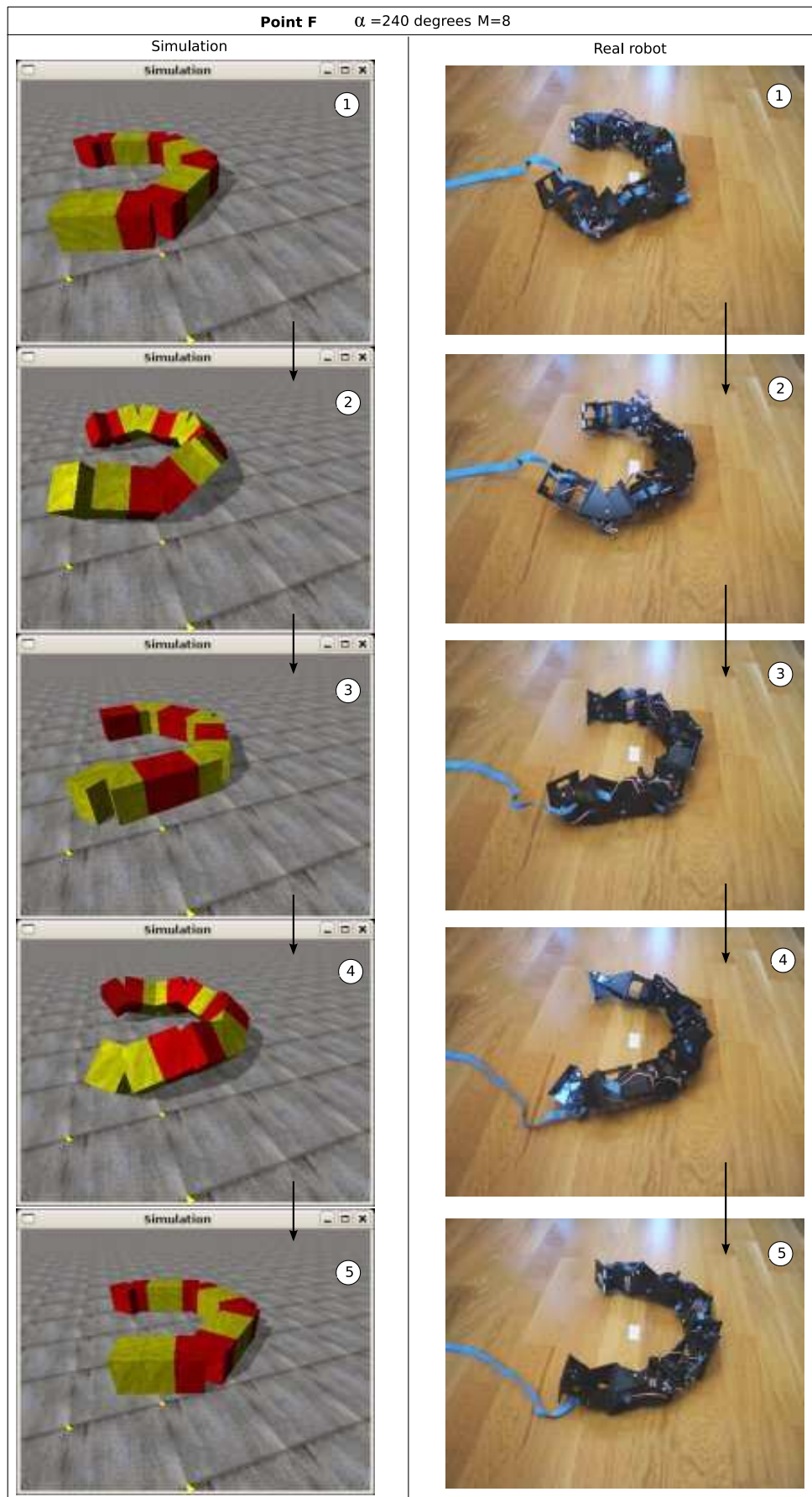


Figure 7.56: Experiment 30: Rolling gait and its simulation in Hypercube, for the working point F

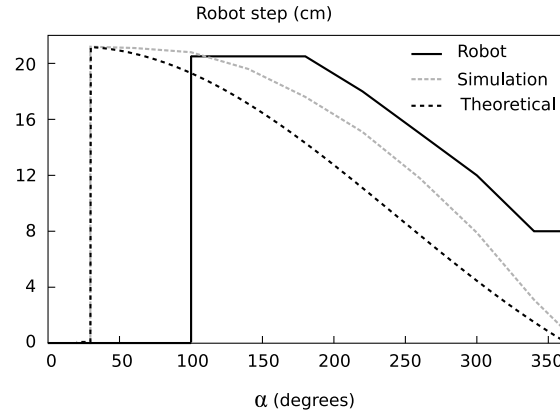


Figure 7.57: Experiment 31: Comparison between the step of the Hypercube Robot and its simulation and theoretical equations

coincide, nevertheless in the case of the real robot this value is greater. Greater amplitudes must be applied so that the robot begins to roll.

Secondly it is noted that the simulation and the real robot are above the theoretical curve. This is due to the fact that the dynamics of the system has not been taken into account. Once the robot begins to roll it acquires an inertia that causes the step to be greater than in the theoretical case, in which only the geometry has been taken into account for its calculation.

It is noted that the variation of the incline of the step in function of α is similar in the three cases.

Points	M	α_v	α_h	k_v	A_v	A_h	$\Delta\phi_v$
S_1	18	40	90	1.5	40	10	60
S_2	18	40	90	2	51	10	80
S_3	18	40	90	2.5	61	10	100
S_4	18	40	90	3	70	10	120
A	18	40	90	3	70	10	120
B	18	40	180	3	70	10	120
C	18	40	360	3	70	10	120
D	8	12	90	1.3	20	22	120
E	8	12	180	1.3	20	44	120
F	8	12	360	1.3	20	90	120

Table 7.9: Selected working points for carrying out the experiments on locomotion in a circular path

7.4.6 Circular path

7.4.6.1 Working points

The working points employed in the experiments of movement in the circular path are shown in table 7.8. The first four, $S_1 - S_4$ are used to test the stability of an 18 module robot, the following three, A, B, and C, are for the simulation of the turn of an 18 module apodal robot and the three last, D, E and F for the movement and simulation of an 8 module Hypercube.

7.4.6.2 Experiment 32: Stability during the turn

The aim of this experiment is to test the criterion of stability expounded in the section 5.5.4.1, according to which the circular path movement of a robot is always stable if the parameter k is greater than or equal to 3 (valid for the wired model). An 18 module apodal robot is simulated when it moves using the points $S_1 - S_4$. They are all equal, only k changes its value. To test the stability we measure the evolution of the angle of inclination (roll) of the robot with time. The results are shown in the figure 7.58. In the point S_1 ($k = 1.5$) the robot overturns. The angle of inclination decreases until it reaches a point of no return. In the point S_2 it does not overturn but there is a strong oscillation which causes the movement to be very abrupt. In S_3 the oscillation persists but is mitigated. Finally in S_4 , the inclination, while existing, does not affect the movement, being quite uniform. Values greater than k will cause the oscillation to diminish even more.

In the figure 7.59 the position of the robot for the three different phases is shown, in all the working points $S_1 - S_4$.

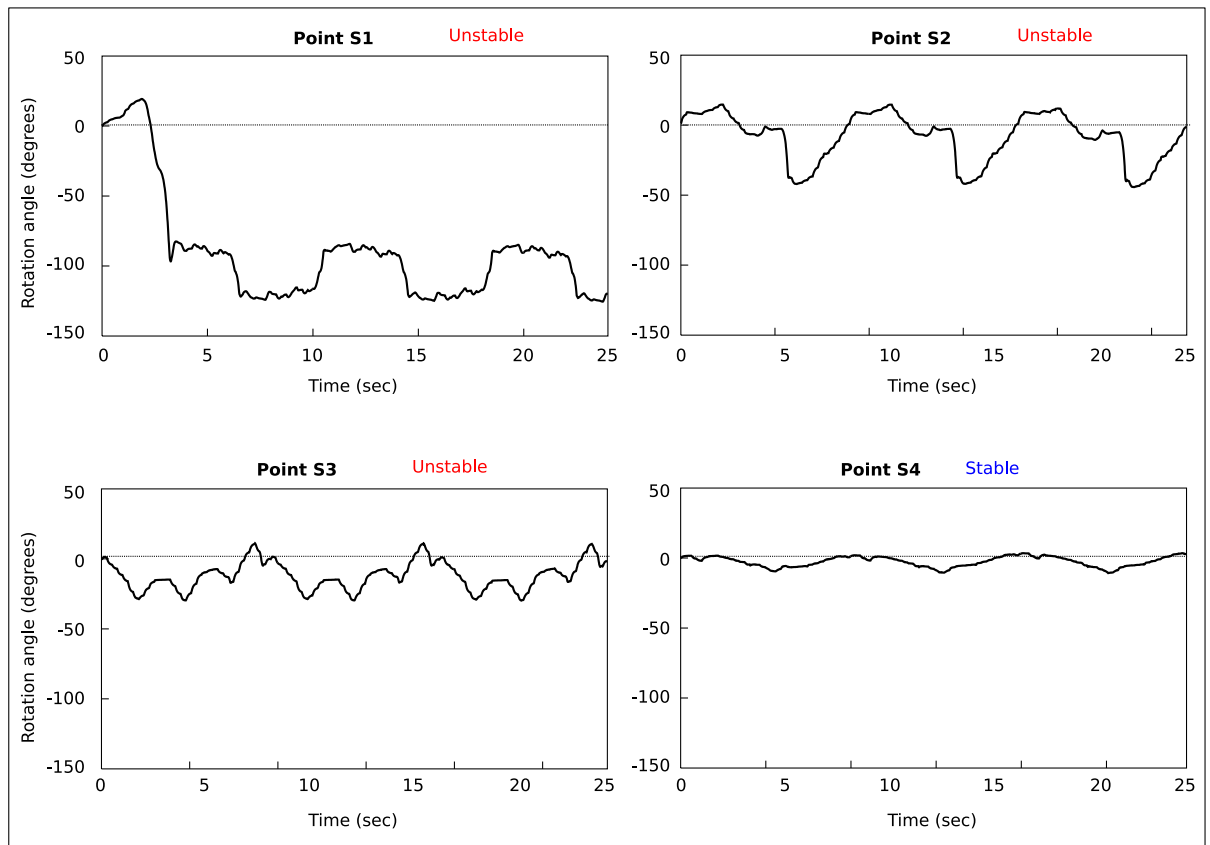


Figure 7.58: Experiment 32: Results of the stability tests. Inclination angle of the robot in function of time

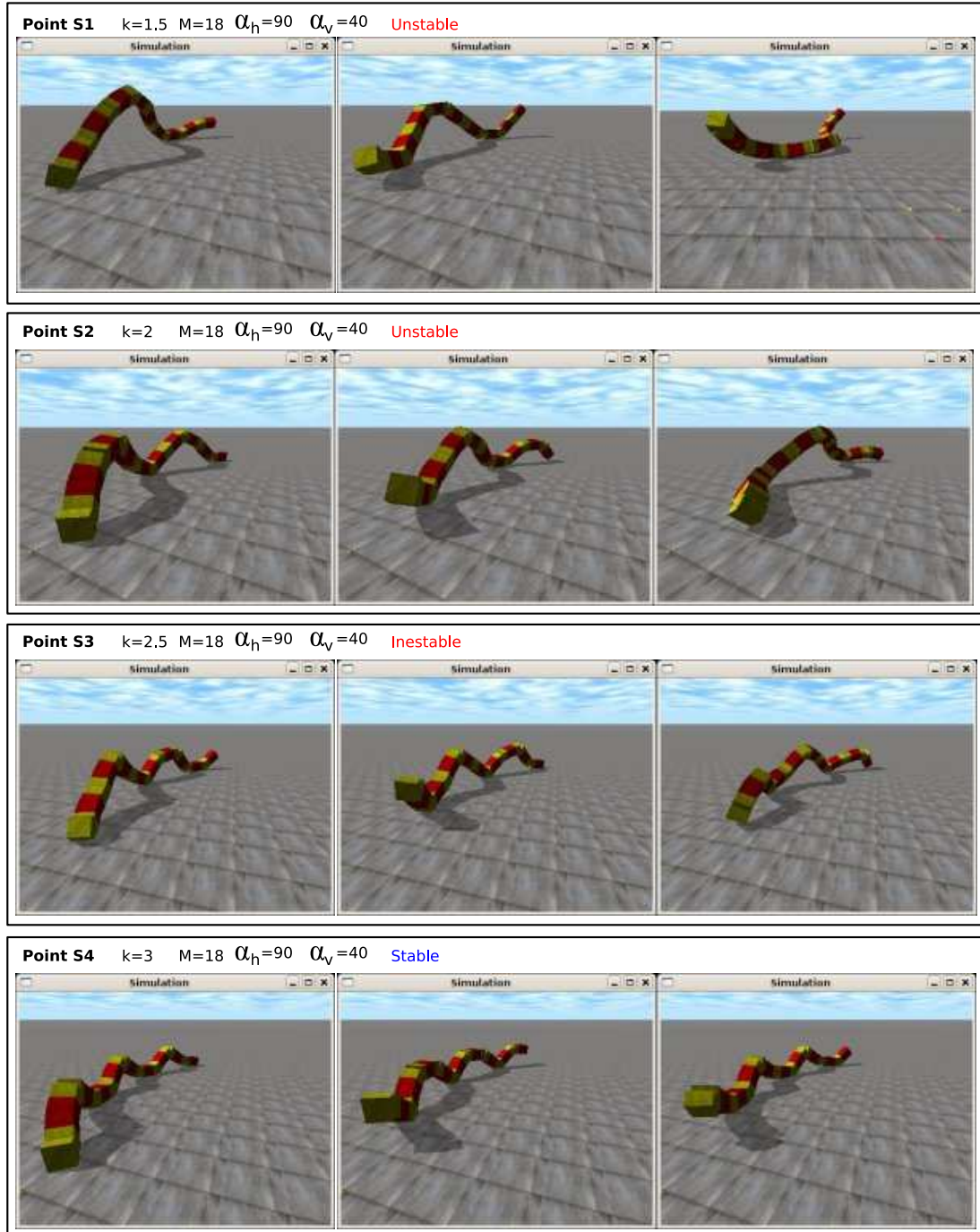


Figure 7.59: Experiment 32: Stability of the circular path gait of an 18 modules apodal robot for different values of k

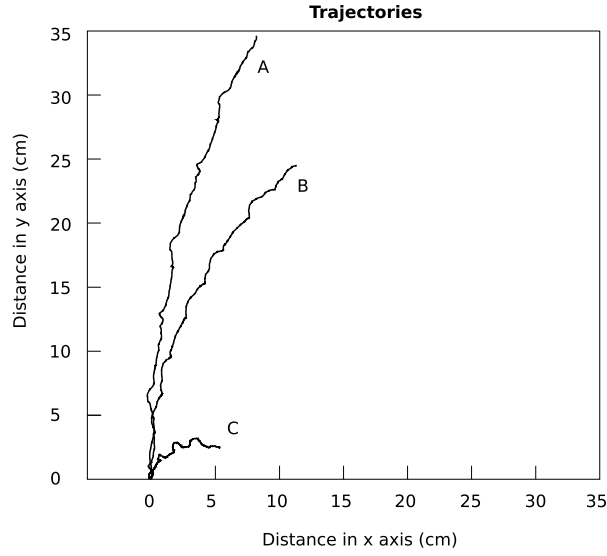


Figure 7.60: Experiment 33: Trajectory of the mid-point of an 18 modules apodal robot for the working points A,B and C

7.4.6.3 Experiments 33: Paths

In the figure 7.60 the positions of the mid-point of an 18 module robot is shown in function of time, for the working points A, B and C. It can be seen that the radius of turn is different according to the point.

In the figure 7.61 the screenshots that correspond to five moments during the movement in a cycle of the robot are shown for the three working points. To appreciate better the movement of the robot, in the figure 7.62 the positions of the robot in four cycles are shown, all of them corresponding to the same phase.

7.4.6.4 Experiment 34: Movement and simulation of Hypercube

The circular path movement of Hypercube as also its simulation in the working points D, E and F is shown in the figures 7.64 and 7.63 respectively.

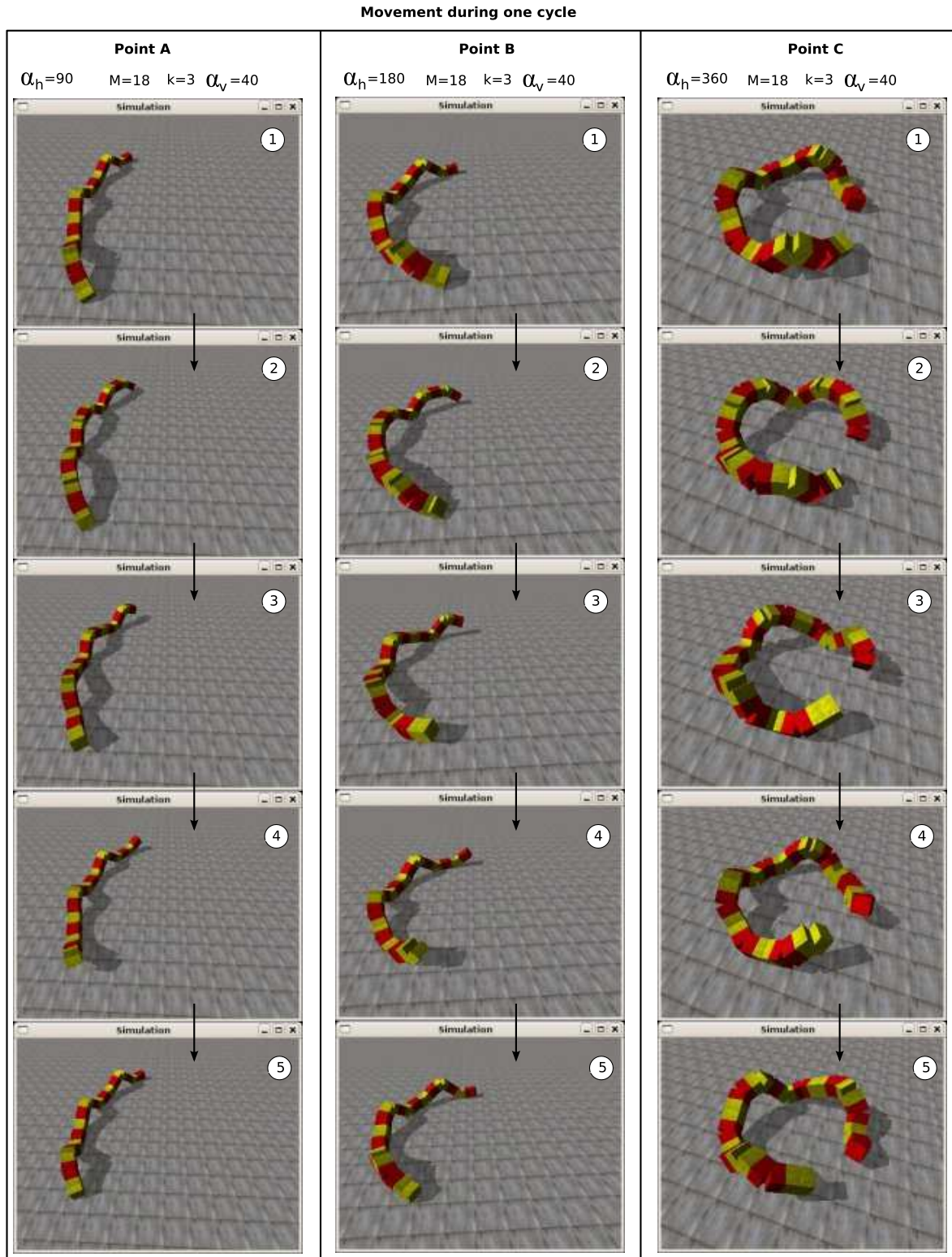


Figure 7.61: Experiment 33: Simulation of the circular path gait of an 18 modules apodal robot for the working points A,B and C, during one cycle

Movement during four cycles

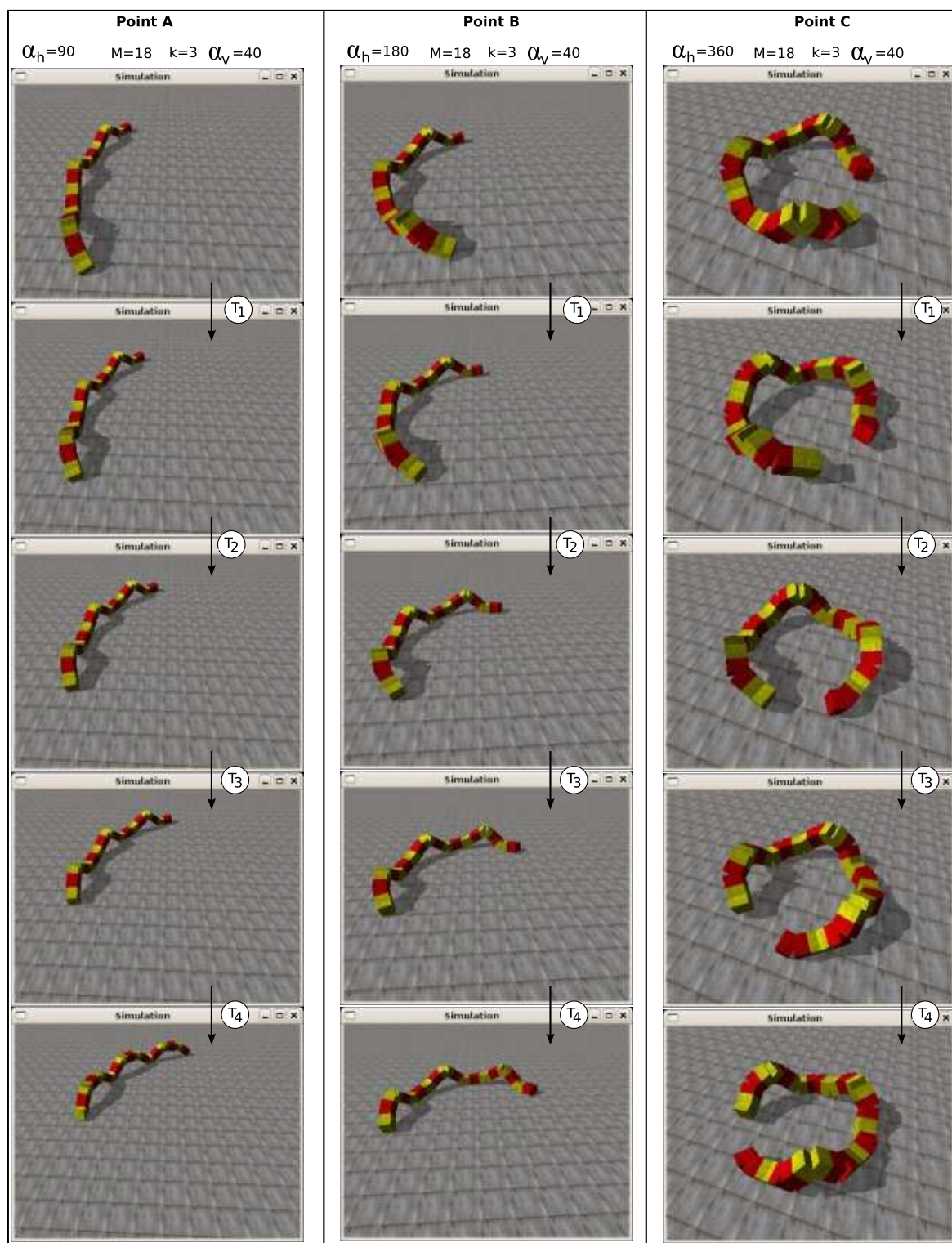


Figure 7.62: Experiment 33: Simulation of the circular path gait of an 18 modules apodal robot for the working points A,B and C, during four cycles

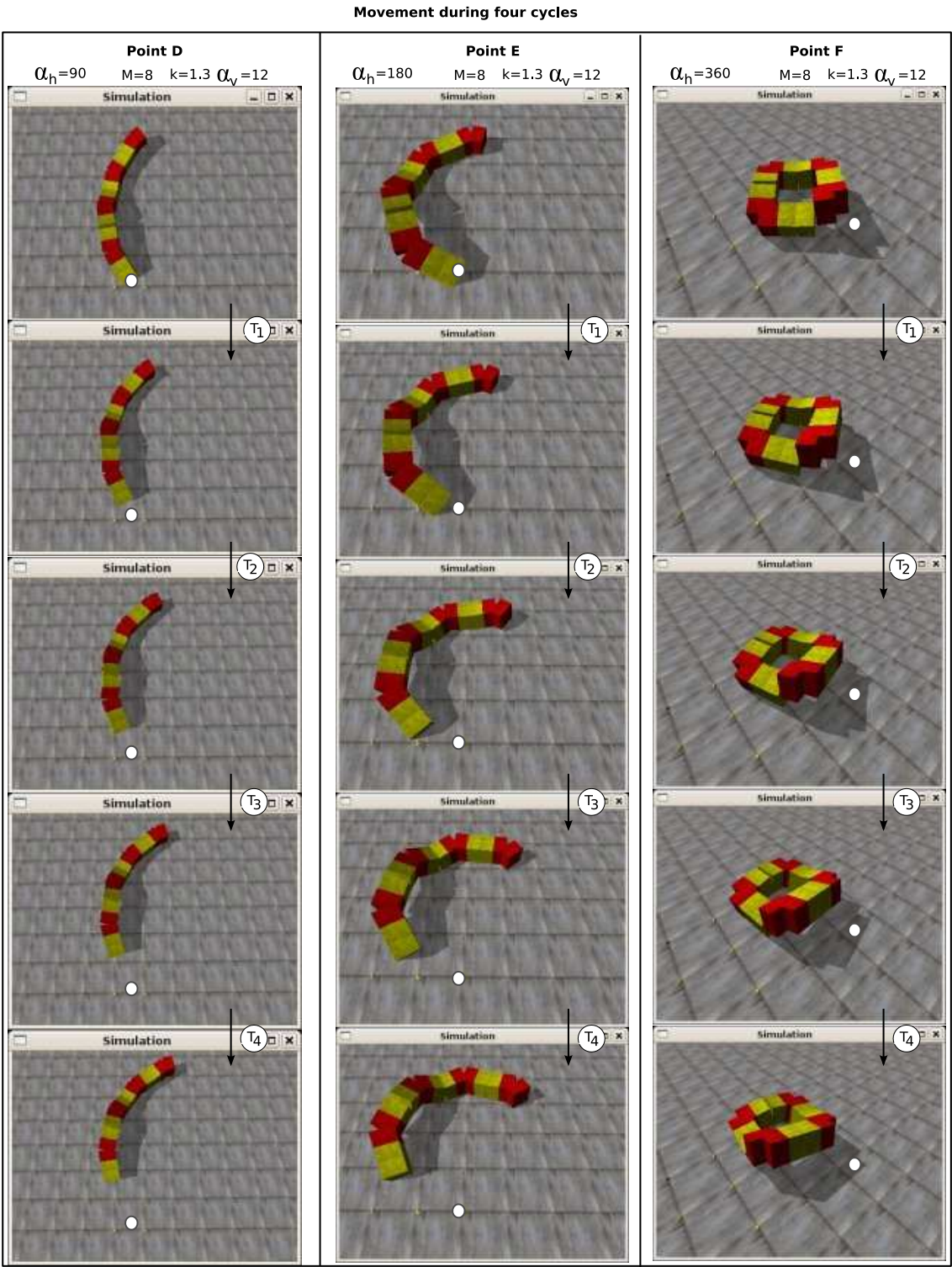


Figure 7.63: Experiment 34: Simulation of the circular path gait in the working points D,E and F



Figure 7.64: Experiment 34: The Hypercube robot moving in a circular path, in the working points D,E and F

7.5 Experiments of the movement of the minimum configurations

7.5.1 Movement in a straight line

7.5.1.1 Experiment 35: Robot's shape

In this experiment the shape of the wired model of the PP configuration given by the theoretical equations is compared with that of the real robot and the simulation. The position vectors of the four principal points of the PP configuration, $\vec{r}_0, \vec{r}_1, \vec{r}_2$ and \vec{r}_3 are calculated in the section 6.4.3.1. Starting with the phase ϕ , the stage in which the robot is found is deduced (section 6.6.2.5) and for each stage the value of the angle of orientation φ_0 is calculated (section 6.6.2.4). From this data the wired model is drawn and is superimposed with the screenshots of the simulation (figure 7.65) taken in the same phases and with the photos of the robot Minicube-I (figure 7.66) also in these same phases. The wired model is scaled so that the length L of its modules is equal to those with which it is desired to compare.

It is shown that the theoretical equations obtained faithfully represent the wired model, in both the simulation and the real robots.

7.5.1.2 Experiment 36: Movement and simulation of Minicube-I

Experiment to prove that the robot Minicube-I (PP configuration) moves in a straight line. The working point where the co-ordination is best has been chosen ($\Delta\phi = 109$), and as amplitude the half of the range has been taken ($A = 45$). In the figure 7.67 the screenshots of the simulation are shown and in the figure 7.68 the photos of the movement of the real robot.

7.5.1.3 Experiment 37: Step of the wired model

In this experiment the simulation of the step of the wired model of the PP configuration is compared with the theoretical equation (eq. 6.17). In the figure 7.69 the results are shown. The simulation has been realised with the “flat” model in which the height of the module is negligible in relation to its width and length. In the graph on the left the variation of the step with the phase is shown. For $\Delta\phi \geq 90$ both models behave in a similar way, with an error relatively minor of 6%. In the zone $\Delta\phi < 90$ the distance between the supporting points during stage 2 increases, therefore the movement does not depend on the co-ordination but rather on the friction between the supporting points and the ground. This zone is of no interest as it does not fulfil the criterion of co-ordination (section 6.6.3.2). The theoretical equation of the step, therefore, is only valid for $\Delta\phi \geq 90$.

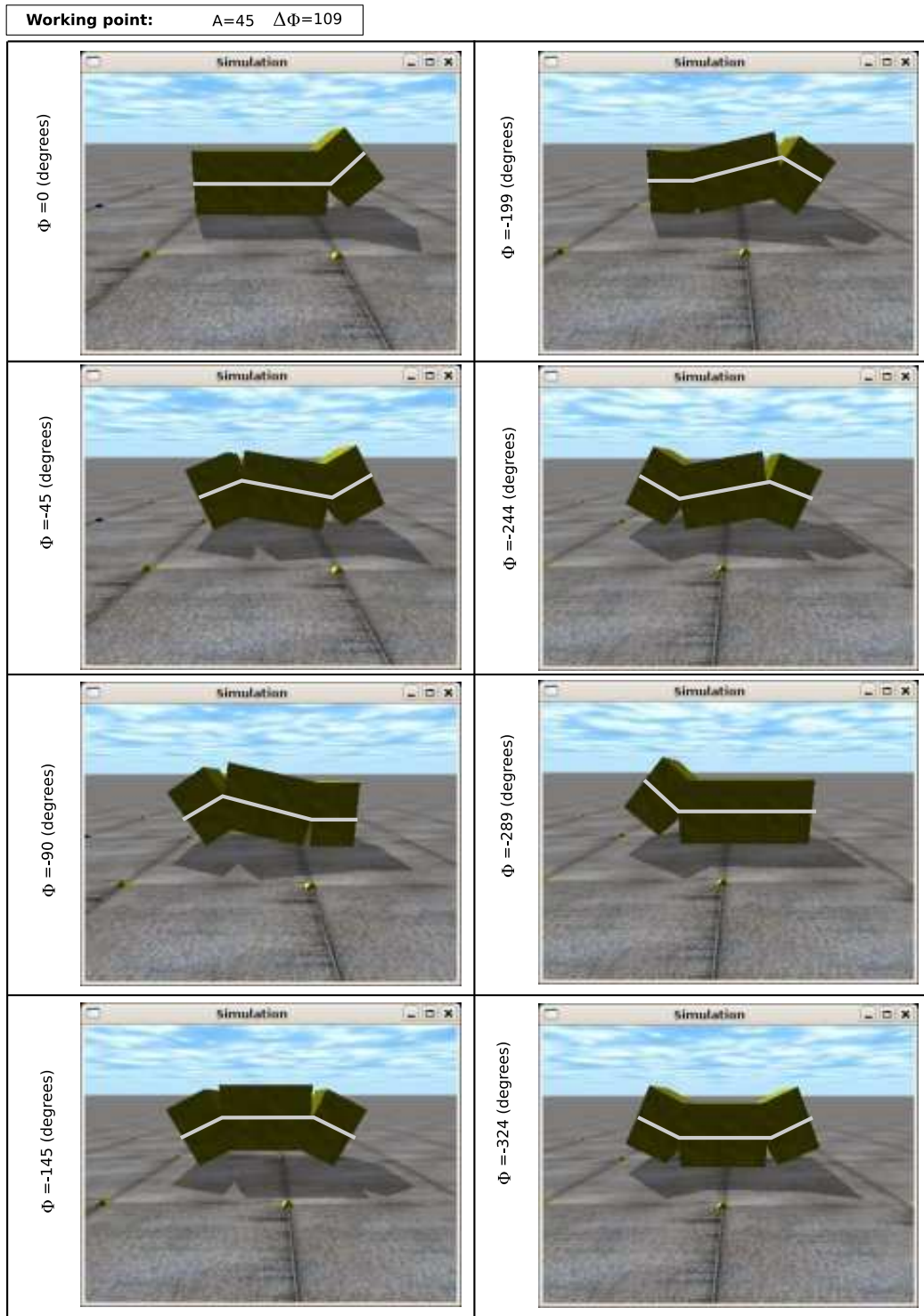


Figure 7.65: Experiment 35: Comparison between the shape of the PP configuration in simulation and the theoretical equations

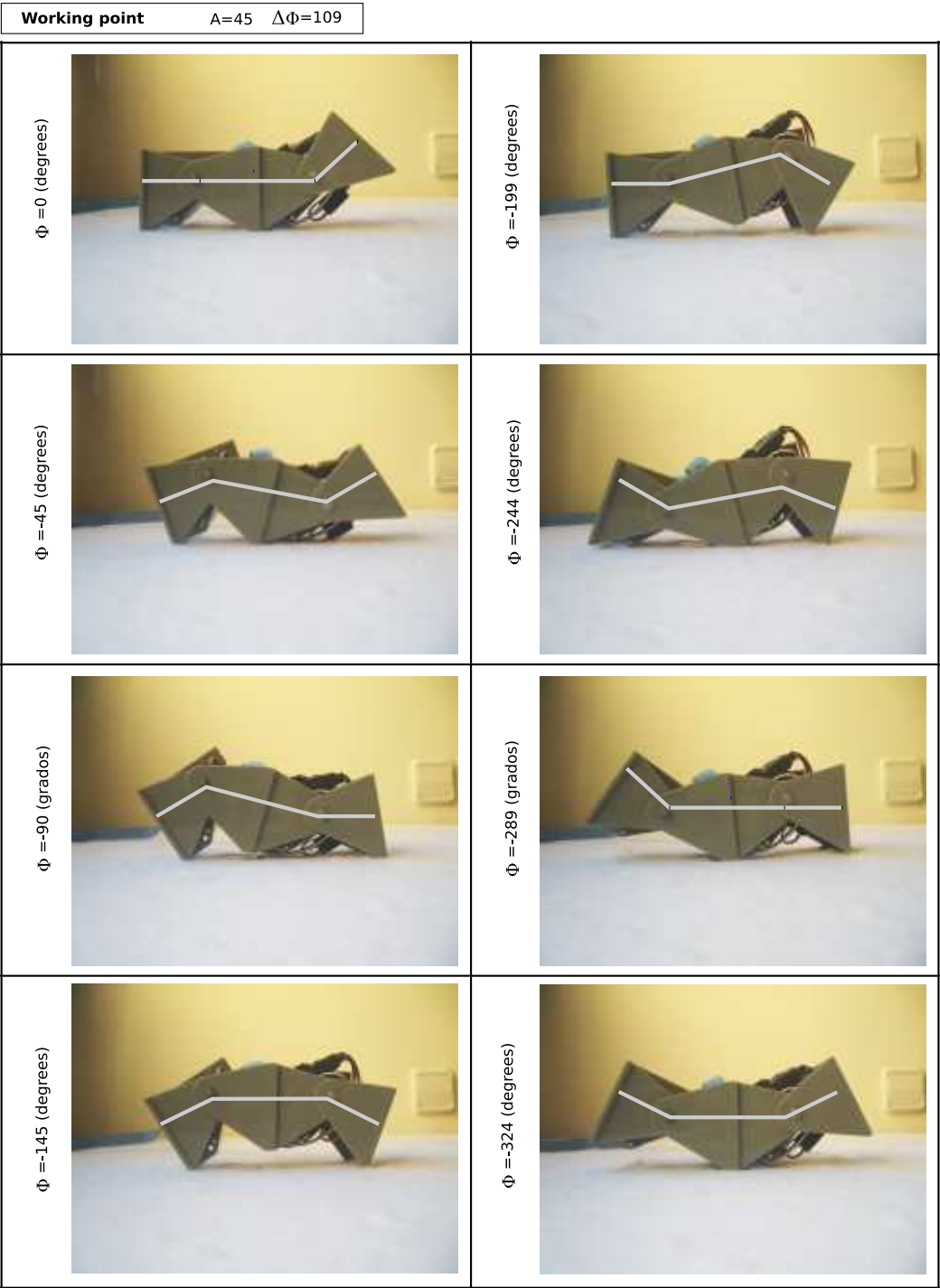


Figure 7.66: Experiment 35: Comparison between the shape of the Minicube-I robot and theoretical equations

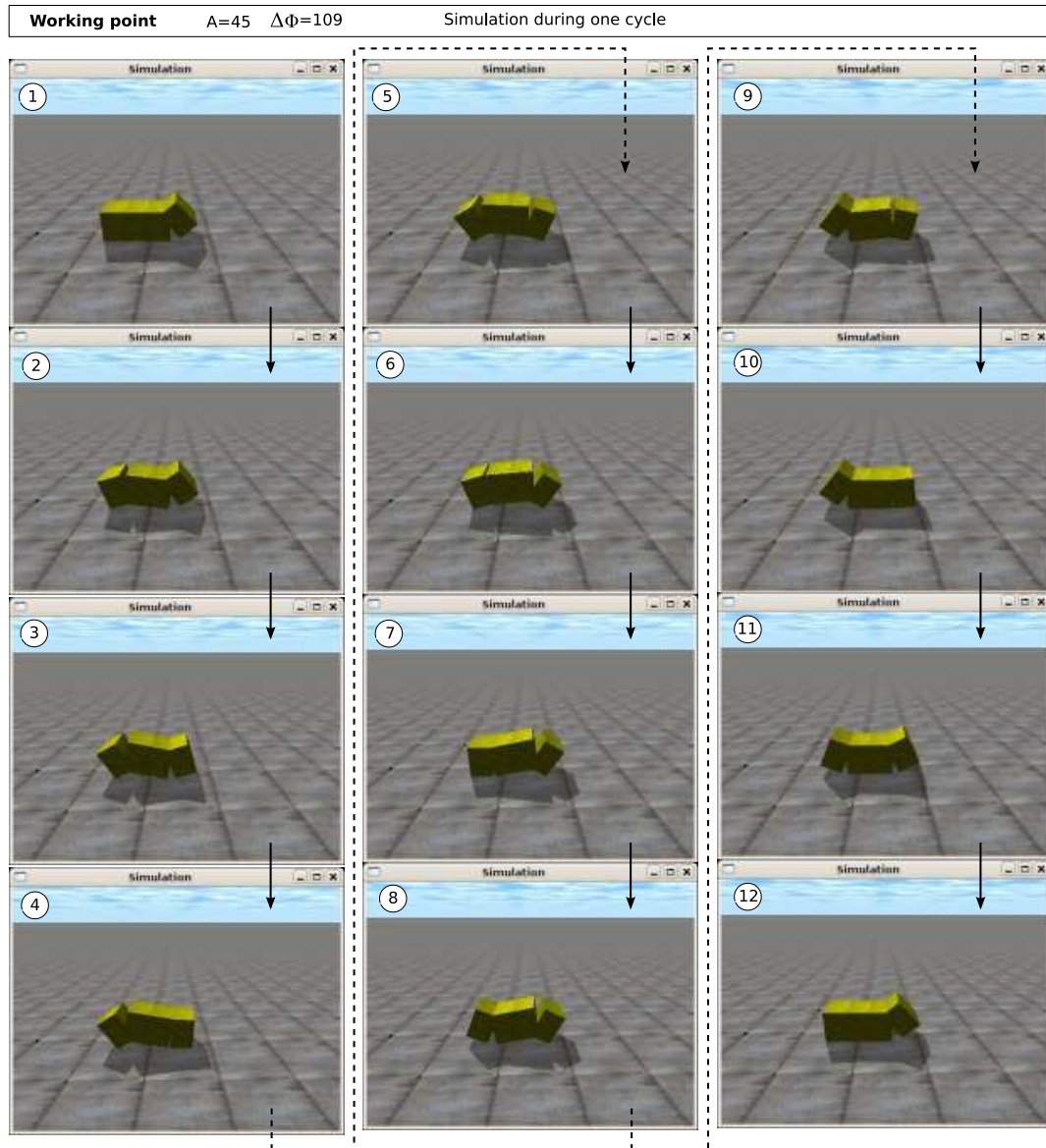


Figure 7.67: Experiment 36: Simulation of the movement in a straight line of the Minicube-I robot

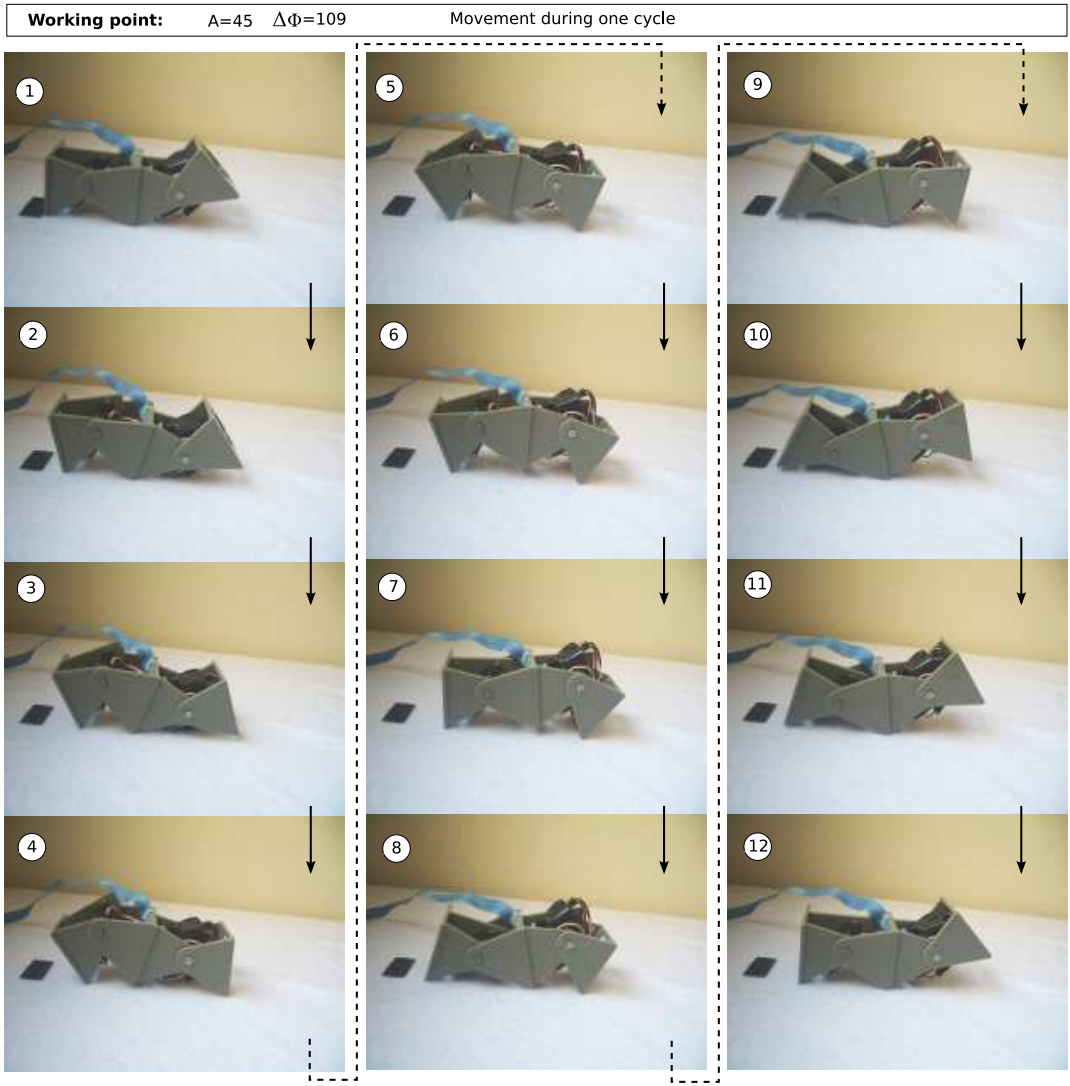


Figure 7.68: Experiment 36: Movement in a straight line of the Minicube-I robot, during one cycle

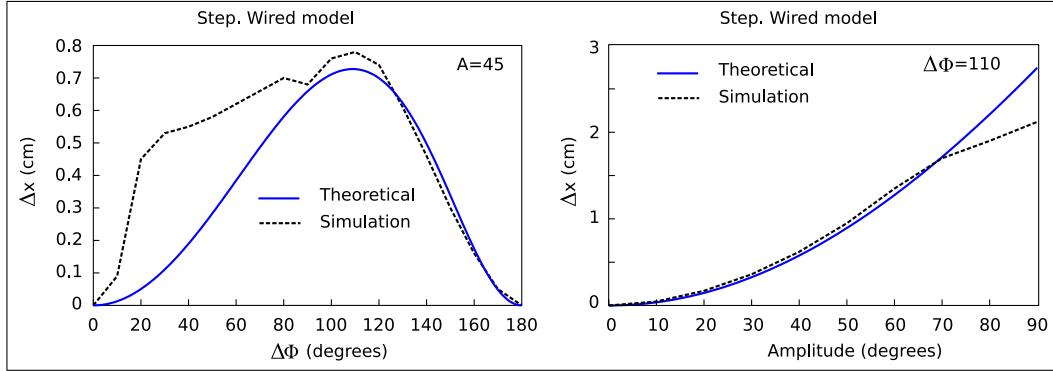


Figure 7.69: Experiment 37: Comparison between the steps give by the wired model of the PP configuration and the theoretical equation

In the graph at the right the variation of the step is compared with the amplitude, for the phase of $\Delta\phi = 110$, where the co-ordination is best. The graphs are similar for $A < 70$. From this amplitude the step in the simulation continues growing with A , but at a slower rhythm than that indicated by the theoretical equation.

7.5.1.4 Experiment 38: Step of the hexahedral model

In this experiment the step of the hexahedric model is obtained from the simulation and it is compared with the wired model and the real robot. The results are shown in the graphs of the figure 7.70.

In the upper graphs the wired model is compared with the hexahedric. Firstly it is seen that the step taken by the hexahedric model is greater than in the case of the wired model. This is due to the supporting points of the extremities. In the hexahedric model the segments that unite the joints with the supporting points have greater length L and therefore the step is greater. The graph of the step in function of $\Delta\phi$ shows a movement to the right. The maximum that exists in $\Delta\phi = 110$ in the case of the wired model, has been transferred to the point $\Delta\phi = 150$ in the hexahedric. The top right hand side graph shows the variation of the step with the amplitude of the two models. They behave in a similar way. When A increases the step increases.

In the lower part the hexahedric model is compared with the results obtained of the real robot's movement. The behaviour in the zone $\Delta\phi > 110$ is qualitatively similar. The step increases until it reaches a maximum, then abruptly diminishes. Quantitatively the step taken by the real robot is greater in the same zone $\Delta\phi > 110$. This is due to the geometry that is not hexahedric in the real robot. The differences can be seen in the screenshots taken of the experiment 36.

In the graph on the lower right the variation of the step with the amplitude is shown when the difference of phase is 110 degrees. It is seen that the variation is similar: the increase in the amplitude causes the step to be greater.

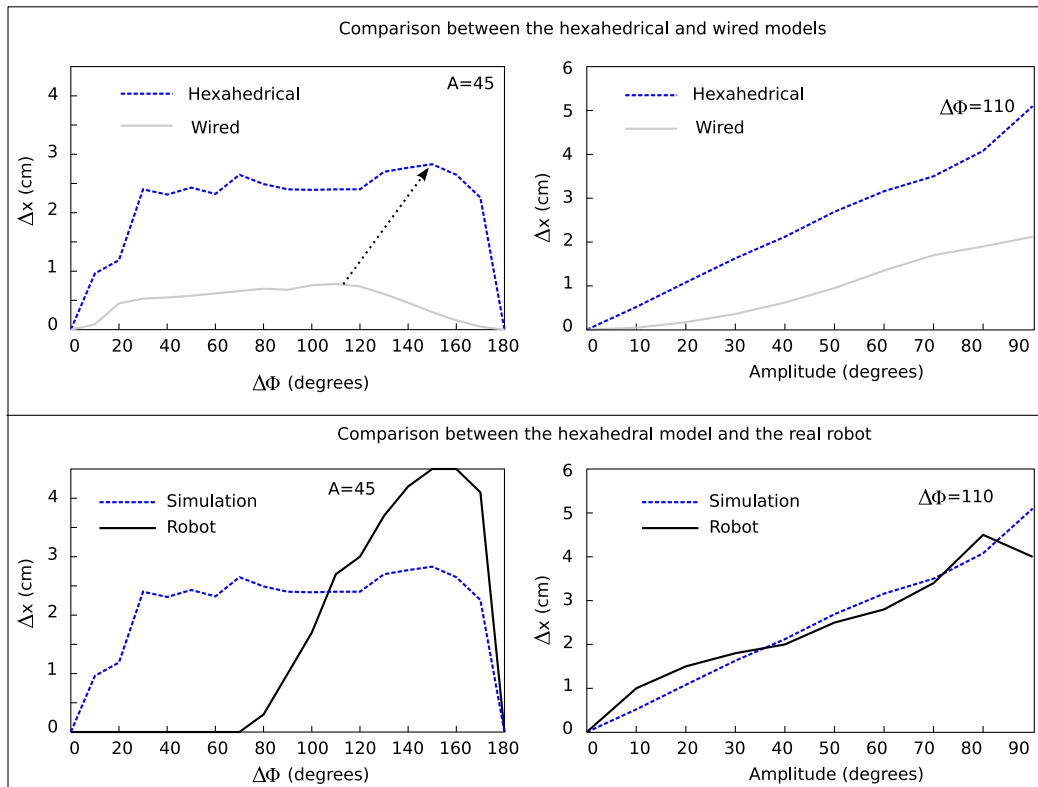


Figure 7.70: Experiment 38: Comparison between the step given by both the wired and hexahedral model and the real robot

Independently of whether it be the wired model, the hexahedric or the geometry of the real robot, a point exists where the co-ordination is the best and the step is maximised. In all these cases the step increases with the amplitude A .

7.5.1.5 Experiment 39: movement of the configuration PYP

This experiment proves that the robot Minicube II (configuration PYP) moves in a straight line when the same co-ordination is applied as in the case of the PP configuration. In the figure 7.71 the shape of the robot at different moments is shown. In the column on the left the movement during a period is seen and on the right the simulation of 4 cycles.

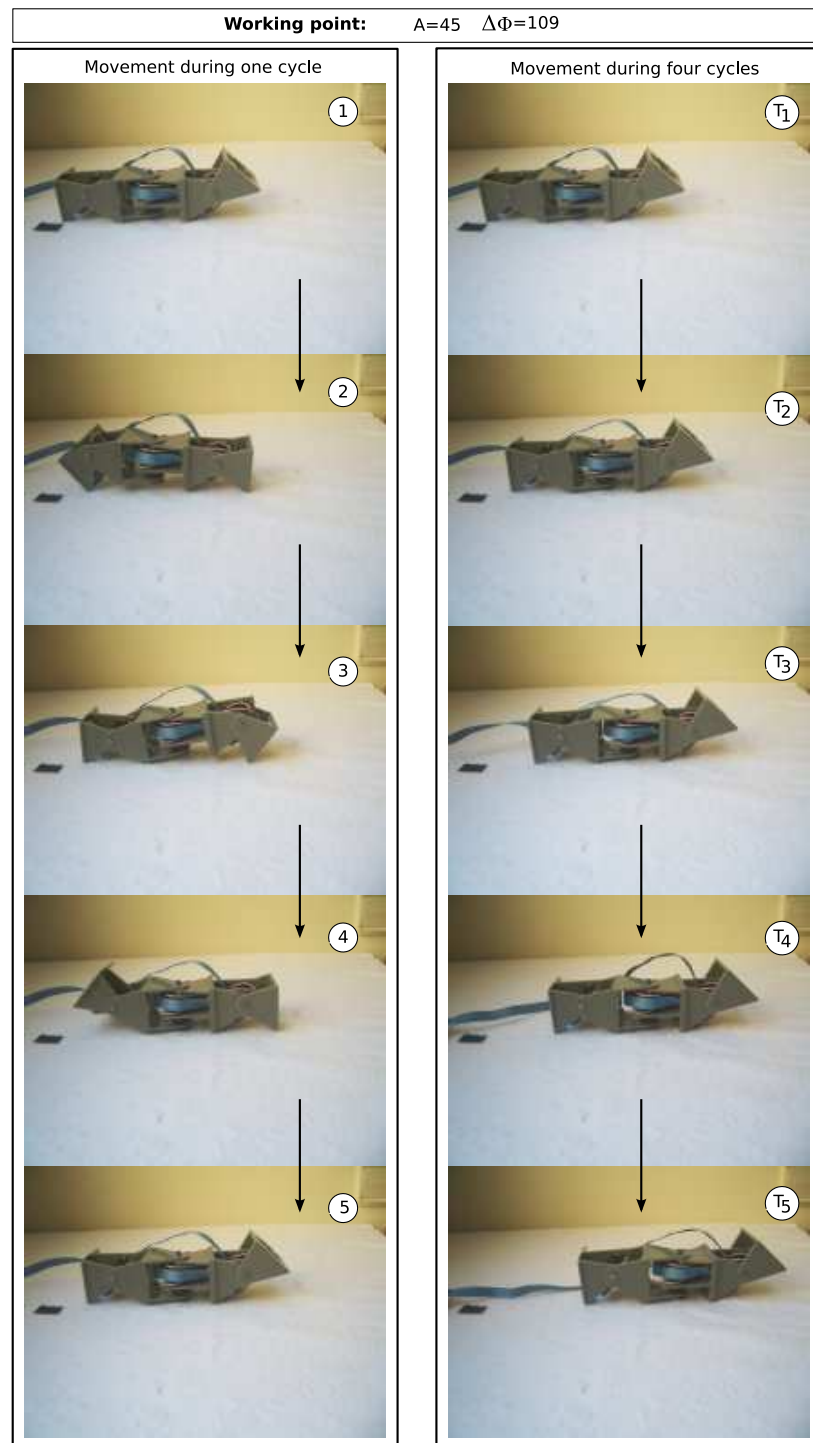


Figure 7.71: Experiment 39: Movement of the Minicube-II robot in a straight line

Working points	A_v	A_h	$\Delta\phi_v$	$\Delta\phi_{vh}$
Point A	30	40	180	90
Point B	30	80	180	90

Table 7.10: Working points for the experiments on rolling of the PYP configuration

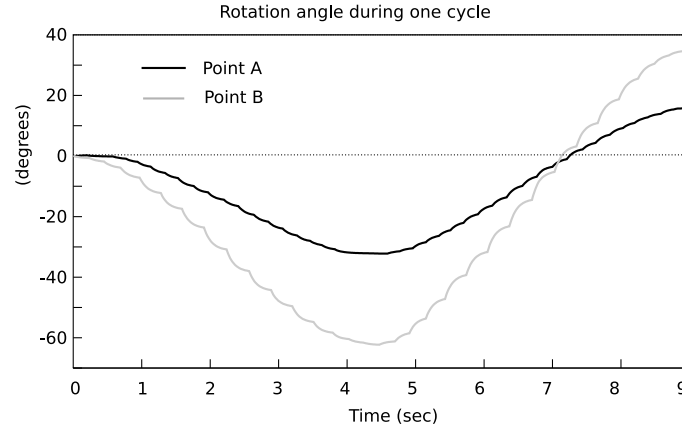


Figure 7.72: Experiment 40: Angle of rotation in function of time

7.5.2 Rotation

7.5.2.1 Working points

The working points for the experiments of rotation of the configuration PYP is shown in the table 7.10. The only difference is the amplitude of the central module.

7.5.2.2 Experiment 40: Variation of the angle of rotation

In the figure 7.72 the variation of orientation of the robot's central module with the time is shown during a cycle. In the initial state the angle of zero degrees is taken as reference. The central module oscillates to both sides, but at the end of a cycle the net result is that its orientation has varied a quantity equal to the angular step. It is also observed that the rotation at the point A is less than at B, because it depends on the parameter A_h . When it is increased the angular step increases.

7.5.2.3 Experiment 41: Path of the centre of mass

The path of the centre of mass during a cycle for the two working points A and B, is shown in the figure 7.73. To the left it is shown in greater detail and to the right referred to the robot's total length, that is approximately 22 cm. It is observed that for the point B the movement of the central module is greater and that at the end of a cycle it is not placed in the original position but it has been displaced a certain distance. For point B this movement represents a 9% of its total length.

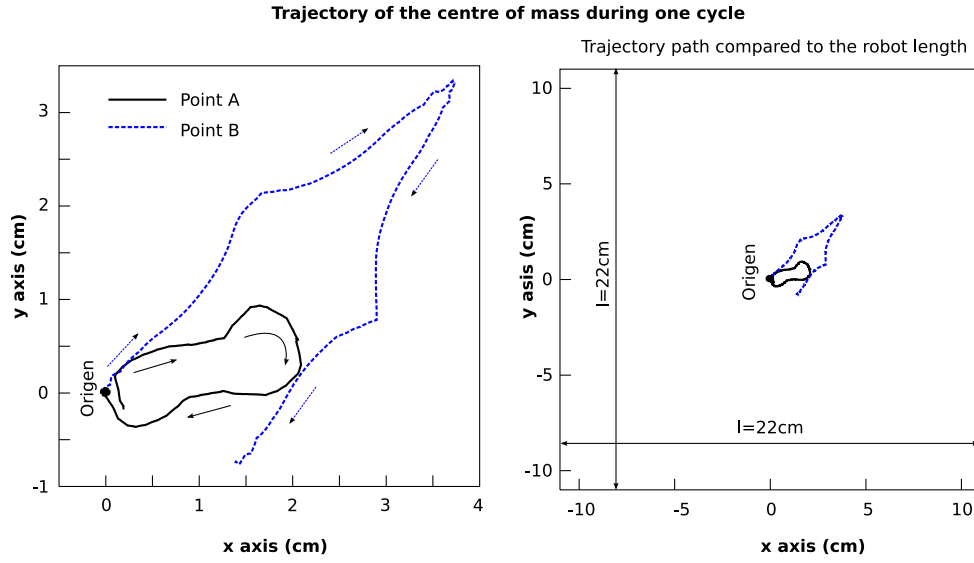


Figure 7.73: Experiment 41: Trajectory of the centre of mass during the rotation

7.5.2.4 Experiment 42: Rotation of Minicube-II and its simulation

Minicube II's rotation and its simulation in the working points A and B is shown in the figures 7.74 and 7.75 respectively. On the left the shape of the robot can be seen in 5 screenshots of the same cycle, for both the real robot and the simulation. On the right the variation of the position of the robot during 4 cycles is shown to display how it goes rotating.

7.5.2.5 Experiment 43: Comparison of the theoretical angular step, simulated and real

In this experiment the angular step is represented in function of the parameter A_h for the real, the simulated robot and the theoretical equation (eq. 6.37) when they are at the working point A. It is observed that in all the cases the angular step increases with the horizontal amplitude in a very similar way.

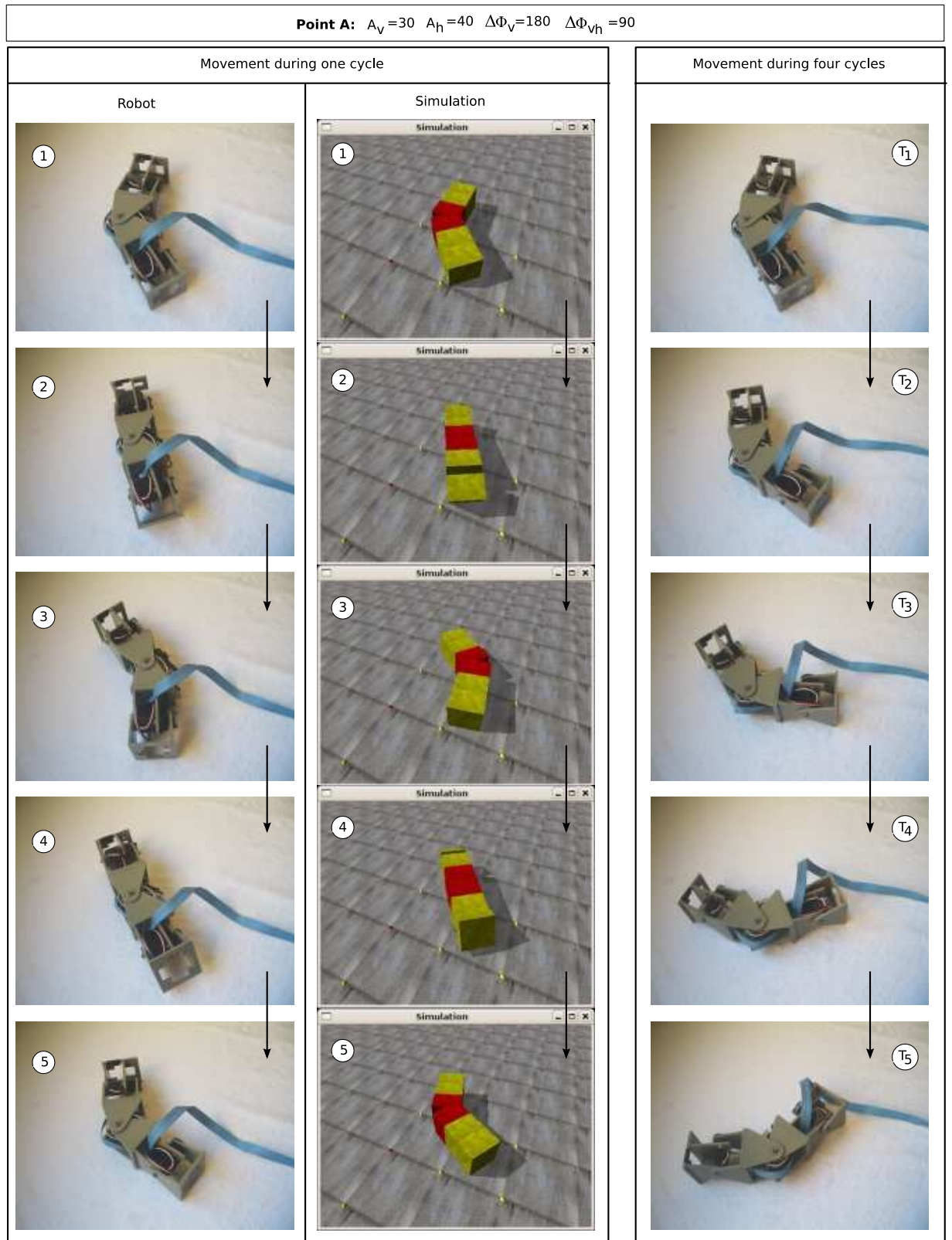


Figure 7.74: Experiment 42: Minicube II performing the rotation gait in the working point A

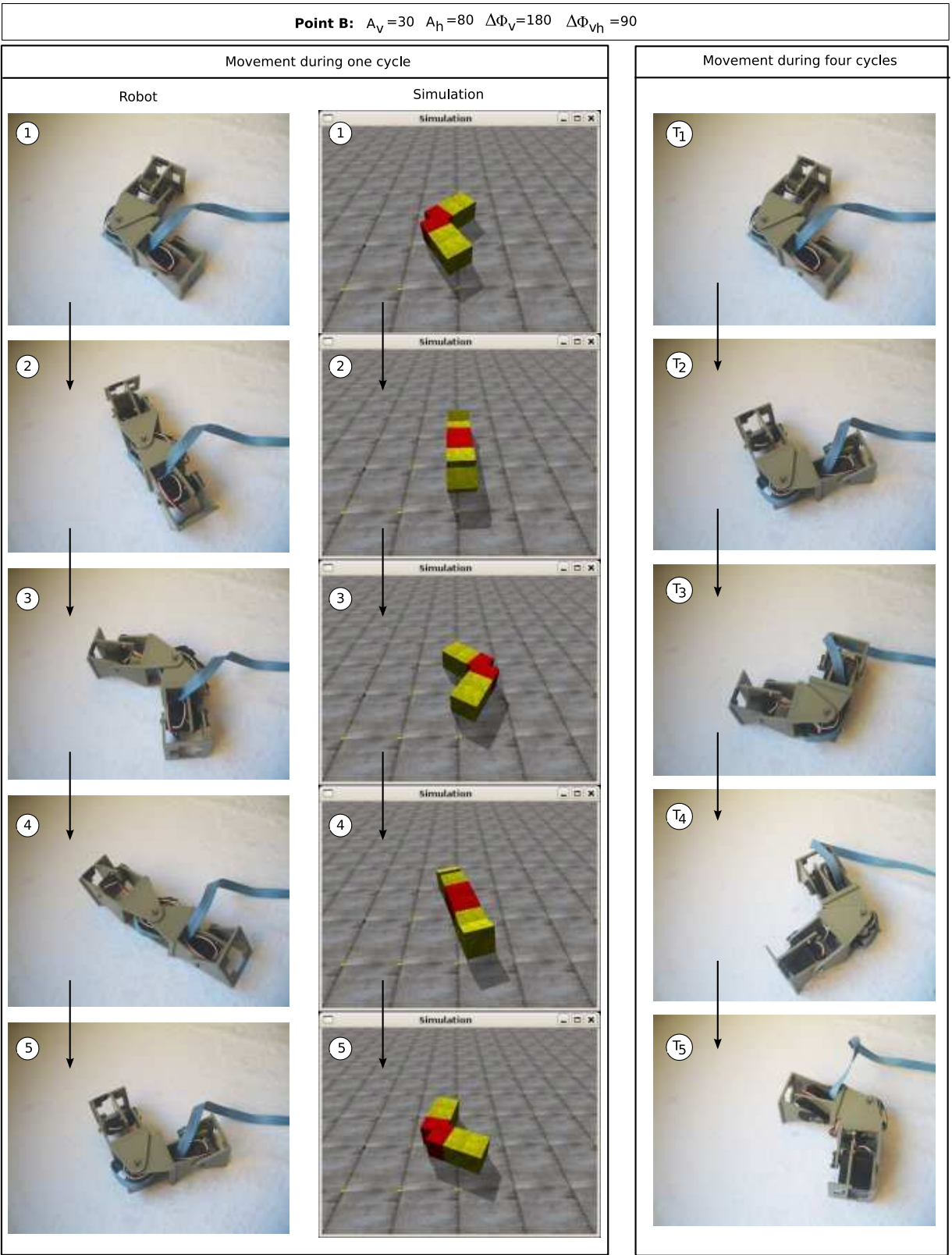


Figure 7.75: Experiment 42: Minicube-II performing the rotation gait in the working point B

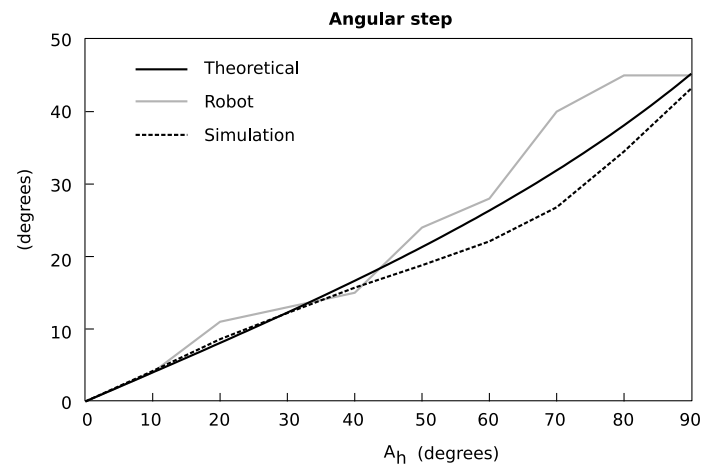


Figure 7.76: Experiment 43: Comparison between the angular step of both the simulated and the real robot and the theoretical equation, for the working point A

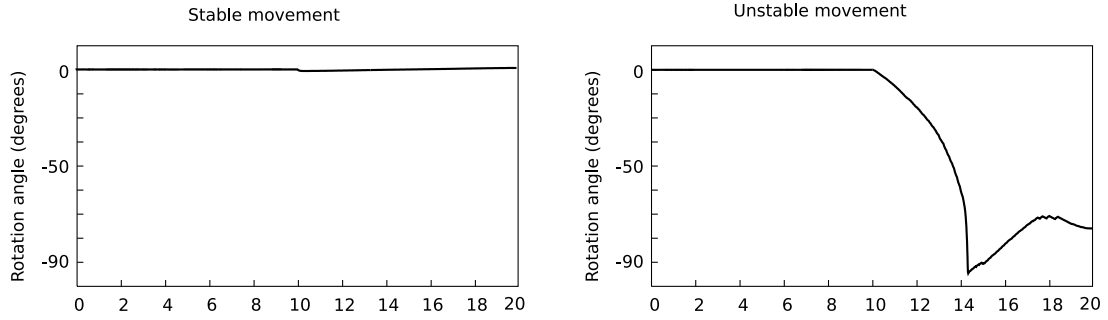


Figure 7.77: Experiment 44: Stability of the sideways movement of the Minicube-II robot

7.5.3 Sideways movement

7.5.3.1 Experiment 44: Stability

The sideways movement is realised applying the same co-ordination as in the case of the rolling movement. The difference is in the value of the parameter A_h , that according to the criterion of the section 6.8.2, if it is less than A_{hL} it will produce movement or to the contrary it will roll. The value of A_{hL} for the hexahedric model of the configuration PYP is of 51.4 degrees (Table 6.2).

This experiment tests what happens for the two working points with $A_h = 60$ and 30. With the first the robot will roll, therefore we consider it unstable for sideways movement. With the second the correct movement is realised. In the figure 7.77 the angle of rotation (roll) of the central module has been represented. It can be seen that when the movement is stable, this angle always remains at zero. Nevertheless, in the case of instability the angle varies, reaching -90 degrees (it has turned over).

In the figure 7.78 the robot Minicube II and its simulation is shown during the realisation of the sideways movement in these two working points.

7.5.3.2 Experiment 45: Sideways movement of Minicube-II and its simulation

In the figure 7.79 Minicube II's sideways movement and its simulation is shown. On the left the robot can be seen in 5 moments during a cycle. On the right the robot is shown in 5 moments corresponding to the start of each period, of a total of 4 cycles.

7.5.3.3 Experiment 46: Step and path

In the figure 7.80 the position of the centre of mass of the robot is shown, for the duration of four cycles. It is observed that when the sign of the parameter $\Delta\phi_{vh}$ is changed the robot moves in the opposite direction, but in the same way.

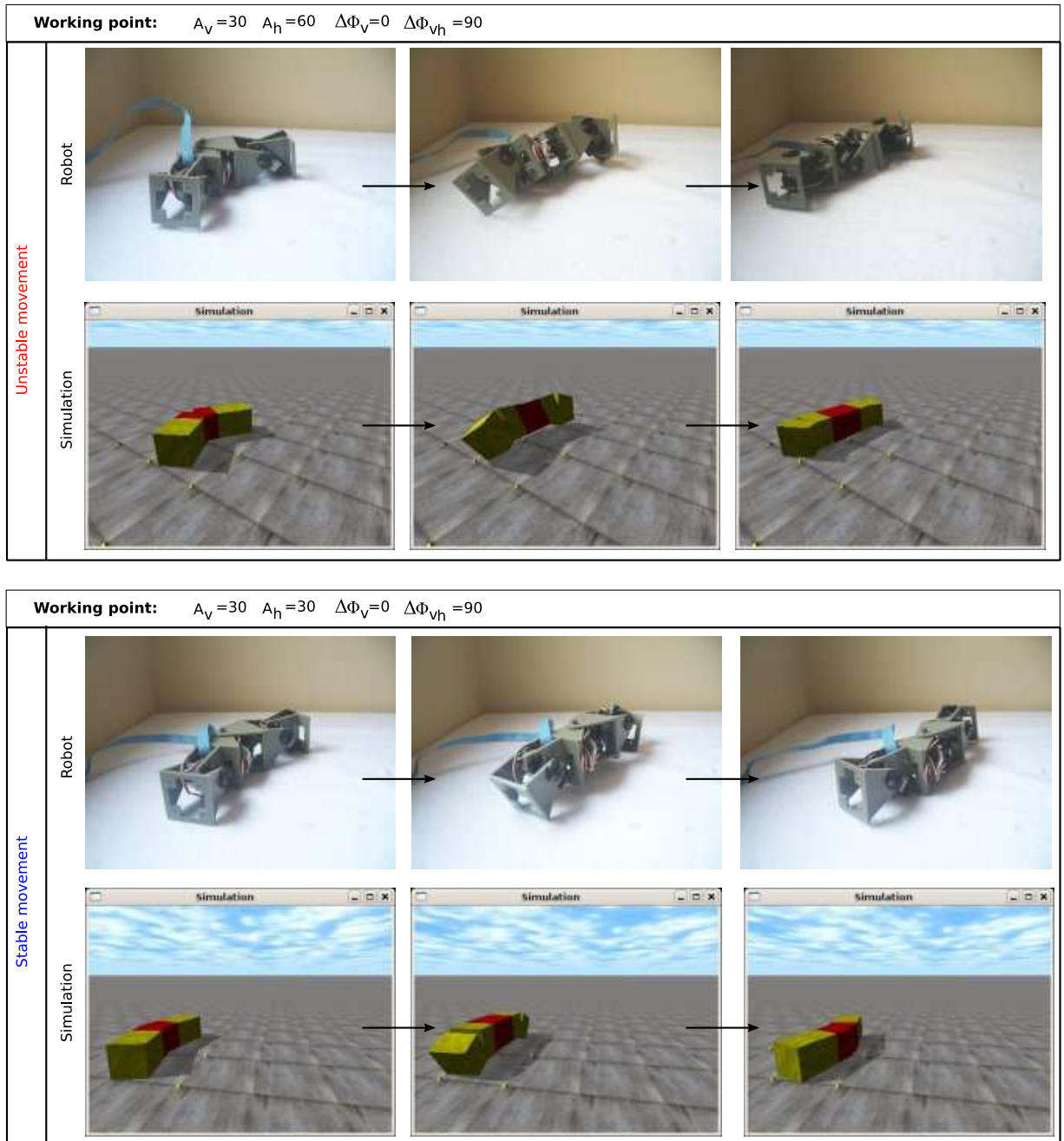


Figure 7.78: Experiment 44: Stability of the sideways movement of the Minicube-II robot

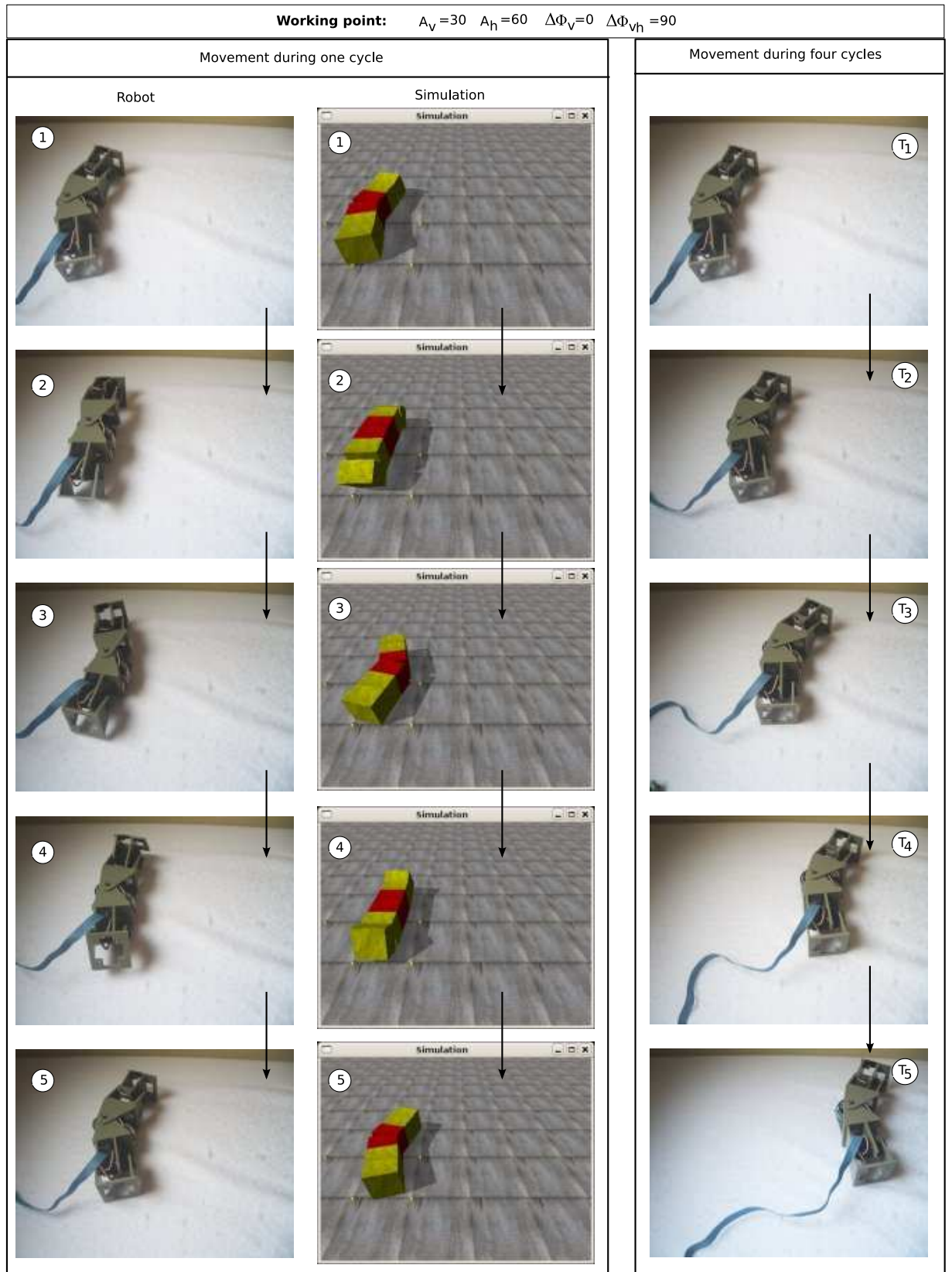


Figure 7.79: Experiment 45: Sideways movement of Minicube-II and its simulation

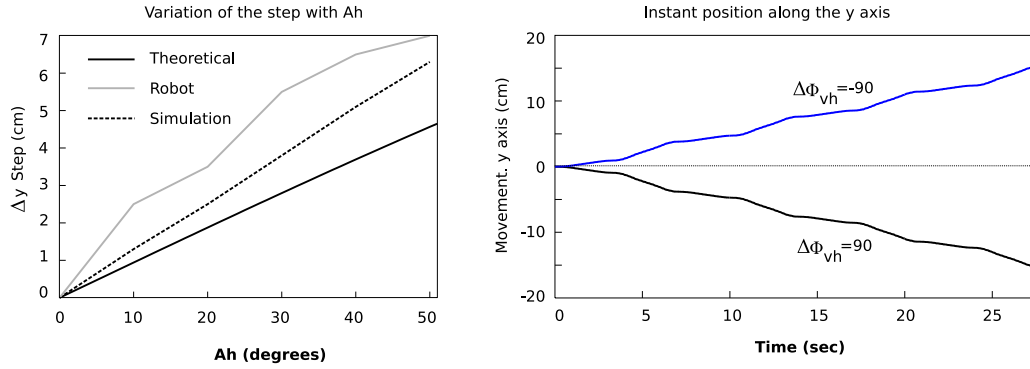


Figure 7.80: Experiment 46: Step and path of the sideways movement of Minicube-II

In the graph on the right the graph of the step given in function of A_h for the real robot, the simulated and the theoretical equation (eq. 6.35) are compared. In all of these cases the step increases with A_h . Both the simulation and the real robot have a step greater than the theoretical. This is because the equation has been calculated for the wired model and the dynamic of the supporting points has not been taken into account.

7.5.4 Rolling movement

7.5.4.1 Experiment 47: Rolling movement of Minicube-II and its simulation

The rolling movement of Minicube II and its simulation are shown in the figures 7.82 and 7.81 respectively, during a period. An amplitude A of 60 degrees is used, The step taken by both robots differs by 3%. Their values are below the maximum of 20.8 that would be obtained if the robot could roll in extended position.

7.5.4.2 Experiment 48: Path and angle of rotation

The angle of rotation in function of time is shown in the graph on the right of the figure 7.83. When the sign of the parameter $\Delta\phi_{vh}$ is changed the direction of rotation changes.

This rotation causes the robot to move along the length of the y axis and, varying the position of its centre of mass as indicated in the figure on the left. It proves, also, that the movement is symmetric with respect to the sign of $\Delta\phi_{vh}$. The movement tends to be uniformly rectilinear, but with superimposed oscillations of small amplitude.

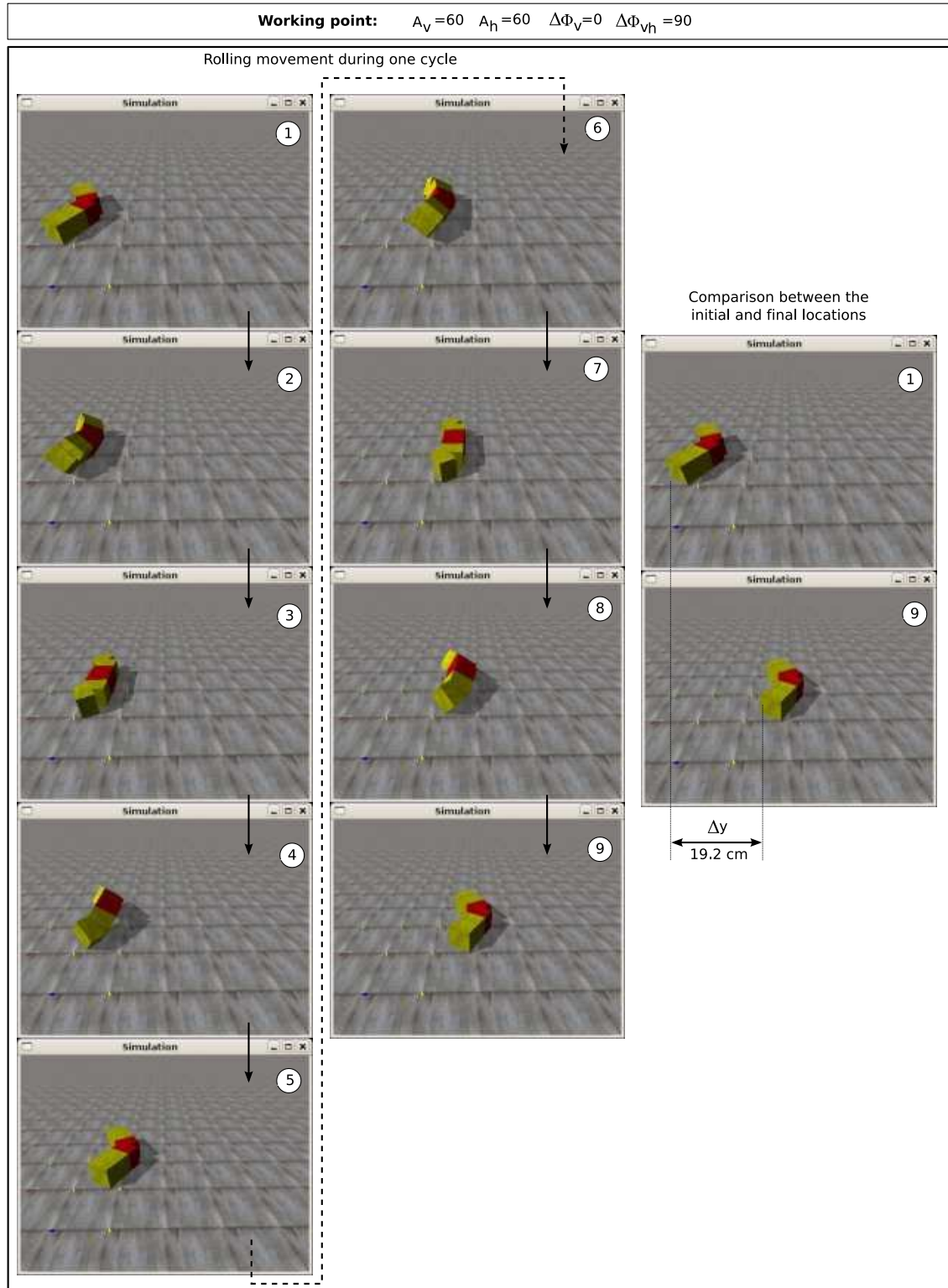


Figure 7.81: Experiment 47: Simulation of the rolling one of Minicube-II, during one cycle

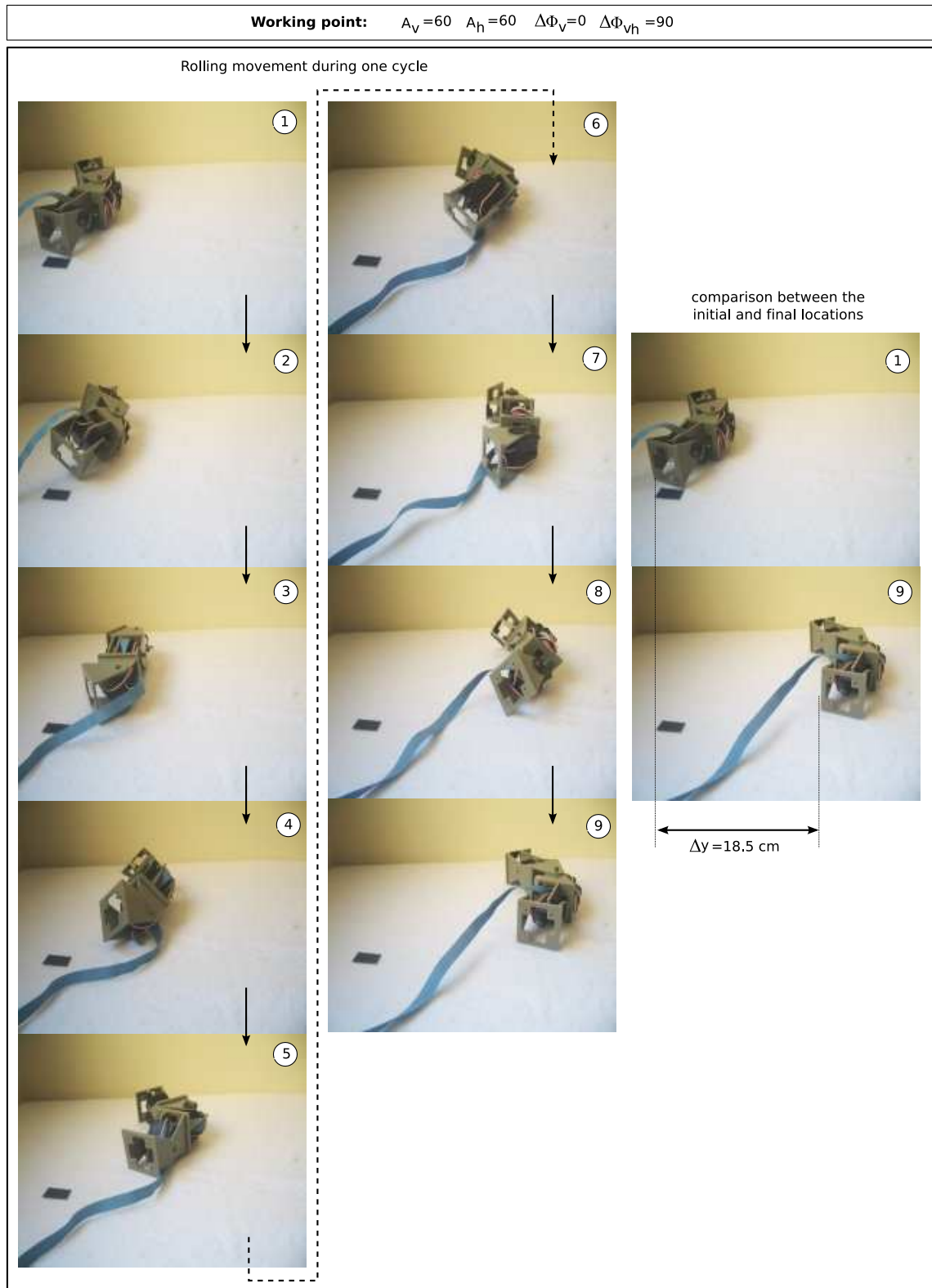


Figure 7.82: Experiment 47: Minicube-II performing the rolling gait, during one cycle

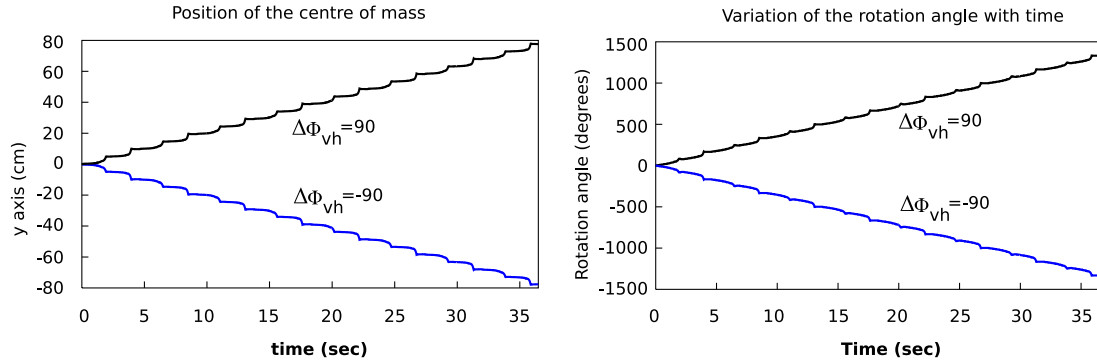


Figure 7.83: Experiment 48: Trajectories and angle of rotation

7.5.5 Circular path

7.5.5.1 Experiment 49: Movement of Minicube-II in circular path

In the figure 7.84 the movement of the robot following a circular path during 4 cycles is shown.

7.6 Conclusions

We have developed a **simulator to confirm the validity of the solutions proposed** for the problem of the co-ordination of the apodal robots of M modules of the pitch-pitch and pitch-yaw groups. This tool allows us to simulate the movement of the apodal robots of any length, with the following aims:

1. Confirm qualitatively the viability of a solution, by mean of the visualisation of the movement of the virtual robot.
2. Obtain quantitative and empirical data about the kinematics of the movement: step, path of the centre of mass, speed, etc.
3. Implement functions of evaluation for the realisation of searches by means of genetic algorithms.

Obtaining solutions by means of simulation has its limitations. On the one hand, simplified models are employed. In our case hexahedral models have been used. On the other hand solutions appear that function very well in the simulation but are not viable in real robots.

One of the aims of the thesis is **to find valid solutions which can be implemented in real robots.** Therefore we have **designed our own modules**, denominated *Y1 Modules* and we have **constructed four prototypes of apodal robots**. Two of them belong to the pitch-pitch group and are the 8 module

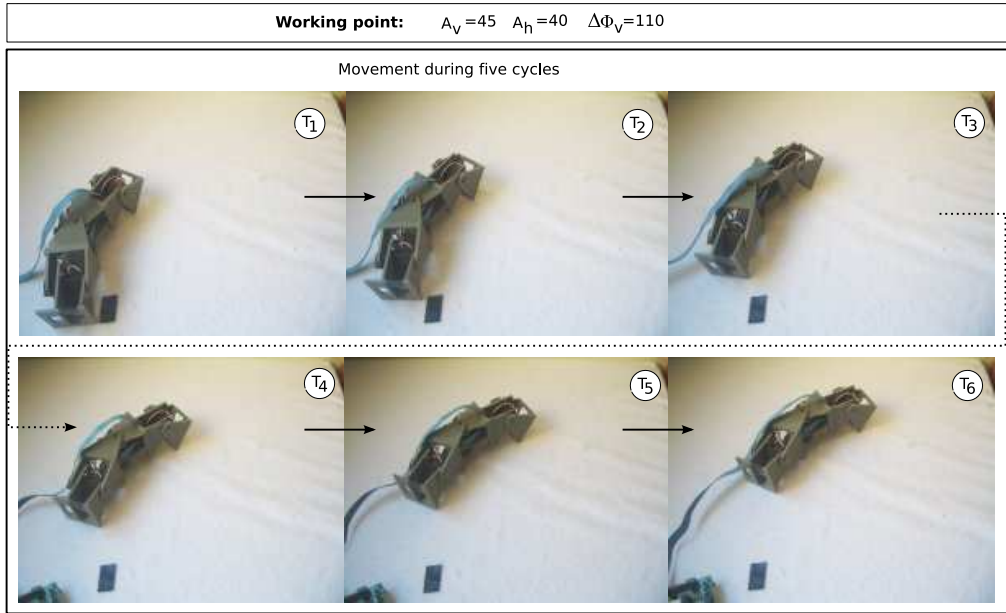


Figure 7.84: Experiment 49: Minicube-II performing a circular path

robot *Cube Revolutions* and the two module *Minicube-I* (being the minimum configuration). The other two belong to the pitch-yaw group. They are the 8 module *Hypercube* and the 3 module (the minimum configuration) *Minicube II*.

The experiments have been placed into three groups of movement: the pitch-pitch group of robots, the pitch-yaw group and the minimum configurations. For all of them the viability of the solutions has been demonstrated both in the simulation and for the real robots.

The principal conclusion is **the qualitative demonstration of the viability of the control model based on sinusoidal generators** for the movement of apodal robots belonging to the pitch-pitch and pitch-yaw groups. We have confirmed that this method is valid for the movement of real robots. What is more, the experimental relationship between the parameters of the generators and the step taken by the robot has been demonstrated and has been compared with the proposed theoretical formulas.

Finally, to allow other investigators to continue or repeat these experiments, when possible **we have only used free technologies**: all the software that we have used and developed, and the hardware we have designed and the modules we have created is free. Anybody is free to study our robots, build them, modify them and redistribute them.

Chapter 8

Conclusions

”It’s the question that drives us. It’s the question that brought you here.”

– Trinity, in the film “Matrix”

This last chapter is divided into three sections. We begin presenting the principal contributions of this thesis together with a brief discussion of its implications. Then we sum up the particular conclusions of each chapter. Finally we indicate some of the possible future lines of investigation that will give continuity to this work.

8.1 Main contributions

After asking the initial questions, developing the mathematical models, obtaining the results and testing them both in simulation and real robots, we arrive at the following conclusions:

1. *The viability of the sinusoidal generators as controllers for movement in one or two dimensions of the apodal robots of the groups pitch-pitch and pitch-yaw, in the steady state on level homogeneous surfaces without obstacles is proved*

This controller is valid for robots with a number of modules greater or equal to two or three, according to whether the connection is of pitch-pitch or pitch-yaw type respectively. In reply to the question made in the aims, “Is movement of the robot obtained?” the answer is “yes”. What is more the movements obtained are very smooth and natural, giving the sensation that the robot is alive.

The controller based on sinusoidal generators has three main advantages. One is its scalability. To carry out the movement of an apodal robot of M modules there is nothing to add except the

same number of generators as there are modules. The other is the economy of resources. Very few calculations are required which permits the implementation of them in low range micro-controllers. The third advantage is their implementation in various technologies: software, digital electronic circuits or even analogue circuits.

By means of the use of FPGAs, specific circuits can be designed that allow the robot to move ‘by hardware’ in the same way that lizard tails move when they are sectioned.

2. *It has been demonstrated that the apodal robots belonging to the pitch-yaw group, with a number of modules greater than or equal to three, can move using at least five different gaits: straight line, circular path, sideways, rolling and rotation. When the number of modules is increased new movements appear such as sideways movement in S, sideways inclined and the rotation in S.*

The model of sinusoidal generators presented as hypothesis is not only viable but allows a variety of movements greater than the anticipated, given the simplicity of the controller. The author of this thesis never ceases to be surprised when observing the robot moving with this variety of movements, knowing that the servos are simply oscillating.

With the gaits obtained all apodal robots of the pitch-yaw group of more than two modules can reach whatever point (x,y) of the plane, with any orientation. What is more, thanks to the rolling movement, it can recover its original position if it tips over.

3. *The minimum dimension of the control space for the movement of the apodal robots of the pitch-yaw group with more than two modules on a surface is five.* That is to say, that only five parameters are necessary so that any robot with a pitch-yaw connection of more than two modules can move employing at least the five gaits discovered. The parameters are the amplitudes of the generators associated to the vertical and horizontal modules, their phase differences and the phase difference between the vertical and horizontal ones.

For the movement in a straight line the dimension is two. Only two parameters are needed to move any robot of the pitch-pitch group which has more than one module. They are the amplitude and the phase difference.

For the movement of a concrete apodal robot of M modules more control parameters can be employed, such as for example the utilisation of different amplitudes for the different modules. In this case the solution is not general, but particular to that robot. In these spaces of greater dimension more than one solution to movement can exist. In this thesis we have concentrated on looking for the space of minimum dimension that allows movement independent of the number of modules

4. *Three novel gaits have been found, that had not previously been studied by other researchers nor realised in any apodal robot, as far as we know. They are the inclined sideways movement and the rotation in S and in U.* The movements of rotation are specially important as they allow the apodal robots to change their orientation to point to any direction. Just by employing the

movement in a straight line and the rotation the robot can reach any point of the plane and is can be orientated in the desired direction

Any robot of the pitch-yaw group with more than two modules can execute the rotation in U. The rotation in S with an undulation can be carried out by all those robots that have 8 or more modules.

5. *The problem of the minimum configurations has been presented for the topologies of one dimension and has been resolved. The two minimum configurations have been found, of two and three modules that are capable of moving in one or two dimensions respectively.* It is, therefore, possible to answer the question asked in the aims: “Which are the robots with the least number of modules that have the capability of movement?” The answer are these minimum configurations. To move in a straight line two modules are necessary. To do so in a plane, three.

This is a novel problem that had not previously been presented. it was proposed in 2005 in [43]. The article was selected as one of the seven best of the congress and received the “Industrial Robot Highly Commended Award”. The two minimum configurations found with one dimension topologies are made up of two modules with pitch-pitch connection (configuration PP) and that made up of three, the central one being yaw and the two extremities pitch (PYP configuration).

These configurations are important for the following reasons. 1) They constitute the atomic units of movement (AUM), that are capable of movement in a plane, reaching whatever point (x,y) of its surface and with any orientation. 2) They maximise the number of sub-robots into which a self configuring modular robot can divide itself. 3) They are the most efficient in relation to the energy necessary to move them. 4) They allow the study of movement of other robots by means of the identification of their structures in them, finding new gaits and deducing the viability of the movement of certain configurations that would not be known *a priori* if they could move.

6. *The relationships between the parameters of the generators and the kinematic parameters of the robots of the study group have been obtained.* For some gaits the theoretical equations have been proposed and for others the empirical relationships are shown.

These relationships show how each generator affects movement. Generally speaking the amplitudes are related to the size of the robot’s step (linear or angular) during a period and the phase difference with the co-ordination and the type of gait. It is important to know them so that the controllers of the superior levels can react to the external stimuli modifying the kinematics of the robot, as for example to reduce the amplitudes to be able to go under an obstacle or through a tube. Doing it, thanks to these relationships, we know that the robot’s step will diminish, but if the phase differences are not modified, the gait will be the same.

7. *Knowledge of movement of apodal robots of the study group has been summed up in 27 fundamental principles, 11 for movement in one dimension, another 11 for the movement in a plane and 5 for the minimum configurations.*

With these principles it is hoped that other researchers or engineers of applications can move any 1D topology modular robot of the mentioned groups, both in simulation and in reality, easily and rapidly. What is more, these principles can be applied to the movement of the self-propelled apodal robots, even though they use wheels or caterpillar tracks as their main means of movement they can also do it by means of corporal movements.

8. *It has been demonstrated that the solutions found to the problems of the co-ordination to obtain movement of the apodal robots are valid for their use in real robots.* They have been tested in four apodal robot prototypes, constructed from the union of the Y1 Modules, designed specifically for this thesis. The verification for robots with different number of modules has been carried out using the simulator developed for this purpose.

8.2 Other contributions

8.2.1 About methodologies

The study of movement of the modular robots in general is a titanic task due to the existence of an infinity of possible configurations. What is more, the number of them grows exponentially with the quantity of modules employed.

To address the problem a classification into three large families of the chain type modular robots has been proposed, according to their size and topology. Then a sub-division into three groups of robots with one dimension topology (apodal robots) has been proposed, according to the type of connection between the modules, This results in the group with connection yaw-yaw, pitch-pitch and pitch-yaw. This thesis addresses in detail the last two groups named.

To study each one of these groups a methodology has been proposed based on identifying the continuous corporal waves that define the shape of all the members of each group. These waves are parametrised and are described by means of points in a shape space.

A method for resolving the problems of direct and inverse kinematics has been proposed establishing relations between the control spaces and that of the shapes, for each one of the gaits found. The search for these gaits has been done by means of genetic algorithms on the control space.

The problem of the minimum configurations has been formulated and the methodology employed to resolve it described, based on iterating on the number of modules and realising searches with genetic algorithms.

A technique has been proposed for analysing and synthesising movements based on identifying the minimum configurations in the wired model of other robots. This allows finding new gaits as well as deducing the viability of the movement of certain configurations which *a priori* it is not known if they would be able to move.

8.2.2 About movement in one dimension

The study of movement in one dimension has been completed for the robots of the pitch-pitch group, though it is applicable also to the pitch-yaw group thanks to the idea proposed of blocks. The equations have been calculated using generic blocks of parameters d and d_0 . Each study groups has different values for these parameters that when substituting them in the generic equations permits obtaining particular expressions for them.

It has been shown that only two parameters are necessary α and k to describe the shape of the apodal robots of this group of any length and to determine its properties of movement. Both the stability and the step depend on them. The dimensions of the control space are 2. By means of the relationships established the amplitude of the generators (A) and the phase difference ($\Delta\phi$) in the control space are obtained.

An equation has been proposed to calculate the robot's step and a criteria to determine the stability. Both can be expressed using either the parameters of the shape space (α, k) or the control space ($A, \Delta\phi$).

The mechanism that makes movement in a straight line possible is the appearance of a corporal wave that passes through the body of the robot. This wave is of the serpenoid type. The parameters α, k describe this global wave. The shape space is very useful to specify the restrictions in the dimensions of the robot, as for example, limiting the height so that it can advance through a tube.

8.2.3 About movement in a plane

The study of movement in a plane has been carried out for the robots of the pitch-yaw group. Only five parameters are necessary to characterise the movement of at least the eight gaits discovered. Expressed in the shape space they are: $\alpha_v, \alpha_h, k_v, k_h, \Delta\phi_{vh}$, and in the control space: $A_v, A_h, \Delta\phi_v, \Delta\phi_h$ and $\Delta\phi_{vh}$.

The mechanism that allows the movement of the robots is due to the appearance of a three-dimensional corporal wave that is the result of the superimposition of the two-dimensional waves that are applied to the vertical and horizontal joints. The size of the robot during the movement, the supporting points on the ground that give it stability and the deduction of the equations for the kinematic parameters are known through the study of the corporal waves.

A classification into different families of the types of three-dimensional waves has been proposed, according to the way they are propagated and the shape they adopt. Each gait is associated to a wave of a different family.

The gaits found have been studied in detail from the shape of the three-dimensional wave. They have between 1 and 3 degrees of freedom. For all of them either theoretical equations have been proposed to calculate the kinematic parameters or they have been deduced empirically from the experiments.

The movement in a circular path is obtained by means of the superimposition of a serpenoid wave in the vertical joints and a circular curve in the horizontal ones. They have three degrees of freedom, the angle of the arc of the path and the parameters α and k of the vertical serpenoid wave.

The rolling movement is characterised by the superimposition of two equal circular waves which are out of phase 90 degrees. They have only one degree of freedom, α , to specify the angle of the arc of the body. From analysing the wired model it has been proved that the rotation is executed for any value of α . Nevertheless, if the section of the robot is square, which happens in the real robots, the threshold value is calculated from α_{min} and defines if the movement will be rolling or flapping type.

The sideways movement is characterised by the superimposition of two serpenoid waves with the same number of undulations. The three-dimensional wave is of the isomorphic type. It has two degrees of freedom α and k that correspond to those of the horizontal wave. This movement can be executed in the inclined version in which a new parameter appears (β) to specify the inclination.

The movement of rotation allows the robot to change the orientation of its longitudinal axis. Two variants of the rotation exist, in S and in U. The first is characterised by the superimposition of two serpenoid waves (giving a three-dimensional non-isomorphic wave) and the second by a serpenoid and another circular. Both have two degrees of liberty.

8.2.4 About minimum configurations

The two minimum configurations that move in one or two dimensions have been found. The configuration PP is constituted of two pitch modules and the PYP of three, two of pitch and the central one of yaw. The first moves in a straight line, forwards or backwards and the second can execute five different gaits: straight line, circular path, sideways movement, rolling and rotation

All the gaits of the PYP configuration are characterised by the equations of their control sub-spaces that establish relations between the four parameters A_v , A_h , $\Delta\phi_v$ and $\Delta\phi_{vh}$. The free parameters are the degrees of freedom of movement. The kinematics of all the movements has been studied and equations proposed to calculate the step in function of its control parameters.

The movement in straight line has two degrees of freedom, A and $\Delta\phi$. A criteria has been proposed to establish the working point with the best co-ordination. It has been shown that, for the wired model, the best co-ordination is obtained in the range of $\Delta\phi$ between 108° and 110° .

The rolling movement has been studied in detail and the value of the minimum amplitude that has to be applied to execute it deduced, in function of the size of the modules. It has only one degree of

freedom, A , that determines the shape that the robot adopts during the movement. To execute it the two vertical joints are in phase and the horizontal one out of phase 90 degrees.

The sideways movement allows the robot to move sideways maintaining the same orientation of its body. The co-ordination is exactly the same as in the case of the rolling movement. According to the amplitude chosen one or other of the movements is executed.

The movement of rotation permits the robot to change the orientation of its body. It has one degree of freedom, A , that decides the angular step when it rotates. The two vertical joints are in opposition of phase, and the horizontal one out of phase 90 degrees.

8.2.5 About the robotic platform developed

As indicated in the introduction of the thesis, a platform has been developed, constituted of mechanics, hardware and software to prove the validity of the proposed solutions.

The Y1 modules designed for the construction of the apodal robot prototypes, in contrast to modules developed in other centres of investigation, are very cheap and easy to build. They consist of six pieces of plastic that are obtained by cutting manually (for the prototypes) or by laser (for greater quantities). They are designed to be used with the servos Futaba 3003 or compatibles, one of the cheapest and most widespread models. What is more, they are free modules. The blueprints for their construction are freely available.

The electronics used in positioning the servos is also free hardware. All the schemes, printed circuit boards (PCB) and *Gerber* files (for manufacturing) are available. Among other things, this allows other researchers or engineers to modify the electronics to include it in the modules, with the idea of building autonomous robots or to add sensors.

The software environment developed allows the simulation of any apodal robot with one dimensional topology. Also the software is free which means that other researchers can reproduce the experiments described in this thesis or create their own.

8.3 Future lines of investigation

As is common in science, the work of investigation presents more questions than those that are answered. This is the case with this thesis. The author has finished it with a certain feeling that it is unfinished. In truth it is so. So much remains to be investigated that the contribution of this work seems insignificant. Professor Juan Pablo Rozas of the University of Castilla la Mancha said to me once: “You must know that thesis are never finished, rather they are killed. Kill yours now.”

Some of the lines of investigation that give continuity to this thesis are:

- *Dynamic/energy study of one dimension topologies.* This thesis presents the movement of apodal robots by means of working points in the shape and control spaces, that define the shape of the robot during the movement, as well as its step (linear or angular). Nevertheless, no energy study has been carried out. It is proposed to find the equation of consumption and energy efficiency in function of the working point. In this way the movements where the consumption is less or the efficiency greater can be chosen. It is a very important problem to bring about the movement of autonomous robots.
- *Implementation of the controllers in hardware, using FPGA.* The controllers based on sinusoidal generators have the advantage that they can be produced in different technologies, amongst them digital circuits. The use of FPGA allows the materialisation of these controllers “by hardware”. This focus of movement “by means of hardware” is more similar to the biological systems where all the neurons and muscles function in parallel and are synchronised by means of connections between them.
- *Development of new controllers with feedback.* The problem of the co-ordination has been resolved, in such a way that the type of oscillations of the modules is known for the execution of the different movements. The next problem to be resolved is how to maintain this co-ordination constant though the means by which the robot moves changes. To maintain a constant rhythm, it will be necessary to include feedback. Two alternatives are proposed to address the design of the controller.

One is the study of the bio-inspired controllers, of CPG type, that take into account this feedback when generating the exit oscillations. This is being studied at this moment by the group of Computational Neuroscience of the UAM, in charge of Professor Pablo Varona. In a preliminary work, Herrero et al. [50] have proved the viability of the different architectures of CPG for movement in a straight line of robots of the pitch-pitch group. Recently they are adding feedback to the position of the servos. To carry out these experiments they have constructed a prototype of 8 joints from the Y1 Modules created in this thesis and are adding the electronics necessary for reading the positions of the servos.

On the other hand, following the ideas developed by Matellán et al. [93], the development of a controller has been proposed to obtain reactive behaviours. The idea is not the design of this controller, but its automatic generation by means of fuzzy logic and genetic algorithms.

- *Design of new modules.* The Y1 modules Y1 created for the construction of the apodal robot prototypes of this thesis are just the first generation. For the investigation of movement of new configurations more robust modules are needed, that incorporate servos with greater torque, as well as the electronics and batteries for the creation of autonomous robots. This is the aim of the new generation: the modules *GZ-I*¹ that are being developed in collaboration with the TAMS group of the university of Hamburg [180]. The prototypes are made of aluminium (figure 8.1).

¹<http://tams-www.informatik.uni-hamburg.de/people/hzhang/projects/modularrobot/index.php>

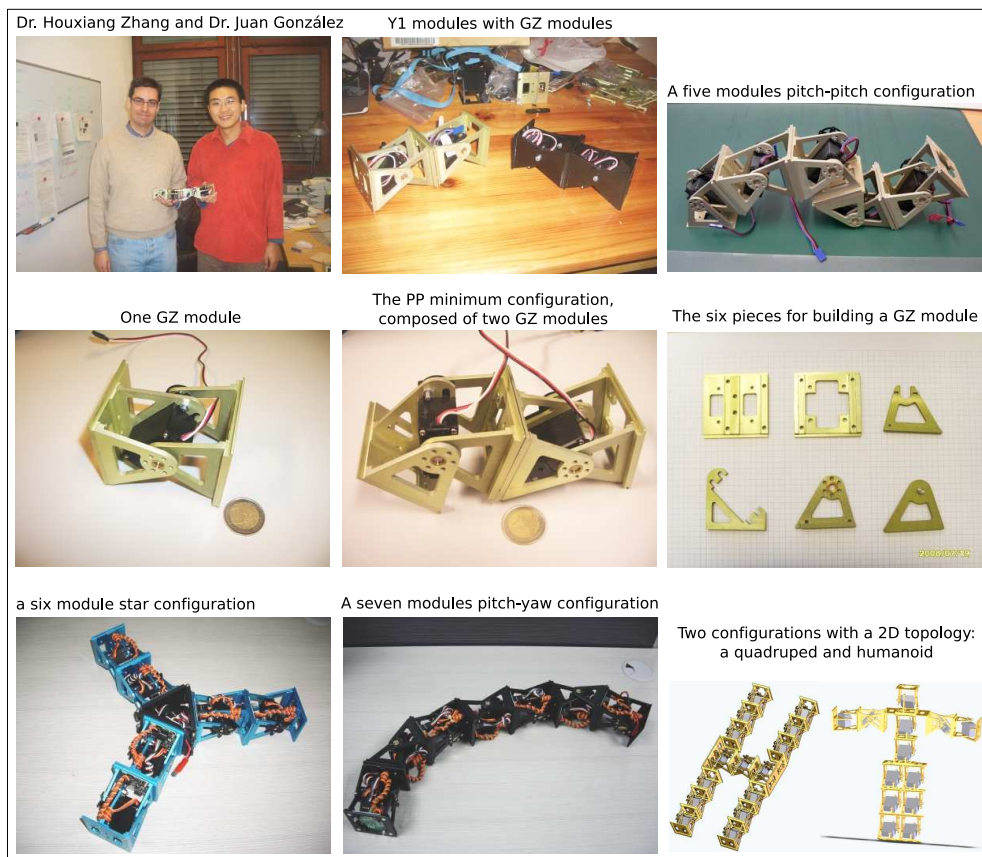


Figure 8.1: The next generation GZ-I modules

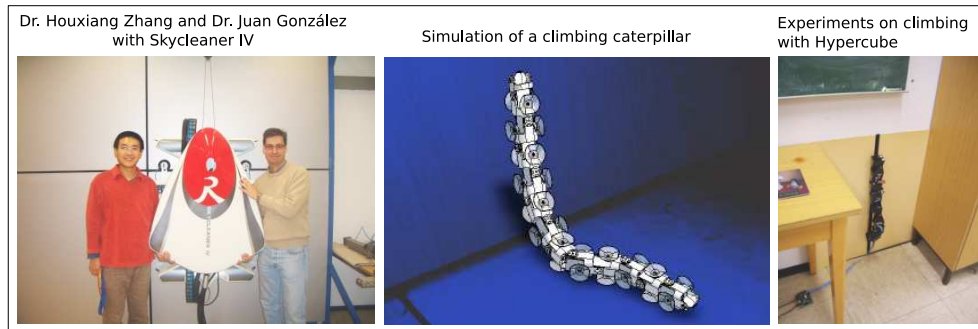


Figure 8.2: Climbing robot *Skycleaner* (left). Prototype of the climbing caterpillar that use passive suckers (middle). Experiments on climbing with Hypercube (right)

- *Study of the movement of the configurations with other topologies.* In this work the study of the movement of modular robots has been addressed, starting with the topologies of one dimension. The study of topologies of two or three dimensions is pending. New classifications have to be established, their properties of locomotion investigated and the minimum configurations of the new groups found. In previous articles [43] a minimum configuration of three modules was found with a two dimension topology capable of moving in three possible directions of the plane as well as rotating to change its orientation. In [180] experiments have been executed with a star shape topology of 6 modules, composed of the modules GZ.
- *The development of climbing caterpillar tracks.* One of the areas of robotics with industrial applications is that of climbing robots, where robots capable of moving on vertical surfaces are investigated and developed to carry out inspections, find leaks or execute cleaning tasks. One group as yet not explored is that of climbing robots with caterpillar tracks. They have the advantage that the body can flex to introduce itself into tubes or to change between surfaces with different slopes. The study of movement of the topologies of 1D can apply to the creation of this type of robot. In collaboration with the group TAMS of the University of Hamburg we are working on a prototype that uses passive suckers to grip on vertical surfaces [179]. In the figure 8.2 the cleaning robot, *Skycleaner*, designed by Houxiang Zhang, is shown, In the middle a drawing of the prototype of the climbing caterpillar and to the right can be seen a photo of the preliminary experiments realised with the robot Hypercube, created in this thesis.

The simulation tool designed in this thesis is only for 1D topologies, nevertheless, Rafael Treviño [149], in his bachelors thesis, has created the software MRSuite that also permits the simulation of topologies in 2D.

- *The development of climbing caterpillar.* One of the areas of robotics with industrial applications is that of climbing robots, where robots capable of moving on vertical surfaces are investigated and developed to carry out inspections, find leaks or execute cleaning tasks. One group as yet not explored is that of climbing caterpillar. They have the advantage that the body can flex to introduce itself into tubes or to change between surfaces with different slopes. The study of movement of the topologies of 1D can apply to the creation of this type of robot. In

collaboration with the group TAMS of the University of Hamburg we are working on a prototype that uses passive suckers to grip on vertical surfaces [179]. In the figure 8.2 the cleaning robot, Skycleaner, designed by Houxiang Zhang, is shown, In the middle a drawing of the prototype of the climbing caterpillar and to the right can be seen a photo of the preliminary experiments realised with the robot Hypercube, created in this thesis.

- *Development and implementation of behaviours.* With the contributions of this thesis an apodal robot of M modules can be converted into a mobile system capable of moving to any point (x,y) of the ground and with any orientation. The following step is to give it sensors and implement behaviours so that it becomes autonomous. One line of work will follow the employment of an architecture based on Dynamic schema hierarchies[7], developed by José María Cañas in his doctoral thesis[6] and implemented on an open source software platform for the development of applications with mobile robots². It is proposed to add to this environment the necessary component to support the modular robots.

²http://jde.gsync.es/index.php/Main_Page

Appendix A

Demonstrations and developments

A.1 Centre of mass of an apodal robot

Taking the equation 3.5 and substituting in it the value of the position vectors for those calculated in 3.1 the result is:

$$\vec{r} = \frac{1}{4M} \sum_{i=1}^M (\vec{I}_i + 2\vec{r}_i + \vec{D}_i)$$

This expression has to remain in function of the position vectors \vec{r}_i (i between 0 and $M + 1$).

The connection between the modules is such that the part on the right of the module i is connected to the left part of the following module $i + 1$. Therefore, (in the wired model) $\vec{D}_i = \vec{I}_{i+1}$ for i between 1 and $M - 1$. If from the previous equation the addend M is subtracted from the summation:

$$\vec{r} = \frac{1}{4M} \left(\sum_{i=1}^{M-1} (\vec{I}_i + 2\vec{r}_i + \vec{D}_i) + \vec{I}_M + 2\vec{r}_M + \vec{D}_M \right)$$

Substituting \vec{D}_i for \vec{I}_{i+1} and using the definition of $\vec{D}_M = \vec{r}_{M+1}$ gives:

$$\vec{r} = \frac{1}{4M} \left(\sum_{i=1}^{M-1} (\vec{I}_i + 2\vec{r}_i + \vec{I}_{i+1}) + \vec{I}_M + 2\vec{r}_M + \vec{r}_{M+1} \right)$$

Removing the terms \vec{I}_1 , $2\vec{r}_1$ and \vec{I}_m from the summation, the expression can be reordered like this:

$$\vec{r} = \frac{1}{4M} \left(\vec{T}_1 + 2\vec{r}_1 + \sum_{i \geq 2}^{M-1} (2\vec{T}_i + 2\vec{r}_i) + \vec{T}_M + \vec{T}_M + 2\vec{r}_M + \vec{r}_{M+1} \right)$$

Operating and applying the definition $\vec{T}_1 = \vec{r}_0$:

$$\vec{r}_{cm_i} = \frac{1}{4M} \left(\vec{r}_0 + 2\vec{r}_1 + \sum_{i \geq 2}^{M-1} (2\vec{T}_i + 2\vec{r}_i) + 2\vec{T}_M + 2\vec{r}_M + \vec{r}_{M+1} \right)$$

The value of the position vector of the extreme left \vec{T}_i can be expressed in function of the position vectors of the module $i - 1$ and i :

$$\vec{T}_i = \frac{\vec{r}_{i-1} + \vec{r}_i}{2}, i \in [2, M]$$

Substituting in the previous equation:

$$\vec{r} = \frac{1}{4M} \left(\vec{r}_0 + 2\vec{r}_1 + \sum_{i \geq 2}^{M-1} (\vec{r}_{i-1} + 3\vec{r}_i) + \vec{r}_{M-1} + 3\vec{r}_M + \vec{r}_{M+1} \right)$$

Subtracting from the summation the term \vec{r}_1 and introducing \vec{r}_{M-1} the final expression is arrived at:

$$\vec{r} = \frac{1}{4M} \left(\vec{r}_0 + 3\vec{r}_1 + 4 \sum_{i \geq 2}^{M-1} \vec{r}_i + 3\vec{r}_M + \vec{r}_{M+1} \right)$$

q.e.d

A.2 Supporting segments of the PP configuration

A.2.1 Supporting segment 1

Starting with the expression:

$$Sa_1 = z_0 + z_1 = Le^{j\varphi_0} \left(\frac{1}{2} + e^{j\varphi_1} \right)$$

Calculation of the module:

$$\|Sa_1\| = L \left\| \frac{1}{2} + e^{j\varphi_1} \right\|$$

Using the property that $\|z\|^2 = z \cdot \bar{z}$, we get:

$$\left\| \frac{1}{2} + e^{j\varphi_1} \right\|^2 = \left(\frac{1}{2} + e^{j\varphi_1} \right) \left(\frac{1}{2} + e^{-j\varphi_1} \right) = \frac{1}{4} + \frac{e^{-j\varphi_1}}{2} + \frac{e^{j\varphi_1}}{2} + 1 = \frac{5}{4} + \cos(\varphi_1)$$

The final expression is:

$$\|Sa_1\| = L \sqrt{\frac{5}{4} + \cos(\varphi_1)}$$

Calculation of the argument:

$$\text{Arg}(Sa_1) = \varphi_0 + \text{Arg}\left(\frac{1}{2} + e^{j\varphi_1}\right)$$

and knowing that the argument is the arc tangent of the imaginary part divided by the real:

$$\text{Arg}\left(\frac{1}{2} + e^{j\varphi_1}\right) = \arctan\left(\frac{\sin(\varphi_1)}{\frac{1}{2} + \cos(\varphi_1)}\right)$$

The result is:

$$\text{Arg}(Sa_1) = \varphi_0 + \arctan\left(\frac{\sin(\varphi_1)}{\frac{1}{2} + \cos(\varphi_1)}\right)$$

A.2.2 Calculation of the supporting segment 2

$$Sa_2 = z_0 + z_1 + z_2 = Le^{j\varphi_0} \left(\frac{1}{2} + e^{j\varphi_1} + \frac{1}{2} e^{j(\varphi_1 + \varphi_2)} \right)$$

The module is calculated in this way:

$$\|Sa_2\| = L \left\| \left(\frac{1}{2} + e^{j\varphi_1} + \frac{1}{2} e^{j(\varphi_1 + \varphi_2)} \right) \right\|$$

and developing the module of the right part using the property: $\|z\|^2 = z \cdot \bar{z}$,

$$\begin{aligned} &= \left(\frac{1}{2} + e^{j\varphi_1} + \frac{1}{2} e^{j(\varphi_1 + \varphi_2)} \right) \overline{\left(\frac{1}{2} + e^{j\varphi_1} + \frac{1}{2} e^{j(\varphi_1 + \varphi_2)} \right)} = \\ &= \left(\frac{1}{2} + e^{j\varphi_1} + \frac{1}{2} e^{j(\varphi_1 + \varphi_2)} \right) \left(\frac{1}{2} + e^{-j\varphi_1} + \frac{1}{2} e^{-j(\varphi_1 + \varphi_2)} \right) = \\ &= \frac{1}{4} + \frac{1}{2} e^{-j\varphi_1} + \frac{1}{4} e^{-j(\varphi_1 + \varphi_2)} + \frac{1}{2} e^{j\varphi_1} + 1 + \frac{1}{2} e^{-j\varphi_2} + \frac{1}{4} e^{j(\varphi_1 + \varphi_2)} + \frac{1}{2} e^{j\varphi_2} + \frac{1}{4} = \\ &= \frac{3}{2} + \cos(\varphi_1) + \cos(\varphi_2) + \frac{1}{2} \cos(\varphi_1 + \varphi_2) \end{aligned}$$

Therefore, the final expression is:

$$\|Sa_2\| = L \sqrt{\frac{3}{2} + \cos(\varphi_1) + \cos(\varphi_2) + \frac{1}{2} \cos(\varphi_1 + \varphi_2)}$$

For the calculation of the argument:

$$\text{Arg}(Sa_2) = \varphi_0 + \text{Arg} \left(\frac{1}{2} + e^{j\varphi_1} + \frac{1}{2} e^{j(\varphi_1 + \varphi_2)} \right)$$

And calculating the value of the second term as the arc tangent of the imaginary part between the real the result is:

$$\text{Arg}(Sa_2) = \varphi_0 + \arctan \left(\frac{\sin \varphi_1 + \frac{1}{2} \sin(\varphi_1 + \varphi_2)}{\frac{1}{2} + \cos \varphi_1 + \frac{1}{2} \cos(\varphi_1 + \varphi_2)} \right)$$

A.3 Transitional phase of the PP configuration

We start with the equation:

$$\varphi_0^1 + \varphi_1 + \varphi_2 = 0$$

Substituting in the equation the values of the bending angles for $\phi = \phi_{12}$ the result is:

$$\varphi_0^1(\phi_{12}) + A \sin \phi_{12} + A \sin(\phi_{12} + \Delta\Phi) = 0 \quad (\text{A.1})$$

If, in the previous expression, $\varphi_0^1(\phi_{12})$ is substituted for its expression given in 6.15 it is not trivial to clear ϕ_{12} . Therefore we adopt a different focus. If $\varphi_0^1(\phi_{12})$ is developed in the Fourier series and it is approximated by the first harmonic the result is:

$$\varphi_0^1(\phi_{12}) = -A_0 \sin \phi_{12}$$

where the co-efficient A_0 is given for:

$$A_0 = \arctan \left(\frac{\sin A}{\frac{1}{2} + \cos A} \right)$$

The equation A.1 remains as:

$$-A_0 \sin \phi_{12} + A \sin \phi_{12} + A \sin(\phi_{12} + \Delta\Phi) = 0$$

Grouping terms:

$$(A - \alpha) \sin \phi_{12} + A \sin(\phi_{12} + \Delta\Phi) = 0$$

This expression can be stated as:

$$B \sin(\phi_{12} + C) = 0 \quad (\text{A.2})$$

where the constants B and C have the values:

$$B = \sqrt{(A - A_0)^2 + A^2 + 2(A - A_0)A \cos \Delta\Phi}$$

$$C = \arctan \left(\frac{\sin \Delta\Phi}{\left(1 - \frac{A_0}{A}\right) + \cos \Delta\Phi} \right)$$

To fulfil the equation A.2, the term $\Phi_{12} + C$ has to be zero which allows us to obtain the final value for Φ_{12} :

$$\Phi_{12} = -\arctan \left(\frac{\sin \Delta\Phi}{\left(1 - \frac{A_0}{A}\right) + \cos \Delta\Phi} \right)$$

A.4 Rotation angle of the PYP configuration

A.4.1 Stage 1

We will calculate the rotation angle θ_1 of stage 1 of the rolling movement of the PYP configuration.

Starting with the definition of the following homogeneous transformations:

$$H_0^1 = \begin{pmatrix} \cos \theta_1 & 0 & \sin \theta_1 & 0 \\ 0 & 1 & 0 & 0 \\ -\sin \theta_1 & 0 & \cos \theta_1 & 0 \\ 0 & 0 & 0 & 1 \end{pmatrix}, H_1^2 = \begin{pmatrix} \cos \theta_2 & -\sin \theta_2 & 0 & 0 \\ \sin \theta_2 & \cos \theta_2 & 0 & 0 \\ 0 & 0 & 1 & 0 \\ 0 & 0 & 0 & 1 \end{pmatrix}, H_2^3 = \begin{pmatrix} 1 & 0 & 0 & 0 \\ 0 & \cos \theta_3 & -\sin \theta_3 & L \\ 0 & \sin \theta_3 & \cos \theta_3 & 0 \\ 0 & 0 & 0 & 1 \end{pmatrix}$$

We obtain the matrix H_1^3 :

$$H_1^3 = H_1^2 H_2^3 = \begin{pmatrix} \cos \theta_2 & -\sin \theta_2 \cos \theta_3 & \sin \theta_2 \sin \theta_3 & -L \sin \theta_2 \\ \sin \theta_2 & \cos \theta_2 \cos \theta_3 & -\cos \theta_2 \sin \theta_3 & L \cos \theta_2 \\ 0 & \sin \theta_3 & \cos \theta_3 & 0 \\ 0 & 0 & 0 & 1 \end{pmatrix}$$

The position vector of the extreme right is $\vec{r}_3^A = \frac{L}{2} \hat{y}_3$.

Referred to the frame R0 is:

$$\vec{r}_4 = H_0^1 H_1^2 H_2^3 \vec{r}_3^4 = H_0^1 H_1^3 \vec{r}_3^4$$

To simplify the calculations we will do it in parts. First we calculate:

$$\vec{r}_1^4 = H_1^3 \vec{r}_3^4 = H_1^3 \begin{pmatrix} 0 \\ \frac{L}{2} \\ 0 \\ 1 \end{pmatrix} = \begin{pmatrix} -\frac{L}{2} \sin \theta_2 \cos \theta_3 - L \sin \theta_2 \\ \frac{L}{2} \cos \theta_2 \cos \theta_3 + L \cos \theta_2 \\ \frac{L}{2} \sin \theta_3 \\ 1 \end{pmatrix} = \begin{pmatrix} a \\ b \\ c \\ d \end{pmatrix}$$

The components of \vec{r}_1^4 we denote by a,b,c,and d. Separately we calculate \vec{r}_4 :

$$\vec{r}_4 = H_0^1 \vec{r}_1^4 = \begin{pmatrix} a \cos \theta_1 - c \sin \theta_1 \\ b \\ -a \sin \theta_1 + c \cos \theta_1 \\ d \end{pmatrix}$$

We impose the restriction $\vec{r}_4 \cdot \hat{z}_0 = 0$, which gives us the expression:

$$-a \sin \theta_1 + c \cos \theta_1 = 0$$

Clearing θ_1 we have:

$$\tan \theta_1 = \frac{c}{a}$$

Substituting the values of c and a by their corresponding previously calculated values:

$$\tan \theta_1 = \frac{\frac{L}{2} \sin \theta_3}{-\frac{L}{2} \sin \theta_2 \cos \theta_3 - L \sin \theta_2} = -\frac{\sin \theta_3}{(2 + \cos \theta_3) \sin \theta_2}$$

We obtain the expression for θ_1 in function of θ_2 and θ_3 .

A.4.2 Stage 2

The procedure is similar to the section A.4.1, but in dealing with stage 2 matrix H_{-90} has to be added:

$$H_{-90} = \begin{pmatrix} 0 & 0 & -1 & 0 \\ 0 & 1 & 0 & 0 \\ 1 & 0 & 0 & 0 \\ 0 & 0 & 0 & 1 \end{pmatrix}$$

The right segment, referred to the frame R3 is: $\vec{d}_3^4 = \frac{L}{2}\hat{y}_3$.

Its expression referred to R0 is:

$$\vec{d}_4 = H_{-90}H_0^1H_1^2H_2^3\vec{d}_3^4 = H_{-90}H_0^1H_1^3\vec{d}_3^4$$

To simplify the calculations we will do it in parts. First we calculate:

$$\vec{d}_1^4 = H_1^3\vec{d}_3^4 = H_1^3 \begin{pmatrix} 0 \\ \frac{L}{2} \\ 0 \\ 0 \end{pmatrix} = \begin{pmatrix} -\frac{L}{2}\sin\theta_2\cos\theta_3 \\ \frac{L}{2}\cos\theta_2\cos\theta_3 \\ \frac{L}{2}\sin\theta_3 \\ 0 \end{pmatrix} = \begin{pmatrix} a \\ b \\ c \\ 0 \end{pmatrix}$$

The components of \vec{d}_1^4 we denote by a, b and c. On the other hand we calculate \vec{d}_4 :

$$\vec{d}_4 = H_{-90}H_0^1\vec{d}_1^4 = \begin{pmatrix} a\sin\theta_1 - c\cos\theta_1 \\ b \\ a\cos\theta_1 + c\sin\theta_1 \\ 0 \end{pmatrix}$$

We impose the restriction $\vec{d}_4 \cdot \hat{z}_0 = 0$, which gives us the expression:

$$a\cos\theta_1 + c\sin\theta_1 = 0$$

Clearing θ_1 we have:

$$\tan \theta_1 = -\frac{a}{c}$$

Substituting the values of c and a for their corresponding values previously calculated:

$$\tan \theta_1 = -\frac{\frac{L}{2} \sin \theta_2 \cos \theta_3}{\frac{L}{2} \sin \theta_3} = -\frac{\sin \theta_2}{\tan \theta_3}$$

We obtain the expression for θ_1 in function of θ_2 and θ_3 .

Appendix B

Genetic Algorithms

B.1 Description

In the search for solutions by means of genetic algorithms the software packet PGAPack¹ has been used, with the options by default. In the table B.1 the parameters employed are summarised.

The individuals are represented by means of chains of integers, ordered in the form: $A_v, A_h, \Delta\Phi_v, \Delta\Phi_h$ and $\Delta\Phi_{vh}$, with the restrictions: $A_v, A_h \in [0, 90]$ and $\Delta\Phi_v, \Delta\Phi_h, \Delta\Phi_{vh} \in [-180, 180]$.

The evaluation functions employed are the step along the length of the x axis (Δx), of the y axis (Δy), rotation angle around the z axis (yaw) and the inclined angle (roll). For its implementation the physical simulator ODE (Open Dynamics Engine) has been used. Two cycles are completed so that the robot reaches its stationary regime and the step is calculated (linear or angular) in the following cycle. The solution looked for is that which maximises the step.

¹http://www-fp.mcs.anl.gov/CCST/research/reports_pre1998/comp_bio/stalk/pgapack.html

Population size	100
Generations	100
Data types:	String of integers (PGA_DATATYPE_INTEGER)
Selection:	Tournament. Probability: 0.6
Crossover:	Two points
Population replacement:	SSGA.Replaced 10% of individuals
Mutation:	Probability: 0.001

Table B.1: Parameters employed for the genetic algorithms

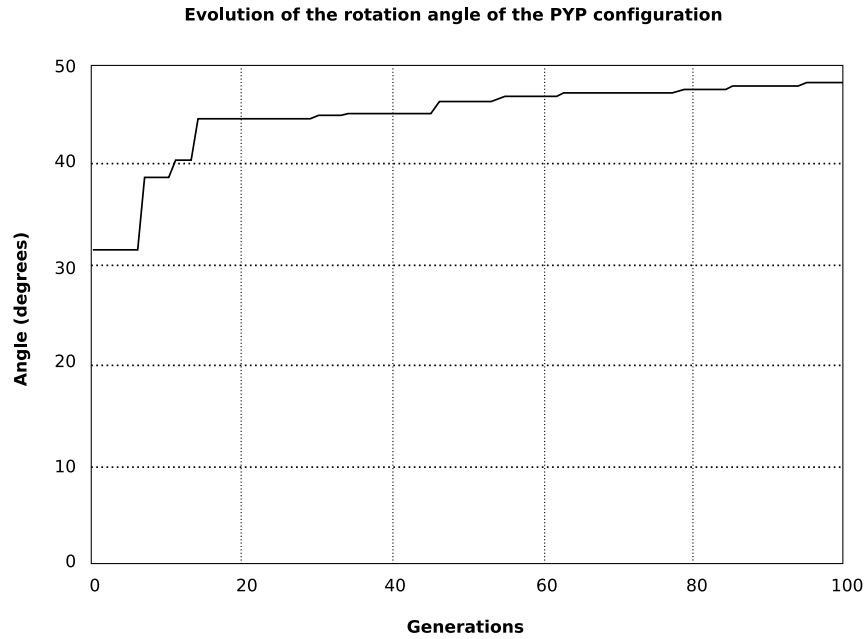


Figure B.1: Evolution of the rotation angle of the PYP configuration

B.2 Example

The functioning of the developed application is illustrated with an example. It is necessary to obtain the solutions so that the minimum PYP configuration carries out a rotation of the greatest possible angle per cycle. Therefore execute:

```
./GA_PYn 2 1 YAW 3 100 100
```

In the machine where the tests have been realised, a Dell Latitude D810 laptop, with 512MB of RAM and Intel Pentium processor of 1.73ghz, it takes 13 minutes approximately to complete.

The results are returned in two files. One of text that contains all the individuals of all the generations. The other is a script in Octave that draws the evolution of the step with the generations. The graph that corresponds to this example is shown in the figure B.1. In the initial population, generated randomly at least one individual has appeared that rotates around 30 degrees. This does not mean that it executes a good movement, but that at the end of a cycle its orientation has varied 30 degrees, but it could refer to a chaotic movement. As the generations progress individuals appear that each time rotate more and with a better co-ordinated movement.

Appendix C

Y1 modules

C.1 Plans

The plans shown here are not to a scale of 1:1, they have been reduced 20% enabling their correct integration into this appendix¹. The plans included are the following:

1. Futaba 3003 servo
2. Piece F
3. Piece E
4. Pieces B1 and B2
5. Piece FE
6. Mounted module (I)
7. Mounted module (II)
8. Four Y1 modules with pitch-pitch connection
9. Screws used

¹All the information is available in: http://www.learobotics.com/wiki/index.php?title=M%C3%B3dulos_Y1

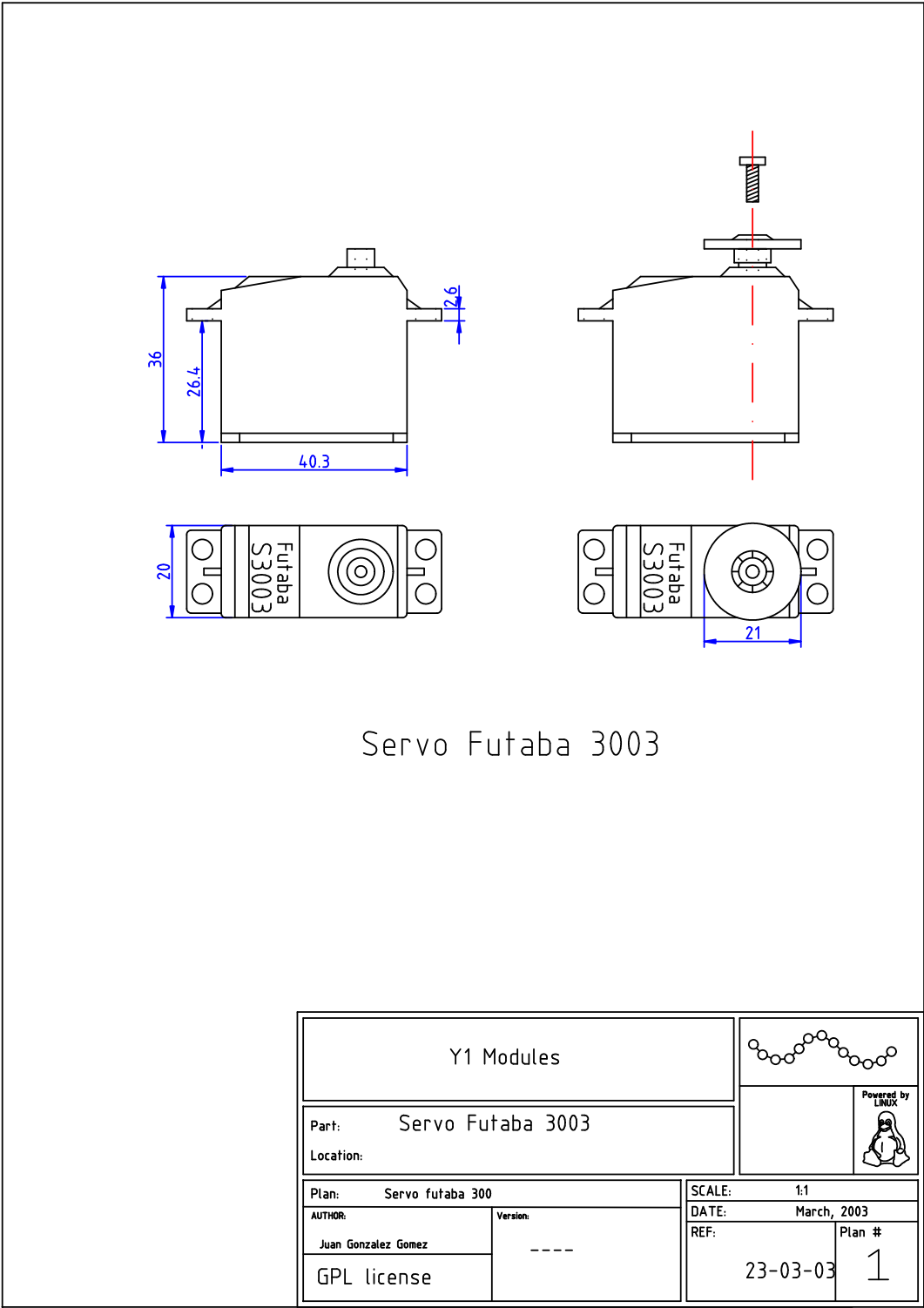


Figure C.1: Plan 1: Servo Futaba 3003

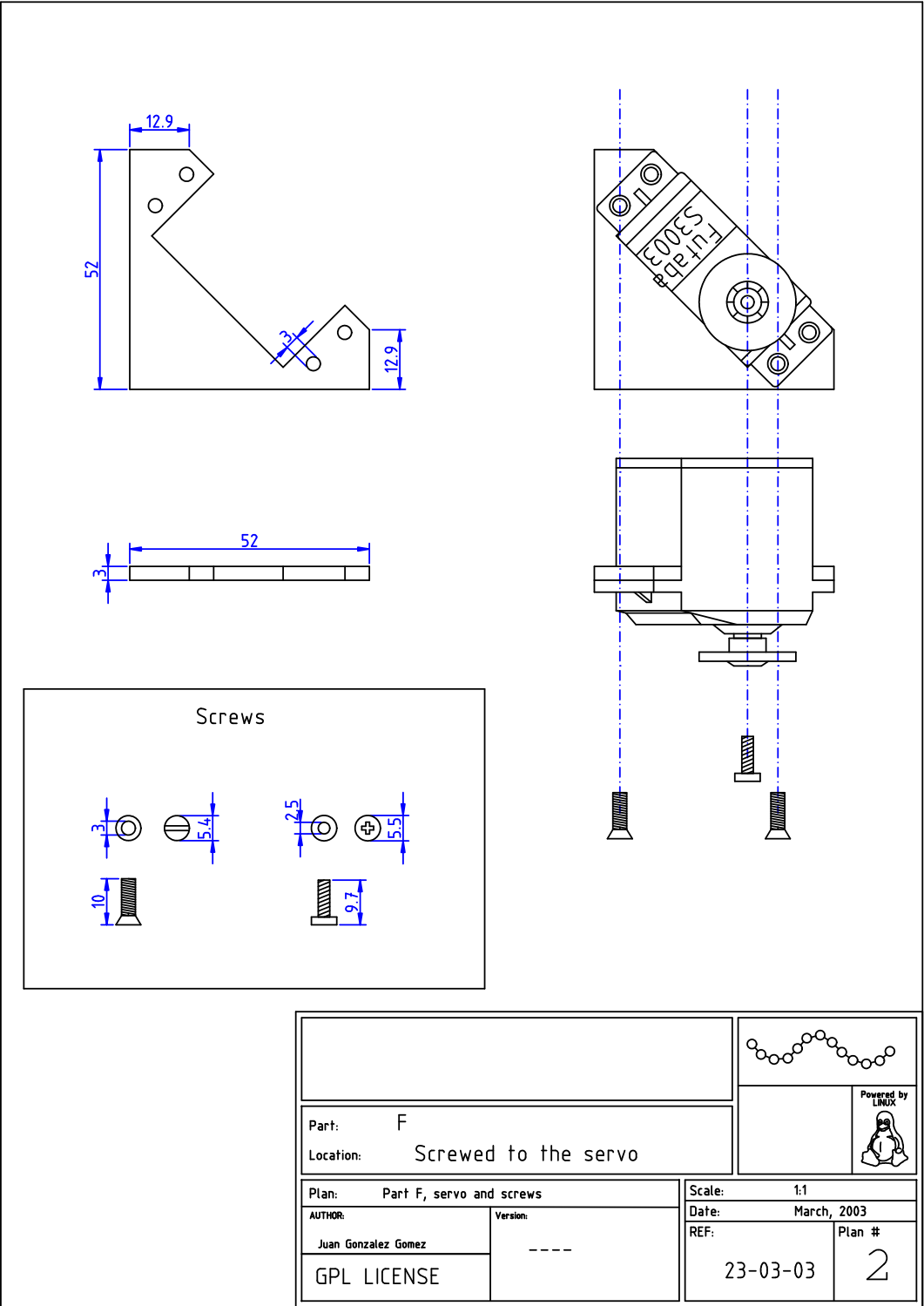


Figure C.2: Plan 2: Piece F

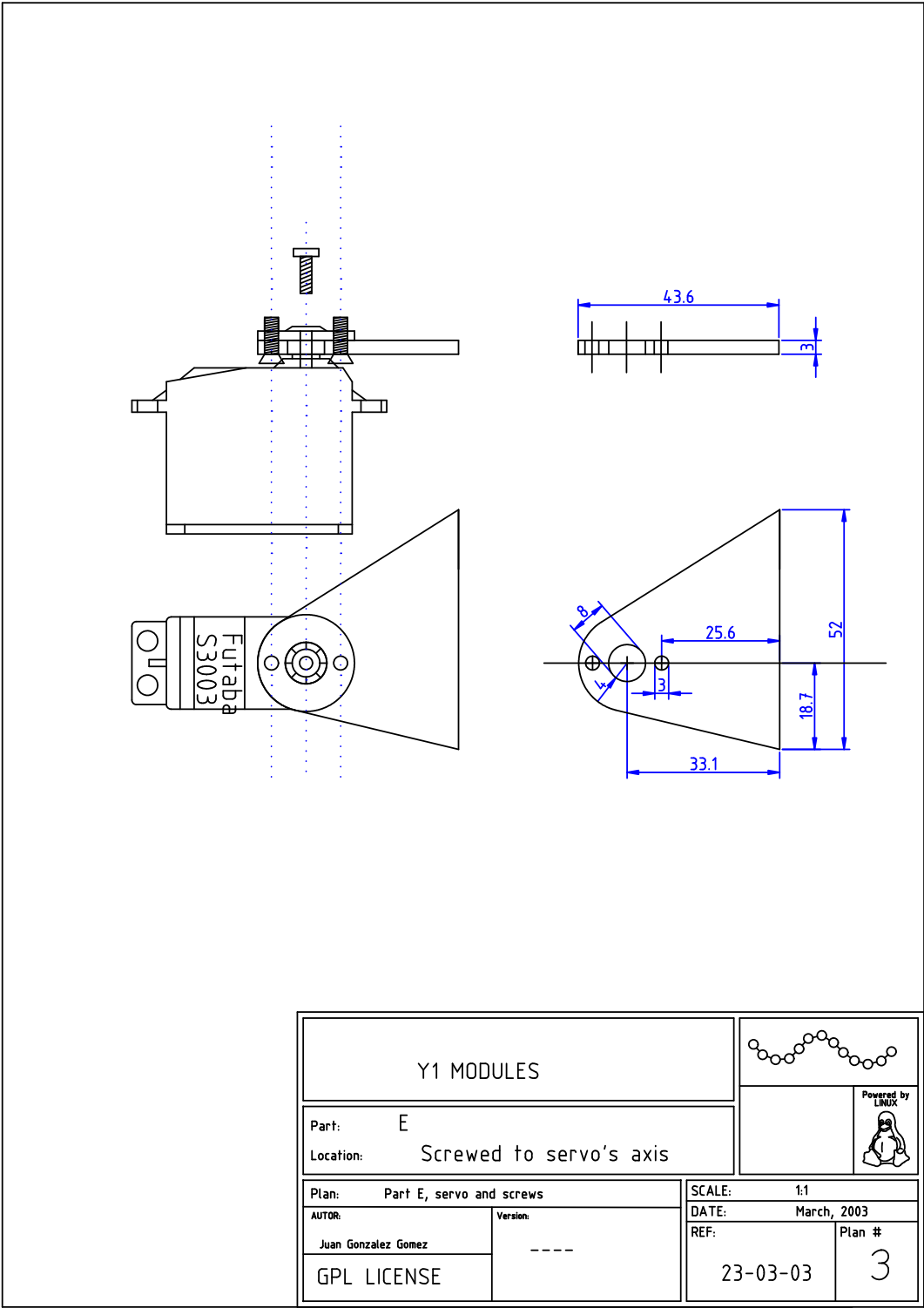


Figure C.3: Plan 3: Piece E

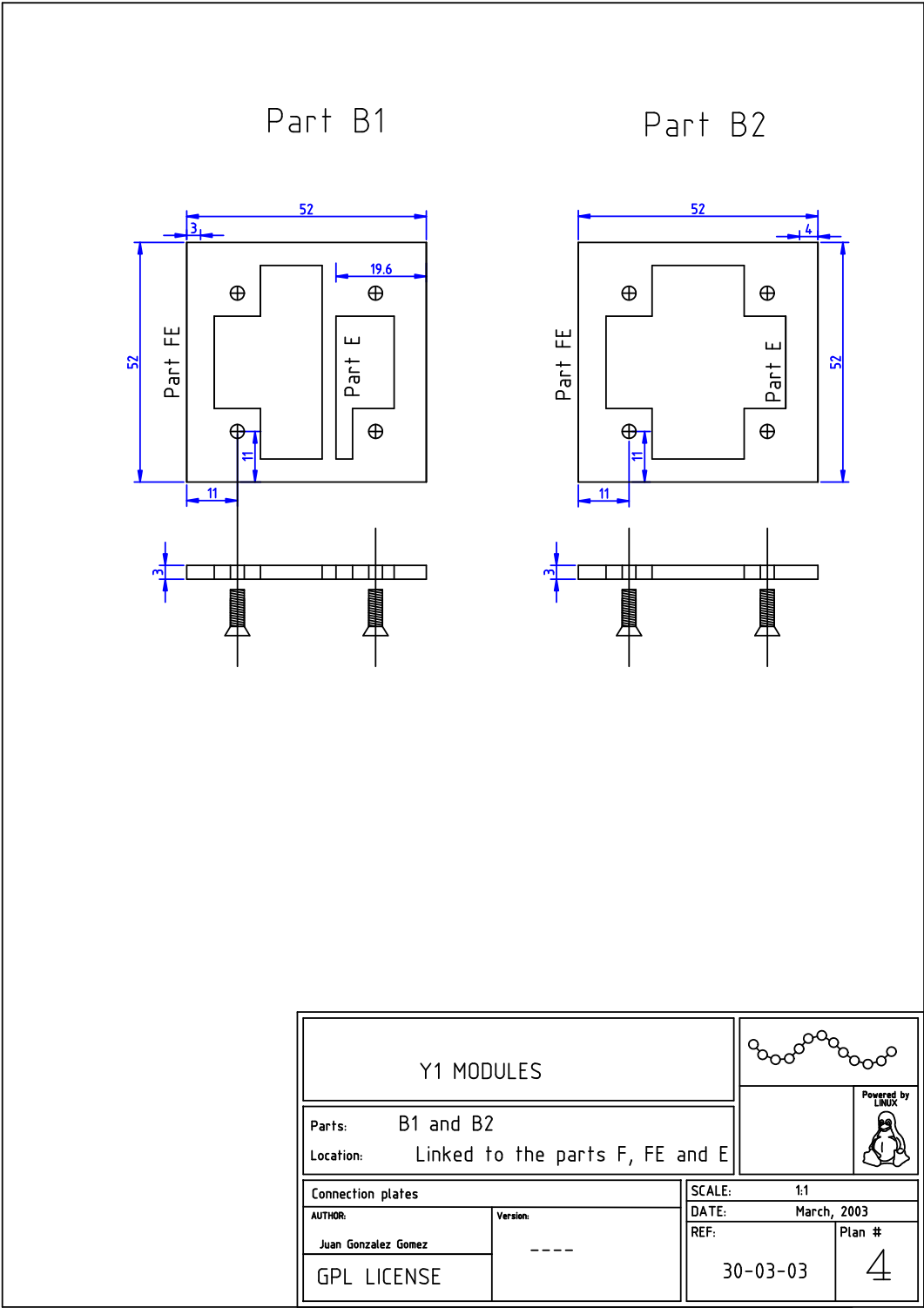


Figure C.4: Plan 4: Pieces B1 and B2

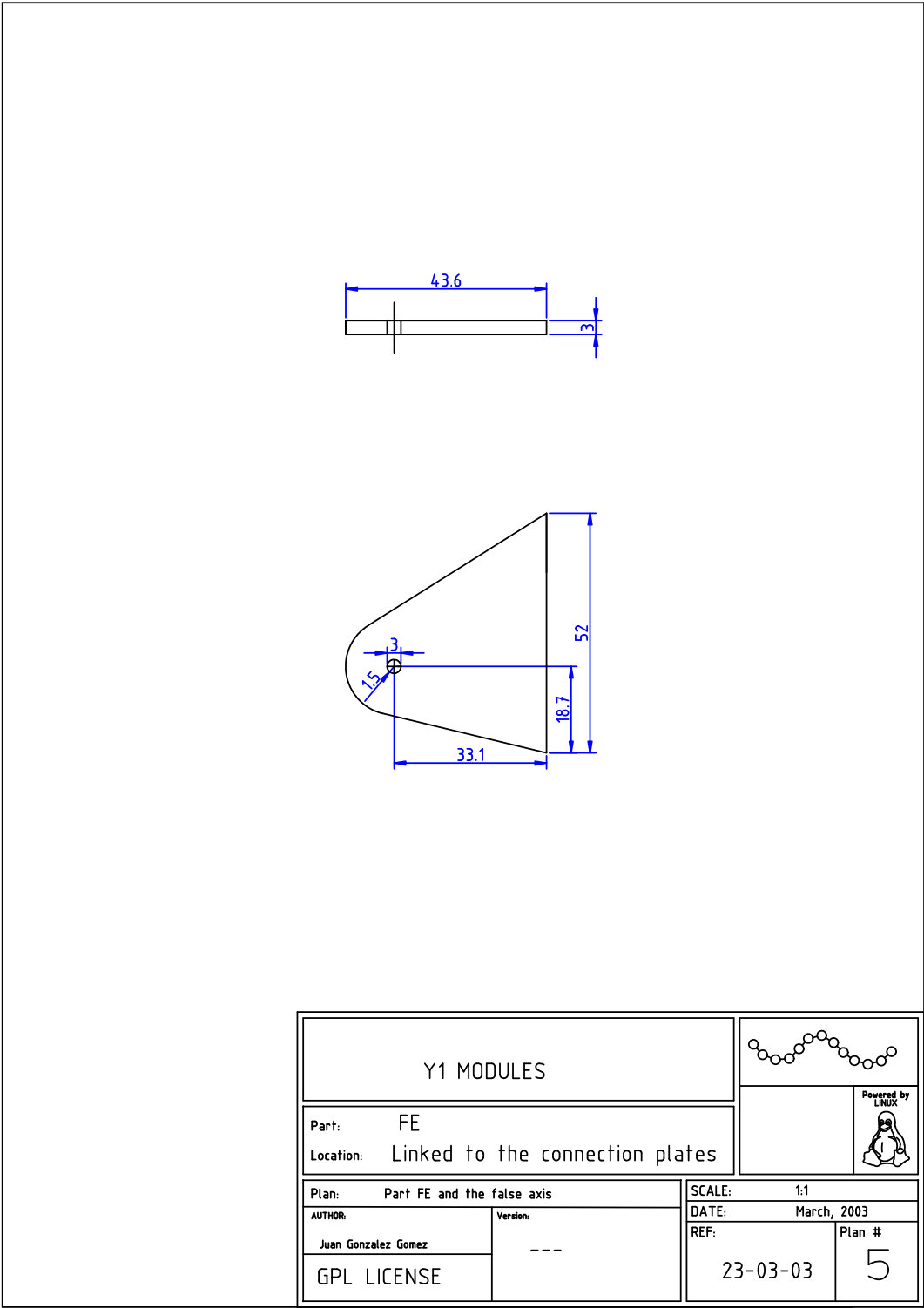


Figure C.5: Plan 5: Piece FE

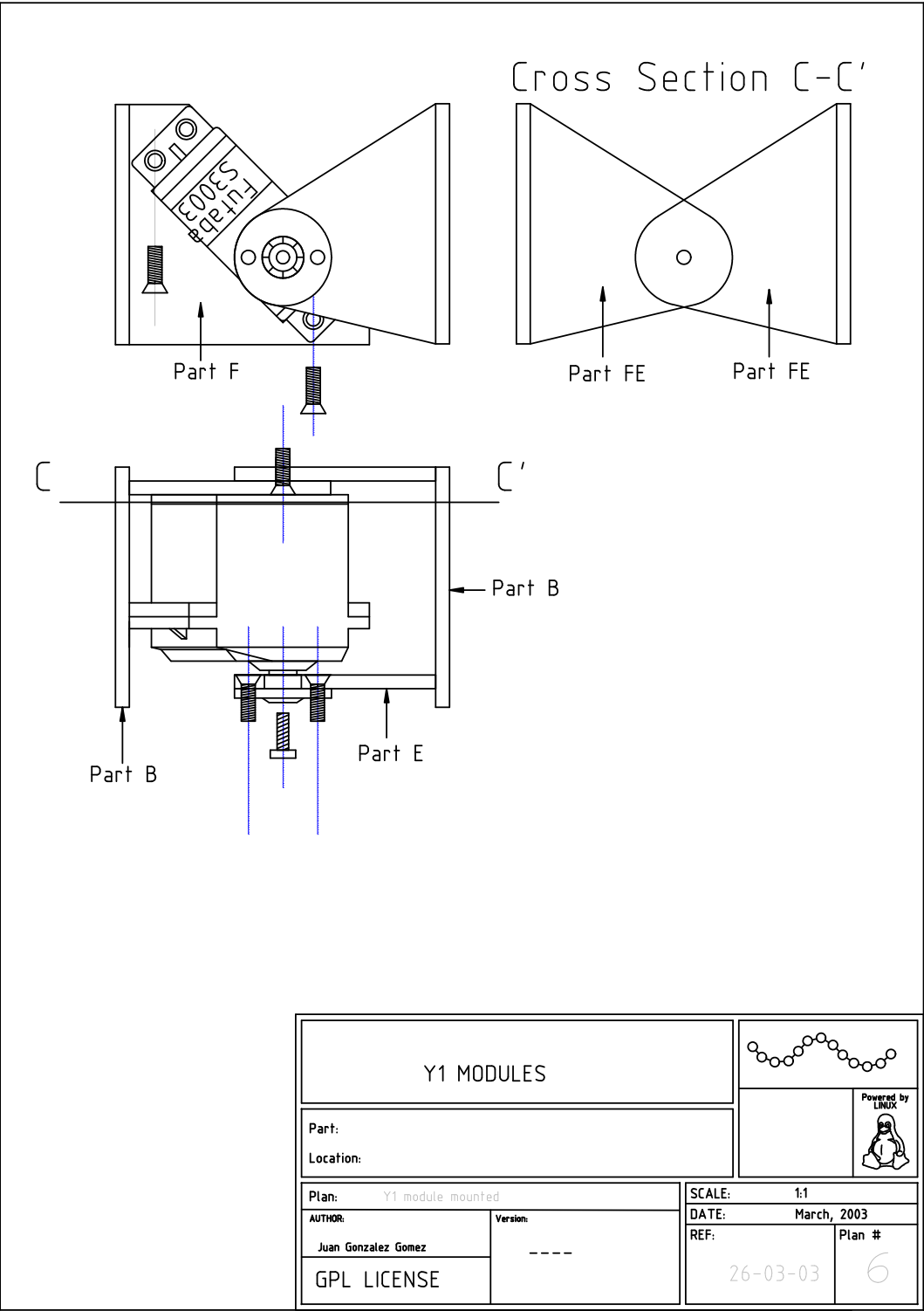


Figure C.6: Plan 6: Mounted module (I)

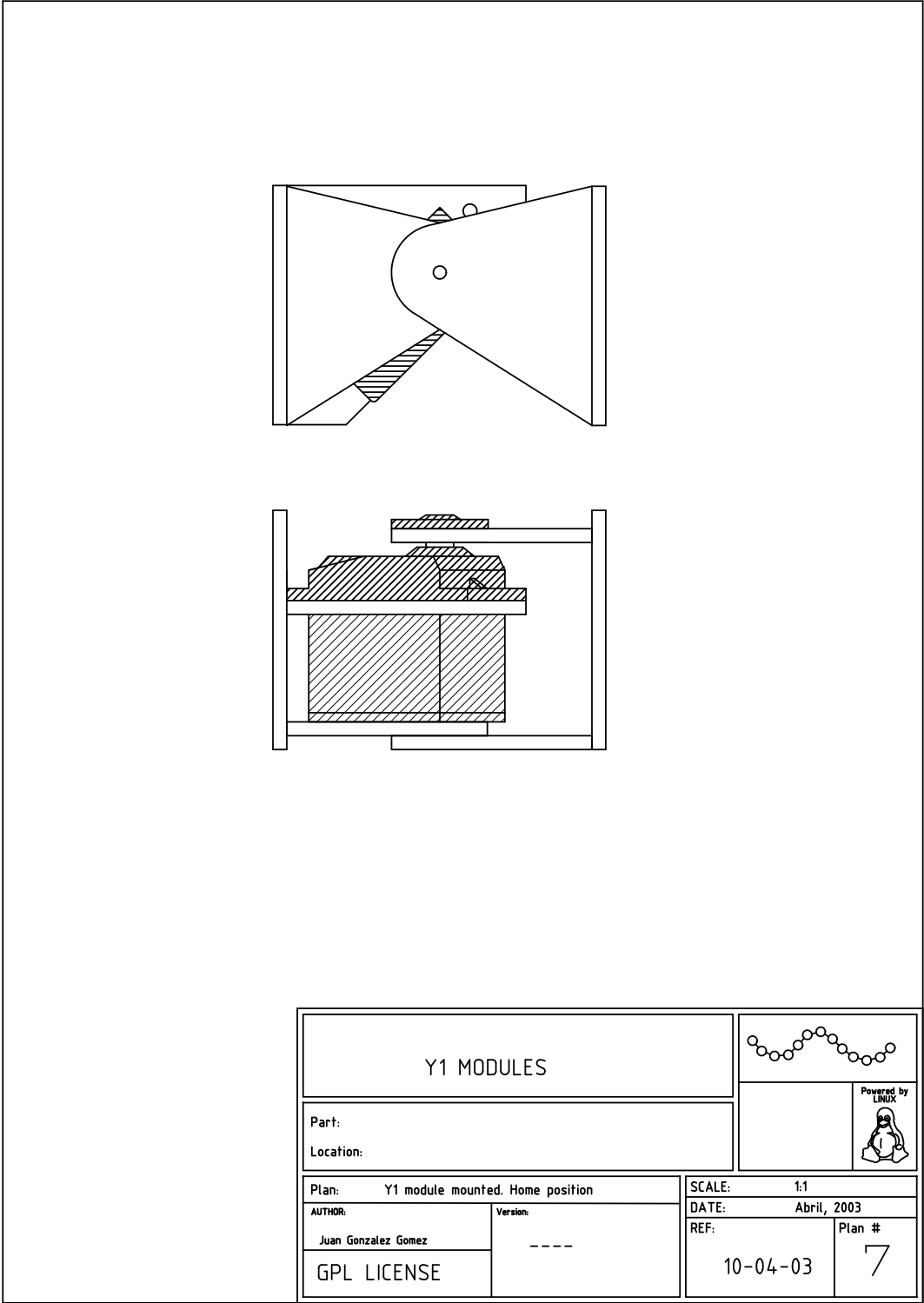


Figure C.7: Plan 7: Mounted module (II)

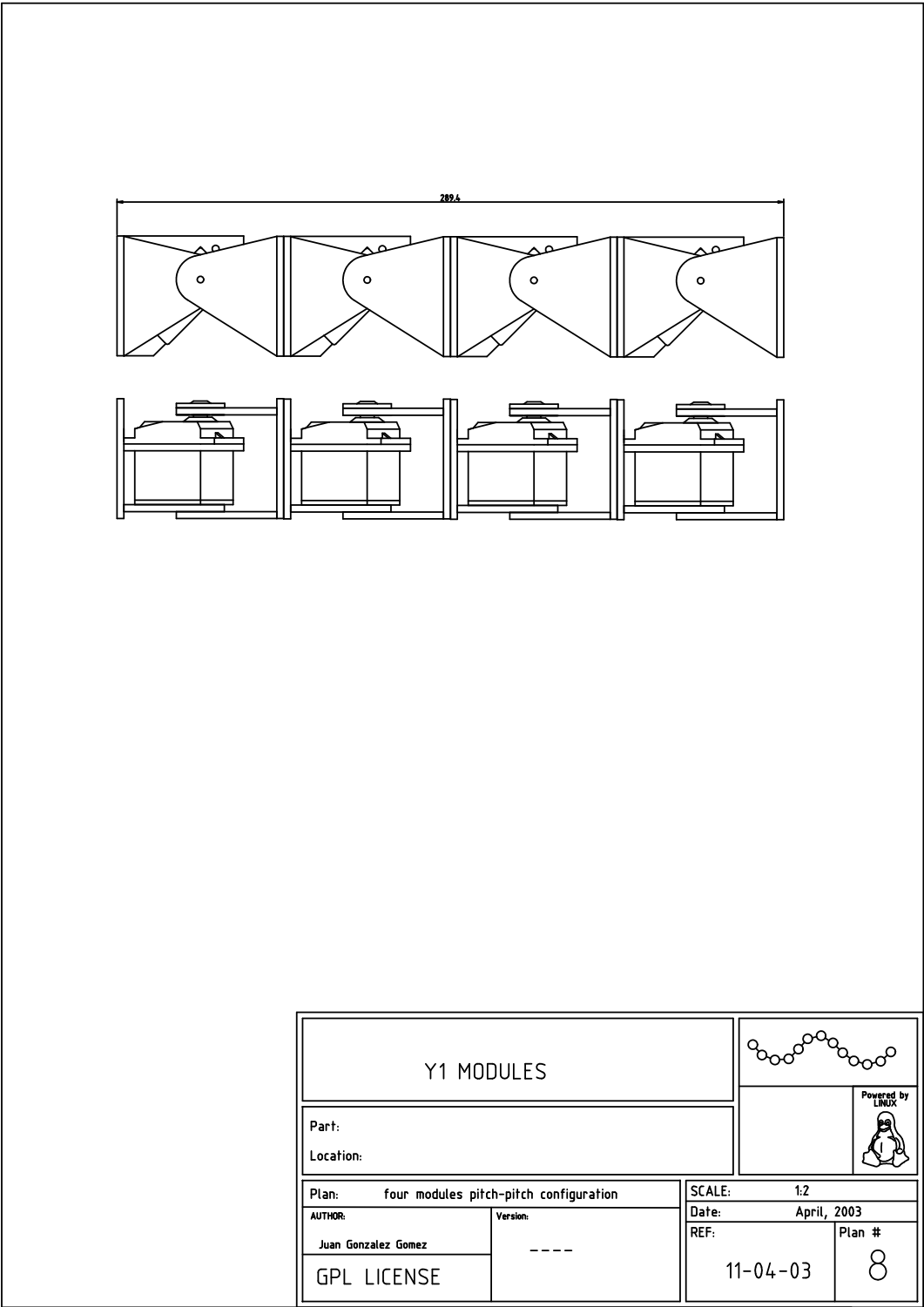


Figure C.8: Plan 8: 4 Y1 modules with pitch-pitch connection.

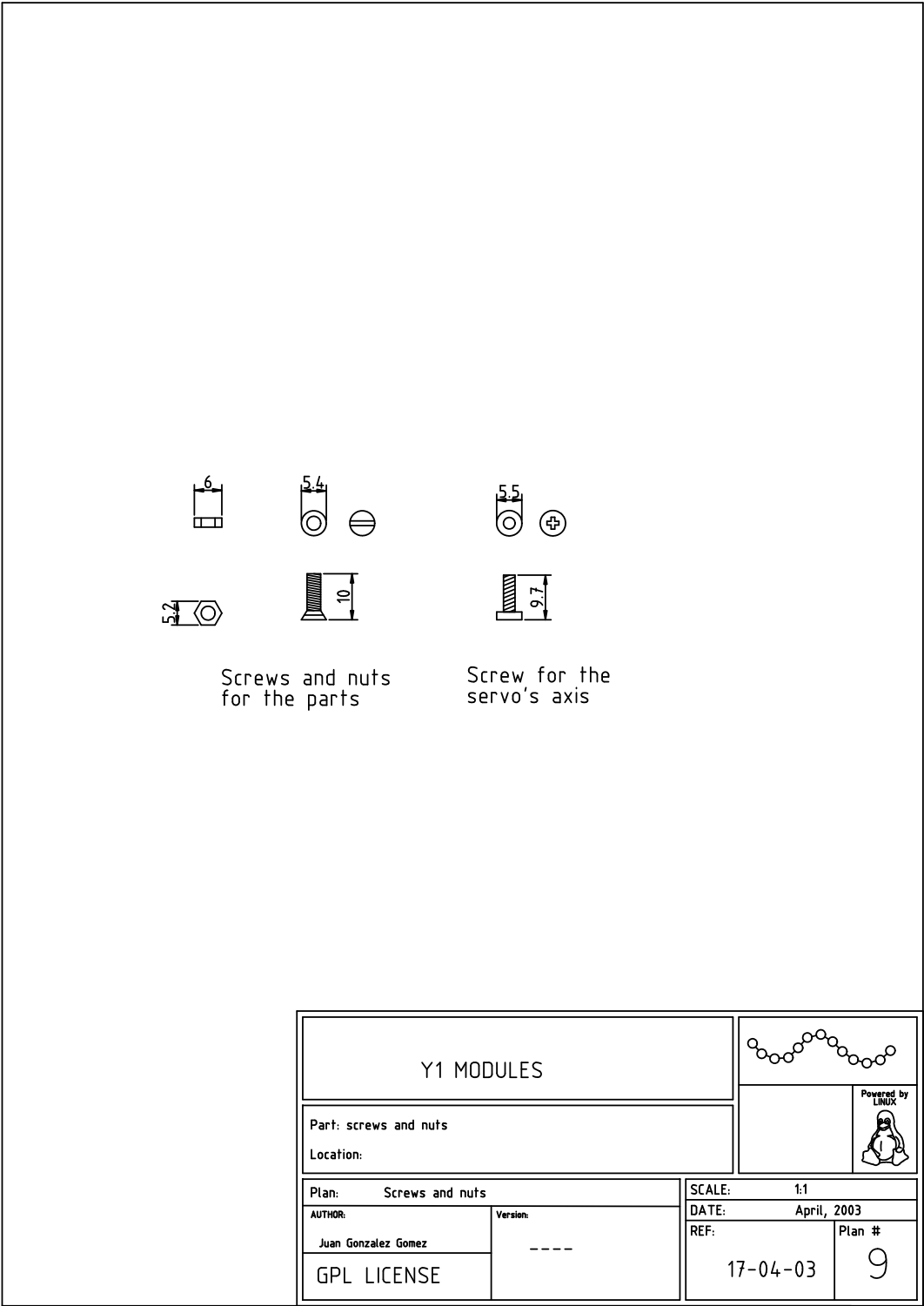


Figure C.9: Plan 9: Screws employed

C.2 Assembling

This appendix describes how to mount the Y1 modules from the basic pieces. The pieces can be obtained in the following way:

- Construct them oneself. For this the best is to print the templates of the pieces on an A4 transparent adhesive paper. Stick it on the sheet of material employed for its construction (expanded PVC, methacrylate, etc.). Cut the pieces and make the drills, For the first prototypes we have used a hacksaw of the type used to cut wood.
- Give the template to a workshop where they do the cutting. This is the best solution for making many modules.

Once all the pieces are available, the assembling can begin, summarised in the following steps (see figure C.10):

1. Material needed. Two pieces FE, one E, one F, one B1 and one B2. In total 6. A servo of the type Futaba 3003 with a crown of $\Phi 21\text{mm}$ and its screws (included with the servo). Also 5 screws of $\Phi 3\text{mm}$ and 10mm long and 6 bolts for these screws.
2. The pieces B1 and F are glued using a special adhesive for plastics.
3. One of the pieces FE is also glued to the base B1. Be careful not to fix it to the edge, but a few millimetres from it.
4. The piece E is glued to the B2, but not on the edge, but aligned with the inside face.
5. The other piece FE is also glued to the B2, but this one aligned to the outside face. A screw is put on the other piece FE, that will serve as a false axis.
6. The crown of the servo is screwed to the piece E.
7. The servo is screwed to the piece F. With this one of the two mobile parts of the module is obtained. This part is denominated the body of the module. The other part, that screws to the axis of the servo and the false axis, is called the head of the module.
8. Finally the body and the head are joined to complete the module. The two bolts are put on the false axis. Before joining it is necessary to calibrate the servo. It has to be in its central position (0 degrees), in such a way that when finished, the head can turn 90 degrees in both directions.

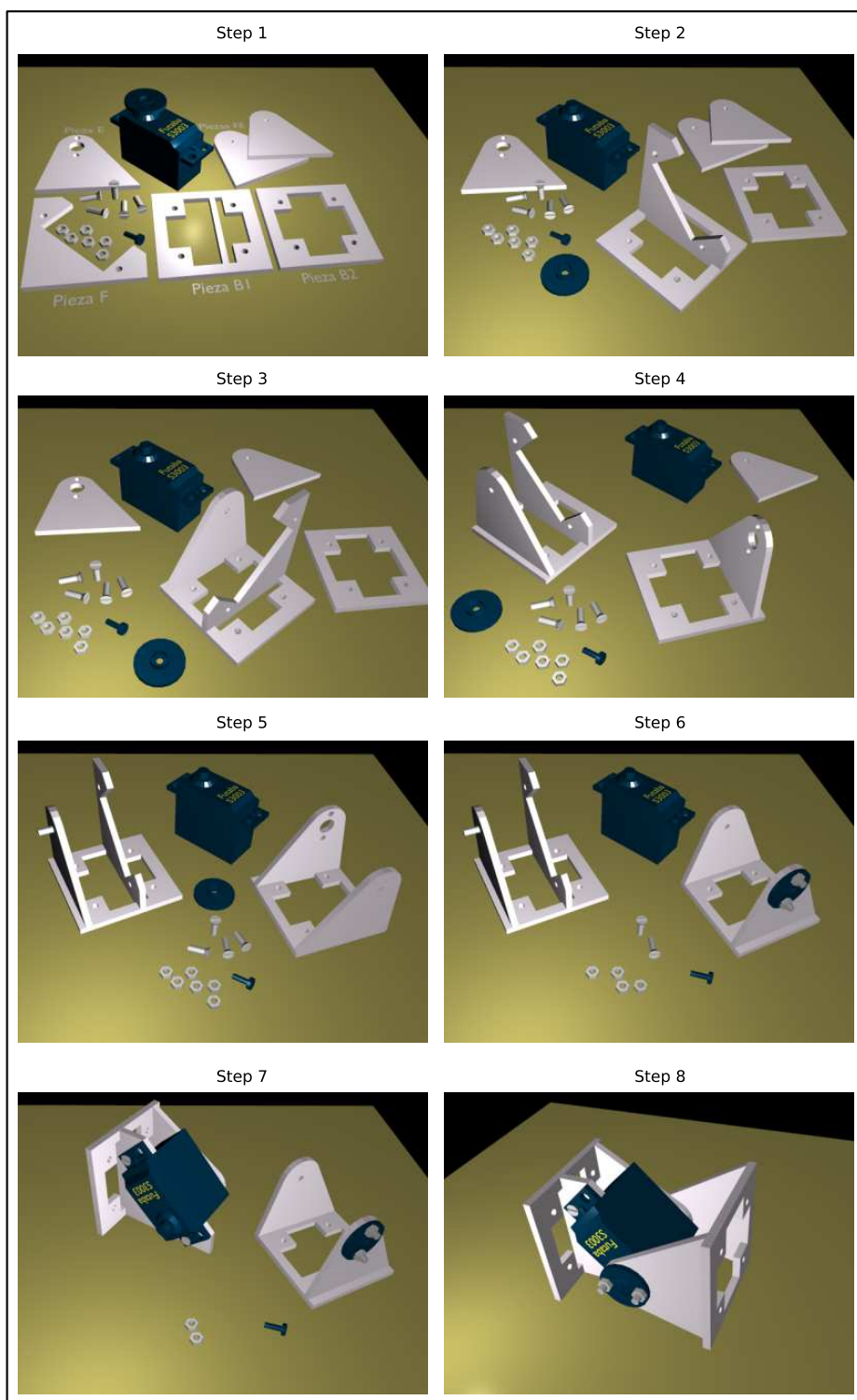


Figure C.10: Steps to assemble the Y1 module

Appendix D

Simulation

D.1 ODE Parameters

For the simulations the physical engine ODE¹ (Open Dynamics Engine) has been employed. It is a library that carries out all the physical calculations from the definition of the bodies of study. In each step of simulation the kinematic and dynamic parameters of all the elements are calculated.

The values employed for the parameters of the ODE are shown in the table D.1.

D.2 Simulation of the Y1 modules

For the simulation of the servos the recommendations indicated in the manual of the ODE have been followed. A proportional type controller has been employed, given by the equation D.1, where $w(t)$ is the angular speed, $\varphi(t)$ the bending angle, p the position of reference and K_p the gain.

¹<http://www.ode.org/>

Gravity	-9.81
CFM	10^{-5}
ERP	0.2
MaxCorrectingVel	0.1
SurfaceLayer	0.0001
Mu	0.2
Simulation step	0.01 Sec
AutodisableFlag	1

Table D.1: Values of the ODE parameters employed in the simulations

Parameter	Value	Units	Description
E_{min}	5	degrees	Minimum error ($\frac{\pi}{36}$ Rad)
L	72	mm	Module length
Width	52	mm	Module width
Height	52	mm	Module height
M	50	gr	Total mass
P_{max}	0.314	N.m	Servo Maximum torque
K_p	8.6	—	Servo gain (P controller)
W_{max}	$\frac{13}{9}\pi$	Rad/sec	Maximum angular speed (260 grad/Sec)

Table D.2: Parameters of both the module and servo employed in the simulations

$$w(t) = K_p[\varphi(t) - p] \quad (D.1)$$

The parameters used for the simulation of the Y1 modules are shown in the table D.2. The constant K_p has been adjusted empirically so that the settling time approximates to that of the Futaba 3003 servos.

The parameter E_{min} is the minimum error allowed between the desired position p and the bending angle $\varphi(t)$. When the condition is fulfilled D.2

$$|p - E_{min}| < |\varphi(t)| < |p + E_{min}| \quad (D.2)$$

it is considered that the servo has reached the position of reference and therefore can be sent to a new position. If E_{min} is near to 0, the servo reaches the position of reference with a low speed. The effect that this has when reproducing a sequence of movements constituted by a list of positions of reference, is that the movement is executed in jumps. To increase the fluidity a greater value of E_{min} is needed.

In the figure D.1 the response to the step function is represented. In the upper part the position of reference p is shown, that is 0 until at a certain moment it changes to 90 degrees (the step function), together with the output angle $\varphi(t)$. In the lower part the angular speed is shown. It can never be greater than the allowed maximum by the servo (W_{max}).

To implement the oscillation of the servos sequences of positions of references obtained from a sampling of a sine function are sent. The bending angle does not describe a perfect sinusoid but as shown in the figure D.2, where 8 samples are being used.

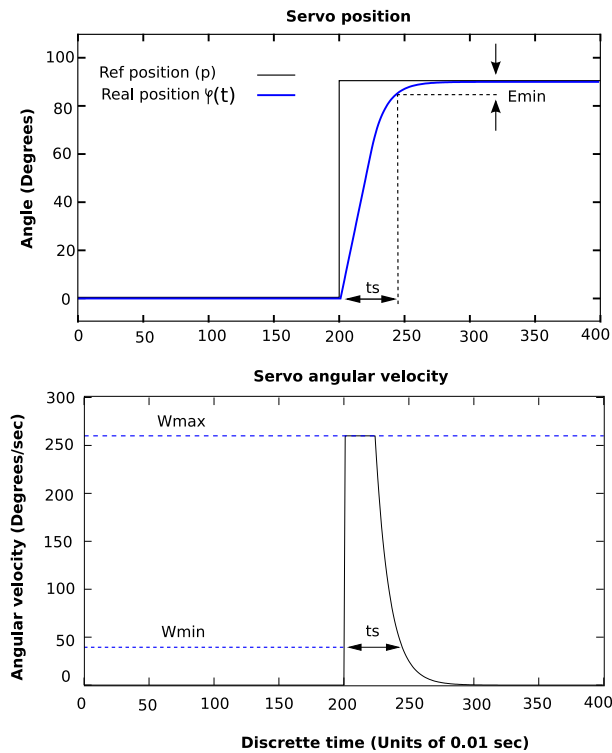


Figure D.1: Response to the step function of the simulated servo

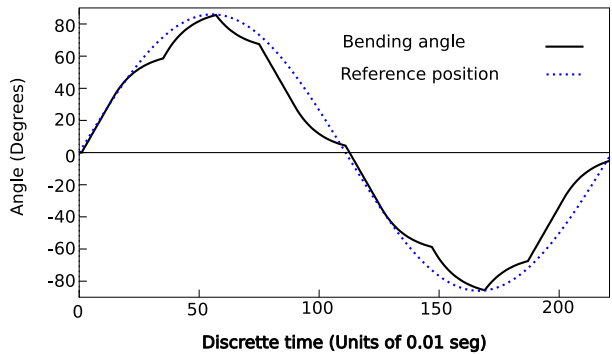


Figure D.2: Comparison between the real bending angle and the sinusoidal function, when 8 samples per period are used

Movement	Command
Pitch-pitch group	
Straight line. 32 Modules.	<code>./View './Pn 32 12 32 23 0'</code>
Straight line. Cube Revolution.	<code>./View './Pn 8 85 32 90 0'</code>
Straight line. Minicube-I	<code>./View './Pn 2 60 32 110 0'</code>
Pitch-yaw group	
Straight line. 32 Modules	<code>./View './PYn 32 32 20 0 0 0 45 0 0'</code>
Straight line. Hypercube	<code>./View './PYn 8 32 45 0 0 0 135 0 0'</code>
Straight line. Minicube-II	<code>./View './PYn 3 32 60 0 0 0 110 0 0'</code>
Turning. 18 Modules	<code>./View './PYn 18 32 70 0 0 10 120 0 0'</code>
Turning. Hypercube	<code>./View './PYn 8 32 20 0 0 22 120 0 0'</code>
Rolling. 20 Modules	<code>./View './PYn 20 32 10 10 0 0 0 0 90'</code>
Rolling. Hypercube	<code>./View './PYn 8 32 30 30 0 0 0 0 90'</code>
Rolling. Minicube-II	<code>./View './PYn 3 32 60 60 0 0 0 0 90'</code>
Rotation. 32 modules	<code>./View './PYn 32 32 10 40 0 0 90 45 0'</code>
Rotation. Hypercube	<code>./View './PYn 8 32 20 40 0 0 180 90 -45'</code>
Rotation. Minicube-II	<code>./View './PYn 3 32 30 40 0 0 180 0 90'</code>
Rotation in U. 16 Modules	<code>./View './PYn 16 32 10 20 0 0 90 0 90'</code>
Rotation in U. 8 Modules	<code>./View './PYn 8 32 10 40 0 0 180 0 90'</code>
Sideways movement. 32 Modules	<code>./View './PYn 32 20 5 40 0 0 -45 -45 112'</code>
Sideways movement. Hypercube	<code>./View './PYn 8 32 10 40 0 0 90 90 45'</code>
Inclined sideways movement. 32 Modules	<code>./View './PYn 32 32 20 20 0 0 -22 -22 0'</code>
Inclined sideways movement. Hypercube	<code>./View './PYn 8 24 40 40 0 0 -90 -90 60'</code>
Flapping. 16 modules	<code>./View './PYn 16 32 2 2 0 0 0 0 90'</code>
Flapping. Hypercube	<code>./View './PYn 8 32 7 7 0 0 0 0 90'</code>
Flapping. Minicube-II	<code>./View './PYn 3 100 30 30 0 0 0 0 90'</code>

Table D.3: Examples of use of the simulation of all the robots built in this dissertation

D.3 Examples of use

The simulator developed to analyse the movement of the apodal robots is formed by a set of utilities executed from the command line. One of them is *View*, that allows the visualisation of the movement in a three-dimensional setting. In the table D.3 some of the movements that the robots can execute have been compiled for the experiments of the thesis: Cube Revolutions, Hypercube, Minicube-I and Minicube-II.

The programme *View* is generic and allows the simulation of any apodal robot of the pitch-pitch type or pitch-yaw with any number of modules and any value for its parameters of the generators. Three blocks of parameters are passed. First the number of modules of the robot, then the values of the Amplitude parameters, Number of examples, Phase and Offset for each module and finally the type of module, using a P if it is pitch and Y if it is yaw.

In this thesis the solutions in the spaces H_1 and H_2 have been studied where all the generators are the same. To simplify the invocation the scripts Pn and Pyn have been used, to simulate the robots of the pitch-pitch and pitch-yaw groups respectively.

Therefore, to visualise the simulations the command employed is in this form:

```
./View './PYn M N Av Ah Ov Oh DFv DFh DFvh'
```

for pitch-yaw configurations or

```
./View './Pn M A N F 0'
```

for the pitch-pitch configurations.

Bibliography

- [1] A. Alonso-Puig. Application of Waves Displacement Algorithms for the Generation of Gaits in an All terrain Hexapod. In *Climbing and Walking Robots*, pages 343–348, September 2005.
- [2] R. Arredondo. Design and simulation of locomotion of self-organising modular robots for adaptive furniture. Master’s thesis, Swiss Federal Institute of Technology Lausanne, Biologically Inspired Robotics Group, July 2006.
- [3] J. Bares and D. Wettergreen. Dante ii: Technical description, results and lessons learned. *International Journal of Robotics Research*, 18(7):621–649, July 1999.
- [4] J. Borenstein, M. Hansen, and H. Nguyen. The OmniTread OT-4 Serpentine Robot for Emergencies and Hazardous Environments. In *Proceeding of the International Joint Topical Meeting: Sharing Solutions for Emergencies and Hazardous Environments*, 12 February 2006.
- [5] Y. Bourkin. Self-Organization of Locomotion in Modular Robots. Master’s thesis, University of Sussex, Brighton, United Kingdom, 2004.
- [6] J. M. Cañas. *Jerarquía dinámica de esquemas para la generación de comportamiento autónomo*. PhD thesis, Escuela Técnica Superior de Ingenieros de Telecomunicación, 2003.
- [7] J. M. Cañas and V. Matellán. From bio-inspired vs. psycho-inspired to etho-inspired robots. *Robotics and Autonomous Systems*, 55:841–850, 2007.
- [8] A. Castano, A. Behar, and P. Will. The Conro modules for reconfigurable robots. *IEEE/ASME Trans. Mechatronics*, 7(4):403–409, December 2002.
- [9] A. Castano, R. Chokkalingam, and P. Will. Autonomous and self-sufficient CONRO modules for reconfigurable robots. In *Proc. 5th Int’l Symp. Distributed Autonomous Robotic Systems*, pages 155–164, Knoxville, TN, 2000. Springer-Verlag.
- [10] A. Castano, W. Shen, and P. Will. CONRO: Towards deployable robots with inter-robots metamorphic capabilities. *Autonomous Robots*, 8(3):309–324, June 2000.
- [11] A. Castano and P. Will. Representing and discovering the configuration of CONRO robots. In *Proc. of IEEE Int. Conf. on Robotics and Automation*, pages 3503–3509, 2001.

- [12] L. Chen, Y. Wang, B. Li, S. Ma, and D Duan. Study on Locomotion of a Crawling Robot for Adaptation to the Environment. In Maki K. Habib, editor, *Bioinspiration and Robotics: Walking and Climbing Robots*, chapter 18, pages 301–316. I-Tech Education and Publishing, September 2007.
- [13] L. Chen, Y. Wang, and S. Ma. Studies on lateral rolling locomotion of a snake robot. In *Robotics and Automation, 2004. Proceedings. ICRA '04. 2004 IEEE International Conference on*, volume 5, pages 5070–5074, April 2004.
- [14] G. S. Chirikjian. Metamorphic Hyper-redundant Manipulators. In *Proceedings of the 1993 JSME International Conference on Advanced Mechatronics*, pages 467–472, August 1993.
- [15] G.S. Chirikjian. Kinematics of a metamorphic robotic system. In *Proceedings of the IEEE Int. Conf. on Robotics and Automation*, volume 1, pages 449–455, May 1994.
- [16] G.S Chirjkjian and J.W Burdick. Kinematically optimal hyperredundant manipulator configurations. *IEEE transactions on Robotics and Automation*, 11:794–806, 1995.
- [17] H. Choset. Coverage for robotics - a survey of recent results. *Annals of Mathematics and Artificial Intelligence*, 31:113 – 126, 2001.
- [18] H. Choset and W. Henning. A follow-the-leader approach to serpentine robot motion planning. In *ASCE Journal of Aerospace Engineering*, 1999.
- [19] D.J Christensen and K. Stoy. Selecting a Meta-Module to Shape-Change the ATRON Self-Reconfigurable Robot. In *Proceedings of IEEE International Conference on Robotics and Automations*, pages 2532–2538, May 2006.
- [20] A. H. Cohen and P.J Holmes. The Nature of the Couplings Between Segmental Oscillators of the Lamprey Spinal Generator for Locomotion: A Mathematical Model. *Journal of Mathematical Biology*, 13:345–369, 1982.
- [21] J. Conradt and P. Varshavskaya. Distributed central pattern generator control for a serpentine robot. In *Proceedings of the International Conference on Artificial Neural Networks and Neural Information Processing*, 2003.
- [22] A. Crespi, A. Badertscher, and A. Guignard. Swimming and crawling with an amphibious snake robot. In *Proceedings of the 2005 IEEE International Conference on Robotics and Automation*, pages 3035–3039, 2005.
- [23] A. Crespi, A. Badertscher, A. Guignard, and A. J. Ijspeert. An amphibious robot capable of snake and lamprey-like locomotion. In *Proceedings of the 35th international symposium on robotics*, 2004.
- [24] A. Crespi, A. Badertscher, A. Guignard, and A. J. Ijspeert. AmphiBot I : an amphibious snake-like robot. *Robotics and Autonomous Systems*, 50(4):163–175, 2005.

- [25] A. Crespi and A. J. Ijspeert. AmphiBot II: an amphibious snake robot that crawls and swims using a central pattern generator. In *Proceedings of the 9th International Conference on Climbing and Walking Robots*, pages 19–27, 2006.
- [26] A. Degani, A. Shapiro, H. Choset, and M. Mason. A dynamic single actuator vertical climbing robot. In *Intelligent Robots and Systems, 2007. IROS 2007. IEEE/RSJ International Conference on*, pages 2901–2906, November 2007.
- [27] F. Delcomyn. Neural basis of rhythmic behavior in animals. *Science*, 210:492–498, 1980.
- [28] S. Dirk and F. Kirchner. The Bio-Inspired SCORPION Robot: Design, Control and Lessons Learned. In Houxiang Zhang, editor, *Climbing and Walking Robots, Towards New Applications*, pages 197–218, Vienna, Austria, October 2007. I-tech Education and Publishing.
- [29] K. Dowling. *Limbless Locomotion: Learning to Crawl with a Snake Robot*. PhD thesis, Robotics Institute, Carnegie Mellon University, Pittsburgh, PA, December 1997.
- [30] G. Endo and J. Nakanishi. Experimental studies of a neural oscillator for biped locomotion with QRIO. In *Proceedings of the 2005 IEEE International Conference on Robotics and Automation*, pages 596–602, April 2005.
- [31] G. Endo, K. Togawa, and S. Hirose. Study on self-contained and Terrain Adaptive Active Cord Mechanism. In *Proc. of the IEEE/RSJ International Conference on Intelligent Robots and System*, pages 1399–1405, 1999.
- [32] G. Figliolini and P. Rea. Mechanics and Simulation of Six-Legged Walking Robots. In Houxiang Zhang, editor, *Climbing and Walking Robots, Towards New Applications*, chapter 1, pages 1–22. I-Tech Education and Publishing, October 2007.
- [33] S. Fukuda, T. Nakagawa. Dynamically reconfigurable robotic system. In *Proc. of the 1988 IEEE Int. Conf. on Robotics and Automation (ICRA)*, pages 1581–1586, April 1988.
- [34] T. Fukuda, S. Nakagawa, and Y. Kawauchi. Self organizing robots based on cell structures—CEBOT. In *Proc. of the IEEE/RSJ int. Conf. Intelligent Robots and Systems (IROS)*, pages 145–150, 1988.
- [35] Y. Fukuoka and H. Kimura. Adaptive dynamic walking of a quadruped robot on irregular terrain based on biological concepts. *The International Journal of Robotics Research*, 22(3-4):187–202, 2003.
- [36] K. Gilpin, K. Kotay, D. Rus, and I. Vasilescu. Miche: Modular shape formation by self-disassembly. *The International Journal of Robotics Research*, 27(3-4):345–372, 2008.
- [37] S. C. Goldstein and T. C. Mowry. Claytronics: A scalable basis for future robots. In *RoboSphere 2004*, Moffett Field, CA, November 2004.
- [38] M.P. Golombek and et al. Selection of the Mars Exploration Rover landing sites. *Journal of Geophysical Research*, 108(E3):ROV13.1–ROV13.48, October 2003.

- [39] A. Golovinsky, M. Yim, Z. Ying, and C. Eldershaw. PolyBot and PolyKinetic System: a modular robotic platform for education. In *Proceedings of the IEEE International Conference on Robotics and Automation*, volume 2, pages 1381–1386, 2004.
- [40] I. González, J. González-Gómez, and F. Gómez-Arribas. Hardware libre: clasificación y desarrollo de hardware reconfigurable en entornos GNU/Linux. In *Actas del VI Congreso de Hispalinux*, September 2003.
- [41] J. González-Gómez. Diseño de Robots Ápodos. Master's thesis, Escuela Politécnica Superiore. Universidad Autónoma de Madrid, July 2003. Available on line: <http://www.learobotics.com/personal/juan/doctorado/tea/tea.html> [Last visit May-14-2008].
- [42] J. Gonzalez-Gomez, Aguayo E., and E. Boemo. Locomotion of a Modular Worm-like Robot Using a FPGA-based Embedded MicroBlaze Soft-processor. In M. Armada and P. Gonzalez, editor, *Climbing and Walking Robots. Proceedings of the 7th International Conference CLAWAR 2004*, number ISBN 978-3-540-22992-6, pages 869–878. Springer Berlin Heidelberg, 2004.
- [43] J. Gonzalez-Gomez and E. Boemo. Motion of Minimal Confiurations of a Modular Robot: Sinusoidal, Lateral Rolling and Lateral shift. In *Proc. of the Int. Conf. on Climbing and Walking Robots*, pages 667–674, September 2005.
- [44] J. Gonzalez-Gomez, I Gonzalez, F. Gomez-Arribas, and E. Boemo. Evaluation of a Locomotion Algorithm for Worm-Like Robots on FPGA-Embedded Processors. In *Lecture Notes in Computer Science*, volume 3985, pages 24–29. Springer Berlin / Heidelberg, March 2006.
- [45] J. González-Gómez and A. Prieto-Moreno. Hardware libre: la Tarjeta Skypic, una Entrenadora para Microcontroladores PIC. In *Actas del I Congreso de Tecnologías del Software Libre*, pages 57–66, 7 July 2005.
- [46] J. Gonzalez-Gomez, H. Zhang, E. Boemo, and J. Zhang. Locomotion capabilities of a Modular Robot with Eighth Pitch-Yaw-Connecting Modules. In *Proc. of the Int. Conf. on Climbing and Walking machines*, pages 150–157, September 2006.
- [47] G. Granosik, M. G. Hansen, and J. Borenstein. The Omnitread Serpentine Robot for Industrial Inspection and Surveillance. *Industrial Robot*, 32(2):139–148, 2005.
- [48] R. Groß, M. Bonani, F. Mondada, and M. Dorigo. Autonomous self-assembly in a swarm-bot. In K. Murase, K. Sekiyama, N. Kubota, T. Naniwa, and J. Sitte, editors, *Proc. of the 3rd Int. Symp. on Autonomous Minirobots for Research and Edutainment (AMiRE 2005)*, pages 314–322. Springer, Berlin, Germany, 2006.
- [49] G.J. Hamlin and A.C. Sanderson. TETROBOT modular robotics: prototype and experiments. In *Proc. of the. IEEE/RSJ Int. Conf. on Intelligent Robots and Systems*, volume 2, pages 390 – 395, November 1996.

- [50] F. Herrero Carrón. Study and application of central patten generators to the control of a modular robot. Master's thesis, Escuela Politécnica Superior, Universidad Autónoma de Madrid, 30 August 2007.
- [51] S. Hirose. *Biologically Inspired Robots (Snake-like Locomotor and Manipulator)*. Oxford Science Press, 1993.
- [52] S. Hirose and G. Endo. Development of Autonomous Snake-Like Robot ACM R-1. In *Proc. Annual Conf. Robotics and Mechatronics*, page 1997, 1997. (in Japanese).
- [53] S. Hirose and E.F. Fukushima. Snakes and Strings: New Robotic Components for Rescue Operations. *The International Journal of Robotics Research*, 23(4-5):341–349, 2004.
- [54] S. Hirose, Imazato M., Kudo Y., and Umetani Y. Internally-balanced magnet unit. *Advanced robotics*, 1(3):225–242, 1986.
- [55] S. Hirose and A. Morishima. Articulated Body Mobile Robot. In *Proc. 7th RoManSy Symp*, pages 1–8, 1988.
- [56] S. Hirose and A. Morishima. Design and control of a mobile robot with an articulated body. *The International Journal of Robotics Research*, 9(2):99–113, 1990.
- [57] S. Hirose, A. Morishima, and S. Tukagosi. Design of Practical Snake Vehicle: Articulated Body Mobile Robot KR-II. In *Proc. 5th Int. Conf. Advanced Robotics*, volume 1, pages 833–838, 1991.
- [58] K. Hosokawa, T. Tsujimori, and T. Fujii. Self-organizing collective robots with morphogenesis in a verticalplane. In *Proc. of the IEEE Int. Conf. on Robotics and Automation*, volume 4, pages 2858–2863, 1998.
- [59] A. J. Ijspeert. *Design of artificial neural oscillatory circuits for the control of lamprey- and salamander-like locomotion using evolutionary algorithms*. PhD thesis, University of Edimburg, 1998.
- [60] A.J. Ijspeert and J.M. Cabelguen. Gait transition from swimming to walking: investigation of salamander locomotion control using non-linear oscillators. In *Adaptive Motion of Animals and Machines*, pages 177–188. Springer Tokyo, July 2006.
- [61] A.J. Ijspeert and A. Crespi. Simulation and robotics studies of salamander locomotion. Applying neurobiological principles to the control of locomotion in robots. *Neuroinformatics*, 3(3):171–196, 2005.
- [62] A.J. Ijspeert and A. Crespi. Online trajectory generation in an amphibious snake robot using a lamprey-like central pattern generator model. In *Proceedings of the 2007 IEEE International Conference on Robotics and Automation*, pages 262–268, 2007.
- [63] A.J. Ijspeert and J. Kodjabachian. Evolution and development of a central pattern generator for the swimming of a lamprey. *Artificial Life*, 5(3):247–269, 1999.

- [64] M.W. Jorgensen, E.H. Ostergaard, and H.H. Lund. Modular ATRON: modules for a self-reconfigurable robot. In *Proceedings of the IEEE/RSJ International Conference on Intelligent Robots and Systems*, volume 2, pages 2068–2073, 2004.
- [65] T. Kamegawa, T. Yamasaki, H. Igarashi, and F. Matsuno. Development of the snake-like rescue robot. In *Proc. of the IEEE Int. Conf. on Robotics and Automation*, volume 5, pages 5081–5086, April 2004.
- [66] A. Kamimura, H. Kurokawa, E. Toshida, K. Tomita, S. Murata, and S. Kokaji. Automatic locomotion pattern generation for modular robots. In *Proceedings of the IEEE International Conference on Robotics and Automation*, volume 1, pages 714–720, September 2003.
- [67] A. Kamimura, H. Kurokawa, and E. Yoshida. Automatic locomotion design and experiments for a modular robotic system. *IEEE/ASME Transactions on Mechatronics*, 10(3):314–325, June 2005.
- [68] A. Kamimura, H. Kurokawa, and T. Yoshida. Distributed adaptive locomotion by a modular robotic system, M-TRAN II. In *Proceedings of the IEEE/RSJ International Conference on Intelligent Robots and Systems, 2004. (IROS 2004).*, volume 3, pages 2370–2377, September 2004.
- [69] A. Kamimura, S. Murata, and E. Yoshida. Self-reconfigurable modular robot. Experiments on reconfiguration and locomotion. In *Proceedings of 2001 IEEE/RSJ International Conference on Intelligent Robots and Systems*, pages 606–612, 2001.
- [70] A. Kamimura, S. Murata, E. Yoshida, H. Kurokawa, K. Tomita, and S. Kokaji. Self-reconfigurable modular robot - experiments on reconfiguration and locomotion. In *Proceedings of the IEEE/RSJ International Conference on intelligent Robots and Systems*, volume 1, pages 606–612, 2001.
- [71] H. Kimura and S. Hirose. Development of Genbu : Active wheel passive joint articulated mobile robot. In *Proc. of the IEEE/RSJ Int. Conf. on Intelligent Robots and System*, volume 1, pages 823–828, 2002.
- [72] B. Kirby, J. D. Campbell, B. Aksak, P. Pillai, J. F. Hoburg, T. C. Mowry, and S. Goldstein. Catoms: Moving robots without moving parts. In *AAAI (Robot Exhibition)*, pages 1730–1, Pittsburgh, PA, July 2005.
- [73] B. Klaassen and K.L. Paap. GMD-SNAKE2: a snake-like robot driven by wheels and a method for motion control. In *Proceedings of IEEE International Conference on Robotics and Automation*, pages 3014–3019, 1999.
- [74] K. Kotay. *Self-Reconfiguring Robots: Designs, Algorithms, and Applications*. PhD thesis, Dartmouth College, Computer Science Department, 2003.
- [75] K. Kotay and D. Rus. Efficient Locomotion for a Self-Reconfiguring Robot. In *Proc. of the IEEE Int. Conf. on Robotics and Automation*, pages 2963–2969, 2005.

- [76] K. Kotay, D. Rus, and M. Vona. The Self-reconfiguring Robotic Molecule. In *Proc. of the IEEE Int. Conf. on Robotics and Automation*, pages 424–431, 1998.
- [77] E. Krotkov, R. Simmons, and W. Whittaker. Ambler: Performance of a six-legged planetary rover. *Acta Astronautica*, 35(1):75–81, 1995.
- [78] H. Kurokawa, A. Kamimura, and T. Yoshida. M-TRAN II: metamorphosis from a four-legged walker to a caterpillar. In *Proceedings of the IEEE/RSJ International Conference on Intelligent Robots and Systems*, volume 3, pages 2454–2459, September 2003.
- [79] H. Kurokawa, K. Tomita, and A. Kamimura. Distributed Metamorphosis Control of a Modular Robotic System M-TRAN. In *Distributed Autonomous Robotic Systems 7*, pages 115–124. Springer Japan, 2006.
- [80] H. Kurokawa, K. Tomita, and T. Yoshida. Motion simulation of a modular robotic system. In *IProceedings of the 26th Annual Conference of the IEEE Industrial Electronics Society*, volume 4, pages 2473–2478, 2000.
- [81] H. Kurokawaa, E. Yoshidaa, and K. Tomita. Self-reconfigurable M-TRAN structures and walker generation. *Robotics and Autonomous Systems*, 54(2):142–149, February 2006.
- [82] S. J. Lawrence, G. J. Taylor, R. C. F. Lentz, L. M. Martel, W. Shen, M. Will, M. H. Sims, S. Colombano, D. Kortenkamp, B. Damer, and W. Chun. SuperBots on the lunar surface: A habitat operations and maintenance system (HOMS). In *Lunar Exploration Analysis Group (LEAG)*, 2005.
- [83] C. Leger. *Darwin 2k: An Evolutionary Approach to Automated Design for Robotics*. Kluwer Academic Publishers, Norwell, MA, USA, 2000.
- [84] R. C. F. Lentz, G. J. Taylor, S. J. Lawrence, L. M. Martel, Wei-Min Shen, Peter M. Will, M. H. Sims, S. Colombano, D. Kortenkamp, B. Damer, and W. Chun. SuperBots on the lunar surface: A robotic multi-use lunar explorer (MULE). In *Lunar Exploration Analysis Group (LEAG)*, 2005.
- [85] R.A. Lindemann and C.J. Voorhees. Mars Exploration Rover mobility assembly design, test and performance. In *IEEE International Conference on Systems, Man and Cybernetics*, volume 1, pages 450–455, October 2005.
- [86] K. Lipkin, I. Brown, A. Peck, H. Choset, J. Rembisz, P. Gianfortoni, and A. Naaktgeboren. Differentiable and piecewise differentiable gaits for snake robots. In *Proc. of the IEEE/RSJ Int. Conf. on Intelligent Robots and Systems*, pages 1864–1869, October 2007.
- [87] S. Ma, H. Araya, and L. Li. Development of a creeping snake-robot. In *Proceedings of the IEEE International Symposium on Computational Intelligence in Robotics and Automation*, pages 77–82, 2001.

- [88] S. Ma, W.J. Li, and Y. Wang. A simulator to analyze creeping locomotion of a snake-like robot. In *Proceedings of IEEE International Conference on Robotics and Automation*, volume 4, pages 3656–3661, 2001.
- [89] S. Ma and Y. Ohmameuda. Control of a 3-dimensional snake-like robot. In *Proceedings of the IEEE International Conference on Robotics and Automation*, volume 2, pages 2067–2072, September 2003.
- [90] S. Ma and N. Tadokoro. Analysis of Creeping Locomotion of a Snake-like Robot on a Slope. *Autonomous Robots*, 20(1):15–23, January 2006.
- [91] D. Marbach. Evolution and Online Optimization of Central Pattern Generators for Modular Robot Locomotion. Master’s thesis, School of Computer and Communication Sciences, Swiss Federal Institute of Technology Lausanne., 7 January 2005.
- [92] D. Marbach and A.J. Ijspeert. Online Optimization of Modular Robot Locomotion. In *Proceedings of the IEEE International Conference on Mechatronics & Automation*, pages 248–253, June 2005.
- [93] V. Matellán, C. Fernández, and J. M. Molina. Genetic Learning of Fuzzy Reactive Controllers. *Robotics and Autonomous Systems*, 25(1-2):33–41, October 1998.
- [94] K. Matsuoka. Mechanisms of frequency and pattern control in the neural rhythm generators. *Biological Cybernetics*, 56(5-6):345–353, 1987.
- [95] J. Maye. Control of Locomotion in Modular Robotics. Master’s thesis, School of Computer and Communication Science. Swiss Federal Institute of Technology Lausanne, 23 February 2007.
- [96] P.G Miller. Snake Robots for Search and Rescue. In *Neurotechnology for Biomimetic Robots*, pages 271–284. MIT Press, 2002.
- [97] R. Moeckel, C. Jaquier, K. Drapel, E. Dittrich, A. Upegui, and A.J. Ijspeert. Exploring adaptive locomotion with YaMoR, a novel autonomous modular robot with Bluetooth interface. *Industrial Robot*, 33(4):285–290, 2006.
- [98] R. Moeckel, C. Jaquier, K. Drapel, A. Upegui, and A. Ijspeert. YaMoR and bluemove – an autonomous modular robot with bluetooth interface for exploring adaptive locomotion. In *Proceedings CLAWAR 2005*, pages 685–692, 2005.
- [99] F. Mondada, G. C. Pettinaro, A. Guignard, I. Kwee, D. Floreano, J.-L. Deneubourg, S. Nolfi, L.M. Gambardella, and M. Dorigo. Swarm-bot: a new distributed robotic concept. *Autonomous Robots*, 17(2–3):193–221, 2004.
- [100] F. Mondada, G. C. Pettinaro, I. Kwee, A. Guignard, L. Gambardella, D. Floreano, S. Nolfi, J.-L. Deneubourg, and M. Dorigo. SWARM-BOT: A swarm of autonomous mobile robots with self-assembling capabilities. In C.K. Hemelrijk and E. Bonabeau, editors, *Proceedings*

- of the International Workshop on Self-organisation and Evolution of Social Behaviour*, pages 307–312, Monte Verità, Ascona, Switzerland, September 8-13, 2002. University of Zurich.
- [101] M. Mori and S. Hirose. Development of Active Cord Mechanism ACM-R3 with Agile 3D mobility. In *Proc. of the IEEE/RSJ International Conference on Intelligent Robots and System*, pages 1552–1557, 2001.
- [102] M. Mori and S. Hirose. Three-dimensional serpentine motion and lateral rolling by Active Cord Mechanism ACM-R3. In *Proc. of IEEE/RSJ Int. Conf. on intelligent Robots and Systems*, pages 829–834, 2002.
- [103] J.M. Morrey, B. Lambrecht, A.D. Horchler, R.E. Ritzmann, and R.D. Quinn. Highly mobile and robust small quadruped robots. In *Proceedings. 2003 IEEE/RSJ International Conference on Intelligent Robots and Systems, 2003. (IROS 2003).*, volume 1, pages 82–87, October 2003.
- [104] S. Murata, K. Kakomura, and H. Kurokawa. Docking Experiments of a Modular Robot by Visual Feedback. In *Proceeding of the IEEE/RSJ International Conference on Intelligent Robots and Systems*, pages 625–630, October 2006.
- [105] S. Murata and H. Kurokawa. Self-Reconfigurable Robot. *IEEE Robotics and Automation Magazine*, 14(1):71–78, March 2007.
- [106] S. Murata, H. Kurokawa, and S. Kokaji. Self-assembling machine. In *Proc. of Int. Conf. on Robotics and Automation*, volume 1, pages 441–448, 1994.
- [107] S. Murata, H. Kurokawa, E. Yoshida, K. Tomita, and S. Kokaji. A 3-D self-reconfigurable structure. In *Proc. of the IEEE Int. Conf. on Robotics and Automation*, volume 1, pages 432–439, May 1998.
- [108] S. Murata, E. Yoshida, A. Kamimura, H. Kurokawa, K. Tomita, and S. Kokaji. M-TRAN: self-reconfigurable modular robotic system. *IEEE/ASME Transactions on Mechatronics*, 7(4):431–441, December 2002.
- [109] S. Murata, E. Yoshida, and H. Kurokawa. Self-Repairing Mechanical Systems. *Autonomous Robots*, 10(1):7–21, January 2001.
- [110] S. Murata, E. Yoshida, K. Tomita, H. Kurokawa, A. Kamimura, and S. Kokaji. Hardware design of modular robotic system. In *Proceedings of the IEEE/RSJ International Conference on Intelligent Robots and Systems*, volume 3, pages 2210–2217, November 2000.
- [111] Paap K.L., T. Christaller, and F. Kirchner. A robot snake to inspect broken buildings. In *Proceeding of the 2000 IEEE/RSJ International Conference on Intelligent Robots and Systems*, pages 2079–2082, 2000.
- [112] A. Pamecha, C. Chiang, D. Stein, and G. Chirikjian. Design and implementation of metamorphic robots. In *Proceedings of the 1996 ASME Design Engineering Technical Conference and Computers in Engineering Conference*, August 1996.

- [113] M. Park, S. Chitta, A. Teichman, and M. Yim. Automatic Configuration Recognition Methods in Modular Robots. *The International Journal of Robotics Research*, 27(3-4):403–421, 2008.
- [114] A. Prieto-Moreno. Diseño, construcción y control de un robot articulado mediante una red de microcontroladores. Proyecto fin de carrera, UPM, February 2001.
- [115] A. Prieto-Moreno. Estudio de la locomoción de un robot cuadrúpedo mediante la generación de patrones biológicos. Master's thesis, Escuela Politécnica superior. Universidad Autónoma de Madrid, October 2007.
- [116] R.D. Quinn, J.T. Offi, D.A. Kingsley, and R.E. Ritzmann. Improved mobility through abstracted biological principles. In *IEEE/RSJ International Conference on Intelligent Robots and System*, 2002., volume 3, pages 2652–2657, 2002.
- [117] E. Rome, J. Hertzberg, F. Kirchner, U. Licht, and T. Christaller. Towards autonomous sewer robots: the MAKRO project. *Urban Water*, 1(1):57–70, 1999.
- [118] K. Roufas, Y. Zhang, D. Duff, and M. Yim. Six Degree of Freedom Sensing For Docking Using IR LED Emitters. In *Experimental Robotics VII*, volume 271, pages 91–100. Springer Berlin / Heidelberg, 2001.
- [119] C. M Rovainen. Neurobiology of lampreys. *Physiological Reviews*, 59(4):1007–1077, 1 October 1979.
- [120] M. Rubenstein, K. Payne, P. Will, and W. Shen. Docking among independent and autonomous CONRO self-reconfigurable robots. In *Proc. of the IEEE Int. conf. on Robotics and Automation*, pages 2877–2882, New Orleans, USA, April/May 2004.
- [121] N. F Rulkov. Modeling of spiking-bursting neural behavior using two-dimensional map. *Physical Review E*, 65(4):041922, April 2002.
- [122] D. Rus and M. Vona. Self-reconfiguration planning with compressible unit modules. In *Proceedings of the IEEE Intl. Conference on Robotics and Automation*, volume 4, pages 2513–2520, Detroit, MI, USA, 1999.
- [123] D. Rus and M. Vona. Crystalline robots: Self-reconfiguration with compressible unit modules. *Autonomous Robots*, 10(1):107–124, 2001.
- [124] B. Salemi, M. Moll, and W. Shen. SUPERBOT: A deployable, multi-functional, and modular self-reconfigurable robotic system. In *Proc. of the IEEE/RSJ Int. Conf. on Intelligent Robots and Systems*, Beijing, China, October 2006. To appear.
- [125] B. Salemi, W. Shen, and P. Will. Hormone-controlled metamorphic robots. In *Proc. of the Int. Conf. on Robotics and Automation*, volume 4, pages 4194–419, 2001.
- [126] B. Salemi, P. Will, and W. Shen. Autonomous discovery and functional response to topology change in self-reconfigurable robots. In Dan Braha, Ali A. Minai, and Yaneer Bar-Yam, editors, *Complex Engineering Systems: Science Meets Technology*, pages 364–384. Springer, 2006.

- [127] J. Sastra, S. Chitta, and M. Yim. Dynamic Rolling for a Modular Loop Robot. In *Experimental Robotics*, volume 39 of *Springer Tracts in Advanced Robotics*, pages 421–430. Springer Berlin / Heidelberg, 2008.
- [128] J. Sastra, W. Giovanni, B. Heredia, and J. Clark. A biologically-inspired dynamic legged locomotion with a modular reconfigurable robot. In *Proceedings of ASME Dynamic Systems and Control Conference*, October 2008.
- [129] E. Shammas, A. Wolf, and H. Choset. Three degrees-of-freedom joint for spatial hyper-redundant robots. *Journal of Mechanism and Machine Theory*, pages 170 – 190, April 2005.
- [130] W. Shen, J. Bogdanowicz, W. Chun, M. Yim, Peter M. Will, M. Sims, S. Colombano, D. Kortenkamp, S. Vanderzyl, E. Baumgartner, and J. Taylor. SuperBots: Modular, multifunctional, reconfigurable robotic system for space exploration. In *Lunar Exploration Analysis Group (LEAG)*, 2005.
- [131] W. Shen, M. Krivokon, H. Chiu, J. Everist, M. Rubenstein, and J. Venkatesh. Multimode locomotion for reconfigurable robots. *Autonomous Robots*, 20(2):165–177, 2006.
- [132] W. Shen, B. Salemi, and P. Will. Hormone-inspired adaptive communication and distributed control for CONRO self-reconfigurable robots. *Trans. on Robotics and Automation*, 18(5):700–712, October 2002.
- [133] M. L. Shik and Severin. Control of walking and running by means of electrical stimulation of the mid-brain. *Biophysics*, 11:756–765, 1966.
- [134] B. Shirmohammadi, M. Yim, and J. Sastra. Using Smart Cameras to Localize Self-Assembling Modular Robots. In *DFirst ACM/IEEE International Conference on Distributed Smart Cameras*, pages 76–80, September 2007.
- [135] K.A. Sigvardt and T.L. Williams. Effects of local oscillator frequency on intersegmental coordination in the Lamprey locomotor Cpg: theory and experiments. *Journal of Neurophysiology*, 76(6):4094–4103, December 1996.
- [136] D. Spennberg, M. Albrecht, T. Backhaus, J. Hilljegerdes, F. Kirchner, and H. Zschenker. ARAMIES: A Four-legged Climbing and Walking Robot. In *'i-SAIRAS 2005' - The 8th International Symposium on Artificial Intelligence, Robotics and Automation in Space*, volume 603 of *ESA Special Publication*, August 2005.
- [137] D. Spennberg, F. Kirchner, and J. de Gea. Ambulating robots for exploration in rough terrain on future extraterrestrial missions, 2004.
- [138] B. Spranklin. *Design, Analysis, and Fabrication of a Snake-Inspired Robot with a Rectilinear Gait*. PhD thesis, University of Maryland, June 2006.
- [139] A. Sproewitz, R. Moeckel, J. Maye, M. Asadpour, and A.J. Ijspeert. Adaptive locomotion control in modular robotics. In *Workshop on Self-Reconfigurable Robots/Systems and Applications IROS07*, pages 81–84, November 2007.

- [140] A. Sproewitz, R. Moeckel, J. Maye, and A. Ijspeert. Learning to move in modular robots using central pattern generators and online optimization. *Int. J. Rob. Res.*, 27(3-4):423–443, 2008.
- [141] H. Streich and O. Adria. Software approach for the autonomous inspection robot MAKRO. In *Proc. of the IEEE Int. Conf. on Robotics and Automation*, volume 4, pages 3411– 3416, 2004.
- [142] Y. Sugiyama, A. Shiotsu, and M. Yamanaka. Circular/spherical robots for crawling and jumping. In *Proc. of the IEEE Int. Conf. on Robotics and Automation*, pages 3595– 3600, 2005.
- [143] J.W. Suh, S.B. Homans, and M. Yim. Telecubes: mechanical design of a module for self-reconfigurable robotics. In *Proceedings of the IEEE Int. Conf. on Robotics and Automation*, volume 4, pages 4095– 4101, 2002.
- [144] T. Takayama and S. Hirose. Development of Souryu-I connected crawler vehicle for inspection of narrow and winding space. In *Proceeding of the 26th Annual Conference of the IEEE Industrial Electronics Society*, volume 1, pages 143–148, 2000.
- [145] T. Takayama and S. Hirose. Amphibious 3D Active Cord Mechanism "HELIX" with Helical Swimming Motion. In *Proc. of IEEE/RSJ Int. Conf. on intelligent Robots and Systems*, volume 1, pages 775– 780, 2002.
- [146] T. Takayama and S. Hirose. Development of "Souryu I and II" -Connected Crawler Vehicle for Inspection of Narrow and Winding Space. *Robotics and Mechatronics*, 15(1):61–69, 2003.
- [147] G. J. Taylor, R. C. F. Lentz, S. J. Lawrence, L. M. Martel, Wei-Min Shen, Peter M. Will, M. H. Sims, S. Colombano, D. Kortenkamp, B. Damer, and W. Chun. SuperBots on the lunar surface: Mini-mobile investigation system (Mini-MIS). In *Lunar Exploration Analysis Group (LEAG)*, 2005.
- [148] K. Togawa, M. Mori, and S. Hirose. Study on Three-dimensional Active Cord Mechanism: Development of ACM-R2. In *Proc. of the IEEE/RSJ International Conference on Intelligent Robots and System*, pages 2242–2247, 2000.
- [149] R. Treviño. Entorno de simulación para el estudio de la locomoción de robots modulares. Proyecto fin de carrera. Escuela Superior de Informática. Universidad Politécnica de Madrid, 15 October 2007.
- [150] Y. Umetani and S. Hirose. Biomechanical Study of Serpentine Locomotion. In *Proc. of the 1st RoManSySymp*, pages 171–184, 1974.
- [151] C. Unsal. I-Cubes, A Modular Self-Reconfigurable Bipartite System. *Robotics and Machine Perception*, 9(1), March 2000.
- [152] J. Ute and K. Ono. Fast and efficient locomotion of a snake robot based on self-excitation principle. In *Proc. 7th International Workshop on Advanced Motion Control*, pages 532– 539, 2002.

- [153] W. Wang and G. Zong. Analysis on The Mechanics Stability for a New Kind of Robot. *Journal of Robot*, 21(7):642–648, 99.
- [154] T.L. Williams and K.A. Sigvardt. Intersegmental phase lags in the lamprey spinal cord: experimental confirmation of the existence of a boundary region. *Journal of Computational Neuroscience*, 1:61–67, 1994.
- [155] T.L. Williams and K.A. Sigvardt. Spinal cord of Lamprey: generation of locomotor patterns. In *The handbook of brain theory and neural networks*, pages 918–921. MIT Press, 1995.
- [156] D. M. Wilson. The central nervous control of flight in a locust. *Journal of Experimental Biology*, 38:471–490, 1961.
- [157] A. Wolf, H. Brown, R. Casciola, A. Costa, M. Schwerin, E. Shamas, and H. Choset. A mobile hyper redundant mechanism for search and rescue tasks. In *Proceedings of the 2003 IEEE/RSJ International Conference on Intelligent Robots and Systems*, volume 3, pages 2889 – 2895, October 2003.
- [158] C. Wright, A. Johnson, A. Peck, Z. McCord, A. Naaktgeboren, P. Gianfortoni, M. Gonzalez-Rivero, R. Hatton, and H. Choset. Design of a modular snake robot. In *Proc. of the IEEE/RSJ Int. Conf. on Intelligent Robots and Systems*, pages 2609–2614, October 2007.
- [159] H. Yamada, S. Chigisaki, and M. Mori. Development of Amphibious Snake-like Robot ACM-R5. In *The Proc. of 36th Int. Symposium on Robotics*, 2005.
- [160] H. Yamada and S. Hirose. Development of Practical 3-Dimensional Active Cord Mechanism ACM-R4. *Journal of Robotics and Mechatronics*, 18(3), 2006.
- [161] M. Yamakita, M. Hashimoto, and T. Yamada. Control of locomotion and Head Configuration of a 3D Snake Robot. In *ICRA '03. Proc of the IEEE Int. Conf. on Robotics and Automation*, volume 2, pages 2055– 2060, September 2003.
- [162] M. Yerly. YaMoR Lifelong Learning. Master’s thesis, Computer Science Department, University of Fribourg, 2007.
- [163] M. Yim. *Locomotion with a unit-modular reconfigurable robot*. PhD thesis, Stanford University, December 1995. Available on-line: <http://www-db.stanford.edu/TR/CS-TR-95-1536.html> [Last visit May-10-2008].
- [164] M. Yim, D. Duff, and K. Roufas. Modular Reconfigurable Robots, An Aproach to Urban Search and Rescue. In *Proc. of 1st Intl. Workshop on Human-friendly welfare Robotic Systems*, pages 69–76, January 2000.
- [165] M. Yim, D.G. Duff, and K. D. Roufas. PolyBot: a modular reconfigurable robot. In *Proceedings of the IEEE International Conference on Robotics and Automation*, volume 1, pages 514–520, April 2000. Available on-line: <http://www2.parc.com/spl/projects/modrobots/publications/pdf/icra00.pdf> [Last visit: May-14-2008].

- [166] M. Yim, D.G. Duff, and Roufas K.D. Walk on the wild side. *IEEE robotics and automation magazine*, 9(4):49–53, 2002.
- [167] M. Yim, D. Goldberg, and A. Casal. Connectivity planning for closed-chain reconfiguration. In G. T. McKee and P. S. Schenker, editors, *Proc. SPIE Vol. 4196, p. 402-412, Sensor Fusion and Decentralized Control in Robotic Systems III, Gerard T. McKee; Paul S. Schenker; Eds.*, volume 4196 of *Presented at the Society of Photo-Optical Instrumentation Engineers (SPIE) Conference*, pages 402–412, October 2000.
- [168] M. Yim, R. Hinden, C. Conley, C.K. Wang, K. Roufas, and C. Eldershaw. Open Loop Climbing with Modular Robots. In *Video Proceeding of the IEEE International Conference on Robotics and Automation*, 2006.
- [169] M. Yim, S. Homans, and K. Roufas. Climbing with Snake-like Robots. In *Proc. of the IFAC Workshop on Mobile Robot Technology*, 21 May 2001.
- [170] M. Yim, K. Roufas, and D. Duff. Modular Reconfigurable Robots in Space Applications. *Autonomous Robots*, 14(2-3):225–237, March 2003.
- [171] M. Yim, W. M. Shen, and B. Salemi. Modular self-reconfigurable robot systems. *IEEE Robotics and automation Magazine*, 14(1):43–52, 2007.
- [172] M. Yim, B. Shirmohammadi, and J. Sastra. Robustness and self-repair in modular robots. In *IEEE/RSJ International Conference on Intelligent Robots and Systems*, pages 2553–2554, October 2007.
- [173] M. Yim, B. Shirmohammadi, and J. Sastra. Towards robotic self-reassembly after explosion. In *IEEE/RSJ International Conference on Intelligent Robots and Systems*, pages 2767–2772, October 2007.
- [174] M. Yim, Y. Zhang, and D. Duff. Modular robots. *IEEE Spectrum*, 39(2):30–34, February 2002.
- [175] M. Yim, Y. Zhang, K. Roufas, D. Duff, and C. Eldershaw. Connecting and disconnecting for chain self-reconfiguration with PolyBot. *IEEE/ASME Transactions on Mechatronics*, 7(4):442–451, December 2002.
- [176] E. Yoshida, A. Kamimura, and K. Tomita. A Self-Reconfigurable Modular Robot: Reconfiguration Planning and Experiments. *The International Journal of Robotics Research*, 21(10-11):903–915, 2002.
- [177] E. Yoshida, S. Murata, A. Kamimura, K. Tomita, H. Kurokawa, and S. Kokaji. A motion planning method for a self-reconfigurable modular robot. In *Proceedings of the IEEE/RSJ International Conference on Intelligent Robots and Systems*, volume 1, pages 590–597, 2001.
- [178] H. Zhang, Z. Deng, and W. Wang. Novel Reconfigurable Robot with 3 DOF Active Joints for Rugged Terrain. In *Proceedings of the IEEE/RSJ International Conference on Intelligent Robots and Systems*, pages 5588 – 5593, October 2006.

- [179] H. Zhang, J. Gonzalez-Gomez, S. Chen, W. Wang, R. Lin, D Li, and J. Zhang. A Novel Modular Climbing Caterpillar Using Low-Frequency Vibrating Passive Suckers. In *Proc. of the IEEE/ASME International Conference on Advanced Intelligent Mechatronics*, 4 September 2007.
- [180] H. Zhang, J. Gonzalez-Gomez, Z. Xie, S. Cheng, and J. Zhang. Development of a Low-cost Flexible Modular Robot GZ-I. In *Proc. of the IEEE/ASME International Conference on Advanced Intelligent Mechatronics*, pages 223–228, 4 June 2008.
- [181] H. Zhang, W. Wang, and Z. Deng. A Novel Reconfigurable Robot for Urban Search and Rescue. *International Journal of Advanced Robotic Systems*, 3(4):359–366, 2006.
- [182] Y. Zhang, A. Golovinsky, C. Eldershaw, and M. Yim. An XML-based scripting language for chain-type modular robotic systems. In *Proc of 8th Conference on Intelligent Autonomous Systems*, 2004.
- [183] Y. Zhang, K.D. Roufas, and M. Yim. Software architecture for modular self-reconfigurable robots. In *Proceedings of the IEEE/RSJ International Conference on Intelligent Robots and Systems*, volume 4, pages 2355–2360, 2001.
- [184] Y. Zhang, M. Yim, C. Eldershaw, D. Duff, and K. Roufas. Phase automata: a programming model of locomotion gaits for scalable chain-type modular robots. In *IProceedings. of the IEEE/RSJ International Conference on intelligent Robots and Systems*, volume 3, pages 2442–2447, 2003.
- [185] G. Zong, Z. Deng, and W. Wang. Realization of a Modular Reconfigurable Robot for Rough Terrain. In *Proceedings of the 2006 IEEE International Conference on Mechatronics and Automation*, pages 289–294, 2006.
- [186] V. Zykov, A. Chan, and H. Lipson. Molecubes: An Open-Source Modular Robotics Kit. In *Proc. of the IEEE Int. Conf. on Intelligent Robots and systems*, 2007.
- [187] V. Zykov, E. Mytilinaios, B. Adams, and H. Lipson. Self-reproducing machines. *Nature*, 435(7039):163–164, 2005.